SAR

Synthetic Aperture Radar

EARTH OBSERVING SYSTEM

Volume IIf

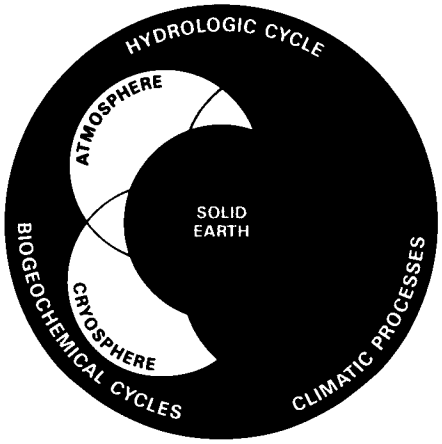

INSTRUMENT PANEL REPORT

NASA
National Aeronautics and
Space Administration

EARTH OBSERVING SYSTEM REPORTS

Volume I	Science and Mission Requirements Working Group Report
Volume II	From Pattern to Process: The Strategy of the Earth Observing System Science Steering Committee Report
Volume IIa	Data and Information System Data Panel Report
Volume IIb	MODIS Moderate-Resolution Imaging Spectrometer Instrument Panel Report
Volume IIc	HIRIS High-Resolution Imaging Spectrometer: Science Opportunities for the 1990s Instrument Panel Report
Volume IId	LASA Lidar Atmospheric Sounder and Altimeter Instrument Panel Report
Volume IIe	HMMR High-Resolution Multifrequency Microwave Radiometer Instrument Panel Report
Volume IIf	SAR Synthetic Aperture Radar Instrument Panel Report
Volume IIg	LAWS Laser Atmospheric Wind Sounder Instrument Panel Report
Volume IIh	Altimetric System Panel Report

SYNTHETIC APERTURE RADAR INSTRUMENT PANEL FOR THE EARTH OBSERVING SYSTEM

Keith Carver, Chairman
JoBea Cimino, Co-Chairman
Charles Elachi, Co-Chairman
Marguerite Syvertson, Executive Secretary
Robert Beal, Oceanography Team Leader
Theodore Engman, Hydrology Team Leader
Gerald Schaber, Geology Team Leader
Fawwaz Ulaby, Vegetation Science Team Leader
Wilford Weeks, Glaciology Team Leader
William Campbell
Frank Carsey
John Curlander
Craig Dobson
Lee-Lueng Fu
Robert Gurney
Benjamin Holt
Robert Murphy
Robert Shuchman
Calvin Swift
James Taranik
Diane Wickland
Paul Zinke

COVER PHOTOGRAPH:

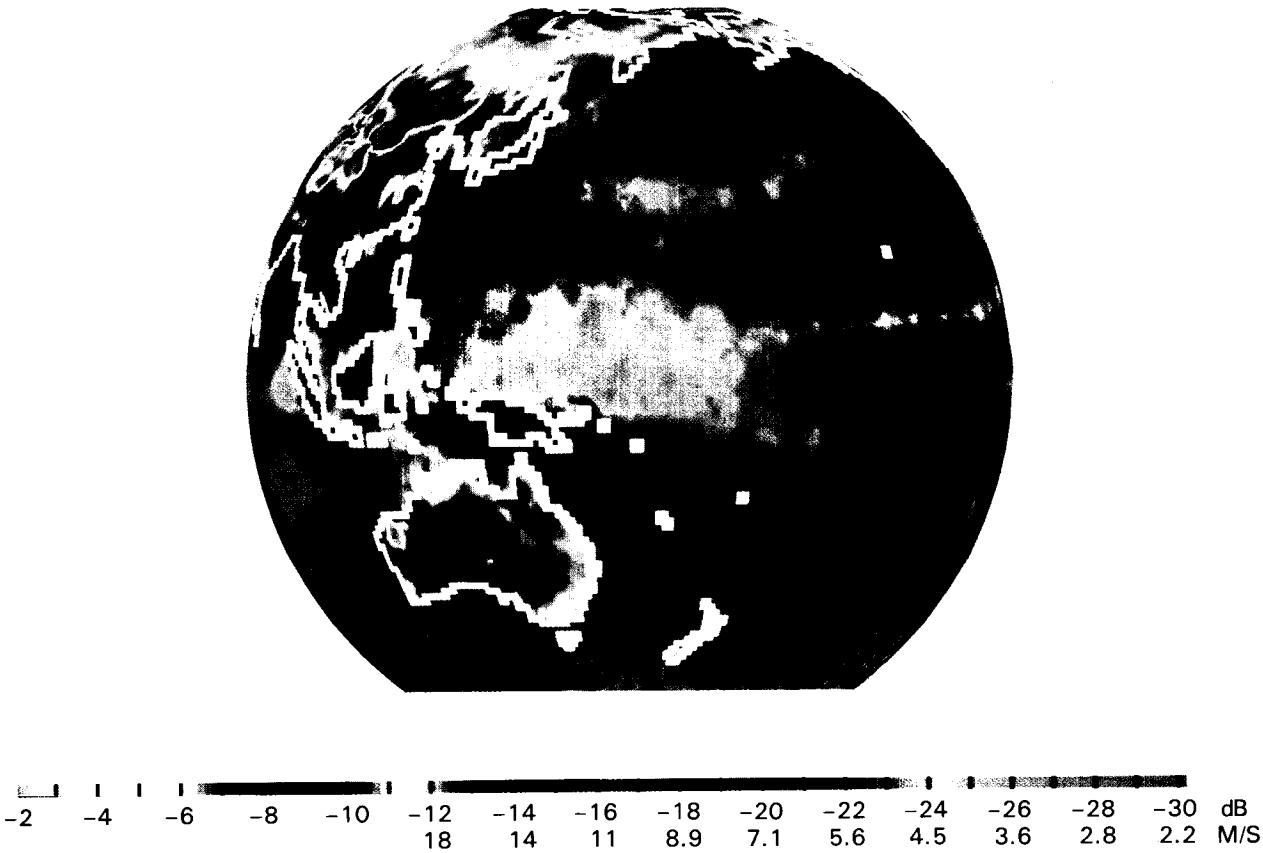

The cover photograph presents images made from various spaceborne radar systems. The global picture in the center view is a radar image of the world as seen in 1978 by the Seasat K_u-band Scatterometer System (SASS). Over the land is shown the mean vertically polarized backscatter coefficient at 45° incidence angle averaged over the mission duration (July 7 through October 9, 1978). This backscatter depends mainly on vegetation type and moisture. The top scale on the color bar shows the backscatter coefficient in dB.

Over the oceans are shown the mean wind speeds averaged over the mission duration derived from the backscatter coefficients measured at multiple azimuth angles and a 45° incidence angle at each location. The bottom scale on the color bar shows the wind speed. Regions around the poles have been omitted because of no coverage by SASS or because of the existence of sea ice. This global map is indicative of the observations expected from the Eos Synthetic Aperture Radar in its global mapping mode.

The four radar images surrounding the global map provide examples of the spatial detail that can be expected from the Eos SAR in its highest resolution mode. The upper left image, acquired by the Shuttle Imaging Radar-A (SIR-A), shows buried paleodrainages of the Eastern Sahara. The upper right image, acquired by the SIR-B, shows oceanic eddy features. In the lower left image, acquired by the Seasat SAR, detail of sea ice morphology in the Beaufort Sea region is shown. The lower right image illustrates landform details obtained from multipolarization data; this image was acquired by the Jet Propulsion Laboratory (JPL) aircraft L-band multipolarization SAR.

Rosemary Kennett, JPL

PREFACE

The objective of the Synthetic Aperture Radar (SAR) Panel has been to establish scientific and engineering requirements for a SAR instrument to be included as part of NASA's Earth Observing System (Eos). The SAR Panel members were selected by the Earth Science and Applications Division of NASA Headquarters. The general role of SAR within the context of Eos has been described in the Earth Observing System Reports (Butler *et al.*, 1984) and by the Earth System Sciences Committee (Bretherton *et al.*, 1986).

Through a series of meetings held over a period of 2½ years, the SAR Panel has developed scientific and engineering requirements for a SAR instrument as described in this report. The Panel was organized into five geoscientific teams (glaciology, hydrology, vegetation science, oceanography, and geology). Each discipline team, headed by a Team Leader, was asked to develop general scientific requirements for SAR data, specific geoscientific observational needs, and corresponding instrument requirements.

The SAR Panel wishes to acknowledge the assistance of a number of individuals not on the Panel but who made substantial contributions to this report. Valuable scientific contributions and suggestions were made by Miriam Baltuck, Carol Breed, Art Bloom, John Crawford, Jeff Dozier, Diane Evans, Tom Farr, John Ford, Marc Imhoff, Rosemary Kennett, Mike Kobrick, John Norman, Manfred Owe, Jack Paris, Martin Ruzek, Mike Thomas, Steve Wall, and Jacob van Zyl. Preliminary SAR system design calculations were made by Ed Caro, Dan Held, Neil Herman, and Rolando Jordan. The SAR Data Acquisition Plan and detailed data rate computations were contributed by Daren Casey; other data and information system concepts were provided by Steve Wall, Dave Nichols, and Mike Thomas. Important contributions were made by Elizabeth Smith to the discussions on altitude effects and the computations of average data rates. Valuable insights into synergism and multi-instrument concepts were provided by Harry Press, Jim Graf, Deborah Vane, Robert Rowley, and Michael Mangano. The Panel also acknowledges the dedicated efforts of Kathy Banwart, Michele Vogt, Margie Olanyk, and Annie Richards, all of whom were instrumental in the preparation of report drafts, and the assistance in preparation of illustrations provided by Joe Kelly and Marysha Cleary and the JPL Graphics and Photolab. The Panel expresses its gratitude for the efforts of Debby Critchfield, Dawn Cardascia, and Brenda Moldawer for their skillful handling of the final manuscript.

Keith R. Carver
Chairman, SAR Instrument Panel
Amherst, Massachusetts

EXECUTIVE SUMMARY

One of the main objectives of the Earth Observing System (Eos) is to understand the processes and interactions that lead to large-scale changes in the Earth's environment, and to monitor these changes on a global basis over a significant time period of at least a decade. In order to observe and monitor the different features of the Earth's environment, sensing over a wide range of the electromagnetic spectrum is necessary. Visible and infrared sensing is mostly sensitive to the chemical and thermal properties of the observed medium, while microwave sensing is mostly sensitive to the physical and electrical properties of the surface, its covering, and subsurface.

In order to achieve Eos objectives, a suite of instruments is required for large-scale coverage and high (spatial and spectral) resolution, in-depth analysis. In the optical and near-infrared spectral region, surface observations are met with MODIS, for large-scale coverage, and HIRIS for high spectral and spatial resolution. In the active microwave region, similar functions are incorporated in one single instrument, the Synthetic Aperture Radar (SAR). SAR has two fundamental capabilities. The first one allows large-scale coverage (global coverage every 3 days) at a moderate resolution (a few hundred meters). This capability complements MODIS for global monitoring. The second capability allows multispectral, multipolarization, high resolution (tens of meters) imaging to study the details of surface processes, and thus complements HIRIS. The combination of SAR, HIRIS, and MODIS will provide a very powerful tool to observe global surface changes and to understand the processes and interactions behind these changes.

This report provides the scientific and engineering requirements for the Eos imaging radar. We define an imaging radar instrument as that which, in conjunction with other sensors, would provide the measurements needed to meet the Eos objectives and document the different scientific research disciplines that heavily depend on the radar measurements. The Panel consisted of scientists representing the disciplines of glaciology, hydrology, vegetation science, oceanography, and geology as well as researchers familiar with imaging radar sensors and associated data systems. Although the report is organized by scientific discipline, it is recognized that Eos is an interdisciplinary enterprise that will require that the radar be used in synergism with other Eos sensors to study phenomena that cross the boundaries between the traditional Earth science disciplines.

SAR provides imagery that characterizes the physical properties (morphology, roughness, dielectric properties, geometric shapes, etc.) of the surface, its cover, and the near subsurface volume. These observations are acquired independent of cloud cover and solar illumination, thus allowing the capability of all time observation, which is a key requirement for observing dynamic phenomena.

INSTRUMENT DESCRIPTION

The SAR sensor recommended by the Panel is based upon the technology inherited from the Shuttle Imaging Radar-C (SIR-C). The Eos SAR would include three frequencies: 1.25 Gigahertz (L-band), 5.3 Gigahertz (C-band), and 9.6 Gigahertz (X-band); selectable polarizations for both transmit and receive channels; and selectable incidence angles from 15° to 55°. There would be three main viewing modes: a local high-resolution mode with typically 25 meter resolution and 50 kilometer swath width; a regional mapping mode with 100 meter resolution and up to 200 kilometer swath width; and a global mapping mode with typically 500 meter resolution and up to 700 kilometer swath width. This latter mode allows global coverage in 3 days.

EVOLUTION OF Eos SAR

The Eos SAR will be the first orbital imaging radar to provide multifrequency, multipolarization, multiple incidence angle observations of the entire Earth. This instrument will be derived from the SIR-C design. The Eos SAR mission will also take advantage of experience gained from Seasat, SIR-A, SIR-B, as well as other international SAR missions expected over the next several years. These include the Earth Resources Satellite-1 (ERS-1), a polar orbiting 3-day repeat cycle platform with a C-band radar; Radarsat, a Canadian platform also with a C-band radar; and Japan's Earth Remote Sensing Satellite (JERS-1), which includes an L-band radar. These different missions, taken together, would provide continuous radar observation capability spanning the whole decade of the 1990s with the Eos SAR continuing into the next century.

GLACIOLOGY

Sea ice serves as an insulating layer between the frigid polar winter air masses and the relatively warm ocean beneath the ice. Heat fluxes through open leads can be 100 times those through the ice; small changes in ice compactness and extent can have major climatic effects. The distribution of snow is also important for weather and climate modeling because it efficiently reflects shortwave solar radiation during the day and serves as a nearly perfect blackbody radiator during the night. Ice shelves and sheets also have an impact on atmospheric and hydrologic cycles,

although the associated time scales are generally longer than for sea ice and snow. Thus, an understanding of global effects associated with the world's snow and ice masses requires information about small-scale internal processes. Due to the high variability of snow and ice, these measurements must be made frequently and consistently. In particular, measurements must be made in the higher latitudes when sun angles are low and cloud cover is at its peak.

SAR is the only instrument that can provide consistent observations through all seasons, at high latitudes, and with high spatial resolution (20 to 30 meters). SAR observations can lead to an improved understanding of these processes, including (1) spatial distribution of ice, (2) ice dynamics, and (3) ice and snow geophysical properties.

Eos SAR will be able to provide information about the distribution of ice masses, their boundaries, and ice characteristics within these masses. The multifrequency capability of SAR will also be useful for delineation of the extent, water equivalent, and the presence of free water within snowpacks. By repetitive observation, SAR will also provide information about the motion and deformation of sea ice that results from wind and current forcing within the constraints imposed by nearby land masses. It will be necessary to acquire synoptic scale observations over a period of several years that include sufficient detail so that specific ice characteristics can be observed, tracked, and compared with model predictions. Similar requirements exist for observations of lake and river ice. In addition to mapping the areal extent and dynamics of snow and ice masses, it is essential to monitor their geophysical state. The multifrequency, multipolarization capabilities of Eos SAR will provide valuable information about ice composition and structure, as well as metamorphic changes in the density, grain sizes and shapes, layering, and distribution of liquid water within snowpacks.

HYDROLOGY

An improved understanding of the hydrologic cycle requires measurements of the processes of precipitation, evaporation, evapotranspiration, and runoff on a global scale, determination of the controlling factors for the hydrologic cycle, and quantification of the interactions between the vegetation, soil, and topographic characteristics of the land surface and the components of the hydrologic cycle. To meet these objectives, it will be necessary to focus Eos observations on water storages (soil moisture, snow, and surface water), water fluxes (precipitation as input, surface runoff and ground water as redistribution, and evapotranspiration as output), and chemical fluxes (including the chemical balance of wetlands).

Eos SAR will monitor soil moisture, frozen soil boundaries, snowpack extent and condition, landwater boundaries, and vegetation cover (both extent and moisture content). The high-resolution measurements of soil moisture within and between watersheds by SAR are complementary to the low-resolution regional and global measurements by the passive microwave radiometer (ESTAR). Both instruments respond to changes in the dielectric constant as a result of varying moisture content. As water freezes, there is a marked change in its dielectric constant in the microwave spectrum; thus, it is expected that Eos SAR will provide information about frozen soil extent and boundaries. The measurement of water storage in snowpacks may be possible with the multifrequency capability of Eos SAR, if a repetitive series of observations can be made. Inversion algorithms for determination of snow water equivalent (SWE) have been proposed for use with the L-, C-, and X-band channels of SAR; with sufficient absolute calibration, a ± 10 centimeter accuracy in snow water equivalent can be expected. The multipolarization capability of SAR will be useful for delineation of water storage in lakes, reservoirs, and wetlands, including standing water boundaries in forested areas.

Our understanding of terrestrial water fluxes will be enhanced with SAR data, especially precipitation (SAR observations of soil moisture changes resulting from rain event), evaporative moisture flux (diurnal observations of soil and canopy moisture levels), and runoff (repetitive imaging of soil moisture within watersheds could help identify runoff-producing areas).

Although SAR cannot directly identify chemical fluxes, it will provide information which is indirectly useful. Because surface runoff and interflow are the primary transport vehicles for the movement of chemicals in an ecosystem, the spatial detail, topographic sensitivity, and soil moisture sensitivity provided by SAR may be useful for identifying runoff flow paths. Soil erosion by wind or water is a major mechanism for chemical flux; Eos SAR may provide valuable data for monitoring erosion by observing temporal changes in surface roughness and slope. Finally, SAR images will be useful for detection of wetlands boundaries, even including standing water under trees. This will be valuable for studies of wetlands, which produce conditions which allow reducing chemistry to occur. Wetlands produce several environmentally important gases, particularly methane.

VEGETATION SCIENCE

Eos SAR has the potential to monitor canopy moisture, biomass and morphology, and surface boundary conditions. Although the use of data for vegetation measurements is not as mature as for ice dynamics or geological mapping, it has been demonstrated by field and aircraft radar experiments that radar backscatter in the microwave range exhibits a unique sensitivity to plant canopy morphology. In

particular, by carefully selecting the right combination of frequency, polarization, and incidence angle, it may be possible to (1) observe the backscattering from the canopy alone, or (2) to look through a canopy and observe the condition of the underlying surface. Backscattering from a canopy is dominated by the geometry of leaves, stems, and trunks as well as the moisture content within the canopy. It is expected that the multipolarization, multifrequency capability of Eos SAR (especially the C- and X-band channels at higher incidence angles) will be especially useful for measurement of biomass, geometry, and moisture of canopies; the L- and C-band channels at near-nadir incidence angles will be used to monitor the surface boundary layer state.

OCEANOGRAPHY

SAR will be useful for several Eos studies in the area of oceanography. In combination with other planned Eos sensors, it could contribute to: (1) measurement of mesoscale to large-scale circulation of the ocean including long-term variability, (2) determination of global heat, mass, and momentum coupling between the ocean and atmosphere, (3) determination of the upper ocean response to thermal and atmospheric forcing, including the effects of persistent horizontal variability in the ocean and atmosphere, and (4) improvement of our understanding of the interaction of physical and biological processes, including the effects of horizontal and vertical variability. SAR is expected to provide information about the locations and boundaries of currents, eddies and fronts, surface and internal waves, bathymetric features, and mesoscale atmospheric features. Our understanding of the basis by which imaging radars reveal these various geophysical processes is only rudimentary at present, but it is clear that expressions of surface and subsurface phenomena abound in all existing data sets from Seasat, SIR-A, and SIR-B. Furthermore, it is expected that repetitive SAR observations of these features will provide information about their dynamic behavior which, coupled with other Eos sensor data, will lead to a much improved understanding of physical and biological processes.

Repetitive observations of current and frontal boundaries as well as a wide range of scales of eddy fields would be especially useful for studies of ocean circulation features. In fact, for many regional studies, SAR could provide the only observational method for detection of the features. For example, SAR could provide observations of energetic regions that are remote and subject to extensive cloud cover (such as the Gulf of Mexico) where visible and infrared sea surface temperature instruments are less useful.

Observations of internal waves, bathymetric signatures, and wind stress will also be possible with Eos SAR. Imagery obtained from Seasat, SIR-A, and SIR-B show expressions of surface atmospheric structure resulting from Bragg scattering from wind-roughened, small-scale ocean surface waves. SAR imagery often shows spatial structure suggesting a strong relation to horizontal stress at the boundary layer, such as due to rain squalls or thunderstorms. This information from Eos SAR imagery will be on a much finer scale than that available from Radar scatterometer (SCATT), which will also be sensitive to surface wind stress but with a resolution of about 10 kilometers. Thus, SAR can be used synergistically with SCATT by providing fine detail for targets of opportunity.

GEOLOGY

Since the early 1950s imaging radars have been used for geologic mapping, especially for determination of structural information in regions obscured by cloud cover, vegetation, or sand. Eos SAR is expected to be especially useful for studies of global crustal structure and tectonics, arid lands geology and desertification, soil erosion from arable and grazing lands, and other geologic studies.

Radar imagery is sensitive to surface morphologic indicators of tectonic and crustal activity; this is principally due to the strong dependence of radar backscatter on changes in surface roughness, slope, or dielectric constant. Eos SAR data will be synergistic with HIRIS and TIMS data, which will provide information about surface chemistry and emissivity, respectively. Taken together, these instruments will provide an improved understanding of crustal evolution and plate tectonics.

It will be possible to improve models of the Pleistocene history of the world's larger and more arid desert regions with Eos SAR data, especially where little but eolian sand deposition has occurred since the late Pleistocene; the L-band channel will be especially useful for penetration of these sand mantles in very arid regions to reveal alluvial deposits as well as other subsurface structures (to depths of about 2 to 6 meters). Measurements of desertification boundaries and rates may be possible with SAR data when consistently acquired over a period of years. Similarly, Eos SAR data acquired over a period of years may be useful for detection and tracking of soil erosion, due to the sensitivity of radar to surface morphology at the scales of interest in erosional processes. This would further our understanding of the climatic changes in the last thousand to million years by looking at this effect on surface erosional properties.

DATA AND INFORMATION SYSTEM

One key element of the total Eos system is the implementation of a data and information system that would allow the broad scientific community to quickly access the multitude of data sets acquired by

the different Eos sensors. Access must be possible in a timely fashion to different levels of processed data. This aspect is a major driver in high rate sensors such as SAR where average bit rates of a few tens of megabits are expected. A sample scenario of data acquisition for research and monitoring showed that the SAR average data rate for the high-resolution and regional mapping modes could be about 10 megabits per second. The global mapping mode will double that data rate unless onboard processing is included.

This data needs to be processed and reformatted in order to be useful to the general scientific community. The techniques and technology required for such processing have been a major limitation in previous missions. However, recent and ongoing developments in the U.S. and Europe will allow real time data processing to be achieved on a routine basis. The main challenges will be not in the data processing, but rather in the data calibration to geophysical parameters and in the distribution to a large spectrum of users in a timely fashion. Both of these aspects will be addressed intensively by pre-Eos missions such as SIR-C, ERS-1, Radarsat, and JERS-1.

SUMMARY

In summary, Eos SAR is expected to be a key and essential element of the Eos by providing the equivalent of both MODIS and HIRIS in the microwave region. It will play a key role in both monitoring surface global changes by using its global coverage capability, and in investigating detailed surface processes by using its multispectral and multipolarization high-resolution imaging capability. It is based on extensive inheritance from the shuttle imaging radar series (SIR-A, -B, and -C), and the interpretation and data handling techniques will be well advanced after the experiences of the SIR-A, B, C, ERS-1, JERS-1, and Radarsat.

CONTENTS

CONTENTS (continued)

CONTENTS (Continued)

CONTENTS (continued)

CONTENTS (continued)

CONTENTS (continued)

CONTENTS (continued)

CONTENTS (continued)

LIST OF TABLES

LIST OF FIGURES

LIST OF FIGURES (continued)

LIST OF FIGURES (continued)

LIST OF FIGURES (continued)

LIST OF FIGURES (Continued)

ACRONYMS

A/D	Analog to Digital Converter
ADCLS	Advanced Data Collection and Location System
ADSP	Advanced Digital SAR Processor
AI	Artificial Intelligence
AIS	Airborne Imaging Spectrometer
ALT	Altimeter
AMSR	Advanced Microwave Scanning Radiometer
AMSU	Advanced Microwave Sounding Unit
ASF	Alaska SAR Facility
AVHRR	Advanced Very High-Resolution Radiometer
AVIRIS	Airborne Visible and Infrared Imaging Spectrometer
BFPQ	Block Floating Point Quantizer
DDHA	Digital Data Handling Assembly
DFVLR	German Aerospace Research Establishment (Deutsche Forshcungs-und Versuchsanstalt für Luft-und Raumfahrt)
DN	Digital Number
DOY	Day of Year
DTM	Digital Terrain Model
Eos	Earth Observing System
ERS-1	Earth Remote Sensing Satellite-1
ESA	European Space Agency
ESMR	Electronically Scanned Microwave Radiometer
ESSC	Earth System Science Committee
ESTAR	Electronically Scanned Thinned Array Radiometer
FDMCN	Flight Data Management and Communications Network
FFT	Fast Fourier Transform
FOV	Field-of-View
GDMCN	Ground Data Management and Communications Network
GEOSAT	Geodynamic Experimental Ocean Satellite
GLAI	Green Leaf Area Index
GLORI	Global and Local Radar Imager
GLRS	Geodynamics Laser Ranging System
GOES	Geostationary Operational Environmental Satellite
GPS	Global Positioning System
GSFC	Goddard Space Flight Center
HDDR	High-Density Digital Recorders
HDDT	High-Density Digital Tapes
HH	Horizontally Polarized Transmit, Horizontally Polarized Receive
HIRIS	High-Resolution Imaging Spectrometer
HPA	High-Power Amplifier
HV	Horizontally Polarized Transmit, Vertically Polarized Receive
ICC	Instrument Control Center
IOC	Initial Operating Configuration

ACRONYMS (continued)

IR	Infrared
JERS-1	Japanese Earth Remote Sensing Satellite-1
JPL	Jet Propulsion Laboratory
LACIE/ AgRISTARS	Large Area Crop Inventory Experiment/Agriculture and Resources Inventory Surveys Through Aerospace Remote Sensing
LAI	Leaf Area Index
LASA	Lidar Atmospheric Sounder and Altimeter
LIMEX	Labrador Ice Margin Experiment
LNA	Low-Noise Amplifier
MIZEX	Marginal Ice Zone Experiment
MODIS	Moderate-Resolution Imaging Spectrometer
MSS	Multispectral Scanner
NASA	National Aeronautics and Space Administration
NIR	Near Infrared
NOAA	National Oceanic and Atmospheric Administration
NROSS	Naval Remote Ocean Sensing System
PIPOR	Programme for International Polar Oceans Research
PRF	Pulse Repetition Frequency
PSC	NASA Program Support Communications
RF	Radio Frequency
SAR	Synthetic Aperture Radar
SASS	Seasat Scatterometer System
SBL	Surface Boundary Layer
SCANSAR	SAR Mode Utilizing Electronic Steering to Create Wide Swaths
SCAT/SCATT	Scatterometer
SDAP	SAR Data Acquisition Plan
SIR-A	Shuttle Imaging Radar-A
SIR-B	Shuttle Imaging Radar-B
SIR-C	Shuttle Imaging Radar-C
SIR-D	Shuttle Imaging Radar-D
SLAR	Side-Looking Airborne Radar
SLR	Side-Looking Radar
SMRWG	Science and Mission Requirements Working Group
SNR	Signal-to-Noise Ratio
SPOT	System Probatoire d'Observation de la Terre
SSC	Science Steering Committee
SST	Sea Surface Temperature
SWE	Snow Water Equivalent
SWIR	Shortwave Infrared
TDRS	Tracking and Data Relay Satellite
TIMS	Thermal Infrared Multispectral Scanner
TM	Thematic Mapper
T/R	Transmit/Receive

ACRONYMS (continued)

TOPEX	Ocean Topography Experiment
UCOWR	University Council on Water Resources
VH	Vertically Polarized Transmit, Horizontally Polarized Receive
VIS	Visible
VV	Vertically Polarized Transmit, Vertically Polarized Receive
WMO	World Meteorological Organization

I. RADAR IMAGING FROM SPACE

INTRODUCTION

Purpose of the Report

The purposes of this report are to (1) establish geoscientific observational requirements for an Earth Observing System (Eos) Synthetic Aperture Radar (SAR), (2) outline the characteristics of an Eos SAR instrument that can acquire these required data sets, (3) show how SAR can be used synergistically with other Eos instruments, and (4) discuss SAR data requirements strategy and a management strategy that will meet these needs. SAR is viewed as one component of a multi-instrument Earth Observing System that can provide an enhanced understanding of the global processes that comprise the Earth system.

Scope

The Eos concept has been described in three reports by the Science and Mission Requirements Working Group (SMRWG) (Butler *et al.*, 1984), the Eos Science Steering Committee (SSC) (Butler *et al.*, 1987) and the Earth System Science Committee (ESSC) (Bretherton *et al.*, 1986). The concept envisions the synergistic use of various remote sensing instruments such as SAR, the High-Resolution Imaging Spectrometer (HIRIS), the Thermal Infrared Multispectral Scanner (TIMS), the Moderate-Resolution Imaging Spectrometer (MODIS), the Advanced Microwave Scanning Radiometer (AMSR), and others. These sensors, along with an international data and information system (Chase *et al.*, 1986) would provide global data sets to further our understanding of the hydrological cycle, biogeochemical cycles, and climatic processes as well as many problems within the traditional disciplines of Earth science. Various instrument panels, including the SAR Instrument Panel, have been formed to articulate the specific geoscientific data needs for Eos sensors, and to outline an instrument design that would meet those needs. The SAR Instrument Panel Report provides a specific assessment of scientific needs as well as a full description of the SAR instrument and data system requirements for the Eos era.

The Eos SAR Instrument Panel in coordination with the Eos Science Steering Committee has defined SAR as a multifrequency (L-, C-, and X-bands), multipolarization system capable of observing the Earth using a variety of imaging geometries. The frequency bands are shown in Figure 1. SAR will provide multiparameter high-resolution observations in the microwave spectrum, a capability that is expected

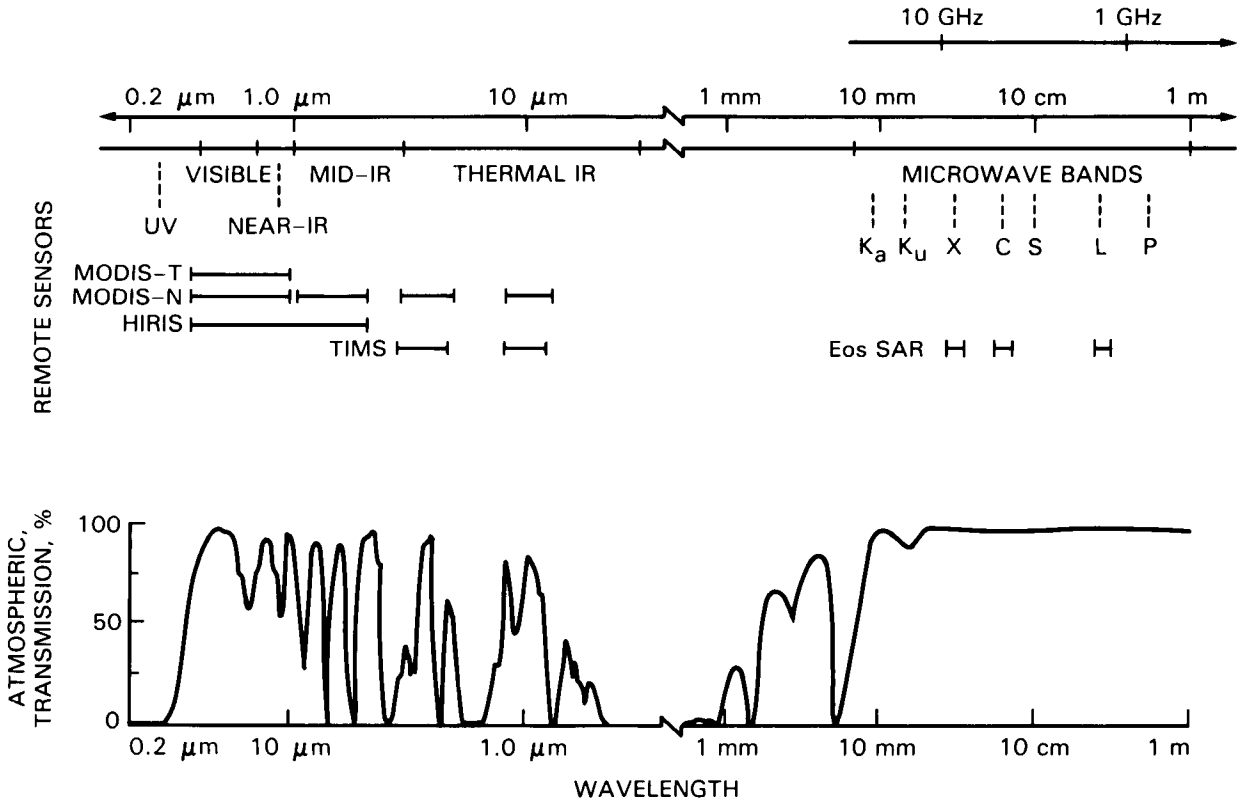

Figure 1. Electromagnetic spectrum showing atmospheric transmission windows, the microwave, IR, and visible bands. The Eos SAR frequencies are L- band (1.278 GHz, 24 cm wavelength), C-band (5.3 GHz, 5.7 cm), and X-band (9.6 GHz, 3.1 cm).

to provide unique information about polar ice dynamics and ice morphology, crustal structure and plate tectonics, soil moisture, desertification and soil erosion processes, vegetation canopy structure, and oceanic circulation features, to name just a few. When used synergistically with the other Eos instruments, the information potential is much greater than with SAR acting alone. The data management problems inherent in global data sets from a very high-resolution instrument such as SAR must be considered an integral part of the overall instrument design.

THE EVOLUTION OF SAR INSTRUMENTS AND SCIENTIFIC APPLICATIONS

Instrument Heritage

SLAR Development

The first imaging radars were Side-Looking Airborne Radars (SLARs) developed in the early 1950s for military reconnaissance purposes. Because of their long wavelengths, these radars could image the Earth's surface without obscuration from clouds or atmospheric water vapor. Because the radar furnished its own illumination, images could be obtained either during the day or at night, a considerable advantage in reconnaissance missions. The first operational SLARs were the Westinghouse AN/APQ-56 and AN/APQ-55 K_a-band (2 cm wavelength) system, developed in the mid-1950s. SLAR is known as a "real-aperture" radar because its along-track resolution is determined by the ratio of wavelength times the slant range divided by the along-track antenna length; fine resolution in the cross-track direction is obtained through the use of pulse compression techniques. For airborne radars operating at K_a-band, this means that resolutions of some tens of meters could be obtained at near-nadir slant ranges.

The first scientific uses of these real-aperture radars were for cartography and geological mapping. Radar returns are quite sensitive to surface slope, surface roughness, and the presence of water. Combined with the capability to penetrate clouds, this provided geologists with a means to map heavily cloud-covered and previously uncharted regions in the Darien Province of Panama and Brazil. A number of studies were undertaken by investigators at the U.S. Geological Survey, the University of Kansas, the U.S. Army Topographic Command, and other institutions to determine how SLAR images could be used in the emerging field of radargrammetry, i.e., the use of radar images for cartographic and topographic mapping. It was also determined that radar imagery was very useful for the study of very near-surface geological features, i.e., to map different surficial materials such as sand, gravel, and glacial deposits, or to delineate contacts between fans and playas or bedrock and alluvial fans.

SAR Development

The principal disadvantage to using SLAR is that its along-track resolution is limited by the antenna length. The development of SAR overcame this disadvantage. Like SLAR, SAR used pulse compression techniques to provide fine range resolution. However, it was determined that if a pulsed coherent radar could be used, then the doppler-shifted radar echoes could be recorded and played back through a coherent SAR image processor to synthesize an along-track antenna length much longer than the antenna's physical length. The first operational SAR was the Goodyear AN/APQ-102, an X-band (3 cm wavelength) horizontally-polarized system that was used on an RF4C aircraft. This yielded resolutions on the order of 15 m in both the along-track and cross-track directions.

A further advantage of SAR over SLAR was that it could be used at longer wavelengths.

Seasat

The first spaceborne imaging radar to be used for imaging of the Earth was the L-band SAR on Seasat, an instrument package launched into an 800 km altitude near-polar orbit in June 1978. This horizontally polarized instrument operated at a fixed wavelength (23 cm) and at a fixed look angle (20° from nadir). The Seasat swath width was 100 km and the resolution was approximately 25 m. While SAR was included in the Seasat payload primarily for the purpose of ocean wave imaging, radar images were also acquired over large areas of the Arctic ice pack and over land areas in the Northern Hemisphere. During its 3-month lifetime, Seasat acquired imagery of over 125 million km^2 of Central and North America, western Europe, the North Atlantic, the North Pacific, and the northern polar regions.

Imagery obtained from the Seasat SAR clearly demonstrated its sensitivity to surface roughness, slope, and land-water boundaries. Seasat images have been used to determine the directional spectra of ocean waves, surface manifestations of internal waves, polar ice-cover motion, geological structural features, soil moisture boundaries, vegetation characteristics, urban land-use patterns, and other geoscientific features of interest.

Despite its overall technological and scientific success, Seasat's relatively short lifetime precluded the acquisition of seasonal data sets, for example of polar ice dynamics or of vegetation canopy phenology. Moreover, the Seasat SAR was a "single-parameter" instrument, i.e., it used a fixed wavelength (23 cm), a fixed polarization (HH)[1], and a fixed incidence angle (23°). The near-nadir incidence angle was ideal for acquiring strong oceanic returns, but produced severe geometric layover distortions on terrain images of high-relief regions.

[1]HH = Horizontally polarized transmit, Horizontally polarized receive.

Shuttle Imaging Radar

The next spaceborne SAR to follow Seasat was the Shuttle Imaging Radar-A (SIR-A), ferried into a 57° inclination, 240 km altitude orbit in November 1981 by the Space Shuttle Columbia. The SIR-A SAR technology was derived from Seasat, again using the 23 cm wavelength and HH polarization. However, since the SIR-A mission was to be used principally for geological research, the look angle was changed to a fixed angle of 47°. The higher incidence angle (50°) provided enhanced sensitivity to geological structural features such as faults and folds. The SIR-A swath width was approximately 50 km, and the resolution was 40 m. SIR-A provided much improved image data for geological analyses as they were relatively free of the layover distortion that accompanied Seasat images of high-relief regions. SIR-A also led to the discovery of buried and previously uncharted dry river beds beneath the Sahara Desert in Sudan and Egypt. This demonstrated the ability of an L-band radar to penetrate up to several meters in hyperarid sand sheets. During its 2-day mission, SIR-A acquired images over about 10 million km^2 of the Earth's surface, mostly over land. All SIR-A raw data were optically processed at the Jet Propulsion Laboratory (JPL).

The next NASA SAR mission was SIR-B, launched in October 1984 on the Space Shuttle Challenger. SIR-B also used the Seasat/SIR-A technology with the same 23 cm wavelength and HH polarization. However, SIR-B was equipped with an articulating antenna so that selectable incidence angles could be obtained over the 15° to 60° range. This provided the first multi-incidence angle data set, useful in extracting geophysical information where there is a strong illumination angle signature. SIR-B data were digitally-encoded and processed. Despite problems with the shuttle's K_u-band antenna and with an intermittent fault in the radar's antenna cable, SIR-B provided good quality data over a number of sites and demonstrated the potential for mapping surface features (particularly forests) using multiple-incidence angle backscatter signatures and for topographic mapping. SIR-B data were also used to demonstrate the sensitivity of L-band radar images to soil moisture, to geological structural and lithologic features, and to oceanic directional wave spectra.

SIR-B data were the first to be digitally encoded and digitally processed. The SIR-B data echoes were digitized and recorded on a high-density tape recorder onboard the shuttle at a data rate of 30 Mbps. The data could then be stored on tapes onboard the shuttle or transmitted to the ground by placing the entire shuttle in a Tracking and Data Relay Satellite (TDRS) tracking mode to accommodate the mechanical K_u-band antenna failure. The tapes (both those carried onboard the shuttle and those containing data transmitted to the ground through TDRS) were transported to JPL for digital processing. This has provided digitally encoded SAR images for more precise quantitative analysis by geoscientists, and represents a significant advance in SAR image processing technology.

The successes of the SIR-A and SIR-B missions have led to a second generation SAR design that will be used both for later shuttle flights and on Eos. The SIR-C SAR mission, scheduled for two flights in the early 1990s, will incorporate a multifrequency, multipolarization, variable incidence angle SAR, which will provide valuable new scientific information hitherto not obtainable from either aircraft or space platforms. The SIR-C instrument will incorporate new distributed solid-state SAR technology in order to provide the power levels necessary for imaging at L-band (23 cm) and C-band (6 cm) in the cross-polarization mode. An X-band, VV[2] channel will also be included; this system will be provided by the German Aerospace Research Establishment (DFVLR). SIR-C will provide for recording the amplitude of the horizontally, vertically, and both cross-polarized radar echoes, as well as the electrical phase angle between the HH and VV echoes. These amplitude and phase data are expected to dramatically increase the information content in a set of radar images and to lead to expanded geoscientific applications. SIR-C will also provide electronic beam steering to minimize mechanical antenna and shuttle rotations; electronic beam steering will also allow acquisition of swath widths in excess of 200 km.

Aircraft and Truck-Mounted Radars

Most of the systematic studies of radar backscattering sensitivity to Earth surface features with frequency, polarization, and illumination angles as parameters have been made using ground-based truck radar scatterometers and airborne scatterometers and imaging radars. These are the essential laboratory case-study instruments of the trade, and have provided valuable information on the optimum radar parameters for different geoscientific purposes. For example, it has been determined from truck radar scatterometer data that L- and C-band radars are better suited to soil moisture discrimination than are X-band radars, and that X- or K-band radars are better for discriminating snowpack properties than are L- or C-band radars. Similar findings on the roles of polarization and incidence angle have been chronicled in the literature.

SAR image data has found its most mature and clear-cut applications in the fields of geology, cartography, and glaciology. The potential of SAR data for hydrology (especially soil moisture measurements), vegetation science, and oceanography has also been demonstrated, although the lack of well-calibrated SAR image data sets, including coincident ground-truth measurements over extended periods of time (months or years), has slowed the development of these applications.

[2]VV = Vertically polarized transmit, Vertically polarized receive.

Researchers have used airborne and truck radar data to determine the optimum parameters for vegetation discrimination and soil moisture delineation as well as oceanic wind speeds and wave energy spectra. Although these data sets have greatly advanced our understanding of the radar physics involved, they have not been able to serve as an adequate surrogate for high-quality high-resolution radar images that demonstrate the capability to quantify the geophysical information needed. However, the limited data sets obtained from Seasat and the SIR-A and SIR-B missions have tended to confirm the predictions made from truck and airborne data. This means that the quantitative truck and airborne radar studies of the dependence of the radar backscattering coefficient on soil moisture, plant canopy structure, ice type, snowpack properties, etc., must serve as the scientific basis for designing the Eos SAR. It is expected that images obtained from SIR-C will further confirm these ground-based studies.

Other Future Spaceborne SAR Missions

There are several future spaceborne SAR missions planned that will greatly assist in the development of techniques and algorithms for use with the Eos SAR. The SIR-C mission will offer an opportunity to acquire multichannel SAR data from sites as far north or south as 57° latitude. The Earth Resources Satellite (ERS-1) will provide C-band SAR data from a polar orbit with a 3-day repeat cycle; Canada's Radarsat will likewise provide C-band SAR data from polar orbit. The Japanese Earth Remote Sensing Satellite (JERS-1) will provide L-band SAR data from polar orbit.

Summary of SAR Technology Development

The new generation of imaging radar technology envisioned for SIR-C and Eos provides the potential of greatly enhanced information-gathering capabilities through the use of multiparameter SAR designs (Figure 2). These multiparameter radars are to Seasat, SIR-A, and SIR-B SARs as Landsat Multispectral Scanner (MSS) or Thematic Mapper (TM) imagers are to older monochromatic imagers, but with the further enhancement of full polarization and electronic beam steering. Images obtained through these "color radars" will provide detailed information on the surface and volume scattering processes that underlie the extraction of useful quantitative geoscientific data (Figures 3 and 4). However, this comes at a cost. First, the data rates will easily exceed 200 Mbps, so that very large data channel bandwidths will be required for Eos. Second, the processing of raw data into image form will require ground processors with speeds of the order of 1 GFlop/s. Third, after processing, an image storage and retrieval mechanism must be developed so that users have the capability to browse through very large global data sets and select specific areas, time periods, or frequencies for further examination or

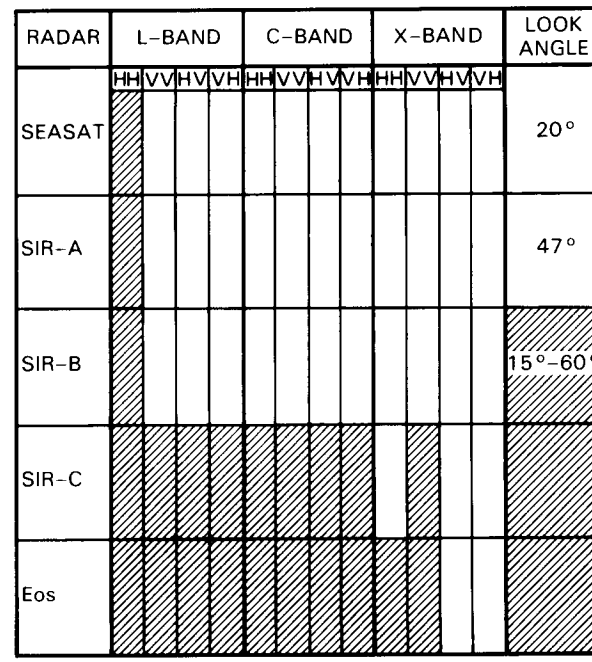

Figure 2. Evolution of the imaging parameters of the Spaceborne Imaging Radar from Seasat to Eos.

for additional data acquisition. Finally, the enormous volume of high-resolution image data that can be acquired by a polar-orbiting SAR threatens to overwhelm the ability of human interpreters to extract the needed information (such as ice or soil moisture dynamics). This means that a considerable effort must be expended on development of advanced techniques for automated image segmentation, co-registration, and change detection. In addition, inversion algorithms must be in place to analyze the SAR data at the same rate it is being processed.

These latter data management problems could easily be more challenging than the design of the radar instrument itself. The efficient acquisition, processing, storage, and retrieval of global high-resolution calibrated SAR data sets poses problems of a scale not previously addressed. Chapter IX of this report attempts to outline some of the more significant of these data management issues and proposes some solutions.

Scientific Applications of SAR Data

The scientific applications of SAR data have been extensively documented in the literature. It is useful at this point to present a brief, albeit highly oversimplified, summary of what has been learned about the principal sensitivities of SAR to geophysical parameters. Chapters II through VI present detailed discussions of the role a future Eos SAR may play in geoscientific research. Table 1 summarizes the geophysical and biophysical parameters expected to be measured by SAR, both alone and in conjunction with other Eos instruments.

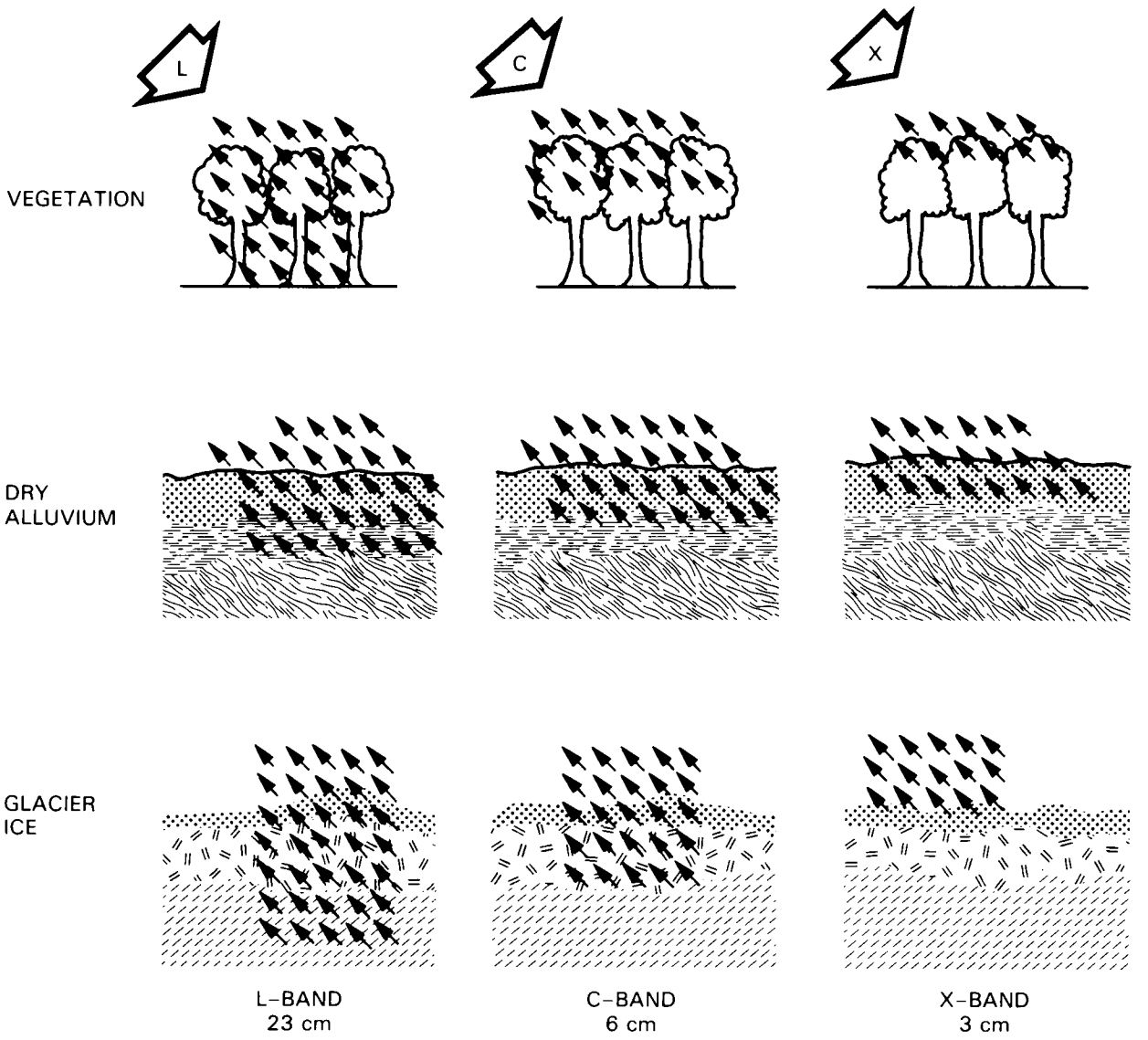

Figure 3. Penetration capability of multifrequency radar system through vegetation, dry alluvium, and glacier ice.

Glaciology

Seasat SAR data obtained in the summer of 1978 demonstrated that radar images are very useful for studying ice dynamics and for providing information on the character and features of sea ice. More than 100 passes over the Beaufort Sea were recorded on nearly a daily basis, enabling sequential imagery to be analyzed for detailed ice motion and changes in the character, distribution, and surface properties of sea ice. Sea ice is formed as slush ice or thin sheets and gradually thickens into large plates called floes. Winds and surface currents move the floes, and by compressive and shearing forces from other floes, pressure ridges are formed in the floes. If a floe survives the summer melt season to become multiyear ice, such floes will have further increases in surface roughness principally resulting from melt pond formation. Thus, some SAR image discrimination between first-year and multiyear ice can be made on the basis of surface roughness. The addition of a multifrequency capability (especially with a channel at X-band or higher frequency) will further enhance the ability of SAR for ice type discrimination based on surface roughness. Other radar studies have shown that shorter-wavelength, multifrequency radars should be able to provide information on snowpack extent, snow wetness, and snow liquid water content. SAR images should also provide valuable information on freshwater ice and glacier morphology.

Hydrology

L- and C-band radars are sensitive to soil moisture, although the response is also modulated by surface roughness, slope, and vegetation. Nonetheless,

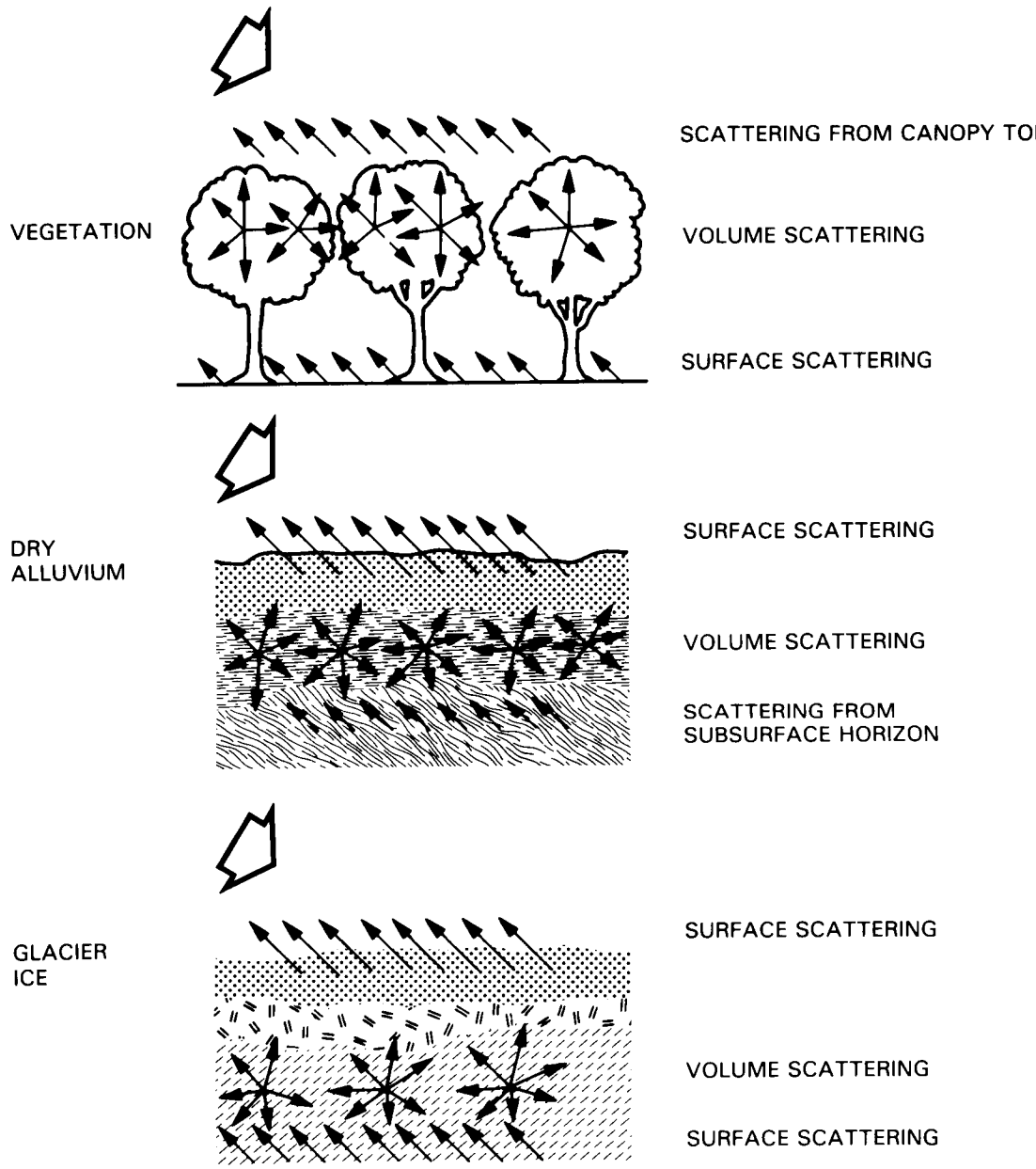

Figure 4. Like- and cross-polarized surface and volume scattering expected from vegetated surfaces, dry alluvium, and glacier ice.

both Seasat and SIR-B data have shown that SAR images can clearly delineate soil moisture boundaries and be used to estimate soil moisture levels, at least for agricultural fields with low relief. When the wavelength becomes shorter than about 3 cm, radar returns from snowpacks are enhanced as described previously. Thus, an L-, C-, and X-band SAR could provide high-resolution soil moisture and snow data if a calibrated time-series data set could be obtained.

It should also be noted that the application of SAR data to hydrology is not as well demonstrated as in the cases of geology and glaciology. This is partly because of the confusing effects that surface roughness, slope, and vegetation cover have on extracting quantitative estimates of soil moisture and because ground-truth data collection is essential for any significant analysis. Nonetheless, it is expected that well-calibrated time-series data sets will provide a means for minimizing these confusing effects and for extracting quantitative soil moisture and snow cover data.

SAR responds to soil moisture for the same reason that an L- or C-band passive radiometer responds to soil moisture, namely the sensitivity of the soil surface dielectric constant to the presence of water. However, SAR data from space provide much

Table 1. Geophysical and Biophysical Parameters from SAR Observations

Observation Parameter	Units
Glaciology	
Sea ice type discrimination	area (km^2)
Sea ice dynamics	velocity (m/day)
Lake and river ice extent	area (km^2)
Ice sheets and shelf dynamics	velocity (m/year)
Snowpack properties	
extent	area (km^2) and shape
snow water equivalent	height (cm)
wetness	fraction (cm^3/cm^3)
Hydrology	
Soil moisture	percent (cm^3/cm^3)
Surface roughness	height (cm)
Erosion	area (km^2)
Landform patterns	area (km^2) and shape
Land-water boundaries	pattern shape
Snowpack properties	see above
Vegetation Science	
Canopy moisture	volume of water per unit area
Canopy geometry	linear and angular
Change in canopy biomass	mass/unit area/season
Surface boundary layer state	extent (km^2)
Oceanography	
Currents and fronts	boundary velocity (m/s)
Rings and eddies	boundary velocity (m/s)
Internal waves	boundary velocity (m/s)
Bathymetric boundaries	boundary velocity (m/s)
Surface wind field	velocity (m/s)
Geology	
Landforms	areal extent (km^2)
Drainage patterns	areal and linear extent
Surface cover boundaries	extent (km^2)

higher resolution (tens of meters) than passive radiometer data from space (tens of kilometers). Radar data appear to be more sensitive to surface roughness and slope than do radiometer data. Both instruments (SAR and the Electronically Scanned Thinned Array Radiometer (ESTAR)) should be viewed as a highly complementary pair, with the passive instrument providing more accurate soil moisture predictions over 10 km cell sizes, and the active instrument yielding finer-grain (20 m to 500 m resolution) information on both soil moisture and vegetation cover. The same argument applies to X- or K-band sensing of snowpack properties, where both radars and radiometers are complementary.

Vegetation Science

It has been shown that when L-band Seasat SAR data is added as a channel to Landsat data acquired over corn and sorghum fields, the agricultural crop classification accuracy increases dramatically. This is because of the unique sensitivity of radar to plant canopy moisture and geometric structure. It has also been shown that there is a direct correspondence between the seasonal variation of a plant canopy's leaf area index (LAI) and the radar backscattering coefficient.

Thus, the radar is sensitive to plant canopy geometric structure, moisture content, and LAI. SAR images of plant canopies should be used with optical/infrared (IR) images, and viewed simply as additional data channels. In the Eos era, inversion algorithms to calculate canopy biophysical properties will incorporate both SAR and HIRIS data.

Time-series data of canopy scattering properties at different frequencies and polarizations could provide information about annual foliar biomass in

forests and annual above-ground productivity in grasslands and agricultural systems.

Oceanography

It has been shown that SAR images are sensitive to oceanic winds, currents, fronts, eddies, surface and internal waves, and bathymetric features. Moreover, SAR imagery obtained from Seasat and SIR-B have been used to derive ocean wave and wave directional information. Wave directional spectra are much more clearly discerned in low-altitude (under 250 km altitude) SARs than in high-altitude SARs (e.g., Seasat or Eos altitudes). The mechanism by which these oceanic features find expression in SAR imagery is not completely understood, although it is generally assumed that it is related to Bragg scattering from gravity waves with wavelengths of tens of centimeters, which in turn are modulated by the features themselves in somewhat characteristic ways.

The application of SAR images to physical oceanography has been slowed by the lack of physically based models for extracting quantitative geophysical information, particularly involving the imaging mechanisms for the various oceanic features. This includes wave energy spectra (which involves both azimuth direction spectra and wave heights) and circulation studies. These difficulties may be relieved when calibrated time series of SAR images of oceanic circulation features become available from Eos (e.g., week- or month-long SAR movies of oceanic circulation features). This will permit studies of the fine-scale dynamic behavior of these numerous features in a manner heretofore not possible.

Geology

The utility of both aircraft and satellite SAR imagery for geologic mapping and cartography has been well documented, and the techniques for application of SAR imagery to these disciplines are mature. The sensitivity of SAR to surface roughness, slope, and the presence of water makes it an ideal instrument for geomorphological studies, for delineating structural and tectonic features, for discriminating lithologic boundaries, and when stereo pairs are available, for radargrammetric mapping. Longer-wavelength SARs (e.g., L-band) are also capable of penetrating up to several meters in very dry eolian sand sheets, such as found in the eastern Sahara. Furthermore, the use of SAR to characterize effects of faster-paced geologic phenomena such as volcanic activity and earthquake effects (e.g., fault movement, landslides, avalanches) could be invaluable, particularly where cloud cover such as is commonly associated with active volcanoes limits the use of optical data.

Because geological features will in general not change over the lifetime of Eos, the rationale for using Eos for geologic studies could be questioned. However, in order to acquire one global map of the Earth's land mass once in each of the four seasons at two incidence angles, 16 to 20 dedicated shuttle missions would be required.

RATIONALE FOR Eos SAR OBSERVATIONS

SAR is a high-resolution, moderate-swath instrument that can be used both for targeted, site-specific research and for global mapping. The main reasons for using SAR are (1) its unique sensitivity to surficial morphology (e.g., global crustal structure, sea ice morphology, or plant canopy geometry), (2) its sensitivity to the dielectric constants of surface materials, especially water, and (3) its ability to obtain images independent of weather conditions or sun angle.

Eos SAR will be synergistic with a number of other Eos instruments, especially HIRIS, the Scatterometer (SCATT), AMSR, ESTAR, and MODIS. However, the information obtainable by SAR is fundamentally different from that obtained by HIRIS and MODIS in the visible/infrared (VIS/IR) spectrum, where the sensitivity is to surface chemistry and fine, cellular structure (visible/shortwave infrared (SWIR)) or to surface IR emissivity and temperature (thermal IR). SAR, by contrast, is sensitive to: (1) the geometrical arrangement of centimeter-scale scatterers; (2) to the dielectric constant of vegetation, soil, ice, rocks, and snow; and (3) to the presence of water in vegetation, soil, or snow, as well as the boundaries of ponded water. Passive microwave radiometers (e.g., AMSR or ESTAR) are also sensitive to these parameters, and in fact for a specular surface the passive microwave emissivity is equal to one minus the radar reflection coefficient. Because of their inherently poorer resolution (typically 1 to 10 km), spaceborne microwave radiometers are useful for global surveys, whereas SAR provides finer detail in particular regions of interest and will be available with more frequencies and at shorter wavelengths. The unique information obtained in the microwave spectrum is of fundamental importance to an improved understanding of global processes.

The ability of SAR to provide high-resolution imagery independent of weather or sun angle is especially important for regions of the Earth where there is a large percentage of cloud cover (e.g., the Amazon forest) or where solar illumination is insufficient (e.g., Artic Ocean in winter) to obtain VIS/IR imagery. Figure 5 illustrates the loss of coverage of the northern latitudes during the winter for various minimum required sun angles; SAR will be useful for imaging these regions when coverage cannot be obtained by MODIS or HIRIS.

Eos SAR INSTRUMENT CAPABILITIES

The Eos SAR is envisioned as a three-frequency multipolarization instrument with capabilities for

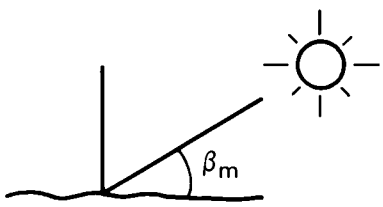

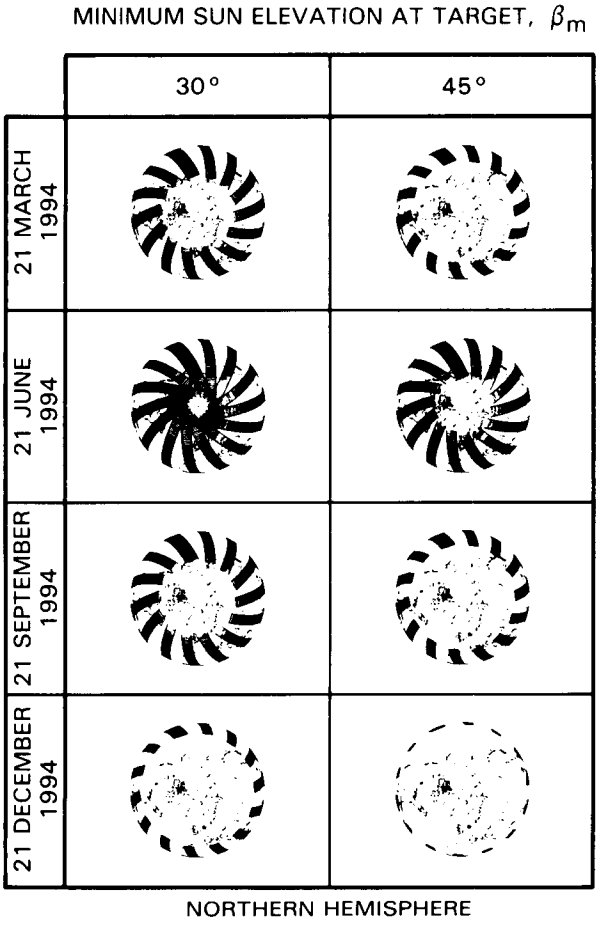

Figure 5. Northern hemisphere coverage by HIRIS or MODIS for various minimum sun angles during four seasons.

electronically scanning the beam through incidence angles of 15° to 55°. The three frequencies are L-, C-, and X-band.

The L- and C-band channels will provide full polarimetric capability, which means that the polarization states (axial ratio and tilt angle of the polarization ellipse) for both the transmit and receive signals may be synthesized. This means in principle that targets can be enhanced by proper selection of polarization states. In practice, however, the intensity of the cross-polarized radar returns (especially for specular targets) may be too weak for use. The majority of the data will be acquired for like polarization (amplitude of HH and VV returns as well as the phase between HH and VV), although the cross-polarization returns (HV[3] and VH[4]) will be used for investigation of volume-scattering mechanisms associated with vegetation, ice, and snow. It is expected that the X-band channel will provide both HH and VV polarizations, but not cross polarization. Although it is not included in the current SAR baseline, there is a desire for P-band (75 cm wavelength) in the post-initial operating configuration (IOC) era. The Eos SAR will utilize electronic beam steering so that images may be acquired at selectable incidence angles (in the cross-track direction) from 15° out to about 55°. It may also be possible to mechanically rotate the entire SAR antenna through about 90° so that images may be acquired looking either east or west of the ground track.

Three basic viewing modes of operation are envisioned: a *local high-resolution mode* with narrow swaths (typically 30 km to 50 km) and highest resolution (20 to 30 m) in which up to six simultaneous frequency-polarization combinations can be recorded, a *regional mapping mode* with wide swath (100 to 200 km) in which only two or three simultaneous frequency-polarization combinations would be used, and a *global mapping mode* with a very wide swath (up to 700 km) and low resolution (500 m) in which only one or two simultaneous channels would be collected.

A more complete discussion of the Eos SAR system design is provided in Chapter VIII. Figure 6 shows the expected evolution of SAR instruments since the 1981 SIR-A mission and extending through Eos.

ORGANIZATION OF THE REPORT

The heart of this report is Chapters II through VI, wherein the requirements for SAR data are discussed for the disciplines of glaciology, hydrology, vegetation science, oceanography, and geology. Each of these chapters is organized in an identical fashion and seeks to answer the following questions:

- What are the broad Eos-related science issues, and what are the specific SAR-related science issues?
- What are the observational requirements? Specifically, what are the observational parameters (geophysical properties) and observational regimes (regions of the world) to be measured by SAR alone or in conjunction with other Eos instruments?

[3]HV = Horizontally polarized transmit, Vertically polarized receive.
[4]VH = Vertically polarized transmit, Horizontally polarized receive.

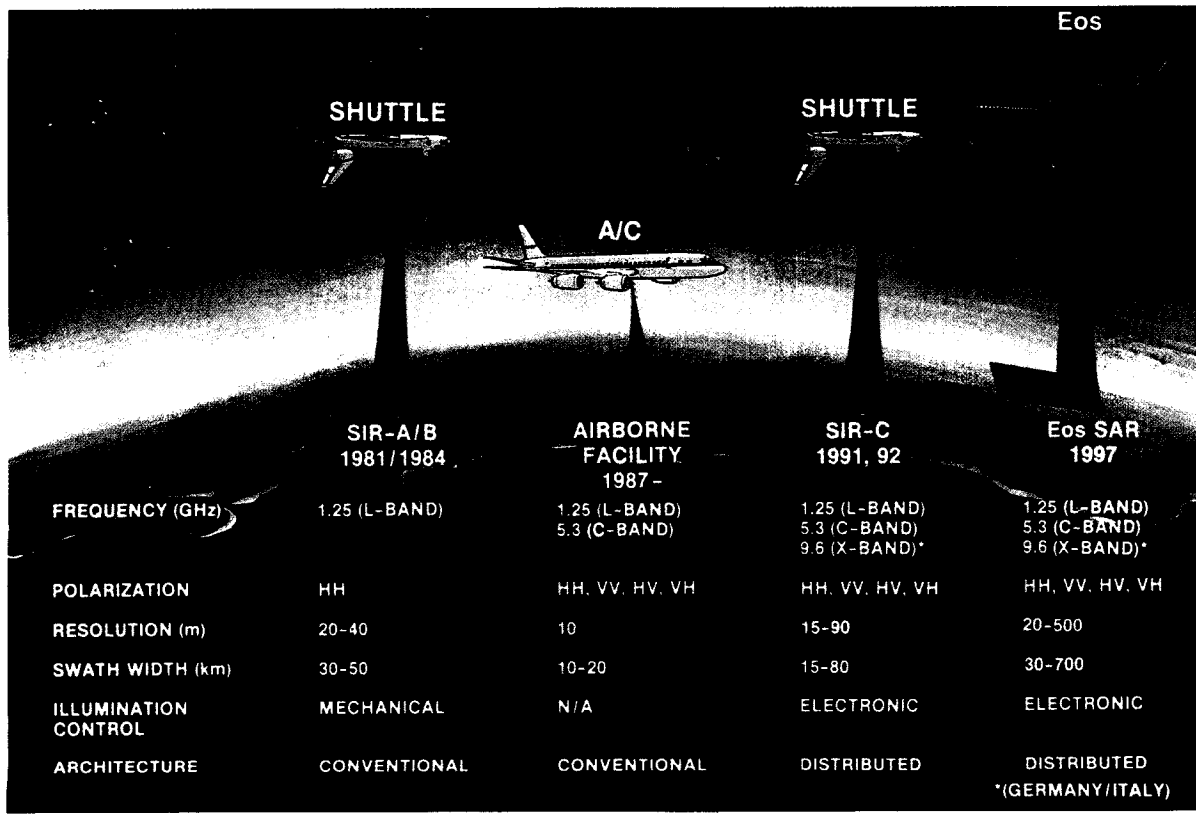

	SIR-A/B 1981/1984	AIRBORNE FACILITY 1987-	SIR-C 1991, 92	Eos SAR 1997
FREQUENCY (GHz)	1.25 (L-BAND)	1.25 (L-BAND) 5.3 (C-BAND)	1.25 (L-BAND) 5.3 (C-BAND) 9.6 (X-BAND)*	1.25 (L-BAND) 5.3 (C-BAND) 9.6 (X-BAND)*
POLARIZATION	HH	HH, VV, HV, VH	HH, VV, HV, VH	HH, VV, HV, VH
RESOLUTION (m)	20-40	10	15-90	20-500
SWATH WIDTH (km)	30-50	10-20	15-80	30-700
ILLUMINATION CONTROL	MECHANICAL	N/A	ELECTRONIC	ELECTRONIC
ARCHITECTURE	CONVENTIONAL	CONVENTIONAL	DISTRIBUTED	DISTRIBUTED *(GERMANY/ITALY)

(a)

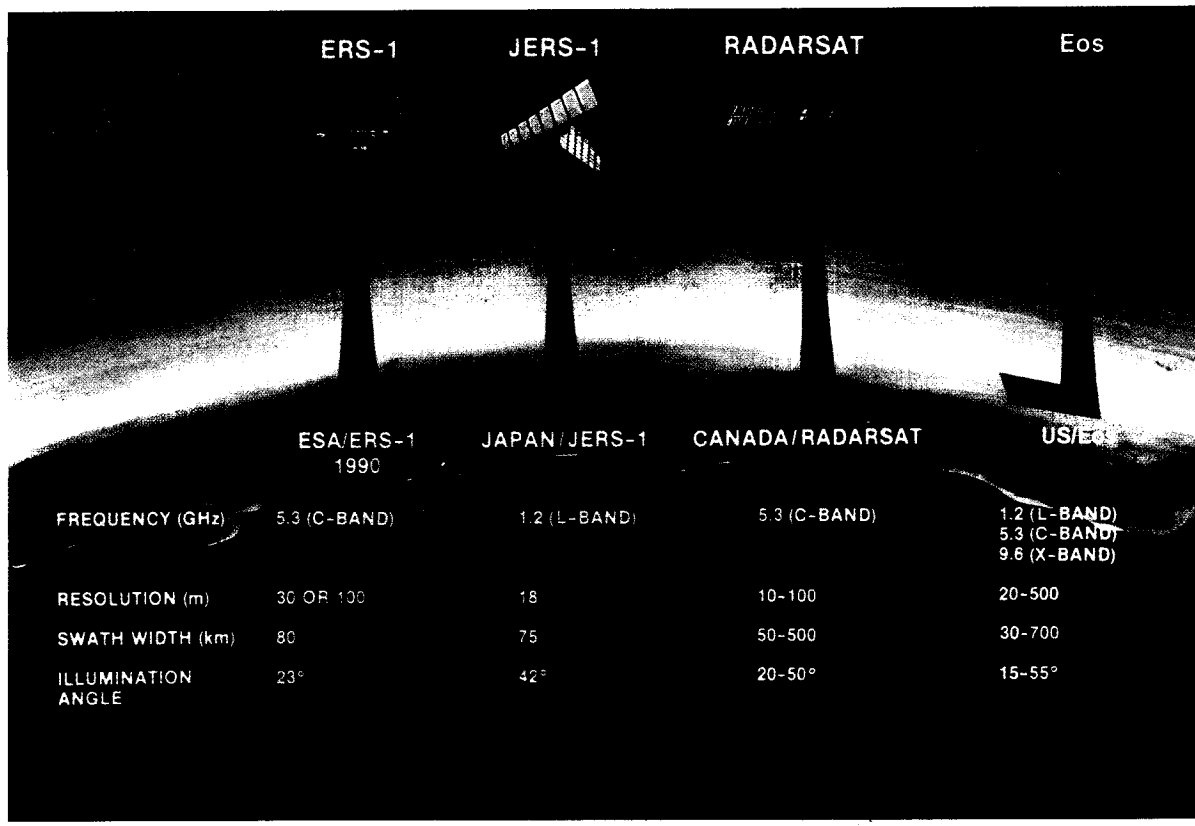

	ESA/ERS-1 1990	JAPAN/JERS-1	CANADA/RADARSAT	US/E
FREQUENCY (GHz)	5.3 (C-BAND)	1.2 (L-BAND)	5.3 (C-BAND)	1.2 (L-BAND) 5.3 (C-BAND) 9.6 (X-BAND)
RESOLUTION (m)	30 OR 100	18	10-100	20-500
SWATH WIDTH (km)	80	75	50-500	30-700
ILLUMINATION ANGLE	23°	42°	20-50°	15-55°

(b)

Figure 6. (a) Schedule for the SIR system from Seasat to Eos SAR; (b) Also shown are ERS-1 and JERS-1.

- What is the rationale for using SAR? What are the fundamental physical processes that relate to radar backscatter, and how may they be exploited with an Eos SAR?
- What are some relevant case histories that demonstrate that SAR can be used to acquire the needed data? (Detailed examples are included in the appendices.)
- What is the Eos SAR mission strategy in terms of instrument and viewing parameters, synergism with other instruments, and data and information requirements for each specific science objective?

Chapter VII then summarizes the instrument and viewing parameters necessary to cover all of the high-priority scientific objectives. Chapter VIII provides a description of the SAR instrument, including the system and hardware description, the calibration strategy, and the onboard data system. The impact of altitude on the performance of SAR is also discussed in detail.

Because the processing, delivery, archiving, and analysis of global high-resolution SAR data sets is a problem that has not heretofore been addressed, this strategy is crucial. The Eos Data Panel has provided a much more detailed study of the fundamental issues involved, which include both technological data processing and delivery problems and the need for a data management structure that addresses the needs of researchers. Chapter IX discusses the SAR data system and approaches for information extraction. Chapter X presents a summary of SAR synergism with other instruments. Chapter XI summarizes some of the high-priority research programs for SAR required before the launch of Eos.

II. GLACIOLOGY

SCIENCE ISSUES

The volume of ice and snow on Earth is enormous: enough to cover its entire surface with a layer roughly 60 m thick. Roughly 50 percent of Earth's surface is, at present, covered by snow or ice during some time of the year. Ice is not uniformly distributed over the Earth but is instead concentrated in the polar regions and mountains, attaining thicknesses of over 4,000 m; snow is concentrated in the mid- to high-latitude regions. More important in a geophysical sense, however, is the areal extent and the variability of the ice and snow cover. Approximately 11 percent of Earth's land surface is covered by glacier ice containing over 88 percent of the world's available freshwater. On a time scale of a few years, this area and the associated ice volume are relatively constant. On a time scale of hundreds to thousands of years, however, large changes in the amounts and coverage of glacial ice occur with the maxima corresponding to so-called "ice ages." One must add to the present area covered by glacier ice the highly variable coverage by sea ice and snow: sea ice covers between 3 and 10 percent of the world ocean, while snow covers between 11 and 46 percent of the land surface. These thin layers of sea ice and snow are the most ephemeral features of the Earth's surface undergoing large fluctuations annually as well as on time scales of decades to centuries.

Broad Eos Science Issues[5]

An understanding of the geophysics of snow and ice masses is essential to the comprehension of various interdisciplinary science problems of global importance. Sea ice serves as an insulating layer between the frigid polar air masses and the relatively warm ocean beneath the ice. Heat fluxes through open leads can be 100 times those through the ice; thus small changes in ice compactness extent can have major climatic effects. In addition, present climatic models suggest that any CO_2-induced atmospheric warming would be largest in the polar regions and that sea ice extent is probably the most sensitive natural indicator of such a temperature change. Furthermore, the brine rejection process associated with the growth of sea ice is believed to be an essential component in the formation of the cold, saline bottom water of the World Ocean. This growth takes place principally in the leads and polynyas and at the ice margins. Understanding this process is essential to understanding large-scale circulation and ventilation of the deep ocean. Bottom water is rich in CO_2 and its formation removes CO_2 from the atmosphere; an understanding of these complex processes is vital to improved forecasts of atmospheric CO_2 buildup. The sea ice edge "steers" intense localized storms and is associated with ocean eddies that contribute to vertical mixing.

In weather and climate modeling, the distribution of snow is important because it efficiently reflects short-wave solar radiation during the day and serves as a nearly perfect black-body radiator during the night. Snow is also an excellent insulator, with insulative and radiative properties changing as the snow cover ages and compacts. In addition, the deposition of large quantities of snow in non-polar regions results in storage for up to several months before the water released from the atmosphere actually becomes available to the land.

Ice shelves and ice sheets have similar impacts on atmospheric and hydrologic cycles, although in general, the associated time scales are significantly longer. For instance, an increase in the rate of discharge of ice from the West Antarctic Ice Sheet as a result of climatic warming could cause the balance of this vast sheet to become negative. With time this would result in a thinning of the sheet, a retreat of the grounding line, and a transfer of ice from the land to the sea. Some current studies within the glaciological community (Lingle and Brown, 1987) suggest that this retreat, once initiated, may be irreversible, resulting in a significant increase in the already bothersome gradual rise in sea level. Such changes would affect many low-lying areas of the Earth's surface.

Specific SAR Science Issues

To understand the global effects associated with the presence of, or changes in, the world's snow and ice masses, it is important to understand the small-scale internal processes that lead to behaviors and interactions. A variety of measurements, including both high- and low-resolution spaceborne observations and continuous *in situ* observations are necessary. Due to the large variation of snow and ice, these measurements must be made frequently and consistently. In addition, the measurements must be made in the higher latitudes during the spring, fall, and winter seasons when sun angles are low and cloud cover is at its peak. Therefore, microwave instruments are essential. In addition, high-resolution SAR can provide valuable operational support to ships and platforms located in and near the ice.

SAR observations can lead to an improved understanding of these processes, including the spatial distribution of ice, ice dynamics, and ice and snow geophysical properties. The electromagnetic and structural characteristics of the various types of ice bodies are strikingly different, ranging from low loss/low scatter (lake ice), to high loss/low scatter (first-year sea ice), to low loss/high scatter (multiyear

[5]See review by Untersteiner, 1984.

sea ice and glacier ice). Therefore, when dealing with different types of ice masses, both the geophysical problems and the appropriate remote sensing techniques may change.

Spatial Distribution of Snow and Ice

Determining the spatial distribution of snow and ice includes mapping the boundaries of snow and ice masses and the distribution of ice characteristics within these masses. Of particular interest is the detailed geometry of the sea ice margins where a number of complex, poorly understood processes are occurring, for example the generation of large eddies. In the seasonal snow cover there is great interest in not only the extent of the snowpack, but also in its thickness, its density, and the presence of free water. All of these parameters can rapidly change both spatially and temporally. The location of the borders of even such slowly varying entities as ice shelves and glaciers are in many cases not well known. For instance, in the Antarctic much of the coast is composed either of ice shelves or of ice tongues that discharge directly into the sea. In the past, a number of instances of large ice masses (on the order of 50 to 100 km in diameter) calving into the sea have been reported. The exact times of these calvings are not known to better than a several-year interval. The same lack of knowledge applies to the drift tracks of the icebergs once they leave their region of origin. SAR will clearly provide an ideal tool for monitoring such origins and movements.

Ice Dynamics

Studies in ice dynamics include the specification of the motion and deformation field of sea ice that results from wind and current forcing within the constraints imposed by nearby land masses. Associated with the deformation are the problems of describing the redistribution of ice thickness via the mechanisms of lead and pressure ridge formation, the changes in the drag coefficients of the upper and lower ice surfaces as the result of deformation and differential ablation, and the mechanisms accounting for brine drainage from sea ice. The latter process is believed to be the initial step in the formation of bottom water. The amount of brine drainage, as well as the initial amount of salt rejected by growing sea ice, is in turn related to the ice growth rate, a function of the surface heat balance and the ice thickness. Also, the strength of the ice (which determines its susceptibility to cracking and ridge formation) is a complex function of ice thickness. A system model diagrammatically showing process interrelations in winter sea ice behavior is given in Figure 7 (Butler *et al.*, 1987).

At present, there exist several models of different degrees of complexity that describe the coupled dynamics and thermodynamics of pack ice behavior. There are even models that begin to treat interactions between the ice and the ocean. Missing, however, are synoptic-scale observations taken over a period of several years that include sufficient detail such that specific ice characteristics can be observed, tracked, and compared with model predictions. Such observations are required not only for model verification, but also to gain insights into processes occurring within the pack.

Similar geophysical problems exist in lake and river ice, differing only in the relative importance of various factors. For instance, in most lakes and rivers the dissolved and particulate material content of the water is sufficiently low that impurity rejection during ice growth ceases to be of interest. In rivers, the currents and the geometry of the land boundaries are of primary importance. In large lakes, such as Lake Superior, a stable ice cover only forms in protected bays, with the great majority of the ice continually drifting during the winter. Although the processes occurring in packs of lake ice are presumed to be similar to those occurring in pack ice in the sea, the observational support for such an assumption is limited. Clearly the mechanistic details of many of the processes must be different. Spaceborne SAR observations would clearly fill a major observational gap in this field of study.

Understanding the motion and deformation field is also important when glaciers, ice sheets, and ice shelves are considered. In these cases leads are replaced by crevasses, and the 1 to 10 km/day drift of the sea ice pack is changed to a 0.001 to 1 km/year glacial creep. To date SAR observations have not be utilized in the studies of these slowly moving ice masses. However, the limited data that do exist suggest a number of possible applications, particularly in areas where glacial ice motions are relatively rapid (several meters per year or greater). For instance, installation of passive radar reflectors on the ice surface would allow the determination of the general motion field from observations made one to several years apart. Also, mapping the distribution of crevasses should permit the location of fast-moving ice streams that course through more slowly moving ice sheets and shelves. Such observations would be invaluable in developing and verifying more realistic models of glacier flow.

Ice and Snow Geophysical Properties

In addition to mapping the areal extent and dynamics of snow and ice masses, it is essential to monitor their geophysical state. We need to develop and verify improved quantitative models that predict the surface and volume scattering contributions expected from different ice types and geometries. For instance, the limited Seasat SAR data from large ice sheets show anisotropic returns and wavelike patterns from regions with featureless, apparently isotropic snow surfaces. The exact causes of these patterns are, as yet, unknown (Swift *et al.*, 1985a). Sea ice shows characteristic changes in radar return as it ages (particularly as it undergoes partial melting). Although some aspects of the physics of these

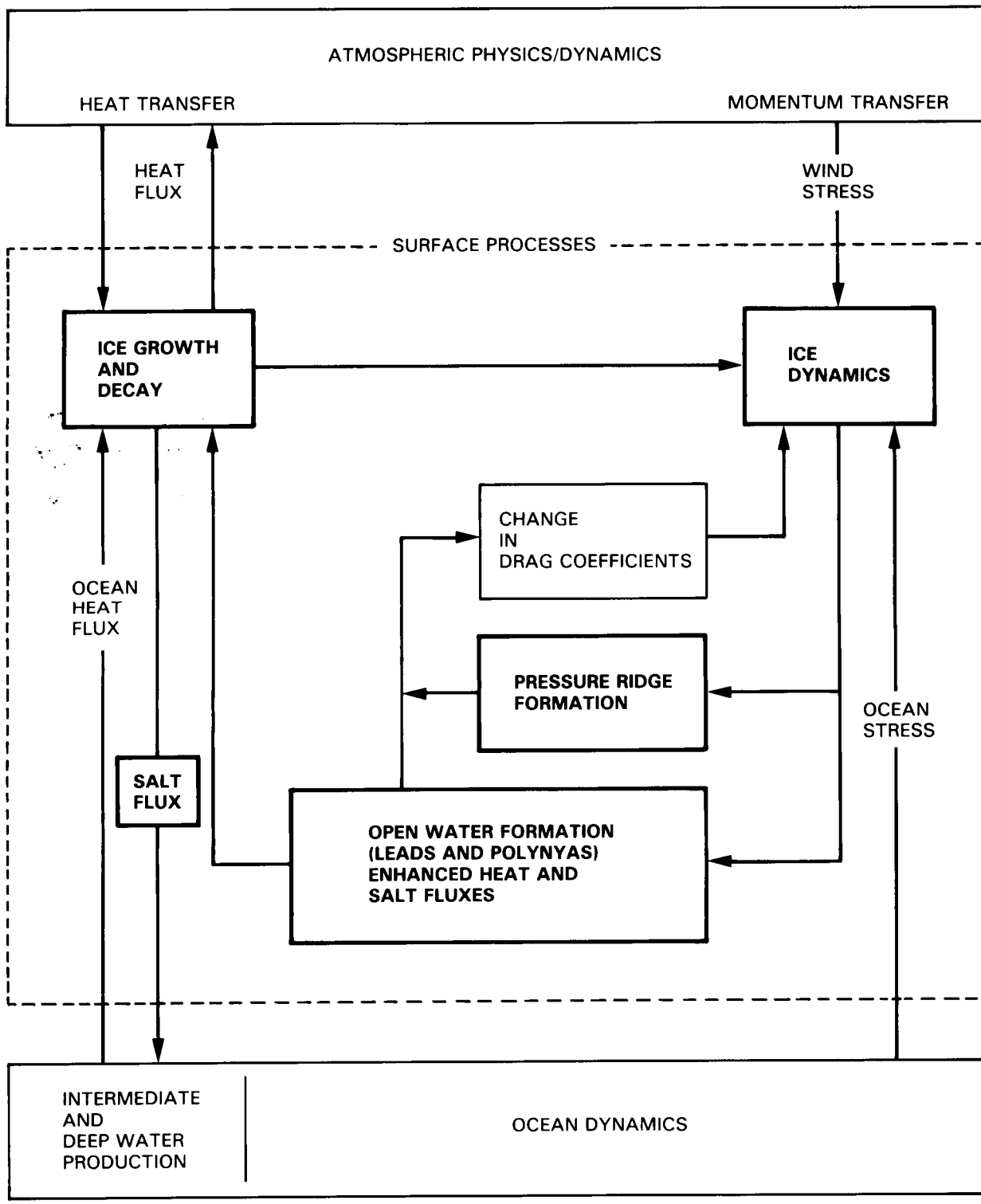

Figure 7. A system model for winter sea ice behavior (Butler *et al.*, 1987). Parameters in bold face represent those that can be measured by SAR.

changes are understood in terms of changes in ice composition and structure, the level of understanding is far less than desired (Holt and Digby, 1985). Advances in the understanding of this class of problems will require frequent SAR coverage of identifiable and trackable ice features combined with *in situ* observations of ice properties and modeling.

The primary science problem for snow is related: analyzing the continued metamorphic changes in the density, grain sizes and shapes, layering, and

distribution of liquid water (if present) in terms of the associated environmental forcing, and developing models relating these changes to observed differences in scattering.

In monitoring floating ice masses, we also see a variety of return patterns that cannot be adequately interpreted at present. For example, Seasat SAR imagery of the ice island T-3 (Figure 8) shows regions of extremely strong returns that do not correlate with what is known of the surface topography of the island. Perhaps the regions of strong returns correspond to some specific ice type of structure. It is important to establish if such strong returns are characteristic of all ice islands, as this would aid in identifying and tracking these hazardous ice masses. Icebergs also can show a characteristic strong return that is spatially displaced from the actual location of the berg. The exact combination of radar frequency and iceberg geometry requisite for such focused returns is not well understood.

Operational Applications

Information collected by the Eos SAR system will clearly be of major operational usefulness. This is especially true if arrangements are made both to process imagery within a few hours of data collection and to transmit either the imagery or selected information extracted from it directly to the concerned operator. Examples of problems where SAR data could be particularly useful include:

- Determining ship routes through pack ice
- Determining when to move non-ice-strengthened drill-ships
- Accurate location of ice edge
- Tracking ice islands, icebergs, floebergs
- Identification of thin ice areas within the ice pack

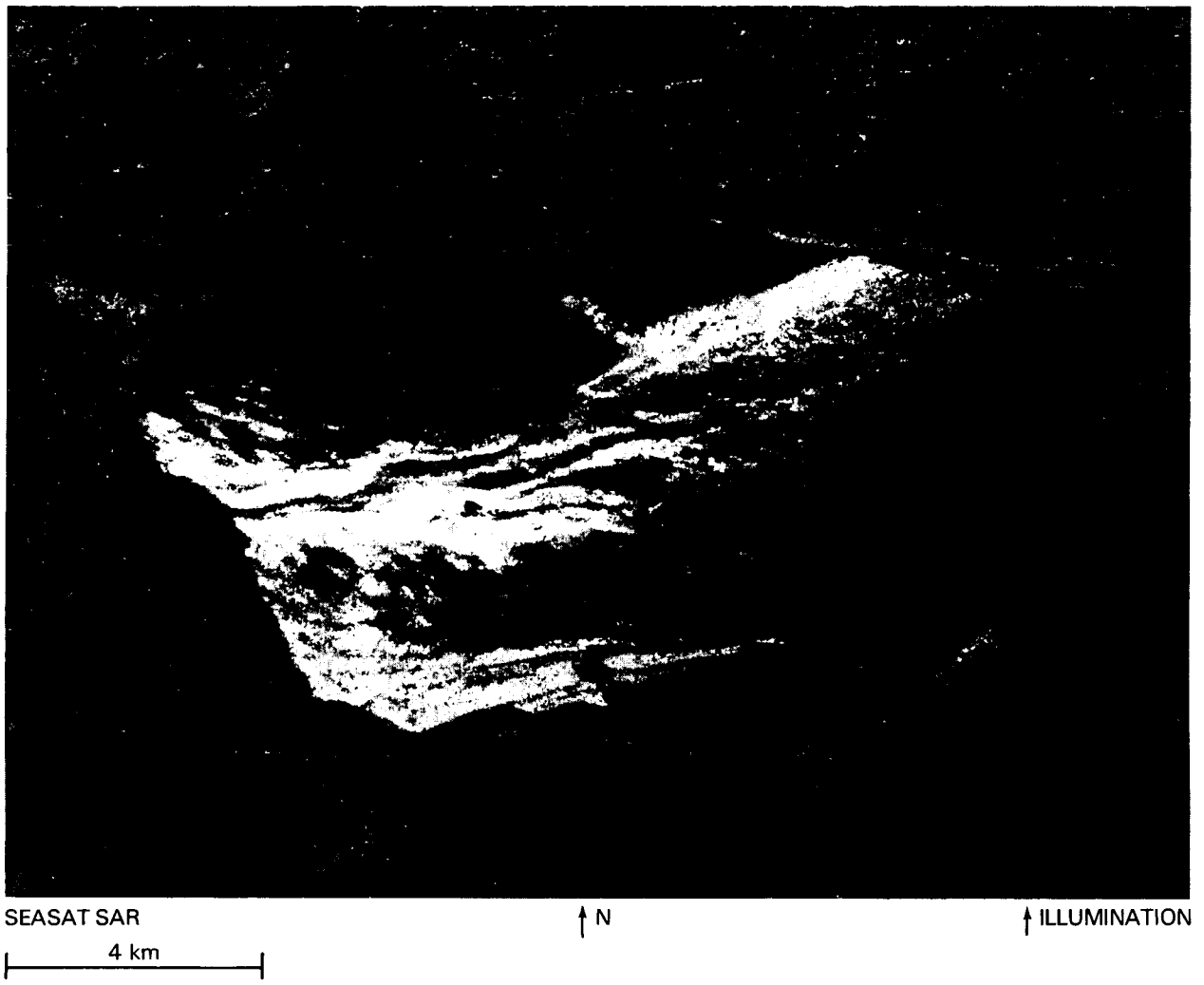

Figure 8. Seasat SAR image of the ice island T-3, Rev. 1452, October 6, 1978.

Table 2. Science and Operational Instrument Requirements for Glaciology

Glaciological Regime/ Observational Parameter	Usefulness of SAR	Other Applicable Eos Sensors
Sea Ice		
Pack ice edge	Yes*	MODIS, HIRIS, AMSR
Fast ice edge	Yes*	MODIS, HIRIS
First year ice concentration	Yes	AMSR*
Multiyear ice concentration	Yes*	AMSR*
Compactness	Yes	AMSR*
Floe size distribution	Yes*	HIRIS
Ridging Patterns	Yes*	
Surface roughness	Yes	GLRS*
Lead orientations and occurrence	Yes*	MODIS, HIRIS
Ice thickness	Yes (indirect)	TIMS*, MODIS, AMSR
Ice motion	Yes*	HIRIS
Albedo	No	MODIS*, AMSR
Surface melt	No	TIMS*, MODIS, AMSR
Surface temperature	No	TIMS*, MODIS
Ice islands	Yes*	MODIS, HIRIS, AMSR
Icebergs	Yes*	HIRIS
Wind velocity	No	SCATT*
Ocean wave characteristics	Yes*	
Lake and River Ice		
Ice edge	Yes*	MODIS, HIRIS, AMSR
Fast ice edge	Yes*	MODIS, HIRIS
Compactness	Yes	AMSR*
Floe size distributions	Yes*	HIRIS
Ridging patterns	Yes*	
Lead orientations and occurrence	Yes*	MODIS, HIRIS
Ice thickness	Yes (indirect)	TIMS*, MODIS, AMSR
Ice motion	Yes*	HIRIS
Ice jam locations	Yes*	HIRIS
Albedo	No	MODIS*, AMSR
Surface melt	No	TIMS*, MODIS, AMSR
Surface temperature	No	TIMS*, MODIS
Wave characteristics	Yes*	
Wind velocity	No	SCATT*
Ice Sheets, Shelves, and Glaciers		
Ice mass boundaries	Yes*	HIRIS, ALT*
Surface elevation	No	GLRS*, ALT
Accumulation rate	No	AMSR*
Mean surface temperature	No	TIMS, MODIS*
Surface velocity field	Yes*	GLRS
Ice streams	Yes*	
Internal velocity field	No	
Surface melt	Yes	TIMS*, AMSR
Crevasse patterns	Yes*	HIRIS
Iceberg discharge	Yes*	HIRIS
Snowpack		
Thickness	No	GLRS
Density	No	AMSR*
Water equivalent	Yes	AMSR
Free water content	Yes	AMSR
Extent	Yes	HIRIS*, MODIS
Mean grain size	Yes*	AMSR, HIRIS, MODIS
Surface temperature	No	TIMS*, MODIS
Albedo	No	MODIS*, TIMS

*Indicates instrument(s) of choice.

- Identification of ice jam formation and breakup on large river systems
- Mapping snow cover characteristics for hydrological forecasting
- Mapping crevasse fields in ice shelves and sheets
- Mapping ice shelf and ice sheet boundaries (particularly needed in the Antarctic)
- Mapping ice streams within ice sheets

Operational utilization of the imagery will undoubtedly grow with time as the applications community, through hands-on experience, gradually becomes aware of the potential of SAR.

OBSERVATIONAL REQUIREMENTS

Observational Parameters

A thorough study of sea ice information requirements in terms of features to observe and associated instruments for both scientific and operational needs has been made as part of the planning effort for the Radarsat mission (Carsey *et al.,* 1982). Similar listings have been developed by the Eos SMRWG (Butler *et al.,* 1984) and the Committee on Earth Sciences of the Space Science Board (NRC, 1985). Table 2 is largely based on this information. The applicability of SAR to each of the four primary observational regimes is indicated, as is the applicability of other potential Eos sensing systems. Table 2 indicates that of all the proposed Eos instruments, SAR predominates overall as the sensor of choice for studies of sea ice, of lake and river ice, and also of ice sheets, shelves, and glaciers, although less strikingly so. It is only in studies of the seasonal snowpack that SAR would be replaced as the primary instrument by the proposed 3 to 6 km resolution AMSR, a multifrequency suite of passive microwave radiometers. The altimeter (ALT) will also be an important instrument for ice sheet studies. If only three instruments were availale for glaciological studies, they should be SAR, AMSR, and ALT. This conclusion is true even without taking into consideration that SAR and AMSR are the only two imaging instruments that are not limited by either darkness, weather, or both.

The primary reason SAR is viewed as the instrument of choice is its high resolution as well as its all-weather capability. Ice extent is satisfactorily monitored by passive microwave techniques; however, the observations of open water areas, leads, and polynyas will require the resolution of imaging radar. Leads in the Arctic Ocean range from meters to kilometers in width and are typically tens of kilometers in length. Winter photographic data (Hall, 1980) suggest that a 30 m wide lead is typical for deformation; thus, leads of this size should be observed. Radar images also supply ice motion data on a spatially fine grid through the tracking of features in sequential images. Such features call for radar resolution no coarser than about 200 m as errors in the motion become significant if they exceed about 100 m/day.

Spatial Distribution of Snow and Ice

In studies of rapidly varying snow, sea, lake, and river ice covers, systematic detailed observations of the location and nature of the boundaries are required. Of particular interest here is the changing nature of the ice pack margins as revealed by shifting ice bands and streamers, as well as by large eddies and wave forms. The advantages of SAR in such studies are its high resolution coupled with its lack of cloud and lighting constraints. Even in the case of slowly varying ice masses, such as ice sheets and shelves, boundaries can be fixed via SAR observations to sufficient positional accuracy for most mapping and ice inventory purposes.

Ice Dynamics

In sea ice studies, observational parameters include determination of the edge of both the back and the fast ice, the compactness and the concentration of first-year and multiyear ice, the distribution of floe sizes, the ridging patterns, and the occurrence and orientation of leads (Figure 9). Most important, direct, detailed observations of ice drift and tracking of icebergs and ice islands are essential (Figure 10). All the basic observations necessary for studies of ice dynamics are possible with SAR. When these observations are augmented with data from the other Eos instruments, the set of observations will be nearly ideal (it is still not possible to directly measure sea ice thickness from space). The situation for studies of lake and river ice dynamics is similar to that for sea ice.

For ice sheets, shelves, and glaciers, information on ice mass boundaries, on the surface velocity field, on the discharge and drift of icebergs, and on the location of crevasses and ice streams is required (Thomas *et al.,* 1985) (Figure 11). This information is available from SAR. When coupled with laser determinations (Lidar Atmospheric Sounder and Altimeter (LASA)) of ice surface elevations and passive microwave (AMSR) estimates of annual accumulation rates, it should serve as the basis for a variety of investigations of the dynamics of large ice sheets and shelves.

Ice and Snow Geophysical Properties

Observational parameters for ice feature interpretation include the distribution of first-year and multiyear ice, the changing patterns of ridges and rubble, the presence of open water and of leads, icebergs, and ice islands. Of particular interest in river ice studies is the location and movement of ice jams. In glaciers, ice sheets, and shelves, identification of

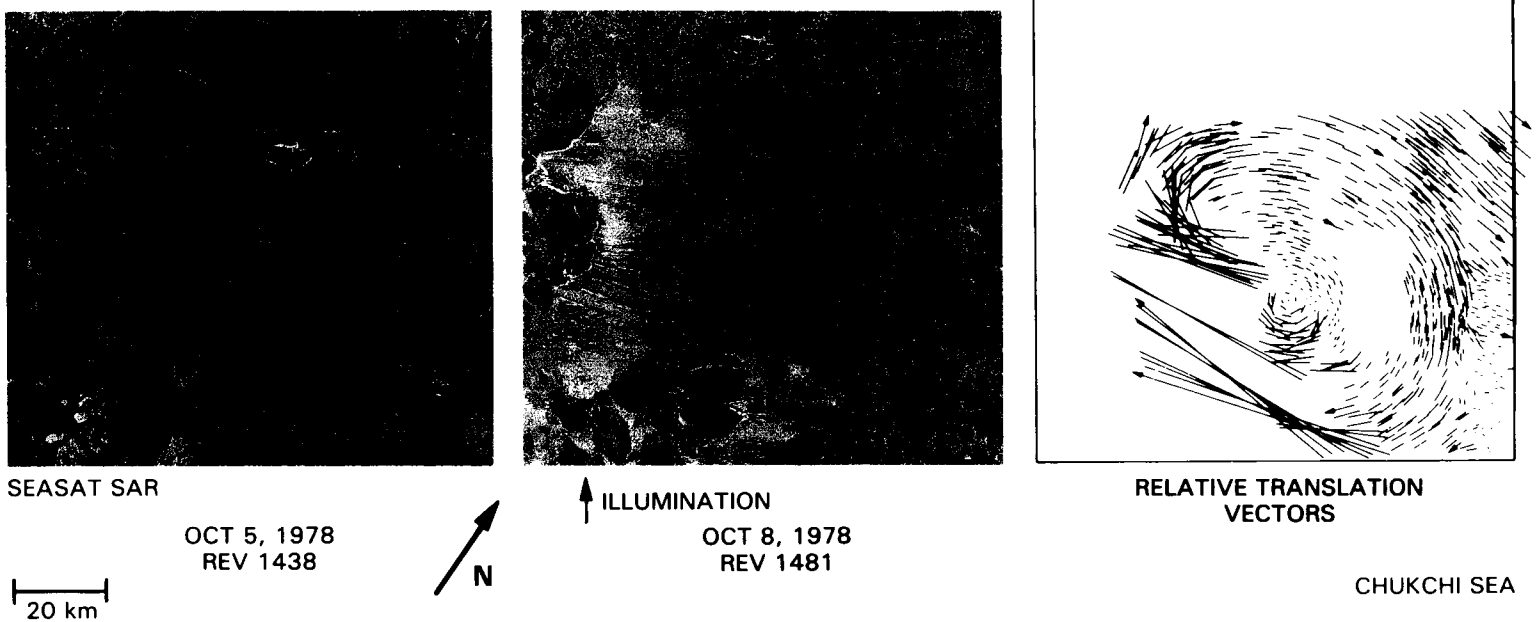

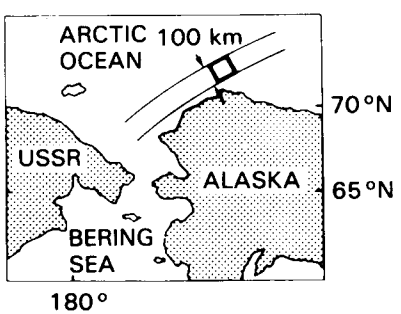

Figure 9. Seasat SAR images of the marginal ice zone in the Chukchi Sea taken 3 days apart. (a) Rev. 1438, October 5, 1978; (b) Rev. 1481, October 8, 1978; (c) relative translation vectors indicating ice motion in (a) and (b) (Carsey and Holt, 1987; courtesy of Holt and Yang, JPL). The vectors show the complexity of motion in an ice field that is the consequence of air stress, ocean surface tilt, water stress, and force transmitted through the ice. The first two stresses are thought to be essentially constant over the 100 km dimension of an image, while the remaining two stresses are known to have spatial variability but unknown form.

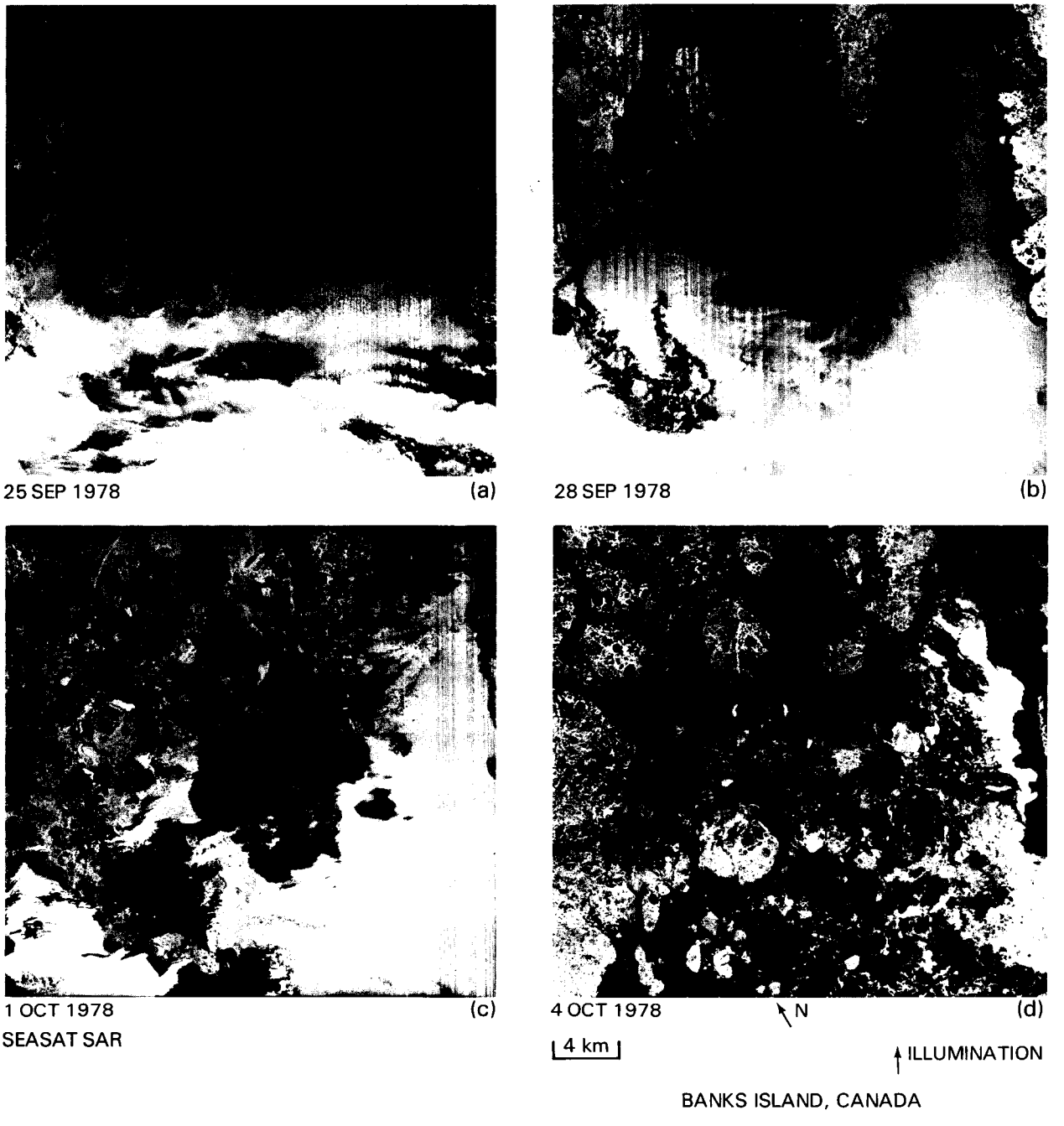

Figure 10. A sequence of Seasat SAR images of the marginal ice zone off Banks Island, Canada each taken 8 days apart. (a) Rev. 1296, September 25, 1978; (b) Rev. 1339, September 28, 1978; (c) Rev. 1382, October 1, 1978; (d) Rev. 1425, October 4, 1978. These images illustrate the dynamic nature of ice motion and rapid ice formation. The open ocean is rapidly covered by multiyear floes and new ice (dark) while a large floe remains grounded over the 12-day period.

large crevasses and, through their patterns, location of ice streams are required (Figure 11). Information on increases in the average grain size of snow is important. The characteristic grain size increase that occurs with melting and refreezing can identify the beginning of the melt season and can serve as an aid in making snowmelt runoff forecasts. SAR provides data on all these observational parameters. Shorter-wavelength imaging radars might, in fact, be used to make high-resolution maps of snowpack metamorphosism, which in areas with complex terrains could greatly enhance the accuracy of the snow water equivalence (SWE) estimates possible from low-resolution passive microwave observations.

Glaciological Regimes

Figure 12 shows the observational regimes discussed in the following section for summer and winter seasons.

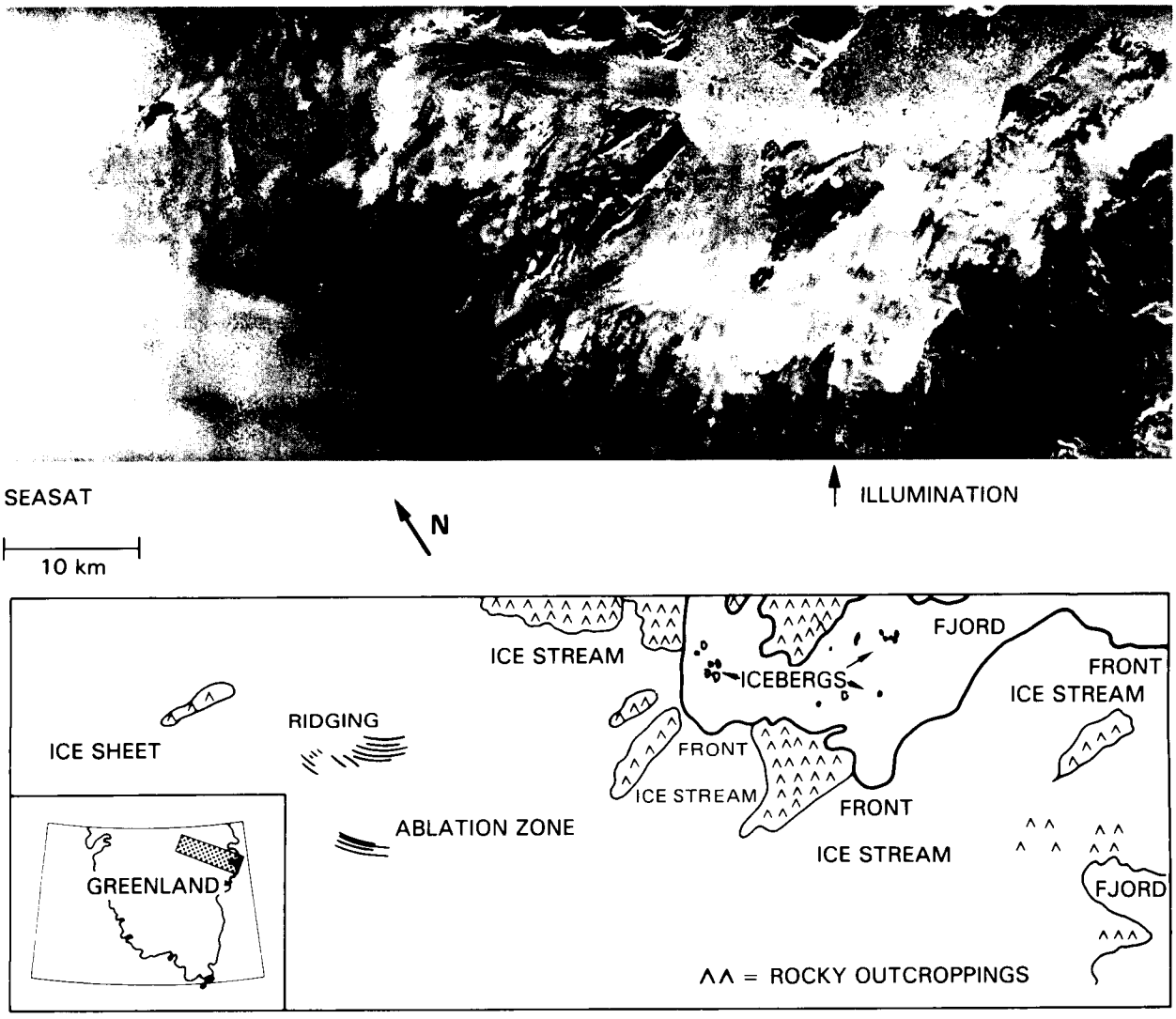

Figure 11. A Seasat SAR image of the southeast coast of Greenland from Rev. 1265, September 23, 1978.

Sea Ice

The total areal coverage of sea ice is both large and annually variable, ranging from 7×10^6 to 14×10^6 km^2 in the northern hemisphere and from 2×10^6 to 20×10^6 km^2 in the southern hemisphere (roughly 13 percent of the World Ocean is affected). Therefore, there are requirements for both large-scale and regional observations. Routine basin-wide coverage can only be obtained with a wide-swath mapping mode. There appear to be three types of regions where high-resolution limited swath observations will be particularly useful. These are:

1. Areas where *in situ* field observations are taking place
2. Areas where interesting small-scale ice processes are occurring, such as at the ice margins
3. Areas where specific operational information is required

Lake and River Ice

The total areas involved in lake and river ice studies are small but scattered over the globe. Of course the occurrence of lake and river ice increases toward the poles and in winter. The period of sampling for any given ice feature is relatively short; it is desirable to obtain observations at as fine a spatial resolution as possible and with revisit intervals as frequent as possible.

Glaciers, Ice Sheets, and Shelves

In many studies, it would be useful to have coverage over complete glacier or ice sheet drainage basins, which can range in size from a few kilometers for mountain glaciers to hundreds of kilometers for the Antarctic.

Snow

For research purposes, particular attention should be paid to obtaining SAR coverage over a

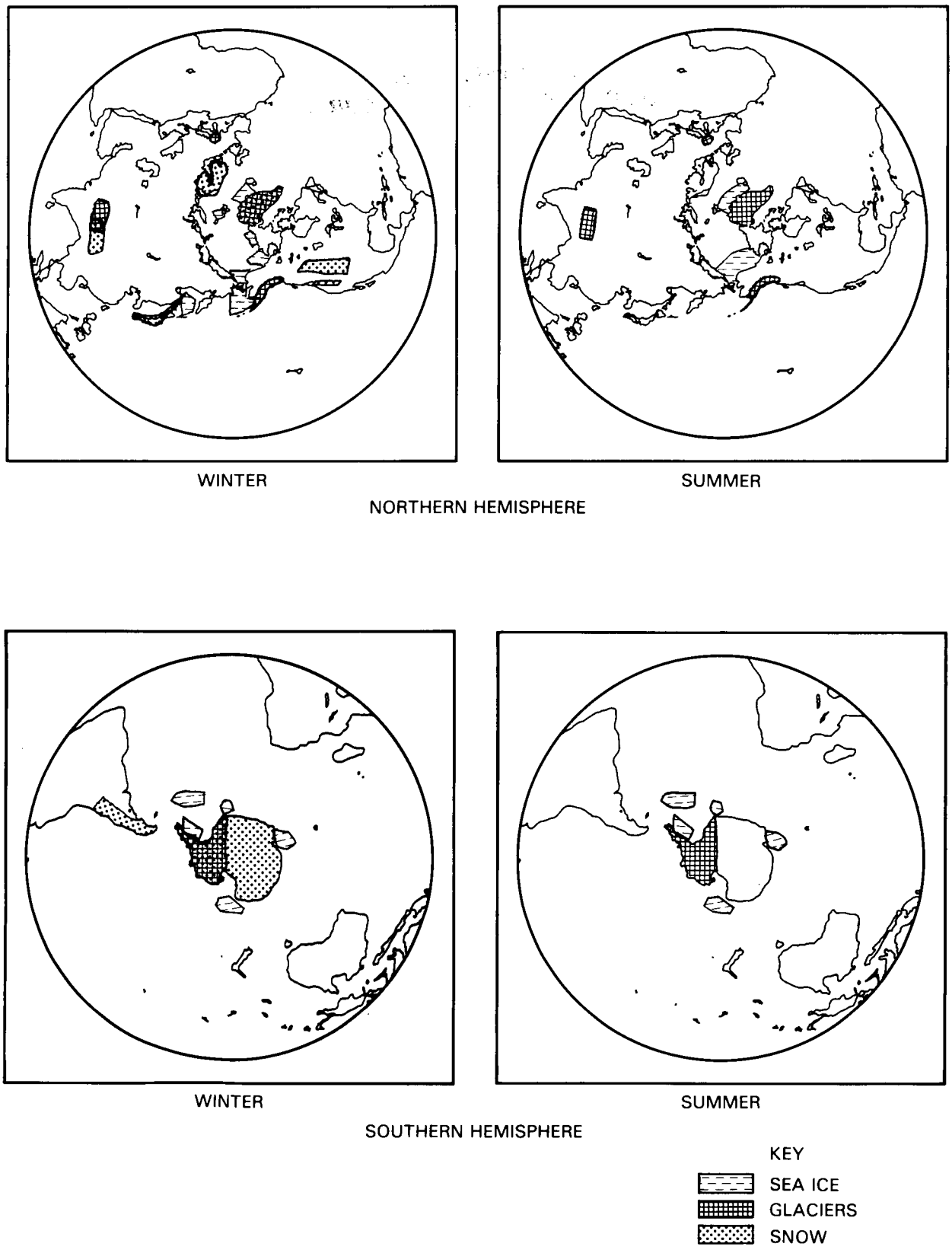

Figure 12. Sea ice, glaciers and snow regimes for the northern and southern hemisphere. These maps form the basis for the yearly average data rate estimate given in Chapter IX.

variety of instrumented watersheds in climatically different areas where snow melt is a significant factor in the overall runoff. Experience gained from these observations then can be expanded to studies of larger, unmonitored watersheds in remote regions of the globe. It is also desirable to measure the spatial extent, water equivalent, and wetness of snow over ice. Snow wetness information may also be useful for avalanche prediction in high-relief regions.

Operational Requirements

As possible operational requirements are extremely varied, we will not attempt to discuss them in detail. Most operational problems, however, are focused on small, localized areas and occur during fairly short periods of time. Accessibility to all higher latitudes is key in meeting operational needs.

RATIONALE FOR SAR OBSERVATIONS

There are two principal reasons why SAR is the sensor of choice for glaciological observations: (1) the unique surface morphology and material properties information revealed in fine detail by radar backscatter, and (2) the all-weather capability of imaging radars.

Electromagnetic Interactions

This section provides a short discussion of our current understanding of the reasons for the wide range of interactions that different ice types have with the electromagnetic pulses generated by SAR. These differences are the result of pronounced changes in the electromagnetic characteristics of the ice itself and in differences in the surface geometry and roughness of the ice bodies relative to the wavelength of the electromagnetic radiation that is used. For instance, sea ice is not pure ice; it contains entrapped sea salt in the form of both brine and solid salt crystals. The exact amount of salt depends on the rate at which the ice grew, its age, and its thermal history. Of particular interest is whether the ice has survived one or more summers; during the summer melt period most of the salt is flushed out of the portions of the ice that are above sea level. If the ice contains an appreciable amount of salt (first-year ice), it is a very lossy dielectric and the electromagnetic radiation penetrates at the most a few millimeters. In such cases, the strength of the radar return is almost completely controlled by the roughness of the upper ice surface. If the surface is flat, as is the case in undeformed first-year ice, the return will be low, as the electromagnetic energy will be reflected away from the radar receiver. If the surface is rough, as in the case of pressure ridges, a strong return from diffuse scattering will occur. This is a somewhat similar situation to the return from an ice-free ocean, in that at incidence angles greater than 20° a calm sea gives a low return while Bragg scattering from a rough sea gives a strong return. Fortunately, it is usually possible to distinguish between ice and open water because the patterns and textures of their returns are invariably different. Because the upper portion of multiyear ice is characteristically of low salinity as the result of brine drainage, the electromagnetic energy penetrates deeper than with first-year ice and reaches a depth where it undergoes volume scattering. In volume scattering, the radar wave is scattered by inhomogeneities (air bubbles, cracks, brine drainage tubes) within the ice mass. Therefore, for a given surface roughness, multiyear ice commonly gives a stronger return than does first-year ice. The interest in this distinction is that multiyear ice is invariably thicker and stronger than first-year ice and is, therefore, a better insulator as well as a more imposing operational hazard. A schematic drawing indicating the nature of radar returns from sea ice is given as Figure 13.

Although sea ice is a high-loss dielectric, lake and river ice are low-loss dielectrics. This is because lake and river ice consist of freshwater. Therefore, radiation normally penetrates completely through the ice, and the strength of the return is a complex function of the roughness of *both* the upper and the lower surfaces of the ice, and the volume scattering within the ice. In fact, in shallow lakes, such as those on the North Slope of Alaska, radar returns clearly indicate the portions of these lakes where the ice is frozen completely to the bottom.

Glaciers, ice sheets, and ice shelvese also consist of freshwater ice. The electromagnetic radiation penecurs. This volume scattering is primarily associated with the presence of air bubbles and rock and dust layers. However, as these ice masses are usually quite thick (hundreds to several thousand meters), at typical radar frequencies there is commonly no return from the bottom of the ice mass (from the ice-rock or ice-ocean interface). Therefore, the return strength is a function of the upper ice surface roughness, of the internal volume scattering, and of the geometry of large discontinuities within the ice such as crevasses or major changes in ice types. The general nature of the radar return from glaciers and ice sheets, and from lake ice, is also shown in Figure 13.

Seasonal snow layers are invariably thin (<5 m), chemically pure (compared to sea ice), and of a low density. Therefore, they usually give a low return and, as a result, are normally invisible at longer wavelengths (e.g., at L-band). However, if the snow is thick or wet or has densified as the result of freeze-thaw processes, and if the included air bubbles or ice lenses are of the appropriate size to serve as effective volume scatterers, moderate returns can result. Also, the upper snow surface can change from very rough (such as for sastrugi and irregular ablation features) to perfectly smooth in the matter of a few hours. Therefore, the radar return from snow is sometimes strong and sometimes very weak; for dry snow, there is minimal dependence on the roughness of the snow-air interface.

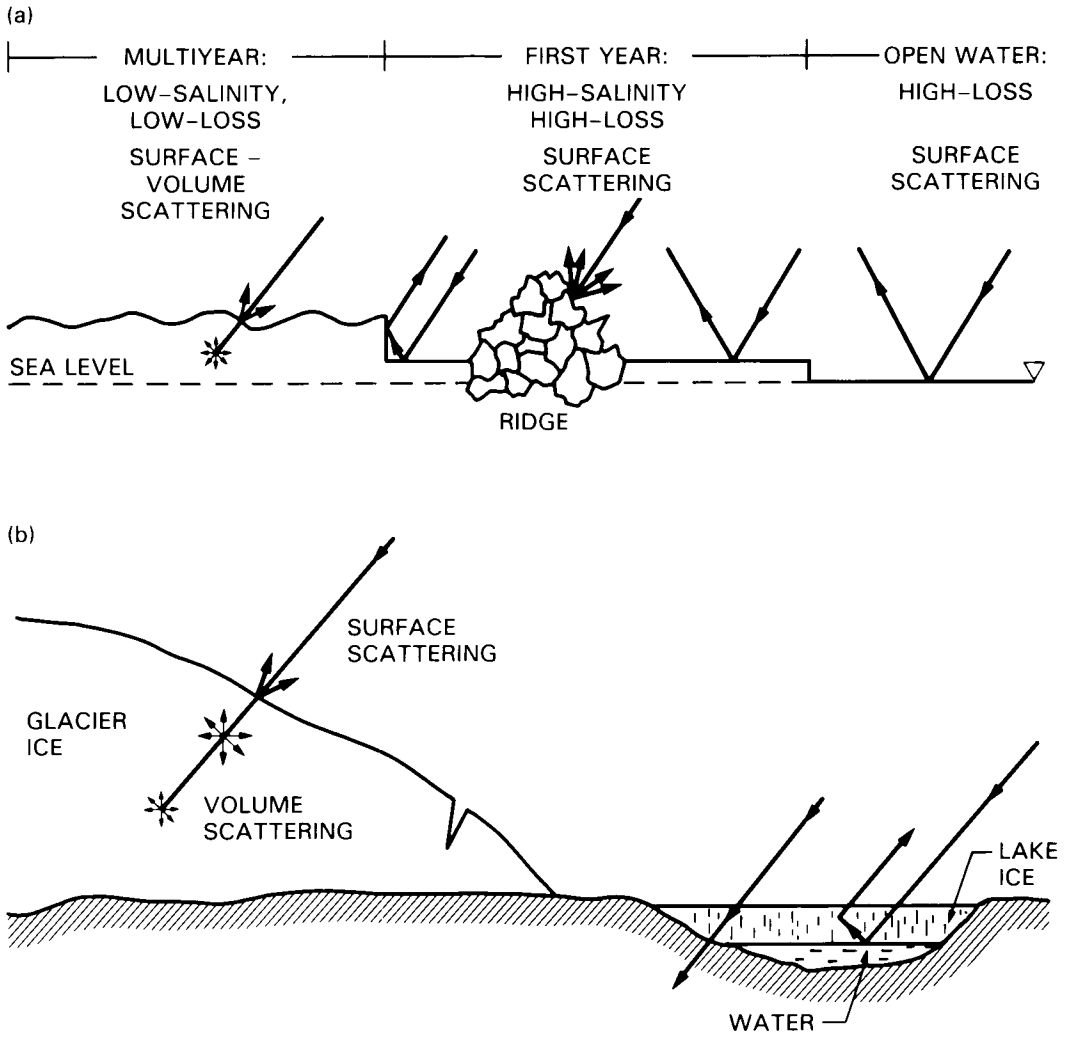

Figure 13. Interactions between radar and different ice types: (a) sea ice and (b) glaciers, ice sheets, and lake ice.

Of particular interest is that as snowpacks approach their melt season the average crystal size can greatly increase, thus increasing the pack's ability to scatter. In the Colorado Basin, large snowpacks metamorphose from having 0.1 to 0.2 mm crystals to crystals as large as 4 to 5 mm. This metamorphosis has been observed to change the 19 GHz and 37 GHz passive microwave emissions from the snowpack, an effect that is being studied in an effort to measure snow water equivalents from space as an aid to increasing the accuracy of snowmelt runoff forecasts. Short wavelength radars might be used to make high-resolution maps of snowpack metamorphosis, which in areas having complex terrains could greatly enhance the accuracy of snow water equivalence estimates. This is discussed further in Appendix A. Preliminary analyses indicate that by using all three Eos SAR channels (L-, C-, and X-bands) and by monitoring the snowpack over the season, it should be possible to extract the SWE. Based on models of backscattering and empirical results obtained from field data, an algorithm for determining the SWE (in cm) and the radar backscattering coefficient at C-band, σ° (θ_{50}, C), has been suggested (f. Ulaby, private communication):

$$SWE = \frac{\cos\theta}{2\,k_{em}} \log_e \left[\frac{\sigma^\circ_G(\theta_{50},C) - \frac{3}{4}\omega(C,r)\cos\theta}{\sigma^\circ(\theta_{50},C) - \frac{3}{4}\omega(C,r)\cos\theta} \right] \qquad (1)$$

where k_{em} is the extinction coefficient (cm^{-1}) and ω is the microwave albedo (a known function of the frequency, here noted with the letter C as 5 GHz, and a function of the ice particle radius r). By observation at 50° using both C- and X-bands, we can find the effective radius r and then the SWE. The numerator term σ°_G refers to the radar scattering coefficient from the underlying ice or soil; this term can be obtained by comparing the C-band measurement to the L-band measurement, as described further in Appendix A.

Variable frequency and polarization features of SAR provide a capability to extract the various properties of glaciers, ice, and snow discussed above. In addition, the high-resolution features of SAR allow fine structural features of ice to be discerned.

Multifrequency

In studies of ice masses, a multifrequency radar capability is of primary usefulness in determining the relative sizes of the effective volume scatterers within ice bodies where there is a significant penetration of electromagnetic energy (i.e., multiyear sea ice, lake and river ice, glacier ice, and snow). If the size of the scatterers is small compared to the electromagnetic wavelength, these inclusions will act as Rayleigh scatterers with radar cross-sections inversely proportional to a power of the wavelength (λ). For metallic spheres the scattering behaves as λ^{-4}, whereas for water it behaves as λ^{-2}, a result of the wavelength dependency of the dielectric constant of the water. Thus a comparison of the wavelength dependence of the scattering will be useful for determining the distribution of tiny brine pockets and much larger brine drainage tubes.

Multipolarization

The prime use of multipolarized SAR data is in separating surface scattering from volume scattering and in gaining further clues to the specific mechanisms involved. For surface scattering there are two well established mechanisms: geometric optics and resonant or Bragg scattering. Over the open ocean, the near-nadir return is governed by geometric optics scattering from the large-scale surface roughness elements and is a function of the average tilt of these elements. This process is independent of polarization. At larger grazing angles Bragg scattering dominates, and it is dependent on polarization being determined by the surface roughness component whose wavelength is of the order of the electromagnetic wavelength. Even in the case of the radar return from sea ice and from glacial ice, experimental data indicates that geometric optics dominates for viewing angles less than 30° to nadir and that Bragg scattering will be expected at larger angles if all the return is from the surface. Therefore, HH and VV polarization will help in discriminating volume scattering from surface scattering at large viewing angles ($>30°$), in that surface (Bragg) scattering is stronger for VV than for HH. It would also be interesting to generate images showing the phase difference between HH and VV, in that, for reasons that are still not well understood, volume scattering produces a near 0° relative phase shift while surface scattering can produce a 180° phase shift.

The potential scientific value of cross-polarized data (HV and VH) is not well quantified at the present time because of difficulties in the details of modeling the backscattering process. However, it is reasonable to expect that the cross-polarized returns (especially at X-band) would be strongly modulated by volume scattering within the ice pack and snow cover.

High Resolution

Typical resolutions obtainable via SAR systems (20 to 30 m) are sufficiently high so that a variety of individual features of natural ice masses can be observed; for instance, leads, individual floes, pressure ridges, and crevasses. These features provide innumerable points that can be identified on sequential images facilitating comparative studies with time and through the use of other sensor systems. The high resolution of SAR is in striking contrast to the low resolution (>2 km) of passive microwave sensors (e.g., AMSR).

All-Weather Observations

SAR observations can be made during periods of darkness, cloud cover, and fog. These capabilities are essential for systematic studies of snow and ice masses, in that the polar regions are characterized by long periods of darkness and twilight during the winter, and an extensive cloud and fog cover during the summer and fall. If observations can only be made during clear periods, the resulting record would be both sparse and biased.

Previous Experimental Results

Available satellite SAR high-resolution images of ice are currently limited to two main sets: Seasat coverage of the Beaufort Sea (summer 1978) and SIR-B coverage of the Antarctic sea ice margin (October 1984), both L-band with HH polarization and about 30 m resolution. In addition, the Soviet Kosmos-1500 Satellite (launched in December 1983) carries an X-band real-aperture radar (SLAR) with 1 km resolution.

In addition to radar images acquired by these satellite instruments, a number of measurements have been made using either *in situ* or airborne scatterometers and SLARs. The most detailed quantitative assessments of the optimum frequencies, polarizations, and illumination angles have been made using data from these scatterometers and SLARs.

Appendix A presents a more detailed discussion of the snow water equivalent algorithm as well as some relevant case histories for ice observations based on satellite, airborne, and *in situ* radar measurements.

RECOMMENDED MISSION STRATEGY

The scientific objective of the Eos SAR instrument for glaciology is to arrive at an improved understanding of the global effects associated with

the world's snow and ice masses by measurement of (1) ice dynamics, especially the specification of the motion and deformation field of sea ice as well as glaciers and ice sheets, and (2) the spatial distribution of snow and ice including their boundaries and characteristics. In addition, information collected by the Eos SAR will clearly be of operational value for ship routing, iceberg hazard tracking, and snow cover monitoring for hydrological forecasting.

The mission strategy recommended for Eos is based on specification of (1) the SAR instrument parameters, (2) the viewing parameters, (3) needs for synergism, (4) data rates and volume, and (5) information extraction techniques. Each of these is discussed below.

Instrument Parameters

Frequencies

Higher frequencies (K- down to C-band) are desirable for sea ice studies since radar backscatter at shorter wavelengths provides the strongest discrimination between ice types. The Eos SAR frequencies for sea ice in order of decreasing desirability are X-, C-, and L-band. The study of old ice structure is a possible approach to estimating ice thickness, an extremely important quantity not obtainable by any means; it is modeled. Thus for this observation the use of low frequency SAR, possibly P-band (75 cm wavelength), would be desirable.[6]

For lake and river ice studies, a wider range of frequencies is desired since the lower frequencies (e.g., L-band) provide better penetration and allow features of the ice bottom to be more readily discerned; by contrast, the higher frequencies (e.g., X-band) allow the best discrimination capability.

There is little information to guide frequency selection for studies of ice sheets and shelves, but the deeper penetration available at L-band will be of interest.

Snowpacks are essentially invisible at L-band, marginally visible at C-band, and quite visible at X-band; therefore the X-band channel will be necessary for snow studies (see Appendix A). If there were adequate image quality (low signal-to-noise ratio (SNR)), a shorter wavelength K-band channel would also be desirable; unfortunately, this does not appear to be feasible with the Eos SAR, due to insufficient transmit power.

Polarization and Phase

Like-polarization images (HH and VV) will be preferred in order to maximize the strength of the return signal for all ice studies. The use of both HH and VV data (and their ratio) should help discriminate volume scattering from surface scattering at large viewing angles ($>30°$), in that surface (Bragg) scattering is stronger for VV than for HH.

Although very little experimental data exists for sea ice, scattering theory suggests that additional information about the distribution of volume scatterers (brine pockets, etc.) should be obtainable from cross-polarization (HV) images. Cross-polarization data has been measured for snowpacks, confirming that HV is sensitive to volume scattering by liquid water and larger snowgrains.

The polarimetric capabilities of the Eos SAR may also provide a means to discriminate surface scattering from volume scattering, although no measurements along these lines have yet been made.

The narrow-swath local high-resolution mode will be used for investigating the utility of the cross-polarization, polarimeter, and phase difference channels for ice type and snowpack information.

Radiometric Calibration

An absolute calibration of at least ± 1 dB and a relative calibration (instrument stability) of 1 dB is desired; this derives principally from the need to measure snow water equivalent to ± 20 cm (see Appendix A). In addition, the radiometric fidelity within a scene (both along- and cross-track) should be within a fraction of a dB; this is necessary to allow quantitative studies of ice dynamics and type over larger areas (several hundred kilometers) using a mosaic of several Eos SAR images.

Viewing Parameters

Incidence and Azimuth Angles

Useful sea ice information can be obtained over a wide range of incidence angles (20° to 65°). However, the details of the information obtained varies with angle. For instance, SAR observations made with incidence angles of less than about 35° allow for the clear discrimination between first-year and multiyear ice and water. At higher incidence angles ($>35°$), discrimination between first-year ice and water becomes increasingly difficult, although it is still possible to easily identify multiyear ice. The fact that multiyear ice continues as a strong scatterer at these high angles is the result of its return being largely due to volume scattering as opposed to surface scattering. Therefore, variable incidence angles give investigators the opportunity to study regional and seasonal variations in the relative surface and volume backscattering contributions. There are no specific science requirements for multi-azimuth angle data.

As in the case of sea ice, the details of lake and river ice returns vary with viewing angle. At shallow incidence angles (nadir to 20°), the backscatter signature is principally coupled with the roughness of the ice-water interface and the bulk attenuation within the ice layer. At angles greater than 20°, the scattering process is determined largely by surface roughness effects. Here, the average surface slopes, which

[6]It is of course recognized that there may be engineering difficulties, such as antenna size, in implementing a P-band SAR, and that Farady rotation effects from the ionosphere may degrade image quality.

determine the degree of scattering, can be extreme due to ice upheavals resulting from a variety of deformation processes. The study of lake and river ice will require more selectivity in targeting than for sea ice. The squint mode will be essential to the accurate targeting of selected lake and river ice study sites at desirable incidence angles.

For studies of ice sheets and shelves, shallow incidence angles (nadir to 20°) will give a measure of the surface roughness. Steeper angles appear to give a unique response to volume scattering effects that are directly proportional to the number density of scatterers.

Experimental data (Stiles and Ulaby, 1980) indicate that at the higher frequencies, the difference in the relative backscatter between wet and dry snow is almost invariant with incidence angles from 10° to 70°. However, incidence angle flexibility for snow studies is required to provide wide-area mosaics of SAR images acquired within a relatively short time span.

Revisit Time

Well inside the boundaries of the polar ice packs, where the ice movements are primarily in response to the movement of large-scale weather systems, observations made every 3 to 6 days are presumably adequate. Clearly it is important to image both the entire Arctic and Antarctic sea ice packs at these short time intervals so that realistic characterizations of the ice kinematics can be obtained. Low-resolution data (500 m), however, is sufficient for these purposes. It will also be important to monitor a variety of different ice processes occurring within the ice packs during different seasons. In these studies specific time periods would be chosen for more detailed observations. Specific locations (i.e., incidence angle selection) should be chosen in advance (a day or two) using the low-resolution synoptic data.

Many processes that occur near the edges of the packs proceed more rapidly. In the Arctic, these processes are limited to Greenland, the Labrador, and the Bering Seas, and should be monitored on a daily basis. In the Antarctic, the processes are very poorly studied at present, but presumably require frequent (1- to 2-day) repeat coverage in selected regions. More information on the sampling frequency of both polar regions will be acquired with ERS-1 in 1990.

As mentioned earlier, ice navigation problems peak in the late summer when ice is at a minimum. Therefore, it will undoubtedly prove operationally important to provide SAR imagery of certain critical areas such as the southern Beaufort Sea on as frequent a basis as possible. Fortunately, regions of operational interest are usually spatially restricted at any given time.

The sampling intervals for studies of the dynamics of ice packs in large lakes are similar to those needed for sea ice (observations every 3 to 6 days). The sampling of selected rivers should also proceed on a similar temporal spacing. However, as most lakes and rivers of interest are located in temperate regions, the total length of the observational periods will be about 3 months per year. It will be particularly desirable to obtain data as frequently as possible during periods of ice jam formation and breakup.

On alpine glaciers, bimonthly observations should be sufficient. On large continental ice sheets, yearly observations near the margins would be adequate to delineate major calving events. In the interior of the large ice sheets, biyearly observations might be required for the investigation of accumulation processes and grain growth in the near-surface layers. On the other hand, if radar techniques are being applied to ice movements, observations every 10 years may well be sufficient. An exception to this timing should be made for regions where more rapidly moving ice streams are anticipated (i.e., on the Ross Ice Shelf). For such areas, observations as frequently as bimonthly might prove to be useful at locations where passive radar reflectors have been deployed. For these phenomena, available data sets are so spatially and temporally limited, there is little guidance for the most efficient temporal sampling scheme.

Selected "representative" snowpacks should be observed both during their accumulation and melt. Monthly imaging during accumulation would seem adequate. Since SAR should give excellent data on snowmelt pattern progression, which is required for most snowmelt runoff models, selected snowpacks should be imaged approximately every 4 days during the melt period. If possible, observations should be made diurnally, since this would allow both dry (nighttime) and wet (daytime) snowpack observations, which are critical for the algorithm presented in Appendix A. Observations of snow on sea ice are essential for estimates of heat transfer through ice; the accumulation should be monitored every few days.

Operational exercises invariably require frequent observations. It is often desirable to acquire images several times per day; this may be possible with SAR at higher latitudes.

Swath Width and Resolution

As discussed in Chapter I, three observational modes are envisioned for SAR: (1) a global mapping or survey mode (700 km swath and 500 m resolution) for coverage of the Arctic and Antarctic, (2) a regional mapping mode (100 km swath and 100 m resolution) for more detailed regional sea ice studies, and (3) a local high-resolution mode (50 km swath and 30 m resolution) for detailed observations around the margins and in specific locations within the polar ice packs, especially individual pressure ridges and other fine details of sea ice. The global and regional mapping modes will also be important in regions of rapid ice motion, where features may move completely outside of the field-of-view if a 3-day sampling interval is used.

Because of the generally smaller scales of lake and river ice, the majority of these studies would be able to obtain an adequate sample with a swath width of 100 km or less. Studies of ice sheets and shelves, where rapid repeat sampling is not important, would require a 100 km swath width.

Synergism

SAR will be particularly useful in the monitoring of sea ice, lake and river ice, ice sheets, shelves, and glaciers. However, in order to understand more fully the processes involved, data from other sensors must be utilized. Table 2 lists these data requirements.

The polar regions, locations of the majority of the ice studies, are characterized by darkness in winter and haze in summer. This therefore restricts the instruments used with SAR in ice studies primarily to those operationg in the microwave frequencies (AMSR, Advanced Microwave Sounding Unit (AMSU), ALT, SCATT) as well as telemetry instruments such as the Advanced Data Collection and Location System (ADCLS). See Chapter X for a further discussion of each of these instruments.

Simultaneity requirements may be on the order of hours for ice data as conditions, especially in terms of sea ice, will change rapidly. It is believed that synergism will play a critical initial role in ice research as SAR capabilities are refined; however, this need may decrease somewhat once SAR's ice monitoring becomes more operational.

SAR and AMSR

As pointed out previously, the most synergistic instrument pair for glaciological studies will be SAR and the AMSR.

In terms of operational capabilities, AMSR is the only short-wavelength microwave instrument besides SAR; neither is limited by weather or darkness. AMSR will be complementary to SAR, providing a total low-resolution overview of the pack ice in contrast to the focused, high-resolution SAR view. The AMSR data can thus be processed to yield the following information: the ice edge position, the first and multiyear ice concentration, and the location and persistence of polynyas. The AMSR is most useful in studies of the seasonal snowpack, especially in terms of density, water equivalent, and free-water content (wetness). SAR, on the other hand, can monitor snowpack metamorphosis, sensing an increase in grain size prior to melt. Together these microwave instruments could provde a more accurate "early warning system" of snowmelt.

AMSR will provide 1,400 km swath, contiguous-coverage, moderate-resolution, (2 to 20 km) passive microwave data with horizontal and vertical polarizations at six frequencies ranging from 6 to 91 GHz. The 18 GHz (6 km resolution), 37 GHz (3 km resolution), and 91 GHz (1.2 km resolution) channels are expected to be useful for estimates of snow cover amounts on land; when supplemented by the 10 GHz (10 km resolution) channel, moderate resolution estimations of the amount, age, and thickness of sea ice can be made.

The 6 GHz AMSR channel is very close in frequency to the C-band SAR channel and is expected to be useful for estimation of sea surface temperature. This information will be useful when combined with SAR images of the sea ice margin.

SAR, HIRIS, and MODIS

Under clear skies, MODIS and HIRIS can provide information on the optical properties of snow and ice, the ice edge position, snow covered area, the snow and ice optical albedo, and in spring and summer, information on the presence and magnitude of biological productivity at the ice edge. In mountainous terrain, the fine spatial resolution provided by SAR and HIRIS will be necessary to interpret data from AMSR, ESTAR, and MODIS. However, both MODIS and HIRIS coverage of the polar regions are extremely limited by both darkness and weather, especially during the winter months.

The thermal information provided by the MODIS thermal IR channels will be especially valuable in combination with SAR data for studies of sea ice dynamics and boundaries.

SAR and ADCLS

ADCLS will also be crucial to ice studies. ADCLS will provide the linkage between buoys mounted on the ice that transmit their position, and a variety of other data such as surface pressure, temperature, and related oceanographic data from suspended instruments. In particular, velocities derived from the buoys can be used as both a check and a tie point for the velocities derived from SAR.

SAR, ALT, GLRS, and SCATT

ALT and, to a lesser extent, the Geodynamics Laser Ranging System (GLRS) will yield ridging statistics and scalar information on the wave fields within the open-water areas within the ice pack. In terms of ancillary data, SCATT will be useful in estimating wind velocities as well as for large-scale backscatter measurements over ice sheets (Thomas *et al.*, 1985). SAR itself will also be a source of ancillary data, measuring wave characteristics necessary for sea ice studies.

Data Parameters

Contiguous single-channel SAR coverage once of the northern polar sea ice pack would require the equivalent of 700 SAR images (100 km on a side) for the summer and 1,400 for the winter; in the southern hemisphere, this number ranges from 200 in summer to 2,000 in winter. The total number of SAR images

required for complete sea ice coverage could be many times this, depending on the number of channels (frequencies, polarizations, etc.) and the number of revisits.

It is clear that such a complete, high-resolution, multichannel coverage scheme would quickly overwhelm the ability of investigators to digest and analyze, to say nothing of the demands on the data transmission and image processing systems. However, much of the polar sea ice is not sufficiently dynamic to require frequent 30 m resolution coverage. Single frequency, 100 m resolution coverage, involving 1/16 of the data, would be sufficient for monitoring ice; the global mapping mode with 500 m resolution will also be useful and will cut the data rate even more. It is paramount that the investigator be able to quickly browse through these low-resolution SAR images of ice or snow scenes in near real time to select scenes for further, more detailed examination. Thus, the low-resolution mapping modes will be useful for surveys; identified study areas will then be covered in the high-resolution (30 m) local mode. This may amount to 10 percent of the total sea ice area, e.g., 20 to 200 SAR images per channel within a short time period.

Research glaciologists using Eos data will combine image products with other collateral data sets taken for study sites. A high degree of investigator interaction with the data system will be required; requests will be made for (1) SAR data, (2) image browsing, (3) radar parameter selection, (4) engineering and system data such as orbital parameters and image radiometric calibration, (5) data from AMSR and other Eos instruments, and (6) collateral data from *in situ* and ancillary data sources. Moreover, this information and data must be made available to investigators at remote locations such as the Beaufort Sea or on research vessels at the Antarctic ice margin. Finally, all images must be radiometrically calibrated and geocoded; this is especially critical for polar ice studies where ground control points are non-existent.

Information Parameters

The specific geophysical information that SAR can provide is summarized in Table 2, along with other applicable Eos sensors.

As pointed out earlier, the extraction of useful geophysical information from the Eos SAR images assumes a high degree of radiometric and geometric calibration. Some of this information is geometrical in nature—e.g., ice pack features and seasonal morphology—and some is directly usable in understanding the processes of heat and mass transfer. The analysis of these images will range from reasonably straightforward task (e.g., tracking of ice leads using single-channel data) to more sophisticated procedures (e.g., extraction of the water equivalent from a snowpack).

Since global multifrequency, multipolarization SAR coverage has not heretofore been possible, it is expected that the first phase of the Eos SAR activity will be to develop and refine algorithms for information extraction using these advanced capabilities. Emphasis will be placed on ice type discrimination, snow water equivalent estimation, and synergistic use of SAR data with AMSR and other Eos instruments.

III. HYDROLOGY

SCIENCE ISSUES

Broad Eos Science Issues

The scientific questions to be addressed by Eos require an improved understanding of the global hydrologic cycle. The components of the hydrologic cycle are so strongly coupled to the mechanisms of atmospheric circulation and the climate cycle that none of these can be meaningfully studied independently. In addition, the fluxes that make up the hydrologic cycle are the primary forces for shaping the landscape and the primary transport mechanisms in the biogeochemical cycles.

The terrestrial component of the global water cycle is characterized by enormous spatial and temporal variability. Hydrologists have very little understanding of the water balance fluxes and storages at catchment and basin scales. Such understanding will be required for inputs into global climate models and large-scale meteorological models.

SAR has the potential for providing micro- to macro-scale information about areas of standing water, soil mositure, snow water equivalent, vegetation moisture, and topography. This information is synergistic with the regional-scale response to soil moisture and soil temperature to be obtained from ESTAR and MODIS, respectively; it is also synergistic with small-scale vegetation and soil moisture information from HIRIS and TIMS. However, SAR is the only sensor with the potential to provide fine-resolution information about soil moisture and snow liquid water and snow water equivalent, at any latitude at any time of the year, and about standing water extent independent of vegetation cover.

The three main hydrologic objectives of the Eos program are (Butler *et al.*, 1984):

1. To quantify the processes of precipitation, evaporation, evapotranspiration, and runoff on a global basis
2. To identify the factors that control the hydrologic cycle
3. To quantify the interactions between the vegetation, soil and topographic characteristics of the land surface and the components of the hydrologic cycle

To meet these objectives, we must focus our research on three key elements of hydrologic models: water storages, water fluxes, and chemical fluxes. These elements are the basis of hydrologic modeling; it is possible using SAR to obtain experimental data that can lead to their definition. The model elements must be quantified in order for hydrologists to make the bridge between contemporary hydrological knowledge and global-scale processes.

Water storages are in the form of soil moisture, snow, and surface water. The storages are highly variable spatially and temporally.

Water fluxes are into and out of the surfaces that define the terrestrial water balance, and include precipitation as an input flux, surface runoff and ground water as redistribution fluxes, and evapotranspiration as the outward flux.

Chemical fluxes include the chemical balance of wetlands. The chemical fluxes depend on hydrologic fluxes and storages because, for the most part, water is the transporting medium. Standing water areas also are the main places in the environment where anaerobic biological processes occur, producing chemically-reduced as opposed to oxidized products (e.g., CH_4).

Specific SAR Science Issues

Many hydrologic processes such as infiltration and evapotranspiration at point locations are quite well understood. In spite of this, several problems in hydrology have proven to be almost impossible to solve using historic point modeling approaches. One of the most important deficiencies in our knowledge is the spatial and temporal variability of factors that affect the hydrology and water balance of a basin or catchment whose feature sizes may range from tens to hundreds of meters. These factors include soil properties and moisture, snowpack properties, topographic features, drainage patterns, land use, areas of standing water, and subsurface water storage (see Butler *et al.*, 1987, Chapter IV). Rainfall, streamflow, soil moisture, evaporation, and snow cover are the major hydrologic variables that have historically been measured at point locations; our hydrologic concepts reflect this point perspective. Scientists have long recognized that hydrologic processes are spatially variable, but there have been feasible alternatives to point data collection. The detailed resolution (30 m) available with SAR in its high-resolution mode, supplemented by HIRIS and TIMS data, will be necessary for hydrologists to bridge point data to micro- and macro-scales, to large-scale areally averaged representative basin processes. Both SAR—in the global and regional mapping modes (500 m, 700 km swath)—and MODIS will then bridge the basin-wide processes to continental scales. The ESTAR passive microwave L-band radiometer will provide global-scale information on soil moisture at 10 km resolution. The scales addressed by SAR in comparison to the ESTAR passive microwave radiometer are shown in Figure 14. The ESTAR response to soil moisture will be less affected by slope than will the SAR response, due in part to larger scale spatial averaging, but only SAR will provide soil moisture and snow water information (by using change detection procedures) at the moderate

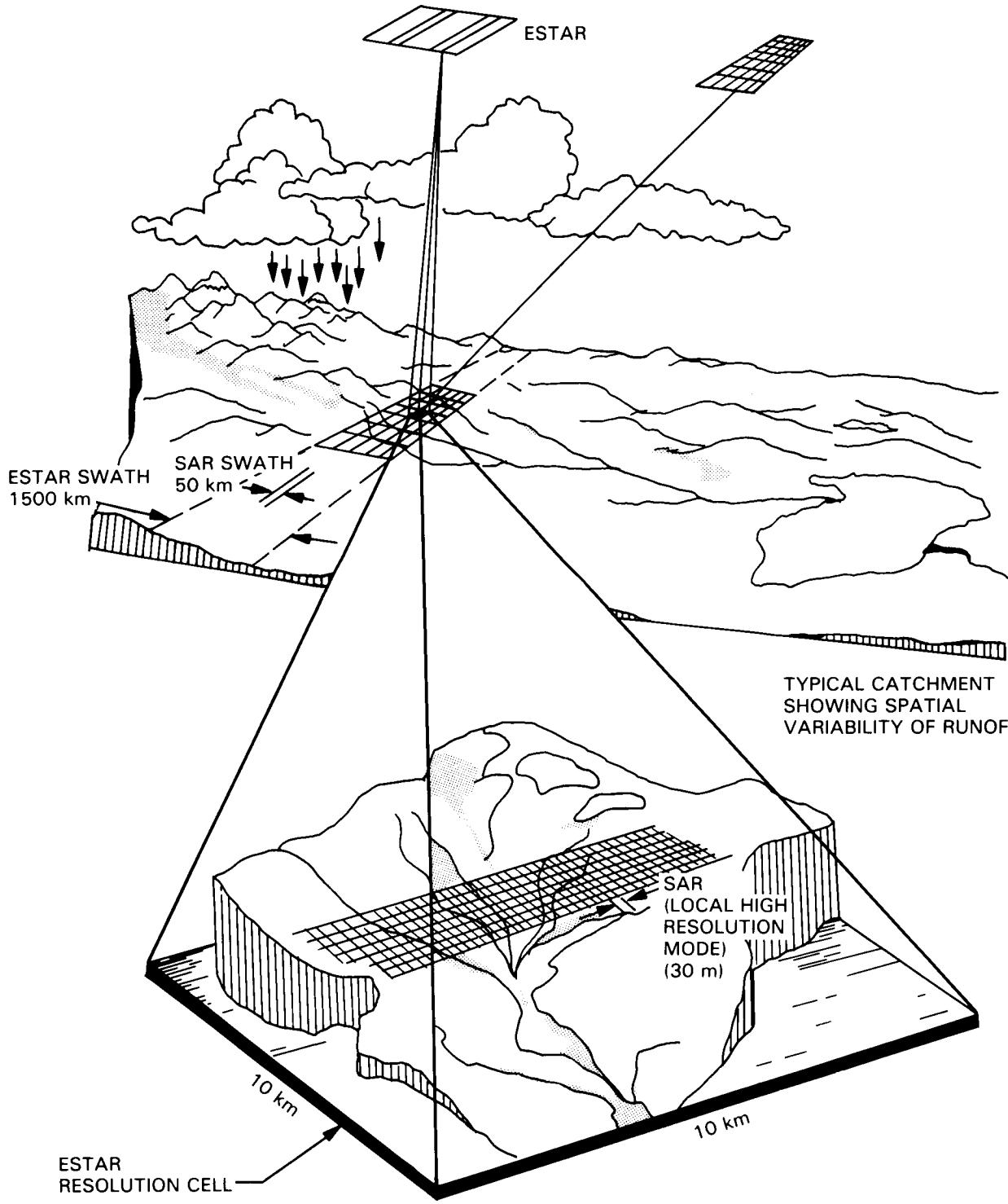

Figure 14. Schematic showing synergistic operation of SAR in the high-resolution mode and ESTAR.

to high spatial resolutions needed for process studies at catchment and regional scales.

OBSERVATIONAL REQUIREMENTS

Observational Parameters

Hydrologists use remotely sensed data to infer specific scene properties; only rarely can these properties be measured directly from the data products. The water and chemical fluxes in the terrestrial ecosystem cannot be measured directly and there is no new technology that seems likely to change this. In fact, hydrologists cannot even infer these fluxes based solely upon remote sensing observations. Nonetheless, remote sensing data will play an important role by providing new types of spatial and temporal data to use in hydrologic system models that will in turn yield information about these fluxes.

Some of the important hydrologic model parameters that are directly observable via radar remote sensing are land use and basin characteristics such as channel geometry and slope information, and areal extent of standing water (Table 3). Procedures for using this type of information have been developed and modified for use in current hydrologic models and procedures (Engman, 1981).

Table 3. Hydrologic Observational Parameters

Terrain Characteristics
Land use
Channel geometry/drainage patterns
Slope/topography
Areal Exent of Standing Water
Lakes
Rivers
Reservoirs
Wetlands
Flooded regions
Soil Moisture
Soil water content
Frozen soil boundaries
Snow
Snow water equivalent
Areal extent
Snowpack conditions (grain size, presence of liquid water)
Vegetation Moisture
Woody components
Foliar components
Surface boundary layer

Soil moisture, snowpack conditions (including snow water equivalent), frozen soil boundaries, and vegetation moisture content are important terrestrial conditions that affect the terrestrial water balance (Table 3). There is strong evidence that these land process state variables may be measured directly from radar data because of the sensitivity of radar backscatter to the widely varying dielectric constants of water, moist and frozen soil, and snow (Figure 15). Although other factors such as surface roughness and vegetation cover also affect the radar backscatter, changes in the dielectric constant of surface materials strongly modulate SAR image intensity.

The temporal behavior of the hydrologic process is another extremely important observational parameter. The Eos program has the potential for making frequent measurements over long periods to develop an understanding of the temporal behavior of hydrologic processes. The use of Eos radar data to track various hydrologic state variables in time may enable hydrologists to define the dynamic nature of these variables over large areas.

There are two temporal scales of interest in the study of hydrologic processes. The first is the diurnal, or daily and short-term variability. The second is seasonal or long-term changes such as those associated with reservoir storage and wetland boundaries. The Eos SAR will provide a means to collect data over both of these time scales and will also provide data for rare hydrologic events such as floods or droughts.

The discussion in this section summarizes the key elements of water balance models, especially fluxes (e.g., precipitation, runoff, or evapotranspiration) and system storages (e.g., ground water, soil moisture, snowpack water equivalent). The role of remote sensing data, especially from SAR, in quantifying these water balance elements is discussed. Since chemical fluxes often have a strong relationship to water fluxes, these are also summarized. Although Eos radar data will not be sensitive to chemical composition, it may provide valuable insight into chemical transport and the extent of regions dominated by chemical reducing reactions.

Equation 2 describes the land phase of the terrestrial water balance:

$$P(t) = Q(t) + ET(t) \pm \Delta GW(t) \pm \Delta S(t) \pm \Delta SM(t) \quad (2)$$

where P = precipitation; Q = runoff; ET = evapotranspiration; ΔGW = change in ground water; ΔS = change in storage such as lakes, snow, plant moisture, etc.; ΔSM = change in soil moisture (including frozen soil boundaries); and t = time. P, Q, and ET are usually considered fluxes whereas GW, S, and SM may be considered storages or system states at a given time (t).

The water balance of natural and controlled vegetation (agriculture) in normal topographic settings is difficult to quantify because of the spatial

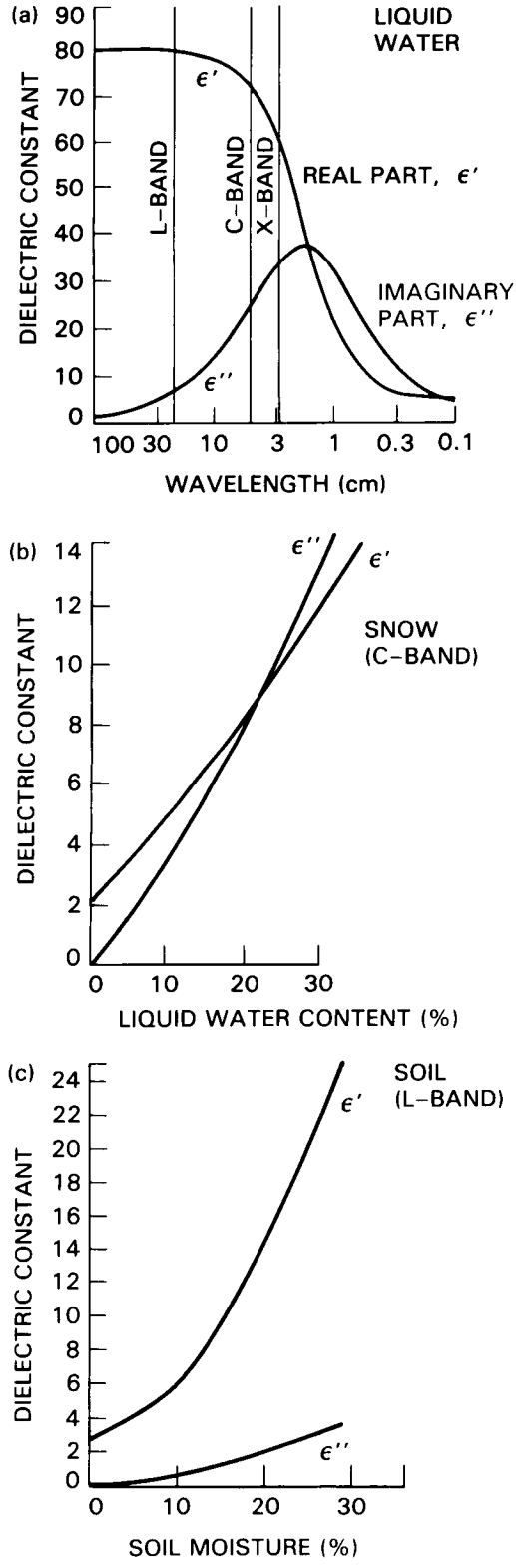

Figure 15. Dielectric properties of (a) liquid water as a function of wavelength, (b) snow as a function of snow liquid water content, and (c) soil as a function of soil moisture. Here, ϵ' and ϵ'' indicate the real and imaginary parts, respectively, of the dielectric constant (Ulaby *et al.*, 1986).

and temporal variability of system states and fluxes. Man's impact, such as in irrigated agriculture, confounds things further. In addition, boundary or edge effects (i.e., forest/cropland, natural vegetation/urban development) complicate the situation and prohibit simple extrapolation of point measurements. However, water balance studies are necessary on a small scale (e.g., basin or catchment size) to understand hydrologic processes and water requirements for various vegetation communities, including crops. In addition, water balance studies become extremely important on a large or global scale. It is at this scale that fluxes between land and the atmosphere must be quantified and understood if we are to understand global climate.

The following sections discuss the terrestrial water fluxes and storages in Equation 2.

Terrestrial Water Storages

In any global circulation study it is imperative to quantify stored water. It is also important to define the storage at a scale concomitant with the process being studied. Four of these storage mechanisms of particular relevance to the Eos SAR are discussed below.

Soil Moisture—Soil moisture is the temporary subsurface storage of precipitation often limited to the zone of aeration, that approximately coincides with the root zone. If this soil moisture freezes, the subsurface storage period is generally much longer in duration, the extreme being permafrost that has trapped soil moisture for many hundreds of years. From the soil, the moisture will either be returned to the atmosphere, temporarily stored in surface vegetation, or percolated to the phreatic (saturation) zone and eventually transmitted to surface channels as streamflow. Soil moisture is a highly variable quantity often resulting from the inhomogeneity of soil properties, topography, and land cover, and is difficult to measure in a way that is representative of a large area. Typically, averages of point measurements of varying density are generally used to quantify moisture over large areas, but seldom yield areal estimates representative to the process (i.e., ET, runoff, etc.) being studied.

There is a need to develop ways to quantify the spatial variability of soil moisture; to determine the scale (size) of hydrologic units essential to various hydrologic processes, and to develop criteria for delineating areas that can be treated as hydrologically uniform. Remotely sensed data have great potential to provide representative areal estimates rather than point measurements. Because hydrologic concepts have been developed from point measurements, i.e., soil columns, rain gauges, etc., hydrologists have been largely unsuccessful in treating spatial variability. This is perhaps the single most important reason why infiltration theory has not been successfully adapted by practicing hydrologists.

The spatial and temporal information derived from remote sensing data coupled with direct measurements of hydrologic state variables such as soil moisture may lead to entirely new types of hydrologic data or model parameters. For example, a time series of soil moisture measurements in a spatial context may depict the dynamic nature of a watershed and reveal new hydrologic characteristics of a watershed. Observations of how soil moisture changes during a drying cycle of several days (10 or so) may provide new insight into the storage and changes of storage in a watershed. It may also provide new insights into hydrologic performance, as opposed to hydrologic properties, of soils, i.e., retention times and watershed lag. (A hydrologic property is a scalar quantity that has no spatial context within a basin, and possibly little relation to dynamic processes. The hydrologic performance of a soil, on the other hand, is a vector quantity that reflects not only the physical characteristics of the soil but also how it relates spatially to the hydrology of the basin.) The spatial distribution of soil moisture with respect to elevation, flowing streams, and soil type would be combined to define its hydrologic performance.

There is also a value in acquiring continental-scale soil moisture maps on a frequent basis; thus trading frequent, global coverage for spatial resolution. These continental-scale soil moisture maps would be used to isolate regions with strong soil moisture gradients in both time and space and would therefore be applied to determine specific areas for high-resolution soil moisture mapping. In addition, the global-scale maps are sufficient to monitor variation in soil moisture due to precipitation as an input to meteorological models. Both SAR in the global and regional mapping modes and ESTAR could efficiently provide continental- to global-scale soil moisture maps.

Snow—Snow is another form of temporary storage with a major impact on local and regional water balances. In many areas of the world, the majority of freshwater available for consumption and irrigation results from snowmelt runoff. Snowpacks providing domestic water supplies are found in various landforms: many in rugged mountainous terrain, others in higher latitude moderate-relief plains areas. Determination of available water in the snowpack just prior to melt season is important for reservoir regulation. A typical snowpack is highly variable in depth (and water equivalent) and it changes dramatically in time and space. These temporal and spatial changes make this storage component very difficult to monitor, especially at the various scales necessary to use it in any process studies. There are three specific snowpack measurements of interest: (1) areal extent, (2) snow water equivalent, and (3) condition of the snowpack (grain size and presence of liquid water).

Historically, snow hydrologists have used a few point measurements that amount to little more than indices as input to snowmelt runoff forecasting procedures. Recent use of visible and near infrared (NIR) data have defined the spatial coverage of the snow but provided little information on the water equivalent—the most critical data needed. Truck and aircraft microwave studies have shown the potential for measuring two of the three important system states of a snowpack: the water equivalent and the condition (wetness). In addition, the all-weather capability of microwave instruments provides a unique capability to continue measurements through cloud cover that may be frequent during the snow season, and independent of sun angle, which is essential for medium to high latitudes during the winter months. The underlying soil moisture, and whether or not it is frozen, are equally important states to be determined. High soil moisture at the start of the melt season will result in larger runoff volumes (Figure 16).

Typically, a snowpack builds up slowly during the winter; the buildup consists of small-grain, dry snow crystals that gradually become compressed by new snow, and may undergo some intermittent thawing and refreezing. A cold, dry snowpack is susceptible to penetration by radar to the underlying ground, and the depth and density of the snow affect the radar brightness. Once the melt season starts there are periods when there is liquid water between the frozen snow crystals. This case severely restricts the penetration of radar and its ability to measure the total water equivalent of the snowpack. However, this case does provide important information on the state of the snowpack, in that the presence of liquid water indicates that additional energy input can produce melt water.

A time series of SAR measurements throughout the winter accumulation period may be able to provide data to estimate the total water equivalent up to the period of melting. During melt sequences the diurnal capabilities of SAR may be able to use night data to monitor the total snowpack water content when the pack refreezes.

Appendix A presents a discussion of an algorithm that could be used for extraction of SWE and snow wetness. This would require the use of L-, C-, and X-band channels in order to separate the effect of the underlying soil from that of the snowpack itself. The relationship used for determination of SWE was presented earlier in Equation 1 and is described in detail in Appendix A.

Detention—At any given time, a certain percentage of the total water in a hydrologic basin is stored in lakes, reservoirs, and wetlands. SAR images can provide very accurate delineations of land-water boundaries at a small scale and for any vegetation canopy cover. The capability to delineate standing water boundaries in forested areas has been recently demonstrated using SIR-B and aircraft SAR quad-polarization data in the polarimetry mode. SIR-B data proved that L-band microwaves undergo a scat-

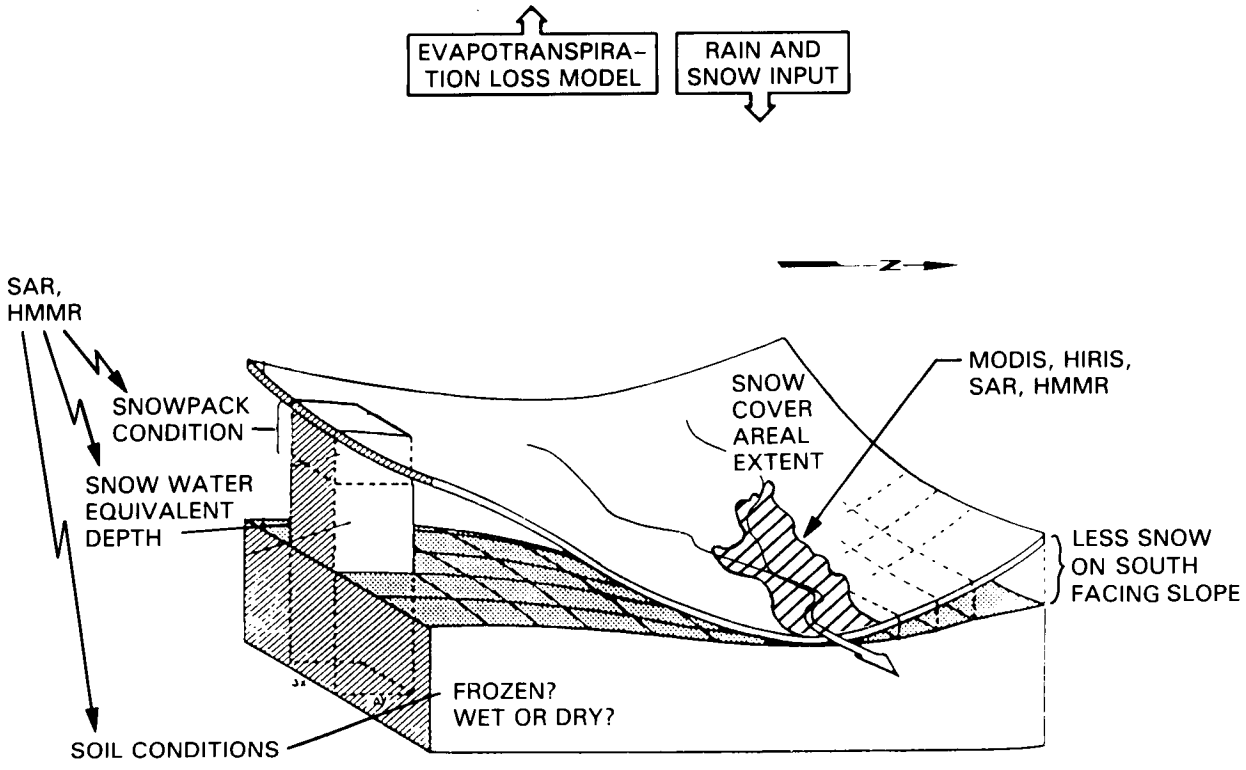

Figure 16. Schematic of snowmelt model showing where SAR and other Eos instruments could be used synergistically (from Jensen and Jonch-Clausen, 1982; modified to show remote sensing inputs).

tering pathway whereby the signal is scattered from the trunk to the flooded surface and back to the sensor (and vice-versa). Flooded surfaces beneath tree canopies have been shown to produce highly characteristic responses in both quad-polarized airborne SAR data and multifrequency SAR data.

Flood water is a form of temporary storage that does not have a major impact on global water balance but does play an important role in regional water balance as well as human affairs. The Eos SAR, especially with its all-weather capability, will provide an excellent source of data for studying the spatial extent and duration of floods due to intermittent storms and periodic events such as seasonal monsoons and tidal cycles, and their relation to regional water balance. This would be useful not only for open areas but also for standing water under forest canopies.

Ground Water—Ground water is an important temporary storage and flux path for chemicals. SAR and other remote sensing instruments have a very limited capability for the direct measurement of ground water because the depth of penetration is limited to a few centimeters except in extremely arid regions. However, there are a number of ground water information needs that can utilize surface water responses. These include the identification of ground water recharge/discharge areas in complex watersheds, the development of methods for conducting resource inventory of ground water by identifying seeps and springs, and quantifying seasonal changes of ground water elevation. The Eos SAR data may be useful for inferring these ground water characteristics by the measurement of changes in surface soil moisture; these remotely sensed data would be coupled with ancillary topographic and geologic structure data. SAR images would be responsive to these recharge/discharge soil moisture zones (whose sizes are of the order of 100 m) and their temporal behavior.

Vegetation Moisture Content—Vegetation stores moisture in both its woody and foliar components; the amount of moisture stored in the woody components of all canopies and the foliar components of coniferous species increases steadily on an annual basis as the canopy ages. The foliar moisture storage varies on a seasonal basis for all deciduous species and shows an annual increase as the canopy ages. The amount of water stored in any vegetated terrain depends on the vegetation species, its age, its micro-environment (water supply), its health, and the season.

Radar returns from the Earth are sensitive to changes in the dielectric constant of the surface. The

dielectric constant of water is about 80 and that of dry soil and dry biomass is about 3 or 4. Thus, the presence of water either in soil or vegetation canopies strongly modulates radar returns. For this reason, the SAR is expected to play a major role in monitoring the moisture content, and especially variations in the moisture of vegetated terrain by component. By careful selection of frequency, polarization, and incidence angle, and by combining seasonal observations, the SAR can potentially measure canopy moisture by component: woody and foliar. It is the only Eos sensor that is likely to be sensitive to the entire canopy volume and to the surface below the canopy. (Chapter IV and Appendix C provide further discussions of the measurement of vegetation moisture content.)

Terrestrial Water Fluxes

Precipitation—Precipitation is the major water flux into the terrestrial surface and, unfortunately, the least well measured. Rainfall is conventionally measured over land by *in situ* gauges, of which there are about 25,000 in the U.S. and perhaps 100,000 throughout the world. World Meteorological Organization (WMO) requirements for rain gauge densities are not met in most areas of the world, including much of the U.S. Although ground-based radar appears operationally useful for weather forecasting, rainfall estimates based on these data are grossly inadequate for most hydrologic purposes. Current spaceborne optical sensors, such as the Landsat and the National Oceanic and Atmospheric Administration (NOAA) satellites, produce marginally useful rainfall information for hydrologic purposes by relating cloud climatology, which may be remotely sensed, to precipitation climatology. Studies of water balance on any scale must be able to determine the rainfall input to a relatively high degree of accuracy.

Rainfall rates should be sensed directly on Eos with other instruments, and it is hoped their measurement accuracies will be suitable for hydrologic studies. Continuous rain-rate sampling, however, is not possible from low-Earth orbiting platforms. The Eos SAR operating in its normal configuration will not be able to directly measure precipitation because of insufficient atmospheric absorption and scattering from rainfall at L-, C-, or X-bands. However, at L-band and C-band, SAR images will be strongly sensitive to changes in surface backscattering due to rain-induced soil moisture changes. This offers the possibility that Eos SAR data may be useful for inferring antecedent rainfall indices. In particular, SAR image-change detection schemes based on post-rainfall repeat visits to sites with decreasing levels of soil moisture may complement rainfall data from other sources by estimating rainfall distribution after the fact. Calibration could then be accomplished with only a limited number of ground-based precipitation stations.

The X-band channel of the Eos SAR may also provide a high-resolution capability for inferring rain rates associated with intense precipitation cells. This would require positioning the antenna beam toward the nadir and range-gating out surface returns.

Evaporative Moisture Flux—The evaporative moisture flux quantifies a major path of water movement from land into the atmosphere. It is imperative to understand evapotranspiration on the spatial scales over which it varies significantly. For example, consider a natural drainage basin in a humid region with an area of several hundred square kilometers. Immediately after a heavy rain, the total basin is wet enough to assume that the evapotranspiration flux is its potential rate associated with a saturated surface. At some later time, due to redistribution of stored water (soil moisture), some areas of the basin will be losing water at rates less than the potential. At this same time there will be other areas in the basin where the moisture flux rate is still at the potential. The location of variable evaporative flux rates will depend on relative topography, soil type, and land cover in some as yet poorly understood way. The potential ET rate, which is essentially a function of the atmospheric state (temperature, wind speed, vapor pressure deficit, etc.) can be determined with reasonable accuracy. Actual ET can be represented as a physically-based function of the soil moisture relative to the soil moisture storage capacity (plant available water) (Figure 17). The Eos SAR high-resolution images will provide essential soil moisture and topographic information within these different areas of the basins.

The evaporative moisture flux follows a well-defined diurnal pattern in response to the input of solar energy. The SAR capability to make nighttime measurements can provide additional information on soil moisture and canopy moisture content that will assist in understanding the water balance of the Earth. Thermal gradients can cause upward movement of soil water during the night that, if monitored, can provide information on the deeper profile soil moisture.

Runoff—Runoff is the result of both rainfall or snowmelt that cannot be stored as soil moisture, and of the delayed release of subsurface or ground water. The moisture flux from a heterogeneous basin results in an uneven distribution of soil moisture, which in turn affects the eventual distribution of subsequent rainfall. Not every storm returns a basin to a uniformly wet condition and not all of the water loss is through the evaporative flux from the surface: storm or surface runoff to stream and river channels can be the primary path of water movement after rainfall. The amount of storm runoff can vary from practically nil to nearly all of the input, depending on the moisture conditions in the basin and the characteristics of the storm. Scientific studies of the water flux

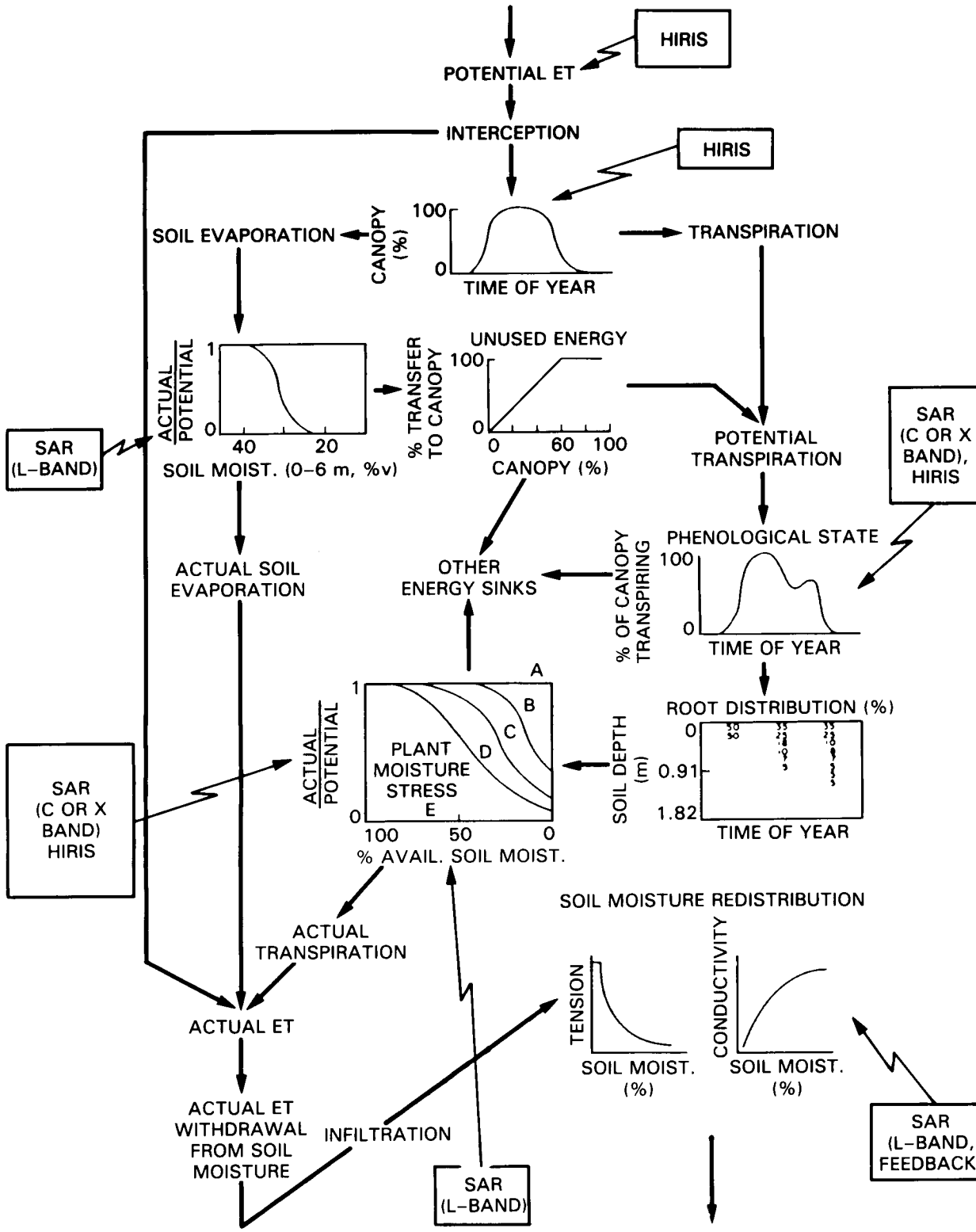

Figure 17. Schematic of water balance modeling showing where SAR and other Eos instruments could be used synergistically (from Saxton *et al.*, 1974; modified to show remote sensing inputs).

depend on an accurate description of the runoff process and its relation to an entire basin.

Field experiments in small watersheds have shown that those parts of the watershed where infiltration capacity is relatively low are probably the areas contributing most to runoff during a storm. The reason certain parts of a watershed have lower infiltration capacity are: (1) soil properties are such that they do not allow rapid water movement; (2) ground water seepage zones maintain near-saturated conditions and thus very little storage is available for rainfall; and (3) high-antecedent moisture reduces the infiltration capacity of certain soils within the watershed.

eous nature of natural watershed systems. If repetitive SAR images of a watershed could be obtained over a period of days or weeks after a storm, it may be possible to partition the basin into similarly contributing areas by examining SAR intensity changes due to surface soil moisture (Figure 18).

Chemical Fluxes

Chemicals and their movement within the biosphere are an integral part of our terrestrial ecosystem. Many chemical fluxes, whether the result of natural weathering processes or of man's actions, depend on water as their transporting agent. The

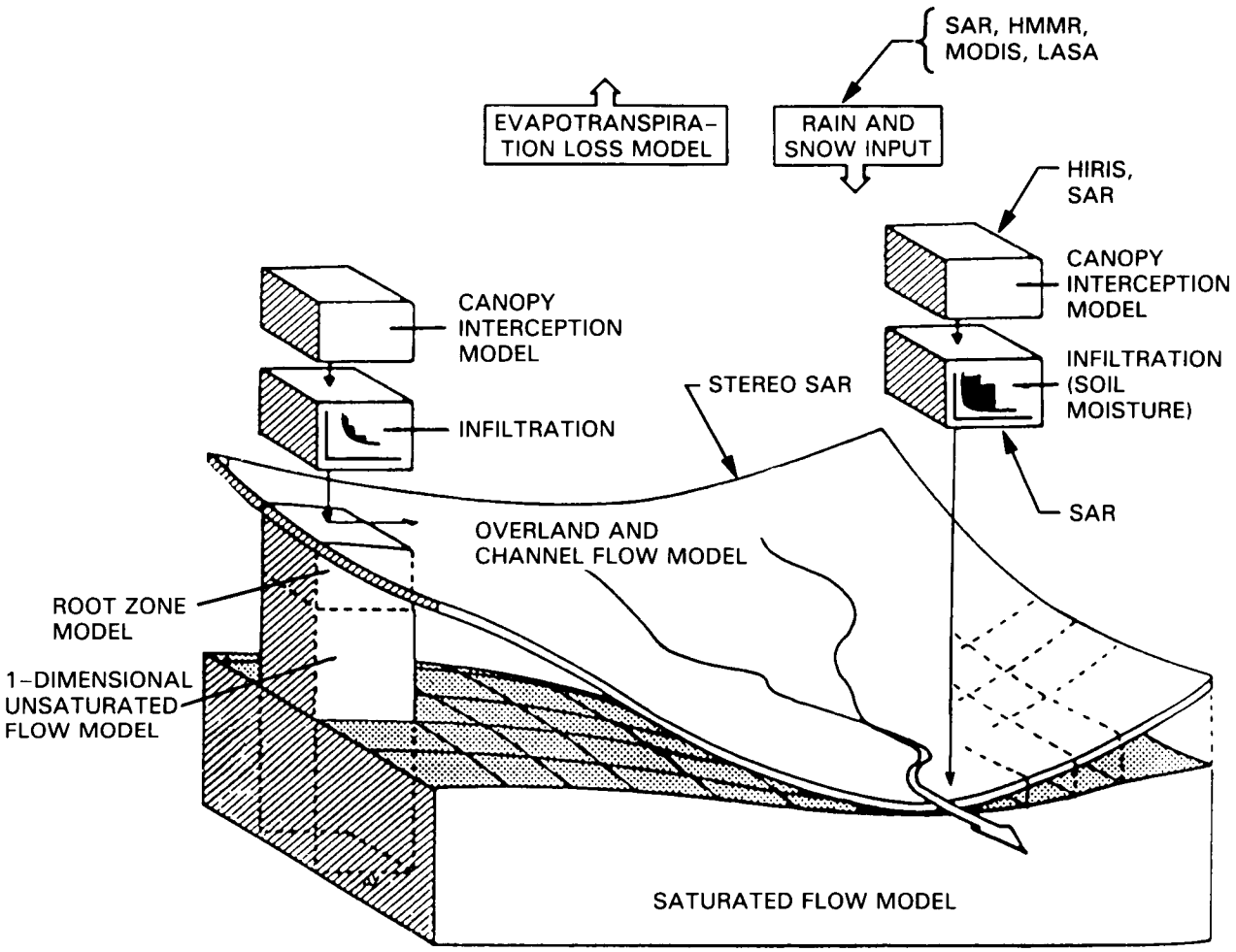

Figure 18. Schematic of runoff process model showing where SAR and other Eos instruments could be used synergistically (Saxton *et al.*, 1974).

An approach to a better understanding of the runoff process could be developed using repetitive Eos SAR imaging of a dynamic watershed; the SAR response to soil moisture coupled with change detection procedures could help identify runoff-producing areas. This concept would focus on the heterogen-

presence of water or soil moisture, in addition to heat, is usually necessary for chemical and biological reactions to occur in the terrestrial ecosystem.

It is unlikely that Eos will be able to directly measure these chemical fluxes, although observations from space of hydrologic processes, especially

runoff and erosion, will provide useful information about the relation of chemical fluxes to water and soil transport. Components of the water balance, and other hydrologic processes, will serve as surrogates to the actual chemical fluxes. This reinforces the need to quantify hydrologic fluxes and storages.

Runoff—Surface runoff and interflow are the primary transport vehicles for the movement of chemicals in the ecosystem. It is imperative that flow paths be clearly identified if we are to understand the relation of chemical fluxes to pollution of streams and ground water supplies. An ideal model should describe where the runoff is likely to originate and how it reaches the stream. The spatial detail needed to study chemical fluxes in the terrestrial ecosystem is perhaps even greater than that needed for adequate representation of water fluxes and storages alone.

Erosion—Erosion of the soil by wind or water is a major mechanism for chemical flux with serious ramifications for the world ecosystem. For example, the most serious conservation problem facing U.S. and world agriculture is the control of erosion. One form of erosion, the formation of ephemeral gullies, is not easily measurable nor are there any general models available for predicting the total soil loss. An ephemeral gully is a drainage channel produced by runoff in agricultural fields during the growing season, but that is periodically filled in by the farmer's tillage operation. Although relatively little quantitative data are available on the amount of soil lost by the formation of ephemeral gullies, it is now realized that estimates derived from current technology are not able to account for gully erosion. Consequently, serious errors in the estimates of soil lost may occur. The quantification of ephemeral gully erosion requires highly accurate measurements at critical periods. The high-resolution mode of SAR should provide adequate delineation of ephemeral gullies with sizes greater than about 100 m. The understanding of erosion from nonagricultural lands involves the same questions and is plagued by the same lack of knowledge. Deforestation in many underdeveloped countries has also resulted in serious and often catastrophic losses of topsoil, which occurred in the U.S. in the 19th and early 20th centuries. The sensitivity of radar to surface roughness may be used as a direct measure of erosion. Thus, the Eos SAR may provide valuable data for monitoring erosion by observing the temporal changes of surface roughness and slopes.

Wetlands—Wetlands are environmentally important because they produce conditions that allow reducing chemistry to occur. Several environmentally significant gases, particularly methane (a greenhouse gas), are produced in wetlands. At present there is no routine operational technique for monitoring these processes and no means of estimating these gas fluxes. An estimate of the changes in wetland areal extent would be very helpful in understanding wetlands dynamics and, eventually, quantifying these gas fluxes.

It has been shown that SAR images are very useful for the detection of wetlands boundaries, even including standing water under trees (Imhoff *et al.*, 1986; Hoffer *et al.*, 1986). A time series of the Eos SAR data could be used to estimate the areal change in inundated areas, and could thereby provide an estimate of gas-producing areas. Wetlands are discussed in more detail in Chapter IV.

Observational Strategy and Regimes

The feasibility of using SAR data for quantitative global studies of water balance dynamics, terrestrial storages, and chemical fluxes has yet to be conclusively demonstrated and much has to be learned before this technique can be applied to global studies. However, as previously discussed, SAR has certain unique capabilities that have a great deal of potential for hydrological studies. The observational strategy recommended for the Eos SAR is to use the first several years to acquire and analyze data from representative study sites, to determine the optimum instrument and viewing parameters, and to then expand these studies to global scales. The synergistic use of the Eos SAR in the low-resolution global mapping mode and ESTAR for accurate soil moisture monitoring on a global scale should also be addressed.

It is expected that valuable experience will be obtained with the data from SIR-C, ERS-1, and Radarsat, all in the early 1990s. In particular, the C-band data from ERS-1 and Radarsat will be useful for testing our ability to measure soil moisture using change detection procedures with images acquired every 3 days. The ERS-1 SAR will provide C-band imagery at a 23° incidence angle with a 3-day repeat cycle.

The Panel recommends that for soil moisture measurements, a 3-day exact repeat cycle be used over a period of at least several months. This would allow a test of change detection procedures with multifrequency SAR images acquired every 3 days after a rain event, and with the same angle of incidence. This change detection technique may be essential to obtaining soil moisture information, and would not be possible with an exact 16-day repeat cycle. With a 16-day repeat cycle, a site could be repeatedly observed every few days, but the angles of incidence would be so widely variable that it would be very difficult to compensate for this effect (see Appendix B).

RATIONALE FOR SAR OBSERVATIONS

Instrument and Physics Perspectives

The recommendations for the Eos SAR observations of hydrologic parameters are motivated by two principal factors: (1) SAR is especially sensitive to the presence of water, either in the form of soil moisture, liquid water in a snowpack, or vegetation moisture; and (2) SAR provides both the high- and the low-resolution data necessary to study the micro- and macro-scale behavior of hydrologic processes in hydrologic basins and catchments and continental scales. SAR is not unique in its sensitivity to soil moisture; passive microwave radiometers such as ESTAR (an L-band instrument) are also sensitive to soil moisture. It is also not unique in its sensitivity to snow; the millimeter-wavelength channels of AMSR may also be useful for snow water studies. The advantage of using ESTAR for soil moisture studies is that the roughly 1,400 km swath permits comprehensive, frequent coverage. However, ESTAR and AMSR resolution is far too coarse to provide necessary details within hydrologic basins. For soil moisture studies the ESTAR and SAR sensors are complementary, with ESTAR providing measurements at 10 km resolution and SAR providing finer grain regional and local detail at resolutions of 500 m down to 30 m.

Hydrologic Model Perspectives

Historically, hydrologists have attempted to model what they conceived to be the hydrologic cycle by a variety of techniques, all somewhat influenced by the phenomena they could measure. Hydrologists have modeled the hydrologic system as a "black box," using only input data (e.g., rainfall and potential evaporation) to produce the output hydrograph. The unit hydrograph is a good example of such a hydrologic "black box." The development of comprehensive hydrologic models such as the Stanford Model exposed the interior of the black box and conceptually subdivided the rainfall-runoff process into a number of physical processes. However, from a systems point of view, this refined model was still essentially not internally defined because there were no provisions for monitoring or measuring any of the system states.

SAR has the potential to measure some of these system states at scales small enough to reflect the processes. Measurements of these system state variables will require new models that incorporate the new data types. Such models would structurally resemble contemporary simulation models but would be more capable of accounting for spatial variability and change. Moreover, the subprocess algorithms (e.g., infiltration or evapotranspiration) would be designed to use remote sensing data as well as more conventional inputs.

SAR Response to Two-Layer Systems

Many hydrologic systems of interest can be modeled as two layers composed of an inhomogeneous stratum (e.g., vegetation canopy or snow) overlying a homogenous substrate (e.g., soil) (Figure 19). Vegetation canopies and snowpacks are electromagnetically inhomogeneous because they are a composite of materials with different dielectric properties. The soil layer may be considered homogeneous (in this context) because its dielectric properties vary only slowly in the spatial domain, except for variations due to soil moisture.

Radar waves at shorter wavelengths (e.g., C- or X-band) incident upon an inhomogeneous layer will be subject to strong volume scattering and attenuation by the individual components (e.g., leaves, branches, or liquid water drops in snowpacks). The result is that radar backscattering at these wavelengths from inhomogeneous layers is dominated by the distribution of individual scatterers. By contrast, radar waves backscattered from the underlying soil result from surface scattering that depends principally upon the dielectric constant of the soil and its surface roughness. By using various combinations of wavelength, polarization, and incidence angle, it is possible to isolate either the inhomogeneous or the homogeneous layer. For example, longer wavelengths and near-nadir incidence angles accentuate underlying surface scatter; shorter wavelengths and larger incidence angles accentuate volume scatter from either the vegetation or snow canopy. This means that the Eos SAR with its multiparameter capability may be useful for "windowing" either the vegetation and snow layers or the underlying soil layer.

Vegetation-Covered Soil

In the context of water balance studies, the Eos SAR would play three important roles: (1) to monitor the vegetation moisture changes, (2) to quantify other vegetation properties for other sensors that see these properties as confusing factors in extracting canopy moisture, and (3) to monitor underlying soil moisture and standing water changes. The shorter radar wavelengths, cross-polarization, and higher incidence angles will provide information on the vegetation canopy; the longer wavelengths, like polarization and steeper incidence angles will provide information about the underlying soil. Change detection procedures would emphasize changes in soil moisture, surface roughness, and vegetation properties that could be used as direct input to water balance models or as feedback to correct model parameters.

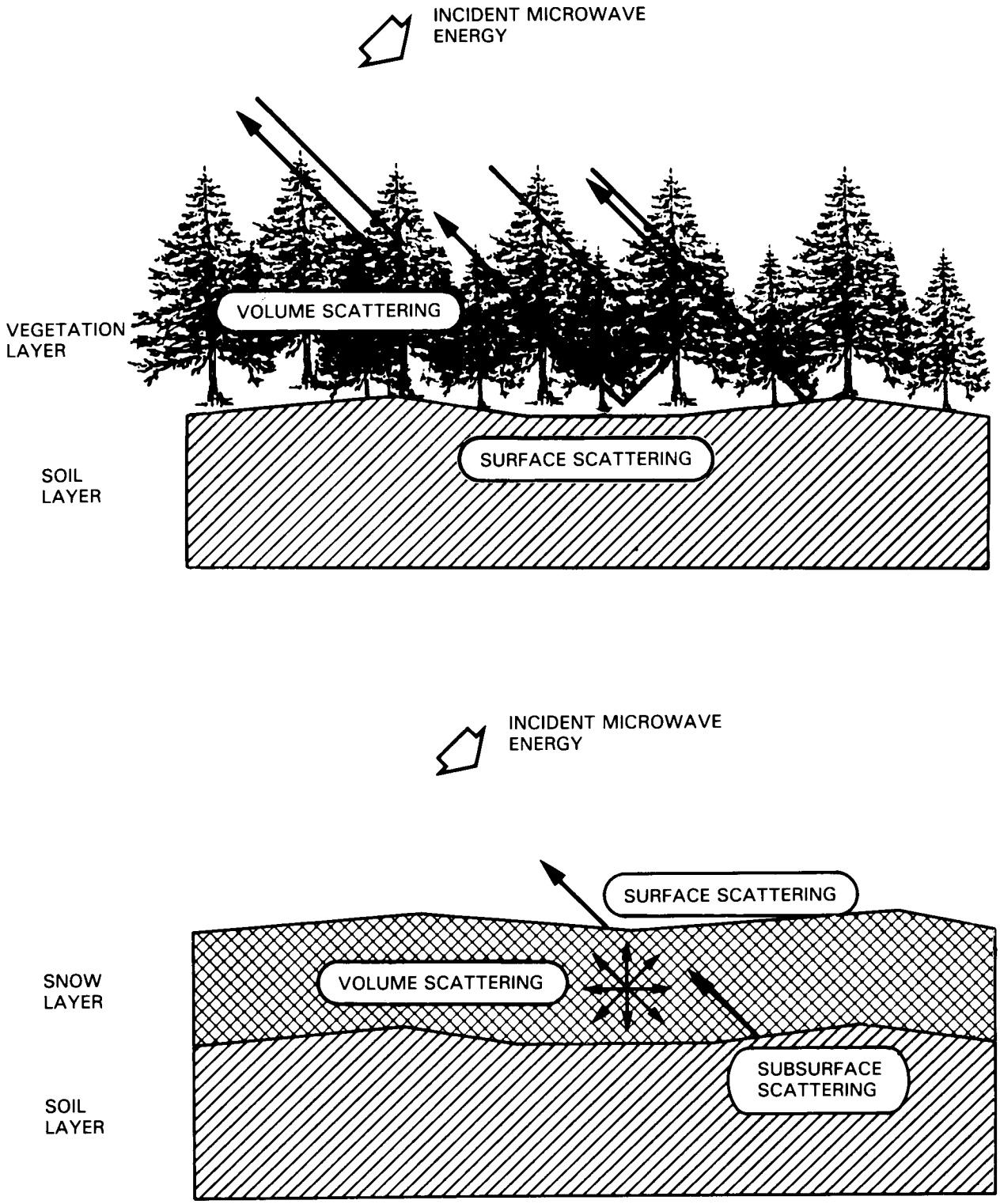

Figure 19. Two examples of two-layer systems: the soil-vegetation system (top) and the soil-snow system (bottom).

Snow-Covered Soil

The soil conditions underlying a snowpack are of interest to hydrologists because the state of the soil can control how much melted snow actually reaches the stream channels. At the longer wavelengths (L- and C-band), snowpacks are essentially transparent (in the absence of free water) so that these longer-wavelength channels may be useful for determining if the underlying soil is dry or near saturation and whether or not it is frozen. At shorter wavelengths (e.g., K- or X-band) the snowpack brightness is dominated by volume scattering from suspended liquid water. This means that both long-wavelength (L) and short-wavelength (X) channels will be needed to determine both snowpack properties and underlying soil conditions.

A further discussion of the radar response to snow is provided in Appendix A.

Previous Experimental Results

The sensitivity of radar backscatter to soil moisture, snow, and vegetation moisture has been clearly demonstrated by data acquired from a number of field, aircraft, and satellite experiments. Exhaustive sets of field measurements were made starting in the mid-1970s using a truck boom-mounted radar spectrometer with a frequency range of 1 to 18 GHz and with full angle and polarization capability. One set of these experiments concentrated on soil moisture in agricultural fields (principally corn, sorghum, wheat, milo, and soybeans) in a variety of midwestern fields ranging from bare to fully vegetated and over the entire growing season; the other principal set of measurements focused on radar sensitivity to snow. The results of these measurements have been widely published; a summary may be found in the three-volume treatise by Ulaby *et al.* (1981; 1982; 1986).

These field results over U.S. test sites have been replicated and extended by other investigators using sites in France, West Germany, the Netherlands, and Canada. Moreover, a substantial body of evidence supporting these results has come from both airborne and spaceborne imaging and non-imaging radar data. Appendix B presents a summary of these experimental results for both soil moisture and snow water equivalent.

RECOMMENDED INSTRUMENT PARAMETERS

The mission strategy for the Eos SAR for hydrologic studies is to gather information about soil moisture, snowpack properties, and vegetation moisture over a wide range of spatial and temporal scales. The principal elements of this strategy are instrument and viewing parameters, synergism, data parameters, and information extraction techniques.

Instrument Parameters

Frequencies

Three frequency bands (L, C, and X) will be required for SAR hydrology studies. It is expected that the L- and C-band channels will be the principal source of soil moisture data and that most of these data will be acquired at near-nadir look angles (20° or less). The shorter wavelength X- and C-band channels will be used primarily for observations of snowpack characteristics and dynamics. The combination of L-, C-, and X-bands will be required to sort out the biophysical canopy and soil properties of a vegetated surface.

Surface roughness information may be obtained by simply ratioing images acquired at different frequencies, e.g., using an image product formed by the ratio of L- to X-band or via analysis of multi-angle observations. This information would be useful for erosion studies, for example.

Polarizations

The use of both polarization amplitude (e.g., HH, VV, or HV) and polarization phase ($\varphi_{hh} - \varphi_{vv}$) available from the Eos SAR is expected to provide a significant enhancement to the information obtained over that from a singly polarized SAR. The ratioing of SAR image amplitude data (e.g., HH or HV) or of phase data provides enhanced sensitivities to snowpack properties or vegetation cover. Cross-polarization data (HV) have added value for making frequent revisit measurements over the same site. Because HV measurements are less dependent on incidence angle, the use of these data may provide the ability to measure soil moisture change from frequent revisits at different incidence angles.

Radiometric Calibration and Sensitivity

As discussed previously, the approach to extracting soil moisture and snowpack information requires the use of time series of SAR images and change detection. Images of a given study site should be acquired every 3 days after a precipitation event. Among other things, this requires that the Eos SAR be radiometrically stable so that the image intensity on day 1 may be compared to the image intensity on day 3. This relative radiometric calibration is crucial to the change detection procedures and means that SAR must exhibit good stability over a period of days or weeks in transmitter power, antenna gain, and receiver gain. To compare moisture content from season to season and year to year, this relative radiometric calibration must also be valid over the lifetime of Eos. The discrimination of five discrete levels of soil moisture from wet to saturated (20 percent variation in each level) corresponds to about 2 dB per level for vegetated areas; these distinctions necessitate a radiometric calibration and fidelity of

less than 1 dB. A relative instrument calibration and stability for each frequency of ±1 dB (and preferably ±0.5 dB) is therefore required for these soil moisture and snowpack studies.

The study of spatial variability and scale within a hydrologic basin will also require that SAR exhibit good cross- and along-track radiometric fidelity. This ensures that the image intensity at the center of a scene can be quantitatively compared to the image intensity at the edge of a scene. It is desired that processed SAR images exhibit cross- and along-track radiometric fidelity to a fraction of a dB. This is based upon the need to establish comparisons to within a few percent of soil moisture levels and surface roughness expressions between various zones across the SAR swath as discussed above.

Surface roughness data may be obtained through the ratio of σ° (L-band) to σ° (C-band), or σ° (X-band). This means that each frequency channel must be absolutely calibrated; ±1 dB is required for this purpose. Good absolute calibration will also be necessary for quantitative comparison of the Eos SAR images to those obtained from SIR-C, ERS-1, JERS-1, and Radarsat.

Viewing Parameters

Incidence and Azimuth Angles

The use of the Eos SAR variable-incidence angle capability provides an opportunity to enhance the separation and measurement of two-layer systems such as vegetation/soil and snow/soil systems. In general, data acquired at incidence angles greater than about 45° and at shorter wavelengths are less affected by underlying surface scatter; conversely, data acquired at near-nadir angles (15° to 20°) and at longer wavelengths more readily penetrate vegetation or snow layers and provide information about the underlying soil surface. Careful choice of the incidence angle will help discrimination and separation of the two layers.

For soil moisture observations, near-nadir observations will be preferred, since vegetation effects will be minimized. When a time series of observations (e.g., every 3 days after a precipitation event), it will be important to maintain the same illumination geometry. For snow observations, the preferred incidence angle will be 50°, supplemented by a second set of observations at 30°; the higher angle will minimize scatter from the underlying soil.

Little is known about the optimum azimuth angles required for hydrological studies. The radar backscatter from straight-line plowed fields depends very strongly upon the azimuth angle with respect to the row direction, especially for like polarization. Since the strategy would be to use change detection, it will be important to closely repeat the azimuth illumination angle for each pass of a time series of SAR images of a study site.

Resolution

The highest spatial resolution (30 m) of the Eos SAR is desired for almost all of the experiments discussed, principally because of the interest in spatial variability of surface moisture and snow, and watershed characteristics. However, the 500 m resolution 700 km swath associated with the global mapping mode will also be useful for basin-scale soil moisture applications including erosion losses, reservoir management, and infiltration studies as well as studies on cultural vegetation stress; this agrees with the 500 m resolution suggested by the NASA Soil Moisture Working Group for these applications (Rango *et al.*, 1980).

Swath Width

A relatively narrow swath width in the 50 to 100 km range would be acceptable for studies of individual sites where the emphasis would be on optimizing channels; once these optimum channels have been identified, regional to global surveys with swath widths in the 100 km to 700 km range could be used. It is noted, however, that the incidence angle ranges from 15 to about 60 across these 700 km swaths; as the radar backscatter can exhibit a drop of 20 dB or more across this angular range (especially for smooth surfaces), we would expect targets nearest the subsatellite track to be relatively bright and those farthest away to be relatively dim. It is possible to compensate for these angular modulation effects, however.

Revisit Interval

A critical requirement is to be able to image a hydrologic study site at frequent intervals after a precipitation event using nearly the same illumination geometry; this is because the extraction of information is based upon the detection of change within a period of days to weeks. The desired revisit interval for most hydrologic parameters is 3 days (5 days is acceptable), although in a few cases (e.g., erosion studies) this interval can be as large as a month. For snow observations, diurnal (day-night) coverage is required.

Longer-term repeat observations of watersheds are needed to monitor both water and chemical fluxes. For these objectives, a 2-year repeat cycle is required to monitor the significant long-term changes in watershed morphology that are not purely the result of variations in soil moisture.

Synergism

The hydrologic cycle is a key to understanding the interactions of the Earth's surface with the atmosphere. Water in all three phases is the main difference between the Earth and the other planets of the solar system, and it enables life to exist. Yet the global hydrologic cycle has been studied very little

because it has been difficult to obtain sufficient global data and to write simple and elegant but general models. It is also difficult to plan with any exactitude for the use of a large number of different types of data together in a model of the global hydrologic cycle. This is because such models do not exist in a way that allows this trade-off between data to be studied. What follows is a suggested strategy for the synergistic use of Eos data.

In principle, the components of the energy balance depend on a set of boundary conditions (incoming radiation, vapor pressure, air temperature, soil moisture content, and temperature of the soil). Some of the functional relationships, such as those for soil hydraulic properties, may be remotely sensed from a time series of soil moisture data, and stomatal resistance may be estimated from visible and NIR spectroscopy. The remotely sensed data that are needed to solve the surface energy balance include visible and NIR data (albedo and stomatal resistance from HIRIS and MODIS), thermal infrared data (surface temperature from TIMS and MODIS), and passive and active microwave data (soil moisture content from SAR and ESTAR).

The mass balance equation components may be considered similarly. Instantaneous precipitation rates may be estimated from space platforms remotely using microwave data, but closely sampled time series of data must be available for biases not to be introduced into the estimates for longer-term integrated measurements. The lack of a spaceborne radiometer or radar with a wavelength that is not receiving a significant signal from the land surface means that the measurement techniques have only been demonstrated for a few aircraft flight experiments over land. Visible and thermal satellite data have also been used for precipitation estimation. Techniques using these data work well for long periods of record, where the cloud climatology and precipitation probability distribution allow the latter to be estimated from the former, and allow empirical relationships between cloud characteristics and precipitation rate to be derived for shorter-period estimates.

Storage of water as snow can be estimated using visible and middle infrared data (HIRIS and MODIS) to get snow extent and active or passive microwave data (very short wavelengths of SAR and AMSR) to estimate snow extent and snow water equivalent. Storage as soil moisture may be estimated using active and passive microwave data to estimate near-surface soil moisture.

Runoff is difficult to estimate except through conventional river gauging. Inundation area, useful for biogeochemical cycling studies, may be estimated using a variety of high-resolution remotely sensed data. Maximum inundation area has been determined using NIR data (such as could be obtained from HIRIS and MODIS) to look at plant stress; in many vegetation types inundation induces plant stress for many days after the flood peak has passed. Radar data may be used to map standing water under vegetation. Rainfall-runoff models either use equations and the application of the remotely sensed data as described above, or use simpler surrogate parameters such as the impervious area of a catchment, which may also be remotely sensed using standard multispectral mapping techniques.

It is therefore expected that SAR data alone will be sufficient for only some of the total required data set. Almost all cases will involve observations from the various instruments within 1 hour of each other because of temporal variability. Thus, synergism will play a crucial role in the hydrology experiments.

SAR and ESTAR

Radar backscatter data obtained by SAR is responsive to the same physical parameters (dielectric constant, surface roughness, and morphology) as brightness temperature data acquired by a passive microwave radiometer. The Eos SAR and ESTAR are thus highly synergistic instruments, with SAR providing high- and medium-resolution (30 m to 500 m) microwave images of spatial details within hydrologic basins and catchments, and regional- and global-scale measurements, and ESTAR providing low-resolution (10 km) microwave images averaged over much larger regions for global-scale estimations (Table 4). SAR and ESTAR should be able to consistently acquire data simultaneously within about an hour. This is driven by rapid changes in canopy moisture in the afternoon during periods of high stress.

SAR and AMSR

For snow studies, the shorter-wavelength SAR channels (especially X-band) will be operated in synergism with AMSR, especially for delineating snowpack areal extent, snowpack wetness, and condition. A number of field studies have shown that both radars and radiometers are sensitive to snow over the range 5 to 40 GHz; as the wavelength shortens, sensitivity to snow increases.

Here again, SAR will have a resolution advantage over AMSR at the expense of increased confusion introduced by surface topography and less extensive coverage. Some of the Electronically Scanned Microwave Radiometer (ESMR) results for snow observations have been quite encouraging, and it is expected that SAR and AMSR observations will be very useful for estimating snow water content. Data for these two sensors should be consistently acquired within a few hours of each other, not necessarily on the same day, to avoid confusion due to daily freezing and thawing of the snowpack.

SAR, HIRIS, MODIS, and TIMS

A fundamental observational goal for hydrologic process studies is to understand the role that

Table 4. Comparison of Remote Sensing Approaches for Estimating Soil Moisture

Approach	Advantages	Limitations	Noise Sources
Active microwave	Independence of the atmosphere High and moderate resolution possible	SAR calibration	Surface roughness Vegetation cover Surface slope
Passive microwave	Independence of the atmosphere Moderate vegetation penetration	Poor spatial resolution -10 km at best Susceptibility to RF interference	Surface roughness Vegetation cover Soil temperature
Reflectance	High resolution possible Basic physics well understood	Cloud cover limits coverage frequency Sensitive to very thin surface layer Organic matter	Vegetation cover Surface roughness Surface topography Mineral content Sun angle Organic matter
Thermal infrared	High resolution possible Basic physics well understood	Cloud cover limits observation frequency	Local meteorological conditions Partial vegetation cover Surface topography

surface cover, especially vegetation, plays in land-atmosphere water flux. The energy and water balances of the land surface are closely coupled, so it is necessary to have information about the albedo and temperature of the surface in order to interpret the moisture data sensed with SAR. These data can be obtained with TIMS and HIRIS on a high-resolution scale and with MODIS on a moderate-resolution scale. For hydrologic process studies, SAR, HIRIS, and TIMS high-resolution images are expected to be highly synergistic for measurements and delineation of vegetation moisture. Data from these three instruments should be consistently acquired within some yet-to-be-determined timing offset.

SAR, LASA, and GLRS

The LASA and GLRS instruments will provide terrain topography to better than 10 cm vertical resolution, however only at point locations. These data may be valuable for reducing the confusion effects introduced into SAR images when generating digital terrain models (DTM) using the stereo mode.

Data Parameters

It is envisioned that SAR data for hydrologic studies will be acquired for a number of global study sites, that images will be processed into geometrically rectified form on a standard cartographic grid (geo-referenced images), mosaicked over the region of interest, and coregistered with SAR data from other dates and other Eos instrument data. These images should be distributed on a near-real-time basis to investigators. The model for this has been discussed at some length in the Eos Data Panel Report (Chase *et al.*, 1986).

It is highly desirable to obtain time-series sets of radiometrically calibrated and georeferenced SAR images using the same (or very nearly the same) incidence angles, and that these image sets be delivered to investigators within a day during rapid moisture changes. These data sets may be requested to coincide with expected storms or other precipitation events in a watershed study site and to continue over a period of days or weeks after the event; in effect, data requests would be automatically tagged to precipitation events monitored by other Eos sensors. For most hydrologic studies, periods where frequent coverage is required cannot be planned far in advance, thus there should be provision for some near-real-time investigator interaction with the SAR instrument.

It will also be necessary to provide collateral data sets such as topographic and land cover maps, precipitation rates, and point-source instruments (e.g., rain gauges). These ancillary data should be furnished along with Eos global observations of soil moisture, surface water distribution, snowpack

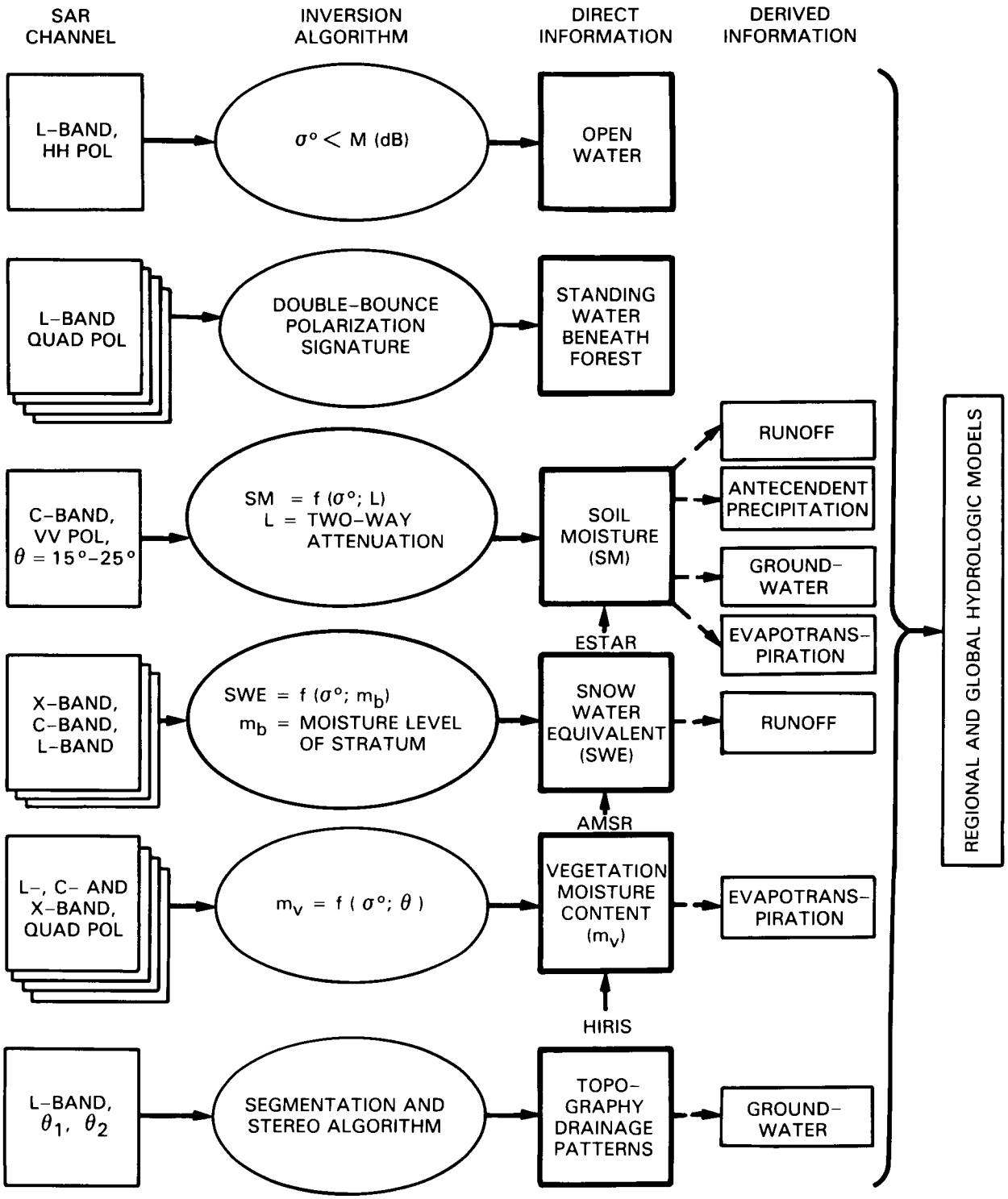

Figure 20. The development and testing of inversion algorithms would allow SAR image data to be converted into useful geophysical information such as soil moisture, snow water equivalent, etc. This geophysical information would be useful for regional and global hydrologic models.

properties, etc., to investigators through the Eos data and information system.

Information Parameters

As discussed above, the desired information consists principally of the spatial and temporal variation of soil moisture, snow, surface roughness, channel geometry, land-water boundaries, and vegetation moisture over a wide range of hydrologic regimes (Figure 20). Since we have relatively little experience with extracting this information from spaceborne SAR images, the first few years of the Eos observations would be focused upon representative global study regions and sites. The emphasis of this initial phase would likely be upon determining optimum instrument (frequency, polarization, etc.) and viewing (illumination geometries, revisit times) parameters, and upon the development of suitable inversion algorithms for filling the missing parts of Figure 20. SAR data would be used with other Eos sensor data (as described previously) to determine optimum sensor combinations and joint inversion algorithm strategies.

The next phase could then consist of the collection and interpretation of SAR time series data sets, with refinement of algorithms for the extraction of soil and canopy moisture, snowpack, and land-water boundary data. These algorithms and instrument parameters could then be used in a number of pilot experiments to determine the extent to which the techniques could be extended from local watershed to the inference of water flux, water storages, and chemical flux at a regional and eventually global level.

Experience with previous spacecraft SAR data, especially Seasat and the SIR-A and SIR-B missions, has taught a clear lesson: the extraction of quantitative information from SAR images will depend critically upon careful radiometric and geometric calibration of the images. For Eos global observations, this requirement will be especially important. Hydrologic investigations of a global scale cannot be conducted if there is continual uncertainty about how to use a set of SAR images of doubtful calibration for studies of spatial and temporal variability.

With calibrated SAR image sets, information extraction can proceed using operational algorithms to extract the geophysical parameters necessary for global hydrologic models. In the case of snowpack studies, the snow surface cover (especially the snowpack water equivalent) is the primary quantity of interest. In the case of soil moisture studies, the confusion effects of vegetation cover and surface roughness must be included in the image analysis algorithms.

IV. VEGETATION SCIENCE

SCIENCE ISSUES

Broad Eos Science Issues

A major goal of Eos is the development of an improved, quantitative understanding of the state and dynamics of Earth's biota and their interaction with the global hydrologic, biogeochemical, and climatic cycles. A key to this understanding is information about the state of global vegetation communities (spatial distribution by type, biomass, and condition) and concerning their dynamics (i.e., the major fluxes of energy and mass to, from, and within their ecosystems). Plants are dynamic in nature and play an important role in all essential global cycles that involve exchanges of energy, water, carbon, and other elements between abiotic reservoirs that comprise, primarily, the atmosphere and sediments, and biotic reservoirs that include both plants and animals. These exchanges are directly related to plant productivity, which is the photosynthetic accumulation of chemicals from the atmosphere and soil into biomass.

Specific Science Issues

The specific issues associated with the interaction of the vegetated terrestrial Earth and the major cycles have been put forth by the Earth System Science Committee (Bretherton *et al.*, 1986) and in several National Academy of Sciences reports (NRC, 1985; NRC, 1986a; NRC, 1986b); those objectives that are related to the terrestrial biosphere and for which SAR will play a role in the measurement are reiterated below:

- To quantify the interactions between vegetation, soil, and topography and the hydrologic cycle.
- To determine the global distribution of biomass, gross primary production, net primary production, respiration, and decomposition; the annual cycles for these processes; and their year-to-year variations.
- To identify the biotic reservoirs for the major biogeochemical cycles (i.e., those of carbon, nitrogen, phosphorus, sulfur); to determine the fluxes among them and between them and the oceans and atmosphere. Included here is the determination of the sources and sinks of radiatively important trace gases.
- To determine the impact of increases or decreases in resource availability on terrestrial ecosystems (e.g., increased atmospheric carbon dioxide concentration, acid precipitation and deposition, long-term drought).
- To quantify the interactions between the vegetation canopy boundary condition and local and regional climate.

In order to understand how the Earth functions as a system and changes over time, the response of ecosystems to natural and anthropogenic environmental changes, the impact on global cycles of these changes in the Earth's ecosystems, and the long-term impacts of changes in the global cycles and the Earth's biota must all be elucidated.

Natural and anthropogenic changes in terrestrial ecosystems can have major impacts on global properties and processes. Examples of current important questions are: Does extensive deforestation, as is now occurring in parts of the tropics, result in a net export of carbon dioxide to the atmosphere? Does extensive deforestation in the tropics or desertification in semi-arid regions significantly alter the regional energy budget and result in changes in regional climate? How do acid precipitation and the associated deposition of nitrogen or sulfur compounds affect the productivity of agricultural and forested ecosystems and how are their fluxes of trace gases to the atmosphere affected?

The response of ecosystems to external forcings, and the responses of their constituent biota, must also be understood as part of the Earth system perspective. Only through detailed study of these responses, do we gain an understanding of the mechanisms involved. At present, most of the mechanisms for ecosystem change are very poorly understood. This is an active area of research in the ecological sciences, and one likely to lead to the development of mechanistic models and an ability to predict ecosystem response to change. In addition to the types of global impacts described above, changes in the structure, function, and composition of terrestrial ecosystems following perturbation can have serious economic or societal consequences. Some important questions related to ecosystems response to perturbation are: Does chronic exposure of agricultural and forested ecosystems to air pollutants and acid precipitation result in a decline in productivity, a complete loss of productivity, or a change in the type of ecosystem (or crop) able to occupy the area? Can secondary tropical forests be as productive as the primary forests, and how do their nutrient-cycling properties (reservoirs, fluxes) vary from those of the primary forest?

The long-term impacts of changes in global properties must also be addressed. Understanding of short-term responses may not always yield insight into long-term effects. It is well-known that plants and presumably ecosystems can acclimate (or adjust) to environmental changes of a chronic nature. Feedback among Earth system components will almost assuredly play a role and it could take years to cen-

turies for the system to equilibrate, if it equilibrates at all. A few questions relevant to this type of interaction are: What will be the net effect of increased atmospheric carbon dioxide on vegetation productivity, given that we know increased carbon dioxide will increase gross productivity, but that increased air temperatures likely to result from increased atmospheric carbon dioxide will increase ecosystem respiration rates and also could cause significant climatic changes for the area in question? We know that vegetation type and productivity in a given area are commonly controlled or limited by one or more of the following environmental constraints: temperature, water, available nutrient concentrations, or atmospheric carbon dioxide concentration; how will the areal extent of various vegetation types and their productivity change when one or more of these environmental constraints ceases to be the controlling or limiting factor?

The answers to the above questions depend on acquiring accurate measurements of the biophysical properties of the Earth's vegetation, including biomass, canopy moisture content, canopy geometry, and the state of the surface beneath, including moisture content, water state, and understory characteristics. In addition, measurements of the areal distribution and boundary location of Earth's biomes as a function of time on seasonal, annual, and decadal time scales are needed. Current uncertainties in the measurements used to address the above issues include (1) the methods for scaling from local well-measured sites to biome-wide estimates, and (2) uncertainties about the natural variation in the extent of different biomes and within a particular biome over the time scales of seasons to centuries.

Clearly a number of measurement capabilities will be required to address these issues; SAR will play a major role due to its sensitivity to canopy moisture, canopy geometry, foliar and woody biomass, and surface boundary condition. In addition, for areas of the world and times of the year for which the use of optical instruments is precluded by sun angle or cloud cover, SAR will provide continuity of observation.

OBSERVATIONAL REQUIREMENTS

Any given vegetated region may be described by biophysical and biochemical parameters associated with three strata: (1) the vegetation layer, (2) the substrate or soil layer, and (3) the atmospheric layer immediately above the canopy. Ecologists have identified the parameters listed in Table 5 as having potential utility for describing characteristics of and inferring processes within the strata. It should be possible to infer some of these parameters from Eos sensor data, as suggested in the right-hand column; other parameters in the table (e.g., atmospheric humidity directly above the canopy) cannot be inferred directly from remotely sensed data. It should also be obvious that even when remotely sensed data have the *potential* to describe these vegetation parameters, the inversion algorithms can be very complex and much basic research work remains to be done on the development of these inversion algorithms. In fact, despite the past decade of remote-sensor data acquisition and analysis, relatively little is known about how to extract quantitative biophysical or biochemical information from optical or microwave sensors. This is partly the result of effort expended in the Landsat era on phenomenological rather than physically based analysis.

In addition, for the purpose of inferring mass, momentum, and energy fluxes it will be necessary to know the areal extent of traditional vegetation cover types (e.g., biomes, communities) and their general pattern on the landscape. It will be necessary also to determine the areal extent of various types of non-traditional vegetation units, defined through their possession of certain biophysical or biochemical attributes, for the purpose of extrapolating site-specific information to regional and global scales. Finally, and perhaps most important, it will be necessary to monitor the temporal variability of these vegetation units and their biophysical and biochemical attributes in order to understand natural phenological patterns and variations as well as directional changes over time. Knowledge of the location of ecotones, the boundaries between vegetation types, and their changes over time will be of great importance for assessment of long-term change. Seasonal, annual, and decadal variations must be monitored in order to extract the long-term effects of directional change in the global ecosystem from short-term seasonal and interannual variations.

Observational Parameters

SAR has the potential to observe several important biophysical parameters, as shown in Table 5. This results fundamentally from the sensitivity of SAR to dielectric discontinuities in the medium, which are represented by the leaves, stems and branches, and trunks (or main stems). The magnitude of the scattering is modulated by the canopy moisture and by the surface scattering from underlying soils (which is also dependent upon soil moisture, standing water, and snow). These physical mechanisms are unique to the microwave spectrum. However, it is envisioned that SAR data will be used synergistically with data from HIRIS, MODIS, TIMS, and other Eos sensors as shown in Table 5.

Canopy Geometry and Biomass

Biomass per unit area is an important variable for understanding ecosystem function and is of obvious importance in predicting food and fiber production in agricultural systems. The biomass per unit area will help determine the size of the pools of biogeochemical compounds. Biomass density is a

Table 5. Vegetation Biophysical Parameters

Layer	Eos Sensors
Vegetation	
Canopy water content	SAR, HIRIS
Canopy structure	
green leaf area index (GLAI)	HIRIS, SAR, MODIS
leaf orientation	SAR, HIRIS
main stem (trunk) geometry and spatial distribution	SAR
stem, branch size, angle distributions	SAR
biomass by component (foliar, higher-order stems and main stem)	SAR
Canopy nitrogen	HIRIS
Canopy phosphorus	HIRIS
Canopy lignin	HIRIS
Canopy temperature	TIMS, MODIS
Soil Surface Boundary	
Soil moisture	SAR, ESTAR*
Soil temperature	TIMS, MODIS, AMSU
Substrate biogeochemistry	HIRIS
Air	
Atmospheric humidity	AMSR, AMSU, LASA, HIRS
Air temperature	AMSU, HIRS, LASA
Precipitation amount and distribution	AMSR
Wind speed directly above canopy	LAWS**
Pollutant influx	atmospheric models

*SAR and ESTAR are the only planned Eos sensors that are directly sensitive to soil moisture; however, the full characterization of soil moisture requires the combined data from many sensors as inputs to soil hydrologic models.

**LAWS is the only Eos sensor that directly measures wind over land, but effective determination will require detailed models of the atmospheric boundary layer using several data sources.

function of the environment and can be used to infer climatic constraints or environmental changes (both beneficial and deleterious). Attempts to estimate biomass by means of remote sensing have focused on the estimation of LAI[7]. LAI, at least at values from about 2 to 7, is highly correlated with above-ground biomass and vegetation water and carbon dioxide exchange. Both optical and radar sensors have provided data from which reasonable estimates have been made for LAIs of up to five. SAR data may provide the means to extend this sensitivity through inference of canopy geometry and vertical extent. Long-wavelength SAR may respond quite differently to wet biomass in the foliar components (leaves) and in the woody components (stems, trunk, stalks, and branches). To SAR, the plant appears to be a seasonally dynamic, three-dimensional water-bearing structure with characteristic morphological organization. It is desirable to be able to estimate biomass densities to within 25 percent (NRC, 1985). Seasonal or yearly estimates of biomass will be adequate for most purposes.

[7]LAI is defined as the total single-side surface area of all leaves contained in a canopy over a unit area of ground.

Canopy Water Content

The hydrologic cycle is of critical importance to understanding the terrestrial ecosystem state and function as discussed in Chapter III. A key ecosystem variable that may be measurable by means of active microwave remote sensing is canopy (or leaf) water content. This variable is of major importance for estimating photosynthetic rates, productivity, biomass, and vegetation vigor. Evapotranspiration is a process of major importance to ecosystem productivity and climate. SAR will be a useful tool for studying evapotranspiration to the extent that it can provide data to infer canopy or soil moisture.

Stand Architecture

For natural ecosystems, the three dimensional stand architecture (i.e., the horizontal and vertical spatial distributions and arrangements of tree

crowns) is indicative of successional state and the nature of disturbance mechanisms. It is expected that the spatial variance of multifrequency SAR data will be highly sensitive to lateral stand heterogeneity due to both spatial variance in canopy biophysical properties and SAR sensitivity to edge effects. Thus, long baseline comparisons of SAR image intensity and high-order spatial statistics will yield useful insights for succession studies, particularly along ecotones, and studies of stand vigor.

Soil Surface Boundary Layer State

As pointed out in Chapter III, L- or C-band SAR images show great sensitivity to soil moisture levels. In fact, the Eos SAR is the only sensor that can provide detailed soil moisture information at the sub-kilometer scale. Estimates of canopy or soil moisture content would be most desirable on a daily, weekly, and/or monthly basis. In addition, longer wavelength radars (e.g., L-band) have the unique capability to penetrate the canopy providing information on the state of the surface boundary layer below a canopy.

Areal Extent of Terrestrial Biomes

One of the basic requirements for all regional and global vegetation studies is for accurate measurements of the amount of land surface covered by each community and the associated location of the ecotones between vegetation types. The synoptic coverage provided by satellite sensors is ideal for this purpose, but the ultimate level of detail achievable in the identification and classification of types is not yet known. Traditionally, vegetation associations have been classified based on such characteristics as species composition, structure (physiognomy), and climatic regime of occurrence.

SAR offers unique sensitivity to canopy morphology or structure and will provide valuable data (along with HIRIS) for identifying and classifying vegetation types, as well as for determining their areal extent (Figure 21). An example of SAR's ability to discriminate forest boundaries was obtained during the SIR-B mission using data acquired along a strong environmental gradient just east of the Andes in southern Argentina (Figure 22). In this case, the sensitivity of the microwave backscatter acquired at different incidence angles provided sufficient information to accurately delineate the boundaries.

Landscape Patterns and Processes

The terrestrial surface is a natural mosaic of vegetation units determined by differences in topography, microclimate, substrate characteristics, and disturbance history. The natural patterns of these regional mosaics and the processes that maintain them have not been investigated in any detail until quite recently. Remotely sensed data from microwave and optical sensors can be used to obtain information on landscape pattern. SAR amplitude and phase data at various incidence angles, frequencies, and polarizations may yield unique information on landscape patch sizes and shapes due to the sensitivity of radar to discontinuities in canopy structure. SAR may be less useful for inferring landscape processes, although a few applications can be envisioned. For example, canopy structure at the edges of forest remnants may provide evidence for patch degradation due to unfavorable microclimatic conditions at the periphery. The scale of the landscape pattern will dictate the scale of SAR coverage required. Amplitude and phase, multiangle, multifrequency, and multipolarization data will all be useful for these purposes. Seasonal coverage will be required to document patterns, and multiyear to decadal coverage will be needed for change detection studies.

Areal Extent of Biophysical Properties Within Each Biome

Measuring and monitoring the spatial variations of the canopy and the surface properties within a biome will be a key use of SAR for Eos. SAR's ability to penetrate the canopy to depths selectable by choice of frequency, polarization, and incidence angle will provide insight into variations of biomass, canopy moisture content, and surface boundary layer state even within a single biome. An example of this is shown in Figure 23 where a coarse-resolution K_u-band image of Africa is contrasted to the fine-resolution SIR-A L-band images of a dense tropical rain forest, a transition zone between the forests and the Sahara (the Sahel), and a region of sand dune encroachment.

Temporal Variability

The use of multidate observations to investigate diurnal and seasonal oscillations related to meteorological and phenological variations, can be documented using the Eos SAR with daily to weekly to monthly repeat coverage. This will improve classification accuracies for vegetation types and will provide consistent frequent coverage for monitoring biome variations and sensitivities to external forcings (Figure 24). It has been demonstrated that radar backscattering is very sensitive to growth patterns (Figure 25) and that the seasonal variation of the radar backscattering coefficient[8] (σ°) tracks the seasonal variation of biomass. In addition, seasonal environmental variations can help to enhance or suppress selected interaction terms in the total microwave backscattering such that the components of the canopy biomass, for example, may be separated.

Observational Strategies and Regimes

Eos is planned for a 15-year time span in order to obtain long-term observations of global change. It

[8]The radar backscattering coefficient, a dimensionless quantity denoted by the symbol (σ°), is defined as the average radar cross section (an area) per unit area; it is a measure of the intensity of the radar echo in relation to the power incident on the Earth's surface.

Figure 21. (a) Radar image of the Amazon Basin obtained from the Seasat scatterometer at K_u-band using VV polarization and 45° incidence angle. The pixels are half-degree (approximately 50 km wide). The boundary between the tropical rain forest (with a backscattering coefficient below -10 dB) is very evident (Kennett, 1987). (b) SIR-A L-band image from east-central Colombia (location A) showing the details of the rain forest/savannah boundary. (c) SIR-A image of deforestation in eastern Brazil (location B). (d) SIR-A image of deforestation in western Brazil (location C).

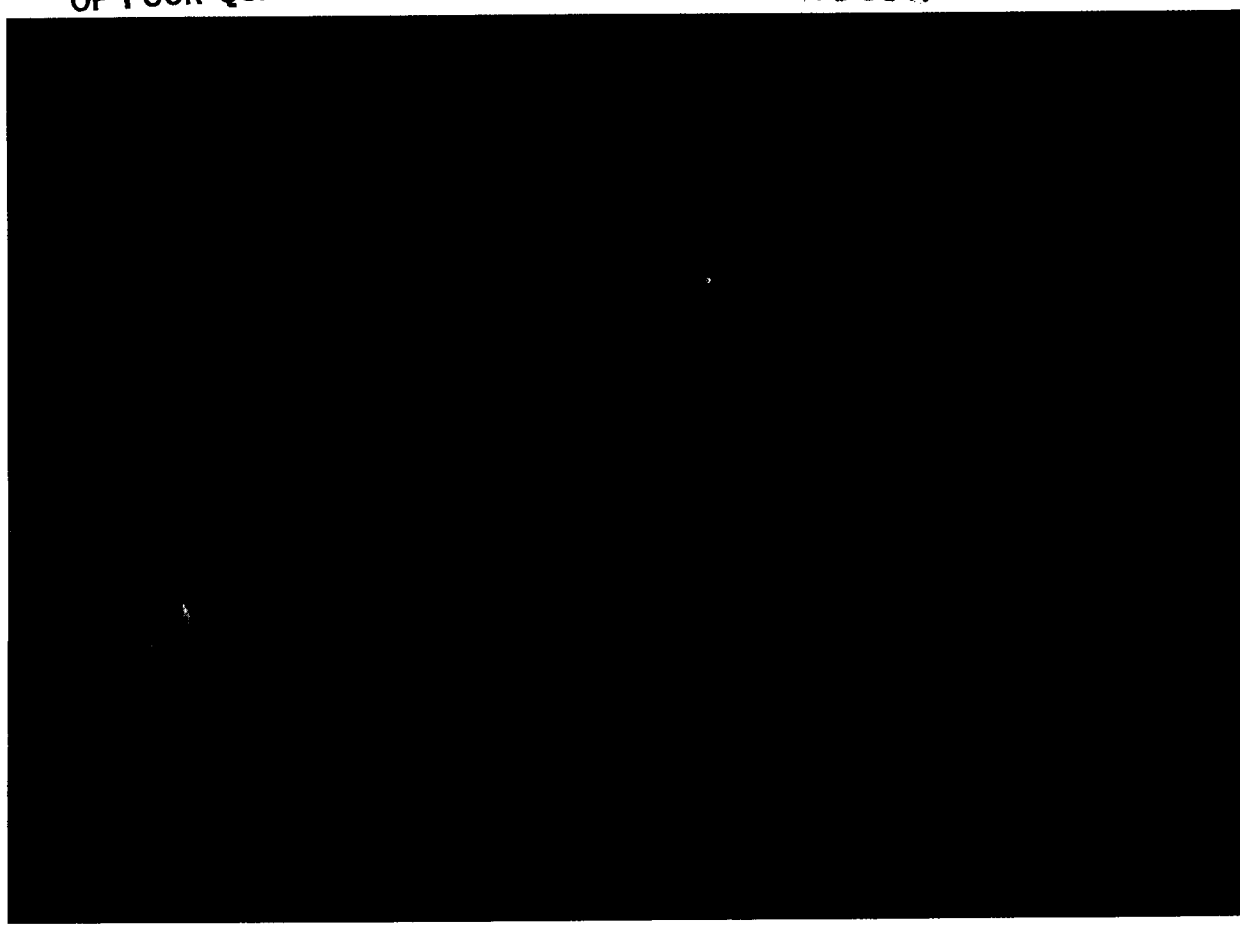

Figure 22. Forest boundaries as determined using multiple incidence angle SIR-B data (Cimino *et al.*, 1986). The region is in the foothills east of the Andes. The boundaries are controlled by sharp rainfall gradients.

is recommended that Eos SAR studies of vegetation concentrate over the first several years on specific sites that are representative of broader ecologic regimes. These initial studies, which would identify optimum instrument and viewing parameters and improve or validate biophysical inversion algorithms, would be followed by broader global surveys. Some of this may be accomplished with single-parameter SARs being flown on ERS-1 and JERS-1 and by the use of Radarsat data.

Eos vegetation studies would initially focus on sites around the world representing four broad regimes: (1) forests, (2) semi-arid ecosystems (grasslands/steppes/desert), (3) agricultural lands, and (4) wetlands (Figure 26).

Approximately one-third of the total world land area is covered with forests, and the total area planted to crops is another 10 percent. This total area for forests and crops is roughly equivalent to 1,500 billion pixels from a single channel of 30 m resolution Landsat data or 6,000 Landsat single-channel images. However, it is unnecessary to acquire high-resolution Eos imagery over the entirety of these vegetated regimes. The essential information required to determine the observational parameters could be obtained from a representative set of sites or biome transects. A large number of representative sites could be chosen for detailed study by SAR and SAR/HIRIS and still give a reasonable average data rate. Some specific scientific objectives for SAR observations are discussed below for each of the four major regimes.

Forests

The objectives of Eos observations of forests using SAR are to:

- Obtain a baseline survey of forest extent by type on a global basis.
- Establish the validity of generalized algorithms for retrieving canopy biophysical information.
- Examine seasonal and interannual variability in forests.
- Monitor the nature and extent of forest responses to such stress agents as diseases, in-

ORIGINAL PAGE IS
OF POOR QUALITY

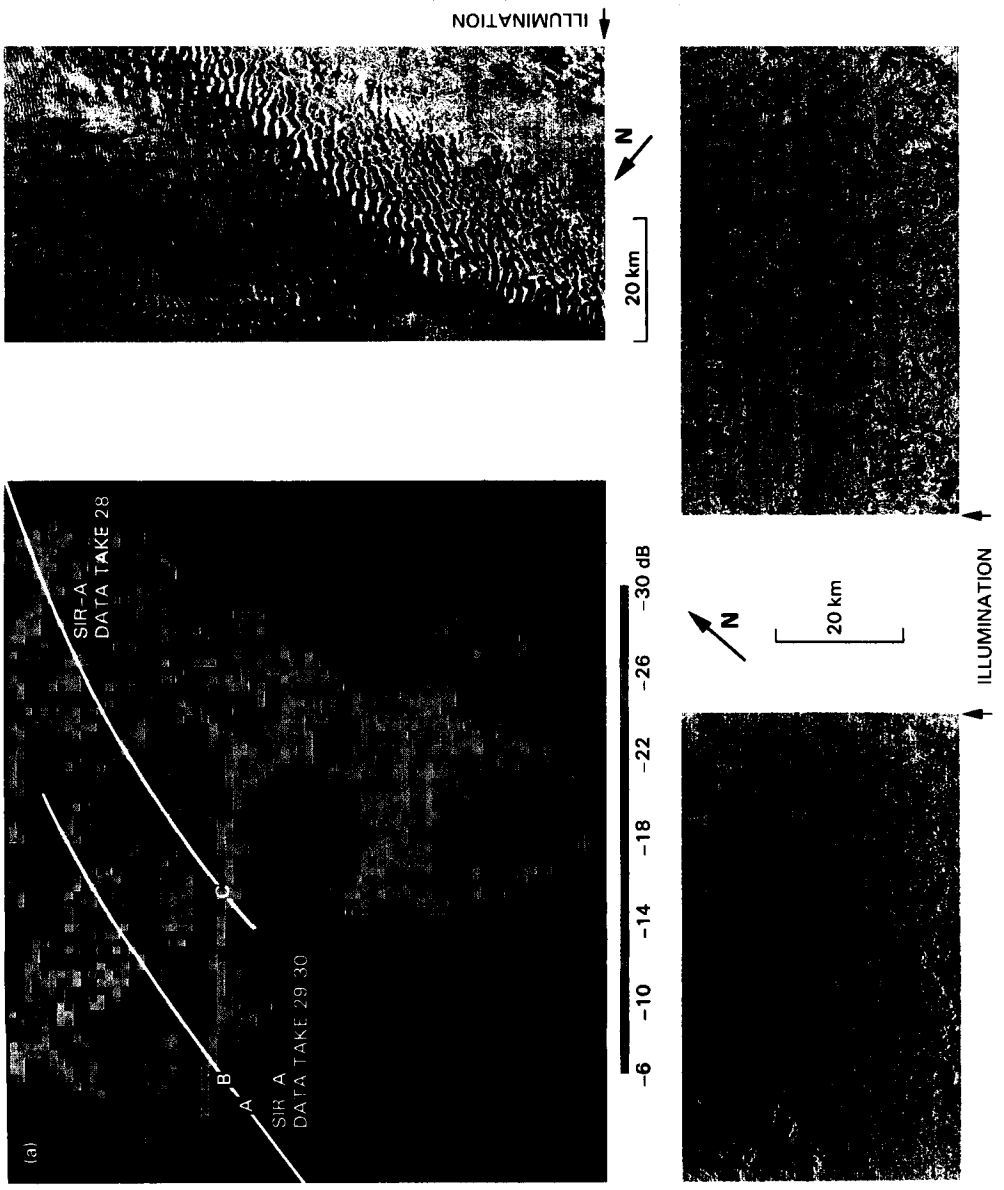

ORIGINAL PAGE
COLOR PHOTOGRAPH

Figure 23. (a) Radar image of the African continent obtained from the Seasat scatterometer at K_u-band using VV polarization and 45° incidence angle (Kennett, 1987). (b) SIR-A L-band image of the dense tropical rain forest (location A on the map). (c) SIR-A image of the Sahelian transition zone between the forests and the Sahara desert (location B). (d) SIR-A image of Lake Chad basin showing the encroachment on sand dunes on the Sahel (location C). These dunes are mostly dark in the image except for the vegetated interdune fields which have a bright response due to a cover of grassy savannah.

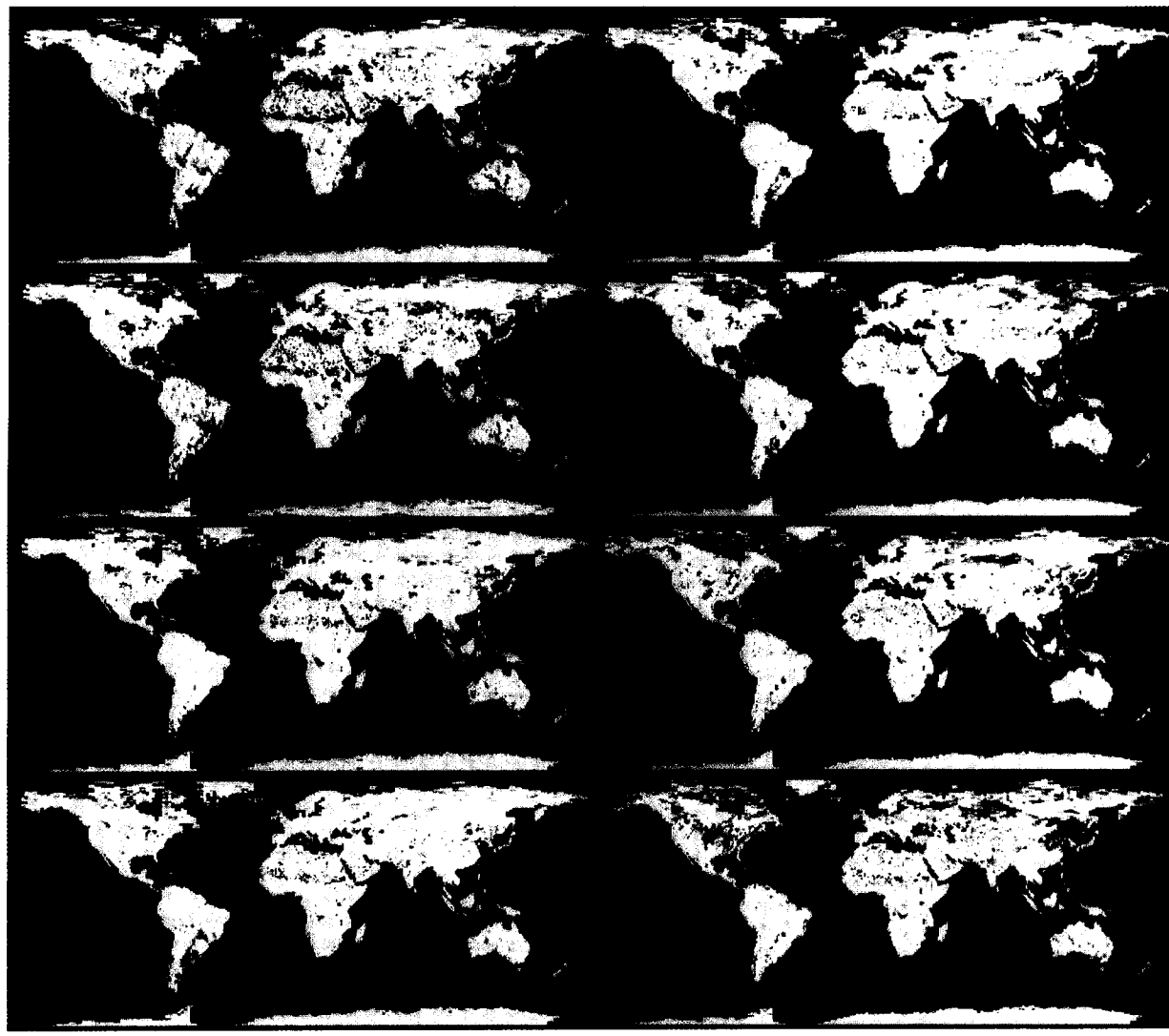

Figure 24. Time dependence of the K_u-band VV-polarized backscatter of the Earth as observed by the Seasat scatterometer. The mean backscatter for the summer of 1978 has been subtracted from the backscatter for each of the following dates: (a) July 7-18, (b) July 19-30, (c) July 31-August 11, (d) August 12-23, (e) August 24-September 4, (f) September 5-16, (g) September 17-28, and (h) September 29-October 9 (Kennett, 1987).

sects, water availability (drought and excess), airborne pollutants, wind damage, frost, fire, and anthropogenic practices.

The realization of these objectives will first require the establishment of selected test sites that collectively cover a range of forest biomes. These test sites will be used to establish the validity of algorithms for retrieving canopy biophysical information. Some of the test sites should include both managed and unmanaged forest stands. Areas should be selected that are in a variety of stages of stress.

Grasslands/Steppes/Deserts

Careful examination of change in grassland, steppe, and desert ecosystems is warranted, especially with respect to desertification, due to their areal extent, economic significance, and particular sensitivity to climatic and anthropogenic stress. There has been very little work done on radar sensitivity to these ecosystems, although it is expected that radar images will provide subtle expressions of the biophysical characteristics for some regions, especially those with larger biomass or strong associations with landforms.

The objectives of Eos observations of grassland/steppe/desert regimes using SAR are to:

- Ascertain the baseline extent and biophysical characteristics of major grassland/steppe regions on a seasonal basis and to infer local and regional primary productivity.
- Examine the seasonal flux of primary productivity (biomass) and relate it to meteorological history.
- Investigate the sources and effects of external stress on primary productivity arising from natural climatic oscillations or change and from anthropogenic factors such as urbaniza-

ORIGINAL PAGE
COLOR PHOTOGRAPH

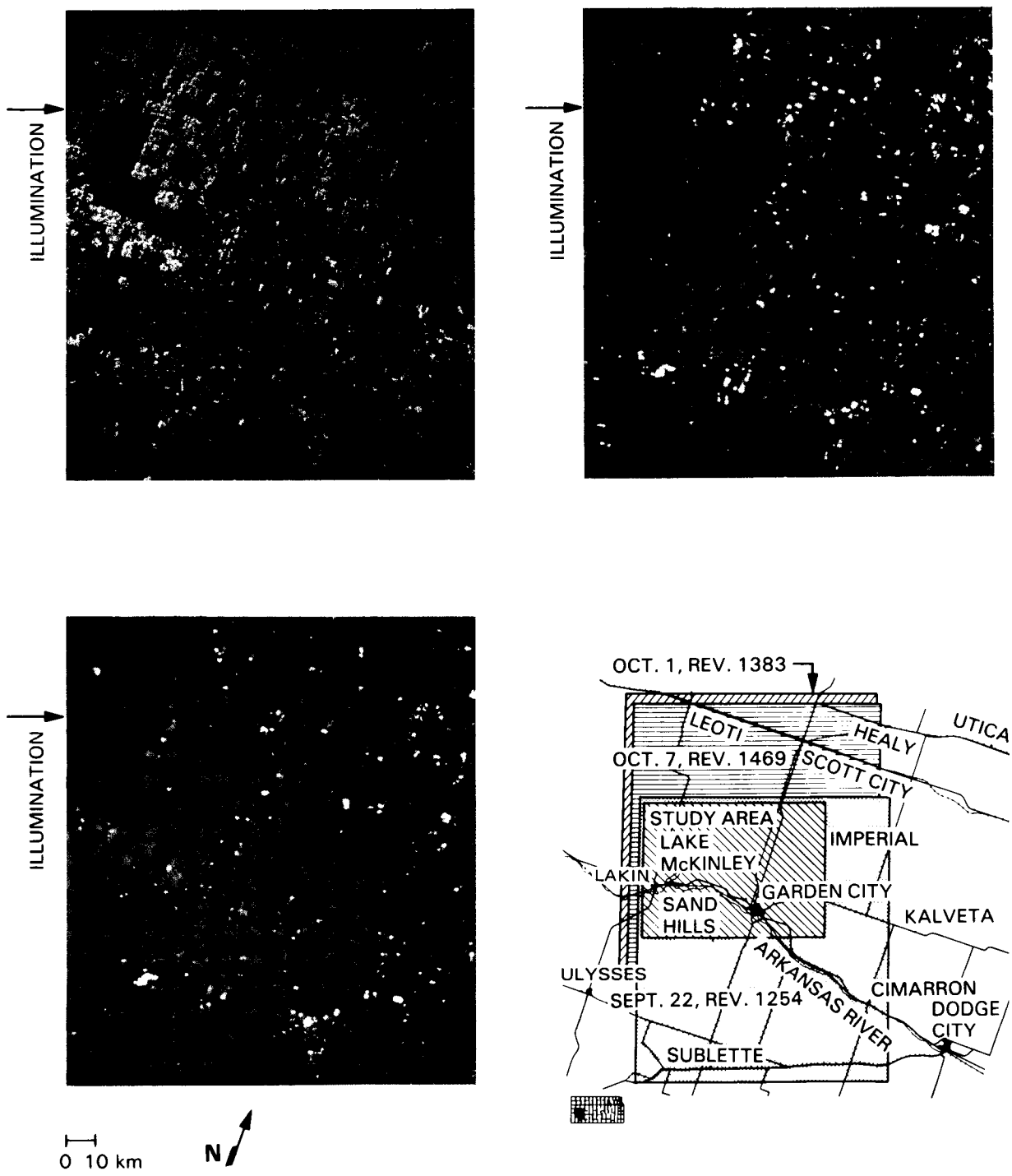

Figure 25. SIR-B multidate observations of Garden City, Kansas.

tion, overgrazing, and conversion to farmland (dryland and irrigated).

- Relate external stresses via their effects on primary productivity to desertification.

These objectives can be approached by initially using a small number of carefully selected test sites characterized by historic and current stress. One such site is the Thar Desert of India and Pakistan, an area of grasslands to desert shrubs under severe anthropogenic stress from grazing. A strong climate/biome interaction mechanism has been suggested. Regions within the North American high plains serve as examples of areas of shortgrass prairie undergoing

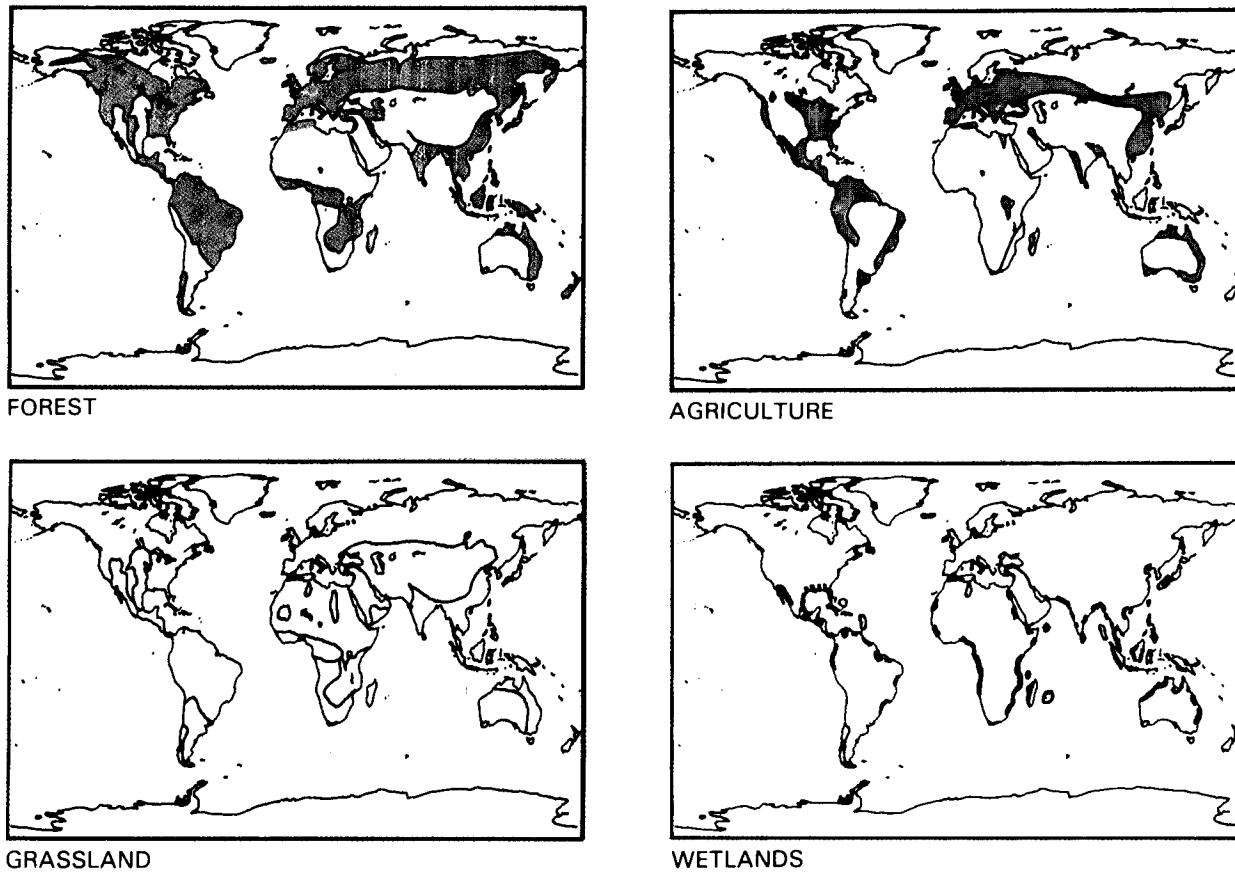

Figure 26. World distribution of forests, grasslands, agricultural lands, and coastal wetlands.

locally intensive conversion to farmland and urbanization. In the Sudan zone of Mali, we find short-grass savannas are undergoing regional climatic stress and grazing pressure. Many other such sites exist, of course. As algorithms are developed and verified, more extensive arid regions will be monitored. The focus for SAR will be on monitoring the boundaries of regions undergoing rapid change as determined by the lower resolution global sensors.

Agricultural Lands

Agricultural crops are managed monospecific stands of plants ranging in size and structural complexity from grasses to orchard plantations. In terms of the spatial variance of microwave scattering properties, the spatial variance of agricultural canopies is not necessarily representative of natural vegetation communities at large; however, the controlled management practices applied to crops makes them ideal experimental test cases for defining the nature of the target/sensor interaction process.

The global distribution of specific crops is the result of the complex interaction of environmental conditions (nutrient and water availability and climate) and anthropogenic factors (fertilization, irrigation, pest control, market forces, and cultural tradition). Global inventory and assessment of agricultural production must unambiguously classify crops (grown using nonuniform cultural practices) and monitor canopy responses to such stress agents as disease, insect infestation, frost, air pollution, or an excess or deficit of moisture.

The objectives of the Eos observations of agricultural regimes using SAR are to:

- Validate crop discrimination and classification accuracy for single-date multifrequency and multipolarization SAR data alone and with HIRIS data.
- Investigate the added information provided by multidate SAR observations with respect to crop classification, crop phenologic development, stress assessment, and change detection resulting from irrigation and tillage practices such as planting and harvest.
- Develop and test retrieval algorithms for extracting canopy biophysical parameters such as LAI, phytomass, canopy productivity, canopy structure, and canopy water content.

Evaluate the sensitivity of these algorithms to background conditions of surface roughness, soil moisture, frost, free water on the canopy (dew or precipitation), and snow cover.

- Evaluate both the temporal and the geographic extensibility of crop classification and assessment algorithms to radically different environmental conditions (e.g., topography and water availability), tillage practices (e.g., planting density and soil-surface roughness), and human settlement patterns (e.g., agricultural field size distribution and the spatial density of cultural features).

These results can then be used to compare, on a global basis, the absolute and relative primary productivity of various cropping practices.

Wetlands

Wetlands play a major role in global biogeochemical cycling through anaerobic production of trace gases and their contributions to the carbon cycle. Many wetlands (freshwater swamps and marshes, salt marshes, and mangroves) serve as major sources of the carbon compounds (detritus) that determine the productivity of riverine and estuarine ecosystems; other wetlands (bogs and northern peatlands) serve as net sinks for carbon.

SAR data may be able to provide valuable baseline information for monitoring and modeling energy and mass fluxes in these wetland ecosystems. The multifrequency, multipolarization capability of the Eos SAR could be used to supply the area and biomass terms to estimate carbon throughput for wetlands having definite seasonal biomass changes. The sensitivity of SAR to surface moisture will be of great utility in determining the areal extent of wetlands and for delineating wetland water regimes, i.e., soil saturation levels. It may be possible to develop models of the backscatter from the canopy which describe the canopy structural components contributing most heavily to litter production. Temporal information on inundation patterns and duration and on biomass accumulation in wetlands may provide the information necessary to make seasonal and annual estimates of the fluxes of carbon, nutrients, and trace gases to the oceans and atmosphere.

The objectives of Eos observations of wetlands using SAR are to:

- Obtain a baseline survey of inland and coastal wetlands extent and to determine their water regimes.
- Examine the seasonal flux of primary productivity and relate it to carbon export to aquatic detrital ecosystems or to *in situ* carbon sequestration as peat.
- Relate temporal information on water regime and productivity to trace gas fluxes.
- Investigate the sources and effects of external stress on productivity and nutrient cycling processes within wetlands.

Human activities such as drainage of wetlands to create arable lands, use of wetlands as dumps for wastes, and channelization of rivers are resulting in a steady loss of wetlands in many parts of the world. A rise in sea level, postulated as a consequence increased atmospheric carbon dioxide, could result in substantial loss of coastal wetlands. Similarly, an increase in mean annual temperature in the northern latitudes could result in profound changes in the rates of biogeochemical cycling and trace gas emissions for the extensive boreal and arctic wetlands. Thus, reductions in the areal extent of wetlands and externally-induced changes in wetlands processes need to be monitored and their impacts assessed.

RATIONALE FOR SAR OBSERVATIONS

Radar observations of vegetation are uniquely sensitive to many biophysical parameters, as discussed in the following sections. Appendix C presents a discussion of some of the backscatter models used for vegetation. These models and their associated experimental data sets form the basis for the assertion that SAR is uniquely sensitive to plant structure, offers substantial penetration of plant canopies, is synergistic with optical data, and provides reliable cloud-free coverage with no sun-angle dependence.

Sensitivity to Plant Structure

Optical sensors are most sensitive to plant structure at the micrometer scale, whereas radar responds to the centimeter and decimeter scales (see Figure 27). A radar operating at a given wavelength (e.g., 6 cm) is most sensitive to scatterers whose sizes are on that order (e.g., leaves). Resonance effects occur when the size of an object is equal to $\lambda/\sqrt{\epsilon}$, where ϵ is the relative dielectric constant associated with the plant material. By combining multiwavelength observations of a vegetation canopy, it is possible to provide useful estimates of the biophysical and morphological parameters of that canopy (see examples in Appendix C). An excellent example of the discrimination capability of the multifrequency SAR is shown in Figure 28.

Most plant canopies are nonisotropic media containing scatterers having specified orientations. Of particular importance to radar are the vertical stems of plants and the trunks of trees because wave propagation through and backscattering from these media are polarization-dependent. Thus, the three polarization configurations—HH, HV, and VV—provide three different views of the canopy's struc-

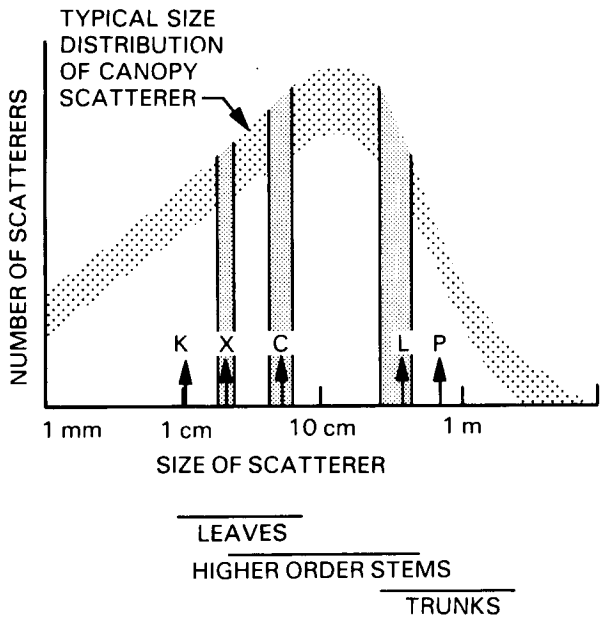

Figure 27. Expected radar response at various wavelengths to the size distribution of canopy scatterers.

ture. This is illustrated by the color variations evident in the false-color multipolarization image shown in Figures 29a and 29b.

For some vegetation conditions, the phase difference between the HH- and VV-polarized backscattering signals may contain useful information about the canopy. This phase information is unique to SAR. Figure 29b is an airborne L-band SAR phase image of an agricultural area in Illinois (Ulaby *et al.*, 1987). In this figure, the color of a given pixel is assigned on the basis of the polarization phase difference. The magenta color in the image, which had been assigned to pixels with zero phase difference, was found to correspond to bare soil surfaces and dry canopies of soybeans, whereas the turquoise pixels, equivalent to a phase difference of 110°, were found to correspond to fields of mature corn. Pixels for which the polarization phase difference is intermediate between those of magenta and turquoise, correspond to cornfields that are about half as tall (due to damage by corn borers) as the mature cornfields. This is a new area of research that should be pursued intensively over the next few years to determine its usefulness as a monitor of both the current and dynamic states of vegetation canopies. Another example of the utility of multipolarization images is shown in Figure 30, which is a color composite of L-band HH, VV, and VH images acquired over the Savannah River Plant, South Carolina.

Canopy Penetration

Optical waves cannot penetrate deeply into thick vegetation canopies, whereas microwaves can penetrate to varying extents, depending upon the frequency, polarization, and incidence angle used (see Figure C.1 in Appendix C).

Synergism with Optical Data

Under clear-sky conditions, SAR observations can be combined with optical observations to yield information of greater accuracy than either type of sensor can provide alone. According to a study (Li *et al.*, 1980) involving the application of Bayes classification to multidate Landsat and X-band radar data of a scene consisting of six classes (water, forest, highways, corn, wheat, and milo), radar provided the greatest separability prior to wheat harvest (Figure 31a) and Landsat bands 5 and 7 provided most of the discrimination after the wheat had been harvested and the fields planted in milo (Figure 31b). In both time intervals, however, the combined use of the optical and radar data provided superior classification accuracies to single sensor observations. Although only a few studies have been conducted to date to establish the quantitative improvement derived from using radar and optical sensors together, the indications are that the information provided by the two types of sensors are complementary in nature.

Cloud-Free Coverage

When cloud cover is present, SAR is the only viable means of obtaining information about vegetation attributes. A simulation illustrating how radar may be used to "substitute" for an optical sensor when cloud conditions do not permit optical observations of the Earth's surface is shown in Figure 32. In Figure 32a, the middle curve represents the multidate classification accuracy obtained by bands 5 and 7 of Landsat. The lower curve shows the results that would have been obtained had the first date (5/20) been cloud-covered. The role of radar is illustrated by the top curve, which shows that if radar data were to be substituted for the missing Landsat observations on 5/20, the overall classification accuracy attained on 6/25 would improve from 70 percent to 90 percent. A similar analysis simulating the absence of Landsat data on the middle date (6/16) is shown in Figure 32b.

Independence from Solar Illumination Angle

In addition to cloud-cover limitations for optical sensors, low sun angles and night limit the available optical data, especially in the high latitudes in the fall, winter, and spring months (see Figure 5). SAR can provide many of the required measurements during these times of the year. In addition, there may be valuable information in comparing day and night time coverage, particularly for assessing moisture stress. SAR can potentially provide these data for situations when dew is absent.

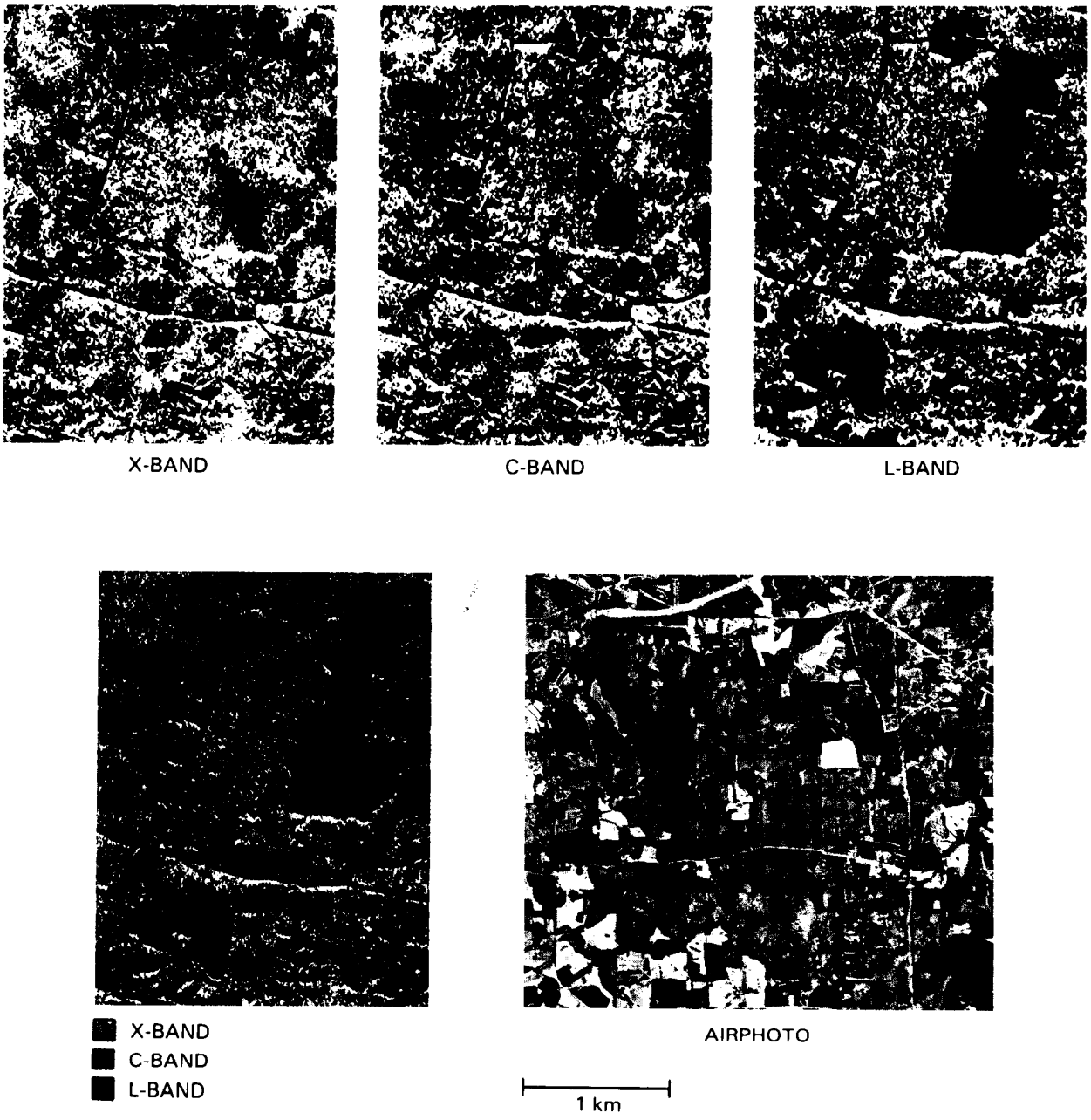

Figure 28. Three-frequency Environmental Research Institute of Michigan (ERIM) aircraft image of the Duke Forest; the bottom left image is a color composite of the combined data with each frequency displayed in a different color. Loblolly pine stands appear red in the SAR image. Direct comparison with an aerial photo show a very high degree of correlation between the image and the ground truth even to the individual tree level (courtesy of E. Kasischke, ERIM).

Multidate Coverage

SAR's ability to provide year-round coverage under any atmospheric conditions will provide a unique high-resolution multidate data set with revisit cycles as short as 1 to 2 days, depending on incidence angle constraints. It should be possible to monitor the occurrence and spatial extent of environmental variations as well as use these variations to improve the information available from a single-date system (see Appendix C).

Previous Experimental Results

It has been demonstrated by a number of field, aircraft, and satellite experiments that radar is sen-

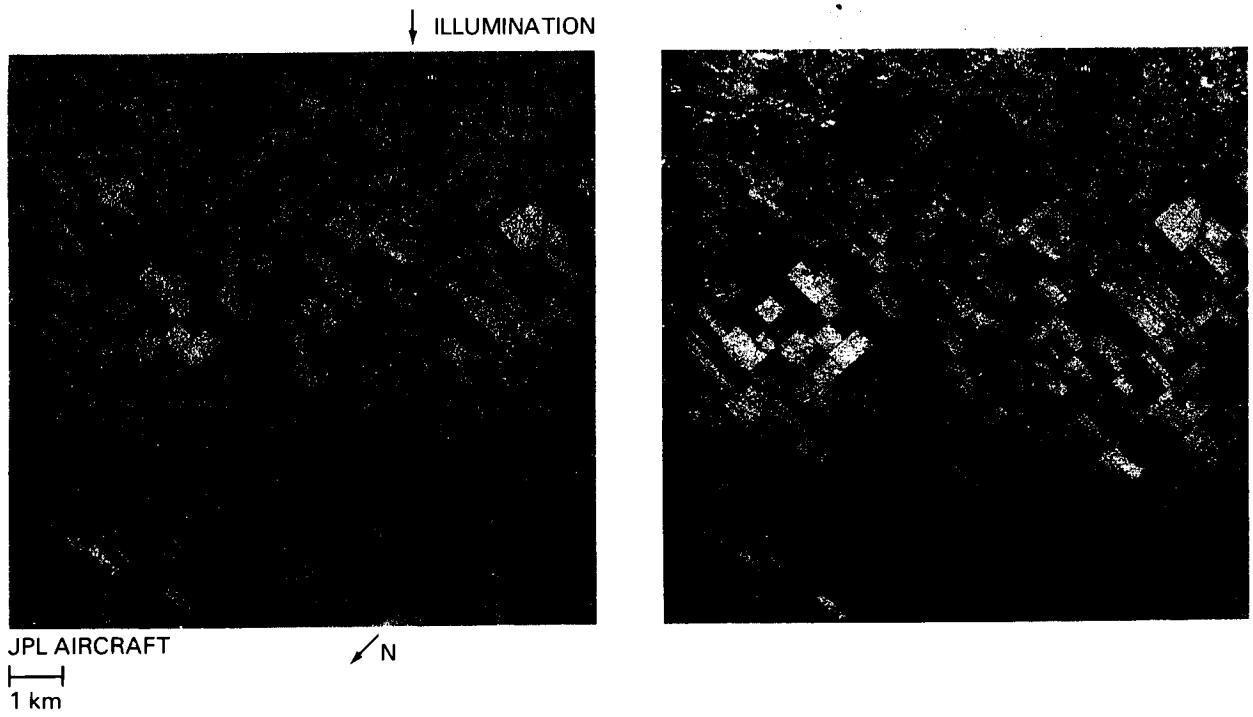

Figure 29. (a) JPL aircraft quad-polarized SAR image (L-band) of an agricultural region in Illinois; this is a polarization phase difference image. Magenta corresponds to no phase difference ($\Delta\phi$ = 0°); turquoise corresponds to $\Delta\phi$ = 110°. (b) Color composite of multipolarization data (Ulaby *et al.*, 1987).

sitive to vegetation canopy structure and underlying surface conditions. Extensive field radar scatterometer measurements of cultural vegetation classes have been made over the past 15 years. These experiments concentrated principally on agricultural targets (principally corn, sorghum, wheat, milo, and soybeans) in a variety of midwestern fields ranging from bare to fully vegetated and over the entire growing season. The results of these measurements have been widely disseminated in the scientific literature; a summary may be found in Ulaby *et al.* (1981; 1982; 1986).

These field results using U.S. test sites have been replicated and extended by other investigators using sites in France, West Germany, the Netherlands, and Canada. In addition, results obtained from the Seasat SAR, SIR-A, and SIR-B have confirmed the sensitivity of radar to vegetation parameters and the underlying soil characteristics. SIR-B results in particular demonstrated the value of SAR in discriminating forest structural differences (Cimino *et al.*, 1986); in penetrating forest canopies and identifying the trunk-ground interaction term (Richards *et al.*, 1987); and monitoring standing water beneath forest canopies (Hoffer *et al.*, 1986; Imhoff *et al.*, 1986); and monitoring changes due to harvest and tillage over short time intervals of roughly 3 days (Ulaby and Dobson, 1986). Appendix C summarizes some of these relevant case histories.

RECOMMENDED MISSION STRATEGY

The objectives of Eos SAR for vegetation science are to achieve an increased understanding of (1) the global distribution of vegetation types, (2) their biophysical properties and temporal variations, and (3) the characteristics of large-scale changes in vegetation communities. To reach these objectives, we must specify the required instrument and viewing parameters, synergistic data sets required, data rates and volume, and a strategy for extracting the required biophysical information. Each of these elements is discussed below.

Instrument Parameters

Frequencies

It has been shown by field scatterometer and aircraft SAR experiments that radar sensitivity to vegetation type is enhanced when the wavelength is roughly equal to the size of the plant canopy components (leaves, stalks, etc.); thus, the ability to select wavelength provides a means of discriminating the scatterers that constitute a plant canopy. Although no spaceborne multifrequency SAR data sets are available to test this hypothesis, preliminary theoretical work and recent field experimental data confirm this general trend.

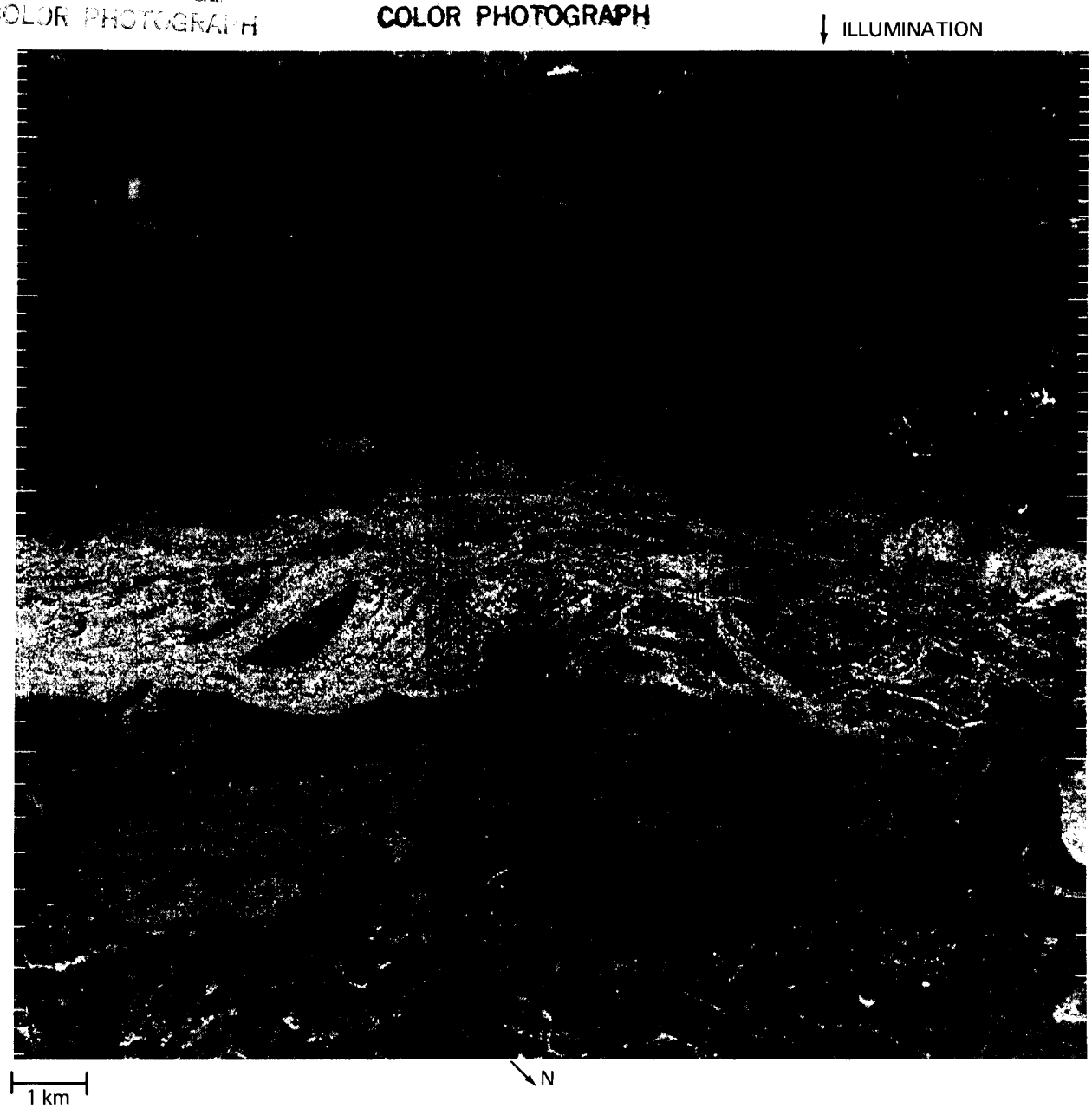

Figure 30. Color composite of L-band HH, VV, and VH images acquired over the Savannah River Plant, South Carolina, shows pine plantations (blue, red) and clear cut areas (black). Swamp areas with standing water beneath canopy produce strong returns in all polarizations (bright yellow to pink) (Evans *et al.*, 1986).

This means that at least three Eos SAR wavelengths (L-, C-, and X-band) will be needed for global observations of vegetation type. The C- and X-band channel combination may be more sensitive to crops and the L- and C-band combination more useful for forest mapping.

Polarization and Phase

Appendix C presents a brief discussion of the sensitivity of radar backscatter to polarization for vegetation. It is very important that both like-polarization (HH and VV) and cross-polarization (HV and VH) amplitude images be obtained. Moreover, phase data ($\varphi_{HH} - \sigma_{vv}$) will also be required. Polarimetry will be used extensively in the first few years of Eos to identify the optimum combination of polarizations such that structural canopy components may be separated.

Radiometric and Geometric Calibration

The approach to extracting vegetation parameters requires the collection of a time series of multiparameter SAR images of a given study site

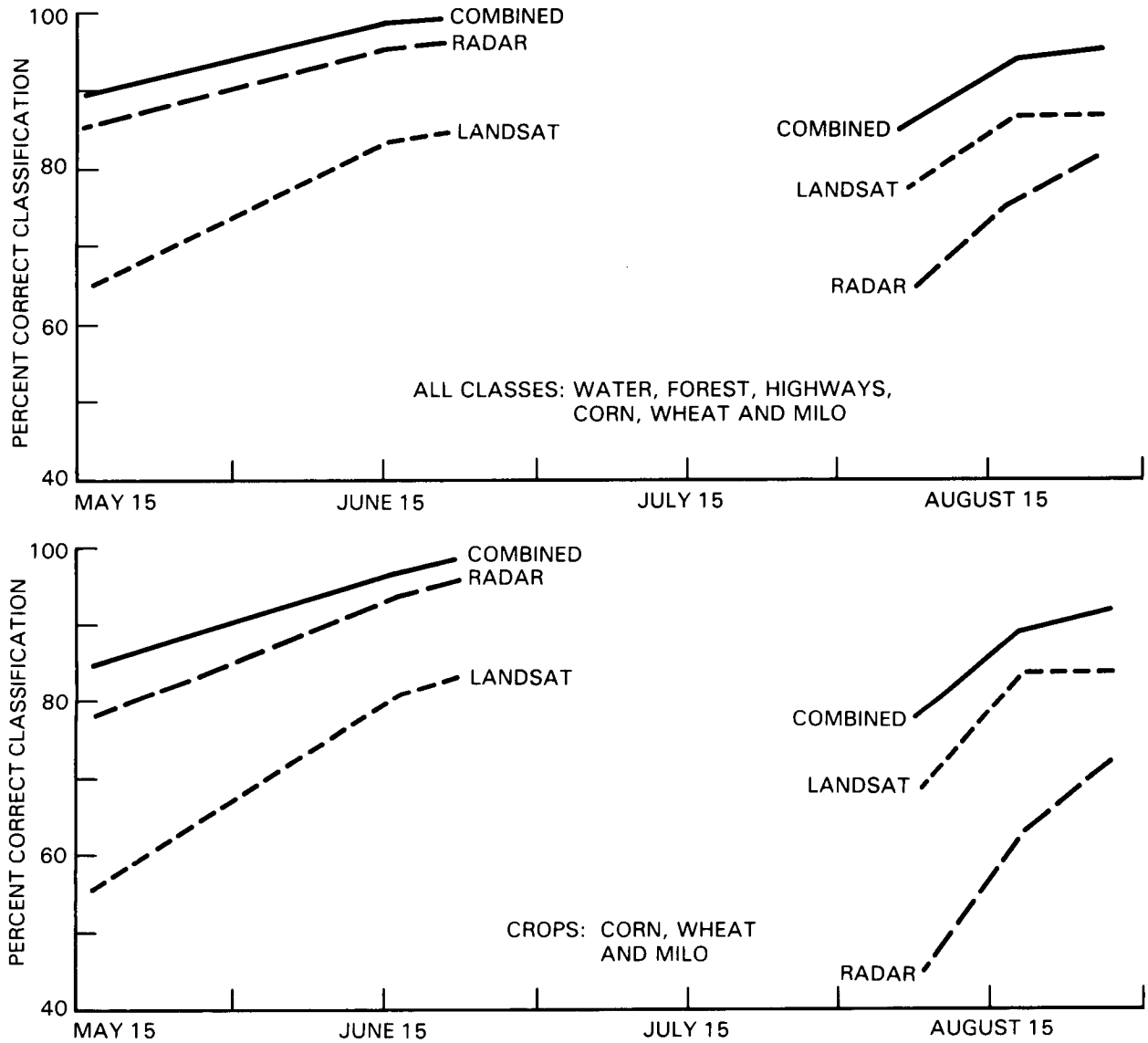

Figure 31. Classification results based on Landsat (bands 5 and 7), and radar (14.2 GHz, VV, and HV) observations of a test area in eastern Kansas (Li *et al.*, 1980).

over a 4-month growing season in the case of crops or a 12-month season in the case of mixed deciduous and coniferous forests. This requires that the Eos SAR be radiometrically calibrated, both on an absolute scale (e.g., for comparison of multifrequency and multipolarization values for a given study site location and for use with SIR-C/X-SAR, ERS-1, and JERS-1 data sets provided that they too are absolutely calibrated) and on a relative scale (e.g., for comparison of image intensity of a given location over a growing season and for comparison of high and low incidence angle data). This means that the SAR must exhibit good stability over a period of weeks to years in transmitter power, antenna gain, and receiver gain. A relative calibration of ± 0.5 dB temporally for 15 years and spatially over the globe is required; an absolute calibration of ± 1 dB is desired for LAI measurements. Good cross- and along-track radiometric fidelity within a scene is also required. This ensures that the image intensity at the center of a scene can be quantitatively compared to the image intensity at the edge of a scene. It is desired that processed SAR images exhibit cross- and along-track radiometric fidelity to a fraction of a dB.

Viewing Parameters

Incidence and Azimuth Angles

Data should be acquired at a minimum of two incidence angles, preferably 20° to 30° and 50° to 60°, such that surface and upper canopy scattering components may be separated. Multiple azimuth angle data are desirable for agricultural canopies and plantations such that row effects may be eliminated. In addition, day/night data should be acquired at the

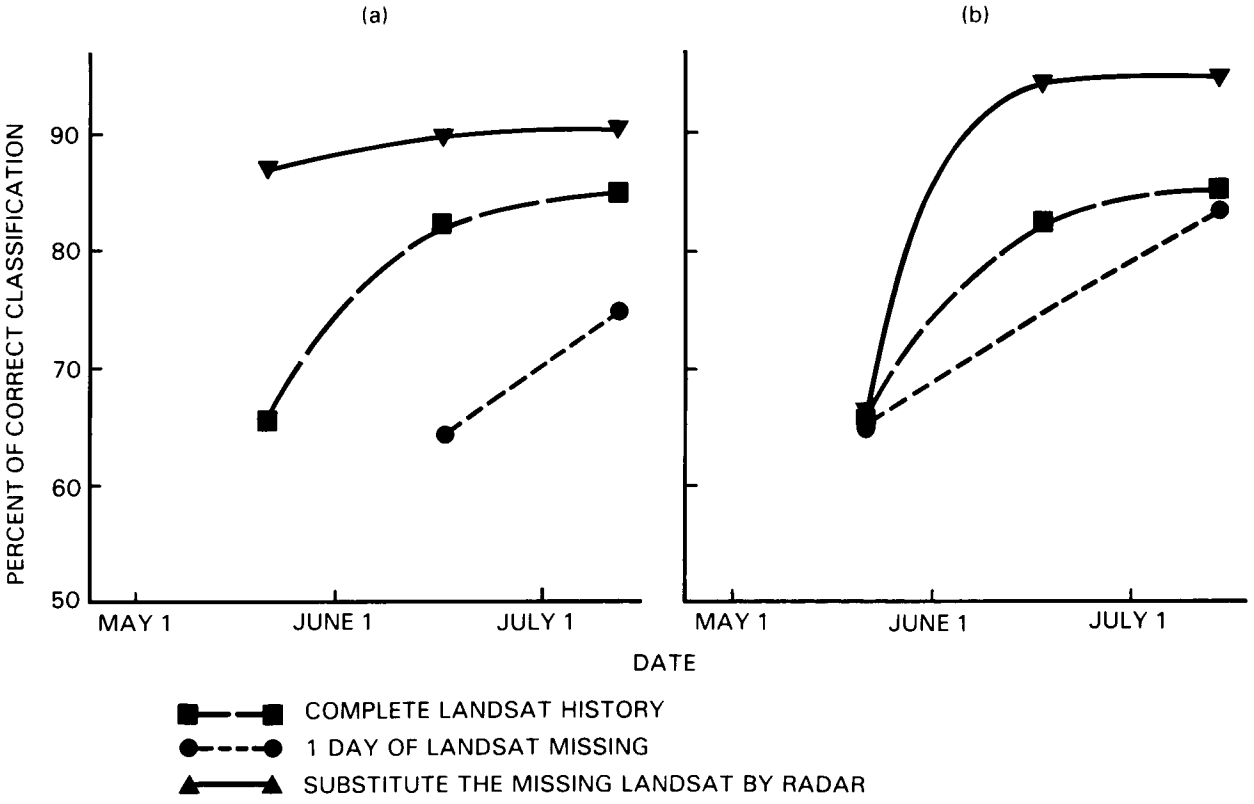

Figure 32. Simulations replacing missing Landsat data with radar data in a multidate classification (courtesy of F.T. Ulaby, University of Michigan).

same azimuth angle such that any azimuth angle effects can be eliminated. This will require a squint on either the ascending or the descending pass of a day/night set.

Resolution

The ESSC recommends two types of coverage for Eos vegetation studies: (1) continuous global coverage with approximately 1 km resolution and coverage two times per month, and (2) high-resolution coverage (30 m pixels) of selected regions within the globally mapped regimes on a more frequent basis. In addition to these general requirements, resolution selection will be based to a large degree on spatial variability within a scene.

Swath Width

Three viewing modes are recommended for vegetation studies: (1) a global mapping mode with 500 m resolution (at least 16-look averaging) and a 700 km swath, (2) a regional mapping mode with 100 m resolution and 100 km swath to be used within large biomes that are undergoing rapid change, and (3) a local high-resolution multichannel mode (4-look averaging) and a 30 to 50 km swath (see cover images) for detailed studies within a biome. The global mapping mode would be used with a minimum number of simultaneous SAR channels (typically one or two) and should provide nearly complete coverage. Data acquired in this mode would be used to select sites for more intensive regional mapping and research mode coverage with narrower swaths, higher resolutions, and more simultaneous SAR channels for extraction of detailed information about canopy morphology and biological parameters. Coverage in the regional mapping mode and the research mode could be along transects that cross the major environmental gradients.

Revisit Times

The revisit interval for the global mapping mode should be weekly and for the research and regional mapping modes every 3 days (for periods of rapid phenologic development or environmental change) to 30 days (for areal extent monitoring). The global and regional mapping modes would be used to define regions of change; a 3-day revisit period would be commensurate with MODIS and would allow direct comparison of SAR and MODIS moderate-resolution images. The high-resolution mode would provide more infrequent but complete multichannel coverage over transects or samples to determine the details of change.

Synergism

Beyond the results of the few studies that have been conducted to date to evaluate the combined use of radar and optical data for crop identification (see Figures 31 and 32), there is no hard evidence that establishes the quantitative improvement that would accrue from the joint observations of radar and optical sensors in connection with vegetation monitoring in general. Moreover, no algorithms or models exist that can merge radar data with optical data to derive biophysical information about the canopy. For the most part, our experience has been limited to color combining of radar and optical images, with the primary driver being the generation of aesthetically pleasing and photointerpretable products. It is, therefore, critical that studies be conducted to:

- Develop models and algorithms for estimating canopy parameters on the basis of input data provided by both radar and optical sensors.
- Establish the degree of simultaneity or optimum time separation required for the optical and radar observations.

In spite of our inexperience with combined microwave/optical observations from space, there are compelling reasons based on fundamental physics for exploiting this synergism. The optical spectral response of vegetation canopies results from molecular resonances and scattering at the micrometer scale, whereas radar backscatter is from plant morphology, i.e., the geometric and bulk dielectric properties of the canopy constituents. Moreover, radar waves penetrate well into the canopy (and in some cases, all the way through it) whereas optically scattered energy results primarily from the top of the canopy. In brief, the two types of sensors are expected to provide complementary information, although a quantitative connection has not yet been defined. In general, MODIS is expected to provide the bulk of the optical data when SAR is operated in the low-resolution global mapping mode for global ecosystem studies, and HIRIS and TIMS are expected to complement SAR when operated in the research mode for specific ecosystem studies.

Synergistic SAR and MODIS data are required on a seasonal (quarterly) basis for each forest site. Synergistic SAR and HIRIS data are required on a weekly to monthly basis for forest process studies. Synergistic SAR, HIRIS, and MODIS data are desired on a semimonthly basis (monthly required) during the growing season and on a seasonal (quarterly) basis otherwise for grassland, steppe, and desert region. Synergistic SAR, HIRIS, and MODIS coverage on a semimonthly basis is desired (monthly basis required) for agricultural regions. Other ancillary data requirements include:

- Meteorological data (temperature, humidity, precipitation, wind, and solar irradiance) should be acquired by Eos sensors and by both a sparse-grid regional network with a maximum/minimum, mean, and rate-measuring capability and by intensive-grid local networks without rate-measuring capabilities at selected locations.
- Hydrologic data pertaining to soil moisture and snow depth should be obtained from other Eos sensors as well as a sparse-grid network of regional reporting stations.
- Canopy biophysical measurements, canopy-growth and phenology, canopy biomass, and leaf area index and soil-boundary conditions (including surface roughness and soil moisture) should be made intensively at selected local sites, particularly in the early years of Eos when algorithms are still under development.

Data Parameters

For baseline surveys using the global mapping mode, it is desirable to acquire as much swath as possible with decreased resolution (100 m) and a minimum number of channels (two or three). In the research mode, a larger number of channels and improved resolution (30 m) is required and swath width can be decreased to 30 km or so.

It is also desirable that all research mode images be geometrically rectified and georeferenced to a standard cartographic grid on an operational basis. All images should be available to investigators within 2 weeks of acquisition, along with documentation on radiometric and geometric calibration. HIRIS images of study sites should also be made available within this period.

A number of collateral data sets will be required to support these studies, including meteorological data, planting dates for mono-specific agricultural vegetation, topographic data, etc. These data sets should be available by investigator query through the Eos information system (Chase *et al.*, 1986).

Information Parameters

The potential of SAR for providing vital and unique information about plant canopy structure and moisture, soil moisture, etc., is based upon its ability to gather data at multiple wavelengths and multiple look angles (especially angles above 40°), with full polarization information (including the phase difference between HH and VV polarizations). Although a very solid case for the potential of SAR for vegetation measurements has been built, it rests largely upon the results of extensive field measurements of agricultural crops and forests using truck and airborne scatterometers. Only a smattering of airborne multipolarization SAR data exist (for L- and X-bands) and all spaceborne SAR data to date are confined to a single wavelength and polarization. In

short, it has not been demonstrated that spaceborne multiparameter SAR data can deliver this unique information. Although there is compelling background evidence for this unique potential of SAR, it will be necessary to acquire synoptic multiparameter multitemporal data sets over test sites before the optimum radar parameters and inversion algorithms can be determined.

The recommended observational strategy is to first acquire global mapping-mode SAR images of deforestation and desertification zones over a 10-year period; the sampling intervals would be seasonal to yearly and the objective would be to measure large-scale changes in global vegetation communities. Regional mapping coverage at approximately 100 m resolution would be acquired along biome margins and in regions of active deforestation. The second part of the strategy would use the higher-resolution research mode to intensively study the processes at selected sites; the objective would be to improve inversion algorithms for extracting vegetation type, canopy structure, biomass, LAI, and other related information, as well as understanding the local processes.

For each specific scientific objective and site, it will be necessary to acquire and analyze multiparameter data sets over periods of weeks, months, and years in order to determine the best algorithms for extracting vegetation type, extent, canopy structure, moisture, etc. For example, it is generally known that radar data at shorter wavelengths (e.g., X-band), larger look angles (e.g., 55°) and multiple polarizations are sensitive to plant canopy structure and morphology. However, quantitative extraction of this information has not been possible because no synoptic multiparameter data sets have been available. It is implicit that to the extent allowed by orbital and instrument clustering considerations, SAR data will be used with that from HIRIS and other sensors. The results of early Eos vegetation studies will be to determine the optimum radar combinations of SAR plus HIRIS data. At a later stage, joint inversion algorithms for the combined use of SAR, HIRIS, and TIMS would be developed to extract more biophysical information.

Analysis of these high-resolution SAR images of test sites such as those described earlier will require very advanced image classification and segmentation algorithms that utilize the inherent information from the multichannel Eos SAR. It is critical that these images be radiometrically and geometrically calibrated because of the very large volume of processed images; investigators will require image sets that can be quantitatively compared for temporal and spatial changes in vegetation parameters. The algorithms developed for the test sites will be used in an operational mode to monitor a large fraction of the world's biomes, concentrating on regions undergoing changes as identified by lower-resolution Eos instruments.

V. OCEANOGRAPHY

SCIENCE ISSUES

Broad Eos Science Issues

The principal goal of Eos is to understand, quantify, and predict the three main cycles of the Earth system: the hydrologic cycle, the biogeochemical cycle, and the climatological cycle. The ocean is a key element in each of these three cycles. Through its large heat capacity, the ocean stores a major portion of the heat content of the Earth system and reduces the temperature extremes, creating a habitable environment for life. The ocean is also the water reservoir for the Earth. Through circulation, evaporation, and precipitation, the ocean regulates the Earth's water supplies. In addition to its influence on the energy and water cycles that are essential to life, the ocean itself is the living environment for marine animals and plants that constitute an important food supply for human beings. It follows that a major objective of Eos is to understand, quantify, and predict the ocean's role in the Earth system.

The ocean is a turbulent global fluid with a rich spectrum of motions on scales ranging from millimeters (small-scale turbulence) to 10,000 km (the width of the Pacific Ocean). Owing to the nature of nonlinear motion, the motions at different scales are linked both dynamically and kinematically. There is no single instrument that can observe this wide range of motion; therefore, the Eos approach must be synergistic, beginning with the use of altimeters for the measurement of large-scale geostrophic currents and scatterometers for measuring ocean surface winds that drive ocean currents. However, these two instruments are useful primarily for large-scale ocean observations. In order to understand ocean dynamics, there is also a need for observations of smaller-scale structure of ocean currents and turbulence. SAR has the unique capability to provide all-weather, high-resolution imagery of the short surface wave field (wavelengths of 1 to 30 cm) of the ocean. Variability in this field is induced by longer waves, currents, and atmospheric conditions. Properly incorporating these small-scale observations with larger-scale observations should significantly improve our understanding of the overall dynamics of the ocean.

Specific SAR Science Issues

The Eos SSC has identified a number of Earth science goals for the 1990s in the area of oceanography. Those goals for which SAR has some applicability, through its ability to sense large-scale surface patterns, are reiterated below.

- To measure the mesoscale to large-scale circulation of the ocean and acquire a better understanding of the long-term variability of the circulation
- To determine the global heat, mass, and momentum coupling between the ocean and atmosphere
- To determine the upper ocean response to thermal and atmospheric forcing, including the effects of persistent horizontal variability in the ocean and atmosphere
- To understand the interaction of physical and biological processes, including the effects of horizontal and vertical variability

Since Seasat was launched in 1978, SAR has been utilized for an increasing number of ocean applications. Although originally planned for global ocean wave monitoring, SAR has also shown promise for monitoring ocean currents, fronts and eddies, internal waves, bottom topography, and the small-scale variability of the surface wind stress (Beal *et al.*, 1981; Fu and Holt, 1982; Kasischke *et al.*, 1984; Vesecky and Stewart, 1982).

The unique information provided by SAR imagery not only on the short surface wave field but on the interaction of this wave field with circulation and upper ocean features can contribute along with other Eos sensors of the oceans to formulating answers to several of the oceanic processes listed above. With the potential for long-term coverage afforded by Eos, most of the temporal characteristics of currents, eddy fields, and frontal boundaries can be revealed by SAR under the proper wind conditions. Variability in these features that are direct means for the transfer of heat, mass, and momentum in the ocean, could be effectively combined with surface topography and sea surface temperature data to further large-scale circulation studies.

The eventual dissipation of tidally generated internal waves over shoaling bottoms is an important mixing mechanism for coastal waters and may also be important for biological production in these regions. Monitoring internal wave activities by the Eos SAR in coastal regions thus has important applications to modeling, predicting, and utilizing the coastal environment, where most of the ocean's productivity occurs.

Surface waves have important effects on upper ocean exchange processes and currents (Price *et al.*, 1987). SAR can monitor the oceanic directional wave spectra as well as provide information on the small-scale surface wind stress, both important parameters that can be effectively combined with sea surface topography measurements by the Eos scatterometer and altimeter.

OBSERVATIONAL REQUIREMENTS

Observational Parameters

The principal observational parameters of interest with SAR are the locations and boundaries of currents, eddies, and fronts, surface and internal waves, bathymetric features, and mesoscale atmospheric features (see Table 6). Each of these phenomena has both short- and long-term variability components of interest. The day-to-day changes in, for example, fronts, surface and internal waves, and atmospheric conditions would provide valuable information on the high-frequency evolution and dynamics involved within any energetic regime. The seasonal occurrence of internal waves within a region, the evolution of rings and eddies, and the gradual changes in bathymetric features are examples of long-range observations that could provide useful information on low-frequency energetic components.

Table 6. Oceanic Geophysical Parameters Observable by Eos SAR

Current boundaries
Frontal boundaries
Eddy fields
Cold water regions
Internal waves
Bathymetric regions
Surface wind field

Our understanding of the basis by which SAR reveals these various geophysical processes is only rudimentary at present, but it is clear that expressions of surface and subsurface phenomena abound in all the existing data sets from Seasat, SIR-A, and SIR-B. Furthermore, many of these expressions are uniquely observable with SAR. In the light of this accumulating evidence, SAR appears to be a valuable adjunct to quantitative altimetry, scatterometry, and radiometry over the ocean. After a brief description of SAR ocean imaging mechanisms, a discussion follows on the various oceanic phenomena that are detectable by a spaceborne SAR. Appendix D presents a short description of the principal mechanisms involved in SAR imaging of the ocean.

Currents, Frontal Boundaries, and Eddy Fields

We have compelling evidence that current and frontal boundaries and a wide range of scales of eddy fields are detectable in SAR imagery. Figures 33 and 34 are characteristic examples of the current structure and eddy variations revealed in Seasat SAR imagery within the Gulf Stream system. Note the sharp linear features, which probably represent regions of

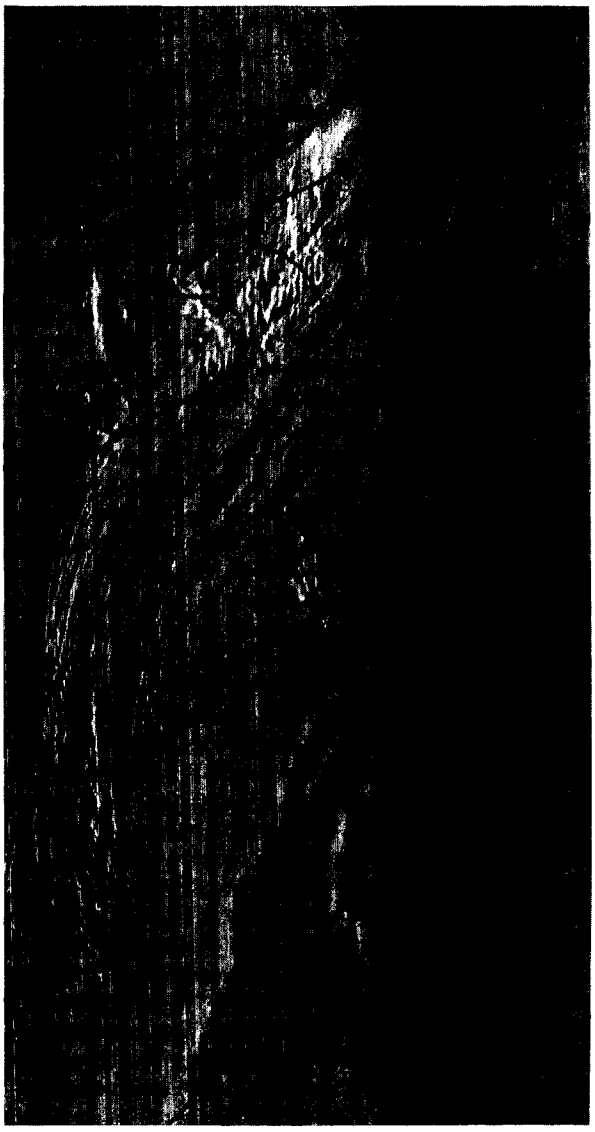

Figure 33. This image shows the Gulf Stream in the eastward deflection zone just northeast of the Charleston Bump. The bathymetric chart, superimposed on the image, shows with dashed lines the Gulf Stream boundaries derived from the Coast Guard Weekly Sea Current Chart prepared on July 26, 1978. The two prominent linear features on the image are probably signatures of the two current boundaries. Note their correlation with the underlying bathymetry. The latitude at which the current axis becomes eastward is about 32.2°N.

Note the small-scale linear striations trapped between the two current boundaries. Their wavelengths range from 300 to 1,200 m, and their long crests are more or less parallel to the current boundaries. Because these features have never been observed by surface measurements, the physics of their generation and interaction with the Gulf Stream is essentially unknown. However, a plausible account was given by Mollo-Christensen (1981), who proposed that these striations were the surface effects of the adjustment of the bottom boundary layer to changes in the interior flow.

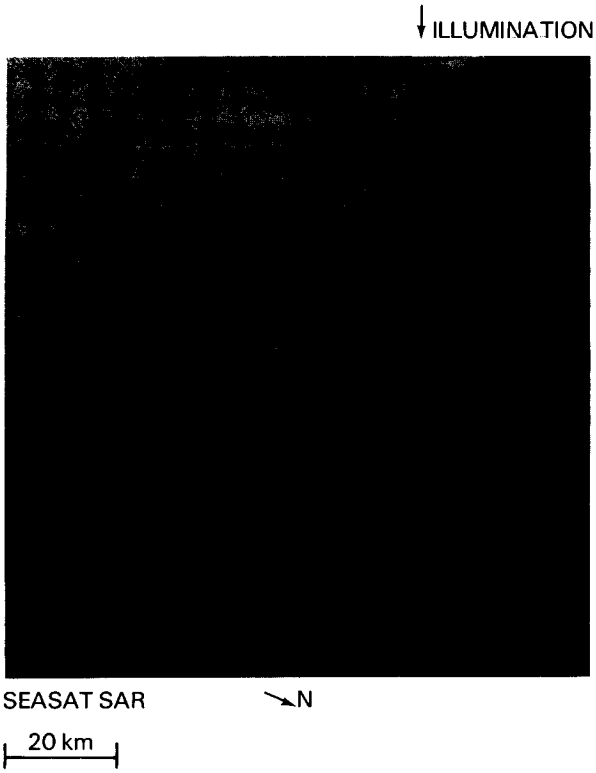

Figure 34. Seasat SAR imagery of current fronts just north of the Gulf Stream Wall (Rev. 1339, September 28, 1978).

high current shear. Also affecting the detection of currents and eddies is the sharp sea surface temperature (SST) gradient that may exist at the edge of the feature. The stability of the air flow across the gradient may be altered, in turn producing a detectable change in the surface roughness at the current boundary. Large, warm-water eddies are reliably detected on SAR (Figure 35) for surface winds up to at least 7 m/s. Like the western boundary currents, these eddies generally have strong thermal signatures as well, although the thermal boundaries may not always coincide with the SAR-observed boundaries. Smaller eddy fields have been seen in both Seasat (Figure 36a) and SIR-B imagery (Figure 36b) principally over coastal shelves (Fu and Holt, 1983; Ford *et al.*, 1986). The narrow dark bands in these two figures are most likely attributable to the presence of surfactants, although recent observations suggest that the dark bands may be associated with high current shear. The appearance of the small eddy fields is quite similar to those recently observed in the glint patterns of visible photography collected during the SIR-B mission (Ford *et al.*, 1986). Cold-water rings, such as are found just south of the Gulf Stream, generally have much more subtle surface thermal signatures, but also have been detected in SAR imagery (Cheney, 1981). Temperature fronts have also been observed (Fu and Holt, 1982).

For many regional studies, SAR could provide the only observational method for detecting circulation features. These include energetic regions that are remote and subject to extensive cloud cover that SST instruments cannot penetrate as well as regions where the surface temperature gradient across circulation features is minimized during seasonal warming, resulting in reduced effectiveness of SST instruments (e.g., the Gulf of Mexico).

Figure 35. Large Gulf Stream warm eddy observed by Seasat SAR. Narrow dimension is 100 km (Rev. 1232, September 21, 1978).

Ocean Waves

The principal use of SAR for oceanography has been for the detection of ocean waves. If SAR could accurately measure waves for direction and even height, this information could be applied in models of wind-wave forecast, which at present are generally inadequate for reliably predicting the surface-wave directional energy spectrum. Major questions exist both in properly specifying the input wind fields and in the associated growth and wave-wave interaction physics. Present theories are based primarily on directionally integrated spectral measurements. There have been few opportunities to verify and refine models with reliable measurements of directional wave spectra such as could be obtained from SAR. Consequently, many forecast models are in

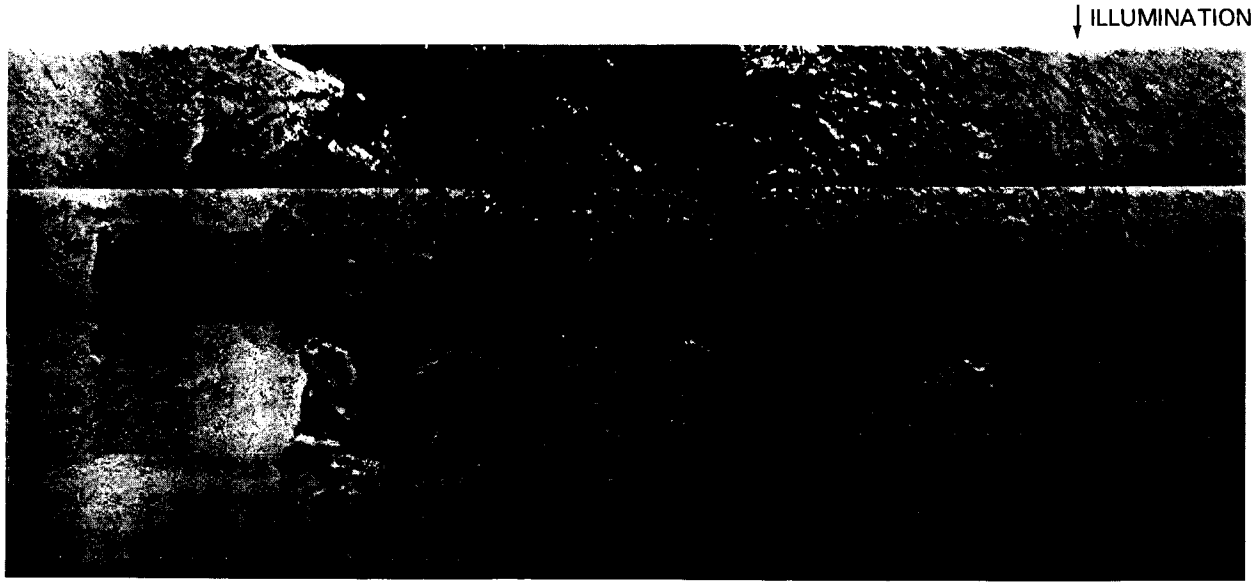

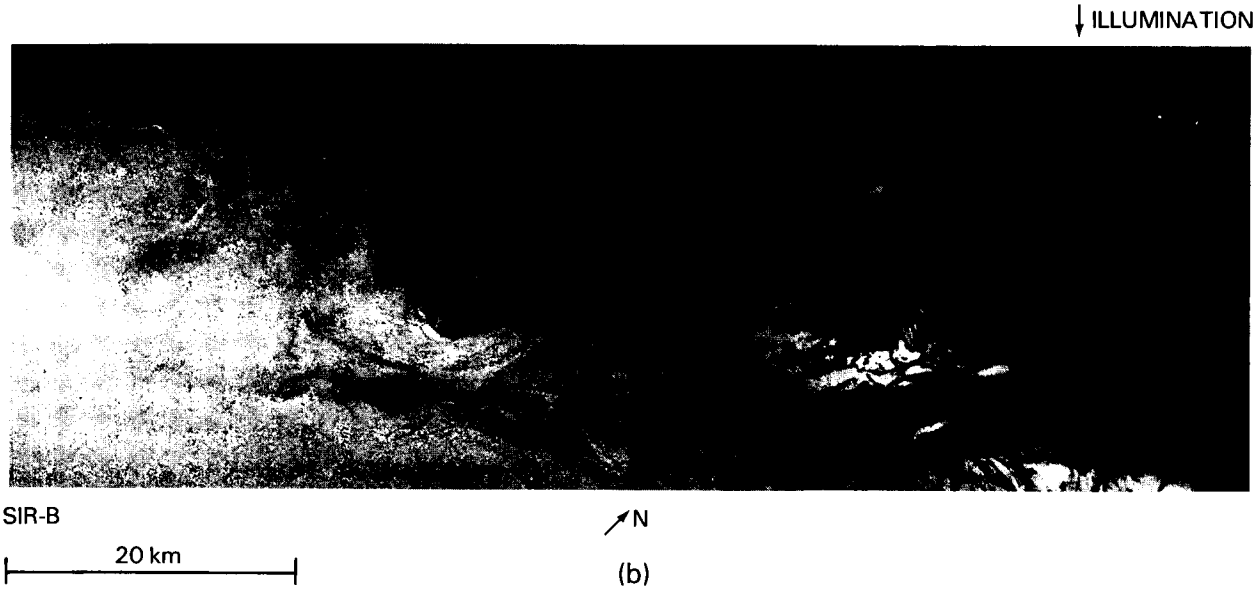

Figure 36. (a) Small-scale circulation signatures in the Caribbean from Seasat SAR, probably indicating concentrations of surfactants. Optically processed imagery. Rev. 1490, October 9, 1978. (b) Small-scale circulation signatures from SIR-B just off the U.S. east coast. Digitally processed imagery. Narrow dimension is 30 km. Data take 96.21, scene 24, October 11, 1984.

gross disagreement, especially in cases of turning or growing winds (The Swamp Group, 1985).

Long surface waves are visible in SAR imagery because they produce an apparent periodic spatial modulation of the local wind-generated 30 cm waves, as shown in Figure 37 and further discussed in Appendix D. The modulation may be much less than the noise on the scale of a single 30 m resolution element, but the spatial spectrum of the wave field is generally well-behaved and homogeneous over tens and even hundreds of kilometers. Extensive averaging over both wavenumber and space, therefore, can reduce a very noisy background by as much as a factor of 30, revealing extremely subtle modulations of only a few percent (Beal *et al.*, 1986b). SIR-B, which had a favorable altitude for wave imaging, accurately measured ocean waves (Alpers *et al.*, 1986) and produced favorable results when compared with a wave forecast model (Beal *et al.*, 1986a). However, as nonlinearities are expected to exist in wave spectra from the Eos SAR due to its higher-than-desired altitude, accurate directional wave spectra will be available principally when the waves are primarily range-traveling and/or long swell is present during low-to-moderate sea state.

However, other applications aside from ocean wave forecasting are possible. These include wave-current refraction, wave-topography refraction, and wave-ice interactions. Such applications may provide ways for determining current velocity, location of bathymetric features, and the effects of incident waves at the ice margins. Finally, some information on SAR directional wave spectra and surface winds from the Eos scatterometer will provide additional insight into the coupling mechanisms of winds and waves and their effect on mixed layer dynamics (Price *et al.*, 1987).

Internal Waves

It has been established by Seasat experience (Fu and Holt, 1982) that internal waves are among the oceanographic phenomena that are most frequently observed by SAR (Figure 38). These waves are most often observed near coastal regions with a sharp, shallow seasonal thermocline where they are generated by the interaction of tidal currents with topographic features, including sea mounts. The amplitudes of these waves are usually very large (10 to 100 m), creating strong divergence/convergence of surface currents that produce SAR signatures (Alpers, 1985; Gasparovic *et al.*, 1986). Internal waves have been detected in winds up to 12 m/s (Fu and Holt, 1984).

If properly calibrated and with accurate modeling of the hydrodynamic interaction and radar scattering, SAR images could be directly used to calculate the wave amplitude and thus the wave energy content.

While optical sensors have imaged internal waves, these techniques are of course limited by cloud cover. One comparative study using Landsat and Seasat imagery indicated that for near coincident coverage, Landsat detected significantly fewer instances of internal waves than Seasat and attributed this to Landsat viewing geometry (Rufenach and

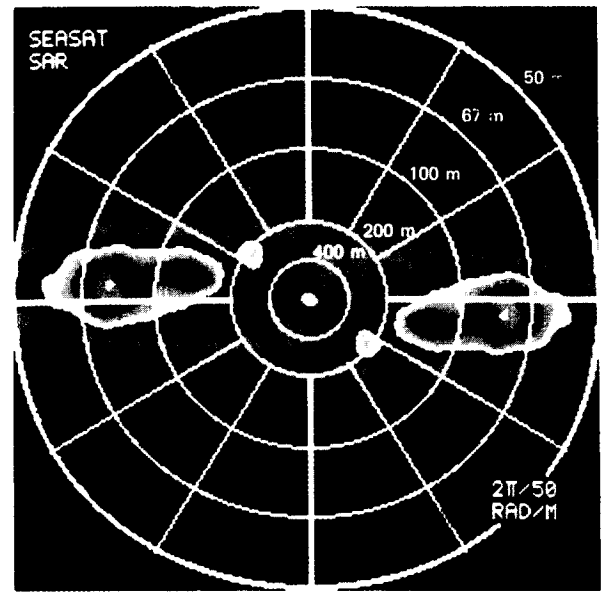

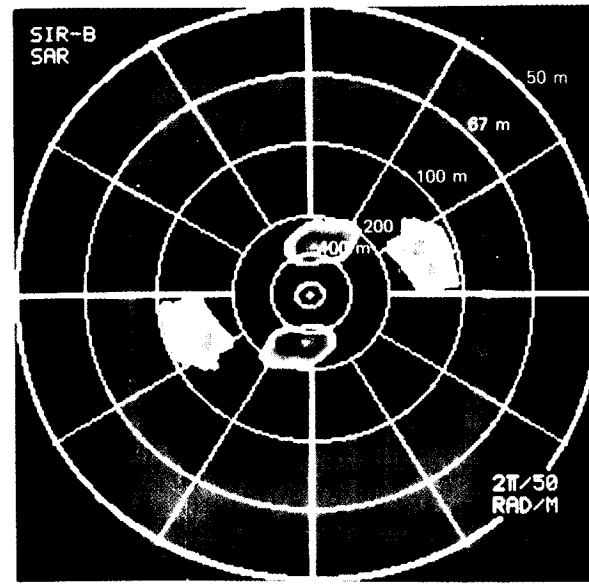

Figure 37. Comparison of typical Seasat (a) and SIR-B (b) ocean wave spectra. Note higher azimuth wavenumber response of SIR-B, resulting from improved (lower) range-to-velocity ratio (Beal *et al.*, 1986a).

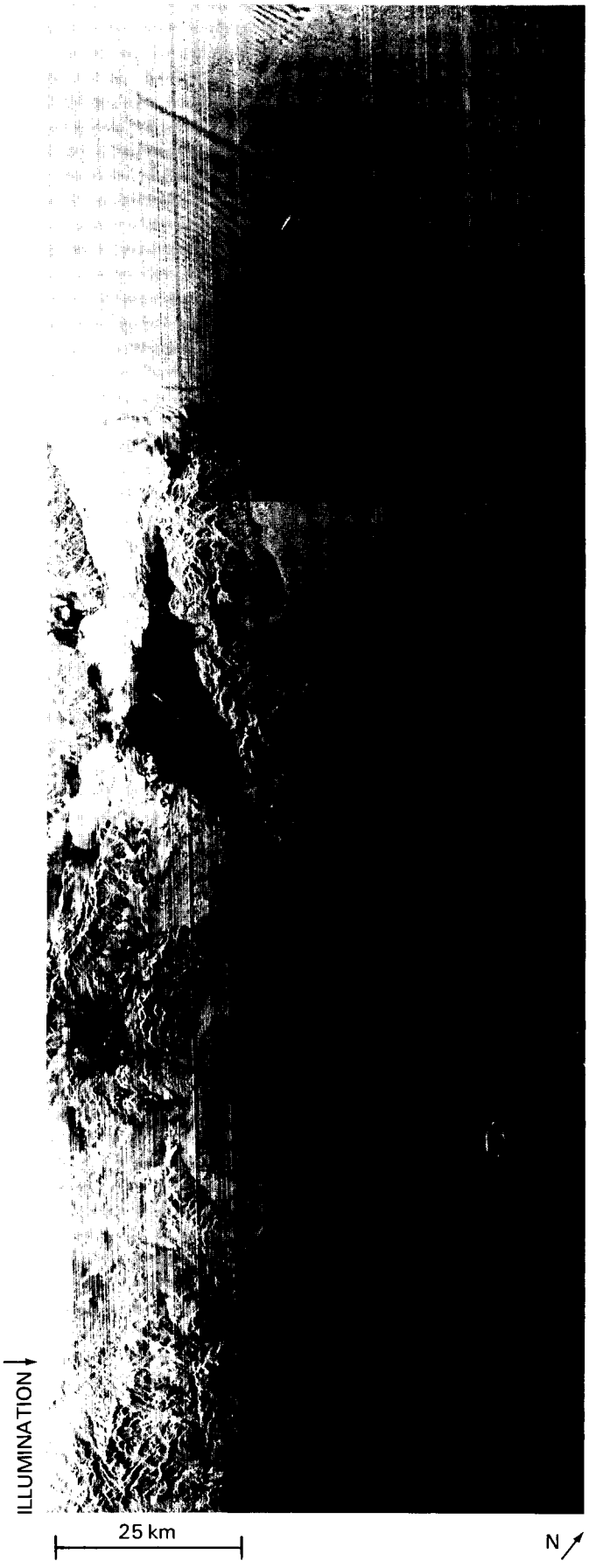

Figure 38. Internal waves in the Gulf of California imaged by Seasat SAR. Digitally processed imagery. Narrow dimension is 100 km (Rev. 1355, September 29, 1978).

Smith, 1985) rather than obliteration of waves by high winds. These results suggest that a SAR is perhaps the ideal sensor for near-surface internal wave observations.

Bathymetric Signatures

Although Seasat was able to sense bathymetric signatures in a few cases, the environmental conditions for optimum surface modulation from these features is not yet understood (Fu and Holt, 1982; Kasischke *et al.*, 1984). If reliable mapping of bottom features could be obtained, an inventory of sometimes rapidly changing shoals would be possible on a global basis. Quantitative extraction of depth information is unlikely from the actual backscatter modulation. Of more likely importance will be the observed changes in spatial structures of the signature itself over time.

Even though radar wavelengths do not penetrate the ocean's surface, imaging radars (both real and synthetic aperture) can detect bottom features due to interactions between physical ocean processes and the features, which result in a modulation of the small-scale ocean-surface scatterers (i.e., the Bragg waves) to which radar is sensitive. These ocean processes include surface gravity waves and currents (Figure 39).

There are two distinct classes of surface patterns caused by gravity waves. First, SAR can often image the surface gravity-wave field itself; from this image, estimates of dominant wavelength and direction of propagation can be extracted. The change in wavelength and direction as a wave field propagates into shallow coastal waters can be measured and used in a linear wave-refraction model to estimate water depth. This technique was demonstrated using Seasat SAR imagery by Shuchman and Kasischke (1981). Also, nonlinear interactions between the surface gravity waves and the Bragg wave sometimes result in distinct changes in radar backscatter. These nonlinear wave-wave interactions occur as the gravity-wave field propagates onto an abrupt depth discontinuity such as a reef or shoal region surrounding an island (Kasischke *et al.*, 1984).

Figure 39. Bathymetric signatures of the English Channel imaged by Seasat SAR. Digitally processed imagery (Rev. 762, August 19, 1978).

Oceanic currents flowing over bottom features are the second major cause of SAR-observed bottom-related surface patterns. The precise mechanism for the appearance of these patterns depends on the water depth. Tidally driven currents flowing over shallow-water features interact directly with the Bragg waves, resulting in a distinct surface pattern (Alpers and Henning, 1984). Tidally driven currents in deep water (>200 m) flowing over bottom features such as seamounts, ridges, shelves, and banks often generate internal waves and areas of upwelling (Kasischke *et al.*, 1984).

Surface Wind Stress

In general, expressions of surface atmospheric structure are in evidence throughout much of the Seasat imagery. These various expressions result from Bragg scattering from the wind-roughened, small-scale ocean surface waves, where a strong correlation exists between local surface winds and the spectral density of short-surface waves. The surface expression of wind rows at high sea states as well as convective patterns associated with low wind states are often seen (Fu and Holt, 1982; Gerling, 1986). SAR imagery (Figure 40) often shows spatial structure suggesting a strong relation to horizontal stress at the boundary layer. The atmospheric conditions that affect the surface roughness in a somewhat characteristic way include rain squalls and storms. The information is present on a much finer scale than is available from conventional scatterometers whose footprints are on the order of tens of kilometers. These SAR expressions of atmospheric effects may be much more ubiquitous than previously thought, and may provide insight into some intrinsically geophysical error sources in scatterometer wind algorithms.

Conventional measurements of the surface wind field are limited to single-point temporal records, which are extremely sparse for most of the ocean. The instantaneous spatial variability of the wind field might be a key ingredient to further refinement of wind-wave generation models, which usually assume spatially homogeneous wind fields.

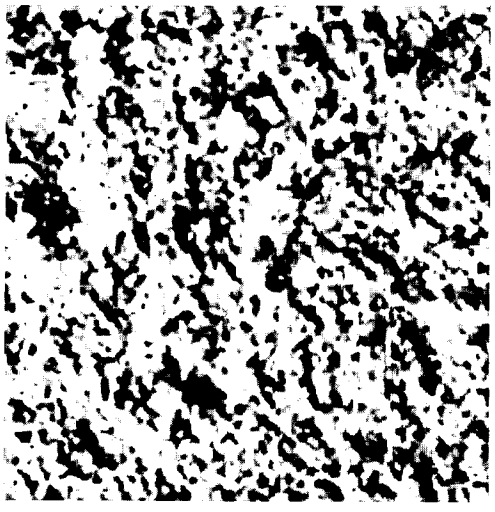

(a)

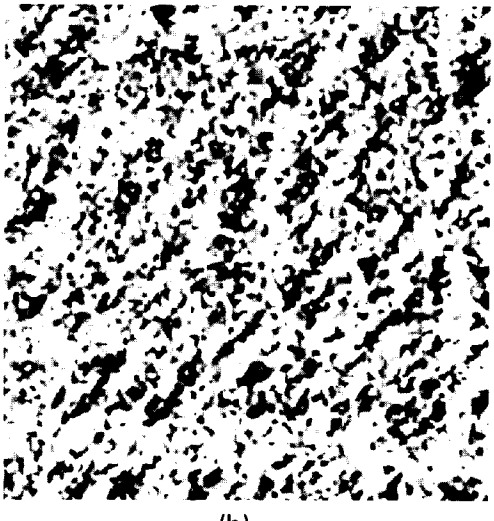

(b)

Figure 40. Two typical SAR surface expressions of wind rows, one of the many examples of atmospheric expressions found in Seasat imagery. Side dimension is 40 km. (a) Weak turning wind field; (b) strong homogeneous wind field (Gerling, 1986).

The principal Eos sensor for surface winds will be the scatterometer, which will provide 50 km resolution and 1,500 km swath. Jones *et al.* (1981) and Gerling (1986) found favorable comparisons of wind speed measurements between Seasat SAR and Seasat Scatterometer (SASS) over a wide range of wind speeds. As shown in Figure 41, the SCATT data nested with spatial variability data from the SAR will provide a better understanding of the surface atmospheric structure and associated wind fields.

Oceanographic Regimes

The data volume resulting from mapping the global oceans with SAR on a continuous basis would rapidly reach an unmanageable size. Thus, a carefully planned sampling strategy is required not only for scientific considerations but also for practical constraints.

SAR imaging of the ocean surface is a relatively uncultivated field. The information content of the imagery and its utility for monitoring oceanic processes are still awaiting a great deal of investigation. A major obstacle for interpreting Seasat SAR ocean imagery is the lack of a consistent sampling scheme and coordinated ocean observations. Therefore, the top priority in developing a sampling strategy for Eos is to identify energetic regions where resources can be pulled together and critical experiments can be performed to gain a full understanding of the imaging processes. Over these regions, time series of imagery should be acquired on a regular basis, especially within the first 2 to 3 years of the Eos mission, with a primary goal of monitoring and understanding the underlying oceanic processes and SAR imaging mechanisms.

There are two considerations for selecting the regions for monitoring. First, the regions must be rich in SAR-detectable features. Second, the regions must be of significant oceanographic interest. Based on Seasat experience, many coastal regions satisfy the first criterion. These regions are also of scientific and practical importance. Thus, a possible strategy is simply to map the coastal oceans of the world (say within 300 km from shore).

Seasat SAR imagery has suggested that features associated with strong boundary currents and energetic eddies are robustly detectable by SAR. These regions have large sea-height variability and have been clearly revealed by Seasat altimetry (Figure 42). As shown in Figure 42, such regions are of somewhat limited geographical extent. If as few as one or two of the highly variable areas are monitored reliably over a long term, our understanding of the underlying ocean dynamics will be considerably enhanced. For example, the highly variable Gulf Stream region just off Cape Hatteras is very well instrumented, and also exhibits excellent conditions in the summer for internal wave generation along the continental shelf, and should serve as one of the primary sites for multiyear Eos observations (Figure 43a). Other such regions of high variability are the Kuroshio Current region of the northwestern Pacific (Figure 43b), and the California Current region of the northeastern Pacific where fronts, eddies, and internal waves are prevalent rather than strong currents.

Many signatures of features in SAR imagery appear to be masked under winds greater than 7 to 10 m/s. The probability of occurrence of low surface winds varies with geographic location and is clearly a function of both season and latitude. Figure 44, derived from Seasat altimeter data, gives a probabil-

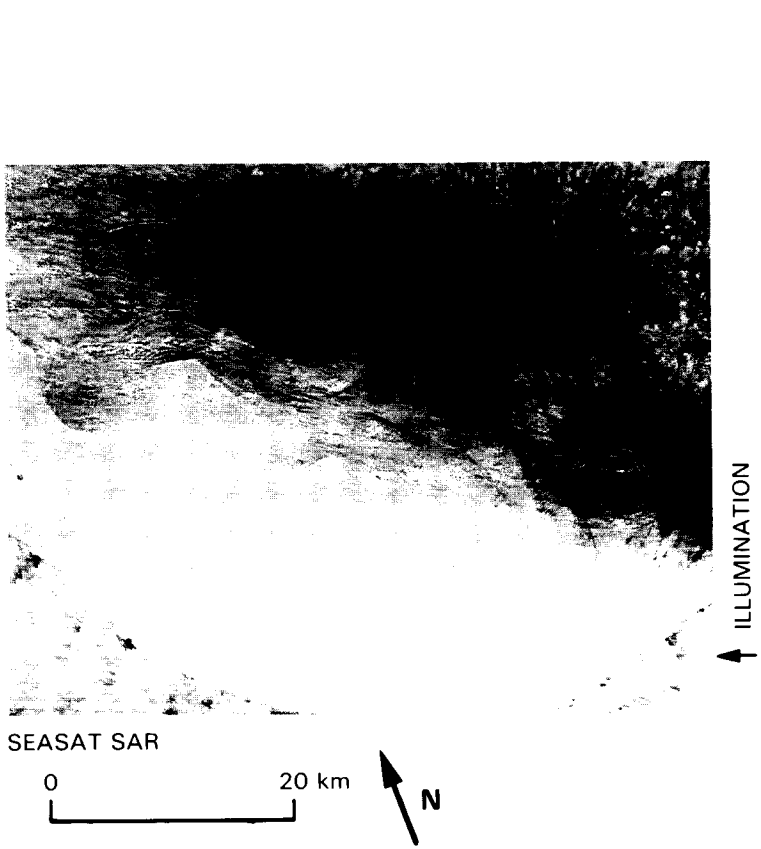

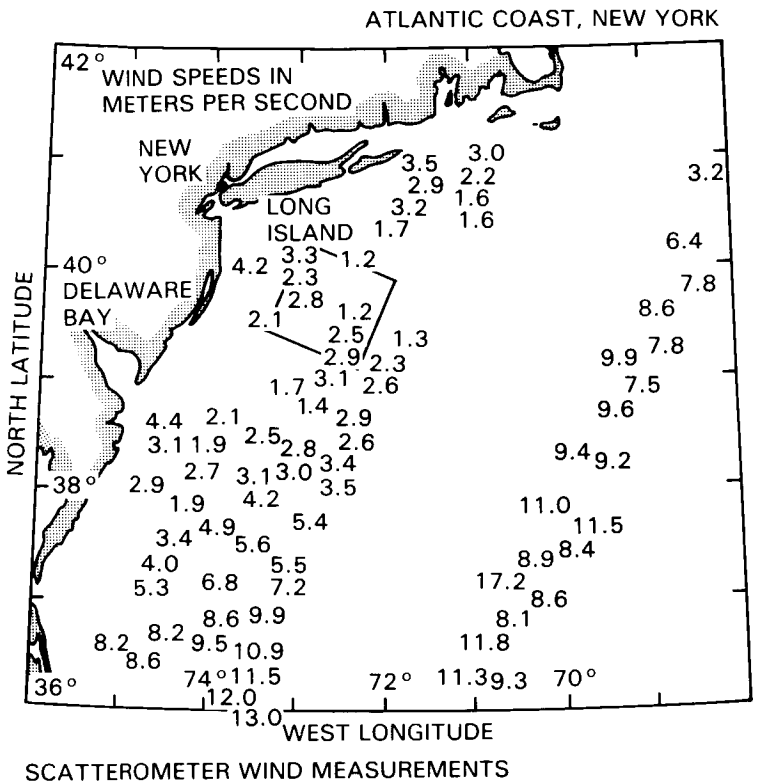

Figure 41. Seasat image of Hudson Canyon with scatterometer wind speed measurements (Fu and Holt, 1982). The area of the SAR image (a) is enclosed by a square in (b).

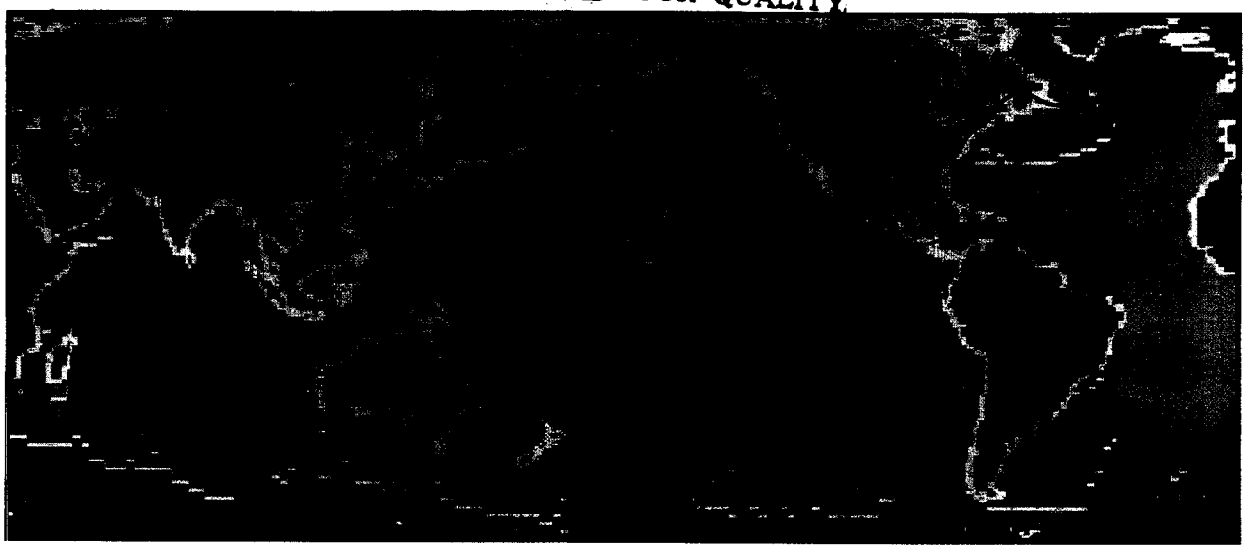

Figure 42. Variability of the global current field, as measured by the Seasat altimeter, August 1978. Most energetic are red-yellow.

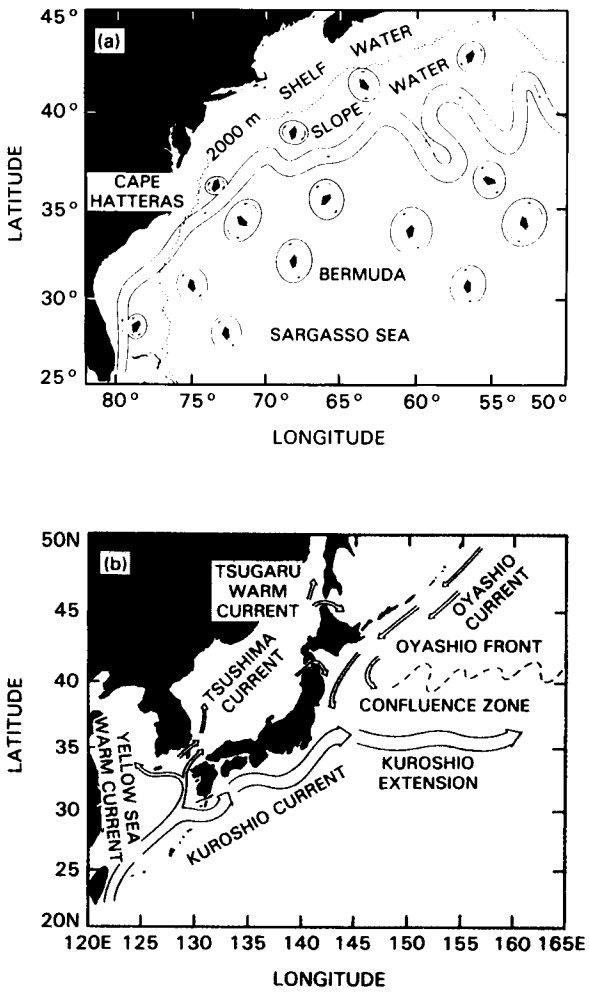

Figure 43. Schematic representation of the Gulf Stream (a) and Kuroshio Current systems (b).

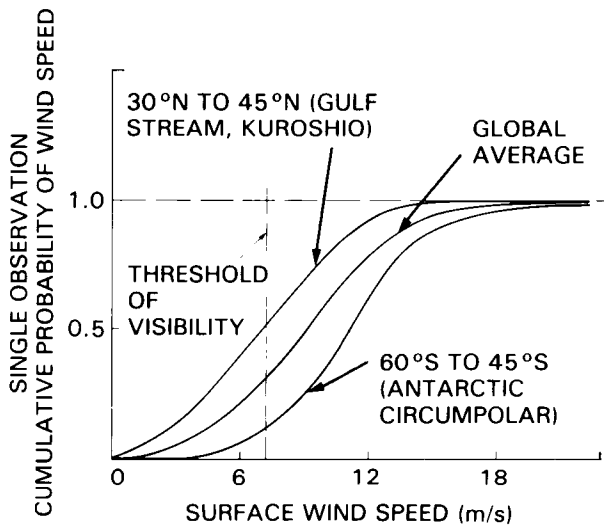

Figure 44. Probability distribution of surface wind magnitude for several key latitude bands, derived from Seasat altimeter data. Data have been corrected for biases of 20 percent reported by Mognard and Campbell (1984).

ity distribution of wind magnitude for several key latitude bands for September 1978. Winds 7 m/s or less are likely to occur several times within 16 days in the Gulf Stream region, except in restricted locales. With repeated observations, the Gulf Stream is likely to be sufficiently observable to track its dynamics in all seasons. The probability of detecting variability in other regions will vary with season and coverage strategy.

Thus, a demonstration-phase data bank would need to encompass only a few of the world's most

energetic and variable regions (see Figure 45). The resulting data could provide boundary conditions for regional circulation models yielding biweekly or monthly estimates of front and eddy locations, internal wave activity, and bottom topography changes due to recent storms. Imaging mechanisms of the various features would be intensively studied. Furthermore, appropriate change detection algorithms, for example, to preserve only current boundaries, which should further reduce data storage requirements, could also be developed and tested.

Once the ocean-SAR interaction mechanisms are well understood and the spatial and temporal observation strategies well determined, the observational regimes could then be expanded to cover additional dynamic regions of the global ocean, particularly including remote regions. Other regions could include the Agulhas-Benguela currents off South Africa, the Brazil-Falkland currents, Drake Passage, and the Northeast Atlantic and the Mediterranean, and the oceans off Peru and Australia (Figure 45).

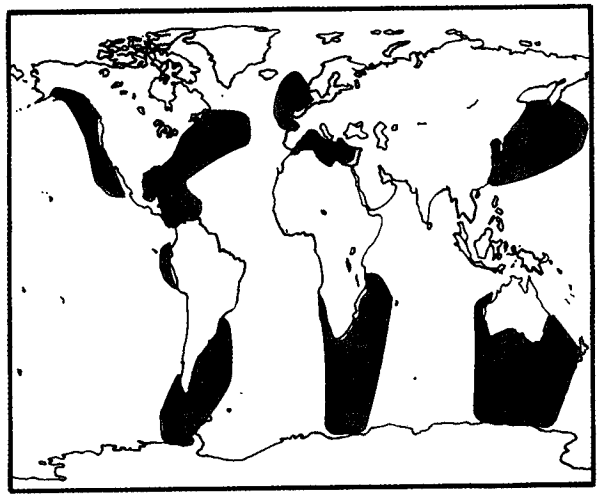

Figure 45. Map of some oceanic study sites for SAR.

RATIONALE FOR SAR OBSERVATIONS

To date, SAR has not been seriously considered for addressing the circulation problem. For examining the large-scale behavior of currents, the precision altimeter (as implemented on Seasat and the Geodynamic Experimental Ocean Satellite (GEOSAT), and planned for ERS-1, and the Ocean Topography Experiment (TOPEX), and the scatterometer (also as implemented on Seasat and planned for ERS-1) have been of primary interest. These two instruments have reached a higher level of maturation in terms of providing quantitative oceanographic data than has SAR, and both have gone through extensive phases of validation. In addition, the SAR backscatter maps cannot yet be related directly to geophysical quantities, largely because of the lack of controlled ocean experiments. Nevertheless, as Figures 33 through 36a and 36b clearly show, SAR can observe detailed structure in the circulation field over synoptic scales that otherwise would be undetectable.

Because the SAR circulation signatures are most likely related to current boundaries (i.e., regions of high shear), and only indirectly to subsurface volume flow, SAR data will be most valuable when used in conjunction with circulation models produced by and refined with scatterometer and altimeter data. In this context, SAR cannot replace proposed strategies for obtaining global circulation information, but it can certainly help to refine and extend them in combination with altimetry, scatterometry, and infrared and visible imagery. For example, the high resolution of SAR can allow monitoring of small-scale turbulence and eddies which may be a significant energy transfer mechanism. As discussed in earlier sections, SAR also can provide unique ocean observations of surface waves, internal waves, bathymetric features, and atmospheric conditions. The ability to clearly and strongly detect these features is due to the high resolution and all-weather characteristics of a spaceborne SAR. Following from this is the capability of SAR to derive highly accurate locational information from the SAR's inherent functional design and operation, an important parameter for imagery of ocean features away from land-reference points.

Previous Experimental Results

Seasat, SIR-A, and SIR-B all acquired spectacular imagery of ocean features. Seasat, however, was flown at a high altitude, which resulted in limited imaging of surface azimuth traveling waves. No simultaneous ocean experiments were conducted during SIR-A. SIR-B was the first mission where extensive ocean data were collected simultaneously with a SAR sensor flown at a favorable altitude, resulting in several studies where accurate SAR wave spectra could be compared with other surface measurements (Beal *et al.*, 1986a; Alpers *et al.*, 1986; Keyte and Macklin, 1986).

It has been possible in several cases to compare Seasat SAR data to ocean and atmosphere data collected by NOAA satellites. Although the mechanisms by which SAR detects ocean phenomena are not well understood, features in the SAR imagery can be correlated to similar features observed in the NOAA data. Such comparisons, especially in the Gulf Stream, have demonstrated that current-system boundaries, oceanic fronts, and mesoscale eddies can be detected by their influence on short gravity waves, which are responsible for modulating L-band backscatter. Internal waves in coastal oceans were also observed with the Seasat SAR, SIR-A, and SIR-B.

Geometric characteristics of internal waves in the Gulf of California were used to estimate the amplitude of the waves and hence their rate of dissipation (Fu and Holt, 1984). Bottom topography has been delineated in many SAR images, including near Nantucket Island and over the English Channel with Seasat. The influence of the atmosphere on the ocean has been observed in several cases for Seasat and SIR-B. Waves associated with hurricanes have also been measured using SIR-B and Seasat imagery.

The examples discussed above are presented in more detail in Appendix D.

RECOMMENDED MISSION STRATEGY

The mission strategy for acquisition of SAR imagery of the ocean to meet the objectives outlined above is discussed in the following sections.

Instrument Parameters

Frequencies and Polarizations

The optimum choice of Eos radar frequencies and polarizations will be better understood after analyzing images acquired by SIR-C. However, it is expected that most observations of oceanic phenomena will require only one frequency and one polarization. This expectation is at variance with most of the other land and ice applications where multifrequency, multipolarization data are useful for classification. It is possible that some oceanic phenomena will respond selectively to changes in radar frequency, but in general, optimizing swath coverage and repeat frequency by limiting multichannel requirements is preferred. It is also possible that phase and polarimetric data will provide unique new information about the ocean, however at this time the value of these modes is unclear and acquisition of data in these modes in the early Eos years will be in a research mode for limited ocean test sites. Certainly HH and VV amplitudes as well as phase data should be acquired in the research mode with user-interactive selection of the frequency band. By collecting data in an area of strong currents and current gradients, raw SAR-signal phase variations may be correlated with surface-current measurements, further exploring the potential of SAR for both relative and absolute current estimates.

Radiometric and Geometric Calibration

Good relative calibration to a fraction of a dB will always be necessary for quantitative ocean applications. This requirement is supported by Seasat SAR analysis of wind fields, which has shown a 1 dB change in backscatter corresponds to an approximate 20 percent change in wind speed (Gerling, 1986). Only with good radiometric calibration can algorithms be reliably used. Geometric calibration is also essential as the ability to accurately locate features in SAR imagery is of primary importance. In the open ocean, where reference markers are nonexistent, absolute location to several hundred meters or less is critical, especially where surface truth data are collected simultaneously with the SAR data.

Observational Modes

The Eos SAR data collected over the ocean will be principally for feature mapping. The capability to switch to a research mode will be necessary particularly to support field observations that have requirements for multifrequency and multipolarization. However, the large majority of the ocean data is expected to be collected in a mapping mode and it is this form of data that will likely be used for deriving quantitative information.

Dynamic Range

As discussed earlier, most of the features detectable by SAR, except surface waves, are masked by high winds. While not precisely known, the high wind speed cutoff is at least 7 m/s but may extend up to about 12 m/s for certain features. At the low end, wind speeds around 2 m/s are necessary in order to generate Bragg scattering waves on L-band SAR imagery. As the radar frequency increases, the Bragg waves that produce ocean backscatter decrease in wavelength and hence form under slightly lower wind speeds. The dynamic range of SAR should be wide enough (20 to 25 dB) to result in an adequate SNR at low wind speeds to produce useful imagery. The backscatter from the highest wind speeds is usually less than for many natural land targets, so saturation is presumably not an issue for ocean imagery.

Viewing Parameters

Incidence Angles

Incidence angles ranging from 15° to 45° are satisfactory, with lower-incidence angles (20° to 30°) preferred to improve SNR from the higher Eos altitudes. This small range of desirable incidence angles enables a certain flexibility in being able to image a specific ocean area more frequently than would be possible with a fixed ocean angle.

Revisit Times

The required sampling interval for oceanography depends on the phenomena to be monitored. For selected regions of intensive ocean dynamics research to be sampled within the first 2 to 3 years, approximately biweekly sampling intervals are required. However, within a biweekly period it is important to ensure nearly complete (>90 percent) coverage within 4 or 5 days. Bathymetric features, on the other hand, may be observed over a period of several months. After the first 2 to 3 years, sampling of a greater number of regions is required on a less fre-

quent period, say nearly complete coverage of a region within 4 or 5 days over a 2-week period but only two to four times a year, but again the regions and sampling frequency might necessarily be limited due to high data rates.

Swath and Resolution

To periodically map these oceanic regions of high variability, all three SAR observational modes would be used, i.e., global and regional mapping as well as the high-resolution local mode. Maximum swath, e.g., several hundred kilometers, is desirable. The regional mapping mode with 100 m resolution should be adequate to reveal principal features of current boundaries, eddies, internal waves, and bathymetric features. For surface waves, the resolution associated with the research mode would be necessary to resolve wavelengths in the 150 to 250 m range, a major component of the wave energy spectrum. These two modes can be alternated over both time and region depending, for example, on wind conditions.

Mission Duration

To provide information on the energetic interannual variabilities in the ocean (e.g., El Niño), we require at least 3 years of observation. A longer mission duration up to 10 years would ensure overlapping at least one and possibly two to three occurrences of El Niño.

Synergism

Since no single instrument can adequately monitor the vast range of motions exhibited by the ocean, the overall Eos approach to gathering oceanographic information must ultimately be a synergistic one. Oceanic circulation models require the observation of large-scale features such as geostrophic currents; an improvement in understanding of the oceanic-atmospheric interface will result from observations of small-scale features such as current boundaries, eddies, etc. A combination of fine-resolution observations of selected oceanic regions with those of other instruments with larger swaths and coarser resolution should significantly improve our understanding of the dynamics of the ocean.

How close to simultaneous must these multisensor observations be? Atmospheric effects can be expected to undergo significant change (over spatial scales corresponding to SAR swath) in hours, current boundaries and eddies in days, and bathymetric signatures in weeks. Each application, therefore, imposes its own set of constraints for simultaneity.

A SAR image of the ocean surface is essentially a map of the energy content of short surface waves that satisfy conditions for Bragg resonance with radar waves. There are numerous factors affecting the Bragg-resonant waves: winds, surface and internal waves, currents, etc. The more we know about ocean surface conditions, the better we can interpret and utilize the SAR image. To realize the full potential of SAR for oceanography, we must therefore study SAR imagery in the context of observations from other sensors collected in approximately the same timeframe.

Four sensor combinations have been identified for synergistic use with SAR: SCATT, ALT, AMSR, and HIRIS/MODIS. Each of these instruments is described in Chapter X.

SAR and SCATT

Ocean surface wind velocity is by far the most important factor determining the performance of SAR over the ocean. Because the time scale for wind variability can be as short as a few hours, SAR should be flown synergistically with SCATT in such a way that the SAR swath is nested within the SCATT swath and data are acquired within 1 hour of each other.

As mentioned earlier, SAR images of ocean surface often reveal fine-scale wind variabilities associated with mesoscale atmospheric conditions providing insight into some geophysical correction sources in SCATT wind algorithms. Hence there is a two-way synergism between SAR and SCATT.

SAR and ALT

ALT provides three useful measurements for interpreting SAR observations: sea surface height, wind speed, and wave height. Sea surface height can be used to compute surface geostrophic current velocities that can be used with SAR images to study large-scale ocean dynamics. Because the time scales of ocean currents are generally longer than 2 weeks, asynchronous sampling of SAR and ALT observations is tolerable. Wave height is a unique ALT measurement that is particularly useful for interpreting SAR data to provide information on the energy of the long surface waves that interact with Bragg-resonant waves. It also provides an independent measurement for comparison with SAR-derived wave height. Because of the short time scales of wind and waves, the ALT observations should be within 1 hour of the SAR observations.

SAR, HIRIS, and MODIS

HIRIS and MODIS provide images of ocean surface in the visible and infrared channels, yielding information on temperature and color of the sea surface. However, since these instruments are affected by cloud cover, SAR can supplement the temperature observation by detecting frontal boundaries when these features are obscured by clouds or the temperature gradients are small. The MODIS information is also useful for differentiating the various complex mechanisms for producing SAR signatures of currents and fronts. It is highly desirable to fly SAR, HIRIS, and MODIS such that the swaths are

consistently overlapping on a biweekly interval within a day of each other.

SAR and AMSR

AMSR has been proposed as a multifrequency instrument that would produce data on a variety of oceanographic conditions including sea surface temperature, wind speed, and atmospheric water vapor above the ocean. The spatial resolution varies with frequency from 1 to 20 km. AMSR will be very useful in conjunction with SAR for wind speed measurements. As with the SCATT-SAR combination, SAR could provide fine-scale wind variabilities which would be useful for comparison with the AMSR wind speed algorithm. This means that SAR and AMSR should have overlapping swaths and be flown as nearly simultaneously to each other as possible. There may also be a synergistic overlap between AMSR sea surface temperature measurements (depending on frequency and radiometer resolution) and SAR, whereby SAR could delineate current boundaries not easily discernible in coarse-resolution cells of AMSR.

Wind Speeds and SAR Ocean Recording

Another mode of synergism could be incorporating wind speed from the most suitable sensor into an onboard automated design where the decision to record SAR ocean imagery would be based on a wind speed threshold measured in real time. This could reduce the amount of recorded data over ocean areas where the instantaneous wind speeds were inappropriate for SAR imaging and no ocean features would be detectable.

Data Parameters

SAR data acquisition for oceanographic studies could initially focus on regions with strong boundary currents and energetic eddies and where there is large current variability. Two regions of particular interest are the Kuroshio region in the northwestern Pacific and the Gulf Stream region east of Cape Hatteras. SAR observations would be made on a biweekly basis. One important objective would be to acquire a time-series set of calibrated SAR images of these features over a period of several years. The area of these regions is about 10^7 km^2.

Research oceanographers using Eos data will combine image products (SAR, MODIS, HIRIS) with ALT and wind (SCATT, HMMR) data and other collateral data (from buoys, ships, etc.). A high degree of investigator interaction with the data system will be required; requests will be made for (1) SAR images (for fine-scale surface features); (2) MODIS and HIRIS images (temperature and color); (3) SCATT and AMSR data (winds); (4) ALT data (current velocity and wave heights); (5) engineering and system data such as orbital parameters and image radiometric calibration; and (6) collateral data from *in situ* instrumented buoys, ships, and aircraft. The SAR data should be processed to imagery within 1 to 2 weeks of acquisition. For some observations, it will be desirable to provide these data in near-real time to investigators at remote locations on research ships or aircraft. All images must be radiometrically calibrated and georeferenced to a standard cartographic grid. SAR images acquired within a 4 to 5 day period should be mosaicked and co-registered to similar image sets acquired on a biweekly basis. The SAR image mosaics should then be co-registered to the other Eos instrument data sets and provided to the oceanographers for analysis.

Information Parameters

SAR images of the ocean are responsive to the centimeter to decimeter Bragg waves, which are in turn modulated by longer gravity waves and currents. Thus, SAR images are sensitive to current boundaries, warm-core eddies, and internal waves, for example.

The question now is how to use this spatial and temporal information to improve our understanding of global oceanic circulation features, the transfer of energy and flux between the oceans and atmosphere, and how to develop better quantitative models of oceanic processes. How can SAR images be used to provide quantitative information about these processes? The short answer is that we do not really know.

A number of detailed studies of Seasat SAR images of the ocean have provided a great deal of insight into the mechanism by which SAR responds to oceanic surface features. However, the Seasat images of the ocean were restricted to a few areas in the northern oceans during one summer season; no large-scale parametric investigations were conducted to establish a conclusive matrix of SAR sensitivity to the various oceanic features in question although a number of site- and event-specific investigations were conducted and have been reported.

If SAR detects current boundaries, warm-core eddies, internal waves, and atmospheric variability, how can this information then be used to improve our understanding of oceanic circulation processes? A central thesis here is that the Eos SAR data, acquired from specific regions of high current variability and with repeat coverage over a period of many months, can be used to form a sequential series of SAR images of these processes. This series of images, coupled with extensive *in situ* and other ancillary observations, can be used to enhance our understanding of the dynamic features of the air-sea interaction. The situation is analogous in some respects to the problem faced by astronomers, i.e., how do we understand energy and matter distribution in the universe? A great deal of understanding has been gained by high-resolution studies of individual galaxies and other stellar objects, with particular attention

to mechanisms of energy generation and distribution. High-resolution instruments such as SAR or HIRIS are not the best sensors for doing global oceanic surveys, but they may well provide the best understanding of the processes of energy and mass transfer in regions of high variability.

To make use of time-lapse SAR imagery of high-variability regions, it is important to acquire SAR images with good radiometric calibration stability over a period of months or years, which can then be used meaningfully in algorithms to derive quantitative oceanographic information.

Data processed into quantitative information results in significant reductions in amount of data and in storage requirements, since only certain types of information would be retained, such as location of current boundaries and eddies, and wind speeds averaged over a selected grid size, as examples. These algorithms could be operated routinely on dedicated hardware and designed in such a way as to provide a variety of output products during a single iteration.

Between Eos and the present, other SAR systems—such as Radarsat, the European Space Agency's ERS-1, and the Japanese JERS-1 missions—can provide extensive information on sampling scenarios, maximum wind speed threshold for detecting SAR ocean features, SAR data processing, and data flow over long-life missions. Perhaps these missions and SIR-C can produce SAR ocean data sets that are radiometrically calibrated. These data would then be extremely valuable for understanding image mechanisms under a large variety of ocean conditions and SAR parameters and for developing SAR ocean algorithms for producing geophysical ocean information.

VI. GEOLOGY

SCIENCE ISSUES

Broad Eos Science Issues

Eos is a program that seeks an improved understanding of how the Earth's subsystems (atmosphere, hydrosphere, biosphere, and lithosphere) interact with one another to control the evolution of the planet. The Eos program is motivated by the data-gathering capabilities of spaceborne and *in situ* observations and measurements. An important aspect of this strategy is the measurement of changes and quantification of the interactions between the Earth's subsystems that occur over a very wide range of time scales. Understanding and quantizing geologic processes that occur over an extremely large range of time scale will be one of the greatest challenges for Eos.

A fundamental goal of Eos is to develop an improved understanding of the processes that control the formation and evolution of the solid Earth. Both the Eos Science and Mission Requirements Working Group (Butler *et al.,* 1984) and the Eos Science Steering Committee (Butler *et al.,* 1987) have identified three broad geologic science issues: (1) the interaction between the crust and mantle; (2) the interaction between the crust, the atmosphere, and the hydrosphere (weathering and wind, water, the shape of the ocean basins, the effect of volcanism on atmospheric chemistry, and ice erosion), including monitoring of selective surface processes; and (3) general chemical evolution of the Earth. These objectives will require a carefully integrated set of multisensor observations as well as coordinated *in situ* surface measurements and observations. SAR, HIRIS, and TIMS will all play pivotal roles in this observational strategy.

Specific SAR Science Issues

The NRC (1982; 1983) has identified several areas of significant geologic importance upon which research should focus in the 1990s. These include the achievement of a global map of lithology and landforms and an understanding of the processes that created these and that currently modify them. An improved understanding of global crustal structure, tectonics, and tectonic history is imperative to this goal. Only with a historical perspective of crustal evolution can the present tectonic configuration be understood and used to anticipate future geologic activity.

A thorough understanding of the processes that change the face of the Earth and a global characterization of geomorphologic and physical geographic features is essential to monitoring global change. Here too, a historic perspective is critical to analysis of present status and to anticipation of change. Key areas of surficial geology research interest in the 1990s include glacial and periglacial geology, including permafrost development/retreat; volcanism and global volcanic activity; coastal geomorphology and processes; arid land geology and desertification, global soil distribution, and soil erosion. Clearly the complete characterization of any of these topics is closely interactive with the hydrologic, vegetation, atmospheric, or climatic setting or to a combination of several of these. The discussion of future surficial geologic research foci will address the latter two as examples of the approach taken when using SAR as one tool in an integrated geologic study.

Global Crustal Structure and Tectonics

One of the most important geoscience objectives for the remainder of the century is the development of a global perspective on the Earth's crustal tectonic framework and the processes that have influenced the development of the Earth's crust through geologic time. Imaging radar has proven to be very useful for the delineation of surface indicators of tectonic and crustal activity as well as for the discrimination of certain kinds of surface lithology. Because of its sensitivity to surface texture radar imagery has been used to discern limestone from other sedimentary rock on the basis of karstic surface texture (Ford *et al.,* 1980), and to discern juxtaposing or adjacent lava flows on the basis of surface roughness (Kaupp *et al.,* 1987). The latter differences have been used both to differentiate between types of lava flow (aa versus pahoehoe) and to derive relative flow ages based upon smoothness of weathering origin.

Radar imagery is sensitive to surface expressions of the margins of discrete igneous-intrusive bodies such as dike swarms, radial faults, and other tensional features. Figure 46a is a SIR-A image of a region of the Sahara Plateau in Mali where a Precambrian gneissic basement has been widely intruded by younger granite plutons and associated dikes. The plutons form circular landforms that appear very bright on the radar image. Figure 46b is a Landsat Band 5 NIR image of the same region; the pluton outlines are moderately clear, although the dike sequences (very clear on the radar image) are obscure.

Radar imagery is also very sensitive to surface expressions of present and past tectonic activity. The neotectonic setting of the San Andreas and Garlock Faults and associated network of smaller faults was described from an imaging radar perspective by Sabins *et al.* (1980). The sensitivity of radar to topographic discontinuity (a key physiographic expression of structural deformation) has been especially useful in areas of heavy vegetation and rainfall. Figure 47 shows six SIR-A images of Indonesian structural features and their corresponding geologic interpretation. The sensitivity to landform expres-

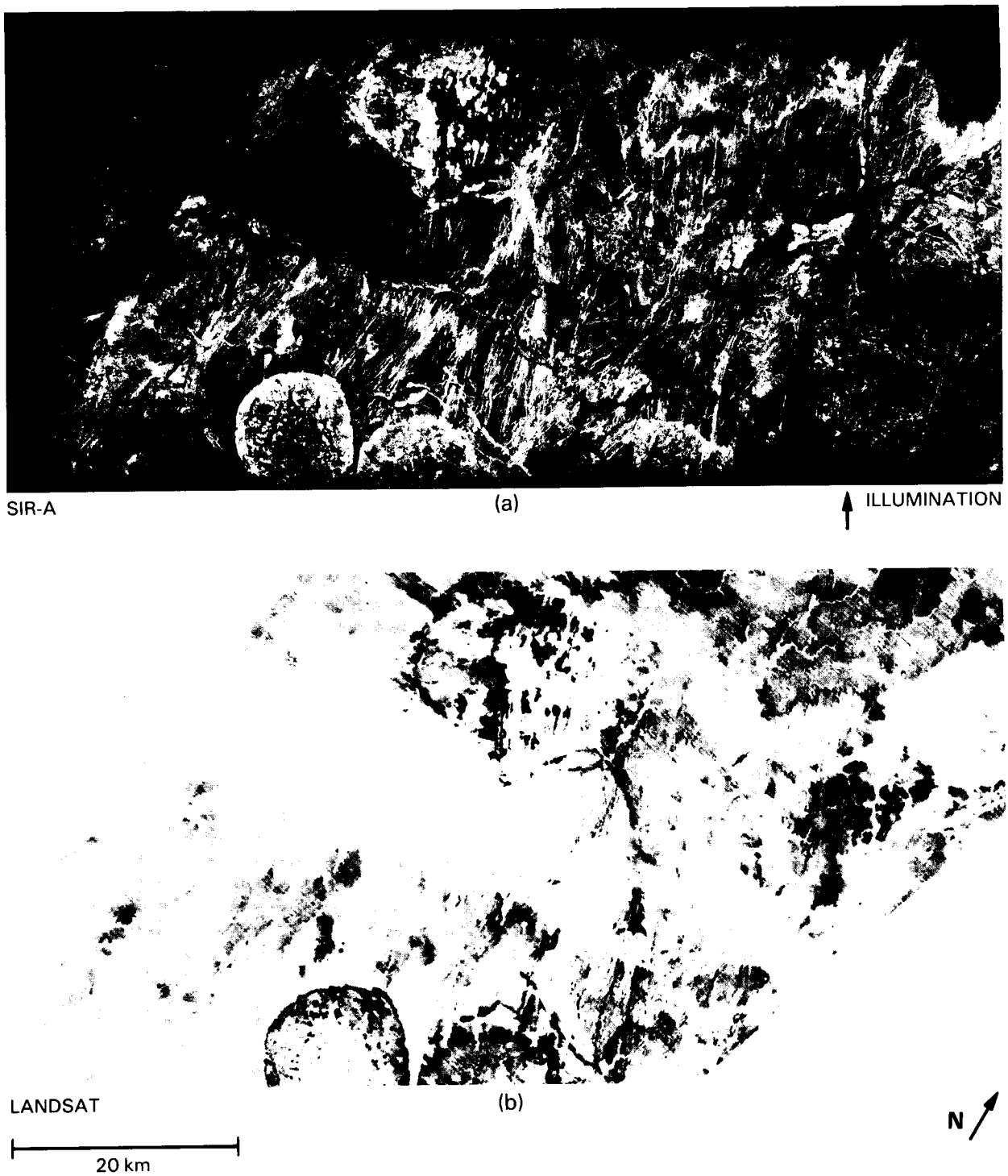

Figure 46. (a) SIR-A image of the Sahara Plateau, Mali (West Africa) (Ford *et al.*, 1983). This exceptionally arid region is underlain by a Precambrian gneissic basement intruded by younger granite plutons and associated dikes. The plutons appear very bright on the SIR-A image, particularly around their margins. Smooth level areas within the plutons are eroded cores that appear dark on the radar image. Thin, bright wavy lines through the plutons conform to the trend of adjacent dikes, which parallel the north-south regional tectonic structure in the area. Level areas of stabilized sand on the Sahara Plateau are very dark on the image. (b) Landsat band 5 near-IR image of the same region.

sions of dipping strata, thrust faulting, strike-slip faulting, and folding even in a tropical rainforest where such features are only very poorly exposed illustrates how global SAR coverage will contribute to the understanding of regions heretofore undocumentable because of difficulty of access or opacity to optical remote sensing techniques.

The maximum geologic information is obtained from radar imagery when it is used synergistically with other techniques. For example, radar stereo

viewing brings a more useful conception of topographic relief into geologic interpretation, and has even been used to construct topographic models. As another example, digital registration of SAR data allows direct comparison and co-registration with other digitally registered data such as Landsat, AVIRIS (Airborne Visible and Infrared Imaging Spectrometer), or the System Probatoire d'Observation de la Terre (SPOT). Figures 48a and 48b are Landsat and Seasat SAR images of the San Francisco volcanic field north of Flagstaff, Arizona. Figure 48c is a composite of (a) and (b) showing the enhancement of surface detail and structure. The synergism in geologic studies that combine the use of Eos SAR, HIRIS, and TIMS data will produce a powerful investigative tool.

The use of radar imagery in economic geologic exploration (the identification of potential petroleum or mineral resources) has been in effect by the private sector for over a decade, particularly in areas of persistent rainfall or cloud cover. As this century draws to a close the identification of new fuel and mineral fields will grow in importance. A global perspective on the Earth's tectonic history and present structural configuration will be essential to a more efficient assessment of the world's petroluem and mineral reserves.

Appendix E presents additional examples of radar images along with a brief discussion, including references, of some of the principal results of radar imaging techniques applied to tectonic and crustal studies.

Arid Lands Geology and Desertification

One-third of the world's land area (excluding the cold polar deserts) has severe moisture limitations. The Eos geologic information needs for these poorly mapped and economically stressed desert regions of the world are to: (1) characterize the surface and shallow subsurface geomorphic, geologic, and tectonic framework, and evaluate the potential for potable, near-surface ground water and other mineral resources; (2) assess climatic changes from the Pleistocene to the present (past 2 million years) by (a) mapping evidence of eolian and fluvial processes (erosion and deposition), (b) reconstructing weathering rates and weathering history of Pleistocene-Recent surfaces; and (3) assess the scope, rates, and geologic affinities of desertification, both human- and climate-induced.

Arid Lands Geologic Framework—Remote sensing investigations of deserts are made more difficult by the presence of pervasive mantles of eolian sand, especially extensive in the hyperarid-to-arid regions; these sand mantles commonly totally obscure characterization of the underlying materials and structures that, given the proper physical conditions (e.g., hyperaridity and less than 2 m sand depth) can be delineated using long-wavelength SAR. An example of this delineation is shown in Figure 49, which compares a SIR-A radar image (a) to a Landsat-3 Band 7 image (b) of a sediment blanket of the Eastern Sahara in northwestern Sudan. This illustrates the penetration capability of the radar, which reveals features beneath a thin dry sand cover.

This sensitivity to surface and subsurface detail is enhanced at longer wavelengths and also can be optimized by careful selection of the incidence angle. It is expected that images of arid regions from the Eos SAR L-band channel will provide important clues to Cenozoic climate changes, desertification, and critical ground water and other mineral resources.

Arid Lands Climatic Distribution and Stress—Figure 50a illustrates the distribution of semi-arid, arid, and extremely arid (hyperarid) regions of the world. Of the world's total land area of 146,300,000 km^2 (excluding the cold polar deserts), about 33 percent has severe moisture limitations. The glacier-free terrestrial area of polar deserts in the northern hemisphere is estimated to be about 4,300,000 km^2 and in Antarctica to be about 600,000 km^2 (Dregne, 1976). It has been estimated that 29 percent (27,991,000 km^2) of the world's land surface areas is characterized by no surface runoff at all (De Martonne, 1927). These regions are socioeconomically the poorest areas of the world, and are also the least well-understood geologically. An important Eos objective is to provide data leading to a better understanding of the associations between desert-forming processes, Quaternary geologic and climatic history, and the potential for development of water resources in these regions.

Climatic changes may be divided into the following types: climatic revolutions (lasting more than a million years), climatic variations (10,000 to a million years), climatic fluctuations (10 to 10,000 years), climatic cycles (less than 10 years), and short-lived usually anthropogenic changes. In those cases where short-term and long-term climatic cycles coincide, the duration of droughts may be extended (Kharin, 1985). This is the case in Africa today.

The Mojave, Sonora, Great Basin, and Chihuahua Deserts of North America, although small in comparison to the world's great deserts, cover a large area of the southwest United States and northern Mexico. The Sonora and Chihuahua Deserts are probably more than a million years old, and yet they have become perceptibly more barren during the past 100 years (Sheridan, 1981). An Eos mission of decadal duration will provide valuable data leading to an improved understanding of the impact of short- and long-term climatic cycles on desertification.

Desertification—Desertification is one of the most serious but least widely reported and researched contemporary problems of global scale. Fortunately, the long mission lifetime of the Eos suite of instruments offers considerable promise for investigating global desertification processes.

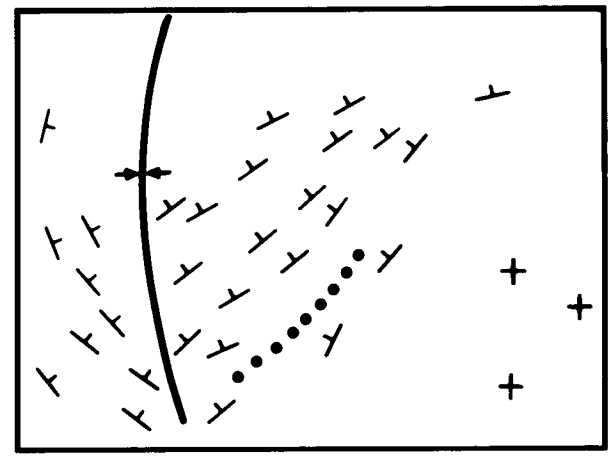

STRIKE AND DIP

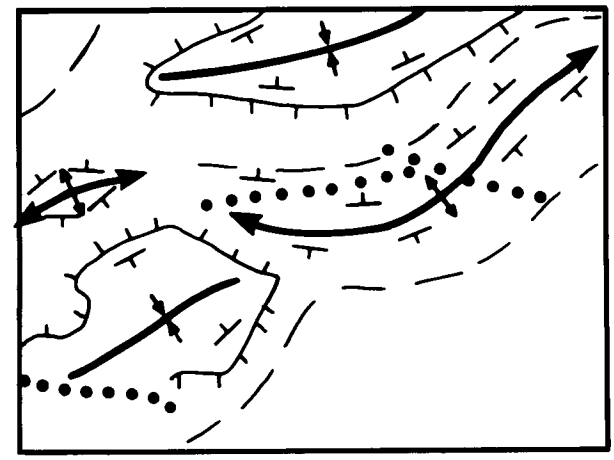

FOLDS, MODERATELY ERODED

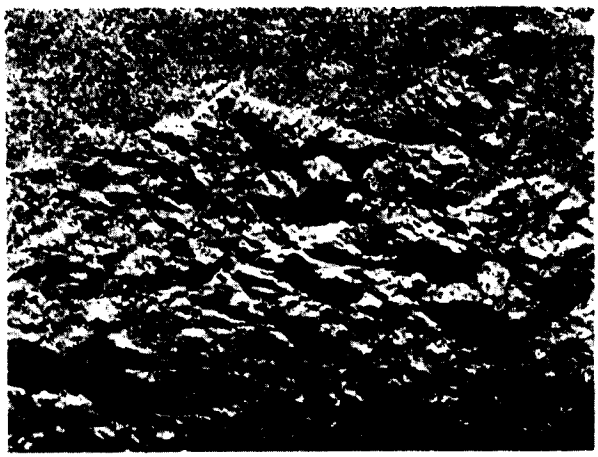

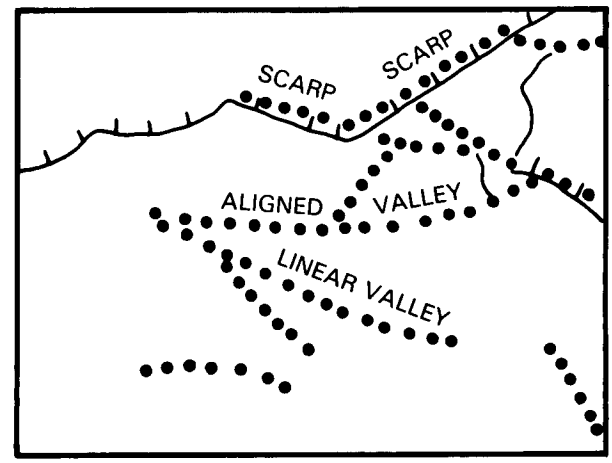

LINEAMENTS

Figure 47. (a-f) SIR-A images of Indonesian structural features. Each image is 28 km wide. Interpretation maps of Indonesian structural features are also shown (Sabins, 1983).

ORIGINAL PAGE
BLACK AND WHITE PHOTOGRAPH

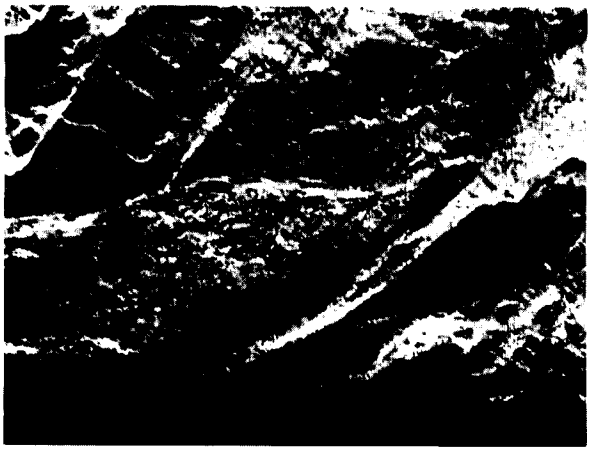

THRUST FAULTS

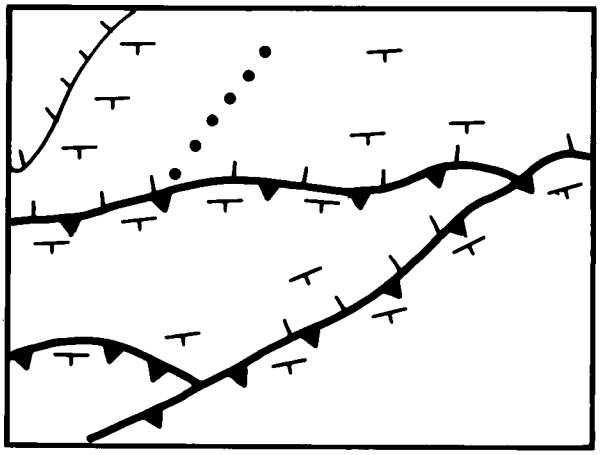

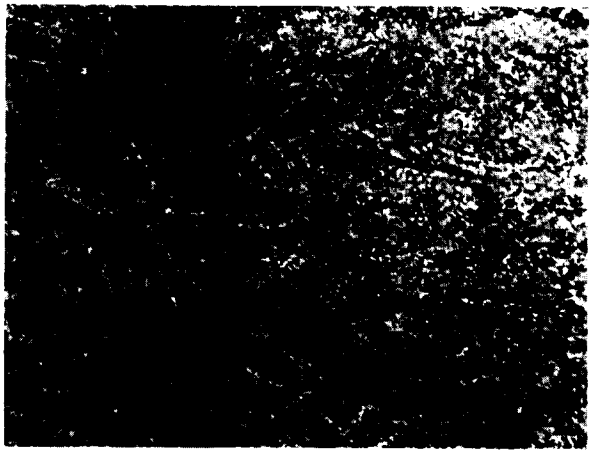

FOLDS, DEEPLY ERODED

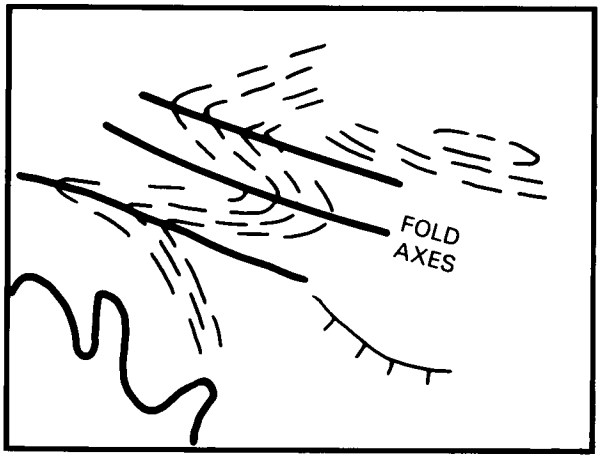

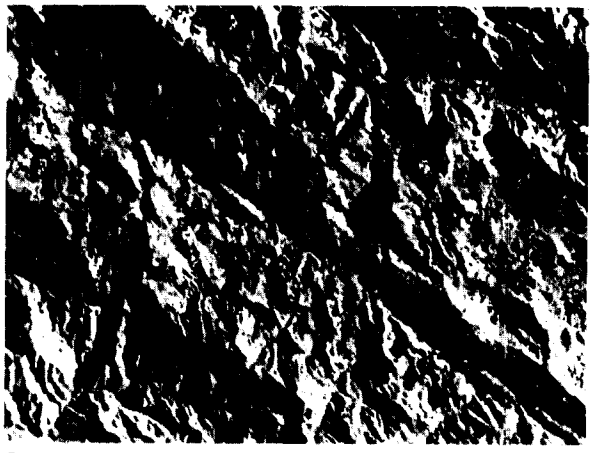

STRIKE-SLIP FAULT

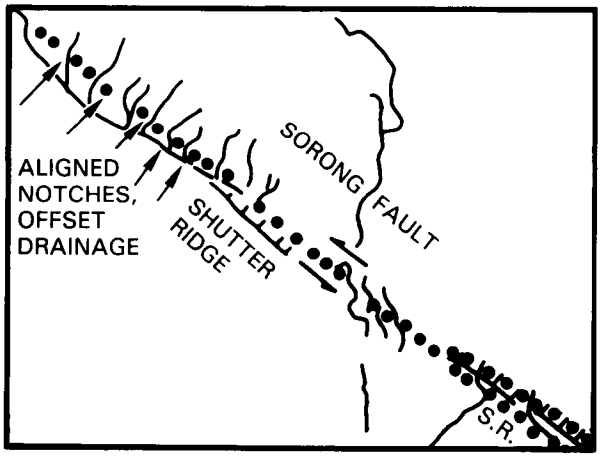

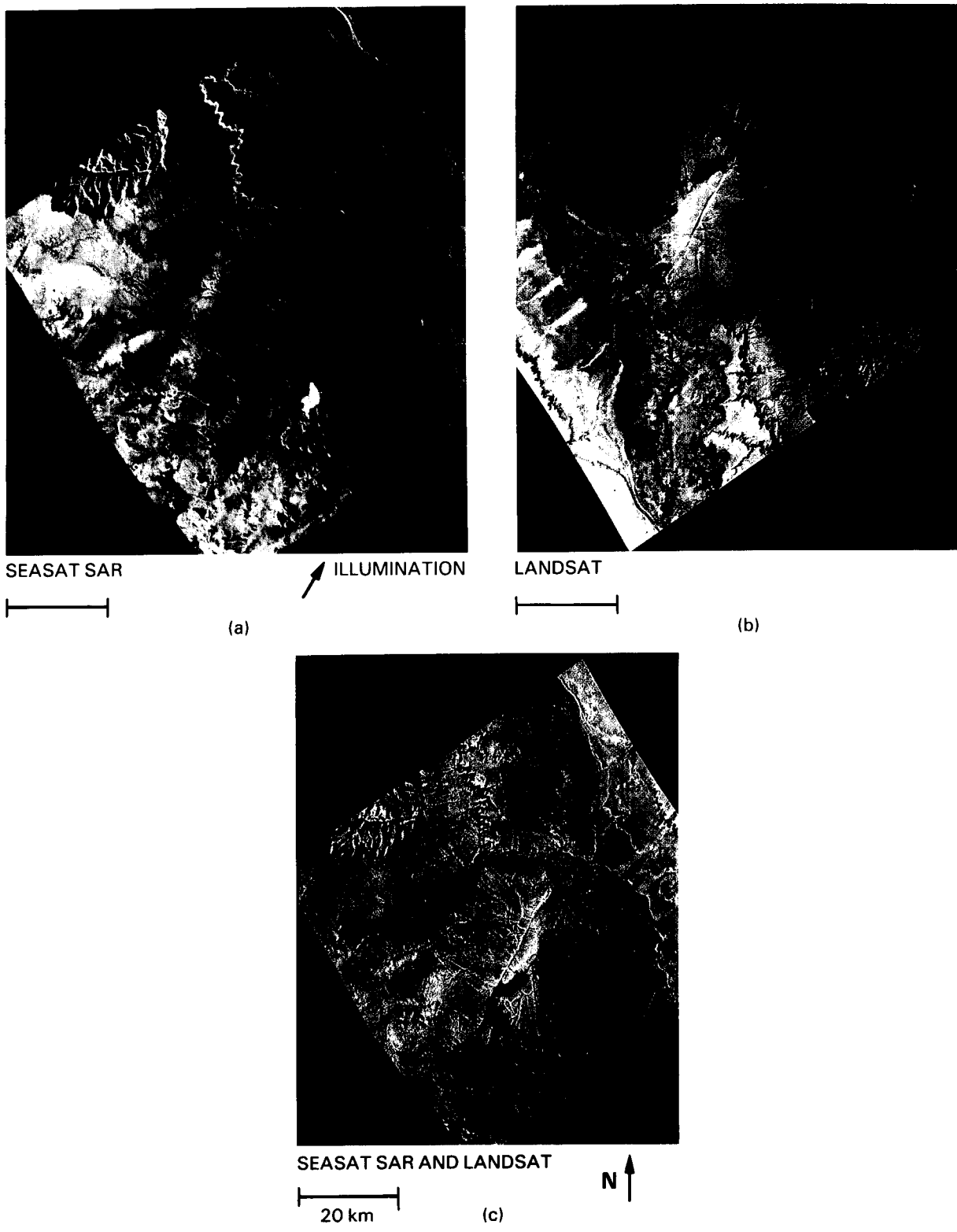

Figure 48. (a) Landsat (bands 4, 5, and 7) image of San Francisco Volcanic Field north of Flagstaff, Arizona showing the S.P. lava flow (1), the Black Point lava flow (2), and part of the Grand Canyon (3). (b) Seasat SAR image of same area. (c) Composite of (a) and (b) showing enhancement of surface detail and structure using synergism of Seasat SAR and Landsat MSS (Chavez and Sanchez, 1981).

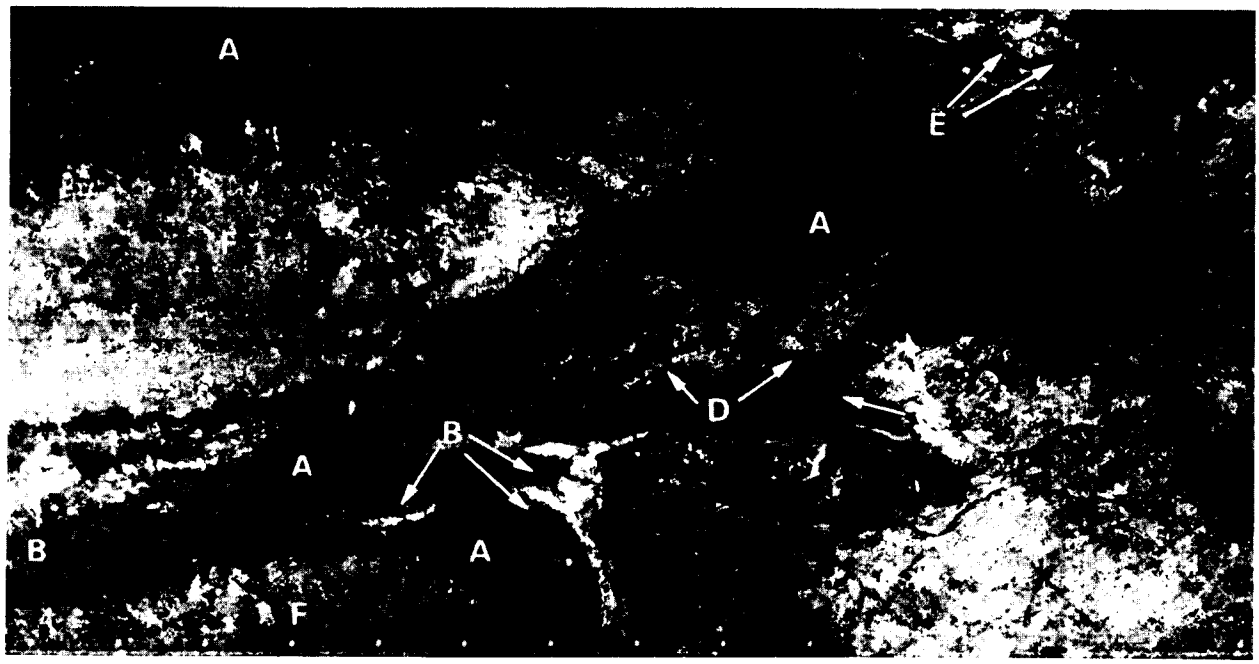

SIR-A (a)

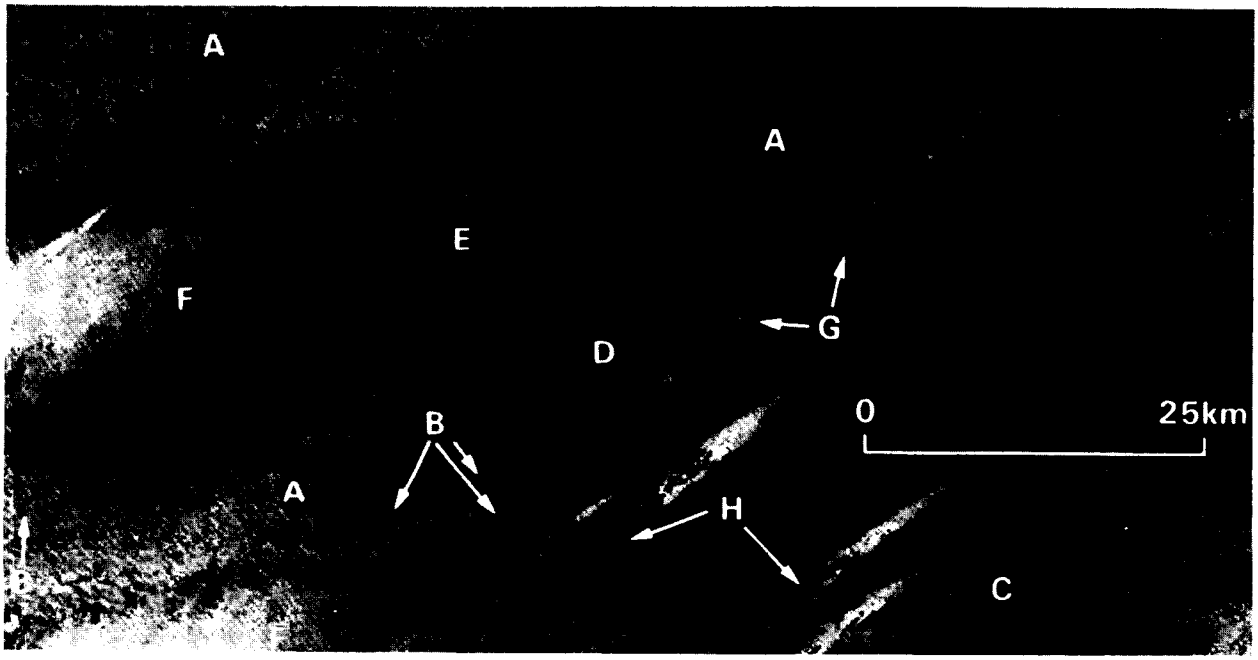

LANDSAT N (b) ILLUMINATION

20 km

Figure 49. Identical areas on the sediment blanket of the eastern Sahara (Schaber *et al.*, 1986). (a) SIR-A image, (b) Landsat MSS band 7 image. A: (dark radar response), areas of confluence of several ancient river systems. B: (bright response), grazing, stream-cut outcrops of iron-rich "Nubia Sandstone" and quartzitic sandstone mantled by thin eolian sand deposits. C: (bright response) terrace or divide mantled by thin sand; isolated outcrops and rubble of "Nubia" rocks; sinuous wadi (dark) of possible Pleistocene age (broad arrows). D: exposures of dense, ground water-deposited calcium carbonate (calcrete) within wide "radar-river" channel. E: (intermediate-mottled response), isolated grazing outcrops and blocky rubble of "Nubia Sandstone." F: (dark mottled response), low denuded interfluves of wide "radar-river" valley; densely cemented below 20 to 50 cm depth by $CaCO_3$ forming radar interface. G: (weak SIR-A return), extensive train of north-trending dunes 10 to 20 m high not penetrated by SIR-A. H: (in (b) only) longitudinal dunes 2 to 3 m high that were penetrated by SIR-A signals.

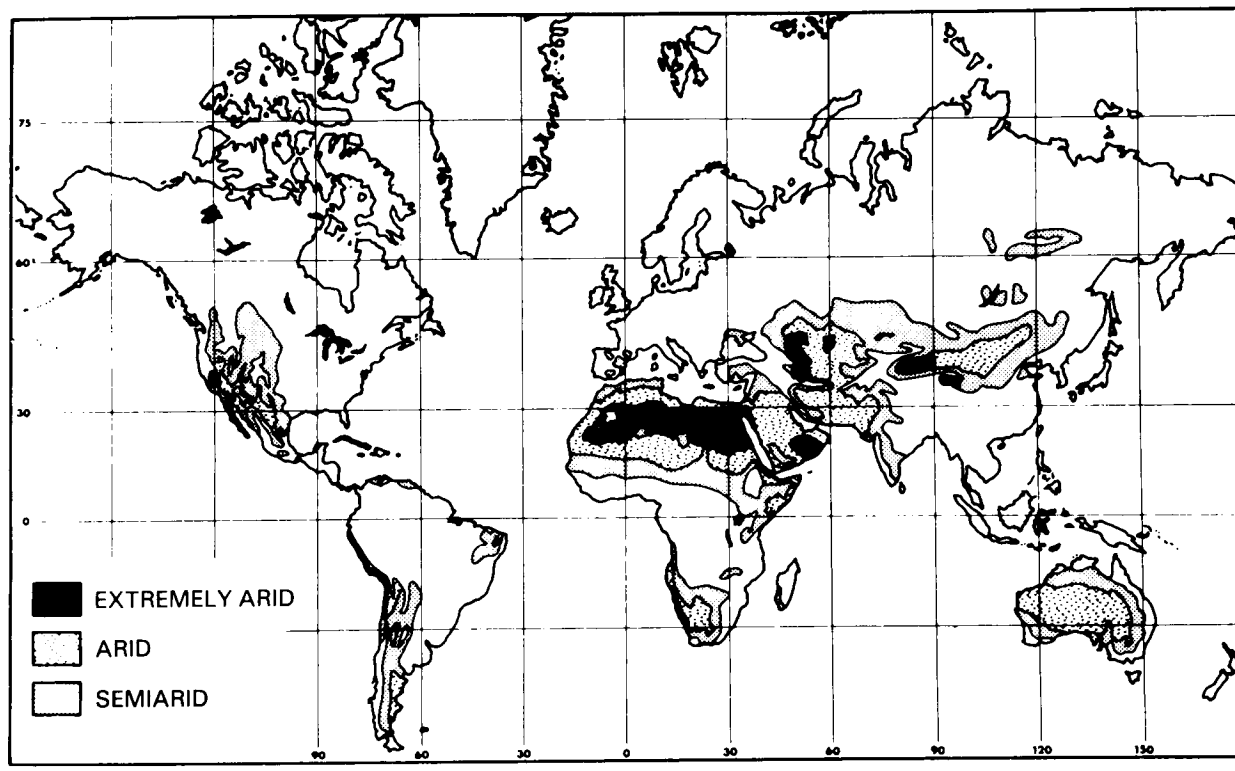

(a)

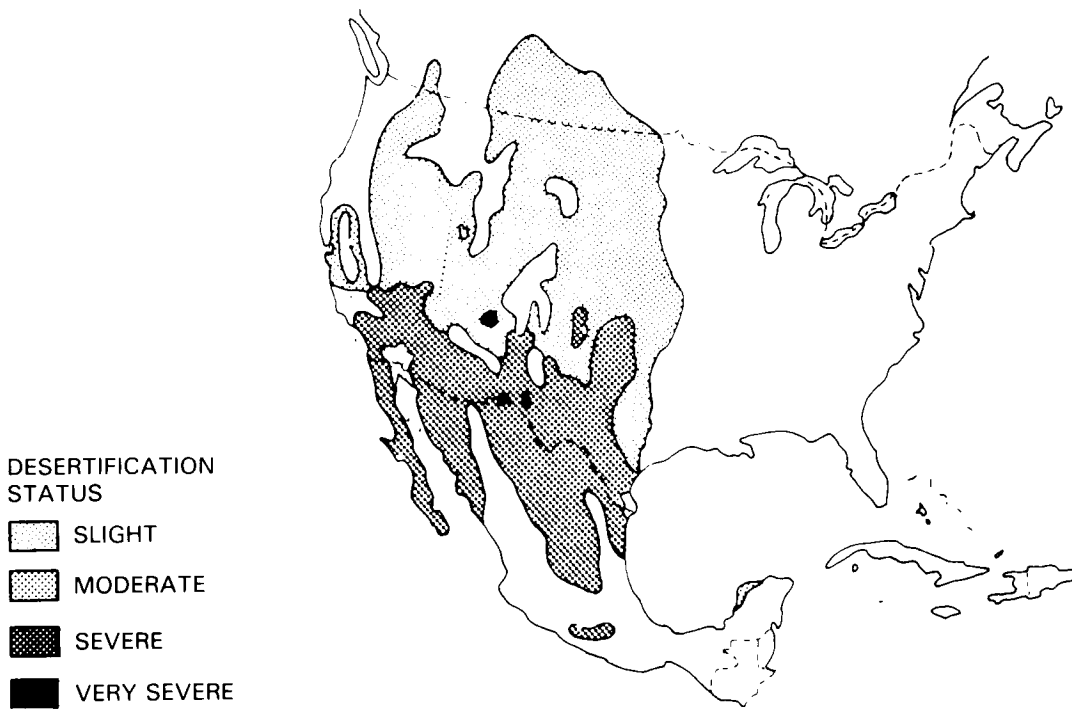

(b)

Figure 50. (a) Arid regions of the world (modified from Meigs, 1953). Polar arid regions not shown (Dregne, 1976). (b) Status of desertification in North America (after Dregne, 1977).

The simplest definition of desertification is the degradation of arid ecosystems accompanied by loss of biological productivity, under the combined pressure of adverse and fluctuating climate and excessive exploitation. Ecosystems adapted to marginal conditions in semi-arid regions are notable for their "fragility" and instability, and they react very rapidly to any interference with or change in the natural environment, such as prolonged drought or the introduction of livestock. Desertification is accompanied by the following processes: degradation of plant cover, wind erosion, water erosion, and salinization of the soil. Additionally, desertification includes reduction of organic substances in the soil, compaction of the soil-surface, accumulation of toxic compounds in the soil, and invasion by windblown sand and dust.

The overall land area affected by desertification in North America is surprisingly large, as shown in Figure 50b. It has been calculated that 12.6 million km^2, or 37 percent of the continent's arid lands, have undergone "severe" desertification and some 27,200 km^2 of the continent have undergone "very severe" desertification. About 225 million acres (10 percent of the land mass) *within* the United States have experienced severe or very severe desertification, with the actual acreage threatened by severe desertification almost twice that amount (Dregne, 1977).

Similar alarming desertification rates have been reported in the Western Desert of Egypt, where sands currently encroach on the fertile Nile delta at a rate of 13 km/year (Babaev and Orlovskii, 1981) and in the northern and northwestern deserts of China. Chinese scientists analyzing numerous historical and archeological data have shown that the 170,000 km^2 of land desertified by man over the last 2,500 years, 50,000 km^2 has been desertified within the past 50 years, yielding the alarming rate of 100,000 hectares per year (Le Houerou, 1984). The Chinese attribute these losses not to climate change but to poor land use practices exacerbated by war, and consider much of the desertized land amenable to reclamation.

The control of desertification will require coordinated international efforts. The application of advanced technology and decadal observations from Eos spaceborne sensors could provide significant help. SAR, HIRIS, and TIMS, for example, could be used to monitor the desertification process over a 10- to 15-year time period, help define the land-atmosphere-cultural processes involved, and provide a mechanism for efficient preventive measures or predictions of long-term effects.

Soil Erosion From Arable and Grazing Lands

The erosion of soil by wind is a critical problem in the United States and the world today and is rapidly becoming worse as the world population expands. Generally, soil erosion by wind is thought to be of consequence only in arid and semi-arid regions; however, it may occur wherever soil, vegetation, and climatic conditions are conducive. Wind erosion is effective when soil is loose, fine, and dry, and has little or no vegetation. In the United States this condition is best known in the Great Plains, but it also occurs in such diverse areas as the Columbia River Basin, the Great Lakes Region, and the Gulf and Atlantic seaboards. On a worldwide basis it affects lands in Africa, the Near East, most of Asia, Australia, southern South America, and much of North America.

SAR data acquired over a period of years may be very useful for detection and tracking soil erosion. The potential of the Eos SAR for soil erosion detection is related to its sensitivity to surface roughness and topography, especially utilizing its multifrequency capability. Although no long-term satellite SAR data sets are available to test the potential for erosion monitoring, there is persuasive evidence from field and aircraft data that SAR is sensitive to surface morphology at the scales of interest in soil erosional processes. Moreover, the radar wavelength provides a "window" on surface roughness scales; the Eos L-band channel will provide images of soil erosion with distinctly different textural and tonal expression than the X-band channel. All three frequency channels in combination should provide unique sensitivity to surface roughness changes due to soil erosion. HIRIS data will also be useful for studies of soil type.

OBSERVATIONAL REQUIREMENTS

Observational Parameters

The observational parameters for geological studies are summarized in Table 7 and discussed in detail below.

Table 7. Observable Geological Parameters

Surface Morphology
Land forms
Drainage networks
Structural Features
Surface
Subsurface
Erosional Features
Fluvial
Pluvial
Buried Alluvial Deposits
Desert/Arid Lands Boundaries and Gradients
Sand Dune Morphology
Drift Sand Migration

Distribution, Morphology, and Structure of Continental Crust

Eos contributions to an improved understanding of Earth's crust and mantle will require one or more global surveys at high resolution in order to establish the framework, morphology, structure, and distribution of crustal rocks on virtually every continent. As previously pointed out, SAR sensors are especially well suited for portraying morphology and structure associated with tectonic deformation of the crust. Surface morphology information from SAR is synergetic with information about petrology or chemical composition obtainable from HIRIS and other sensors.

In the context of the science of geomorphology, morphology is defined as "the external structure, form, and arrangement of rocks in relation to the development of landforms." Structure on the other hand, is defined as the general disposition, attitude, arrangement, or relative position of the rock masses of a region or area: the sum total of the structural features of an area, consequent upon such deformational processes as faulting, folding, and igneous intrusion. Two fundamental morphological attributes of landscapes are analyzed by geologists to develop geological information on the subsurface nature of the continental crust: (1) landforms, e.g., positive elements of terrain such as hills, valleys, mesas, ridges, cones, etc.; and (2) drainages, e.g., negative elements of fluvial-formed terrain described in terms of their geometric arrangement such as rectangular, annular, and dendritic. The geological information developed is used to generate geodynamical models—hypothetical constructs that conceptually explain the development of the three-dimensional crustal framework through time.

By far the most significant utility of the Eos observational capabilities with regard to crustal structure will be to develop an overall global assessment of the spatial and topographic aspects of tectonic landforms (tens of meters to hundreds of kilometers) that have resulted from eons of lithospheric deformation. The ultimate objective for Eos in this regard would be to develop and refine global and regional geodynamical models of crustal evolution that will provide critical data related to plate movements, earthquake prediction, volcanic and other geologic hazard prediction, and mineral depositional environments. Revisions of currently available geologic structure maps on a worldwide basis would be the anticipated interim products.

Arid Lands Geology

The primary objective of the arid lands experiments will be the use of SAR, in conjunction with HIRIS and other sensors, to help develop models of the Pleistocene and Holocene history of the world's larger and more arid desert regions, e.g., the Sahara. These regions, where little but eolian deposition has occurred since the late Pleistocene, are ideal for investigations of the effects of present and past climate change.

Observational requirements for general geologic assessment of the world's semi-arid to hyperarid lands include detection of sand-covered alluvial deposits (potential ground water and placer metal localities) and surface/near-surface structures (e.g., fault traces, synclines, anticlines) that might be the loci of economic mineral deposition. Maps of the surface and shallow subsurface features (perhaps obtained during both the dryest and wettest periods annually) are interim products of the arid lands geologic experiments.

Land Processes Related to Desertification and Soil Erosion

Monitoring selected dynamic land processes will be the major observational requirements for experiments associated with desertification and soil erosion. Remote sensing investigations for these specific purposes have been remarkably few considering the magnitude of these problems on a global scale. The basic difficulty has been the inability to monitor the temporal aspects of such processes, due to difficulty of access and inadequacy of available base maps, and lack of long-term remote sensing data, from which to formulate well-established strategies to address these problems. Data from the Eos orbital platforms will finally provide the required sensors and long-term observations.

Initial Eos SAR observations for this purpose will focus on the potential of SAR for monitoring subtle, slow changes in small-scale geomorphology, such as (1) migration of sand dunes and drift sand onto arable lands in semi-arid and arid terranes, such as illustrated by the L- and X-band SAR images in Figure 51, and (2) changes in surface roughness associated with wind and/or water erosion within arable lands. SAR sensors have enhanced sensitivities to the relevant scales of surface morphology (centimeters to hundreds of meters) and erosional patterns unlike any other Eos sensors. Combined with the high-resolution multispectral information from HIRIS and TIMS and a 10-year lifetime, significant Eos desertification and soil erosion experiments could be conducted with good likelihood of success for monitoring arable lands surface roughness changes due to wind or water erosion. Very high resolution will be required for monitoring the migration of sand dunes, since big dunes move only centimeters per year. Smaller dunes move faster, but may be too small to see unless the SAR is operated in a very high-resolution spotlight mode.

Geological Regimes

Figure 52 illustrates some representative geological regimes of interest for Eos SAR geology experiments. These are included mainly for estimating the yearly average data rate and data volume; other

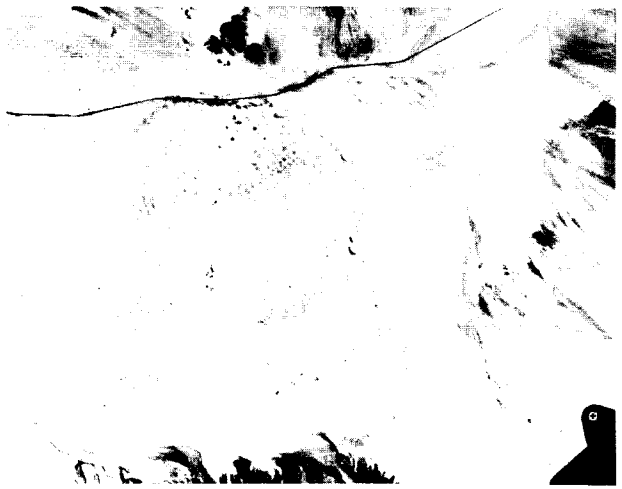

A. AIR PHOTO SUN ILLUMINATION

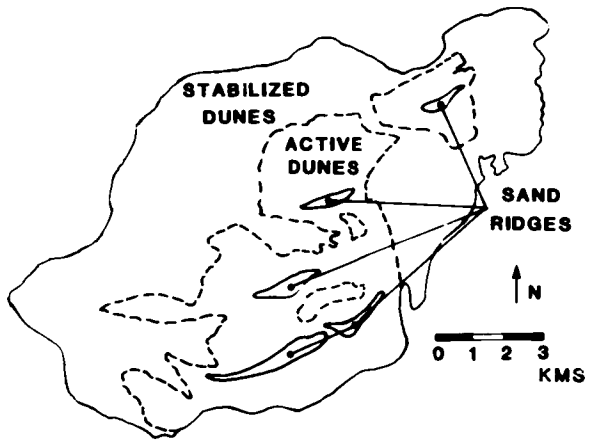

B. SKETCH MAP

C. SEASAT LOOK DIRECTION

D. X-BAND LOOK DIRECTION

Figure 51. Imagery of Kelso Dunes, California (Blom and Elachi, 1981). (a) A high altitude air photo. Principal features of the dunes are marked in the sketch map. (b) The active area consists of the large sand ridges and lesser parallel dunes. The vegetation-stabilized area consists of subdued parallel dunes and irregular dunes. Radar imagery from Seasat is shown in (c). (d) An X-band (60° to 80° incidence angle) image. Note (1) the contrast between the Seasat and the X-band images and (2) that the boundary between the stabilized area and the active dune area is accurately located by a tone change in the X-band (higher frequency) image.

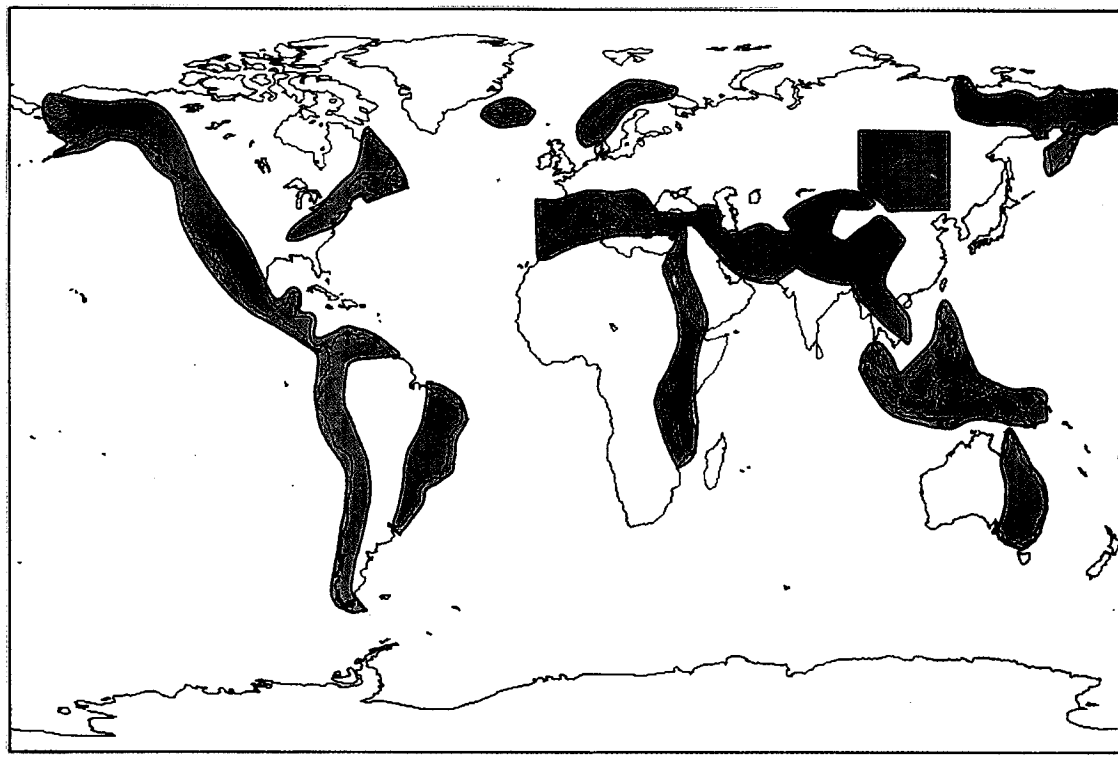

CRUSTAL TECTONICS

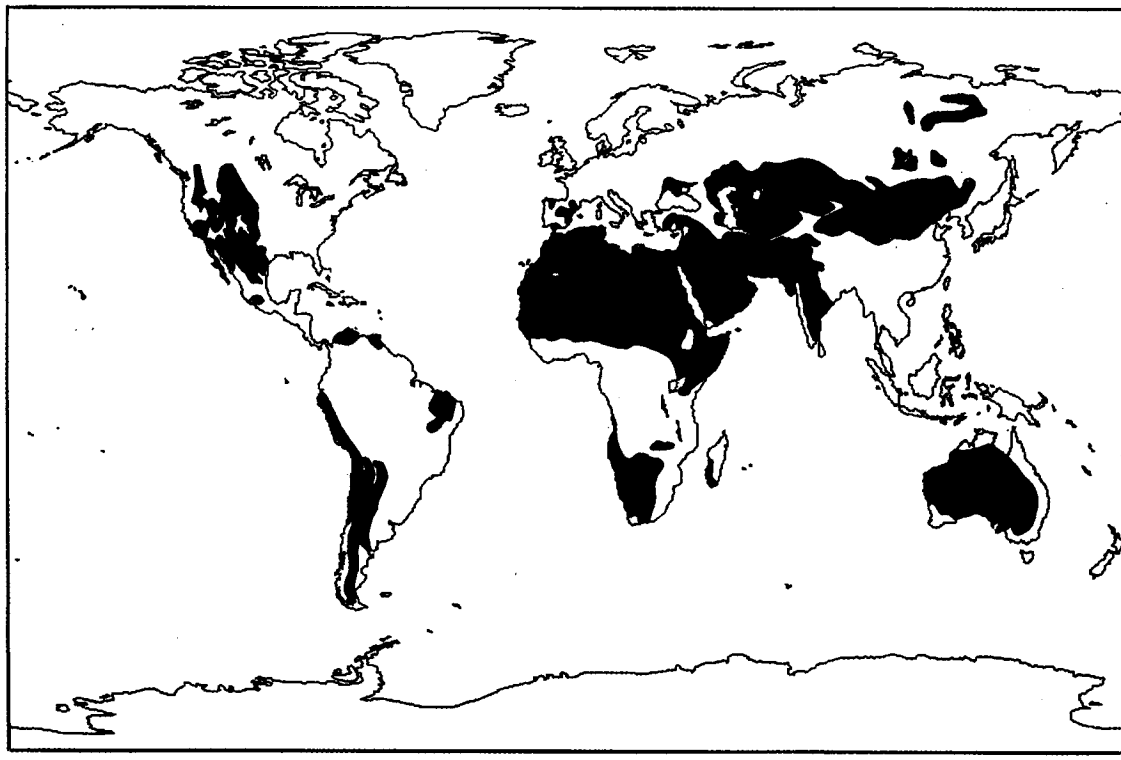

ARID LANDS AND DESERTIFICATION

Figure 52. Map of some representative geologic regimes.

regions not shown may also be of interest. The acquisition, processing, and interpretation of high-resolution SAR imagery for such large global regions will obviously require careful planning with a realistic assessment of the volumes of both image processing and image analysis. On the other hand, SAR coverage for geological processes can proceed at a much more leisurely pace than for other geoscientific studies. Once seasonal responses are recorded, repeat coverage may be required only every few years.

Global Crustal Structure and Tectonics

Areas of interest for this objective would include the major tectonically active regions associated with the edges of plate boundaries, especially where there are seismic hazards. This includes the western edge of the North American plate (3,450,000 km^2), the subduction zone associated with the western edge of the South American plate (4,150,000 km^2), the African rift valley (3,750,000 km^2), the Himalayas (5,200,000 km^2), the Alpine chains and suture, the complex microplates and subduction zones of the Mediterranean and the Caribbean regions, the Antarctic continent, and the circum-Pacific convergent plate boundaries, including those of the Aleutians, Japan, Indonesia, New Zealand, and the Andes.

Arid Lands Geology and Desertification

Typical areas of interest for arid lands geology and desertification processes would be the western interior United States; northeast Africa, including parts of Egypt, Sudan, Libya, and Chad; southwest Africa, including parts of Namibia and Botswana; and north/northwest China, including parts of the Tarim Basin and Hoshi Corridor.

Soil Erosion

Examples of areas with severe soil erosion are northern China, including parts of the Loess Plateau and Inner Mongolia, the Thar Desert of eastern Pakistan and northwest India, and the U.S. Great Plains, including parts of Texas, Oklahoma, and New Mexico.

These typical study areas are shown in Table 8, and are included here as representative geological regions. Other regions will also be of interest. However, it is useful to calculate the number of SAR images that would be required to cover these land areas. This is discussed further in Chapter VIII.

RATIONALE FOR SAR OBSERVATIONS

There are a number of strong motivations for using Eos radar data for geological studies, among them: (1) the ability to penetrate through cloud cover, particularly in tropical regions; (2) the fact that the illumination geometry can be controlled; (3) sensitivity to surface morphology; (4) longer wavelength penetration of eolian sand veneers that obscure the near-surface geological features of arid lands; and (5) the fact that the polarization and phase capability of SAR offers additional unique geological information. Some of these are discussed more fully below.

Illumination Geometry Control

Aerial photography and Landsat images have been used to successfully analyze topography and surface cover in regions where cloud cover is not a problem and where solar illumination geometry does not significantly bias the interpretation. However, in areas less than 20° latitude north and south of the equator, and greater than 55° latitude, solar illumination and cloud cover does cause significant problems. Near the equator, landscape cover is more uniform and low solar zenith angles (small-incidence angles) cause terrain to be more uniformly illuminated, thus making discrimination of topographic features difficult, without the aid of stereoscopic image data. In tropical areas near the equator, high humidity and cloud cover make observations difficult in the visible and infrared portions of the spectrum. In subequatorial and equatorial desert regions, the high specular reflectance from desert surfaces during times of data acquisition used by Earth resource satellites often poorly displays the subtle topography found in these regions. For northern hemisphere latitudes greater than 55°, the azimuth of solar illumination is more nearly from the south during the data acquisition times for Earth resources satellites. This predominantly southern illumination direction tends to enhance terrain features that have an east-west alignment. Similarly, for larger southern hemisphere latitudes, east-west features tend to be enhanced by a mainly northern illumination direction. Also, for much of the year, north-facing slopes of terrain in moderate-to-high relief areas are not directly illuminated by the sun. Above 65° north or south latitude the sun does not directly illuminate north-facing terrain in high relief. Even in the western United States, many of the major structural trends are aligned parallel to the illumination direction of the sun at the time of Landsat data acquisition. In addition, data acquired at very high incidence angles will highlight terrain topography through shadowing. Optical data, especially for sun-synchronous orbits, will not provide the desired low sun-angle highlighting. Stereo viewing of geologic features is also particularly valuable for structural interpretation.

An important capability of the Eos SAR is the ability to select the illumination geometry, i.e., the incidence and azimuth angles. Both SAR and HIRIS will have the ability to change the illumination geometry, although with different combinations of cross- and along-track pointing. SAR data has a wider total

Table 8. Representative Regions for Eos SAR Geology Studies

Objective	Region	Area (km^2)	Number of SAR Images* (single channel)
Global crustal structure and tectonics	North American plate	3,450,000	87
	South American plate	4,150,000	104
	African rift valley	3,750,000	94
	Indo-Eurasian subduction zone	5,200,000	130
	Mediterranean	3,120,000	78
Arid lands geology and desertification	Northeast Africa (Egypt, Sudan, Libya, Chad)	4,840,000	121
	Southwest Africa (Namibia, Botswana, South Africa)	1,040,000	26
	Northwest China (Tarim Basin)	1,120,000	28
	Western Australia	1,120,000	28
Soil erosion	Thar/Rajasthan (Pakistan/India)	480,000	12
	Loess Plateau/Inner Mongolia (China)	400,000	10
	Chihuahuan & Sonoran Deserts (U.S./Mexico)	160,000	4
	Pampas (Central Argentina)	480,000	12
	Great Plains (Texas-Oklahoma-Colorado)	200,000	5
Total area:			29,510,000 km^2
Total number of single-channel SAR images:			738

*Each SAR image assumed to be 200 km × 200 km.

pointing range than HIRIS and will provide illumination-controlled images independent of local sun angle. Of course, surface morphology data, enhanced on SAR images will be highly synergistic with HIRIS image data, which will provide information about surface chemistry.

Sensitivity to Surface Morphology

The surface roughness and dielectric constant within a ground-resolution cell of a SAR image determine the intensity of the return for that cell. The surface roughness of land has both large- and small-scale components. The large-scale component is related to topographic relief and is comprised of slopes and broad undulations in the landform; at this scale, surface heights vary from tens of meters to several kilometers with a similar range for the horizontal variation. The small-scale surface roughness component, in the radar context, varies over a range of centimeters to several meters.

The most obvious features in a radar image are determined by the large-scale component, e.g., topographic relief. However, the small-scale components also strongly modulate the image brightness and indeed, SAR image intensity has been used routinely by radar geologists to infer small-scale surface roughness or micro-relief. Radar sensitivity to micro-relief is determined by the Rayleigh criterion, which states that a surface will be "electrically" rough if its rms height is greater than the wavelength divided by 8 sin θ, where θ is the local incidence angle; the factor of 8 is approximate. Such a rough surface is said to

be diffuse, and appears bright on the SAR image; an electrically smooth surface is said to be specular and appears dark. At an intermediate incidence angle (e.g., 45°), the surface will begin to appear diffuse (moderately bright) when its height irregularities exceed 10 percent to 20 percent of the wavelength; when the heights exceed 30 percent of the wavelength, the surface will be very bright, and when less than 5 percent of the wavelength, dark.

The roughness of surface cover is an important attribute of landscapes that is often directly related to the underlying geological substrate. Seasat, SIR-A, and Landsat images of Chott Merouane and Chott Melrhir in the Sahara of northeast Algeria illustrate the importance of surface roughness to SAR at various incidence angles, as shown in Figure 53. As another example, buried fault traces can often be well defined on SAR image data because of subtle roughness variations not discernible on visible or infrared image data (Sabins *et al.,* 1980). Surface roughness may be caused by the nature of a material's origin (e.g., volcanic flows and scoria), weathering of natural materials, by the formation of soils, or by the presence of associated vegetation. Figure 54 illustrates how an extremely blocky lava flow with isolated, smoother grassy patches appears quite different on X- and L-band aircraft SAR images. Such variations in surface roughness of importance to geologists cannot commonly be evaluated with visible and infrared, or even multispectral image data, but can be mapped using SAR sensors.

The multifrequency Eos SAR will provide powerful new capabilities for surface morphology studies on global scales. In particular, it is expected that wavelength-ratio images (e.g., ratio of X- to L-band) will be especially useful for quickly discriminating diffuse from specular surfaces, and thereby determining geologic surface morphology.

Surface Penetration and Subsurface Geology

The depth of penetration experienced by electromagnetic waves normally incident from air onto the Earth increases with longer wavelengths and also with a decrease in the attenuation losses and volume scattering within the shallow subsurface. The attenuation in soil is governed by soil moisture and soil texture; dry sandy soils have the lowest attenuation. Volume scattering is determined by randomly spaced inhomogeneities within the soil, usually unconsolidated sediment.

Obliquely incident radar waves are refracted into the soil according to Snell's Law (i.e., the angle of refraction depends on both the incidence angle and the refractive index) for the soil. For example, a radar wave incident at a 45° angle onto a flat dry sand sheet (dielectric constant = 3, refractive index = 1.73) will refract into the sand at an angle of 24° with respect to vertical. These smaller refraction angles tend to enhance radar returns due to volume scattering and subsurface features.

This penetration capability and its importance to arid lands geology was dramatically illustrated by L-band SAR images obtained during the SIR-A overflights of the Eastern Sahara during November 1981 (McCauley *et al.,* 1982; 1986). Subsurface features at depths of several meters have been discerned on SIR-A, Seasat, and other SAR images.

The L-band channel on Eos will provide very useful data for geological studies of hyperarid lands subsurface features; a P-band channel (75 cm wavelength) would be even more valuable. It is expected that data over a range of incidence angles and for both like- and cross-polarized channels will be used to map these geologic features resulting from penetration and subsurface scattering.

Polarization Discrimination

The availability of cross-polarized SAR channels (HV or VH) in addition to like-polarized channels (HH and VV) can often help the geologist to distinguish surfaces that are specular reflectors or highly faceted at or below the wavelength scale, from those surfaces that are diffuse or volume scatterers (Schaber *et al.,* 1980). For example, Figure 55 illustrates two K_a-band (0.86 cm wavelength) aircraft SAR images of a blocky lava flow, showing strong like-polarized (HH) and weak cross-polarized (HV) returns.

Like-Polarized Returns: Physical Mechanisms

The basic physical properties responsible for like-polarized radar returns are (1) quasi-specular surface reflection, and (2) surface or volume scattering (Fung and Ulaby, 1983). The quasi-specular reflection normally accounts for the high returns near vertical incidence. Since most SARs transmit at moderate to large incidence angles, both surface and volume scattering play important roles. Returns due to surface scattering are normally stronger near vertical incidence and decrease with increasing incidence angle, with a slower rate of decrease for rougher surfaces. Returns due to volume scattering from an inhomogeneous medium with a large average dielectric constant tend to be uniform for all incidence angles away from grazing.

Cross-Polarized Returns: Physical Mechanisms

A transmitted radar wave of a given polarization (e.g., H) will be backscattered from the Earth's surface with both horizontal (H) and vertical (V) components, e.g., the radar echo will have both HH and HV components. The like-polarized component (HH) is normally stronger than the cross-polarized component (HV). The scattering process that causes the cross-polarized component is also called the depolarization mechanism.

It is important to understand the depolarization and scattering processes in relation to surface and subsurface geometries and material properties. There

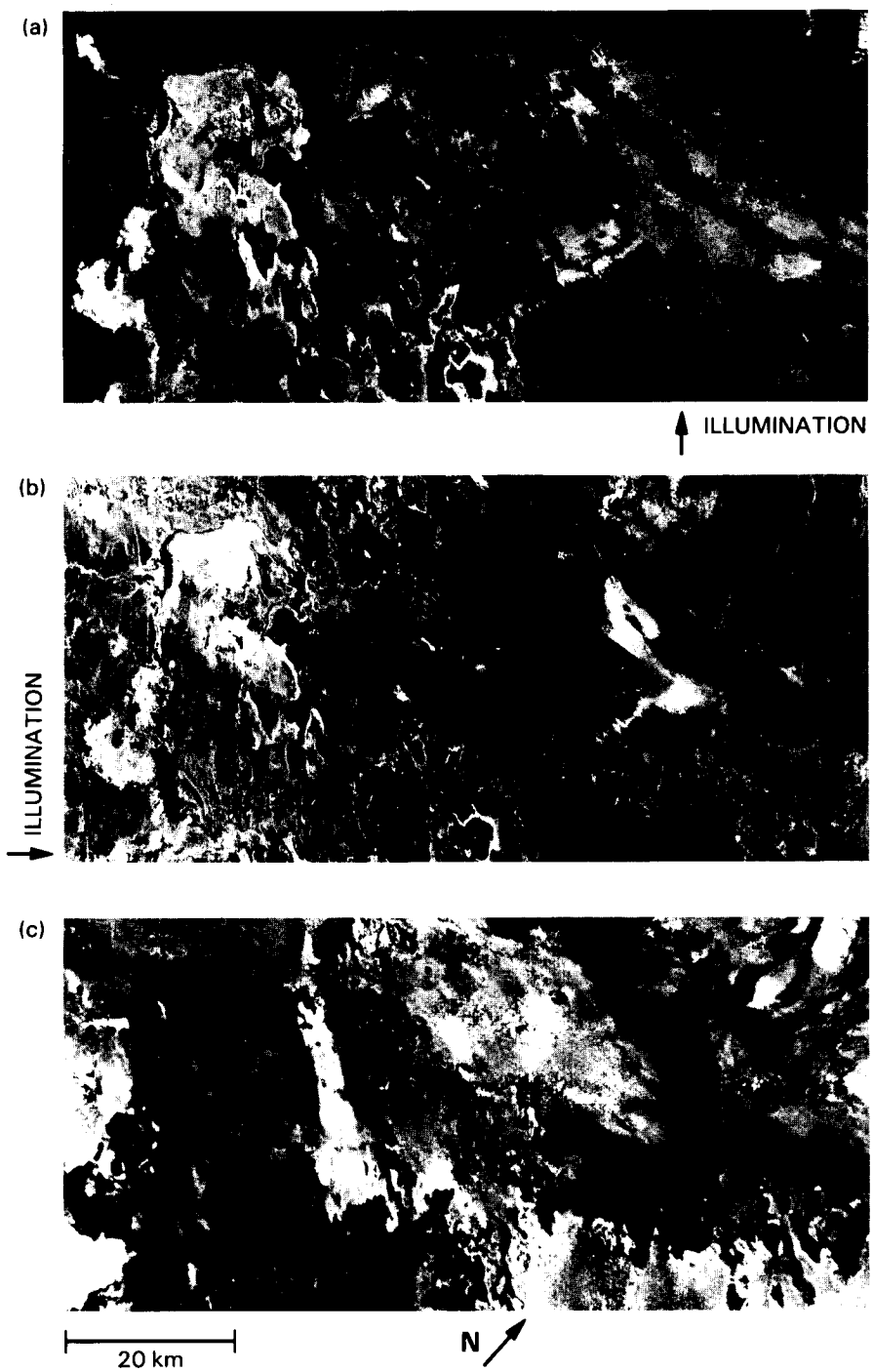

Figure 53. (a) SIR-A image, (b) Seasat SAR image, and (c) Landsat band 4 images of northeast Algeria (Ford *et al.*, 1983; text supplied by Phillippe Rebillard). Chott Merouane (left) and Chott Melrhir (right) are located in the Sahara some 80 km south of the Aures Mountains. The Chotts are playas situated some 40 m below sea level. The bright returns from Chott Merouane suggest a wide range of roughness at the scale of the radar wavelength. The moderate-to-dark returns from Chott Melrhir imply a smoother surface.

The surface of Chott Merouane on the corresponding Seasat SAR image appears quite similar to that on the SIR-A image. However, the floor of Chott Melrhir appears substantially different because it presents a mostly low level of radar backscatter. The differences in backscatter may be due to the difference in incidence angle of the two radar systems or to such seasonal effects as the presence or absence of surface moisture.

The Landsat image in the visible green wavelength was acquired slightly less than 5 years prior to the Seasat image, and almost 9 years before the SIR-A image. Chott Merouane appears moderate to dark, in contrast with the radar images where it is moderate to bright. Chott Melrhir appears moderate to bright on the Landsat image. This suggests a strong reflectance from the salt deposits.

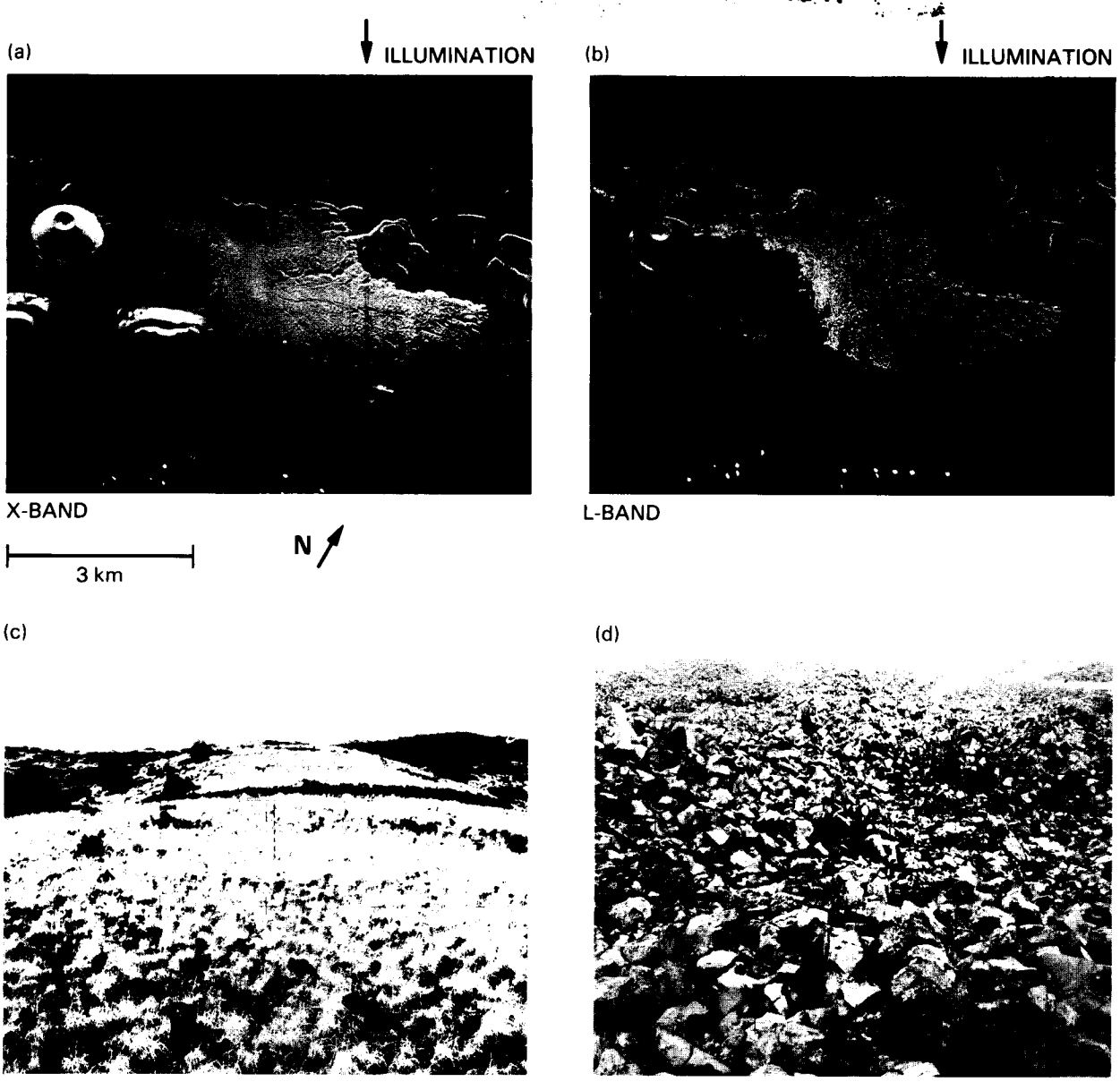

Figure 54. (a) X-band and (b) L-band HV cross-polarized SAR images of S.P. cinder cone and lava flow in north-central Arizona. Note the uniform radar return from the blocky andesitic basalt flow on the X-band image and the presence of two distinct radar tones on the L-band image. The dark areas on (b) represent grassy, smoother regions (c) within the extremely rough lava flow (d).

are four broad mechanisms that cause these waves to become depolarized: (1) quasi-specular reflection as a result of the difference between the Fresnel reflection coefficients for a homogeneous, two-dimensional smoothly undulating surface; (2) multiple scattering as a result of target surface roughness; (3) multiple volume scattering due to inhomogeneities, especially those embedded within a skin-depth of the target surface; and (4) anistropic properties (physical or geometric) of the target (Fung and Ulaby, 1983). The first three mechanisms are the most commonly encountered in remote sensing applications. Much is to be learned about the specific details of target-scene interactions for cross-polarized returns, but practical experience with like- and cross-polarized radar images has shown that the geologic value of radar imagery is greatly enhanced by including the cross-polarized channel (Daily *et al.*, 1978; Schaber *et al.*, 1980).

The combination of like- and cross-polarized channels will greatly enhance the potential of the Eos SAR for geologic investigations. It is expected that experience gained with these channels on SIR-C and with additional aircraft SAR data will be valuable in planning for Eos SAR acquisition of data for surface and subsurface morphology studies.

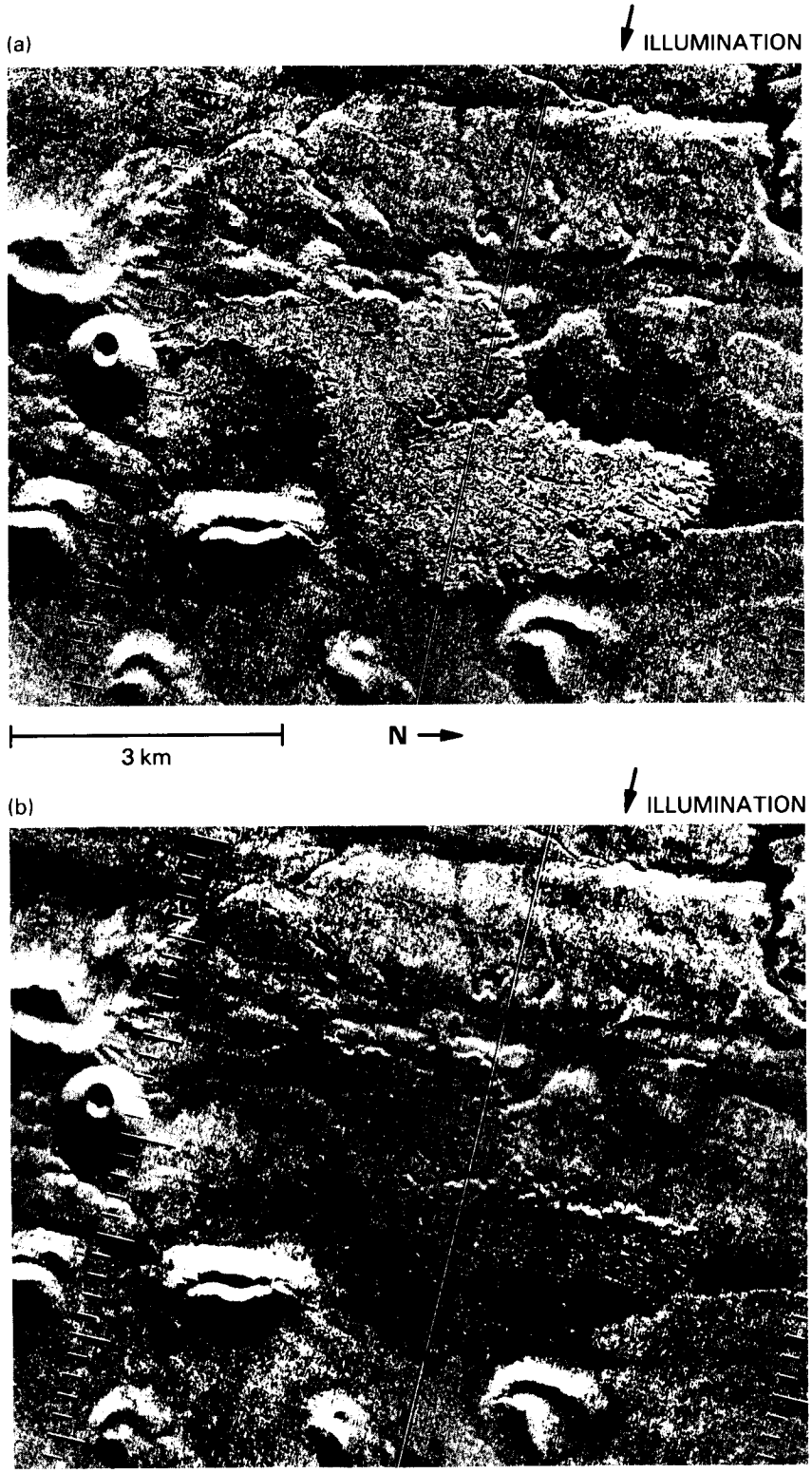

Figure 55. (a) K_a-band, HH polarization real aperture radar image of S.P. cinder cone and lava flow described in Figure 54. (b) Simultaneously obtained HV polarization image. Note the strong response of S.P. flow in the direct return image and the weak return on the cross-polarized image indicating the blocky flow to be highly polarizing; this was suggested by Schaber *et al.* (1980) to be the result of direct reflection from blocks that are large relative to wavelength scale. Note on Figures 54a and 54b that the cross-polarized return from S.P. flow at X- and L-bands both show a strong depolarizing component, unlike the K_a-band image.

Phase Discrimination

Recent data obtained with the JPL L-band aircraft multipolarized SAR have demonstrated that the *phase difference* between the electrical phase angles of the HH and VV radar echoes can be recorded and processed into image form. These phase difference images have been shown to be very responsive to terrain surface morphology and vegetation cover, as well as oceanic surface features (van Zyl *et al.*, 1986).

The mechanisms of the interaction are not yet well understood, although the phase-difference channel is an additional radar geology information source that is independent of any of the amplitude channels. Both SIR-C and the Eos SAR will routinely provide phase-difference images, and it is expected that future aircraft SAR phase-difference data over geologic test sites will provide entirely new and unique geologic information.

Previous Experience with Radar Geology

The first scientific (non-surveillance) uses of imaging radars were made in the early 1950s by geologists using images acquired by SLAR. Over the past three decades, advanced generations of imaging radars such as Seasat, SIR-A, SIR-B, and various aircraft SARs have been used by geologists for lithologic, geomorphologic, and structural mapping. Techniques for extracting information from the map-like images produced by SAR have been developed by geologists to a level of considerable maturity and sophistication, more than by any of the other disciplines of Earth science.

The scientific objectives outlined previously in this chapter are attainable with Eos SAR data. There is compelling evidence that the required observational parameters for these objectives can be determined from SAR data. A discussion of some of the relevant case histories supporting this claim is presented in Appendix E.

RECOMMENDED INSTRUMENT PARAMETERS

The objective of the Eos SAR mission strategy for geology is to provide global data sets and information extraction techniques that will lead to an improved understanding of lithospheric processes.

Perhaps the most formidable of all the challenges to Eos is the analysis and understanding of the information content in a global data set. This is particularly so for both SAR, HIRIS, and TIMS, and any other high-resolution, high data-rate instruments. A large number of calibrated SAR images will be required to meet the geological objectives; however, the analysis can be done over a period of years so the data problem is not especially difficult.

The principal focus of this section is on SAR instrument and viewing parameters. For each of the specific science issues discussed in this chapter, there is a discussion of the preferred combinations of instrument parameters (frequency, polarization, calibration) and viewing parameters (look angles, swath widths, repeat cycles, times of data acquisition, etc.). Table 9 summarizes instrument and viewing parameters recommended for geological observations.

Imaging Parameters

Frequency

X-band radar has been used operationally for many years by most SAR and real aperture radar contractors for acquisition of geologic and structural data. At the 3 cm X-band wavelength, most landscape surfaces appear rough and there is good signal-to-noise return, even at large look angles. There is little or no observable difference between C- and X-band SAR image data for most geological surfaces. Speckle effects, caused by constructive and destructive interference from terrain using SAR sensors, are, however, minimized through the use of the shorter-wavelength (higher frequency) SAR sensors (Ford, 1982). Large variations in surface roughness at L-band as observed with Seasat, SIR-A, and SIR-B are useful in evaluating the nature of weathering and mass-wasting of geological materials, although the speckle effects are greater for L-band than at C-band and higher frequencies (e.g., X-band).

Shorter-wavelength SAR data (e.g., C- and X-band) are also generally most useful for portrayal of the type of desert landforms thought to be indicative of desertification, such as drift sand and dunes.

The highest priority frequencies for soil erosion investigations would be L-band followed by C-band. The L- and C-band frequencies are most sensitive to scales of surface changes (e.g., gulleying) that can occur through soil erosion on a 1-year to 10-year basis (tens of centimeters to tens of meters). L- and P-band are preferred for arid lands investigations because there is greater surface penetration. Scintillation effects at L-band might pose some resolution problems in quantifying observed changes in this application.

Polarization

VV and HH polarizations would both result in useful SAR images for the majority of structural terranes. HH polarization should be slightly favored, however, simply because of its enhanced ability to penetrate thin low-loss mantles of sand, snow, and ice, and the general preference in nature of surfaces configured in a horizontal-dominant manner as opposed to a vertical-dominant manner at the wavelength scale. The suggested preference for structural mapping and topical structure investigations would be HH and VV. However, cross-polarized returns should provide important information permitting separation of specular, diffuse, and volume scattering mechanisms.

Table 9. SAR Parameters and Geology Experiment Requirements

	Crustal Structure and Tectonics	Arid Lands Geology (subsurface mapping)	Desertification
Frequencies (1, 2 priorities)	X, C (1) L (2)	L (1) X, C (2)	X, C (1) L (2)
Polarizations (1, 2 priorities)	HH, VV (1) HV (2)	HH, HV (1) VV (2)	HH, HV (1) VV (2)
Azimuth directions	2 minimum	2 minimum (not orthogonal)	2 minimum (not orthogonal)
Incidence angles	variable 30°–60°	variable 15°–60°	variable 15°–60°
Resolution	<20 m	15–50 m	15–20 m
Swath width	100 km minimum	100 km minimum	50–100 km
Repeat cycle	once each azimuth direction	2 yrs	2 yrs
Time of data acquisition	summer (vegetated) and winter (non-vegetated)	driest and wettest season	driest, wettest, and windiest season
Data encoding	6 bit	4–6 bit	6 bit
Calibration Radiometric Geometric	 2–3 dB absolute best possible	 2–3 dB absolute 500 m	 2–3 dB absolute 200–500 m
Data processing turnaround time	6 mon–1 yr	3 mon	3 mon
Years of data analysis	10 yrs+	10 yrs	10 yrs
Archiving plan	1 complete global data set for both vegetated and non-vegetated seasons	1 complete set (dry season and wet season) every 2 yrs	1 complete data set for wettest and driest and most windy season every 2 yrs
Pre-Eos research (1, 2 priorities)	aircraft over-flights (X, L, C) (1)	aircraft over-flights L, P-bands (1) X, C-bands (2)	aircraft over-flights L, C (1) X (2)
Stereo coverage	yes, <20%	yes, <2%	yes, <5%
Orbital inclination	near polar	near polar	near polar

HH is the polarization of choice for desert geologic mapping given its increased potential for easy refraction into a low-loss unconsolidated sand mantle, as shown by Elachi *et al.* (1984). HH and HV are the dual polarization mode of highest priority, followed by VV. The HV channel should be important for determining the presence of volume scattering from the shallow subsurface, diffuse backscatter from the air/surface interface, or diffuse backscatter from a sand-buried permittivity interface such as bedrock. The fact that HV returns fall in power less sharply than HH with increasing look angle can also be used to good advantage in evaluating the scattering mechanisms.

Thus VV and VH polarizations may suffice for a large percentage of anticipated desertification targets. VV or HV polarization is preferred when signal penetration and subsurface backscatter is desirable.

HH and HV polarization would be first priority with VV secondary for soil erosion studies. The HV channel would be useful for assessing and quantifying the degree of diffuse and volume scattering versus direct reflection and multiple reflection. Most surfaces of agricultural importance affected by soil erosion are characterized in the horizontal-dominant, as opposed to vertical-dominant, relief in the absence of live vegetation. Vegetated (e.g., vertical-dominant structure) fields undergoing soil erosion might be best examined using HH, HV, and VV polarization channels.

Radiometric and Geometric Calibration

An absolute radiometric calibration of 2 to 3 dB is desirable because (1) this will allow development of scattering models that provide quantitative relationships between $\sigma°$ and geophysical parameters, and (2) it allows quantitative comparisons of image intensities at multiple wavelengths. This would also allow quantitative comparisons between Eos SAR data and that of other calibrated airborne and spaceborne SARs.

A georeferencing system accurate to 100 m or less would be required for maximizing structural mapping and quantitative interpretations.

Viewing Parameters

Incidence and Azimuth Angles

For maximum geological information, the Eos SAR should provide a selection of both azimuth angles and incidence angles. Analysis of Seasat SAR image data established that a minimum of two different azimuth illumination angles is desirable for crustal evolution and structure investigations and they should not be orthogonal (MacDonald *et al.*, 1969). Different incidence angles will be needed for varying topographic relief and for stereographic analysis of terrain using SAR images (see Figures 56 and 57). The incidence angles will have to be selected for each terrain type and its average relief. Stereographic SAR data will require imaging from the same azimuth direction at two different incidence angles (Leberl *et al.*, 1986).

The azimuth direction will not be as critical as incidence angle in the initial global mapping and assessment of alluvial and erosional patterns within world desert regions. However, a minimum of two azimuth directions will be required to properly assess linear structural patterns within desert regions, both on the surface and below thin eolian sand cover. Given the results of SIR-A in Egypt and Sudan and the study by Elachi *et al.* (1984), an incidence angle between 40° and 50° may result in maximum efficiency for refraction of the L-band SAR signals while still allowing a positive backscatter from a permittivity contrast below a thin eolian sand mantle of about 1 m to 2 m depth.

Azimuth directions most favorable to normal viewing of encroaching sand dunes and other surface landforms will be of priority in desertification investigations. Sand dune morphology has been shown to be best delineated on SAR image data using small look angles that are sensitive to the quasi-specular component of the return created by the gentle topographic undulations of the landforms (Blom and Elachi, 1981) (Figure 51).

Soil erosion is closely associated with small-scale topography that can be characterized both as highly aligned or patterned (e.g., furrowed agricultural fields), semi-aligned (e.g., dendritic gulley networks), and random (e.g., wind fluting and deflation hollows). Thus, a minimum of two different azimuth directions is desirable over each study site. Again, these azimuth directions should not be orthogonal. Incidence angles must be variable and range from 15° to 60° in order to be able to assess both the gently undulating surface slopes (smaller incidence angles) as well as the higher-relief terrains and small-scale surface roughness (larger look angles). Stereoscopic data will be required for about 10 percent of the data acquired in topographically rough regions.

It is also important for all applications to have the capability to vary the incidence angle from 15° to 60° in order in properly assess the relation between incidence angle and C- and L-band wavelengths, and to derive empirical surface and subsurface scattering models.

Resolution

Spatial resolution of Eos SAR sensors should be 20 m or better to resolve recent fault scarps and allow structural attitudes to be determined. A goal for radar image products should be to produce 1:50,000 scale images that would allow measurements of topography to about 20 m contour accuracy.

For general synoptic mapping and morphologic characterization of world desert regions, the spatial resolution of the Eos SAR need not exceed that of SIR-A (about 40 m). Higher resolutions of 10 to 25

Figure 56. Generation of Mt. Shasta perspective views using two SIR-B images. A stereo pair collected at two different incidence angles was used to generate the topography. A density slice of the image intensity was then done to generate the color (Leberl *et al.*, 1986).

m may be useful for 5 to 10 percent of the required data set. The 500 m to 100 m resolutions associated with the global and regional mapping modes would be useful for preliminary analysis of large desert regions. However, spatial resolution of the SAR sensors for applications in desertification will need to be at least 20 m in order to resolve the details of dune-train movement and sand encroachment onto arable lands as part of desertification investigations. Lower resolution may suffice for 10 to 20 percent of the data during simple monitoring of currently inactive or potential desertification targets.

It is critical that test areas characterized by serious, active soil erosion be imaged by the SAR sensors with as high a spatial resolution as possible, perhaps 15 to 20 m. The categories of information that will be required at each study site will lie at or near this resolution level in possibly 50 to 60 percent of the data acquired. The remaining 40 to 50 percent of the data acquired for soil erosion investigations will involve monitoring and evaluation of sites where soil erosion either has a low level of activity, or a high potential for future activity due to manmade destruction of protective vegetation cover, construction, etc. These sites may require SAR spatial resolutions of the order of 20 to 50 m.

Swath Width

For geologic mapping, swath width is not a critical requirement as long as the images can be mosaicked into scenes on the order of hundreds of kilometers across. High resolution is far more important than swath width for nearly all geologic studies.

Revisit Times

Unlike biota, glaciology, and hydrology investigations, the temporal scale of change in even the most tectonically active regions of the continents are not in accord with the 15-year lifetime proposed for the Eos platforms, with the expection of documenting large-scale fault movements resulting from earthquakes and monitoring of volcanic eruptions.

Seasonal coverage is necessary to assess the effects of maximum contrast in surface moisture (per-

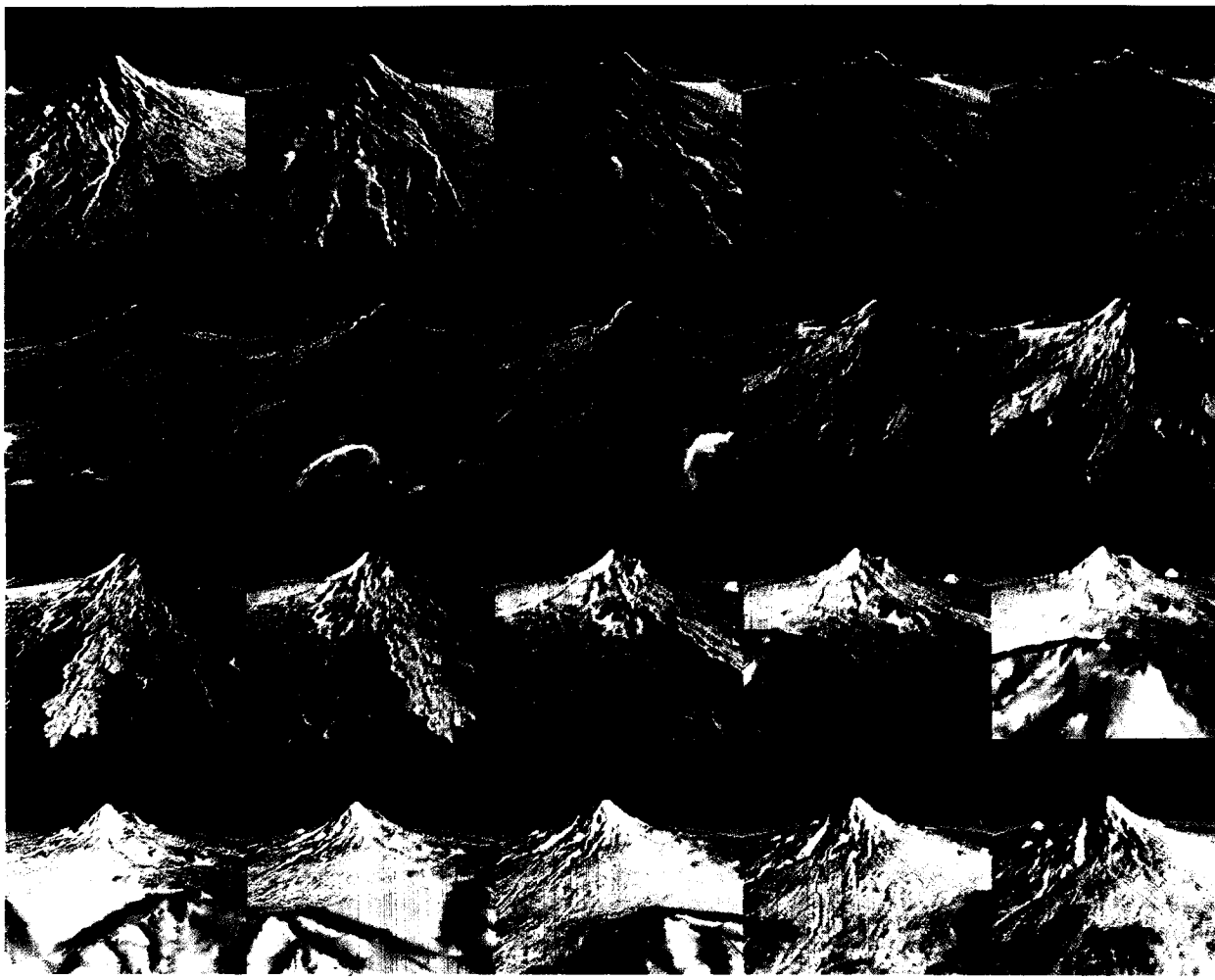

Figure 57. Perspective view of Mt. Shasta generated entirely with SIR-B data.

mittivity changes), vegetation, snow, and ice as they relate to the underlying geological substrate. Once the effects of seasonality are documented with SAR data, there should be few requirements for repeat coverage, except when significant changes in regional or local conditions, or temporal geologic events (earthquakes or volcanic eruptions) dictate.

The temporal aspects of general arid lands geology are not expected to be of importance during the time scale of the Eos spacecrafts with the exception of possible monitoring of hydrologic changes related to near-surface ground water aquifers.

If monitoring and assessment of desert hydrology/geology interactions is the major objective of an experiment, repeat cycles during both the wettest and driest months would be required about every 2 years.

Desertification is of a temporal scale and magnitude that could easily be monitored given the proposed Eos strategy and lifetime. Complete SAR coverage of each desertification target region with at least two look angles (small and large) from the same look direction is desired every 2 years; synergistic HIRIS and TIMS coverage would also be important for 10 to 50 percent of the areas studied. Seasonal coverage will be required as dictated by the most and least windy periods of the year, locally. Seasonal coverage may also be necessary to assess the effects of variations in soil moisture, vegetation, and human activity as they relate, for example, to dune and drift sand movement.

Temporally, soil erosion is generally a slow process but can undergo rapid acceleration leaps during catastropic climatic events such as windstorms and seasonal droughts. Complete coverage of each soil erosion test area with at least two incidence angles from the same azimuth angle is mandatory. A second data set from a second azimuth direction and incidence angle would be very helpful. Repeat coverage every 2 years of major test sites would be required with acquisition to immediately follow the dryest, wettest and/or most windy season, locally. The best season for initial coverage in most temperate latitudes might be early mid-winter and early fall. Synergistically collected HIRIS and SAR data for 10 to 30 percent of the data takes would be very important to successful soil erosion investigations and monitoring.

Synergism

In the area of geology, synergistic measurements with SAR, HIRIS, and TIMS are essential. In general, SAR supplies information about physical properties (structure, texture, and roughness), HIRIS about chemical properties, and TIMS about thermal properties (Figure 58). Information from all three sensors may be used to produced characteristic signatures that include mineralogical as well as geomorphological information (Figure 59). For crustal structure and tectonics, synergistic SAR measurements with GLRS may be valuable in addition to HIRIS and TIMS.

Exact SAR simultaneity (shorter than days or weeks) with any sensor is not required for most envisioned geologic experiments. Possible exceptions might be unanticipated volcanic, earthquake, or landslide events. The requirements for simultaneity and total percent of synergistic data is much less stringent for geology than the other disciplines; however, the importance of HIRIS and TIMS synergism with SAR should not be underestimated. Based on previous results of combined SAR/Landsat data analyses, a 50 to 200 percent increase in science return is anticipated when SAR and HIRIS and/or SAR and TIMS synergism is available versus SAR alone. This will be true for crustal structure and tectonics, arid lands geology, desertification, and soil erosion, in addition to many other geology experiments not specifically described here.

Data Parameters

Table 8 summarizes representative geological regimes of interest, their areas, and the number of SAR images required to produce geological maps at a single frequency, polarization, and illumination angle. It is assumed that each SAR image is 200 km $\times$ 200 km (mapping mode). The total number of SAR images required for each science objective is the product of the number of single channel images (Table 8) times the number of channels required for each scene.

A detailed scenario for the number of channels has not yet been worked out, but a reasonable assumption is that an average of two channels per scene will be needed to meet the science objectives (e.g., L-band HH, C-band HH, both at 50° incidence angles). Moreover, in order to understand the effects of vegetation on the image, it is desirable to acquire two complete data sets, one in the summer and one in the winter. As indicated above, the total number of 200 km $\times$ 200 km single channel SAR scenes required for these regions is about 740. At two channels per scene and two seasons per scene, the total number of processed images would be 740 $\times$ 2 $\times$ 2 = 2,960. If we further assume steady acquisition, processing, and analysis of SAR images for these regions over a 5-year period, this means that about an average of 50 SAR images per month would be processed and analyzed.

The magnitude of this volume of imagery has several major implications for the data system and analysis procedures:

- All images must be processed to georeferenced map-like form, with good cross-track radiometric fidelity (to allow easy mosaicking).
- There must be some provision for "quick browse" by geologists through hundreds of Eos SAR images.

ORIGINAL PAGE
COLOR PHOTOGRAPH

Figure 58. Multisensor imagery of Death Valley, California, simulating SAR (physical), HIRIS (chemical), and TIMS (thermal) data.

- Many more geologists trained in the analysis of SAR images will be required than now exist.

Information Parameters

The geoscientific information extracted from SAR data is displayed in the form of geological maps (e.g., Figure 46). For studies of global crustal structure and tectonics, the principal information obtained from SAR is geometrical in nature, i.e., surficial expressions of crustal structure. For arid lands and desertification studies, the principal information of interest is detection and identification of shallow subsurface structures and topography, including paleodrainage systems. For soil erosion studies, the information sought is in the form of land surface properties, including percent of bare soil, amount and type of vegetation cover, and mobile sand (drifts and dunes).

Extraction of this information from SAR images, or from SAR plus HIRIS or TIMS images,

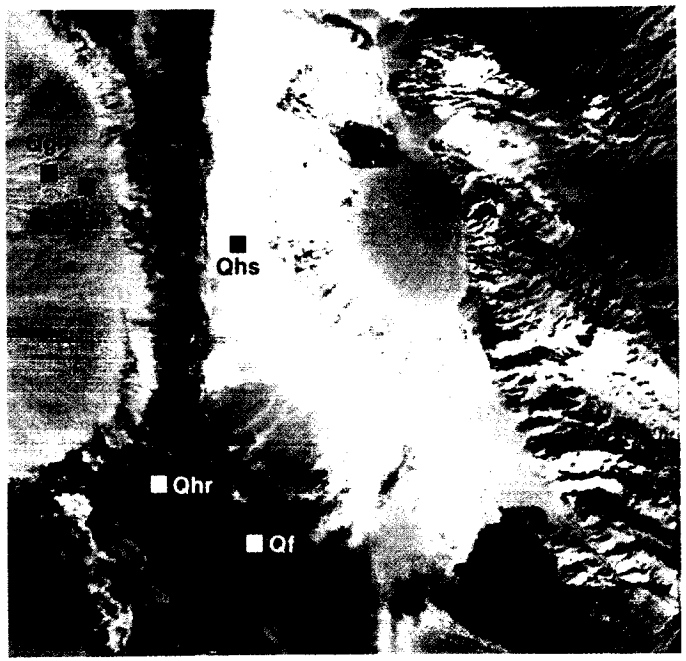

THEMATIC MAPPER IMAGE SHOWING
AREAS USED IN THE ANALYSIS

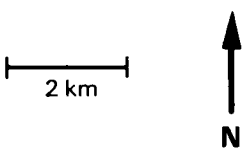

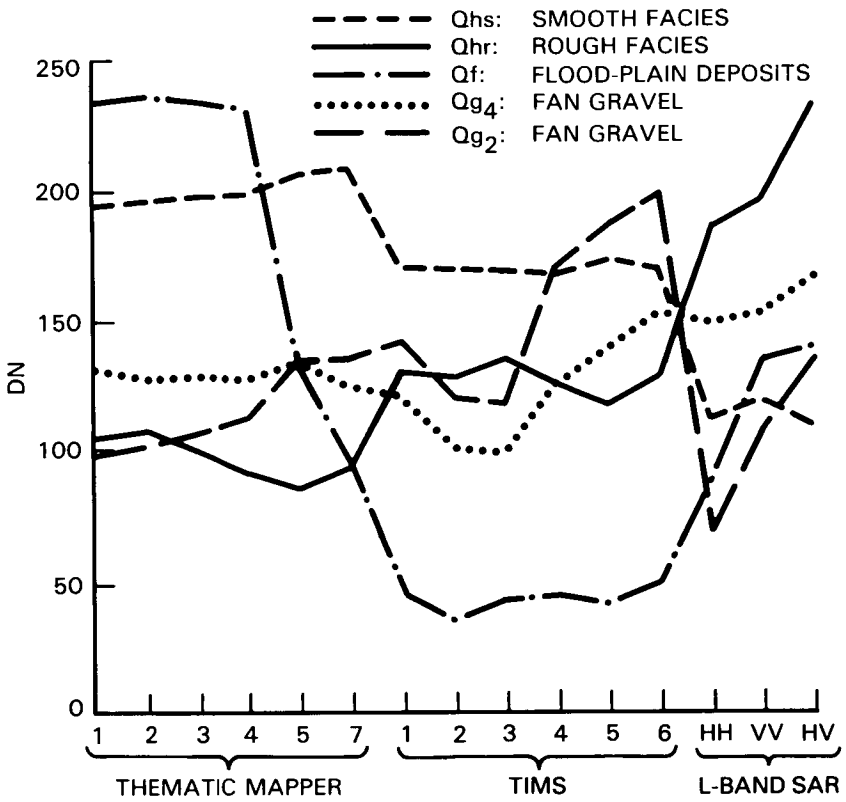

EXTENDED SPECTRAL SIGNATURES
DERIVED FROM COREGISTERED IMAGES

Figure 59. Extended spectral signatures of Death Valley, California. The combination of chemical (visible/near-IR), thermal, and physical data (radar) may produce characteristic spectral signatures used to differentiate facies.

ORIGINAL PAGE
COLOR PHOTOGRAPH

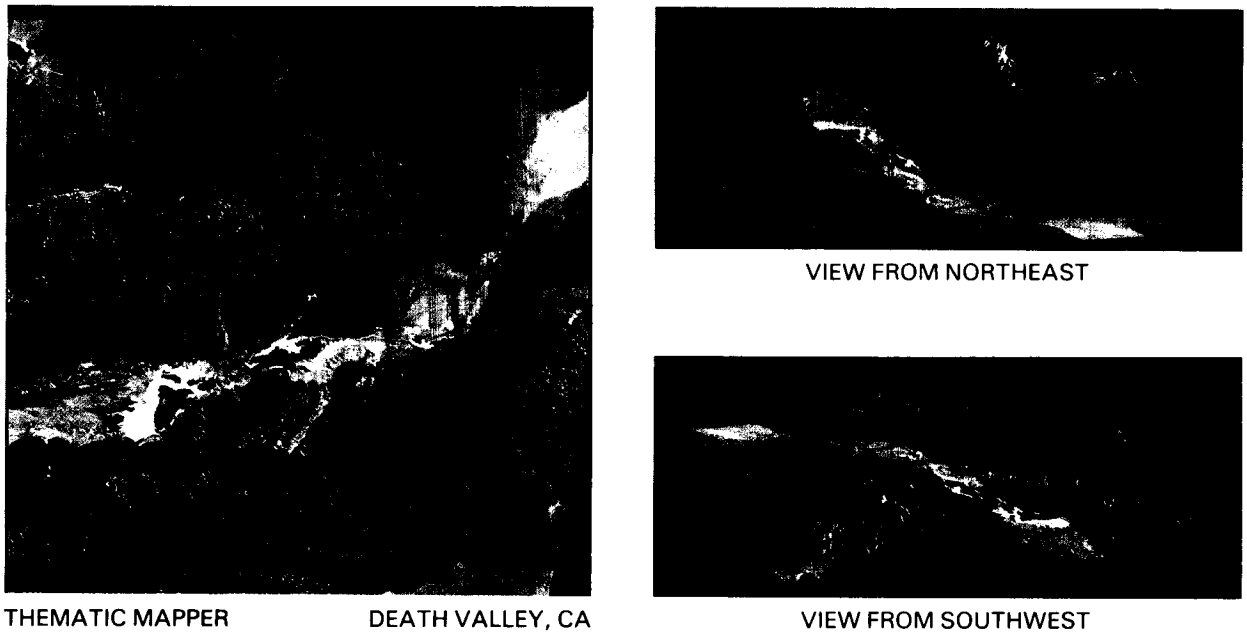

Figure 60. Two-dimensional and three-dimensional images of Death Valley, California.

would be accomplished at several levels of sophistication, beginning with the traditional use of tone, texture, and context (Figure 60) but also using advanced algorithms which incorporate sophisticated scattering models. Study areas would be initially examined using images taken at a single frequency, polarization, and incidence angle. This would provide baseline information about gross structural features, etc. Images acquired at additional frequencies, polarizations, and incidence angles would then be used with algorithms to extract information about surface roughness, vegetation cover, etc.

It is clear from the volume of data implied for global high-resolution mapping that information about global crustal structure, arid lands geology, and soil erosion will require more trained research geologists, very high quality SAR image processing, and possibly the use of artificial intelligence (AI) or knowledge-based systems for use in automation of image analysis.

VII. SUMMARY OF INSTRUMENT AND VIEWING REQUIREMENTS

The principal scientific motivations for acquiring Eos SAR data are outlined in Chapters II through VI. At the conclusion of each chapter, specific requirements for instrument and viewing parameters are discussed, along with synergism and information issues. This chapter summarizes and elaborates further on these instrument and viewing requirements. The principal instrument parameters are frequency, polarization, calibration (radiometric and geometric), and dynamic range; these parameters are determined by the design of the transmitter, receiver, antenna, and data handling system. The principal viewing parameters are revisit intervals, illumination angles (incidence and azimuth angle and look direction), swath width, resolution, and mission lifetime. The first three of these parameters are dependent on the spacecraft altitude and inclination. Swath width and resolution are also dependent on the instrument design. Finally, observational modes are recommended to meet the great variety of science requirements.

INSTRUMENT PARAMETERS

Frequency

The scattering of electromagnetic waves by the Earth's surface is strongly wavelength-dependent. At a given wavelength, the intensity of backscattering is governed by three scene-dependent mechanisms: (1) volume scattering and attenuation by surface cover such as vegetation or snow; (2) surface scattering from soil, rocks, or water; and (3) penetration into sand and volume scattering from within soil or ice. The Eos SAR will allow a new observational strategy that couples multifrequency data to backscattering models, thereby allowing inference of backscattering mechanisms and related biophysical and geophysical properties. In effect, the frequency (along with polarization and illumination angles) can be chosen to enhance surface scattering from the ocean, ice, or soil, to give greater surface penetration, or to enhance volume scattering from vegetation, snow, or sand.

The selection of the L-, C-, and X-band frequency channels for the Eos SAR is based upon previous scientific and radar technology experience, upon constraints of size, weight, and power consumption imposed by the Eos platform, and upon cost. From a purely scientific point of view, it might be desirable to also have a longer wavelength channel (e.g., P-band with 75 cm wavelength) for greater penetration in arid lands studies, and a shorter wavelength channel (e.g., K-band with 1 cm wavelength) for improved snow characterization; however, the P-band antenna would be too large for the Eos platform at IOC and the K-band power requirements would be excessive.

For *glaciology studies*, the best sea ice type discrimination is observed at high frequencies (e.g., X-band) because the shorter wavelengths are similar to the ice grain sizes in the upper ice layers; high frequencies are therefore also best for determining sea ice dynamics. For lake and river ice studies, there is greater penetration and enhancement of ice bottom features at lower frequencies (e.g., L-band). There is little quantitative information on optimum frequencies for ice sheets and shelves, but the greatest penetration can be expected at L-band. Snow cover extent and water equivalent are best observed at C- and X-band or higher (K-band) frequencies along with an L-band channel for characterizing the soil surface.

For *hydrology studies*, sensitivity to soil moisture is enhanced at L- or C- band; some studies have shown that soil moisture is less confused by surface roughness at C-band than at L-band, especially for near-nadir incidence angles. For surface erosion studies, however, surface roughness is itself useful information; it is expected that ratios of images obtained at different frequencies will provide the best estimate of surface roughness. Land-water boundaries are easily identified at any frequency; however, L-band is best to reduce any confusion due to surface winds that may roughen the water surface. As pointed out above, snowpack extent and condition is best revealed by combining C- and X-band or higher (K-band) frequency observations.

Vegetation studies will require a variety of frequencies as canopies are usually composed of a wide variety of scatterers. Foliar vegetation biomass, type, and condition are best observed at shorter wavelengths and higher incidence angles where volume scattering predominates; however, longer wavelengths (L-band) may enhance returns from woody biomass. Canopy moisture is best measured with SAR when the ground surface contribution is eliminated, thus X-band is probably best. The state of the surface boundary layer (i.e., its moisture, snow cover, or flood state) is best observed at L-band where attenuation by the upper canopy is reduced.

For *oceanography studies*, it is expected that both L- and C-band channels will be sensitive to Bragg-scattering from capillary waves of 6 cm to 30 cm wavelength, but there are as yet no definitive models to indicate which of these frequencies would be preferable.

For *geology studies*, a wide range of bare and vegetated surfaces will be of interest so that all three Eos SAR frequency channels (L-, C-, and X-band) are desirable. Some studies have indicated that speckle from terrain is minimized at shorter wavelengths; at X- or C-bands, most landscape surfaces appear rough. Mostly for these reasons, these higher frequency channels are desired for desertification studies as well as investigations of crustal structure

and tectonics. For studies of arid lands geology, however, there will be more interest in the L-band (and P-band) channels where there is greater surface penetration and sensitivity to weathering and mass-wasting of geological materials.

As summarized in Figure 61, L-, C-, and X-bands are desired by all five disciplines except oceanography, which requires only L- or C-bands.

Polarization

In general, radar echoes from either point or extended targets are strong in like-polarization and weak in cross-polarization. It has been known for a number of years that some targets have very distinctive "polarization responses," and that the proper choice of HH, VV, or HV images could enhance features of the Earth's surface. In like-polarized radar systems (HH and VV), strong responses occur when scatterers are oriented in the same direction as the polarization of the incident wave. For example, a wheat field has a much stronger response to a VV system than an HH system due to the presence of vertical stalks. Cross-polarized backscatter results either from multiple scattering within a diffuse volume such as a vegetation canopy or from multiple bounce interactions associated with natural dihedral reflectors such as rock formations. Thus, cross-polarized images, even though weak, may convey valuable information about vegetation canopies, ice or snow layers, or geologic structural features.

The Eos SAR should have full amplitude and phase capability in both horizontally and vertically polarized transmit and receive vectors. This means that it will be possible in principle to synthesize any polarization state for transmitted pulses and also for the received echoes. The received image amplitudes will be the four basic linear polarizations (HH, VV, HV, and VH) and the received image phases would be the phase differences between the linear polarizations. It will then also be possible, for example, to synthetically transmit a right circularly polarized signal and receive a left circularly polarized signal. This polarization synthesis technique is known as polarimetry, and can be used to enhance the response of certain extended and discrete targets.

What polarization states should be chosen to better characterize ice, vegetation communities, or tectonic features? Since all spaceborne SAR data has been limited to HH, we must look to experience gained with images acquired with airborne radars or with scattering coefficients measured by truck-based scatterometers. This limited data base suggests that some very significant new information about the characteristics of the Earth can be obtained by utilizing the full polarization capability. It is expected that most of the Eos SAR data requests for regional and global-scale studies will be for one or two polarizations; however, the full polarization capability of the Eos SAR will likely be used extensively during the first few years of Eos for intensive observations of a few representative study sites such that an educated selection of the polarization channels can be made. This may lead to techniques for separating different layers in vegetated terrain or polar regions with multiyear or snow-covered ice.

For *glaciology studies*, like-polarization images (HH or VV) will be preferred, at least initially, in order to maximize ice return strength. The use of HH, VV, and the ratio HH/VV should help discriminate volume scattering from surface scattering at incidence angles greater than about 30°. Scattering theory suggests that additional information about volume scatterers (brine pockets, etc.) should be obtainable from cross-polarization (HV) targets. Scatterometer observations of snowpacks confirm that cross-polarized returns are sensitive to volume scattering by liquid water and larger snow grains.

For *hydrology studies*, like-polarization (HH and VV) will be used for initial soil moisture and surface morphology studies. However, cross-polarized data may be of primary interest since HV returns are less dependent on incidence angle than like-polarized returns; this property is useful when frequent revisits at different incidence angles are required. Understory land-water boundaries in forested regions would be enhanced with HH polarization.

Vegetation studies will utilize all polarizations to enhance or subdue the various contributions to the total canopy and surface backscatter. VV will be useful for main stem observation; HH will enhance the horizontal canopy structure. Cross-polarization may be useful as an indicator of multiple scattering, which may be related to foliar biomass. The best polarization for canopy moisture determination is yet to be determined. Monitoring of the surface boundary layer state is best done at HH or VV, depending on whether the canopy is dominated by vertical or horizontal stems.

For *oceanography studies*, where little is known about the polarization response of the ocean, initial studies will utilize HH and VV data. The cross-polarized channels are likely to be very weak for the ocean except at the steepest incidence angles.

For *geology studies*, emphasis will also be on HH and VV returns. It is expected that HH polarization will provide enhanced penetration of low-loss sand, snow, and ice mantles and will be more sensitive to landscape surfaces that tend to be more horizontally than vertically oriented. Secondary emphasis will be on VV. Cross-polarized returns may provide important information permitting separation of specular, diffuse, and volume scattering mechanisms.

Figure 62 summarizes the recommendations for polarization states. The reader will note that emphasis here has been on HH and VV returns, i.e., those that we know best. Actually, relatively little is known about optimum polarizations, and it can be safely predicted that both SIR-C and the Eos SAR

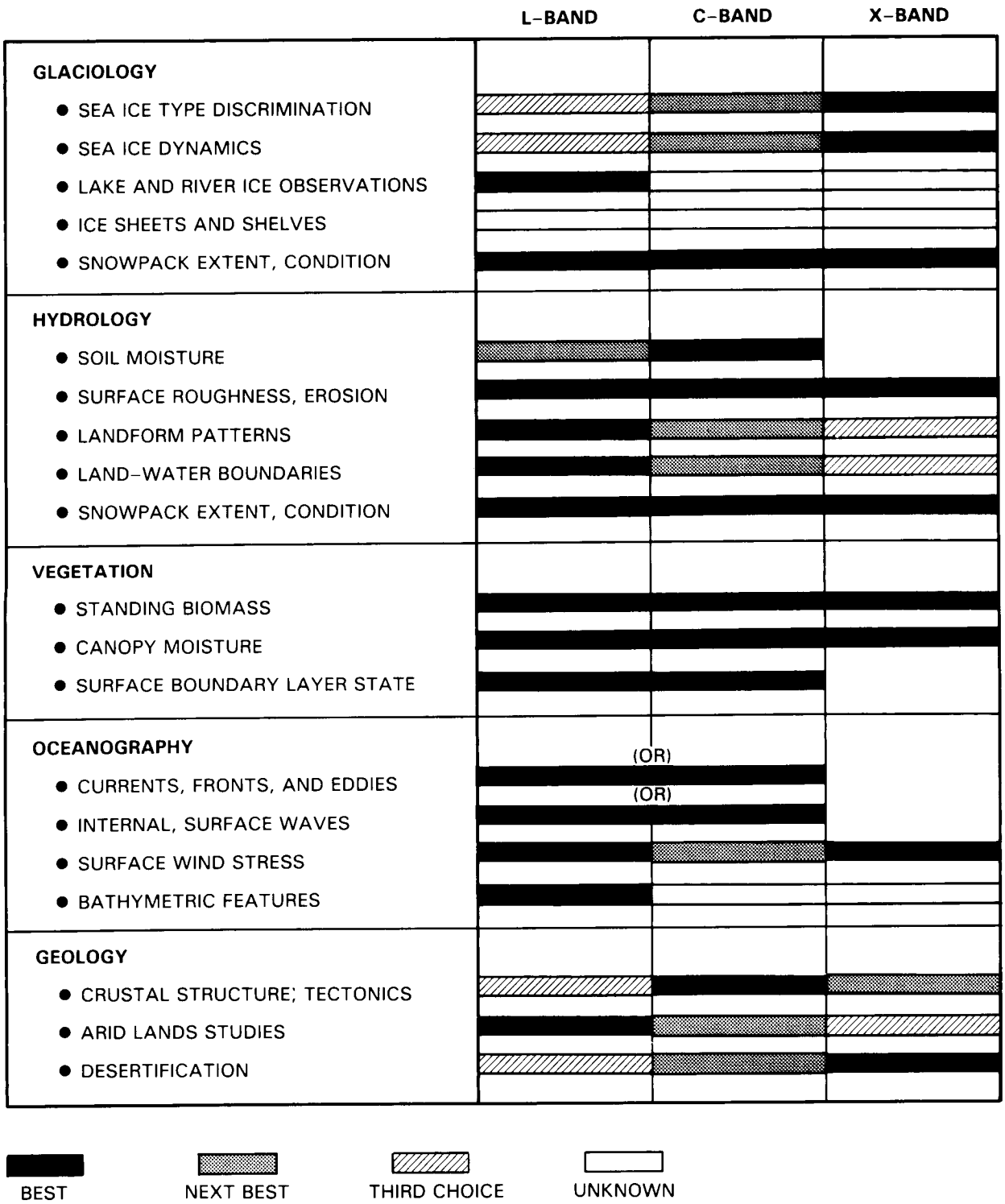

Figure 61. Summary of frequency requirements for the five science disciplines.

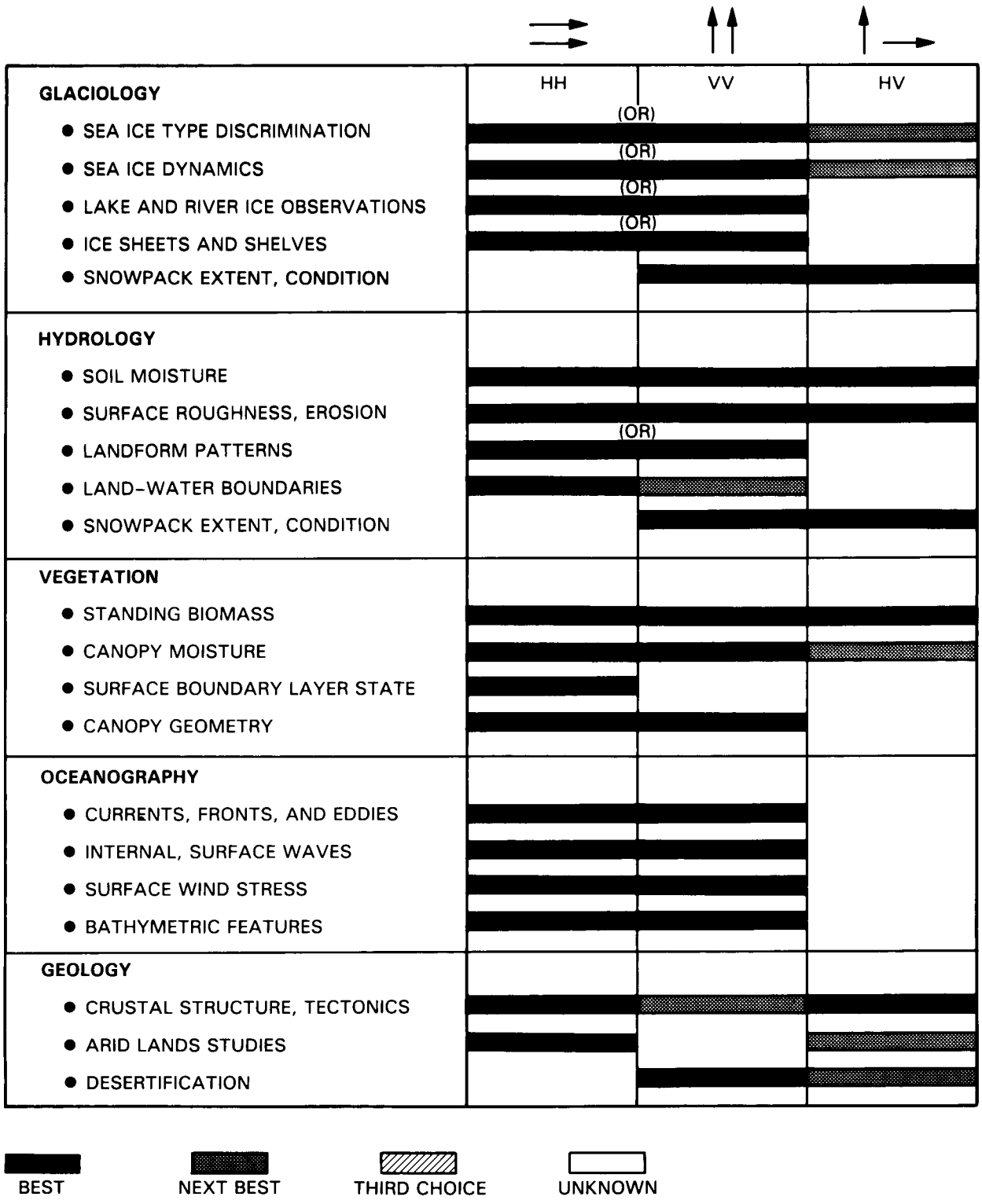

Figure 62. Summary of polarization requirements for the five science disciplines.

will reveal a number of surprises about the response of the Earth's surface.

Calibration

Radiometric Calibration

The radiometric calibration of a SAR establishes a relationship between SAR image intensity and the radar backscattering coefficient (σ°) of the imaged surface. The relative calibration of the SAR establishes how precisely one measurement can be related to another while absolute calibration establishes the accuracy of the measurement of σ°. The relative calibration of a system accounts for changes or instabilities in its subsystem parameters, such as gain drifts in amplifiers. Absolute calibration takes into account the transmitted power level, system biases, and the absolute gain of the antenna and receiver. It establishes the constant K in the relationship $I = K\,\sigma^\circ$, where I is the SAR image intensity.

Absolute Calibration—There are three main reasons why the Eos SAR will need to be accurately calibrated on an absolute scale:

Geophysical Parameter Dependence on σ°—There are at least four geophysical parameters derivable from SAR images that depend on good absolute calibration.

1. *Snow water equivalent.* As shown in Figure A.2, SWE has a unique relationship to σ° dependent on frequency, polarization, incidence angle, and snow wetness. The measurement of SWE would be made for dry snowpacks (night observation); an absolute calibration of ± 1 dB is required to obtain a SWE accuracy of ± 10 cm.
2. *Leaf area index.* LAI also has a unique relationship to σ° dependent on frequency, polarization, incidence angle, and phenologic state. An absolute calibration of ± 1 dB is required to establish an LAI accuracy of ± 0.5 for $0 < \text{LAI} < 2$ (Ulaby *et al.*, 1986).
3. *Soil moisture.* The measurement of soil moisture for bare fields with known roughness and slope may be accomplished directly from a knowledge of σ°. (We may obtain the roughness from observations at three or four incidence angles.) An absolute calibration of ± 1 dB would correspond to an accuracy of ± 0.3 gm/cm^3 in volumetric soil moisture.
4. *Oceanic wind speed.* The measurement of sea surface wind speed will normally be made by SCATT, where there is a relationship between the absolute value of σ° and surface wind speed; however, for comparison of SCATT wind speed profiles to SAR images, it will be desirable to calibrate the SAR to ± 1 dB, which would correspond to an accuracy of about ± 20 percent in wind speed (for wind speeds less than about 7 m/s).

Comparison of Eos SAR Data to Other Radar Data—The second need for absolute calibration derives from a requirement to make quantitative comparisons of Eos SAR image intensities to those obtained by other spaceborne radars such as Radarsat, ERS-1, JERS-1, and as mentioned above the Eos SCATT. This of course presumes that these other sensors will likewise be accurately calibrated.

Multifrequency Comparisons—The multifrequency capability of the Eos SAR can be fully exploited only if we are able to quantitatively ratio σ° at one frequency (e.g., C-band) to that at another frequency (e.g., X-band). Accurate establishment of these ratios will be necessary in order to extract geophysical and biophysical information via quantitative scattering models. An absolute calibration of ± 1 dB will be required for multifrequency comparisons.

Relative Calibration—It will also be necessary to maintain good relative calibration, both spatially and temporally. Good relative spatial calibration within an image means that there is good radiometric fidelity across and along the swath. For studies of ice dynamics and type, it may be necessary to maintain radiometric fidelity to better than ± 1 dB across several hundred kilometer swath widths. Good relative temporal calibration means that the instrument is stable, i.e., the transmit power, receiver gain, and antenna gain do not drift appreciably. It is especially important to maintain good stability over periods of months or years in order to allow quantitative studies of long-term changes such as desertification processes.

Good relative calibration between the HH and VV channels at a given frequency will also be necessary to fully exploit the polarimetric capability of the Eos SAR. It is estimated that a ± 0.2 dB amplitude and 10° phase relative calibration will be required for this purpose.

Unless otherwise specified, the goal is for ± 1 dB absolute calibration and ± 1 dB relative. It is recognized that this level of calibration is not currently available, and that new calibration techniques will need to be developed, most likely using extended ground targets with accurately known scattering properties.

Geometric Calibration

The geometric calibration of a SAR image establishes the relative geometric fidelity of surface features within the image, and the absolute location accuracy of these features on a cartographic grid. This is particularly important in the Eos era, where

analysis of large volumes of SAR and other Eos data will require automatic coregistration and mosaicking routines. The establishment of good relative geometric fidelity in a SAR image involves various routine image-processing steps such as correcting for image skew generated by the data-taking geometry and correcting for the variation of ground-range resolution as a function of the angle of incidence. Good absolute geometric calibration requires accurate knowledge of the platform position to within one resolution cell. Unless otherwise specified, it is required that points within any Eos SAR image be georeferenced to within half a pixel (15 m for the high-resolution mode) such that automatic coregistration with other Eos sensors (especially with HIRIS) and with other Eos SAR images acquired on different dates may be incorporated.

Dynamic Range

The dynamic range of the Eos SAR refers to the ratio of the maximum to minimum measurable radar echo intensities. In general, radar echoes can vary over a 60 dB or larger dynamic range with the weakest returns from calm seas and lakes, and the strongest returns from mountainous, forested, or urbanized regions.

Practical bandwidth-limited space-to-Earth transmission channels, however, make it necessary to trade dynamic range (number of bits) against swath width and resolution. This is because the channel data rate is proportional to the product of the number of bits times the total number of range cells. If the number of bits is too low, image quality suffers.

For the Eos SAR, it is desirable to maintain an effective 60 dB dynamic range, but it is also necessary to achieve large swath widths.

VIEWING PARAMETERS

The principal SAR viewing parameters are the *incidence* and *azimuth angles*, the *swath width*, the *resolution*, and the *revisit times*. The incidence and azimuth angles are set by the SAR antenna beam-pointing angle; for a fixed antenna length, the maximum achievable incidence angle is determined by the altitude and the target scattering properties (σ°). In addition, the wider the swath, the greater the range in incidence angle across the swath. The swath width is determined by the antenna elevation beamwidth, and the available data rate, and the resolution is determined by the bandwidth and the incidence angle. The swath width may be increased using the SCANSAR (SAR mode utilizing electronic steering to create wide swaths) capability; the resolution is reduced by approximately the same factor as the swath is increased. The time interval between revisits (repeat cycle) is set by the spacecraft altitude. It is recommended that a 3-day exact repeat cycle be used for soil moisture investigations over a period of months and that the altitude be changed to a 16-day repeat cycle for the other objectives requiring synergistic observations with HIRIS, etc. This is discussed further below.

It is also recommended that the Eos SAR incorporate an electronic beam-steering capability like that planned for SIR-C, with a 15° to 60° range in elevation. The antenna should also have a capability to be mechanically rotated to look to the left or right of the spacecraft nadir track; thus providing a capability for imaging to either side of the ground track. The Eos SAR should also provide for beam steering in azimuth.

Incidence Angle

In general, there are four advantages to acquiring radar imagery at selectable incidence angles. For a given SAR frequency and polarization, the incidence angle may be used as a variable to generate quantitative scattering models for determining surface geophysical and biophysical properties. Backscatter curves (σ° versus θ) generated from scatterometer data indicate the shapes of the curves for different terrain types are fairly well behaved (Figure 63). In general, there is a rapid decrease in backscatter with increasing incidence angle at small incidence angles. At larger angles, the slopes level off to a slowly decreasing backscatter with increasing incidence angle. In addition, the magnitude and the shape of the backscatter curves vary with surface roughness and volume geometries.

For discrimination of surface roughness in flat terrain, near-nadir incidence angles are preferred. Sea, lake, river ice, desertification, and soil erosion studies fall in this category. For hilly or mountainous terrain, surface roughness is enhanced at larger incidence angles. Even though the sensitivity to surface roughness at any single high-incidence angle is less, variations in slope due to topography will have a minimal impact on the backscatter. For surfaces made up of two layers, for example vegetated or snow-covered surfaces, the combination of large- and small-incidence-angle data can be used to enhance the separation of the two systems. Larger incidence angles allow less penetration, thereby providing a greater contribution from volume scattering by the upper layer. Small-incidence angles are best to minimize the effective length of the scatterers in the upper layer (this applies particularly to vegetated regions) thereby maximizing the return from the lower boundary surface.

For the purpose of characterizing surfaces by the incidence angle signatures of backscatter, at least six incidence angles ranging from 15° to 60° are desired. In many cases, loss of the data at incidence angles greater than 45° will have little impact on the classification; however, in some cases, particularly;

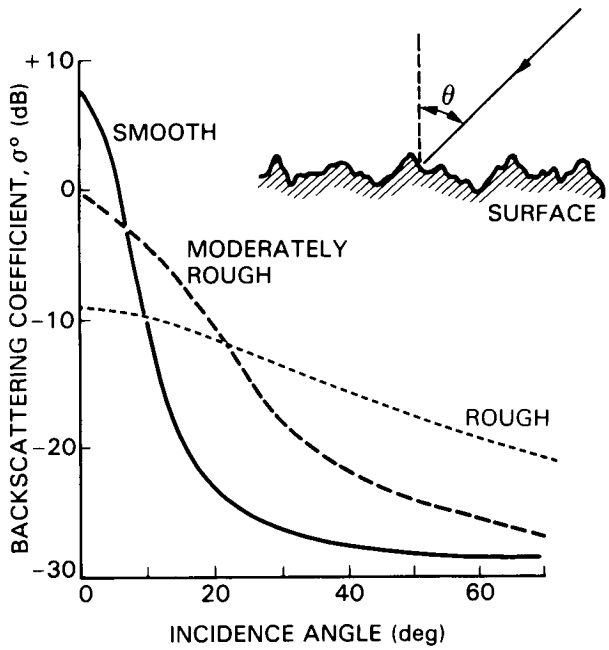

Figure 63. Typical backscatter curves for smooth, moderately rough, and very rough surfaces.

vegetation and snow studies, data acquired at angles greater than 50° are essential.

The number of incidence angles that can be used to view a given site is governed by the satellite repeat cycle (altitude). For a 16-day repeat cycle, several different incidence angles can be employed; however, for a 3-day repeat cycle, only one or two incidence angles are available. This situation is discussed further in Chapter X, Synergism.

Stereo Imagery

There are two main applications of radar and photographic stereo: visual interpretation of topography for geologic or terrain analysis, and production of topographic maps. There are a number of ways of acquiring stereo radar imagery, although multiple incidence angle imaging is the preferred method. The larger the difference in look angles of the stereo pair, the greater the terrain exaggeration. However, preliminary results from the SIR-B mission (Leberl *et al.*, 1986) indicate that generating topographic maps from images acquired with large separation angles causes confusion due to large variations in backscatter with incidence angle.

For the purpose of visual interpretation, images with incidence angles separated by about 20° are most useful. For generating topographic maps, images with incidence angle separations of about 5° to 10° produce the most accurate results. It is desirable in both applications that both the images be acquired at incidence angles greater than about 30° and less than about 50° to avoid confusion from layover and shadowing.

Topographic Highlighting

Topographic highlighting in a radar image is vital for determining surface morphology. For example, geological features such as folds and faults are often expressed topographically in a very subtle manner. High-incidence-angle observations increase the topographic highlighting because of shadowing or low radar return due to the grazing incidence of the radar beam.

In order for a topographic feature to actually cast a radar shadow, its slope must exceed the complement of the radar incidence angle. For example, a slope must exceed 35° to get a shadow with a 55° incidence angle. Inasmuch as there are many more slopes that exceed 30° than 35°, the optimum incidence angle for topographic highlighting is 60° or more.

Small-incidence-angle imagery may also be used for topographic highlighting. Radar backscatter changes rapidly at small incidence angles. This effect provides the desired highlighting in a different way. In this scheme, information is not lost in shadows as is the case at large incidence angles. The penalty is that in steeper terrain, radar images acquired at lower incidence angles are geometrically distorted.

Imagery acquired at incidence angles of 15° to 20° and 55° to 65° is desired for topographic highlighting of subtle terrain features. For flat bare terrain, the radar echoes will be too weak to produce a usable image at the large angles; however, for rough, vegetated terrain a good signal return is expected.

Improved Accessible Field-of-View (FOV)

By steering the antenna beam through a range of selectable incidence angles, flexibility in site selection is significantly enhanced (Figure 64a). Table 10 lists the range of target distances from the platform nadir point which may be imaged as a function of platform altitude; this assumes that SAR image quality is acceptable over a 15° to 60° range of incidence angles. Table 10 also shows the accessible FOVs on each side of the nadir track and the near-nadir coverage gap.

The number of days within the 16-day repeat cycle of the orbit in which a given target may be imaged does not change significantly with altitude. At 824 km and 700 km, targets are lost for 3 days due to the large gap between 15° and nadir (Figure 65). At 542 km targets are lost at the edge of the repeat cycle. The number of imaging days per repeat cycle is also listed in Table 10 for targets at the equator.

At increasingly larger incidence angles, the additional accessible FOV (in kilometers from the nadir track) per degree of angle change increases significantly (Figure 64b), especially at the higher Eos altitudes. Therefore, the larger the maximum incidence angle capability, the greater the improvement

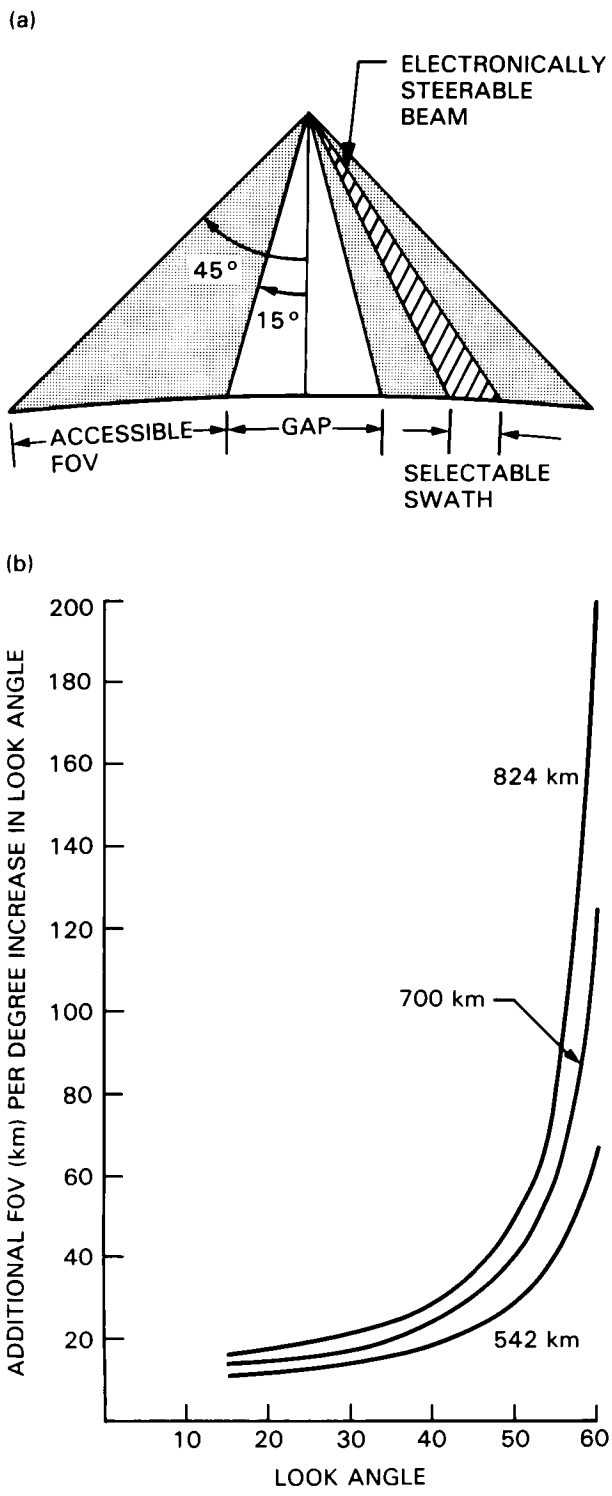

Figure 64. (a) Accessible FOV for a variable look angle and look direction SAR antenna. (b) Additional FOV (km) per degree increase in look angle as a function of look angle.

in accessible FOV. This is generally desired for many of the scientific objectives as long as high quality data can be acquired at the larger angles.

Azimuth Angle

Multiple-azimuth-angle imagery acquired by squinting the SAR antenna beam (to the right or left of the cross-track direction) is desired for three primary reasons (Figure 66):

1. *To acquire near-simultaneous SAR and HIRIS data at selectable SAR incidence angles.* In any platform-instrument sorting scenario, acquisition of simultaneous or near simultaneous SAR and HIRIS data requires flexibility in the look angles of both instruments. With only 1° of freedom in SAR imaging geometry, an investigator requiring near simultaneous SAR and HIRIS data would have no choice in SAR incidence angle. By adding a multiple-azimuth-angle capability, the incidence angle of SAR is selectable.
2. *To provide information on a terrain's scattering properties as a function of azimuth angle.* Multi-azimuth-angle data sets are very useful for any target with a preferred azimuth pattern, (for example faults, ocean waves, or agricultural fields). For faults or other geomorphic lineaments, the direction of the fault determines the optimum viewing angle. Selectable azimuth angles between 0° and 60° in either the forward or reverse direction (only one direction is required) in combination with the capability to image on either side of the platform nadir track and on ascending and descending passes will provide a variety of viewing geometries for a given target (Figure 67).
3. *To provide day/night coverage at the same azimuth angle.* For many studies, particularly in the hydrology and vegetation disciplines, diurnal coverage is required. This can be accomplished by combining ascending afternoon passes and descending midnight passes with SAR. However, since the ascending and descending tracks cross the equator at an angle of approximately 8°, SAR must be squinted approximately 16° in order to acquire the data with the same azimuth angle. Added confusion effects with different day/night azimuth angles will be particularly bothersome with vegetation and hydrology sites, which often have a directional bias due to planting or drainage patterns.

Look Direction

In addition to varying the incidence angle, it is also desirable to vary the look direction from the left to the right side of the platform nadir track for three primary reasons: (1) to increase the number of viewing geometries for geologic studies, as discussed

Table 10. Accessible FOV Versus Altitude

Altitude (km)	Minimum Accessible Distance (km)*	Minimum Accessible Distance (km)**	Accessible FOV (km)	Gap (km)	Imaging Days Repeat Cycle
824	222	1,998	1,776	444	13
700	188	1,554	1,366	376	13
542	146	1,112	966	292	12

* $\theta_i = 15°$
** $\theta_i = 60°$

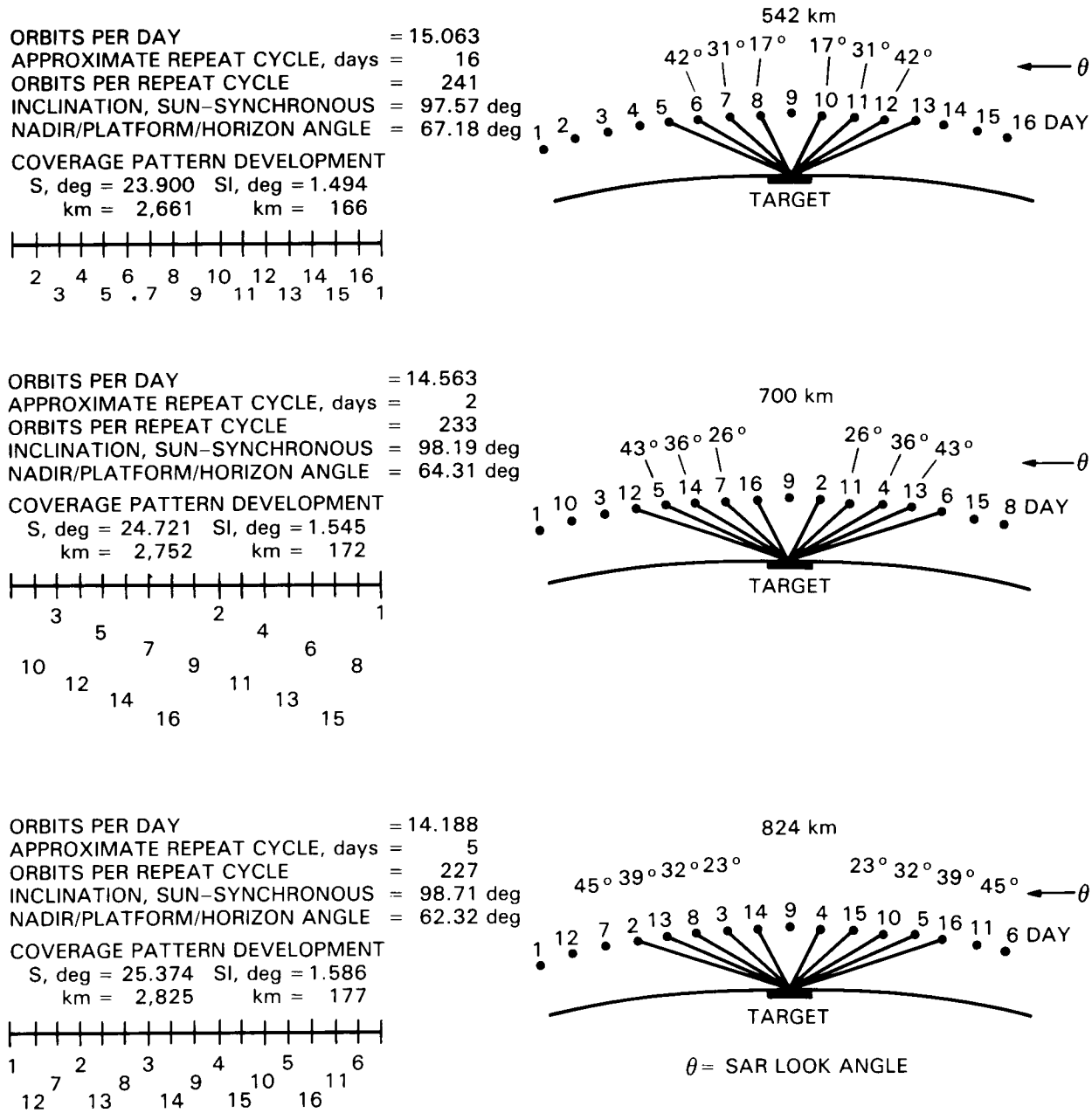

Figure 65. Specific days within the 16-day repeat cycle and corresponding incidence angles that a target may be imaged at three altitudes: 824, 700, and 542 km.

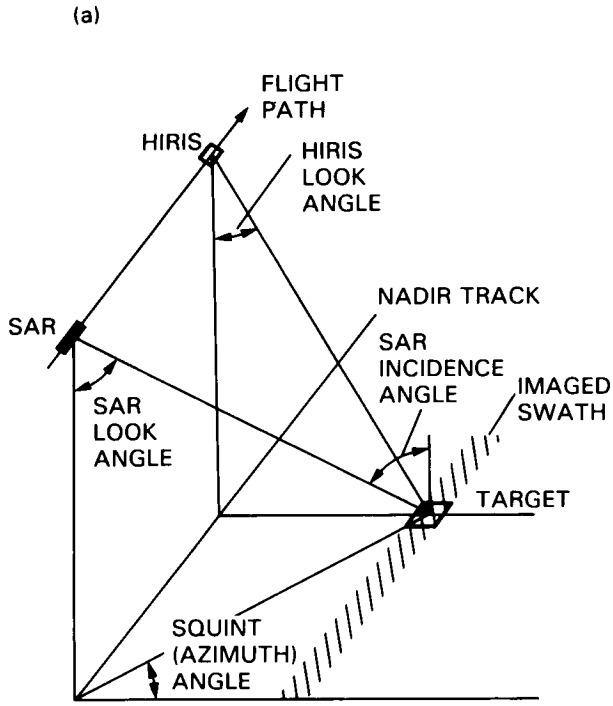

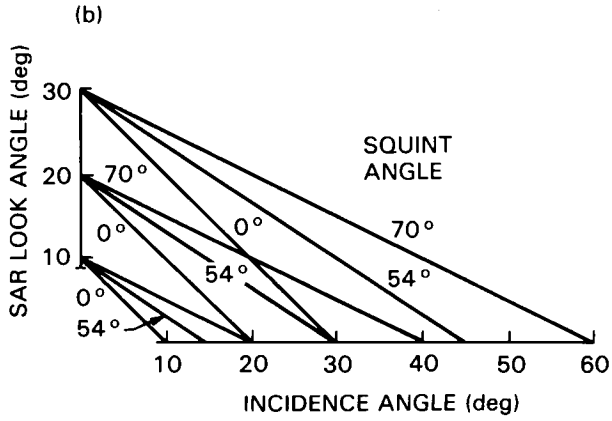

Figure 66. Imaging geometry to acquire simultaneous SAR and HIRIS data at selectable SAR incidence angles.

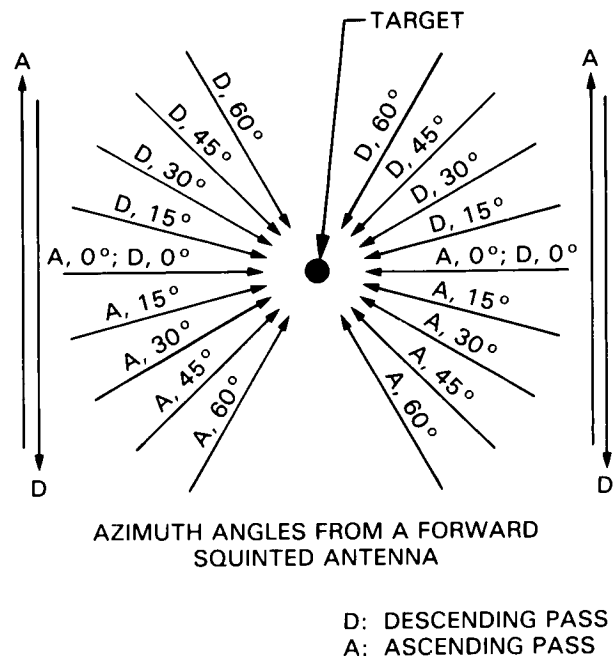

Figure 67. Possible azimuth angles from ascending and descending orbits assuming the SAR can be squinted forward up to 60°.

below and described in Figure 67; (2) to monitor a site for more days within the 16-day repeat cycle; and (3) to optimize viewing of the edges of the polar ice caps.

Resolution

It is recommended that the Eos SAR incorporate a 20 to 30 m high resolution for use in the local mode, a 50 to 100 m medium resolution for use in the regional mapping mode, and a 200 to 500 m low resolution for use in the global mapping mode. The high-resolution mode would be used for detailed studies of sea ice features (especially delineation of pressure ridges), lake ice, recent fault scarps and structural attitudes, and vegetation morphology in rapidly varying terrain. The medium-resolution mode would be used for regional mapping of soil erosion, desertification, soil moisture, sea ice, and for ocean surface surveys. The low-resolution mode would be used for antecedent precipitation studies, global soil moisture surveys, large-scale forest monitoring, and for synoptic mapping and morphologic characterization of world desert regions.

Swath

Although very large swath widths are generally desirable, instrument and data rate limitations require that for high resolution, swath widths be held to a minimum and that mosaicking techniques be implemented to obtain very wide swaths. The parameter most affecting the required swath width then is the temporal variability of the surface feature being studied. For geologic features, changes are not expected to occur within the lifetime of the Eos mission, therefore swath widths may be extremely narrow and mosaicking implemented. For other surface features, for example the polar ice margins, changes are expected to occur on a daily basis. For these applications, wide swaths of several hundred kilometers are required.

Revisit Times

Glaciology studies require very frequent revisit intervals. Inside polar ice pack boundaries, ice movements are primarily in response to the movement of large-scale weather systems. This means that it is desirable to make observations every 3 to 6 days; these observations can be made in the medium-resolution mode. It is important to image both the entire Arctic and Antarctic sea ice packs at sufficiently short time intervals to characterize ice kinematics; the total coverage requirement for each ice pack will vary as a function of time of year. It will also be necessary to monitor a variety of selected ice processes occurring *within* the ice packs, especially at their margins, at higher resolution (20 to 30 m) and on a daily basis during periods of rapid change.

Bimonthly observations of alpine glaciers and yearly observations of large continental ice sheets near the margins are adequate to delineate major calving events. In the interior of large ice sheets, biyearly observations are required for investigations of accumulation processes and grain growth in the near-surface layers. For movement only, observations every 5 years may be sufficient. For regions of rapid movement such as the Ross Ice Shelf and some alpine glaciers, bimonthly observations of deployed passive radar reflectors may be required.

Selected "representative" snowpacks should be observed both during their accumulation and melt. Monthly imaging during accumulation is adequate; observations approximately every 4 days during the melt period, both day and night, are desired.

Some *hydrologic* applications also require frequent revisit intervals. After a precipitation event, soil moisture can vary rapidly depending on soil characteristics; this means that Eos SAR studies of short-term temporal and spatial variability will require frequent observations, preferably every two or three days. The preferred observational strategy is to employ change detection techniques (i.e., comparison of images acquired every 3 days with the same illumination geometry).

Longer-term repeat observations of watersheds are needed to monitor both water and chemical fluxes. For these objectives, a 2-year repeat cycle is required to monitor the significant long-term changes in watershed morphology that are not purely the result of variations in soil moisture.

In the area of *vegetation,* investigations of forest and agriculture phenologic development will require repeat coverage on a weekly basis during periods of rapid phenologic or environmental change, and on a monthly to bimonthly basis the remainder of the year. Semimonthly low-resolution coverage of grasslands is desired, while seasonal high-resolution coverage of these regions is needed. Frequent revisit intervals should be optimized for monitoring the biophysical state of a biome, at the expense of complete mapping. For monitoring the change in areal extent of a biome, such as in monitoring deforestation, complete mapping is required, but only on annual cycles.

The revisit period for *oceanographic studies* varies considerably with scientific objective. For example, meso- and fine-scale currents should be observed every few days, whereas bathymetric measurements can be made over a period of several months. In the early stages of Eos, near-complete cover (90 percent) of a region should be completed in 4 or 5 days and repeated every 2 weeks. In general, however, the temporal scale of many of the oceanic processes is not well understood, so that observations should be made as frequently as possible until the time scales of the processes are better understood.

Geologic time scales are generally much longer than the envisioned 15-year lifetime of Eos. Even the most tectonically active regions of the continents change relatively slowly, except for the effects of earthquakes and volcanic eruptions. This means that for most structural and tectonic studies, only two Eos SAR global coverage data sets are required, one for each season (winter and summer). For geologic hazards studies and to assess the immediate effects of catastrophic geologic phenomena (earthquakes, volcanic eruptions, floods), the flexibility to obtain SAR data during or soon after the event will be essential.

The geology of arid lands will not change perceptibly during the Eos lifetime, with the possible exception of hydrologic changes related to near-surface ground water aquifers. For monitoring and assessment of desert hydrology/geology interactions, coverage during both the wettest and driest months would be required about every 2 years.

Soil erosion is also a very slow process, but can undergo rapid acceleration during catastrophic climatic events such as windstorms and seasonal droughts. Repeat coverage every 2 years of major test sites is required with acquisitions immediately following the driest, wettest, and/or most windy season locally. The best seasons for initial coverage in most temperate latitudes might be midwinter and early fall.

Desertification extent does change on the time scales of the Eos mission. Complete coverage of desert margins, as well as selected transects across the regions, are required several times each year.

STANDARD OPERATING MODES

The Eos sensor we envision will have a very high degree of flexibility in channel and imaging geometry selection. We have identified two kinds of operational parameters which are essentially independent of each other except in determining total data rate: (1) sensor parameters (including frequency and polarization), and (2) viewing parameters (including resolution, swath width, and imaging geometry).

Three general viewing modes are envisioned for the Eos SAR. The first is a *global mapping mode* with up to a 700 km swath width and 500 m resolu-

tion. The second is a *regional mapping mode* with a 50 to 100 m resolution and a 100 to 200 km swath. The third is a *local high-resolution mode* with a narrow swath (30 to 50 km) and 20 to 30 m resolution. At one extreme, the global mapping mode would be used for global-scale surveys of large regions (e.g., the ice dynamics of the polar ice caps or the biomass of the Amazon forest). At the other extreme, the local transect mode would be used for detailed studies of relatively localized sites.

The number of SAR sensor modes or channels (e.g., frequencies and polarizations) that can be simultaneously acquired is determined by the allowable data rate, which is dependent on the viewing mode (swath and resolution). For a given data rate, e.g., 100 Mbps, the product of the swath width, the resolution, and the number of channels must be held to a constant. This tradeoff is discussed further in Chapter IX.

SUMMARY OF INSTRUMENT AND VIEWING REQUIREMENTS

Table 11 summarizes the principal instrument and viewing requirements for the Eos SAR.

Table 11. Summary of Instrument and Viewing Requirements

Frequency	L-, C-, and X-band K- and P-bands also desired
Polarization	Quad (HH, VV, HV, and VH plus phase) for all frequencies
Radiometric calibration	± 1 dB relative ± 1 dB absolute
Geometric calibration	15 m for high-resolution mode ½ pixel for all modes
Dynamic range	60 dB, effective
Incidence angle	15° to 65°, variable per site, 1° increments
Azimuth angle	0° to 60°, fore or aft (not both)
Look direction	Left and right of nadir track
Resolution	20 to 30 m–local high-resolution mode 50 to 100 m–regional mapping mode 200 to 500 m–global mapping mode
Swath width	30 to 50 km–local mode 100 to 200 km–regional mapping mode up to 700 km–global mapping mode
Revisit interval	3 days (hydrology and glaciology) 16 days (other disciplines)
Lifetime	15 years

VIII. SAR SYSTEM DESIGN

This chapter outlines a recommended configuration of the Eos SAR. The design of the SAR should be responsive to the scientific requirements described in previous chapters and also utilize the technology inheritance from SIR-C and X-SAR. In fact, a primary intent of the Shuttle Imaging Radar program has been to develop a SAR that would meet the needs of the Earth observation community in the 1990s. The shuttle has served as a testbed to develop successively more complex spaceborne hardware, as well as to exercise more robust and efficient ground data and operations systems. This program has also demonstrated the value of imaging radar to the scientific community. The evolution of the SIR system parameters from the Seasat SAR to Eos is discussed in Chapter I.

In order to meet the Eos scientific requirements and also take advantage of the SIR-C/X-SAR technology, the Eos SAR should provide three frequency channels (L-, C-, and X-band) with full polarization capability at L- and C-bands; as a minimum the X-band channel should provide like polarizations (HH and VV), and also cross-polarization if technology permits. Electronic beam steering must be provided for all the channels. The SIR-C instrument will also have most of these capabilities and will offer the first spaceborne tests of multiparameter radar technology. Table 12 and Figure 68 compare the main sensor and mission characteristics of the Eos SAR to previous spaceborne SAR missions.

Although other additional scientifically desirable options have been considered by the SAR Panel, the baseline design recommended for the Eos SAR facility instrument has been scaled with consideration for size, weight, power consumption, and cost. For example, a P-band channel (75 cm wavelength) has not been included because of the rather large antenna size and weight and because of potentially severe fading due to ionospheric Faraday rotation. A K_u-band channel (1.5 cm wavelength) has also been excluded because of prohibitive transmitter power requirements. It may be desirable to include these channels in a post-IOC design, however.

The tradeoffs in SAR design discussed in this chapter presume a degree of familiarity with the principles of SAR. Appendix F presents a short tutorial on those principles as they relate to the Eos SAR.

SIR-C TECHNOLOGY INHERITANCE

SIR-C/X-SAR, currently scheduled for launch in the early 1990s, will be the first spaceborne SAR to provide multifrequency, multipolarization, and variable-incidence-angle data simultaneously (or near simultaneously in the case of incidence angle). The L- and C-band radars are being designed and built by JPL as SIR-C; the X-band radar is being provided by the DFVLR as X-SAR. The SIR-C design and much of the hardware can be directly inherited by the Eos SAR. Previous spaceborne SARs (Seasat, SIR-A, and SIR-B) all utilized a single frequency (L-band), a single polarization (HH), and either fixed look angles or mechanically steerable antennas; these radars also utilized a single solid-state 1,000 W transmitter.

The baseline SIR-C instrument will provide both L-band and C-band channels, and will utilize two planar arrays, one for L-band dual-polarized operation and the other for C-band dual-polarized operation. Each array is composed of a uniform grid of dual-polarized microstrip antenna elements and each polarization port is fed by a separate corporate feed network. Each frequency/polarization port is routed to a separate receiver and data channel. This will allow capture of the full polarization matrix, which contains amplitude, phase, and polarization of the radar echoes (HH, VV, HV, VH).

The SIR-C design is based on distributed SAR technology that uses a multiple array of solid-state high-power amplifiers (HPAs), low-noise amplifiers (LNAs), and 4-bit phase shifters distributed across the antenna aperture (Figures 69a and 69b). By positioning the transmit/receive modules immediately behind the radiating elements, this distributed system avoids power losses associated with conventional corporate feedlines, and results in efficiency improvements of up to eightfold. This arrangement results in a more efficient use of transmitter power, and corresponding improvements in the receiver sensitivity. In addition, the inherent redundancy and the extended lifetimes of the distributed systems make them more desirable for the long-duration Eos mission.

The dimensions of the SIR-C antenna are 4.1 m x 12 m. This allows for a 2.9-m wide L-band array, a 75-cm wide C-band array, and a 40-cm wide X-band antenna. The Eos SAR antenna length would be 20.2 m (Figure 69) in order to achieve the desired performance at the higher platform altitude (see Appendix F). The estimated peak radiated power is 6.0 kW, 3.6 kW, and 5.0 kW for L-, C-, and X-band, respectively.

The SIR-C antenna array is configured with a transmit/receive (T/R) module connected to each one of 18 microstrip subarray elements distributed along the elevation axis of the antenna. The phase shifters used with this arrangement allow $\pm 23°$ electronic beam steering in the range (cross-track) direction. This will make it possible to acquire images at selectable incidence angles without tilting the entire antenna (or rolling the shuttle).

Because of current technology limitations, the X-band SAR (to be provided by DFVLR) will provide only VV polarization and will use a passive slot-

Table 12. Evolution of Eos SAR Characteristics

Parameters	Seasat	SIR-A	SIR-B	SIR-C/X-SAR	Eos SAR
Mission month	July-Oct	Nov	Oct	Feb, July	TBD
Mission year	1978	1981	1984	1991, 1992	1995
Altitude (km)	800	259	225	225	542,700, or 824 (824 baseline)
Inclination	108°	38°	57°	57°	sun-synchronous
Frequency (GHz)	1.28	1.28	1.28 5.3 9.6	1.25 5.3 9.6	1.25 5.3 9.6
Polarization	HH	HH	HH	HH (L,C) VV (L,C,X) VH (L,C) HV (L,C)	HH (L,C,X) VV (L,C,X) VH (L,C) HV (L,C)
Incidence angle	23°	50°	15°-65°	15°-55°	15°-55°
Swath width (km)	100	50	20-50	15-90	15-700
Azimuth resolution (m)	25 (4 look)	33 (6 look)	20 (4 look)	40 (4 look)	40 (4 look)
Range resolution (m)	25	40	58-17	60-10	120-10
Peak power (kW)	1	1	1	3.4 (L) 2.7 (C) 3.3 (X)	6.0 (L) 3.6 (C) 5.0 (X)
Bandwidth (MHz)	19	6	12	20, 10	20, 10, 5
Optical data collection (hrs)	42	8	8	none	none
Digital data collection (hrs)	42	none	7	50 h/channel (3 channels)	~25%

ted waveguide array antenna. Thus a tilt mechanism is required to point the X-SAR. An upgraded version of X-SAR with both HH and VV polarizations, and a distributed, electronically steered antenna is desired for Eos. This upgraded X-band system may also be provided by DFVLR as a follow-on to X-SAR.

The transmitter peak power is 3.8 kW at L-band and 2.1 kW at C-band; these are achieved by coherently combining the output from 18-element subarrays of microstrip elements. Each solid state amplifier is driven through a corporate feed network by a central radar exciter; one for each frequency. The exciter output is a train of pulses with 33 μs pulse width and a pulse repetition frequency (PRF) selectable over a range of 1,200 to 1,800 Hz, depending on shuttle altitudes and the system configuration. (The pulse width for Eos would be increased to 50 μs in order to achieve the required SNR at the Eos altitude. The longer antenna (20 m) that is proposed for Eos will permit reduction of the PRF range to 750 to 1,100 Hz.) The bandwidths of the chirp modulator are 10 and 20 Mhz for SIR-C at L-, C-, and X-bands to provide for both high and lower resolution images. A third bandwidth would be added to the Eos system to provide a lower resolution channel for the global mapping mode.

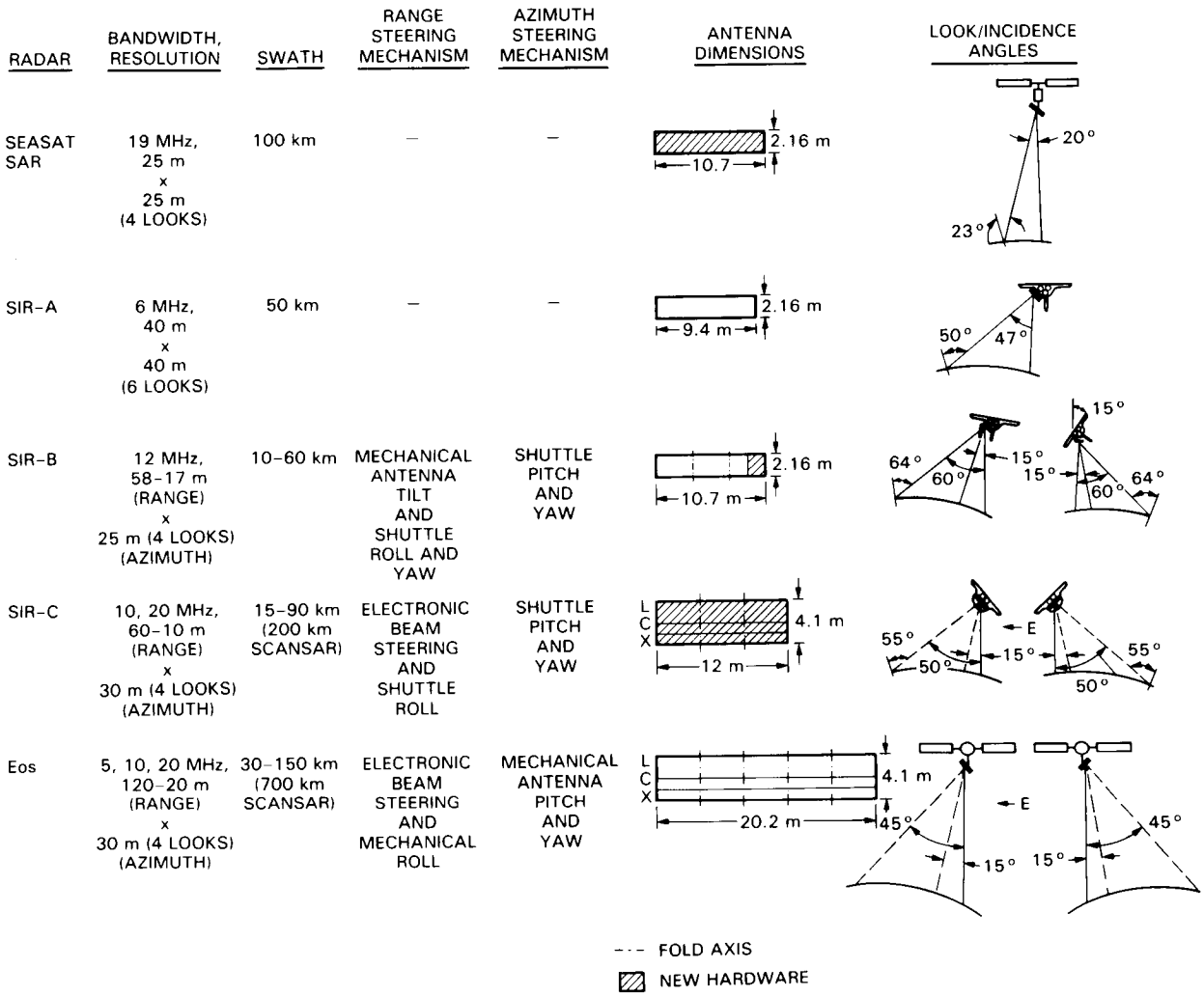

Figure 68. Evolution of the SIR antenna and imaging geometry from Seasat to Eos.

As with SIR-B, SIR-C and X-SAR data may be acquired on either side of the shuttle nadir track by rolling the shuttle 90° or yawing it 180°. It will also be possible to "squint" the antenna beam in azimuth by maneuvering the entire shuttle. The squint mode would allow SAR imaging over a wide range of azimuth angles.

Swath widths for SIR-C will range from 15 to 90 km. The swath widths will be limited primarily by the available data rate and will depend on the number of bands collected on a given pass. A more uniform illumination of the imaged swath over the full range of incidence angles can be achieved by spoiling the beam by means of phase control. A new wide-swath SCANSAR mode will also be implemented by utilizing the beam steering capability. SAR will be operated in a burst mode, with the antenna beam scanned electronically by one beamwidth between bursts. The result is a wider swath width by a factor of two to four, depending on the number of scan steps, with a corresponding degradation of azimuth resolution by this same factor.

Four solid-state receivers are included in the SIR-C system, two for L-band and two for C-band (Figure 70). In the single-frequency, quad-polarization mode one radar antenna is excited so that one polarization (H for example) is transmitted. The resulting echoes are received by both receivers (H and V), resulting in HH and HV data. A subsequent pulse excites the other polarization (V for example) so that it is transmitted, and again the echo is received by both receivers, resulting in VV and VH data. The process is then repeated one pulse repetition period (1/PRF) later. This process provides coherent and fully registered quad-polarization imagery. The dual-frequency, quad-polarization mode is similar with the exception that both L- and C-band H transmitters are activated simultaneously, followed by the V transmitters. The resulting data rate is twice that of the single-frequency, quad-polarization data.

The radar echoes from each receiver are routed through a receiver switching network to four digital data handling assemblies (DDHA), each with a data rate of 45 Mbps. These will then be directed to on-

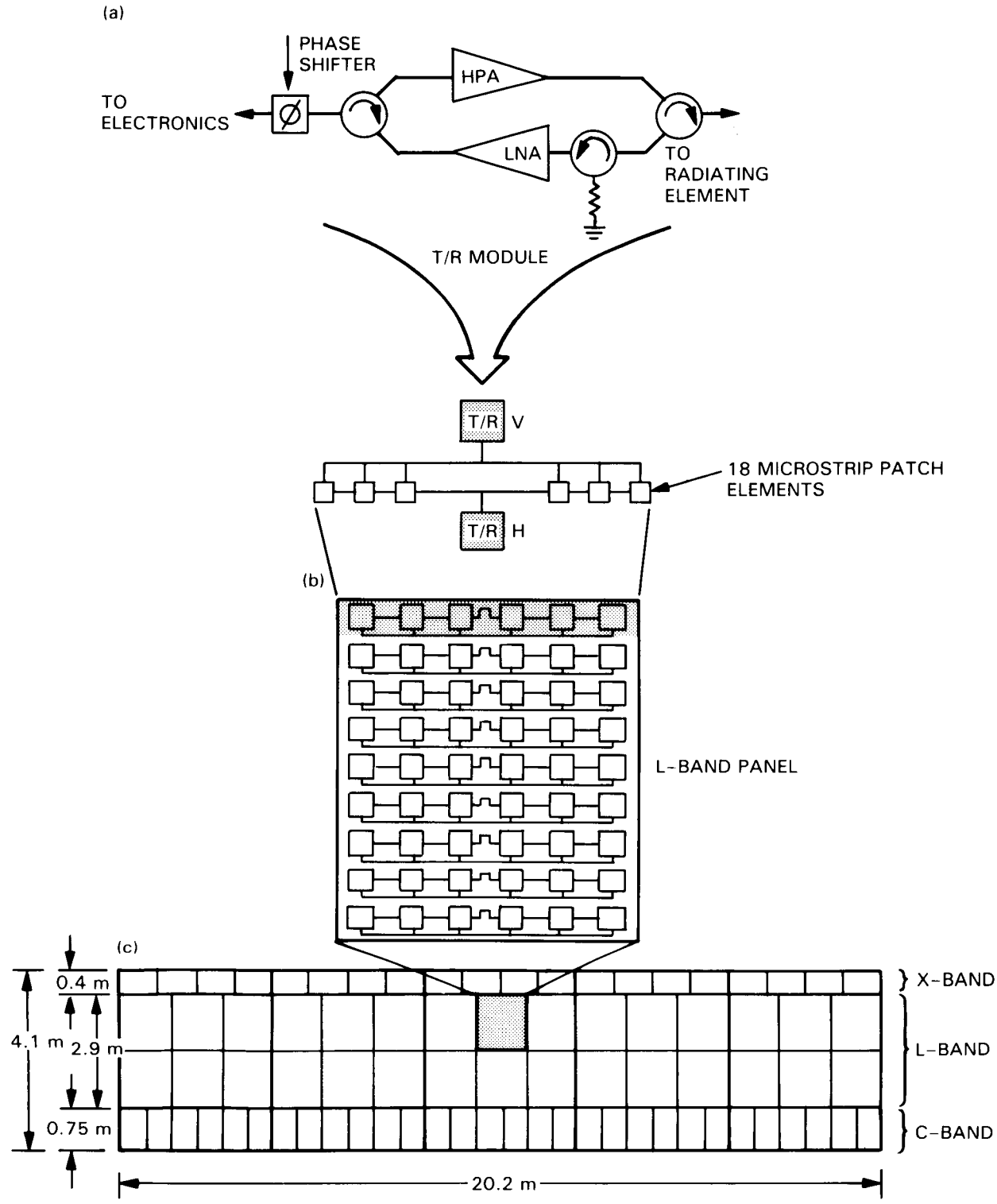

Figure 69. Eos SAR antenna concept. (a) Details of the distributed Eos SAR electronics. (b) L-band antenna panel layout. (c) Antenna array layout for L- , C-, and X-bands.

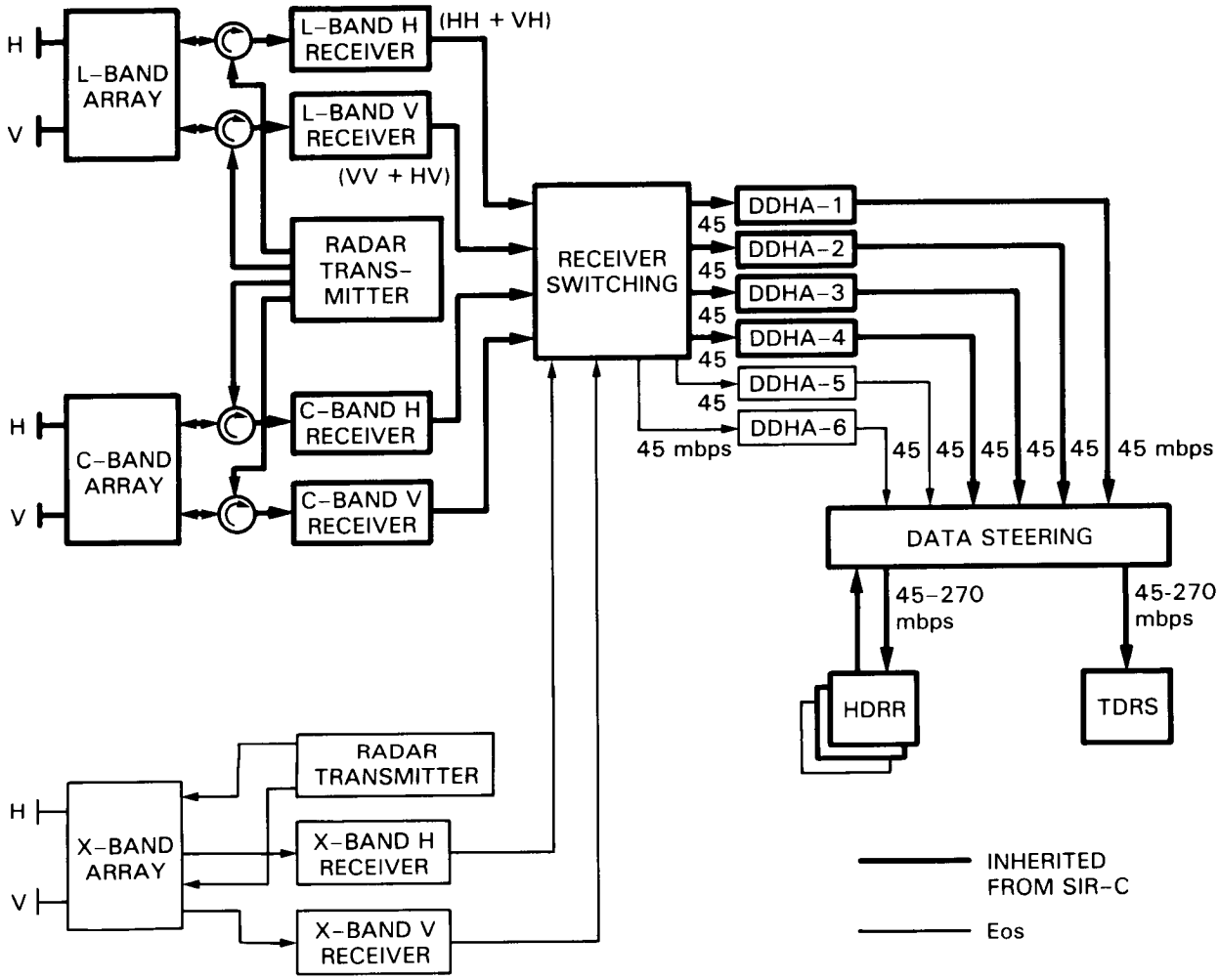

Figure 70. Block diagram of the SIR-C system indicating the new components for the Eos SAR system.

board 100-Mbps tape recorders (three are planned for SIR-C). Any one of the channels can also be routed through the shuttle's K_u-band 45-Mbps data link to TDRS to be recorded in real time on the ground. The tape-recorder capability allows coverage of virtually any location on the Earth. The TDRS system allows selected data to be downlinked in real time or near real time for engineering checks and some science analysis. The equivalent of two additional DDHAs will be added to the Eos system such that the full TDRS capability can be used to provide wide swaths and/or accommodate the additional X-band channels.

SIR-C/X-SAR is scheduled for two flights 18 months apart, starting in early 1991, in order to study seasonal variations of some terrain types. SIR-C should provide data to the archives of the Eos Information System thus expanding the lifetime of Eos with SAR by four years for certain selected locations. It is therefore essential to provide the best achievable calibration for the SIR-C system. The goal is to obtain ± 1 dB relative and ± 3 dB absolute calibration. The techniques used to obtain these high levels of calibration will include preflight calibration, inflight internal calibration, including frequent onboard measurements of transmitted and received power levels, and overall system calibration during the data takes using artificial ground targets with known scattering properties.

Eos SAR DESIGN

The Eos SAR design will be based upon scientific requirements for data, upon the experience gained with SIR-C/X-SAR and aircraft data, and upon expected improvements in technology by the early 1990s. The SIR-C L- and C-band radars should not be changed significantly as SIR-C is designed to meet most of the Eos SAR requirements. The majority of the changes will be to accommodate the higher Eos altitude and longer mission duration. Although a detailed design has not been undertaken, the principal preliminary design features are discussed below.

Figure 71 is a block diagram of the Eos SAR instrument. The sensor would be composed of several subsystems: the antenna, the radio frequency (RF) electronics, the Data Handling Subsystem, the Command and Telemetry Subsystem, and the Power Distribution Subsystems. These all would exist on the Eos spacecraft. The antenna would be mounted on a mechanical gimbal for articulation (Figure 72) and the remainder of the subsystems would be mounted directly on the carrier and require no articulation. In addition, there would be three subsystems which exist on the ground: the SAR processor, the SAR Instrument Control Center (ICC) and the Ground Calibration Network. The SAR processor and ICC subsystems are discussed in subsequent chapters.

The discussion below of recommended instrument and viewing parameters is in response to the Chapter VII summary of the instrument and viewing parameters required to meet the scientific objectives.

Instrument Parameters

The instrument parameters discussed below will meet the majority of the science requirements for all five disciplines. For any single application, only a subset of the parameters will be needed depending on the specific characteristics of the surface and the biophysical and geophysical parameters of interest. Thus, in order to efficiently utilize available power and data rate, and optimize imaging swaths, channel selection is essential. Any combination of channels is selectable.

Frequency

The design inherited from SIR-C and X-SAR includes L-, C-, and X-band frequencies. These three frequencies (1.248, 5.298, and 9.600 GHz) provide an 8:1 spectral range, and will enable research to be conducted on the wavelength-dependent processes of sur-

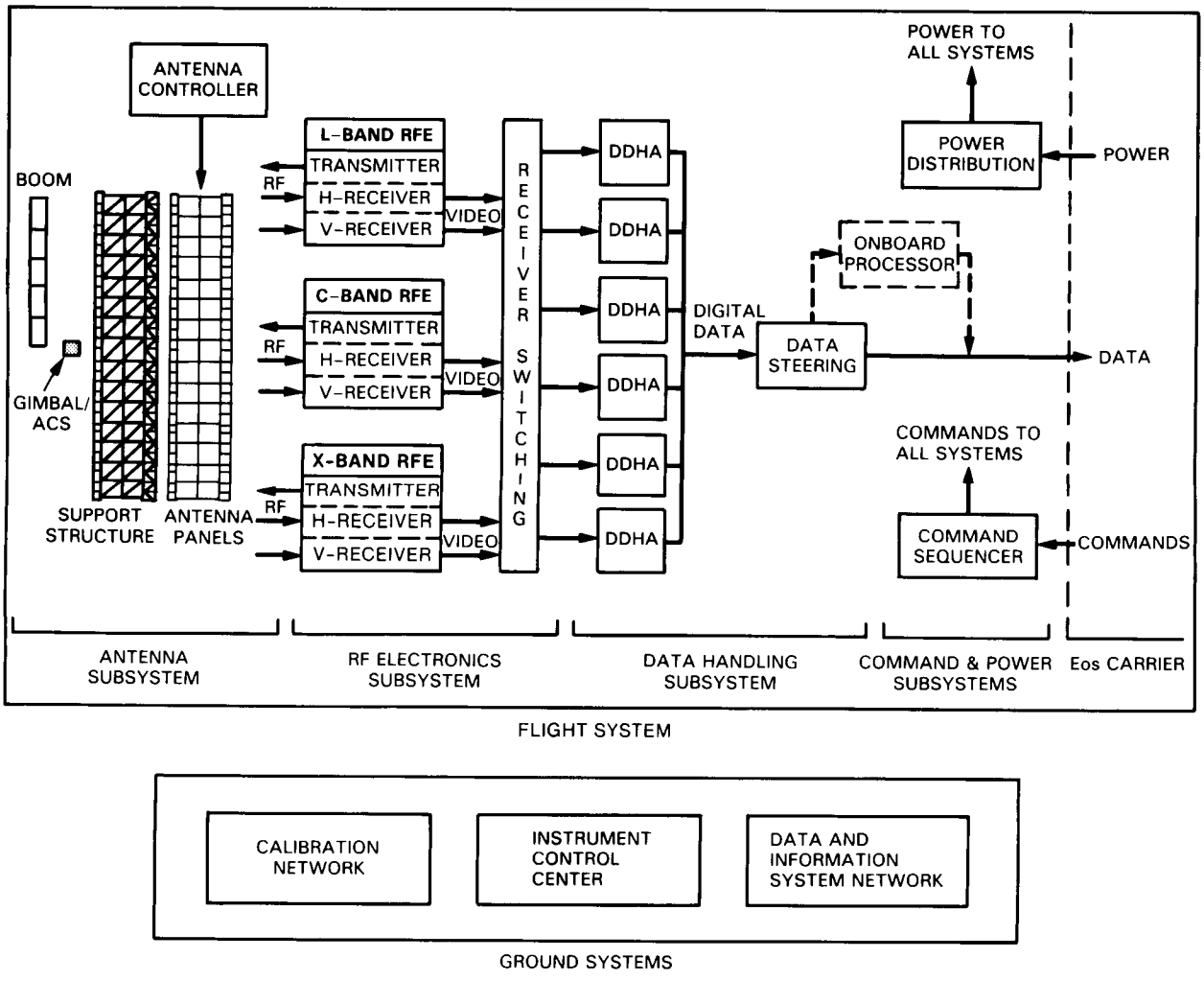

Figure 71. Eos SAR block diagram showing all subsystems including those that will be on the platform and those that will be on the ground.

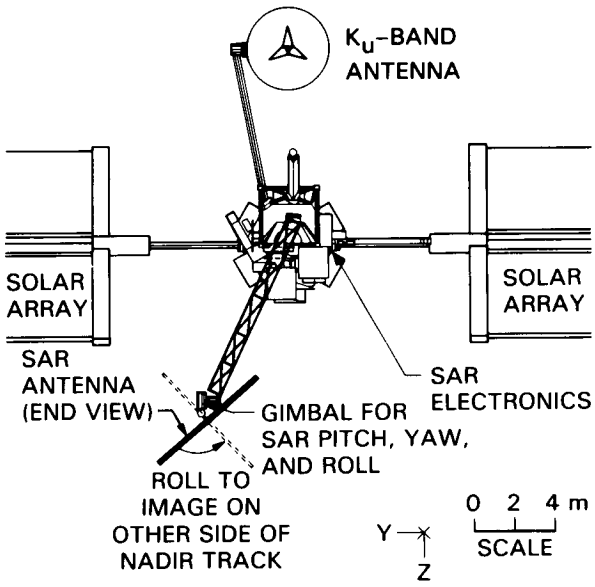

Figure 72. The SAR antenna on the Eos platform; the gimbal and mechanical maneuvering capabilities are shown.

face and volume scatter as well as penetration and absorption.

Polarization

The SIR-C design includes quad-polarized systems for the L- and C-band radars, but only VV polarization for the X-band system. (Here, the term "quad-polarized" refers to the capability to produce both like- and cross-polarized images as well as phase.) The scientific recommendation is for the Eos SAR to include quad-polarization for all three frequencies. However, at IOC the X-band system may not be sufficiently powerful to efficiently utilize the cross-polarized channels due to limitations on transmitter power. Depending on available power and technology at the time of servicing, it is recommended that an upgraded quad-polarization X-band system be added when possible.

There is as yet no clearly documented scientific requirement for the polarimetric mode of the Eos SAR, i.e., the mode that allows arbitrary selection of both transmit and receive polarization state. This is mainly because (1) only a very limited number of polarimetric SAR images have been acquired and made available to the geoscientific community, and (2) these images have been only very recently acquired. Nonetheless, preliminary analyses of these data sets indicate that the polarimetric capability offers considerable potential for geoscientific data, mainly due to its ability to enhance returns from selected targets and scenes.

The primary value for the full polarimetric capability of the Eos SAR will be in the first few years of the Eos mission. It is expected that scientists will utilize the polarimetry capability for selected sites to optimize the selection of channels for regional and global mapping. Recent analyses of polarimetric images obtained with the JPL aircraft L-band SAR suggest that it may be possible to "tune" the polarization vectors to obtain significant enhancement of particular features within a scene. It is expected that Eos scientists will wish to exploit this capability.

Radiometric Calibration

As discussed in the previous chapter, there are scientific requirements for ± 1 dB absolute and ± 1 dB relative radiometric calibration for the Eos SAR. This level is beyond our current capability, which is at best ± 3 dB absolute and ± 1 to ± 2 dB relative. There are two techniques for establishing an absolute calibration. The first is based on the radar range equation that relates the received power to the radar scattering coefficient σ°; this requires that the receiver gain, transmit power, and antenna gain and pointing direction be independently and carefully measured. It is also necessary to relate the receive power to image intensity. The total absolute calibration error is then determined as the root sum squared of all the individual errors. The second technique makes use of ground targets whose backscattering cross section are known; this normally requires that these targets be calibrated by observation with a separate ground-based or airborne scatterometer that is itself well calibrated. This latter technique will be necessary for meeting the calibration requirements of the Eos SAR, and will require considerable efforts involving engineers and the international remote sensing community using a variety of sites. Tests of these calibration procedures should be given high priority for the SIR-C missions. One option for Eos is to deploy several ground calibration stations along one polar orbit swath to calibrate along an orbit, and one similar station common to all orbits (e.g., at the South Pole). These stations would operate a combination of receivers, transponders, and ground scatterometers. Transponders are useful for determining a calibration model at the brighter end of the backscatter range; scatterometers must be used to measure distributed targets at the lower end of the backscatter range (Dobson and Ulaby, 1986).

Geometric Calibration

The geometric calibration of the Eos SAR would provide information to the image user that allows pixel locations to be specified on a cartographic grid. Level 1.1 georeferenced images should provide pixel locations to ± 15 m in the high-resolution local mode and to within one-half pixel for all modes.

Dynamic Range

The quantization of radar echoes for digital transmission to Earth is accomplished by an A/D

converter; the dynamic range is determined by the number of bits in the quantizer. The conversion is at the rate of slightly less than 6 dB/bit, so that a 4-bit A/D converter would give an approximate 21 dB instantaneous dynamic range.

This is suitable for mapping purposes. For calibrated data, an 8-bit A/D conversion is required generating approximately a 30 dB dynamic range. Using a BFPQ technique, it is possible to achieve this dynamic range with an effective swath width corresponding to a 4-bit quantization. This 30 dB dynamic range is selectable within an available 60 dB dynamic range by resetting the antenna or the receiver gain.

Viewing Parameters

Incidence Angles and Look Directions

It is desirable to provide a range of incidence angles from 15° to 60° in 1° increments for all channels, corresponding to look angles of 15° to 53° at 824 km (see Figure 73 and Table 13). The maximum usable incidence angle at a given altitude is determined by how much ambiguity (ghosts or aliases of radar echoes) is acceptable; as the SAR antenna length is increased, the ambiguity noise decreases (see Appendix F). Thus, the maximum incidence angle is determined by the antenna length. To acquire multiple incidence angles, electronic beam steering should be incorporated in all three antennas.

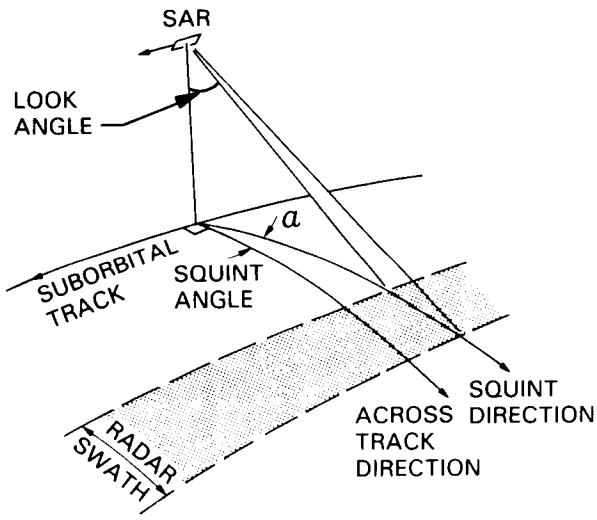

Figure 73. The squint mode.

Also included should be the capability to roll the antenna to the opposite side of the platform nadir track for acquisition of both east-looking and west-looking imagery at these incidence angles (Figure 72). This could be accomplished by mechanically rolling the antenna on its own gimbal.

Table 13. Look Angles for Maximum Accessible Incidence Angles at Three Potential Eos Altitudes

	Incidence Angle				
Altitude (km)	45°	50°	55°	60°	65°
824	39°	43°	47°	50°	53°
700	40°	44°	48°	51°	55°
542	41°	45°	49°	53°	57°

Azimuth Angle

Azimuth angle requirements for the Eos SAR are much more important than for previous SIR missions, because of the need for synergistic SAR and HIRIS imaging and for day/night imaging at the same azimuth angles. Multiple azimuth (or squint) imaging requires pointing the antenna in both pitch and yaw in order to keep the beam aligned with an iso-Doppler line (Figure 73). The use of electronic beam steering to achieve this capability cannot be accomplished with the current SIR-C antenna design, nor is it feasible even with future technology given the mass limitations of the platform. It is therefore recommended that multiple-azimuth imaging be accomplished by mechanically pitching and yawing the antenna on its own gimbal. Thus, the antenna beam could be squinted, relatively slowly, in either the forward or reverse direction; only one direction would ever be necessary. However, squinting should be in the *same* direction on both the east and west sides of the nadir track in order to optimize the available azimuth angles for a given site.

Resolution

It is recommended that a third bandwidth of 5 MHz be added to the dual-bandwidth capability of SIR-C in order to provide for low resolutions. The resulting resolution range of 20 to 500 m would meet all the resolution requirements discussed in Chapters II through VII. Because of data rate limitations, an increase in resolution generally requires a decrease in swath width. However, it is important that investigators be provided with the flexibility to make swath/resolution tradeoffs. Figure 74a illustrates the dependence of the range resolution on incidence angle for an assumed 2×2 look system with a 45 Mbps data rate and 20 m azimuth resolution.

The lower resolutions associated with the regional and global mapping modes would result in lower data rates, but would also provide a greater number of looks (less speckle). In the configuration used for the global mapping mode, onboard processing could significantly reduce the data rates; onboard processing could potentially cut the SAR-to-Earth data rate by a factor approximately equal to the number of looks.

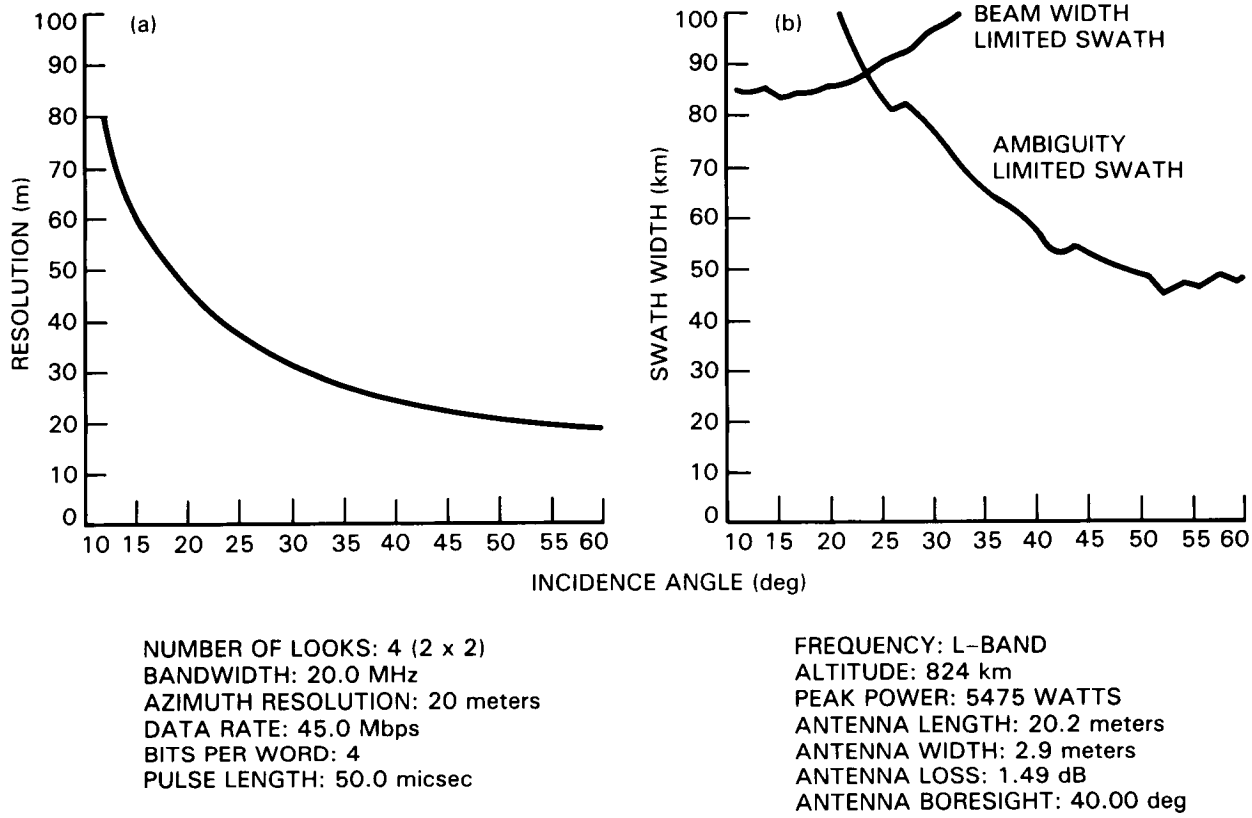

Figure 74. (a) Resolution versus incidence angle for the Eos L-band SAR. (b) Swath width versus incidence angle for the Eos L-band SAR.

Swath

As previously discussed, there is a need for three general viewing modes, the first a narrow-swath "local" mode (30 to 50 km), the second a wider-swath regional mapping mode (100 to 200 km), and the third a global mapping mode with a swath width up to 700 km. Swath widths up to about 150 km are attainable in the nominal SAR configuration. To acquire the wider swaths, a SCANSAR mode must be implemented.

Normal SAR Operation—For a SAR operating in a normal continuous PRF mode, the maximum obtainable swath width is determined by the data rate and by the antenna elevation beamwidth. When the antenna beam is pointed near-nadir (smaller incidence angles), the swath width is governed by the antenna beamwidth in the cross-track direction. For a uniformly illuminated antenna aperture, this beamwidth is given approximately by λ/H_c (radians) where λ is the wavelength and H_c is the width (short dimension) of the antenna. However, when the beam is steered to larger angles, the swath is constrained by the data rate or bandwidth. For a SAR antenna with uniform illumination along its short dimension (such as the case for Seasat or SIR-A), the near-nadir antenna beamwidth limited swath would typically be smaller than the data-rate limited swath obtained at large incidence angles. By only partially illuminating the short dimension of the antenna aperture, an effectively smaller antenna width can be obtained, thus producing a wider near-nadir swath more nearly equal to the swath width at larger incidence angles (Table 14). Figure 74b illustrates the dependence of swath width on incidence angle for an assumed L-band SAR operating at 824 km altitude.

SCANSAR Operation—Swath widths up to 700 km could in principle be obtained by utilizing the SCANSAR mode with 10 beams (Figure 75); it is recommended that this mode be implemented to achieve the global mapping mode for the Eos SAR. The SCANSAR mode is made possible by utilizing the electronic scanning capability of the antenna along with a burst mode. In the burst mode, the high instantaneous PRF rates necessary to prevent azimuth ambiguities can be achieved without exceeding the limitations imposed by the data rate. By electronically scanning the antenna beam up and down in range by a beamwidth between bursts, the effective swath width of the system can be doubled. One price for this capability is degraded azimuth resolution (resulting from the finite burst duration) and/or a reduced number of looks (in comparison to the continuous operating mode) by a factor equal to the increase in swath width. Another penalty is a considerable increase in the complexity of the SAR

Table 14. Beam Limited Swath Widths at 824 km Altitude

Frequency	Polarization	Incidence Angle	Swath Width (km)
L-band	like	15°	140
		45°	150
		56°*	131
L-band	cross	15°	132
		45°	136
		52°	147
C-band	like	15°	122
		45°	162
		60°	150
C-band	cross	15°	94
		45°	57
X-band	like	15°	85
		45°	110
		55°	100

*Maximum ambiguity-limited incidence angle.

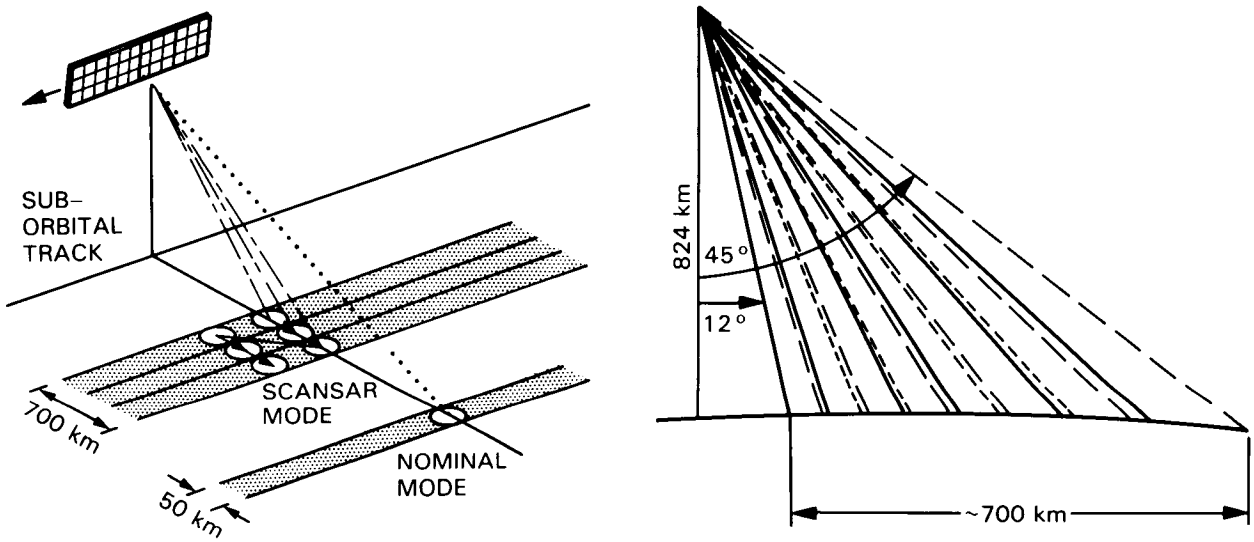

Figure 75. (a) The SCANSAR imaging mode for a 3-beam SCANSAR. (b) Geometry of a 10-beam SCANSAR.

image processor. This mode may be implemented for L- and C-band, but not for X-band due to the narrow X-band illuminated beam on the Earth's surface.

The resolution and swath of the three standard viewing modes of the Eos SAR are summarized in Table 15.

Instrument Configuration States

Several specific instrument configuration states are shown in Table 16. These are included here in order to describe the variety of resolutions, swaths, and looks available to Eos scientists, as well as the associated data rates. The three standard viewing modes are a subset of these states.

Summary of Eos SAR Sensor System Parameters

Table 17 summarizes the principal Eos SAR system parameters.

Table 15. Standard Viewing Modes

Mode	Resolution	Swath Width
Local high-resolution	20–30 m	30–50 km
Regional mapping	50–100 m	100–200 km
Global mapping	200–500 m	up to 700 km

Table 16. Instrument Configuration States (40° Incidence Angle)

State	Band-width (MHz)	Looks	Azimuth Resolution (m)	Range Resolution (m)	Swath (km)	Data Rate (Mbps)
Nominal SAR	20	1(1 × 1)	12	12	26 140	22 90
	10	2(2 × 1)	23	23	26 140	11 45
	5	4(4 × 1)	46	46	30 160	6 22
3-beam	20	3(1 × 3)	35	35	80 415	22 90
	10	6(2 × 3)	70	70	80 530	11 45
	5	12(4 × 3)	140	140	80 415	6 22
10-beam	20	160(4 × 40)	470	480	670	45
	10	80(4 × 20)	470	460	625	22
	5	40(4 × 10)	470	470	695	11

*For SCANSAR a 15% overlap has been assumed.

IMPACT OF ALTITUDE ON Eos SAR PERFORMANCE

The capability of the Eos SAR is very strongly influenced by the platform altitude. For a given frequency, antenna size, and efficiency (or transmit power level), the maximum usable incidence angle decreases as the altitude increases. In addition, the revisit interval is very altitude sensitive. Maximum SAR/HIRIS synergism would be obtained with the two instruments on separate platforms at the same altitude.

Maximum Incidence Angle Limitations

At a given SAR altitude, the maximum usable incidence angle will be reached when the combination of thermal and ambiguity noise begins to mask the desired radar returns. Thus, the maximum incidence angle is determined by the SNR and ambiguity level of the radar system. The SNR is in turn determined by transmitter power level, receiver noise figure, antenna gain, spacecraft altitude, and the radar scattering coefficient σ°. The ambiguity level is determined principally by the PRF and the antenna area.

Table 17. Eos SAR System Parameters

Imaging Parameters
L-, C-, and X-band
HH, VV, HV, and VH for L- and C-bands
HH and VV for X-band

Imaging Geometry

Look angle:	15° to 60°
Look direction:	to either side of the platform ground track
Azimuth angle:	0° to 60°, forward or reverse direction (desirable)

	L-band	C-band	X-band
Electronics			
Frequency (MHz):	1,248	5,298	9,600
Wavelength (cm):	23.9	5.7	3.1
Transmit pulse length (μs):	50*		
Minimum PRF:	750*		
Maximum PRF:	1,100*		
Bandwidths (MHz):	20, 10, 5*		
Instantaneous dynamic range (dB):	30		
Adjustable dynamic range (dB):**	60*		

	L-Band	C-band	X-band	Total
Antenna				
Length (m):	20.2	20.2	20.2	20.2
Width (m):	2.9	0.75	0.4	4.1
Number of antenna panels:	30	30	30	90
Peak radiated power (kw):	6.0	3.6	5.0	
Elevation beam steering:	46°	46°	46°	
Azimuth beam steering (electronic):	4°	2°	2°	

Data System

Maximum data rate (Mbps):	270
Data rate units (Mbps):	45
DDHA bits per word:	8 and 4
DDHA BFPQ (bits in, out):	(8, 4)

Images

Resolution (m):	20 to 500
Swath (km):	30 to 700
Looks:	20 to 160 selectable with resolution

Calibration:

Radiometric (relative):	±1 dB
Radiometric (absolute):	±1 dB
Geometric (m):	0.5 pixel, 15 m

*These parameters hold for L-, C-, and X-bands.
**Obtained by resetting the antenna or receiver gain.

Figures 76a and 76b show the general range of radar returns (σ° versus incidence angle) expected at L-band for geologic (bare soil) and vegetated surfaces. Figures 77a and 77b show the same curves for C-band. The solid lines indicate the range of expected like-polarization (HH, VV) returns, and the dashed lines the expected cross-polarization (HV) returns. The upper line indicates the maximum expected return and the lower line the minimum return. These curves are included to indicate general trends measured with radar scatterometers, and should not be construed as exact. However, several trends can be noted. First, there is a general decrease in σ° with increasing incidence angle. Second, the cross-polarization returns

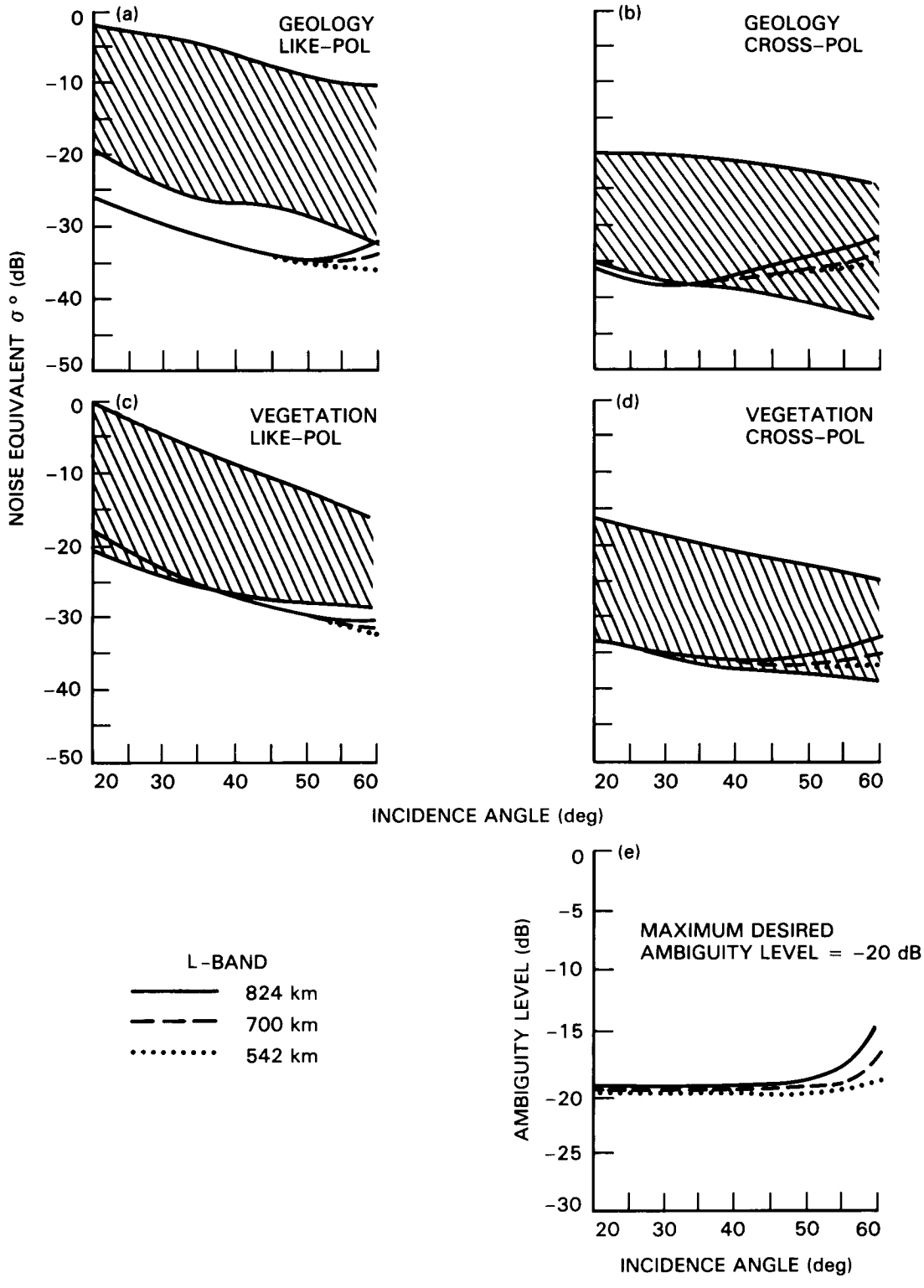

Figure 76. At L-band: The range of expected backscattering coefficient σ° versus incidence angle for geologic (bare soil) targets in the like-pol (a) and cross-pol (b) modes, and vegetation targets in the like-pol (c) and cross-pol (d) modes. The computed noise equivalent σ° versus incidence angle is also shown for three altitudes. High incidence angle limits based on ambiguities are also shown for three possible Eos altitudes (e). The maximum desired ambiguity is −20 dB.

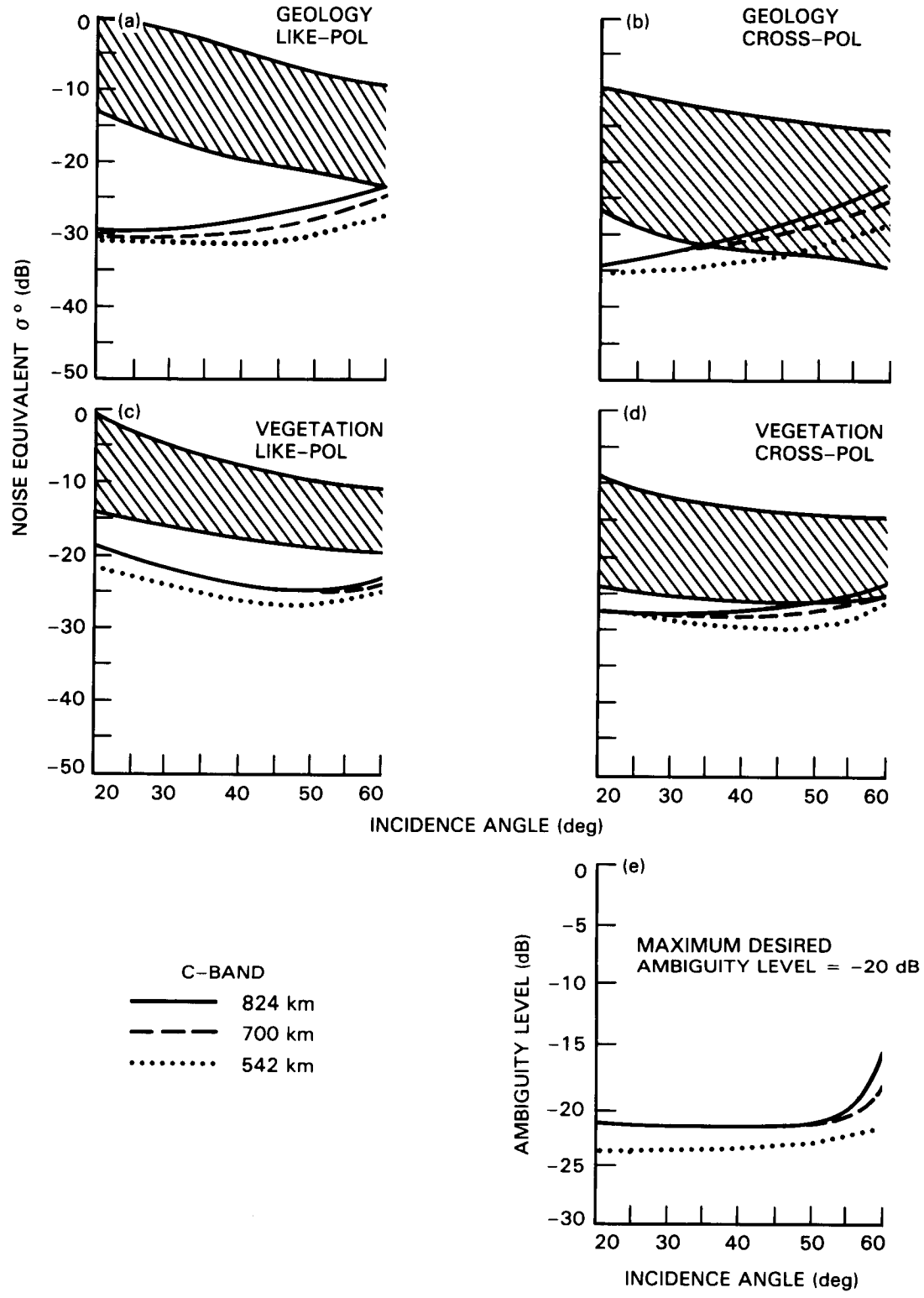

Figure 77. At C-band: The range of expected backscattering coefficient σ° versus incidence angle for geologic (bare soil) targets in the like-pol (a) and cross-pol (b) modes, and vegetation targets in the like-pol (c) and cross-pol (d) modes. The computed noise equivalent σ° versus incidence angle is also shown for three altitudes. High incidence angle limits based on ambiguities are also shown for three possible Eos altitudes (e). The maximum desired ambiguity is -20 dB.

are from 10 to 20 dB weaker than the like-polarized returns. Third, at a given incidence angle and frequency, there is an expected variability of about 15 dB associated with a given range of surfaces.

SNR Limitations

The term "noise equivalent $\sigma°$" refers to the radar backscattering coefficient level that is just barely discernible above the thermal noise; i.e., the minimum detectable $\sigma°$ (Appendix F). This depends principally on the altitude, transmitter power level, antenna size, number of looks, and bandwidth. In effect, the noise equivalent $\sigma°$ describes the radar sensitivity floor. If a particular scene has a backscattering coefficient that is above this floor, it can be detected; otherwise, the radar echoes are below the system noise level and are undetectable.

The noise equivalent $\sigma°$ has been computed as a function of incidence angle for Eos SAR L- and C-band channels, at three assumed altitudes: 824, 700, and 542 km. In these calculations, it was assumed that the peak transmit power was 6.0 kW at L-band and 3.6 kW at C-band. The antenna length was assumed to be 20.2 m; the L-band antenna width was 2.9 m and the C-band width was 0.75 m. An antenna loss of 1.5 dB and a look angle of 35° was used. Additional assumptions were four looks, a 20 MHz bandwidth, a 45 Mbps data rate, 4 bits per word, and a 50 μs pulse length.

Figures 76 and 77 illustrate the range of expected backscattering coefficients for both bare soil and vegetated targets, at L- and C-band. When the average radar return $\sigma°$ (average of minimum and maximum) is at least 3 to 5 dB above both the noise (both thermal and ambiguity), then a subjectively "good" quality image can be expected.

Ambiguity Limitation

In addition to thermal noise, SAR images can be further corrupted by ambiguity noise resulting from ghosts or aliases of radar echoes that are folded into the Doppler bandwidth (see Appendix F). The ambiguity level depends principally upon the altitude, incidence angle, PRF, and antenna length. Figures 76e and 77e illustrate the expected ambiguity level versus incidence angle at L- and C-bands, respectively, and for three different altitudes. In order to keep ambiguity noise acceptably small, an acceptable ambiguity level of -20 dB is recommended (dash-dot line on the figures).

Summary of Maximum Incidence Angle Versus Altitude

Based on ambiguities, it will be possible with Eos SAR to image out to about 49° at L-band and 55° at C-band for an 824 km altitude, out to about 53° (L-band) to 57° (C-band) at 700 km altitude, and out to about 58° (L-band) to 60° at 542 km altitude, as shown in Figures 78a and 78b. These limits are

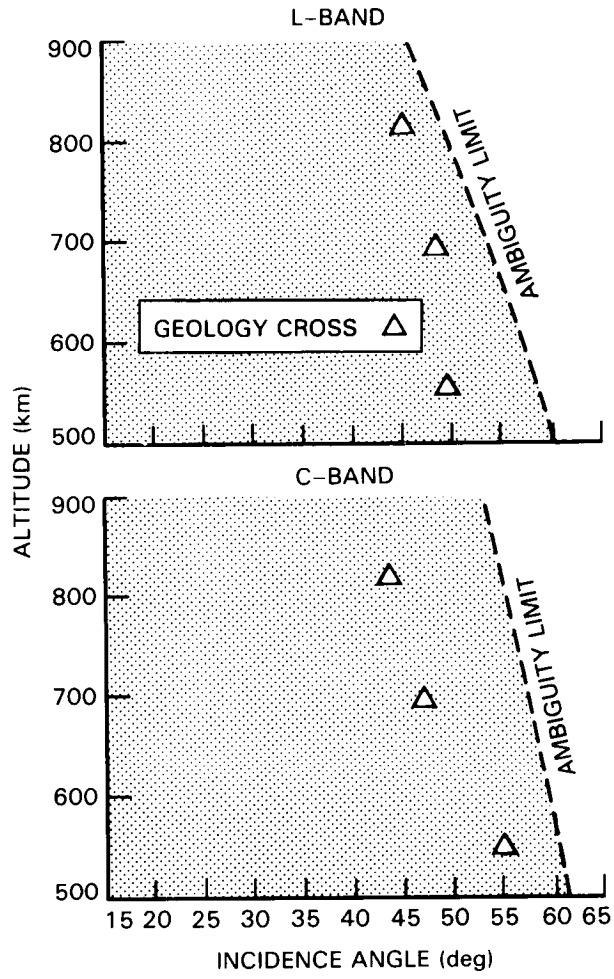

Figure 78. (a) At L-band: Computed maximum incidence angle capability versus altitude based on SNR (triangles) and ambiguity level (shaded region shows acceptable region) for geologic and vegetated surfaces for a 20 m SAR antenna length. (b) At C-band: Computed maximum incidence angle capability versus altitude based on SNR (triangles) and ambiguity level (shaded region shows acceptable region) for geologic and vegetated surfaces for a 20 m SAR antenna length.

governed by the maximum acceptable ambiguity level of -20 dB, and a 20 m antenna length. With the power levels expected for the Eos SAR, like-polarized L- and C-band data with good image quality (SNR) may be expected out to these angles for both geologic and vegetated surfaces (Figure 76a and 76c and 77a and 77c). Good image quality cross-polarized L- and C-band data for vegetated surfaces is also expected out to the ambiguity limit (Figure 76d and 77d).

At L-band, the acquisition of cross-polarized images at high incidence angles for geologic surfaces is limited by SNR (noise equivalent $\sigma°$), not ambiguities. Images at L-band may be required in the cross-polarized mode out to 50° at 542 km, 48° at 700 km and out to 45° at 824 km.

Acquisition of geologic targets at C-band out to 55° at 542 km, to 47° at 700 km, and to only 44° at 824 km, if possible.

Repeat Cycle Limitations

The revisit interval (repeat cycle) is determined by the satellite altitude; at this writing, three sun-synchronous altitudes are under consideration: 824, 700, and 542 km, with 824 km considered the more likely choice based on NOAA requirements. At 824 km, there is an exact repeat cycle of 16 days; this means that SAR imaging of a site with a given illumination geometry would be exactly repeated every 16 days and that the subsatellite track is displaced by 530 km (at the equator) each day. Assuming an acceptable incidence-angle range of 15° to 35°, sites could be acquired at intervals of 1 to 6 days, depending on the period within the 16-day exact repeat cycle. The intervals form a repeating pattern and for 824 km, the days of separation between observation are 1 day, 4 days, 1, 4, 5, 1, 4, 1, 4, 5 days, etc.

At 700 km, the exact repeat cycle is again 16 days with an approximate repeat of 2 days. Sites could be imaged every 2 to 5 days (2, 5, 4, 5, 2, 5, 4, 5, etc.), again depending on the time within the exact 16-day repeat cycle. At 542 km, images will be acquired every (1, 2, 1, 12, 1, 2, 1, 12, etc.) days.

As stated earlier, soil moisture measurements for a given site would be most accurately made if imagery was obtained every 3 days with exactly the same incidence angle; change detection procedures would allow the elimination of surface cover and roughness variables. This is clearly inconsistent with an exact 16-day repeat cycle orbit. With an 824 km altitude with 16-day repeat cycle, the site could be viewed every few days only by repointing the antenna beam and acquiring images over a wide assortment of incidence angles. This would greatly complicate the extraction of soil moisture information.

Fortunately, by changing the altitude just a few kilometers (using platform thrusters), the repeat cycle can be changed to 3 days or 5 days from a nominal altitude of 700 km or 824 km, respectively. A 3-day repeat cycle necessary to use change detection procedures for short-term phenomena, especially soil moisture, and we recommend that the capability to acquire soil moisture data every 3 days over a period of months be incorporated, after which the platform would return to a 16-day repeat cycle. During this period of acquiring 3-day repeat cycle data, synchrony with the other Eos platform would be lost and experiments requiring simultaneity with HIRIS, MODIS, etc., would not be possible. However, upon return to the 16-day repeat cycle altitude, these experiments could be resumed.

IX. DATA AND INFORMATION SYSTEM

In this chapter, we summarize the data volume and rate requirements for each discipline and outline a representative data acquisition scenario for that discipline. These scenarios take into account the spatial scales of the features of interest as well as the temporal scales of change expected to be observed by SAR, and should therefore provide relatively accurate data requirement estimates. We also describe the onboard and ground data systems needed to meet the requirements of all discipline sciences.

The data system for the Eos SAR will be driven by the data rate and volume requirements for each science discipline. The peak data rate is bounded by the satellite-to-ground data link via TDRS, whose current total capacity is 300 Mbps; the peak data rate for SAR is expected to be under 270 Mbps. The yearly average data rate is bounded by the capacity of the Eos data system to accommodate data requests from all Eos instruments; the average SAR data rate is expected to be less than 20 Mbps.

By way of comparison, the SIR-B mission yearly average data rate (i.e., total data collected during the 1-week mission averaged over a year) was 0.3 Mbps; this included data takes at various incidence angles. SIR-C, with frequency, polarization, and incidence angle agility, will increase the yearly average data rate by a factor of four (estimated about eight times the number of channels but only half as many incidence angle requests over a 1-week period), i.e., to 1.2 Mbps.

SCIENCE DATA REQUIREMENTS

A SAR Data Acquisition Plan

An Eos SAR Data Acquisition Plan (SDAP) has been developed for this report, employing procedures and software used with SIR-B. The purpose of the SDAP is to more accurately describe the data requirements for the Eos SAR, especially the number of images required and the yearly average data rate. The procedure begins with the area (square kilometers) for each of a number of representative study regions for the type of research tasks described in Chapters II through VI. Next the required coverage frequency, resolution, swath width, peak data rate, and the number of SAR channels are noted. From this, the yearly average data rate can be computed. The sites, areas, coverage frequency, and number of channels used in this SDAP have been carefully chosen so that a reasonably accurate average data rate could be estimated; however, many other alternate choices could be made.

Sites

In order to estimate the areas likely to be required for each discipline, representative long-term study sites for all scientific disciplines have been chosen (Figure 79). In general, these sites are large compared to sites typically used for shuttle experiments, although in most cases the sites are less than continental in size. The largest sites are the northern and southern polar ice packs. These also have the highest coverage frequency requirements and will therefore constitute a large portion of the SAR data stream.

Coverage Frequency and Time-of-Year Requirements

For each site, a coverage frequency requirement was chosen depending on the time scale of change of that particular surface feature. Coverage frequencies range from every 2 to 3 days for some hydrologic observations to twice only (summer and winter) for the whole Eos mission for some geologic studies. Some observation frequencies would also vary with time of year. Coverage frequency requirements for vegetation, for example, would be much higher in the spring and fall during emergence and senescence than in the summer and winter. Sea ice coverage requirements would be highest in the winter.

Sensor and Viewing Modes

For each site, a fixed number of SAR channels (frequencies and polarizations) were specified based on an estimate of need for the surface feature being observed. Based on the frequency and polarization requirements for each discipline, a set of standard sensor modes have been selected (see Chapter VII). The data rate for each SAR sensor mode depends on the following viewing parameters, which would be selected by the investigator:

- Incidence angle (determines resolution for a given bandwidth and maximum beam-limited swath)
- Bandwidth (20, 10, or 5 MHz, determines resolution)
- Bits per sample
- Swath width

Table 16 defines the approximate data rates for a single channel and a 40° look angle for a variety of instrument configuration states ranging from high resolution, narrow swath, to low resolution, wide swath. It is expected that most investigators will require all desired channels simultaneously, at least initially. Therefore, for most of these modes, the swath width is limited by the data rate. It is expected that most Eos investigators would prefer wide-swath modes, especially for large-scale study sites. Thus the peak data rates for SAR would tend to be the maximum available through TDRS.

Yearly Average Data Rate

Table 18 summarizes the SAR data acquisition plan; this is basically an estimate for each scientific

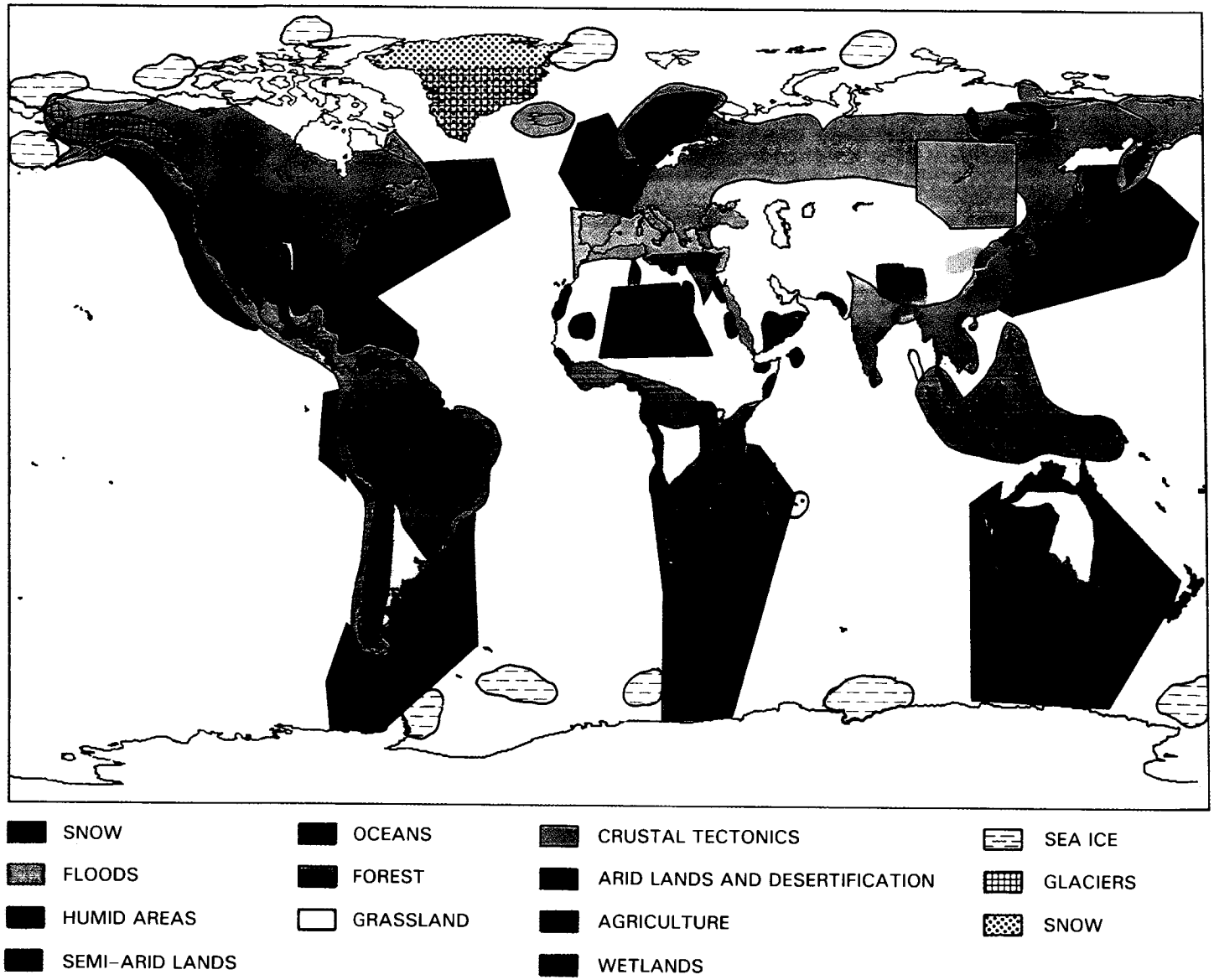

Figure 79. Summary maps of geographical regions for all five science disciplines for high- and moderate-resolution imaging. Sea ice will be imaged completely with the global mapping mode.

Table 18. Summary of SAR Data Acquisition Plan

Experiment	Recommended Sites	Frequency	Polarization	Incidence Angle (deg)	Resolution (m)	Swath	Simultaneous Coverage
Ice							
Sea Ice	Southern Beaufort Sea; Arctic Ocean; Bering Sea; Southern Ocean; Greenland Sea; Great Lakes; North and Baltic Seas	X L,C,X	HH HH,VV,HV,VH	<35 <35	50-100 50-100	Wide Narrow	MODIS, HIRIS AMSR, TIMS, SCATT, ALT
Glacial Ice	Alaska; Greenland; Antarctica; Alps	L	HH,VV,HV	<35	50-100	Wide Wide	MODIS, HIRIS AMSR, TIMS, SCATT, ALT
Snow	Polar Regions	C,X	HH,VV	30,50	20-30	Narrow	HIRIS, MODIS AMSR, TIMS
Hydrology							
Humid	U.S. Southeast; Central Europe; Amazon; East Coast of Australia	L,C,X	HH,VV,HV,VH	30,50	20-30	Narrow	HIRIS, ESTAR
Snow	Andes; United States; Europe; Himalayas; Japan; New Zealand	L,C,X	HH,VV,HV,VH	30,50	20-30	Narrow	HIRIS, MODIS ESTAR, TIMS
Semi-Arid	U.S. Southwest; Australia; India; Africa	L,C	HH,VV,HV,VH	30,50	20-30	Narrow	HIRIS, ESTAR
Floods	India; Mississippi River Basin; Amazon; China; Bangladesh	L	HH	30	20-30	Narrow	HIRIS
Vegetation							
Forests	U.S.; Canada; Northern Asia; West Africa; Upper Volta; Amazon; Peru; Germany; Indonesia	L,C,X	HH,HV,VV,VH	30,50	50-100 20-30	Wide Narrow	HIRIS, MODIS
Grasslands	India; Pakistan; Colorado; Mali; Asia	C C,X	HH,HV,VV,VH HH,HV,VV,VH	30,50 30,50	50-100 20-30	Wide Narrow	HIRIS, MODIS
Agriculture	United States; Canada; West Africa; China	L,C,X	HH,VV,HV,VH	30,50	50-100 20-30	Wide Narrow	HIRIS, MODIS
Wetlands	Mississippi Delta; Venezuela; Botswana Bangladesh; Alaska	L,C	HH,VV,HV,VH	30,50	20-30	Narrow	HIRIS

Table 18. Summary of SAR Data Acquisition Plan (continued)

Experiment	Recommended Sites	Frequency	Polarization	Incidence Angle (deg)	Resolution (m)	Swath	Simultaneous Coverage
Oceans	Western Atlantic and Caribbean Sea; West and East Pacific; South America; South Africa; Australia; Mediterranean	L,C	HH,VV	20-30	50-100 20-30	Wide Wide	MODIS, HIRIS SCATT, ALT
Geology							
Crustal Structure And Tectonics	Global surface land	L,C,X	HH,HV	30-60	20-30	Wide (Mosaic)	HIRIS, ALT, TIMS, GLRS
Arid Lands	North Africa; S.W. U.S.; China; Australia; Middle East; Chile; Peru; S.W. Africa	L	HH,HV	30-60	20-30	Wide (Mosaic)	HIRIS, TIMS, SCATT
Desertification	North Africa; S.W. U.S.; China; Middle East; Australia; South America	C,X	HH,HV	20-35	20-30	Wide (Mosaic)	HIRIS, TIMS
Soil Erosion	Middle East; China; Australia; Brazil; India; North America; Africa; Mexico	L,C	HH,HV	20-35	20-30	Wide (Mosaic)	HIRIS, TIMS

objective of the required resolution, swath width, revisit interval, and synergism requirements. Table 19 summarizes the yearly average data rate; this totals to about 10 Mbps. For all disciplines, it was assumed that the global mapping mode provided a frequent low-resolution coverage of the regimes of interest. The data rates in the tables include *only* the local high-resolution mode and the regional mapping mode. If onboard processing is incorporated into the Eos SAR system, the global mapping mode will add an insignificant amount to the 10 Mbps data rate. If onboard processing is not included, this data rate may double.

This plan would be appropriate to the first few years of Eos. As investigators begin to more fully understand the time scales of surface processes and identify optimum channels, the number of channels and the frequency of observation can be expected to decrease. However, it is also expected that larger sites will be incorporated and the number of investigators will increase. Thus the average yearly data rate for SAR is not expected to change significantly as the Eos mission progresses (Figure 80).

Glaciology

Inside polar ice pack boundaries, ice movements are primarily in response to the movement of large-scale weather systems. Thus observations made every 3 to 6 days are necessary. Spatial resolutions of 200 to 500 m will be adequate for these observations; approximately 90 percent of the Arctic and Antarctic ice packs should be imaged. X-band is the frequency of choice and dual polarization will be valuable for discriminating first-year and multiyear ice, especially at incidence angles greater that 30°. The total areal coverage requirements for each ice pack will vary as a function of time of year.

It will also be important to monitor a variety of different ice processes occurring within the ice packs at higher resolution (50 to 100 m) during periods of rapid change, especially along the ice margins. These observations should be made every day if possible. The location of these observations will change somewhat as the ice pack moves, therefore the lower resolution large-scale maps should be used to determine the exact location of the narrower high-resolution

Table 19. Summary of Average Yearly Data Rate

Discipline	Minutes	Number of Maps	Data Rate/ Channel	Number of Channels	Number of Incidence Angles	Day/ Night	Repeat Cycle	Number of Years	Yearly Average Data Rate
Sea ice/ north winter	55	1	24	2	1	1	every 2 days in winter	15	0.30
Sea ice/ north summer	40	1	24	2	1	1	every 2 days in summer	15	0.22
Sea ice/ south all year	62	1	24	2	1	1	every 2 days	15	0.52
Glaciology north	288	1	45	2	1	1	2-6 per year	15	0.20
Glaciology south	56	1	45	2	1	1	once every 2 years	15	0.005
South polar snow	56	1	24	3	2	2	monthly (variable)	15	0.36
Glaciology (Total)									**1.61**
Humid hydrology	70	1	22	4	1	1	3 days (eighth time)	5	0.18
Semi-arid	150	1	22	4	1	1	3 days (eighth time)	5	0.38
Snow (melt)	75	1	24	3	1	2	4 days	5	0.16
(accumulation)	75	1	24	3	1	2	(1 month) monthly (3 months)	5	0.06
Wetlands	10	1	45	4	1	1	every 2 weeks (1/3 time)	5	0.03
Hydrology (Total)									**0.81**
Forests	123	1	22	6	2	1	every 2 weeks (average)	15	1.61
Agriculture	50	1	22	4	2	1	every 2 weeks (average)	15	0.43
Grassland	65	1	22	4	2	1	every 2 weeks (average)	15	0.57
Vegetation (Total)									**2.61**

Table 19. Summary of Average Yearly Data Rate (continued)

Discipline	Minutes	Number of Maps	Data Rate/ Channel	Number of Channels	Number of Incidence Angles	Day/ Night	Repeat Cycle	Number of Years	Yearly Average Data Rate
Oceans	800	1	90	1	1	1	every 2 weeks	15	3.60
Oceans (Total)									**3.60**
Structural geology	1,232	4	45	6	2	1	twice per year	once only	0.67
Arid lands	417	4	45	4	1	1	once per year	2	0.08
Desertification	335	4	45	2	1	1	2 seasons per year	4	0.12
Soil erosion	379	4	45	4	1	1	2 seasons per year	4	0.26
Geology (Total)									**1.13**
Total									**9.76**

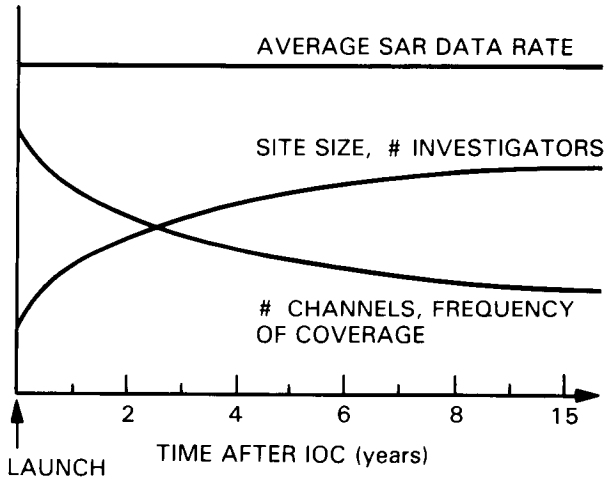

Figure 80. Expected yearly average data rate as a function of year past IOC.

swaths. The high-resolution swaths should be acquired with a greater range of frequencies and polarizations than the low-resolution coverage such that information on the geophysical properties can be acquired.

Figure 81 shows the high-resolution coverage of the northern and southern ice zones for the winter season.

Bimonthly observations of alpine glaciers and yearly observations of large continental ice sheets near the margins are adequate to delineate major calving events. In the interior of large ice sheets, biyearly observations are required if one is investigating accumulation processes and grain growth in the near-surface layers. For movement only, observations every 5 years may be sufficient. For regions of rapid movement such as the Ross Ice Shelf and some alpine glaciers, bimonthly observations of deployed passive radar reflectors may be required.

Selected "representative" snowpacks should be observed both during their accumulation and melt. Monthly imaging during accumulation is adequate; observations approximately every 4 days during the melt period, both day and night, are desired.

Hydrology

Fairly frequent revisit times will be necessary to make optimal use of the SAR data for hydrology studies. Soil moisture is highly variable, and frequent observations with the same illumination geometry, preferably every 2 to 3 days, are needed for accurate monitoring. Global-scale monitoring in the global mapping mode is essential, as well as monitoring of

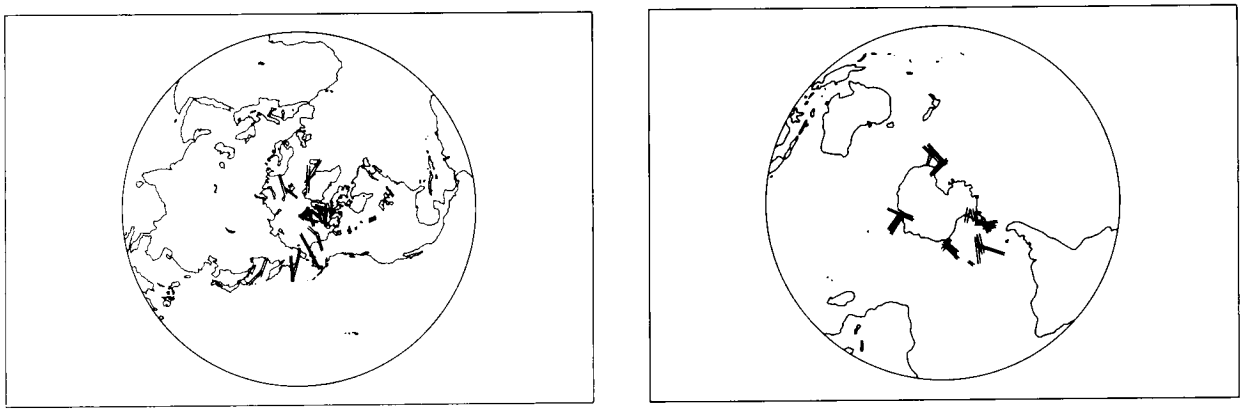

SEA ICE
WINTER
1 day COVERAGE
100 km SWATH
INCIDENCE ANGLE = 30°

Figure 81. SAR swaths over representative glaciology regions used to calculate yearly average data rate.

selected catchments and watersheds using the high-resolution local mode.

In addition, a 2-year repeat cycle is required to monitor the significant long-term changes in watershed morphology that are not simply the result of variations in soil moisture. These data may be acquired over a long period of time and should be acquired at two different incidence angles.

Figure 82 shows the recommended coverage over 4 days for humid hydrology study regions.

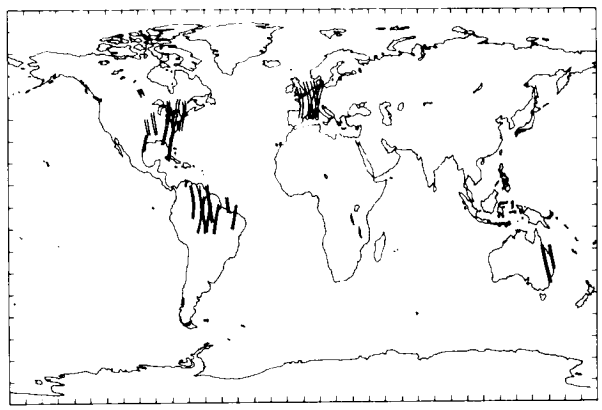

HUMID HYDROLOGY
4 day COVERAGE
100 km SWATH
INCIDENCE ANGLE = 35°

Figure 82. SAR swaths over representative hydrology regions used to calculate yearly average data rate.

Vegetation Science

For most vegetation studies, it is necessary to measure such biophysical parameters as biomass, canopy moisture, canopy geometry, leaf area index, and surface boundary layer (SBL) state or state of the canopy floor (litter, moisture, etc.). This would make use of inversion algorithms that require all frequencies and two to four polarizations at each frequency. Detailed studies designed to gain mechanistic understanding of ecological processes will require high-resolution data in all channels for very limited areas of the Earth's surface. Frequency of coverage however would depend on the type of vegetation.

Coverage is desired on a weekly to monthly to quarterly basis keyed to forest phenologic development. More frequent coverage is desired during leaf flush and leaf fall periods and during the burning seasons. Resolution requirements will depend on the uniformity of the forest and the topography. It would not be necessary to cover the entire forest canopy; only representative transects that cross the major environmental gradients would be required. For the purpose of estimating total data requirements, two winter, two summer, five spring, and five fall data sets with a resolution of 120 m might be requested. For most forest applications, at least two and preferably three incidence angles are required.

In addition to this seasonal monitoring, a complete map of the regions of the world's forests that are sensitive to change will be required each year in order to monitor the ecotones and areal extent of biomes. This coverage would require the high-resolution mode but would only need one channel; this

channel would be selected based on the multichannel transects.

Low-resolution coverage of grasslands would be desired semimonthly, while high-resolution coverage is needed only seasonally, relating to maximal and minimal thermal and precipitation conditions.

Radar coverage of agricultural regions is desirable both in a regional mapping mode with C-band, quad-polarization channels with a weekly revisit interval for soil moisture sensing, and in the high-resolution local mode (30 m) on monthly revisit interval throughout the cropping season, with higher-frequency coverage required during emergence and senescence.

Figure 83 shows representative transects for forest monitoring.

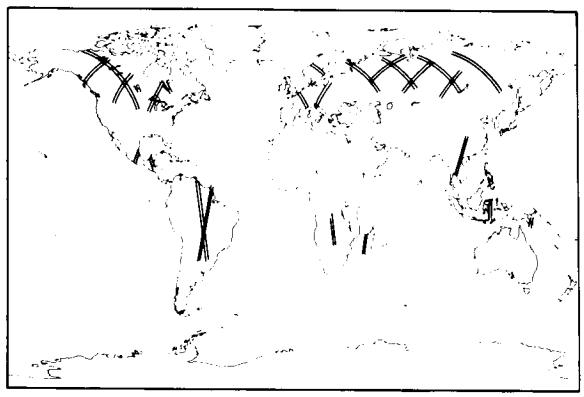

FORESTS
VEGETATION
1 day SELECTED COVERAGE
100 km SWATH
INCIDENCE ANGLE = 45°

Figure 83. SAR swaths over representative vegetated regions used to calculate yearly average data rate.

Oceanography

The revisit interval required for SAR observations of the ocean will depend on the feature being observed. Meso- and fine-scale currents vary on a time scale of a few days, and bathymetric measurements can be made over a period of several weeks. Since the ocean's features vary so greatly with time, observations should be made as frequently as possible until the processes are better understood and this constraint could be relaxed. Resolutions of 100 m are acceptable with 60 m resolution preferred; 90 percent coverage should be acquired and only a single channel is necessary.

Figure 84 shows the coverage over a 4-day period of the major ocean regions suggested in Chapter V.

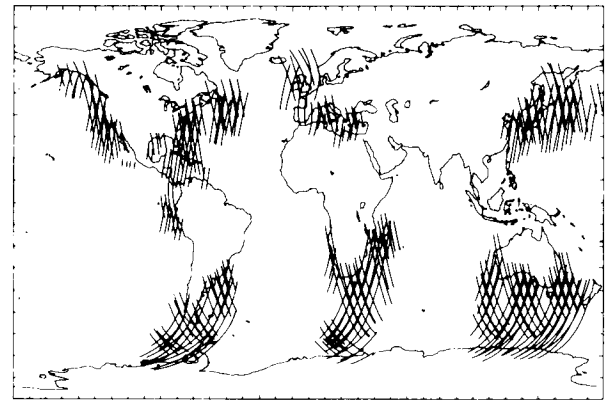

OCEANOGRAPHY
4 day COVERAGE
200 km SWATH
INCIDENCE ANGLE = 30°

Figure 84. SAR swaths over representative oceanography regions used to calculate yearly average data rate.

Geology

Unlike the previous disciplines, the temporal scale of geologic change in even the most tectonically active regions of the continents are not in accord with the 15-year lifetime proposed for Eos operations. The exceptions to this are large-scale fault movements resulting from timely earthquakes and volcanic eruptions. A winter and a summer data set will be necessary to assess the effects of maximum contrast in surface moisture, vegetation, snow, and ice as they relate to the underlying geological surface. One complete map of the suggested structural geology regions (Figure 85) acquired in both the winter and the summer at high resolution will be sufficient for the whole Eos lifetime for tectonic studies. The two maps may be acquired over the lifetime of Eos; however, they should be acquired at two incidence angles, all frequencies and several polarizations.

The temporal aspects of arid lands geology is not expected to be important during the time scale of Eos with the exception of possible monitoring of hydrologic changes related to near-surface ground water aquifers. For monitoring and assessment of desert hydrology/geology interactions, coverage during both the wettest and driest months would be required about every 2 years.

Temporally, soil erosion is generally a slow process but undergoes rapid acceleration during catastrophic climatic events such as windstorms and seasonal droughts. Repeat coverage every 2 years of major test sites is required with acquisitions immediately following the driest, wettest, and/or more windy season locally. The best seasons for initial coverage in most temperate latitudes might be early midwinter and early fall.

Figure 85 shows recommended coverage over an 8-day period for some structural geology sites.

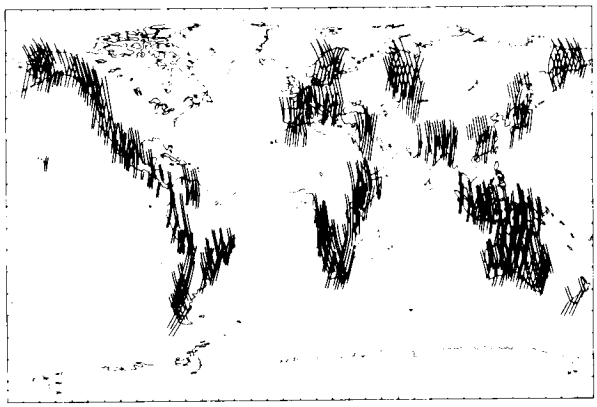

STRUCTURAL GEOLOGY
8 day COVERAGE
100 km SWATH
INCIDENCE ANGLE = 40°

Figure 85. SAR swaths over representative geology regions used to calculate yearly average data rate.

THE DATA SYSTEM

The data system for the Eos SAR is part of a larger Eos data and information system discussed in the Eos Data Panel Report (Chase *et al.*, 1986). The SAR data system will result from Seasat, SIR-A, -B, -C, and the Alaska SAR Facility (ASF) data systems (Figure 86). The data network for the Eos SAR encompasses the flight or onboard data system; the wide-band downlink and data transmission path; the ground image processing subsystem; the archives for raw signal, image, and derived geophysical parameter data; and the data distribution to the user community by means of an online accessible data base system. It will also be essential that the SAR data system include a data analysis network. The data system design must seek to meet user requirements for data product quality and throughput rate, but must also recognize the functional limitations of the platform and the communication links.

SIR-C Inheritance

In preparation for Eos and to accommodate the multiple channels that will be available for the first time, the SIR-C data system will be substantially more advanced and efficient than previous SIR data systems.

The Flight Data System

In order to handle the multipolarization modes for both the L- and the C-band radars which comprise SIR-C, a more efficient onboard data system is required. In the quad polarization mode, the H and V transmitters operate on alternate transmitter pulses. The H and V receivers both receive all return pulses, half of which are vertically transmitted pulses. This procedure requires twice the PRF of a single polarization mode. This means that a multipolarization radar will require four times the data rate as a single polarization radar for the same swath and resolution. If both the L- and C-band channels are operated simultaneously, four 45 Mbps data streams will allow acquisition of all six channels simultaneously with a 30 m resolution and about a 30 km swath. This scenario requires four DDHAs and a data steering network.

The data for SIR-C will be collected by onboard recorders and will nominally be stored onboard on high-density tapes. Selected channels will be transmitted through TDRS for engineering checks and limited real-time processing and distribution. Data sent through TDRS will be recorded at Goddard Space Flight Center (GSFC) and flown to JPL for processing. Data recorded onboard will be flown back to JPL from the landing site at the end of the mission.

The Processor

All SIR-C data will be processed digitally by the Advanced Digital SAR Processor (ADSP) at JPL at or nearl real-time rates. The system includes a SIR-C specific input interface, two high-density digital recorders (HDDRs) for the input and output data, and a scrolling display with a video cassette recorder for quick-look image products.

The input interface contains the necessary logic to decode the subsommutated header data in real time and to perform data quality analysis such as bit-error-rate checks, radar parameter change detection, or data dropout detection. The decoded header data are transferred to a VAX controller for initialization of the autofocus and clutterlock algorithms. In addition, these data are used for determining range-line and reference function sizes as well as for estimating the geometric and radiometric correction parameters (e.g., antenna pattern, angle of incidence, azimuth skew, slant range, etc.)

The correlation algorithm is essentially composed of two one-dimensional matched filtering operations in the frequency domain. The reference functions are determined from the characteristics of the transmitted pulse for the range reference and from the Doppler characteristics of the echo data for the azimuth reference.

The ADSP can perform up to 6 billion floating point operations per second and is designed to process SAR data in strips rather than frame by frame. A special purpose processor has been added to perform geometric and radiometric corrections on the image products as the ADSP has a limited capability for system processing. This system interfaces with the ADSP output and will include mass storage, an array processor, a video display, and a film recorder. Its primary function is to meet the special processing requirements of the SIR-C investigators for selected segments of the image data.

RADAR	# CHANNELS	DATA FORMAT	DATA RATE TO GROUND	DIGITAL DATA RATE TO ONBOARD RECORDERS (TOTAL)	THROUGH-PUT RATE	
SEASAT	1	DIGITAL	110 mbps (ANALOG SIGNAL DIGITIZED ON GROUND)	–	1/400	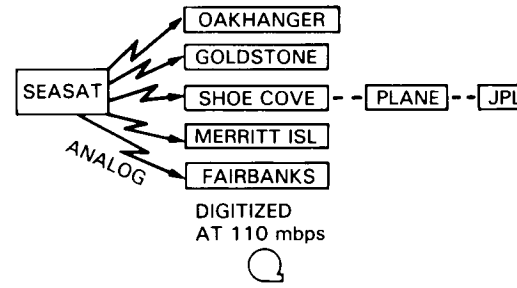
SIR-A	1	OPTICAL	–	–	ONE DATA TAKE PER WEEK	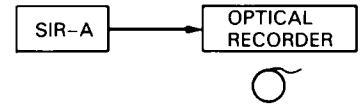
SIR-B	1	DIGITAL AND OPTICAL	45 mbps, 30 mbps	30 mbps	1/360	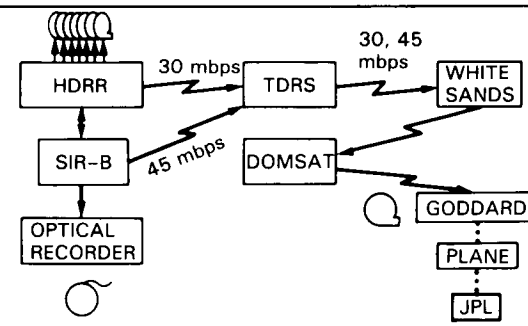
SIR-C	8*	DIGITAL	45 mbps	300 mbps (VARIABLE)	1/6	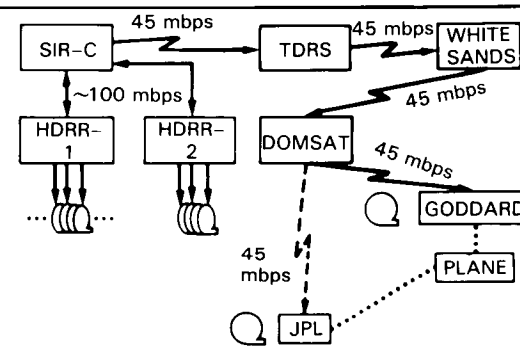
Eos SAR	10	DIGITAL	270 mbps MAXIMUM 10 mbps AVERAGE	270 mbps (VARIABLE)	1/1	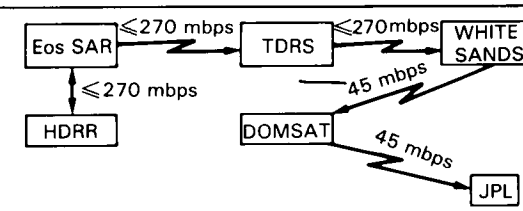

* 9 INCLUDING X-BAND

– – – – DESIRED LINK

····· NON-DIGITAL LINK

Figure 86. Evolution of the Eos SAR data system.

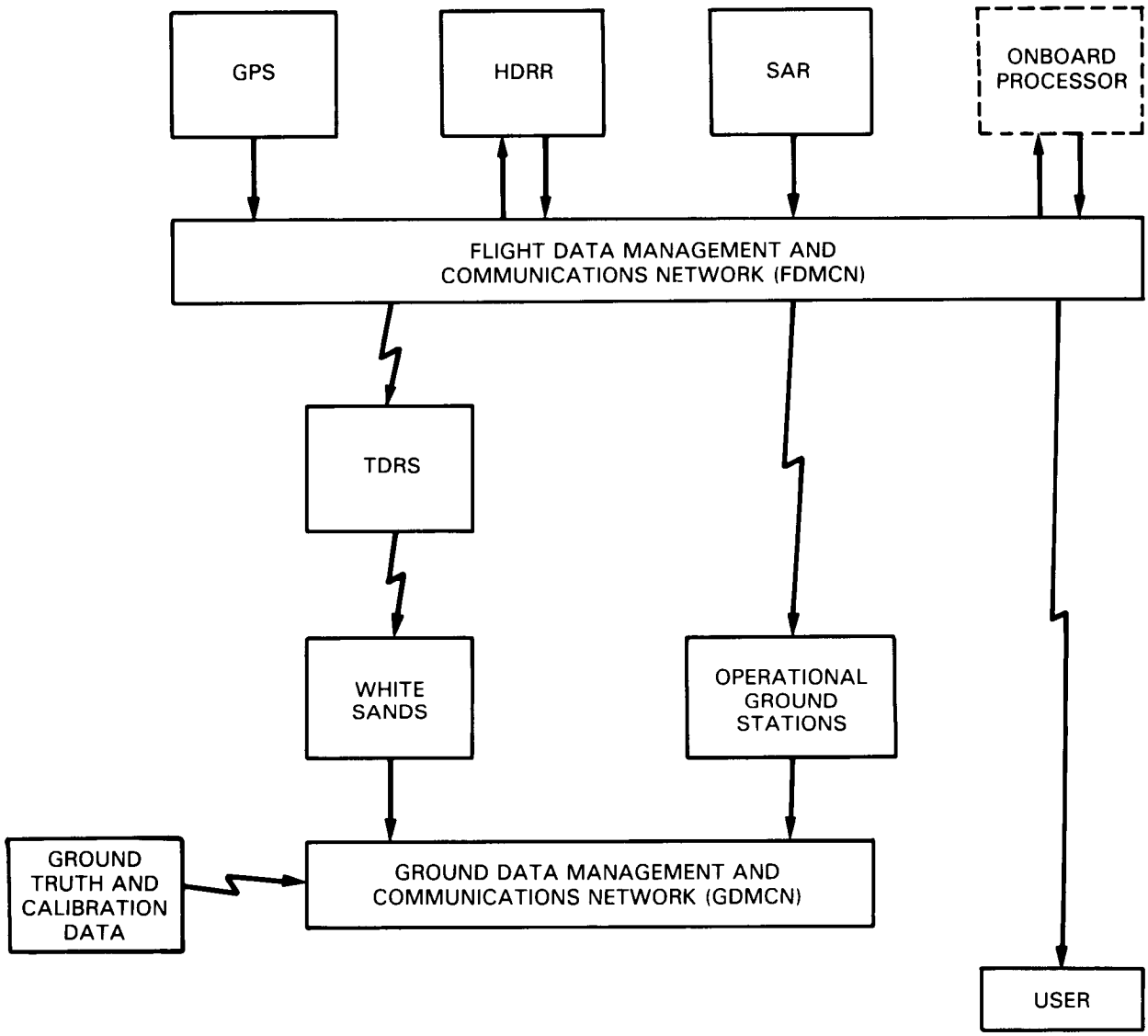

Figure 87. Illustrating the flow of SAR data onboard the Eos platform.

The Alaska SAR Facility Inheritance

ASF, located at the University of Alaska at Fairbanks, will receive, process, and disseminate archived SAR imagery from the ERS-1, JERS-1, and Radarsat satellites beginning in the early 1990s and extending later into the decade (Carsey *et al.*, 1987). The SAR data will be both regional within the ASF receiving station mask and global due to the onboard data storage on both JERS-1 and Radarsat. The SAR image processor will be similar to the ADSP used for SIR-C and is designed for high reliability and automated operation. The ASF processor will have the flexibility to process data from three different SAR sensor/platform systems and to produce a variety of products from full-resolution complex imagery to low-resolution browse imagery for a quick-look survey of the available data.

The Eos SAR Data System

The Eos data system will differ from the SIR-C system principally because of the need for long-term, high data-rate processing, the need to distribute large volumes of calibrated, georeferenced data to a wide variety of users, and the need for operational data analysis systems. In addition, because Eos is a free flyer, the data cannot be recorded onboard (except for temporary storage purposes) and must therefore be downlinked to Earth at very high rates.

The Flight Data System

The hardware for the flight data system for Eos is discussed in Chapter VIII. Once acquired, the data would be routed into six DDHAs, each producing a 45 Mbps digital data stream. These six streams would then be handed over to the Eos Flight Data Management and Communications Network (FDMCN) for transmission to the ground and then the processor (Figure 87). The FDMCN would also be responsible for appending ancillary data such as Global Positioning System (GPS) data to the SAR data streams.

In general, data would be acquired in an organized fashion at the expense of some swath width as described in Figure 88. The single-channel modes (L, HH-pol for example) would use at most three DDHAs because it is expected the swaths will never exceed 150 km due to beam width limitations. The other modes would efficiently utilize all DDHAs.

Wide-Band Downlink and Raw Data Transmission

Eos will take a much needed step toward improving spaceborne data systems by replacing the present 50 Mbps K_u-band link used on the shuttle with a 300 Mbps link. Inasmuch as the TDRS satellite is limited to two 150 Mbps channels, this addition will allow TDRS to be used to its full capacity. Eos will thus be able to use TDRS an average of one-third of the time; this means that the maximum average data rate from Eos through TDRS for all Eos instruments would be 100 Mbps. This new capability is especially important for SAR.

With the current configuration of the Eos platform, data could also be sent directly to operational ground stations or broadcast directly to the users (Figure 87). These routing options will be especially important if onboard processing is implemented for SAR.

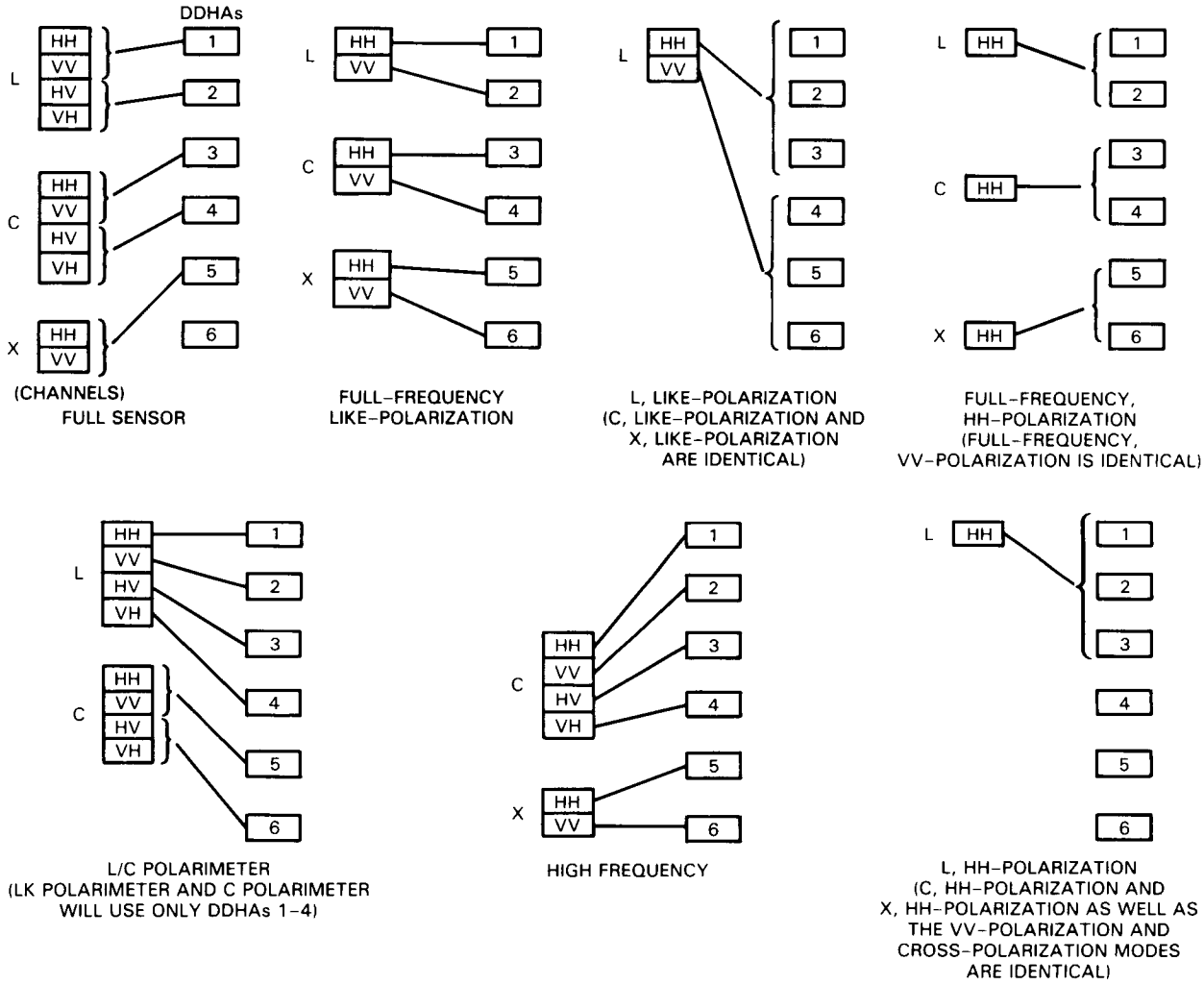

Figure 88. Distribution of channels between DDHAs.

Data arriving at the data relay satellite ground station would have to be buffered to 50 Mbps if it is sent through existing domestic communication satellites. An alternative scenario would be to send the data via a fiber optics land line or to locate the SAR processing facilities at data relay satellite ground stations. The proposed overall routing of the data at all levels is described in Figure 89 and will be handled by the Eos Ground Data Management and Communications Network (GDMCN). The GDMCN would also handle routing ancillary data to the SAR processor such as ephemeris data from the platform and ground calibration data collected in the field.

The raw data should be sent in parallel to the processor and the raw data archive. If the processor is down at the time of data acquisition, the data can then be accessed at a later time from the raw data archive. It is recommended that data arrive at the processor no more than 3 hours after acquisition.

The Ground Image Processing System

The processor for Eos SAR must be capable of processing an average input stream of 10 to 20 Mbps for the lifetime of the Eos mission. Two options for accomplishing this would be a single high-speed processor such as the ADSP, or a series of distributed lower-speed processors with a common catalog system. For the first option, an upgraded ADSP with improved reliability could be implemented. Processed data could be linked directly to the archive via the NASA Program Support Communications (PSC) Network. The new ADSP would require some additional upgrading, including the capability to routinely process squint and SCANSAR data.

For the second option, a SAR processor could be implemented on existing commercial computing systems (e.g., CRAY). These processors could be distributed internationally with a common catalog based in the core Eos information system. Browse imagery would then be linked via a series of land lines and/or satellites to the users. The success of such a system would depend on the cataloging system and the control over the quality of the data products.

In addition to the upgrades to the current processor capability mentioned above, several post processing steps (Level 1) would need to be incorporated on an operational basis and should therefore be included in the operational processor. These include calibration using ground calibration station data, geocoding, georeferencing, and mosaicking. Calibrated, georeferenced image data, including phase

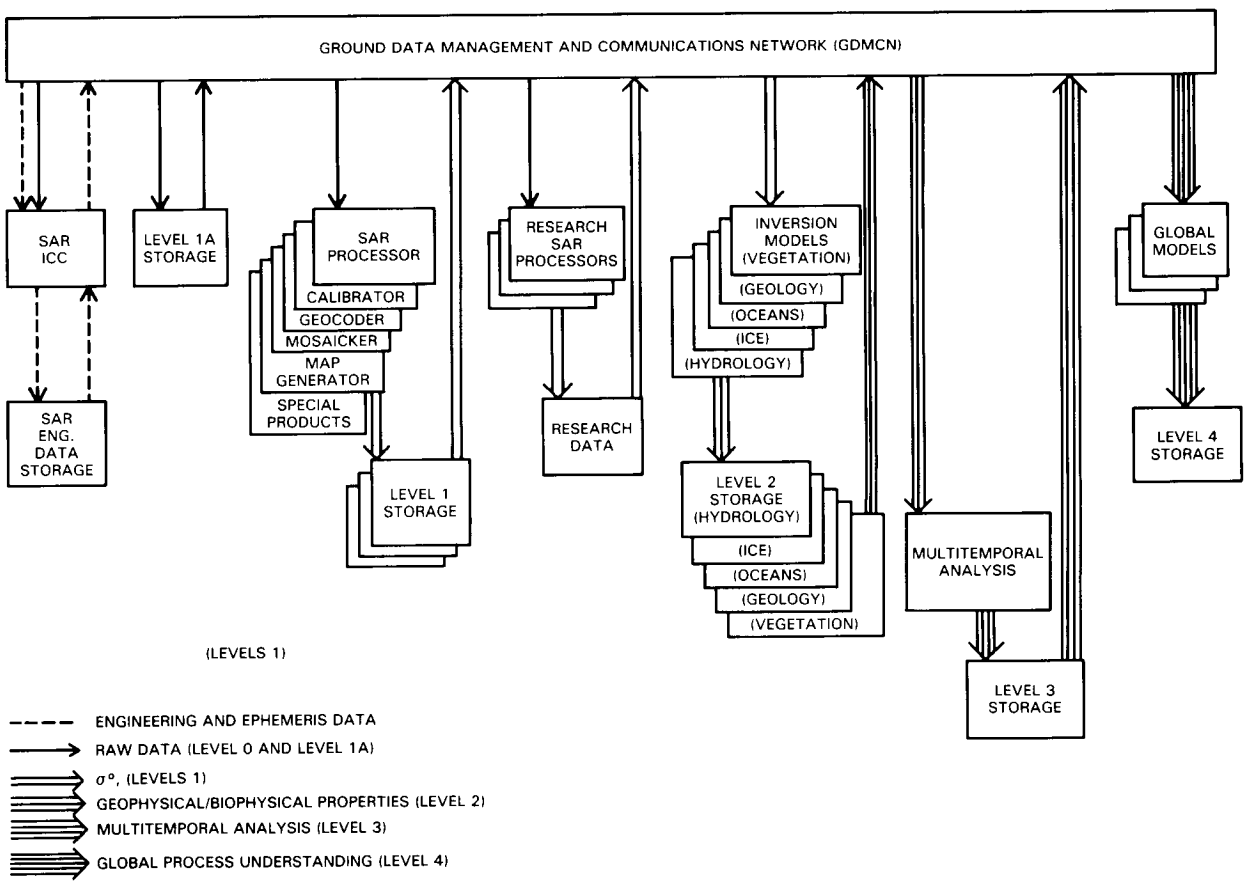

Figure 89. Illustrating the flow of SAR data on the ground.

information, would be sent to the data archives as Level 1.5 products.

There will likely be a number of institutions with their own requirements and capabilities for specialized signal processing and these would be able to routinely access raw data from the SAR data archives. Image products from these processors would be a part of the data archives and listed in the catalogs for other users.

Onboard Processor

An onboard SAR processor has been suggested as a means of reducing the raw SAR data rate. Such a processor would reduce the downlinked data rate by a ratio approximately equal to the number of looks. This capability is very valuable for two reasons: (1) data could be provided to users in remote locations in real time directly from the platform, and (2) the data transmission rate of the SCANSAR mode could be significantly reduced while frequent global mapping could be provided.

Archiving

Eos SAR data must be archived in a manner permitting ready, high-speed distribution of data. It is essential to have one main data catalog for all Eos instrument data which can help scientists can rapidly ascertain whether a required data set exists and the simplest means of access. The Seasat SAR data set, which was stored on high-density digital tapes (HDDTs), offers an important lesson in data archiving; the data on HDDTs were allowed to degrade and portions of a valuable data set were being lost. Improved storage technologies are required. All Level 1 and higher data will be archived by Eos.

Finally, the overall data base available to Eos users should include existing SAR data from Seasat, SIR-A, and SIR-B as well as for all missions between now and the Eos launch (SIR-C, ERS-1, JERS-1, and Radarsat).

DATA PRODUCTS

A number of standard data products have been defined and are described below. These levels are consistent with those defined in the Eos Data Panel Report (Chase *et al.,* 1986). Figure 90 (and Figure 89) describes the location within Eos SAR data flow of the various levels of data products.

Essential to the success of the Eos SAR Data System is specification of international standards for data processing and formatting. These standards must apply to all Level 0 and Level 1 processing, as well as to the inputs to Level 2 post-processing.

The following discussion of data product levels assumes that when data are acquired at more than one polarization amplitude (e.g., HH and VV), the phase (e.g., $\varphi_{vv}-\varphi_{hh}$) will be maintained at all levels of processing.

Data Product Levels

Level 0-Level 0 data represent the basic telemetry stream of raw SAR data as received from the spacecraft. This data stream is time referenced and includes some calibration data that has been directly received by the SAR from ground calibration sites. Level 0 data as it leaves the SAR instrument (specifically the DDHAs) is identical to the Level 0 data as it enters the SAR processor. The data may however go through several sortings between the SAR instrument and the SAR processor in order to more efficiently transmit the data, along with other Eos instrument and carrier data streams, to the ground. It is the responsibility of the Eos Project to ensure the data received at the SAR processor is identical to the data generated by the SAR instrument at the DDHAs.

Level 1A-Level 1A data is identical to Level 0 data except that ephemeris information from the Eos carrier and calibration data not directly provided by the SAR instrument but collected onboard the platform have been added. These ephemeris and calibration data are computed and appended but not applied to the Level 0 data.

Level 1.0-Processing or correlation will produce Level 1.0 data in engineering units of Digital Number (DN). Ephemeris, phase, and calibration data remain appended. This imagery is in raw output form without any corrections (radiometric or geometric) applied.

Level 1.5-Radiometrically and geometrically corrected georeferenced data in sensor units ($\sigma°$) constitute Level 1.5 data. The ephemeris and calibration data are appended.

Level 1.6-Level 1.6 data are geocoded (resampled to grid North) on an Eos-specified Earth-fixed coordinate system with or without terrain correction as required by the topography and the application. Digital terrain models are required for this step of the processing (see Figures 91 and 92).

Level 1.7 (Special Image Products)-Level 1.7 provides images processed into particular formats such as shown in Figure 90. An investigator may choose any one or any combination of these capabilities: polarimetry, generation of backscatter curves (as a function of incidence angle), ratioing, stretches, perspective views, etc.

Level 2.0-Level 2.0 provides geophysical and biophysical parameters in image format. This is based on the use of SAR inversion algorithms as well as algorithms for other Eos instruments. The geophysical and biophysical parameters expected to be derived using SAR data are identified in each science chapter (II through VI) and are presented in Table 1; examples are sea ice type, soil moisture, SBL state,

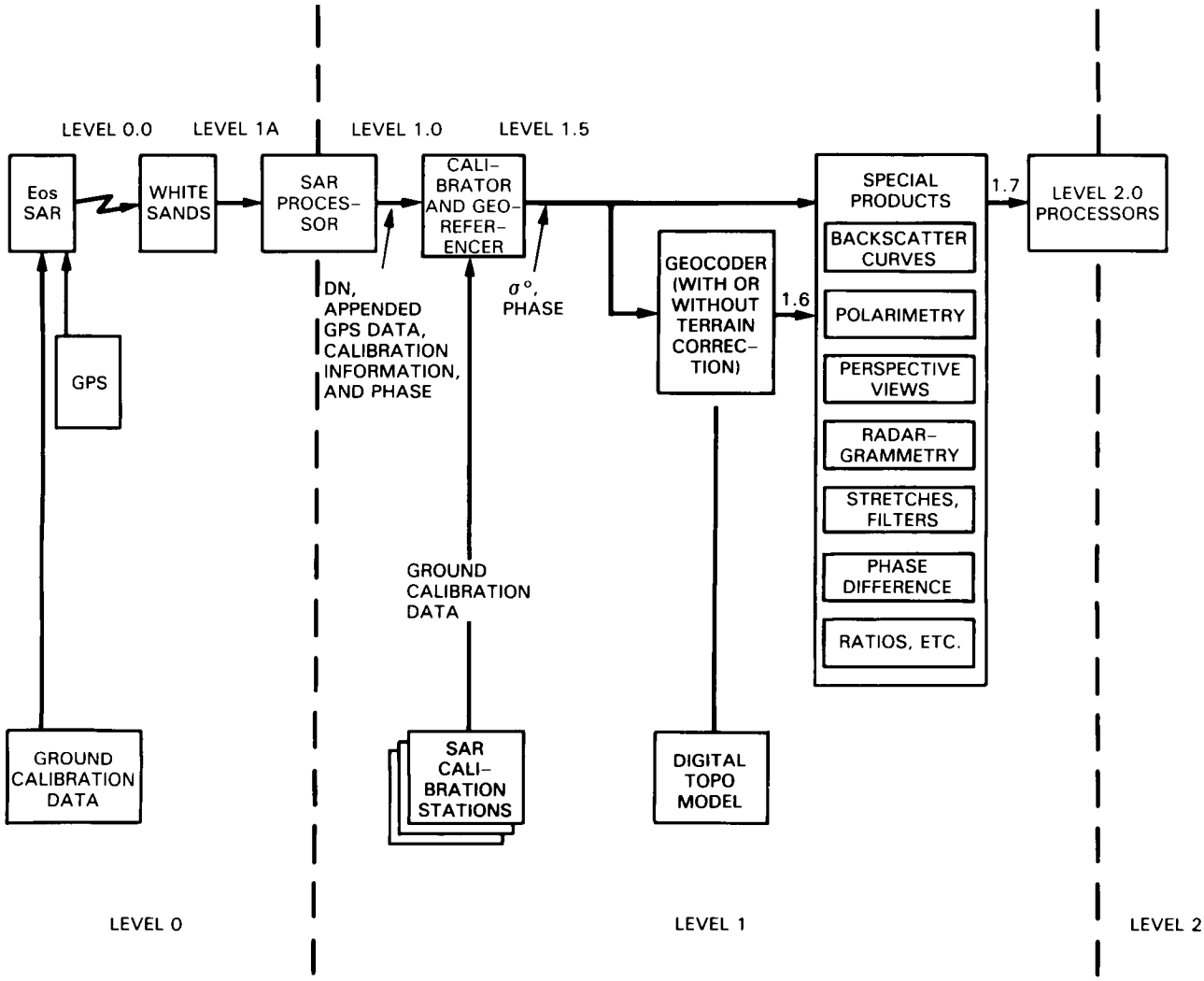

Figure 90. Block diagram describing Levels 0 to 2.

ocean current boundary velocity, or patterns and areas of soil erosion. This level is normally associated with single-date data.

Level 3.0-Level 3.0 provides geophysical and biophysical variables mapped on uniform space-time grid scales; this can include uninterpreted SAR data. Usually some completeness and consistency properties have been applied (e.g., missing points interpolated, etc.). Perspective views of the physical properties may also be accomplished at this level. Level 3.0 is associated with multitemporal data.

Level 3.1 (Incomplete)-Level 3.1 data are mosaicked images. Mosaicking is more easily accomplished within the SAR post-processor. Images are mosaicked and stored until sufficient data are generated to produce map quadrants (Figure 93). Depending on the application and the temporal variability of the region of interest, some investigators may prefer to bypass this step.

Level 3.2 (Complete)-Level 3.2 converts mosaicked images into map quadrants. Margins around the quadrants will indicate the time of acquisition of the various portions of the quadrant. Again, phase information is maintained. Perspective views may be generated at this level.

Level 4.0-The Level 4.0 data is information which can be used directly for understanding global hydrologic, biogeochemical, and climate processes. Level 3.0 SAR data products will be only one of many Level 3.0 inputs to the models needed to generate Level 4.0 products.

INFORMATION SYSTEM

The extraction of usable geophysical and biophysical information on a global scale is one of the most challenging tasks for the Eos system. SAR has

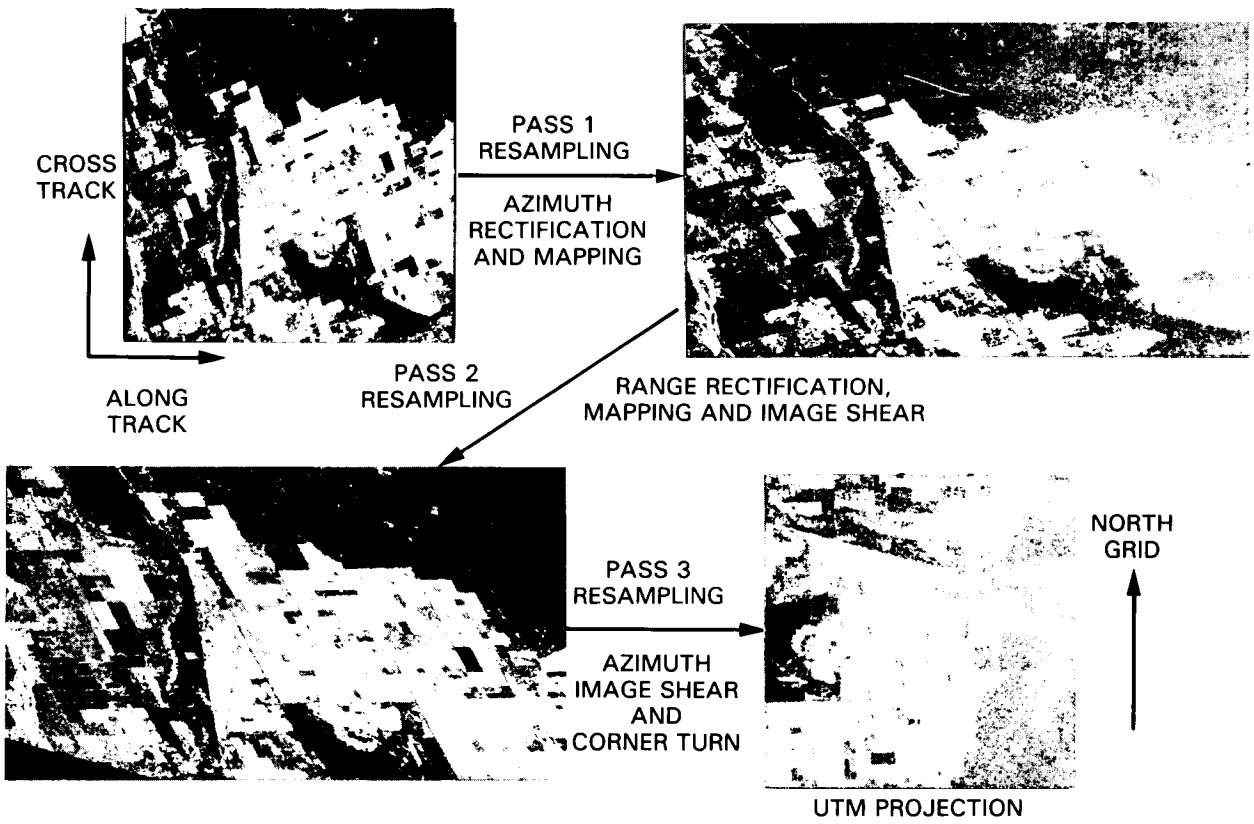

Figure 91. Example of geocoding.

the potential to reveal information not obtainable by other Eos sensors. However, we have little experience with global SAR data sets and many SAR inversion algorithms have not yet been developed and tested from space. Moreover, we have only rudimentary strategies for acquisition, processing, analyzing and distributing global SAR data sets, especially those providing multifrequency, multipolarization SAR imagery.

In order to be effective on a global scale, the Eos SAR system will require that:

- Pre-Eos research be conducted for improved inversion algorithms and techniques for handling global SAR data sets
- Strategies be developed for efficient processing, calibration, distribution, display, and analysis of large volumes of SAR data
- Provisions be made for a high degree of investigator interaction with the SAR data system
- SAR data be readily usable in synergism with other Eos instruments
- Additional geoscientists be trained in the use of Eos SAR data

In the previous chapter, we outline a strategy for data acquisition that would meet the principal scientific objectives but also give a reasonable yearly average data rate. In this chapter, we review the specific geophysical and biophysical information that can potentially be obtained with the help of SAR data and attempt to answer the following questions:

- What institutional frameworks exist for analyzing massive SAR data sets, and what classes of users do we expect?
- What are the particular requirements that SAR levies on the Eos information system design?
- How can we exploit the concept of telescience for efficient user interaction with the Eos SAR data system?

In Chapter XI, we outline some of the critical research issues that must be addressed in the pre-Eos years to develop, improve, and test inversion algorithms for the extraction of information from SAR data.

INFORMATION EXTRACTION TECHNIQUES

Some geophysical and biophysical information can be expressed in scientific units (e.g., snow water equivalent in centimeters or soil moisture in percent

GEOCODED IMAGE

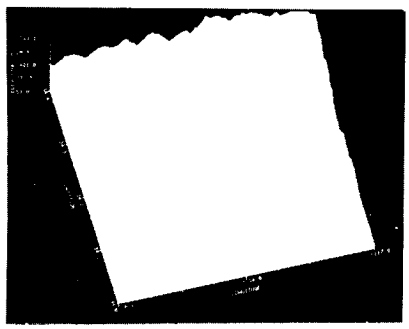

DIGITAL ELEVATION MODEL

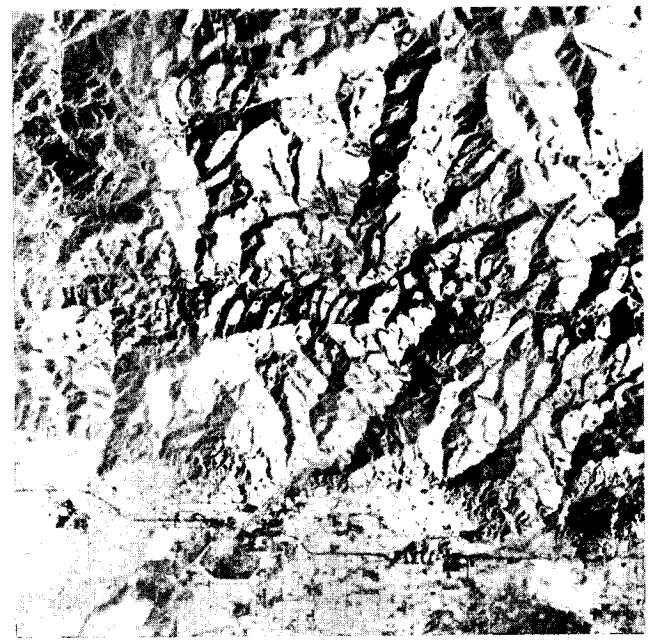

GEOCODED WITH TERRAIN CORRECTION

Figure 92. Example of terrain correction.

of field capacity) whereas other information is derived from patterns, shapes, or linear features (e.g., see Figure 46). The information extraction process for SAR images may be viewed as having three hierarchical levels, as illustrated in Figure 94. The top level, with which we have the most experience, is that of spatial or temporal associations; the next two levels utilize inversion algorithms to extract quantitative information from the SAR data. We have relatively little experience with these more quantitative approaches because very little multiparameter SAR imagery has been acquired.

Spatial or Temporal Association

Information obtainable at this most rudimentary level is derived as a result of the maplike quality of SAR images. Features are directly recognizable as a result of spatial or temporal changes in SAR tone and texture; context also plays an important role at this level. This is essentially the technique that has been used for information extraction from all single-frequency, single-polarization SAR missions such as Seasat or SIR-A. Because only a single set of instrument and viewing parameters is used, there is no need for complex frequency- or polarization-dependent inversion algorithms. Information obtainable at this level from the Eos SAR can be further classified as:

- *Spatial* (e.g., maps of crustal structural features, ice boundaries, soil-water boundaries, vegetation types). Use is made of SAR tone and texture as well as spatial context, to produce maps of surficial features from which geophysical information is obtained. This information may be in the form of linear features (e.g., faults), patterns (e.g., watershed drainage features), or areas (e.g., area of boreal forest). An example of spatial geological information derived from SAR imagery is shown in Figure 46.
- *Temporal* (e.g., ice dynamics, soil moisture, oceanic fronts or eddies, vegetation phenology). By repeated observations over a period of days or months, temporal information is obtained by the use of change detection procedures. One of the best examples of this technique is illustrated in Figure A.5 where Seasat SAR images of central pack ice in the Beaufort Sea were used to obtain velocity vectors from tracking over 750 common floes.

ORIGINAL PAGE
BLACK AND WHITE PHOTOGRAPH

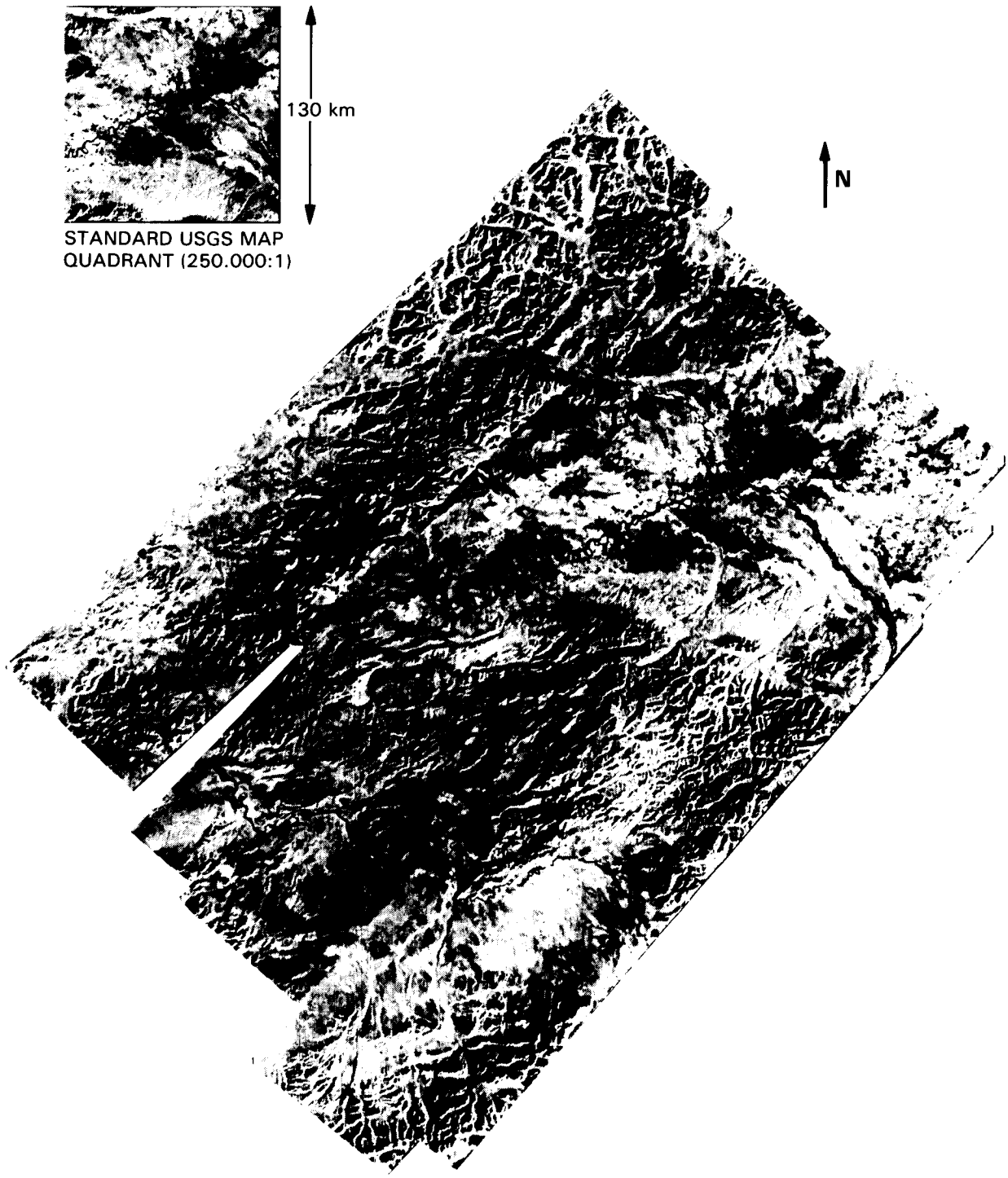

Figure 93. (a) SAR image mosaic of Alaska.

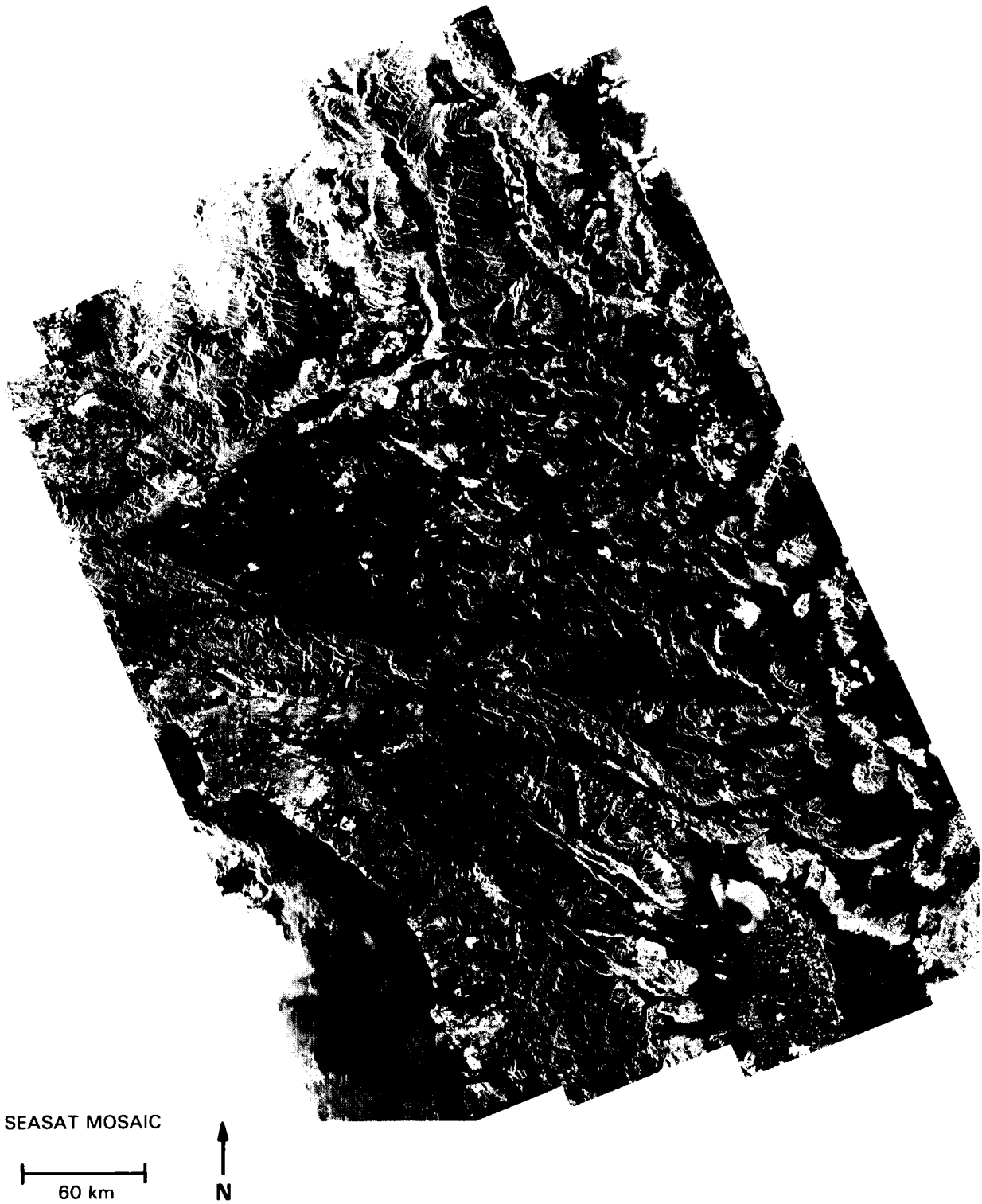

Figure 93. (b) SAR image mosaic of Southern California.

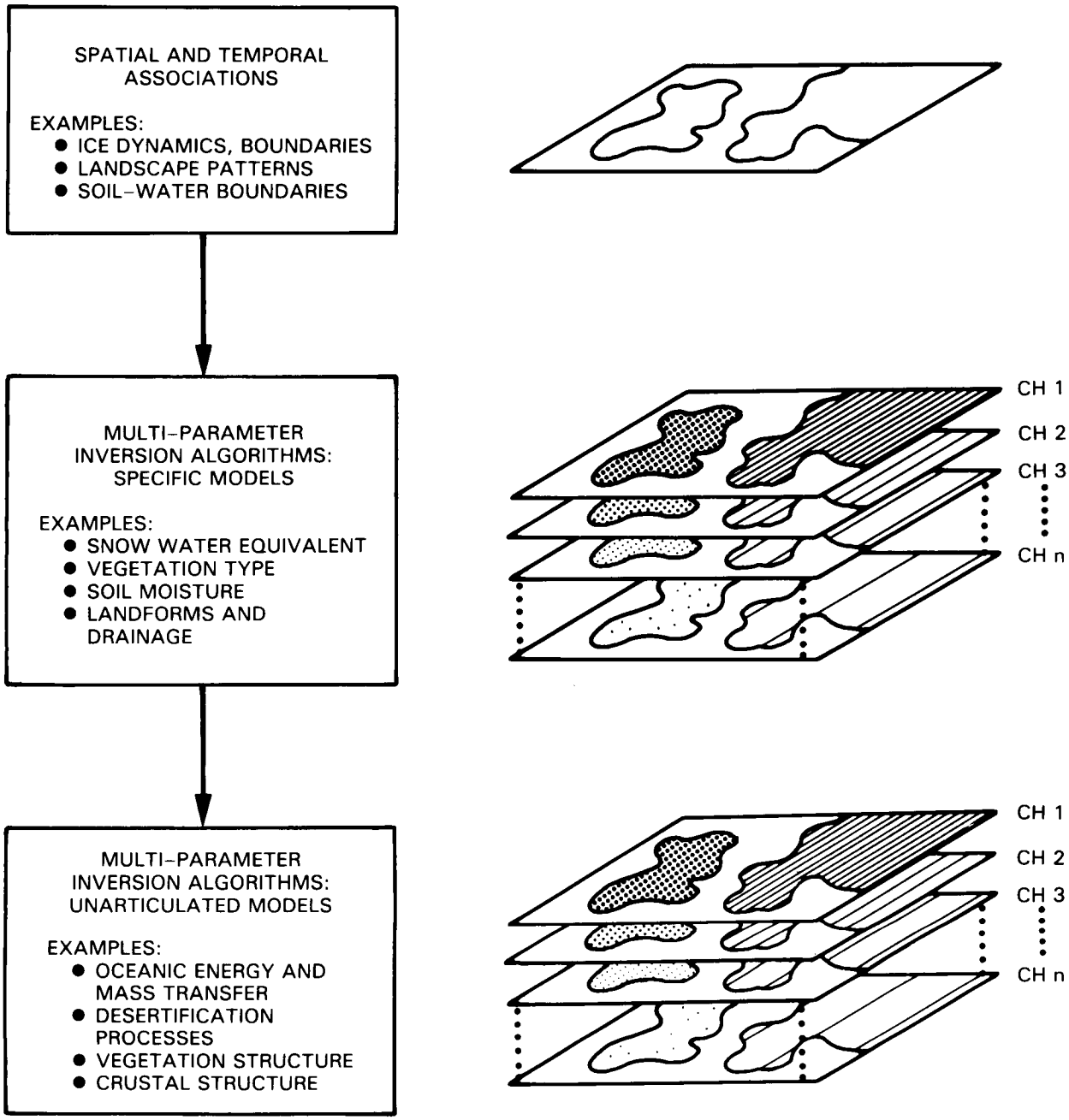

Figure 94. Illustrating a three-level hierarchy of information extraction techniques. At the top level (spatial and temporal associations), the map-like form of SAR is used to derive spatial and temporal pattern information. At the middle level (known inversion algorithms), the multichannel capability of Eos SAR would be used with models to derive specific geophysical and biophysical information. At the bottom level (unarticulated inversion algorithms), the multichannel capability of SAR would be used to extract information via the development of algorithms.

Multiparameter Inversion Algorithms: Specific Models

Information obtainable at this level requires the use of a specific inversion algorithm that already exists and that may in turn require multifrequency, multipolarization, or multi-angle SAR data; it may also require the synergistic use of SAR data with other Eos data, e.g., HIRIS. Information extraction at this level is based on a specific algorithm (formula or technique) that has either been used or hypothesized, and that is based on a specific physically-based model. However, since there have been no multifrequency, multipolarization spaceborne SAR missions, few of these algorithms have been demonstrated on a synoptic basis; SIR-C will offer the first opportunity. At this level, spatial and temporal associations might be used as a starting point, but additional data channels would be required:

- *Multifrequency.* An example of information obtainable from multifrequency association is the extraction of SWE from multifrequency (and multi-angle) data using the algorithm discussed in Appendix A. The L-band data would be used for looking at the stratum under the snow layer, while the C- and X-band channels would be used to extract SWE. While this technique has not been tested from space, it appears to be reasonably straightforward and is based on a good understanding of the physics of scattering from snowpacks. Accuracies of ± 20 cm in SWE may be obtainable.
- *Multipolarization.* On the basis of both models and field radar data, it is expected that multipolarization data will be useful for vegetation morphology (VV for vertical trunk and stem structure and HH for canopy structure), although this has not been tested from space.
- *Multi-angle.* By multi-incidence angle observations of a given site, valuable surface roughness data can be extracted, as was demonstrated with SIR-B. The ratios of SAR images at several incidence angles ranging from 15° to 50° can be used with existing scattering models to classify surfaces from quasi-specular to diffuse.

Multiparameter Inversion Algorithms: Unarticulated Models

Information derived at this third level is based on unarticulated models that are rooted in a general understanding of the scattering process supplemented by some field or aircraft measurements, but that have not yet been articulated in terms of specific formulas or techniques. Even though these models are as yet unarticulated, they nevertheless are based on considerable experience from both measurements and theory. These associations have yet to be tested on any regional or global scale, but have very strong potential for producing geophysical or biophysical information of interest to Eos.

Examples of geophysical information based on unarticulated models include vegetation canopy structure (e.g., differentiation of vegetation woody from foliar components using multifrequency SAR data), oceanographic circulation features (e.g., relationship of multitemporal SAR images of fronts and boundaries to internal processes and oceanic-atmospheric heat and mass transfer), ice types (e.g., use of multipolarization and multifrequency SAR data to differentiate ice type and thickness), and soil moisture (e.g., use of SAR and HIRIS data to minimize effects of vegetation on extraction of soil moisture). Although this level of information extraction is the least well articulated, it is not based on statistical association techniques as was the case in the use of Landsat data for Large Area Crop Inventory Experiment/Agriculture and Resources Inventory Surveys Through Aerospace Remote Sensing (LACIE/AgRISTARS). Quite to the contrary, there is a general understanding of the physics involved in each case but no opportunities to acquire calibrated data sets to test a specific algorithm for extraction of the desired information.

It is of course expected that the first few years of Eos will provide an opportunity to gather selected high-quality data sets that will allow specific inversion algorithms to be developed for these information needs. During this early phase the top two levels of information extraction techniques (e.g., spatial and temporal associations, and the use of specific multiparameter association models) will be used. This means that after the Eos SAR launch, we can expect a very early return of information on a global level for sea ice boundaries and dynamics, of crustal structure, soil-water boundaries, etc., since all of these make direct use of the SAR image spatial and temporal associations with minimal complexity. We can expect a fairly early return of geophysical and biophysical information based on currently known inversion algorithms, among these SWE, soil moisture, and vegetation type. However, information that depends on the articulation of new inversion algorithms may take some years to obtain.

INFORMATION SYSTEM REQUIREMENTS

How many SAR users are there now and how many will there be in the Eos era? Where are these scientists and what approaches will they use to convert Eos SAR data into useful information? To answer these questions, it is important to understand both the categories of users and how they are institutionally clustered.

User Categories

Eos SAR data users can be grouped into four categories (Chase *et al.*, 1986): (1) users at Eos operation centers, who would continuously monitor the SAR instrument, data quality, and calibration accuracy; (2) users such as glaciologists or hydrologists who need real- or near real-time SAR data; (3) users such as vegetation scientists who need archival SAR data with known requirements such as dates, times, or channels; and (4) users who may need archival SAR data whose attributes are known, without regard to when or where the data have been acquired.

User Institutions

The information potential of the Eos SAR is enormous, as we have previously seen, but so is the volume of data. Eos is a research concept, but with very strong implications for operational use of its global data sets. This is nowhere more obvious than with SAR. The initial users of Eos SAR data will very likely be some several dozen researchers who are already familiar with SAR data from the Seasat, SIR, and ERS-1 missions, and who will focus on the use of high-quality data sets from around the globe to enhance their understanding of the physical processes being observed. But it is clear that the volume of the data will demand that hundreds, not dozens, of individuals be involved in converting this data to information. Where are these users and their institutions?

Glaciology

Within the United States there are roughly 25 institutions with substantial capability for, and commitment to, research in sea ice, seasonal snow, glaciers, and ice sheets. At these institutions there are roughly 50 Principal Investigators who would utilize satellite data in a significant way on research and monitoring programs that are supported by a variety of civil, military and industrial groups. In Canada there is also a wide variety of groups involved in ice- and snow-related research, totalling perhaps half of the number of investigators in the U.S.

Of the total list of North American Principal Investigators who will utilize Eos ice and snow data, only a fraction will be interested in the global change programs for which the Eos system has been designed; the other research will be of a retrospective nature often carried out on a small scale. This kind of research is now being conducted with considerable success using Landsat, Seasat, and Nimbus data. Some of this work is in preparation for future data exploitation such as from Eos. Of course, data from the Eos instruments will be far more useful as the data set will be much more complete and the 15-year lifetime will allow international planning for auxiliary surface and oceanographic data collection such as that being initiated by the Programme for International Polar Oceans Research (PIPOR) Group (1985) for the ESA ERS-1 satellite.

There will, however, also be a number of major research programs that will utilize Eos for ice and snow research addressing critical large-scale questions. These research programs will require substantial amounts of data and will primarily be organized by scientists from the geophysics as contrasted with the remote sensing communities. They will also utilize a wide variety of auxiliary data from land stations, remote data buoys, and conventional oceanographic platforms. Over the 15 years of the Eos mission there would perhaps be a dozen such programs with a similar number of Principal Investigators and perhaps 20 to 40 collaborative scientists and 50 to 100 assorted support personnel. A typical lifetime of such a program would be 5 years. Therefore, we estimate that between 250 to 500 man years of effort would be called for over a 15-year period in programs that would heavily exploit the potentials of SAR data as applied to global snow and ice research problems.

Hydrology

There is a large infrastructure of hydrologists in the United States that will be involved in the analysis of Eos data, and in particular, the SAR data. This group is associated primarily with universities, primarily civil engineering and agricultural engineering departments and governmental agencies. There are, for example, at least 50 universities that are members of the University Council on Water Resources (UCOWR). Governmental agencies that have research programs that will eventually be associated with the Eos program include such groups as NOAA, the National Weather Service Flood Forecasting Research Laboratory, the U.S. Geological Survey, the Environmental Protection Agency, Agricultural Research Service, Tennessee Valley Authority, U.S. Bureau of Reclamation, and the U.S. Army Corps of Engineers. Most countries other than the U.S. also have a similar infrastructure of universities and governmental organizations. There are also a large number of private engineering and consulting firms that will utilize Eos data for both research and operational purposes.

The opportunity for intragovernmental and international research is great. An approach that should yield high returns would be one that assembles teams of university, government, and perhaps private researchers to study specific applications and uses of SAR data in depth. Carefully selected field sites would minimize ground data costs through extensive cooperation. Such cooperation should consider international possibilities, both for selection of optimum ground sites as well as to enlist a wide spectrum of highly trained researchers.

Several hundred man-years of effort may be needed to address all possible applications of the Eos

program. As discussed previously, this would include use of a variety of remotely sensed products, not just SAR data. However, it must be reemphasized that easy access to a very large volume of data products is needed to make the gains that can be expected in hydrology. This seemingly large effort is quite achievable. Many existing research groups can and should be redirected to benefit from this program. The potential benefits and potential for scientific breakthrough should be all the incentive necessary for such a redirection.

Vegetation Science

Researchers likely to be interested in extracting canopy structure and water content information from SAR data are spread throughout the United States, and presumably the world. Within the U.S. there are researchers at about a dozen universities interested in canopy structure. Many ecosystem modelers are likely to become involved in SAR data analysis as experience is gained in the use of structural data as model inputs. There is a much larger research community composed of university, government, and private sector scientists interested in canopy moisture. Hundreds of institutions could be involved in the Eos era.

The use of SAR to determine areal extent of vegetation units, to delineate wetlands boundaries and water regimes, and to improve vegetation classification has a potentially large user community. The need for such data and the superiority of SAR for these purposes compared to other sensors will dictate the size of the user community. Tropical studies may profit the most in this regard.

Despite the great potential for SAR in vegetation research, the user community will start quite small and build slowly as ecologists and others who have not traditionally had access to SAR data become familiar with its capabilities. As SAR begins to provide more biophysical information, the community of users will become better defined.

Oceanography

In a 1987 survey by the American Geophysical Society, of 6,000 respondents, about 2,400 listed physical oceanography as one of their areas of interest and 640 listed it as their primary interest area. Most physical oceanography research has traditionally been centered on small scale processes supported by local *in situ* measurements. This is the natural result of the represent sparsity of high quality, geophysically calibrated global data bases. In the absence of viable data bases to confirm, reject, or extend scientific hypotheses, many young oceanographers have found that a career path in global oceanography presents unacceptably high risks. This difficulty has been compounded by the lack of user-friendly data bases for global oceanography.

There are probably at most 1,000 active (publishing) physical oceanographers in the work, perhaps 10 percent or 20 percent of which have used global remote sensors as a primary data source. There are only 20 to 30 government, university, and non-profit institutions in the U.S. that receive the bulk of domestic funding support to perform satellite-oriented physical oceanography. Typical support levels at these institutions are 1 man-year or less. This research includes satellite sensors of all types: imaging, non-imaging, microwave, visible, and infrared.

It is expected that the data acquired from Eos will both increase the number of physical oceanographers using orbital global data and also the percentage of this number who adopt a multi-instrument approach. It is expected, for example, that physical oceanographers who exploit the synergism inherent in the Eos suite of instruments will be able to extract new information about spatial and temporal patterns associated with the ocean-atmosphere interface. Thus a viable approach would be to accrue a critical mass of 20 to 30 researchers (both domestic and foreign) and to encourage them to use this synergism to address fundamental global questions in physical oceanography. Over the lifetime of Eos, this would involve about 300 to 450 man-years of effort.

Geology

Within the United States the major government agency users of the proposed Eos data for geological research will be the Department of the Interior and NASA. University geoscientists from the United States participating in analyses of the Eos data will probably exceed 300 to 500 over the 15-year period. Geoscientists in government agencies and universities of other countries will also play an equally major role in the analysis of Eos data.

Of the total number of geologists who will utilize the Eos SAR data, the greatest percentage can be expected to concentrate on the analysis of SAR images related to crustal structure and tectonics, including mineral resource analysis. Arid lands, desertification, soil erosion, and other geology studies will account for an equal interest among the remaining Eos participants.

Some of the SAR data obtained for desertification and soil erosion experiments will require careful coordination with ground monitoring stations and experiments in order to maximize scientific output. A typical lifetime for desertification and soil erosion experiments would be 15 years while crustal structure and tectonics experiments might last only 1 to 2 years. Over a minimal 15-year lifetime for the Eos sensors, a worldwide total effort of 300 to 500 man-years of investigator participation is likely to be needed for geologic experiments.

User Requirements

The information system for Eos and particularly for SAR is one of the most challenging endeavors for NASA in the 1990s. The primary goal for the information system and the key to the success of Eos in general is to allow an investigator to "focus on (Earth) research rather than on the details of accessing and preparing data for analysis" (Chase *et al.*, 1986). The information system should then be designed by Earth scientists who have developed and understand global models (climate, hydrology, biogeochemical, etc.), not the engineers or image processors.

The information system must be evolutionary. Our knowledge about how to use SAR data will increase significantly with the flights of SIR-C, Radarsat, ERS-1, and JERS-1. It will again advance when Eos is first launched and improve as the Eos mission progresses, especially in the case of SAR where no long-term, multiparameter data sets have ever been acquired. Flexibility and control must be inherent in the system such that improvements may be made but uniformity in long-term data sets is maintained.

The information system is expected to provide a number of products and functions which have been specified in the Eos Data Panel Report, including data, algorithms and analysis tools, documentation, catalogs, engineering data, and instrument operation information. Access to the data archives, the instrument control center, supercomputers, and discipline data center computers and algorithms is essential. The system must also have the capability for electronically and rapidly browsing through the data in selectable dimensions: frequency, polarization, incidence angle, location, geophysical parameter, and time.

X. SYNERGISM

Synergism, in the Eos context, is defined as the cooperative effect resulting from Earth observations by separate instruments that, used together, provide more information than the sum of their individual capabilities. The exploitation of synergism between instruments is a basic idea behind the Eos concept.

Specific requirements for synergistic Earth observations have been discussed for each geoscientific discipline in Chapters II through VI. In this chapter, we collate these requirements and discuss the synergism between SAR and the following instruments: HIRIS, MODIS, TIMS, AMSR, ESTAR, SCATT, ALT, and GLRS.

SAR AND HIRIS

Instrument Description

HIRIS is an Eos facility instrument designed to provide simultaneous imaging in 196 spectral bands over the 0.4 to 2.5 μm wavelength region. HIRIS is a targeting (rather than continuous acquisition) instrument, which can be pointed from -30° to +60° along-track and ±25° cross-track. The swath width is 36 km and the instantaneous FOV is 30 m.

Both SAR and HIRIS will provide high-resolution, map-like images of the Earth; both have very high data rates, and therefore are best not co-located on the same platform. In general, SAR is sensitive to surface morphology (geometrical arrangement of scatterers and dielectric constant of surface materials), whereas HIRIS will be sensitive to surface chemistry and boundaries associated with chemical changes. SAR provides high-resolution images that are essentially unaffected by weather conditions or by sun angle; usable HIRIS images of the Earth's surface will require low cloud cover and sun-synchronous observations.

The SAR and HIRIS coverage and accessible FOV from 824 km altitude are shown in Figure 95.

SAR-HIRIS Synergism

Ice Morphology

SAR will be the primary sensor for both sea ice and ice sheets, owing both to its independence from weather and darkness and to its sensitivity to ice morphology. However, under clear skies, HIRIS (and MODIS) can provide information on the optical properties of ice, the ice edge position, the ice albedo, and in spring and summer, information on the presence and magnitude of biological productivity at the ice edge. This results from the very large variation (seven orders of magnitude) of the absorption coefficient over the spectral range 0.4 to 2.5 μm. Ice and water are optically very similar except for the region between 1.55 to 1.75 μm, where ice is slightly more absorptive. In the visible wavelengths,

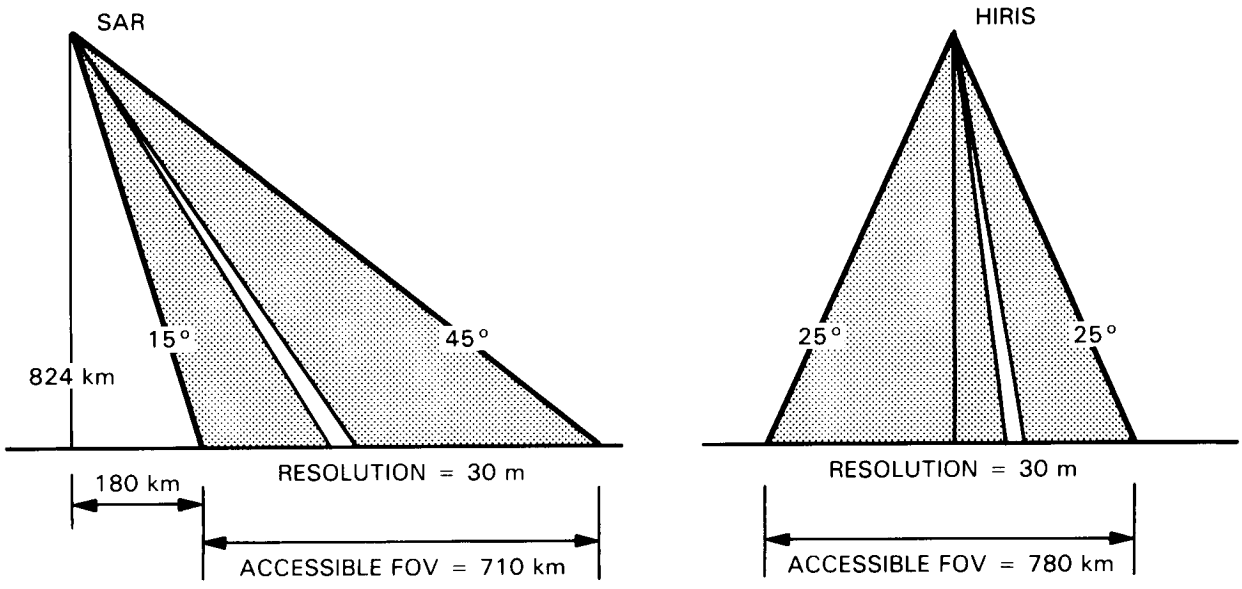

Figure 95. SAR and HIRIS accessible FOVs from an 824 km orbit altitude.

ice is transparent; however, in the near-IR wavelengths, ice is moderately absorptive, and the absorption increases with wavelength.

It is expected that under clear sky conditions, HIRIS data will be useful in conjunction with SAR for delineation of ice edges (both sea and lake ice), for floe size distribution, for lead orientations, ice islands, ice motion, and the mass and crevasse patterns associated with ice sheets, shelves, and glaciers.

Snow Properties

As discussed in Chapter II, snowpack wetness and water equivalent information can in principle be derived by forming the ratio of X- to C-band backscattering coefficients, and from the ratio of daytime to nighttime images at X-band. This algorithm is based upon field measurements and upon models; it has not been possible to test this procedure using aircraft or spacecraft SAR data.

In the near-IR (especially 1.0 to 1.3 μm), the albedo is sensitive to snow grain size. The presence of liquid water in the snow does not itself affect the albedo; however, liquid water causes the grains to form clusters and these apparently behave optically as single grains, causing decreased reflectance in the near-IR wavelengths. It has been shown that minute amounts of absorbing impurities would reduce snow albedo in the visible wavelengths, whereas ice is highly transparent. The visible and near-IR bands of the NOAA-6 satellite have been used to calculate snow albedos (Dozier *et al.*, 1981).

Historically, discrimination of snow from clouds using VIS/IR images has been difficult because of similar reflected radiance. However, some distinction is possible in the 1.55 to 1.75 μm wavelength region.

The principal value of HIRIS for snow observations is thus expected to be in the estimation of snow albedo and, in combination with C- and X-band SAR data, delineation of snowpack extent.

The role of HIRIS, SAR, and other Eos sensors for use in global assessment of energy and mass transfer in global sea ice studies is suggested in Figure 96.

Soil Moisture, Water, and Energy Fluxes

A major objective of Eos is to gain an improved understanding of hydrologic processes, especially the role that surface cover (vegetation) plays in land-atmosphere water flux. Because the energy and water balances of the land surface are closely coupled, it is necessary to acquire information about the surface *albedo* and *temperature* in order to interpret the soil moisture data sensed by SAR and ESTAR.

Thus, HIRIS data (along with MODIS and TIMS) will be required for high-resolution albedo information for use in the estimation of water and energy fluxes within individual watersheds. The high spatial and spectral resolution provided by HIRIS will also be useful for examination of biological productivity and biogeochemical fluxes in inland waters.

Finally, the narrow-band (10 nm) spectral data from HIRIS should be useful for characterizing soils and delineating important soil differences. Although there is much research remaining to be done, HIRIS data may yield quantitative estimation of the physical, chemical, and mineralogical properties of specific soil series and phases within series. Such HIRIS images, in conjunction with SAR images of soil moisture, will provide improved estimates of water and energy fluxes within watersheds.

Vegetation Canopy Morphology

There is evidence that the combination of SAR and optical images of vegetation canopies leads to improved identification of species and vegetation condition over that obtained from either sensor alone. Although quantitative advantages have not yet been established, there are compelling reasons based on fundamental physics for exploiting this synergism.

Several one-dimensional (height) models of the microwave and optical scattering behavior of plant canopies have been developed and published over the past several years. The purpose of these models is to predict either optical radiance or microwave backscatter that would be observable from space, and to relate this to canopy variables such as canopy morphology (including distribution of trunks, branches, and leaves), spatial dispersion of leaves with height, LAI, leaf orientation, leaf dielectric constant, reflectance and transmittance, and soil backscatter or reflectance. Some of these variables (e.g., canopy morphology) are sensible only in the microwave regime, and others (e.g., leaf reflectance) can be obtained only in the optical spectrum.

Considerable information about the state of a plant community can be obtained from its canopy. The SAR response is mainly to plant canopy morphology (geometrical structure) and plant water content, whereas the HIRIS response will be to plant biochemistry. Radar waves penetrate well into the canopy, whereas optical reflectance is primarily from the top of the canopy. The radar backscattering scattering coefficient σ° is sensitive to wet biomass, and when polarization and incidence angle information is used, to plant geometry. The optical reflectance from the canopy responds to leaf chemistry, and with the narrow spectral bands available from HIRIS, may be useful for detection of subtle changes in the vigor of vegetation and rates of various ecosystem functions. Preliminary results from the Airborne Imaging Spectrometer suggest that total canopy nitrogen, water, and lignin may be measurable (Spanner *et al.*, 1985; Fownes and Aber, 1985; Waring *et al.*, 1986).

Synergistic SAR and HIRIS (and MODIS) data are desired every 1 to 2 weeks for most vegetation studies during periods of rapid environmental and phenological change, and are required each month or two during the remainder of the year. For grassland,

steppe, and desert regions, SAR and HIRIS data are only required on a quarterly basis.

Oceanic Frontal Boundaries

The principal use of HIRIS data for oceanographic studies is expected to be in biological process studies of a particular phenomenon in a restricted area for a short duration, such as coastal area phytoplankton blooms. However, HIRIS data may also be useful, in conjunction with SAR data, for physical oceanographic investigations of small-scale phenomena such as fronts. HIRIS images may include glint patterns, which in conjunction with SAR responses to Bragg scattering from short gravity waves, provide valuable information about frontal boundaries.

Geological Structure and Lithology

HIRIS data are expected to provide greatly enhanced discrimination of lithologic units, and in

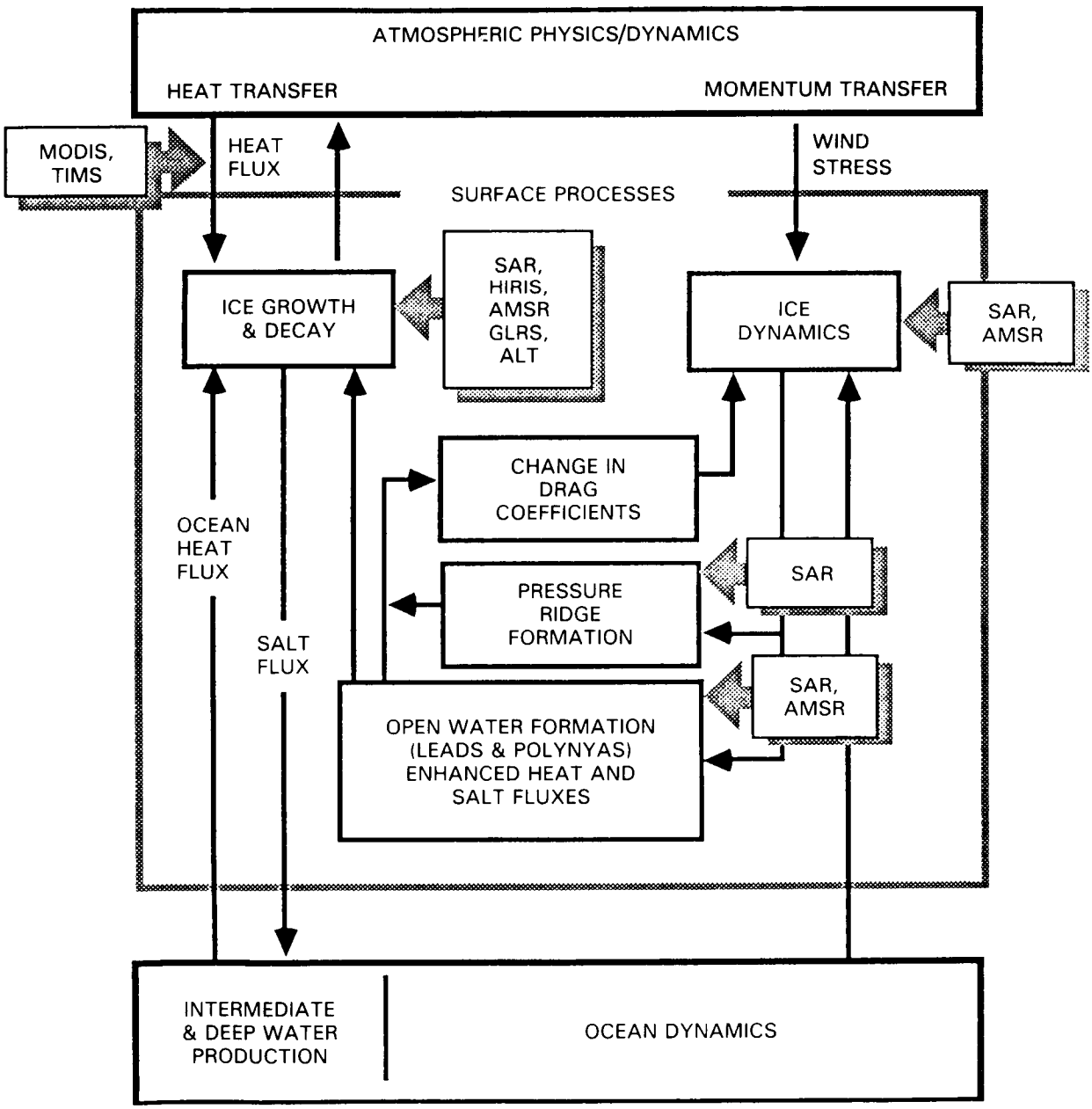

Figure 96. Flow diagram for ice studies.

conjunction with SAR images, to greatly facilitate the analysis of regional- to continental-scale tectonic, magmatic, and depositional features. The high spectral and spatial resolution of HIRIS should enable remote identification and discrimination of certain minerals with diagnostic electronic and vibrational transitions throughout the 0.4 to 2.5 μm region. Over 100 Fe^{2+}, Fe^{3+}, OH, CO_3, and SO_4-bearing minerals have unique spectral characteristics in this wavelength region (Goetz and Herring, 1987). This will enable geologists to map the mineralogy and composition of sedimentary rocks (e.g., limestone, shale, and sandstone), and of hydrothermally altered rocks with alteration intensity expressed by key minerals with diagnostic reflectance spectra; HIRIS data will also be useful for mapping carbonatites (carbonate-rich rocks of magmatic derivation typically containing minerals such as calcite, dolomite, and ankerite).

SAR images, by contrast, are not sensitive to mineral absorption but are very sensitive to surface roughness and dielectric constants. It has been shown that SAR images are very useful for delineation of regions of constant lithology that have undergone different erosional processes, and are especially sensitive to structural features. Taken together, HIRIS data will provide lithologic details within specific structural features delineated by SAR.

SAR AND MODIS

Instrument Description

MODIS is an Eos instrument composed of two mutually-supporting observing modules. One of these modules, called MODIS-N (where N signifies nadir-looking) has a 1,500 km swath and includes 40 spectral bands over the optical, SWIR, and thermal IR wavelengths (0.47 μm to 14.235 μm). The IFOV of MODIS-N ranges from 500 to 1,000 m. The companion instrument to MODIS-N is MODIS-T (where T signifies that the instrument can be tilted $\pm 50°$ along the spacecraft track). MODIS-T also has a 1,500 km swath and includes 64 channels over the range 0.4 μm to 1.04 μm; it is optimized for ocean studies where avoidance of sun glint is important and also for bidirectional reflectance data from land (Salomonson *et al.*, 1987).

MODIS is designed to provide global coverage every 2 days, whereas HIRIS is a targetable instrument which can be used for high-resolution studies of dynamic surface phenomena. MODIS data should also be useful in combination with SAR data, especially the surface temperature information derived from the thermal IR channels. Multistage sampling strategies can in principle make use of the 20:1 resolution ratio (MODIS to SAR or HIRIS), although this technique has never been tested on a global scale.

The SAR accessible FOV and MODIS swath from 824 km altitude are shown in Figure 97.

SAR-MODIS Synergism

Snow, Ice Energy, and Mass Transfer

When cloud cover and solar illumination conditions permit, the moderate-resolution, wide swath coverage of MODIS can be used for 500 m resolution surveys of sea and lake ice edges, leads, and sea ice islands; SAR data would then be used for more detailed studies of ice boundaries and ice dynamics. Although this has not been demonstrated from

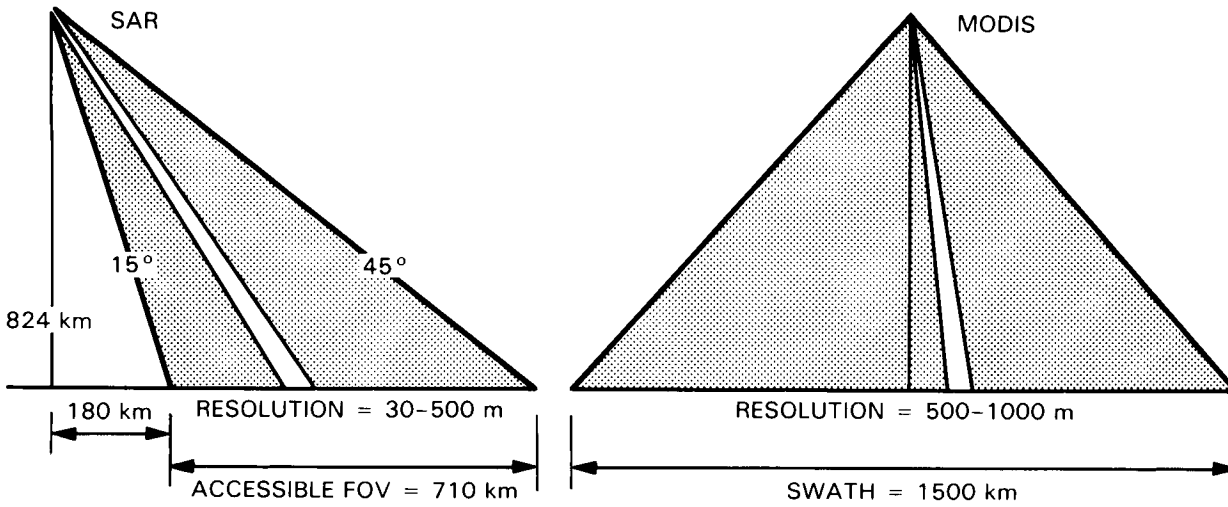

Figure 97. SAR and MODIS accessible FOVs from an 824 km orbit altitude.

space, MODIS has the potential for discrimination of sea ice thickness (up to tens of centimeters) based on spectrally dependent reflectance in the visible region. This complements the ability of SAR to discriminate among first-year and multiyear sea ice by utilizing multiple frequencies and polarizations. MODIS will also provide albedo data for sea ice, lake ice, and snowpacks.

The thermal channels of MODIS should be useful for measurement of the mean surface temperature of snowpacks, sea ice, and of ice sheets, shelves, and glaciers. Thermal data will be useful in conjunction with high-resolution spatial and temporal data from SAR imagery to better understand the processes of sea ice dynamics and energy transfer through snowpacks and ice sheets.

Vegetation Growth and Soil Moisture Stress

An important objective of Eos is to understand the role that surface cover, especially vegetation, plays in land-atmosphere water flux. Because the energy and water balances of the land surface are closely coupled, it is necessary to have information about the surface albedo and temperature in order to interpret the moisture data sensed by SAR. MODIS (and HIRIS) will provide optical reflectance data leading to albedo, and the MODIS thermal channels may be useful for land surface temperature measurements. Little is known, however, about the value of thermal IR data for studies of vegetated regions, other than the potential for regional soil moisture and evapotranspiration estimates (Gurney *et al.*, 1983). The shortwave IR atmospheric window (3.5 to 4.2 μm) permits Earth observations which are about three times more sensitive to surface temperature, and one-third as sensitive to surface emissivity variations, as the longwave IR window (8 to 12 μm). However, shortwave observations are more strongly affected by daytime solar radiation reflectance. This situation is discussed in more detail in the MODIS Report (Esaias *et al.*, 1986).

MODIS will also be used to provide a regional perspective and to identify areas requiring more detailed investigation from higher resolution sensors such as SAR or HIRIS; thus, MODIS is expected to play a major role in a nested sampling approach with HIRIS and SAR.

Large area estimates of soil moisture derived from the thermal bands of MODIS (in conjunction with SAR and ESTAR) will be useful for assessment of vegetation growth and water stress.

Oceanic Frontal Boundaries and Thermal Behavior

MODIS will be utilized for biological oceanography studies (ocean color) and sea surface temperature, whereas SAR will be useful for monitoring physical oceanographic features such as frontal boundaries. However, MODIS-derived sea surface temperatures should be useful with SAR images, especially for studies of the relationship between surface temperature distributions and frontal boundaries.

SAR AND TIMS

Instrument Description

TIMS is envisioned as the thermal IR extension of HIRIS, providing data in the 3 to 5 and 8 to 14 μm wavelength ranges. Like HIRIS, TIMS would be operated as a target of opportunity instrument. The TIMS accessible FOV is similar to that for HIRIS, as shown in Figure 95.

SAR-TIMS Synergism

Ice Thickness, Temperature, and Melt Processes

The high-resolution thermal data obtained from TIMS would be synergistic with SAR data for studies of surface melt processes, surface temperature, and (indirectly) ice thickness for sea ice and lake ice. TIMS data would be valuable, in combination with SAR images, for studies of the mean surface temperature and associated processes of ice sheets, shelves, and glaciers. TIMS-derived data on the surface temperature of snowpacks would be useful in combination with SAR images for estimation of heat transfer.

Geologic Feature Mapping

The synergism between SAR and TIMS has already been demonstrated using combinations of aircraft data (Farr and Evans, 1986). The SAR-HIRIS-TIMS combination will provide an expansion of the electromagnetic spectrum such that a much wider variety of surface phenomena, including chemical (HIRIS), thermal (TIMS), and physical (SAR) information can be extracted and used for mapping geologic features.

SAR AND AMSR

Instrument Description

AMSR would be a multifrequency, dual-polarized radiometer cluster with channels at 6, 10, 18, 21, 37, and 91 GHz and a 1,400 km swath width. This would result in a resolution of 18 km at 6 GHz, 10 km at 10 GHz, 6 km at 18 GHz, 5 km at 21 GHz, 3 km at 37 GHz, and 1.2 km at 90 GHz.

SAR-AMSR Synergism

Sea Ice and Snowpack Metamorphosis

AMSR will offer a very high degree of synergism with SAR, partly because it can provide all-weather, year-around low-resolution viewing of the

sea ice pack, and partly because AMSR will provide valuable snow information. The AMSR data at 10, 18, 37, and 91 GHz should provide the following information: ice edge position, first and multiyear ice concentration, and the location and persistence of polynyas. The 37 and 91 GHz channels will be complementary to the SAR X- and C-band channels for studies of the seasonal snowpack, especially in terms of density, water equivalent, and free water content. SAR will be especially useful for monitoring snowpack metamorphosis, sensing an increase in grain size prior to melt. The combination of SAR and AMSR could provide a more accurate "early warning system" of snowmelt.

Oceanic Wind Speed and Variability

AMSR will provide data on sea surface temperature and wind speeds at the ocean surface (6 and 10 GHz channels). Thus, SAR should be able to provide fine-scale wind variability information that could be used in conjunction with the AMSR wind speed algorithm. This requires that SAR and AMSR have overlapping swaths and be flown as nearly simultaneously to each other as possible.

SAR AND ESTAR

Instrument Description

ESTAR is envisioned as an L-band (1.4 GHz) radiometer utilizing a thinned array antenna approximately 18 m × 18 m in size. This would give a "pushbroom" mode of coverage, with approximately 140 simultaneous cross-track juxtaposed footprints, each with a resolution of about 10 km. The radiometric sensitivity of ESTAR would be less than 1 K, which is adequate for remote sensing of land surface emissivity changes.

SAR-ESTAR Synergism

Soil Moisture

The purpose of ESTAR is to estimate soil moisture; thus, ESTAR would be synergistic with the L- and C-band channels of SAR. ESTAR would provide low-resolution global surveys of soil moisture, whereas SAR would give higher resolution regional and local maps of soil moisture within individual watersheds. Figure 98 compares the SAR accessible FOV to the ESTAR swath.

SAR AND GLRS

Instrument Description

The primary purpose of the GLRS is to provide retroranging data to cube corner targets with centimeter-level precision, mainly for measurement of crustal movements at tectonic plate boundaries. The GLRS beam divergence is 0.1 mrad, i.e., the ground resolution is 80 m from 800 km range (Cohen and Degnan, 1987).

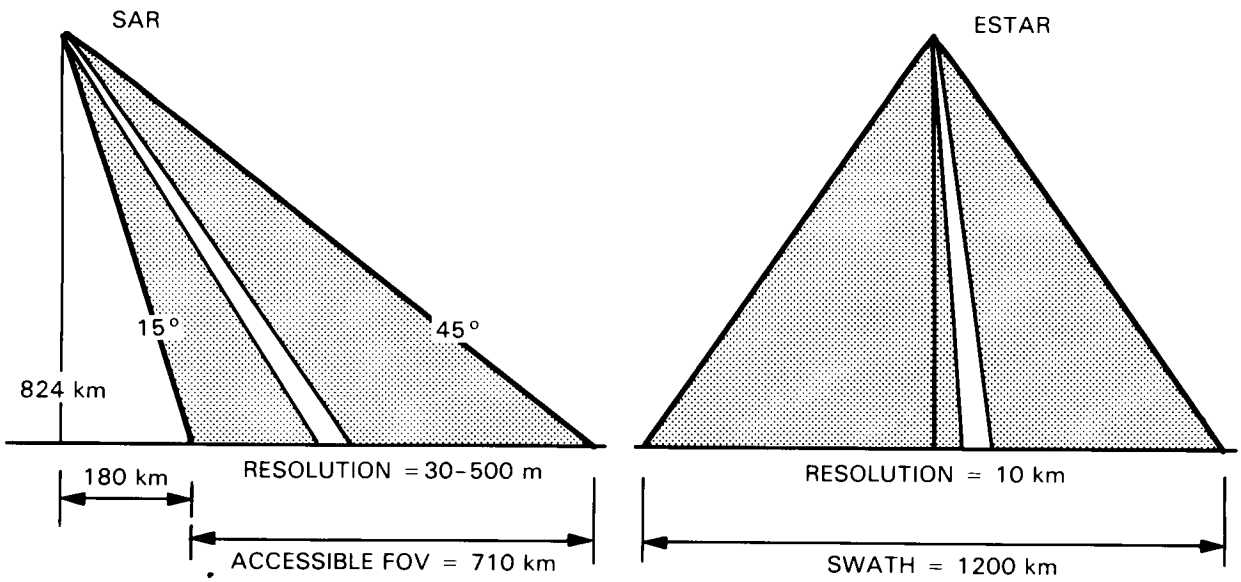

Figure 98. SAR and ESTAR accessible FOVs from an 824 km orbit altitude.

SAR-GLRS Synergism

Crustal Movements

If subcentimeter accuracy can be obtained, GLRS data will be useful for monitoring crustal movements, regional deformations at tectonic plate boundaries, relative motion of small tectonic plates, etc. GLRS data would then be valuable in combination with SAR imaging of the structural features associated with crustal features and tectonic plate boundaries.

Ice Surface Morphology

The major altimetric objective of GLRS for glaciology is to map ice sheet topography with a 10 cm vertical resolution and spatial resolution of 70 to 100 m. Precise ice surface altimetric data are required for determination of changes in ice volume, equivalent to determination of net mass balance (Curran *et al.*, 1987). SAR data would be valuable for identifying the process associated with a rapid change in ice volume. GLRS data, in combination with ALT data, would be also useful for ridging statistics and scalar information on the wave fields within the open water areas within the ice pack; the principal advantage of laser altimetric data over radar altimetric data is a smaller footprint (typically 100 m for the laser and 20 km for the radar altimeter).

SAR AND SCATT

Instrument Description

The Eos SCATT instrument is envisioned as a 13.995 GHz scatterometer with a FOV from 15° to 60° on both sides of the satellite ground trace. The objective of SCATT is to provide oceanic surface wind vector data (with an accuracy of ± 2 m/s) over swaths from 185 km to 785 km on either side of the satellite ground trace; the range resolution is approximately 10°, i.e., about 175 km ground resolution at 824 km altitude. Figure 99 compares the accessible FOV for SAR to the left- and right-side swaths of the scatterometer. Such a spaceborne scatterometer was first flown on Seasat, and later-generation designs are planned for ERS-1, Naval Remote Ocean Sensing System (NROSS), and Radarsat, as well as for Eos.

SAR-SCATT Synergism

Although SCATT is designed principally for oceanic wind vector observations, the data are also useful for very low-resolution global surveys of land surfaces. At K_u-band (13.995 GHz), the Earth appears to be rough and there is enhanced sensitivity to vegetation.

Oceanic Wind Speed and Variability

SAR images of the ocean surface often reveal fine-scale wind variabilities associated with mesoscale atmospheric conditions. This could provide valuable insight into geophysical correction sources for use in SCATT wind algorithms. Because the time scale for wind variability can be as short as a few hours, SAR images should be acquired within a few hours of the SCATT data, and the SAR swath should be imbedded within the SCATT swath.

Snow Distribution and Surface Melt Zones

Over large glaciers and ice sheets, surface roughness characteristics from SAR can be compared to

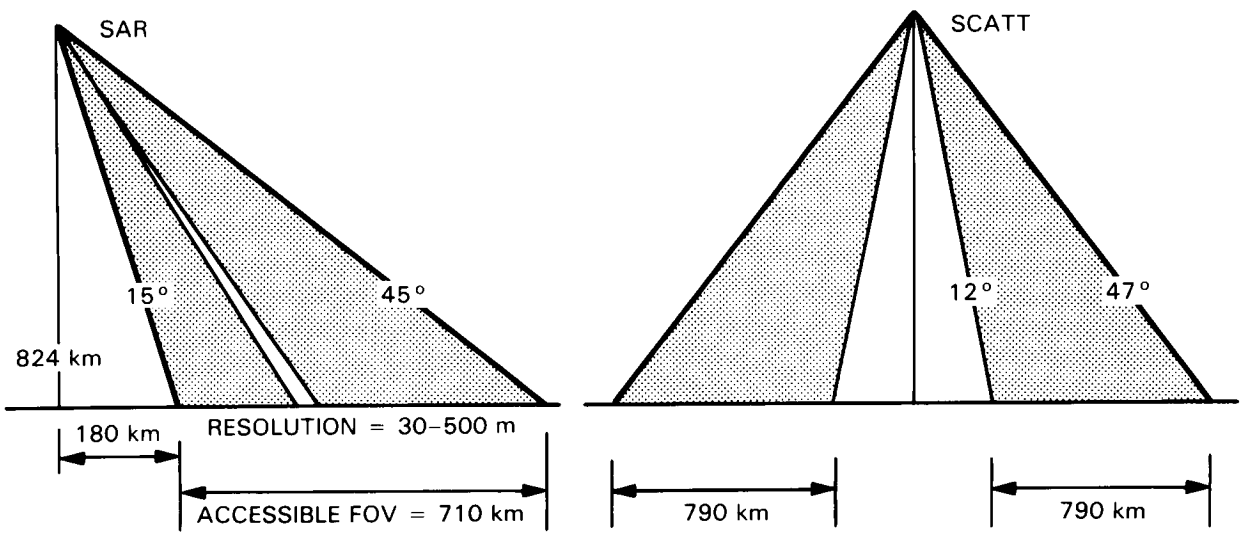

Figure 99. SAR and SCATT accessible FOVs from an 824 km orbit altitude.

the coarser resolution large-scale characteristics of surface roughness and snow measured by SCATT. The information on snow characteristics from SCATT arises from the reduced penetration depth as a result of its higher frequency (in comparison to SAR frequencies). These comparisons should be useful for distinguishing variable snow distributions and zones of surface melting.

Global Crustal Structure and Arid Lands Geology

It would be desirable to exploit SAR-SCATT synergism for global geological investigations. SCATT could be used to produce a first very low-resolution (175 km) K_u-band look at arid lands geology and perhaps global crustal structure. This low-resolution imagery will be useful contextual background for increasingly detailed SAR images of particular regions, depending on the viewing mode chosen. A high priority for SAR-SCATT synergism would be for arid lands geology characterized by large areas of generally low-relief terrains.

SAR AND ALT

Instrument Description

Eos ALT will be based on the TOPEX Altimeter, which is designed to measure ocean surface heights to an accuracy of ± 3 cm. ALT uses two frequencies (K_u- and C-bands) to measure the round trip time for pulses from the satellite to the average sea surface.

SAR-ALT Synergism

Ice Topography

As mentioned above, both ALT and GLRS data should be useful for ice topographic mapping. GLRS would provide much narrower footprints than ALT, but ALT is completely unaffected by weather. The centimeter-scale topographic information about the ice surface would be synergistic with the fine detail in sea ice morphology provided by SAR.

Large-Scale Ocean Dynamics

ALT will provide measurements of sea surface height, wind speed, and wave height, all useful for interpretation of SAR observations. The sea surface height can be used to compute surface geostrophic current velocity, which can be used with SAR images to study large-scale ocean dynamics. Because the time scales of ocean currents are generally longer than 2 weeks, asynchronous sampling of SAR and ALT observations is tolerable. The wave height ALT measurement will be particularly useful for interpretation of SAR data leading to information on the energy of long surface waves that interact with Bragg-resonant waves. For wind and wave studies, ALT observations are needed within 1 day of SAR observations.

Summary of Scientific Values from Synergism

Table 20 summarizes the main scientific objectives for synergistic observations using SAR and other Eos instruments.

EXPLOITATION OF SYNERGISMS ON Eos

The scientific requirements for synergism, described above, make no reference to the strategies for how such multi-instrument observations would be accomplished. In fact, this strategy presents one of the most challenging problems for Eos, since it requires considerations of sensor clustering, multiple platforms, altitude, repeat cycles, time of equatorial crossing, etc.

Altitude Considerations

Altitude Options

The time it takes for a satellite to make one orbital revolution times the relative angular velocity of the Earth yields the distance through which the Earth has travelled in that time. This distance is maximum at the equator and is known as the *fundamental interval* S, as shown in Figure 100a. Once each day over the period of the repeat cycle the fundamental interval S will be crossed by an ascending orbit trace, thus dividing the interval S into D_n (16 for Eos) subintervals of distance SI by the end of the exact repeat cycle, as shown in Figure 100b.

Dependent on the orbit altitude, these crossings can be either *directly drifting* or *skipping,* as shown in Figure 100a for three potential Eos orbits with $D_n = 16$ (16-day exact repeat cycle). In a directly drifting pattern, successive daily crossings of the interval S lie adjacent to one another (Figure 101a). In a skipping coverage pattern, successive daily crossings lie two or more subintervals apart (Figure 101b). Skipping patterns that sweep the interval S in "n" number of days are often referred to as "near 'n' day periodic orbits" because the coverage patterns are similar to exact 'n' day orbits for instruments with sufficiently wide FOV. In the example of Figure 101b, where D_n = 16-day exact repeat cycle, the orbit gives a "near 3-day" periodic coverage (see also Figure 99).

Nominal Orbit Requirements

Since Eos is to be used for observing sites periodically over its mission lifetime, it is necessary to choose a satellite orbit that is exactly repeating. By correctly choosing both the orbit inclination and altitude, an orbit with an exact repeat cycle of D_n nodal days may be obtained. Eos platforms will utilize sun-synchronous orbits, i.e., those that always trace an area of the Earth at the same local time of day.

Table 20. Principal Scientific Measurements for Synergistic Observations

	High-Resolution			Low-Resolution				
	HIRIS	**TIMS**	**GLRS**	**MODIS**	**AMSR**	**ESTAR**	**SCATT**	**ALT**
Glaciology	• Ice albedo • Biological productivity	• Surface temperature	• Ridging statistics	• Ice albedo • Surface temperature • Biological productivity	• Ice edge • Ice concentration • Polynya persistence • Snowpack density, water equivalence, free water content		• Wind velocity (open ocean)	• Ice topography
Hydrology	• Albedo and stomatal resistance • Cloud climatology • Snow extent • Plant moisture stress	• Surface temperature	• Accurate terrain topography		• Regional watershed snowpack density, water equivalent, free water	• Soil moisture (regional scale)		
Vegetation science	• Canopy biophysical properties	• Canopy temperature • Evapotranspiration data		• Canopy biophysical properties		• Soil moisture (regional scale)		
Oceanography	• Ocean color	• Sea surface temperature		• Ocean color • Sea surface temperature	• Wind speed • Wave height		• Sea surface wind vectors	• Large scale ocean dynamics
Geology	• Lithology • Crustal structure and tectonics • Desertification extent	• Lithology • Surface temperature	• Topography • Tectonic activity	• Regional surface temperature		• Soil moisture (regional scale)		

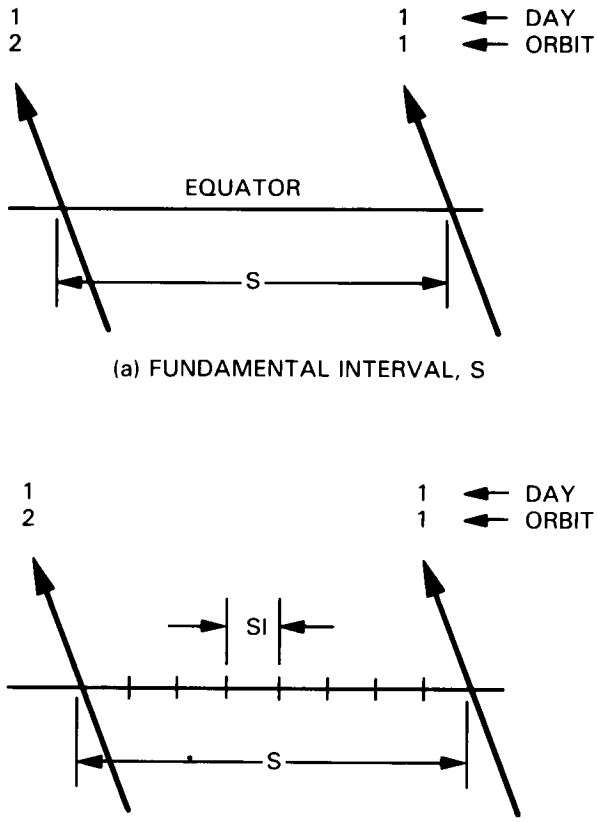

Figure 100. (a) The fundamental interval (length S) at the equator; (b) the subintervals (length SI) produced after one complete repeat cycle.

Although SAR operates day and night, it is sensitive to surface processes that vary on a diurnal cycle and should therefore avoid significant variations in the time of day. Thus, SAR should also be on a sun-synchronous platform.

The exact repeat cycle for Eos has been selected such that narrow FOV instruments such as HIRIS, TIMS, and ALT can eventually either map the globe (HIRIS and TIMS) or generate a dense coverage grid (ALT). This requires a repeat cycle on the order of 16 days; a 16-day repeat cycle has been selected for the platform(s) carrying HIRIS, TIMS, and ALT.

An altitude change of only a few kilometers can change the exact repeat cycle from 16 to a more frequent time period, e.g., 3 days. While a 3-day repeat cycle is not acceptable for HIRIS, given its need to view any location on the globe, it is desirable for SAR when soil moisture experiments are being conducted.

Altitude Requirements for Synergism

The selection of the optimum Eos altitude depends not only on individual instrument and orbit parameters, but also on the synergism between instruments. The main synergism requirement is the ability to consistently acquire simultaneous or near-simultaneous data between instruments.

There are many options for clustering of instruments on the two NASA IOC platforms. However, two key considerations are (1) the need for exact simultaneity between HIRIS and TIMS and MODIS data, and (2) the need to place SAR, HIRIS and TIMS on separate platforms because both instruments have a very high data rate, and the requirement for simultaneous or near simultaneous SAR and HIRIS coverage.

Figure 102 shows the simultaneous accessible FOV of SAR and HIRIS within specified timing offsets for the second platform at a variety of different altitudes. Unless the platforms are placed at the same altitude, a very inconsistent data set will be acquired. A detailed study of the trade-offs at each of these altitudes has been published (Smith *et al.*, 1987). The 824 km altitude has been selected as the baseline Eos altitude for the second platform to provide the optimum synergism between instruments at the expense of instrument performance and cost in some cases.

This of course assumes that both platforms are in synchrony with an exact 16-day repeat cycle. If the SAR platform altitude were slightly changed so as to give a 3-day repeat cycle (e.g., over a period of months), then synchronous near-simultaneous SAR-HIRIS data acquisition would not be possible.

SAR Observations with HIRIS

It is recommended that the SAR platform altitude normally be the same as that of the HIRIS plat-

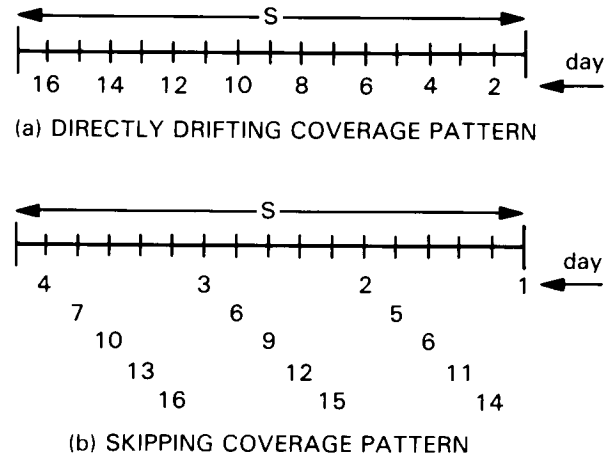

Figure 101. (a) Example of directly drifting pattern for 16-day repeat cycle; (b) example of skipping coverage for 16-day repeat cycle.

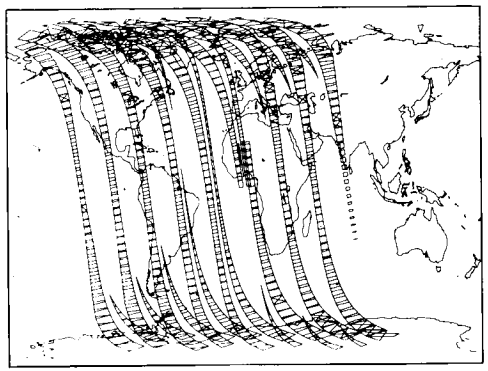

HIRIS 824 km +/−30° FOV
SAR 542 km +/−15–60° FOV
SIMULTANEITY: 30 minutes

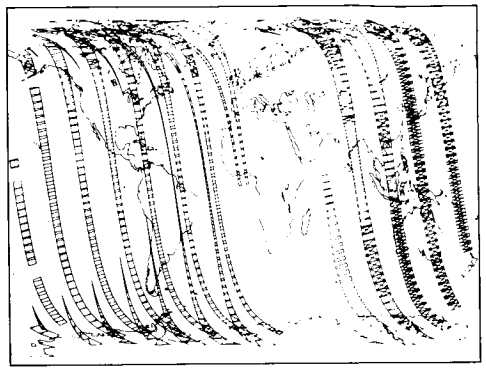

HIRIS 700 km +/−30° FOV
SAR 824 km +/−15–50° FOV
SIMULTANEITY: 30 minutes

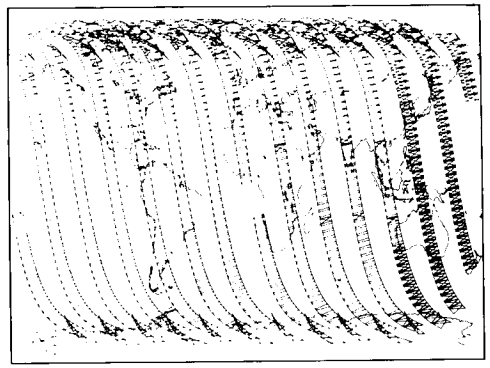

HIRIS 824 km +/−30° FOV
SAR 824 km +/−15–50° FOV
SIMULTANEITY: 30 minutes

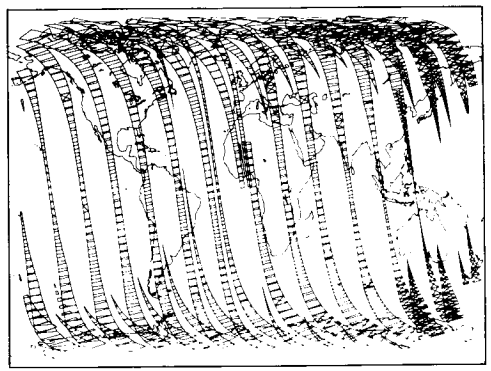

HIRIS 824 km +/−30° FOV
SAR 542 km +/−15–50° FOV
SIMULTANEITY: 60 minutes

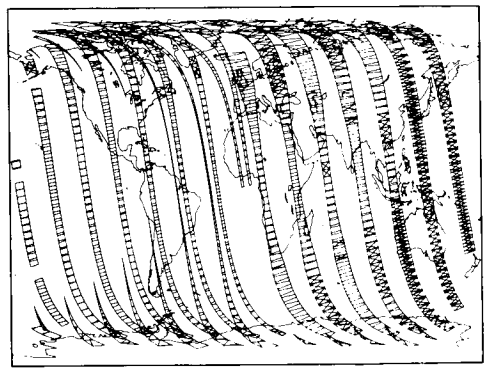

HIRIS 700 km +/−30° FOV
SAR 824 km +/−15–50° FOV
SIMULTANEITY: 60 minutes

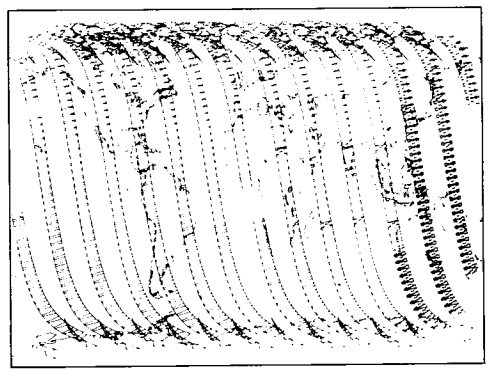

HIRIS 824 km +/−30° FOV
SAR 824 km +/−15–50° FOV
SIMULTANEITY: 60 minutes

Figure 102. SAR and HIRIS simultaneously accessible FOVs for a variety of platform altitudes and specified timing offsets.

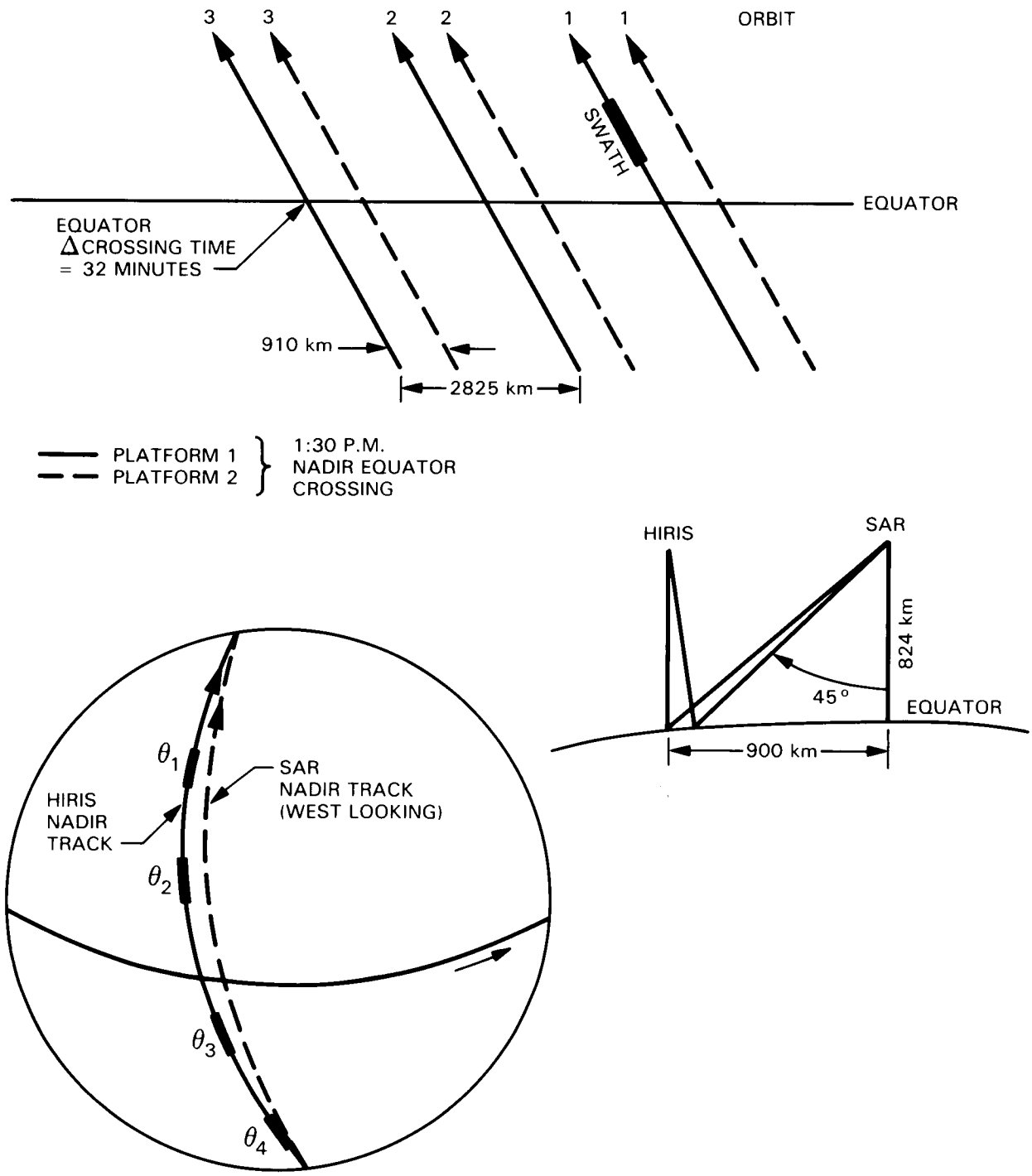

Figure 103. SAR and HIRIS platform configurations for both platforms in the same orbit altitude.

form, in order to maximize SAR-HIRIS synergism.[9] A 524 km or 705 km altitude is preferred for SAR in order to provide acceptable image quality at high incidence angles; however, the 824 km altitude will provide usable data at low to moderate incidence angles.

With an 824/284 im scenario, SAR and HIRIS data could be consistently obtained in the equatorial

[9]As previously discussed, it will also be desirable to fly the SAR platform for several months at a 3-day exact repeat cycle (altitude slightly less than 824 km) in order to confirm the soil moisture change detection procedure.

to moderate latitudes if the two platforms "fly in formation" with equator crossing points offset by the cross-track distance of the SAR swath from its subsatellite ground track. This is illustrated in Figure 103.

To exploit the SAR-HIRIS synergism, the SAR platform should fly first if SAR is usually looking west assuming a 1:30 p.m. equator crossing occurs on ascending passes. In this scenario, SAR will be viewing the south polar region most frequently; a mechanical rotation of the SAR antenna would be required to observe the north polar regions.

On the other hand, if SAR is usually looking east, the HIRIS platform should fly first. Since the majority of simultaneous SAR-HIRIS coverage will be required in the northern hemisphere summer when SAR will also be observing Antarctic ice, the first scenario with the SAR platform flying first would appear to be optimum. In this scenario, SAR would look eastward during most of the northern summer and westward during most of the northern winter.

SAR Observations with SCATT

In the "formation flying scenario" described above, it is desirable for SCATT to fly on the HIRIS platform to allow SCATT-derived surface wind information to be used as a decision basis for turning on SAR to image the ocean only in prespecified wind conditions. This assumes that the SAR platform trails the HIRIS-SCATT platform.

XI. PRE-Eos TECHNIQUE DEVELOPMENT PROGRAMS

The collection of Eos instruments and the associated information system will provide Earth scientists with tools of enormous potential for studies of the Earth system. Eos SAR will have multifrequency, multipolarization, and multi-angle capabilities with a powerful capability to zoom from global mapping wide swaths to narrow swaths with high resolution and multiple channels. This capability is required to address the scientific problems outlined in this report, yet it has never been available to scientists.

It is vitally important that a suite of carefully planned pre-Eos basic research and technique development studies be included as essential elements of the Eos concept. These would include basic research aimed at a better understanding of how electromagnetic scattering reveals geophysical and biophysical parameters of interest, and also would focus on related techniques of inversion algorithms, change detection methods, and data acquisition and processing approaches.

SIR-C will provide the first opportunity for testing these techniques from space using a multifrequency, multipolarization, multi-angle capability, but will not permit acquisition of data at latitudes above about 57°. Radarsat, ERS-1, and JERS-1 will provide valuable experience with single-frequency data and with global coverage. It will be important to continue the acquisition and analysis of airborne SAR data, especially using instruments that replicate the frequency and polarization channels included on SIR-C and Eos. The full polarimetric mode should be further tested using airborne SARs, and additional data should be acquired from field scatterometers.

All of this activity should be accompanied by the development of *useful* inversion algorithms, specifically aimed to yield SWE, ice type, vegetation canopy biomass by parts, soil moisture in the presence of vegetation and surface roughness, ocean-atmosphere energy and mass transfer mechanisms from surface expressions in SAR images, crustal structure and tectonic patterns, desertification and soil erosion patterns, etc. This activity should be pursued with the specific Eos channels in mind.

GLACIOLOGY

It is clear that global, frequent SAR observations are capable of revolutionizing the scientific and operational monitoring of sea ice, snow cover, ice sheets and shelves, and glaciers. It is also clear that the full application of SAR image data to scientific investigations in these areas requires improved algorithms coupled with more rapid analysis procedures. Certain research programs can be carried out in the interval between now and launch to make image analysis both more accurate and faster such that the Eos SAR data can be applied to geophysical problems shortly after collection and, in the long run, be more fully utilized. These research programs should focus on three kinds of investigations: (1) understanding the backscatter properties and processes of ice and snow types formed under a variety of well documented environmental conditions, (2) developing and improving methods of computer-supported image analysis, and (3) exploring the potential information content of novel and specialized SAR data products. The importance of undertaking such studies has been recognized for some time and research is already underway on some problems. Here we stress the need to sustain and strengthen appropriate existing research programs and to initiate new programs as necessary to flesh out a balanced overall program. Such steps are essential in the process of converting SAR data and images into useful geophysical information.

The required improvement in knowledge of the backscatter characteristics of ice and snow can only come from field work in which the physical and chemical aspects of these materials are investigated while the backscatter values of actual natural features are measured. These field projects should be carefully designed to adequately cover the seasonal and regional variations that can be expected to have significance. This would include, for example, sea ice in summer and fall, new ice formation, snow deposits and metamorphosis, snow melt, and firnification. A limited number of such studies have been conducted (Carsey, 1985; Swift *et al.*, 1985a) and can serve as guides in designing future work. Worthy of mention in this regard is the 11-nation Marginal Ice Zone Experiment (MIZEX), a comprehensive, long-term study especially relevant to Eos SAR in that it includes a series of sea ice/ocean remote sensing experiments involving both active and passive microwave techniques. MIZEX will provide important sea ice microwave information for pre-Eos SAR studies and will undoubtedly aid in the development of timely analysis techniques necessary for the effective utilization of the Eos SAR observations in the Arctic and Antarctic. Simultaneously with these field studies, theoretical investigations of backscatter interactions should be conducted to extend our understanding of scattering mechanisms in snow and ice volumes.

HYDROLOGY

Pre-Eos research for hydrology should focus on three primary areas: (1) establishing system parameters, (2) model development, and (3) exploitation of synergism with other Eos instruments. Research needs to be conducted to establish the optimum radar frequencies, incidence angles, polarizations, and spatial resolution for the various hydrologic ap-

plications. This step is needed because each hydrologic application will have unique combinations of sensor and viewing requirements and these will have to be preselected for each experiment.

Existing models of hydrologic processes are not able to use remotely sensed data effectively. These models have been developed to use data collected at the Earth's surface and for the most part, at a point. The spatial nature of remote sensing data and the unique capability of radar to directly measure hydrologic properties such as soil moisture and snow properties provide the hydrologist with information that has never been previously available. New models will have to be developed and tested to take advantage of this new and potentially valuable data. This model development should precede Eos such that operational analysis capabilities are available from the beginning of the Eos mission.

Almost all Eos applications to hydrology will require some synergism with other sensors. The radar is an important component of the hydrologic data needs because of its detailed resolution capabilities and potential for measuring hydrologic properties directly. However, the complexity of the hydrologic cycle needs other data as well. Pre-Eos research should be conducted to learn how to use all data in the various models. Pre-Eos research is also necessary to define spatial and temporal scales needed for various hydrologic applications. The maximum time lag between data collection passes needs to be defined for each hydrologic application.

VEGETATION SCIENCE

Forests

Airborne and/or orbital SAR experiments should be conducted to investigate the following:

- The effect of canopy morphology on radar backscattering as a function of illumination geometry, frequency, and polarization. Test sites should be specifically selected to include extreme examples of canopy geometry as represented by leaf, branch, and trunk shapes (broadleaf versus needle-leaf), sizes (relative to wavelength), and orientation (random versus preferred).
- The influence of overstory leaf area (crown closure and depth), stand density, and stand height upon radar backscattering should be examined as a function of frequency, polarization, and angle from seasonal observations of stands. Observations should correspond to key phenologic stages and include leafless conditions for deciduous species.
- The effects of the understory canopy and soil-surface conditions need to be ascertained. Repeated observations of monospecific stands with variable silvicultural treatments represent one strategy for making these observations.
- Simple empirical expressions need to be developed and tested for the retrieval of stand volume, leaf biomass, and canopy water content.
- Scattering models need to be developed to accommodate the complex structure of forest canopies.
- Dielectric measurements of forest-canopy constituents need to be obtained for use in the scattering models.

Grasslands/Steppes/Deserts

Retrieval algorithms for canopy biophysical parameters need to be derived and tested. Particular attention needs to be given to the confusion effects of soil-boundary conditions (roughness and moisture content) upon parameter retrieval. Multipolarized, multifrequency, and/or multi-angle data can be expected to be critical for these canopy conditions.

Agricultural Lands

- Efforts to describe the target/sensor interaction process via theoretical models should be accelerated in conjunction with experimental measurement programs obtaining simultaneous multifrequency and multipolarized SAR and optical data. The role of canopy morphology with respect to polarization properties merits particular attention.
- A large-area examination of the statistical response of radar backscattering to both diurnal and phenologic cycles needs to be conducted via multitemporal airborne or orbital observations.
- Empirical algorithms for retrieval of simple biophysical parameters need to be defined and tested with respect to variable soil background and geographic conditions.

Wetlands

Experiments similar to those for forests and grasslands should be performed for wetlands. Particular attention should be given to the identification of water boundaries and delineation of the degree of soil saturation in wetlands.

OCEANOGRAPHY

The frequent and long-term monitoring of the ocean surface by Eos SAR will provide important contributions to oceanography in the areas of circulation, oceanic, and coastal processes relating to eddies, fronts, internal waves and bottom feature

mapping, and surface wind variability. Most of these areas require considerable investigation through controlled ocean experiments that include aircraft SAR flights as well as theoretical studies to make full use of the Eos SAR data. Much of this work should be started before Eos is operating and continued into the early Eos data acquisition period. These investigations should include experimental and theoretical studies of SAR imaging mechanisms, synergistic studies with other key instruments, and investigations of air-sea interactions, all pointing toward deriving geophysical information from radar backscatter.

Experimental and theoretical studies of SAR imaging mechanisms should cover the modulation of short waves by the various current conditions in question including ocean boundary currents, eddies, fronts, internal waves, and currents over bottom features, and the variation of these mechanisms with varying radar frequency.

Synergistic studies using SAR should be carried out using ALT, SCATT, and MODIS/HIRIS-like instruments as well as existing data sets to examine all listed oceanographic features, particularly ocean circulation, eddies and fronts, and the surface wind field.

Atmospheric questions should focus on the variation of SAR backscatter across temperature boundaries and under spatially varying wind fields and other atmospheric conditions.

All studies should have the goal of deriving ocean geophysical information from the Eos SAR data and incorporating this information into global ocean data sets.

GEOLOGY

Pre-Eos airborne and/or orbital SAR experiments should be conducted over selected test sites to investigate the following:

Crustal Evolution and Tectonics

The seasonal effect of moisture, snow cover, and vegetation cover on backscatter from terrain surfaces should be determined, as well as the degree to which SAR frequency, polarization, and illumination geometry affect backscatter from such nongeologic ground covers. We need to address the meaningful absolute radiometric calibration requirements for SAR images obtained simultaneously at different frequencies (and between data takes), given variation in moisture and biomass. Test sites should be selected on the basis of accessibility for ground truth with large annual variations in snow and vegetation cover.

Landforms controlled by geologic structure are often strongly aligned or have multiple grain directions; thus, it is important to identify optimum SAR parameters (frequency, polarization, and illumination geometry) to emphasize these trends. Pre-Eos SAR investigations of this type from aircraft and spaceborne platforms may help reduce the number of sites needed during Eos.

It is important to develop usable radar backscatter models for application to specific geologic environments. Accessible test sites should be selected for which detailed surface micro-roughness and other surface measurements can be obtained for backscatter model development. Sites could include, among others: (1) known mineralized regions, (2) igneous (intrusive relief and cover), metamorphic and sedimentary terrains with varying degrees of relief and cover, (3) mass-wasting and alluvial deposits, (4) playas, (5) fold belts and regions of continental rifting or extension, and (6) highly eroded shield complexes (e.g., North American Craton in Canada) and active structural regions (e.g., California-Nevada, Peru).

Pre-Eos investigations of crustal evolution and tectonism will require some synergism with other Eos-like airborne sensors such as TIMS, AVIRIS, NS001 TM simulator, Airborne Imaging Spectrometer (AIS), etc. SAR should be considered as only a single component of a multisensor philosophy to regional and global investigations of crustal development and tectonism.

Arid Lands Investigations

Desert Geologic Mapping

The excellent geologic potential of long-wavelength SAR sensors for geologic mapping of the surface and shallow subsurface of hyperarid desert terrains was shown with the discovery of the paleo-river channels in the Eastern Sahara following SIR-A and SIR-B (McCauley *et al.*, 1982, 1986; Schaber *et al.*, 1986).

The potential of Eos SAR to map regional desert terrains more efficiently than ever before is high because of its multifrequency, multipolarization capability. However, much work remains to be done with airborne and orbital SAR sensors in order to understand the physical processes involved in shallow subsurface mapping. For example, we do not yet know the limitations of subsurface mapping with SAR in regions of less aridity, or more complex soils (e.g., more clay) than encountered in the relatively clean sands of the hyperarid Eastern Sahara.

Acquisition of multifrequency (6 to 75 cm wavelengths) and multipolarization aircraft SAR images over a variety of arid land test sites will be required prior to Eos to model the effect of wavelength, incidence angle, azimuth angle, polarization, and radiated power on signal penetration. The ultimate objective will be to test a variety of backscatter and volume scattering models. Absolute levels of radiometric calibration of SAR data for this application also needs to be addressed. Test sites should be

chosen for accessibility enabling characterization of the surface and shallow subsurface, sampling, and monitoring.

The exploitation of Eos SAR synergism with other instruments requires that we acquire synergistic data sets using airborne SAR or SIR-C along with AVIRIS, TIMS, AIS, NS001 TM simulator, etc. Geometric registration of the SAR and other image data sets will be required to fully exploit these combined data sets. Desert sites selected specifically for penetration studies should be properly instrumented during any pre-Eos overflights. Such ground calibration instruments might include surface and buried signal transponders, repeaters, and/or corner reflectors for proper radiometric and geometric calibration.

Desertification

Pre-Eos desertification investigations are very important because the long-term studies of this type using SAR sensors have not been conducted. Multiple flight aircraft or SIR-C data should be acquired over regions of active desertification in a variety of regional settings (e.g., semi-arid to temperate farmland). Dune sand migration and other forms of sand encroachment onto farmlands and grazing lands should be monitored annually over a 3- to 5-year period using primarily the high-frequency SAR sensors (X- and C-band) coregistered with multispectral sensors such as AVIRIS, TIMS, etc. Examples of suitable pre-Eos desertification sites are areas of Kansas, Nebraska, or Texas in North America, and the Nile River Valley in Egypt.

Pre-Eos investigation of desertification test sites should include the effects of wavelength, polarization, and illumination angles. Minimizing signal penetration depth may prove to be important for investigations of the dominantly surface processes associated with sand migration.

Soil Erosion

As is the case for desertification, there have been no long-term SAR experiments dedicated to the study of soil erosion. It is important in the pre- Eos period to conduct soil erosion experiments using the Eos SAR frequencies, polarizations, and illumination geometries, in combination with co-registered, multispectral images from optical/IR sensors. This would be used to establish the degree to which we can detect surface physical and chemical processes accompanying water, sand, and wind erosion of fertile soil.

The principal surface parameter to be monitored with SAR in soil erosion investigations is small-scale surface roughness resulting from wind fluting and fluvial gulleying. Test sites could include large fallow fields in farmlands currently susceptible to soil erosion (e.g., in Kansas or Nebraska). Additional grazing or farmland sites could be selected in regions of both wind erosion and water erosion of topsoil. Calibrated test fields could be prepared and instrumented prior to overflights.

The basic objective of such investigations is to determine the best combination of SAR and other sensor parameters to monitor soil erosion given different surfaces (physical and chemical) and climatic conditions. The optimum SAR frequencies, polarizations, incidence, and azimuth angles must be understood. Preliminary models, reflecting the rate of soil erosion by wind and water from various test sites, could be tested during Eos. Pre-Eos studies will also be required to determine realistic SAR radiometric calibration needs for soil erosion monitoring.

APPENDIX A: GLACIOLOGY—ADDITIONAL INFORMATION

The first part of this appendix presents an inversion algorithm that could be used for remote sensing of snow water equivalent and snow wetness. The second part reviews some previous relevant sea ice results obtained from Seasat SAR coverage of the Beaufort Sea, SIR-B coverage of the Antarctic sea ice margin, and Soviet Kosmos-1500 radar imagery. Because satellite-based SAR data are not common, much of the analysis of the effectiveness of SAR in studying snow and ice masses is based on the results of either *in situ* or of aircraft-borne scatterometer observations.

REMOTE SENSING OF SNOW PARAMETERS FROM SPACE

The principal desired observable parameters for snowpacks are snowpack extent, snowpack water equivalent, and snowpack wetness. Both SAR and HIRIS will be useful for high-resolution delineation of snowpack extent, SAR because of its sensitivity to scattering from snowpack water, and HIRIS because of its sensitivity at certain wavelengths to snow albedo. However, HIRIS will not be useful for snow delineation either during cloudy conditions or when the sun angle is too low (e.g., winter season at northern latitudes). The 37 and 90 GHz channels of AMSR (passive radiometer) will provide lower resolution (1 to 3 km) delineation of snow cover.

In the microwave spectrum, a snow layer causes both attenuation and scattering of signals, especially at shorter wavelengths. The sensitivity of radar backscatter to snow has been measured using both field equipment (truck-mounted scatterometers) and airborne sensors. Figure A.1 shows that the measured radar scattering coefficient of a 48 cm deep snow layer as a function of frequency for both dry (0 percent moisture by volume) and wet (1.26 percent moisture) snow is less than 1 dB at L-band but increases to about 4 dB at C-band and X-band. Moreover, the radar backscattering coefficient, $\sigma°$, increases with frequency and as the snowpack becomes drier. This indicates that at C- and X-band, a diurnal variation in snow wetness of only about 1 percent should be clearly visible in SAR imagery for snowpacks of about 40 cm in depth or greater.

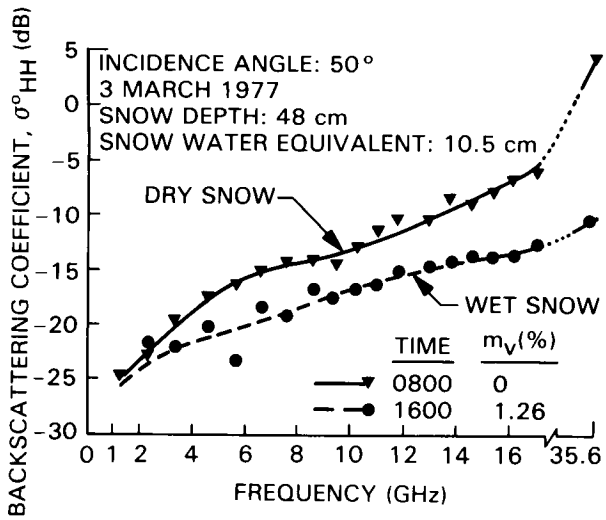

Figure A.1. Spectral response of $\sigma°$ for wet and dry snow (from Ulaby and Stiles, 1980).

The calculated dependence of $\sigma°$, at various frequencies, on the depth of a dry snow layer containing 2 mm diameter ice particles is shown in Figure A.2. Again this is for an HH-polarized radar using a 50° angle of incidence. It is apparent that there is no sensitivity to snow depth at L-band (1.2 GHz) and that even at C-band (5.0 GHz) a 1 m deep snow layer produces only a 2 dB increase in $\sigma°$ over the background provided by the soil (assuming here to have a dielectric constant of 5 and an rms surface roughness of about 1 cm). However, at X-band, a 1 m deep snow layer produces an 8 dB increase in $\sigma°$ over the background soil.

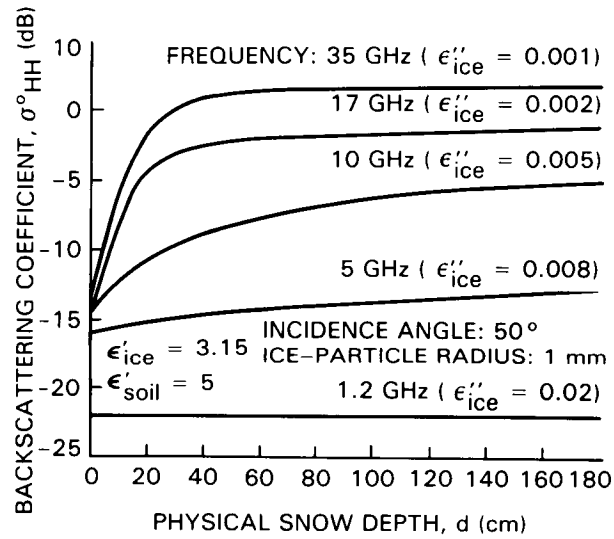

Figure A.2. Calculated variation of $\sigma°$ (HH) with depth for a dry snow layer containing ice particles 1 mm in radius. Note the important role of frequency (after Ulaby *et al.*, 1982).

Characterization of Snow

The characterization of snow depends on whether it is wet (water present in liquid form) or dry.

Dry Snow

We may think of a layer of dry snow as a dielectric medium consisting of ice crystals embedded in an

air background. If we assume that these ice crystals are spherical, we can use Mie scattering to calculate the absorption, scattering, and extinction cross sections of each ice particle in terms of the particle radius r and relative permittivity. The propagation parameters of this snow layer may in turn be characterized by its *volume absorption* and *scattering coefficients* k_a and k_s, respectively. The sum of the absorption and scattering coefficients is defined as the *extinction coefficient* k_e (i.e., $k_e = k_a + k_s$. The *albedo* of the medium is then found by

$$\omega = k_s/k_e \qquad \text{(A-1)}$$

Both the extinction coefficient and the albedo depend on the snow density, the temperature, the ice particle radius, and the wavelength. Figure A.3 shows the calculated dependence of the extinction coefficient and albedo as a function of frequency, for an assumed snow density of 0.24 g cm^{-3} and a temperature of -1°C (Ulaby *et al.*, 1986). As the frequency increases, both the extinction coefficient and albedo increase; the albedo also approaches its asymptotic value of unity as the ice particles become larger.

Wet Snow

As the snowpack heats up during daylight hours, the snow medium becomes a mixture of ice particles, water droplets, and air. The *snow wetness* m_v is the volumetric fraction occupied by the water droplets; these droplets are normally smaller than the ice particles. The extinction coefficient of snow increases with liquid water content.

Radar Backscattering from Snow

Dry snow behaves as an essentially planar layer above ground, with negligible scattering from the air-snow boundary. Radar echoes from dry snow are in general due to both volume scattering from the snow layer and surface scattering from the underlying soil or ice. By contrast, radar scattering from wet snow can be strongly dependent on the surface roughness at the snow-air interface and on the liquid water droplets in the snow layer. The backscattering from both wet and dry snow also depends on the moisture level of the underlying soil.

SWE is the height in centimeters of an imaginary vertical 1 cm^2 column of water resulting from the melting of the snow in that column. The snowpack *wetness* m_v is the volumetric percentage of snow that is in liquid water form.

Figure A.4 shows the dependence of the radar scattering coefficient on the water equivalent for a dry snowpack of various depths, and at a frequency of 9 GHz and a 57° incidence angle.

The presence of liquid water droplets in the snowpack tends to reduce the backscatter from the snow and also greatly decreases the sensitivity of the radar to water equivalent, as shown in Figure A.5 for snow-covered grass. This means that Eos SAR would have to make water equivalent measurements at night (except in the Arctic) when the wetness is essentially zero.

For thicker wet snowpacks (depths greater than about 20 cm), the radar echoes will be essentially independent of snow wetness (depth) and dependent mainly on the snow wetness m_v.

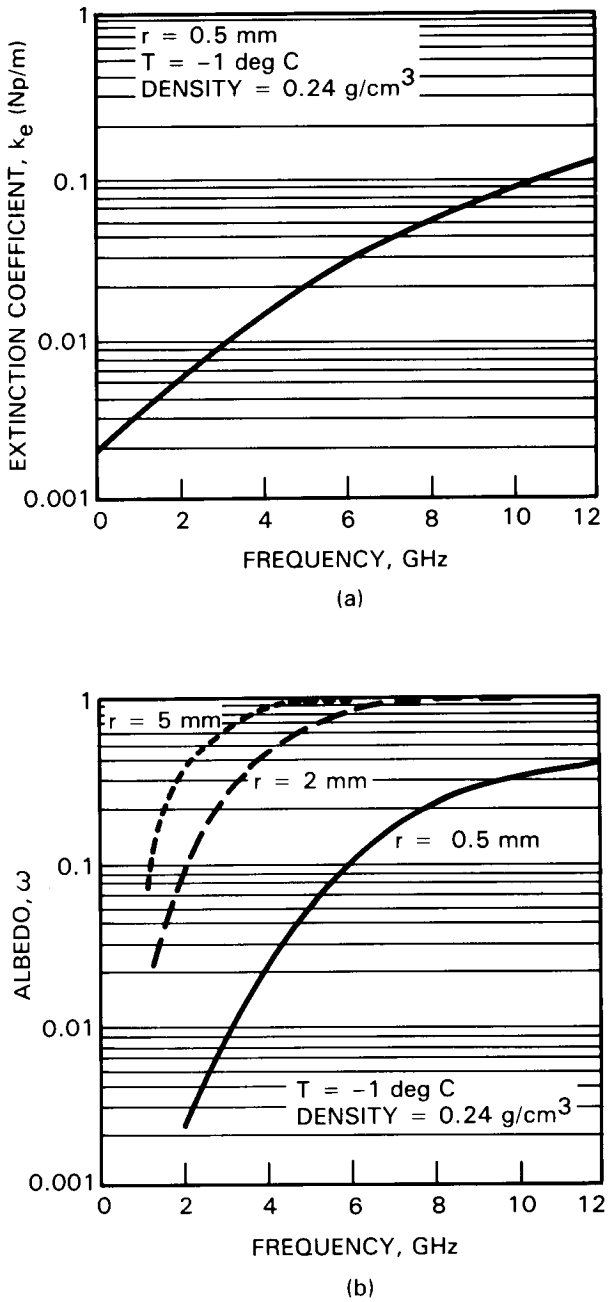

Figure A.3. Calculated extinction coefficient and albedo for dry snow with various radii (after Ulaby *et al.*, 1986).

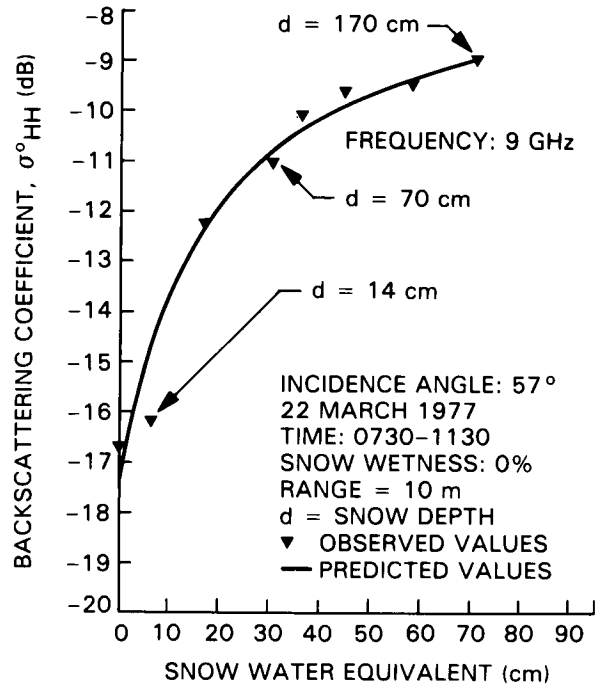

Figure A.4. Example of dependence of radar backscattering coefficient on the water equivalent of a dry snowpack at 9 GHz with HH polarization (after Ulaby *et al.*, 1984a).

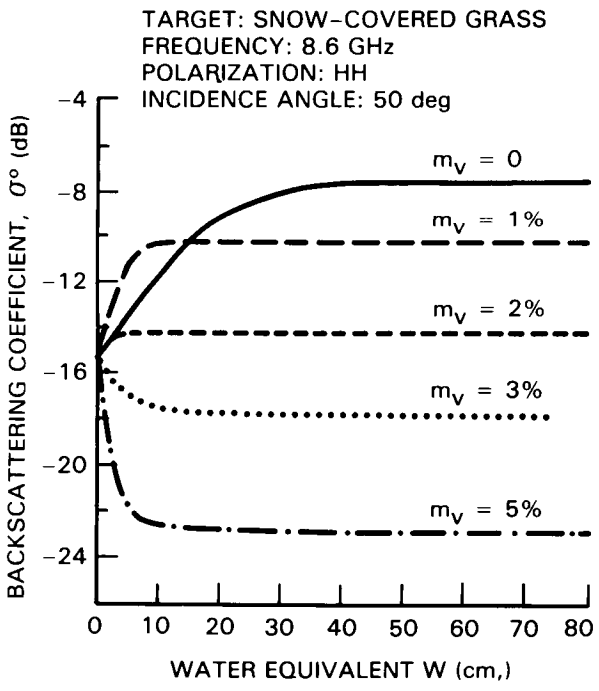

Figure A.5. Effect of snow wetness (m_v) on radar scattering coefficient as a function of water equivalent (after Ulaby *et al.*, 1984a).

Inversion Algorithms for Snow Water Equivalent

The purpose of this section is to describe how SAR data at L-, C-, and X-band might be utilized for the measurement of snowpack water equivalent and snowpack wetness. This inversion algorithm is based upon models of backscattering from snow and empirical results.

Snow Water Equivalent

The Eos SAR strategy for inference of SWE would be to use the L-band channel for monitoring the backscattering coefficient of the underlying soil (since the L-band channel sees entirely through the snowpack) and to use the C- and X-band backscattering coefficients to infer the water equivalent W. These measurements would be made at night (when the snowpack is dry) using VV polarization and at two angles: 50° and 30°. An average of the water equivalent W inferred from both angles is used as the best estimate. Figure A.6 illustrates the principal measurements to be made at a 50° incidence angle.

The first step requires the determination of the backscattering of the underlying material (soil or ice) prior to snowfall:

$$\sigma_G^\circ(\theta_{50},f) = \Gamma_{50}(m_b)[A_{50}-B_{50}e^{-C_{50}(f-1.3)}] \qquad \text{(A-2)}$$

where

σ_G° = radar backscattering coefficient of underlying stratum (soil or ice) (A-3)

$\Gamma_{50}(m_b)$ = Fresnel power reflection coefficient at 50° incidence angle (A-4)

m_b = moisture level of underlying stratum, before snowfall (A-5)

A_{50} = constant for angle 50°

B_{50} = constant for angle 50°

C_{50} = constant for angle 50°

f = frequency (GHz)

θ_{50} = 50° incidence angle

From three frequency observations (1.3, 5, and 9.6 GHz) at 50° of the bare soil or ice before snowfall, we can determine the following constants:

- $\Gamma_{50}(m_b)A_{50}$ (A-6)
- $\Gamma_{50}(m_b)B_{50}$ (A-7)
- C_{50} (A-8)

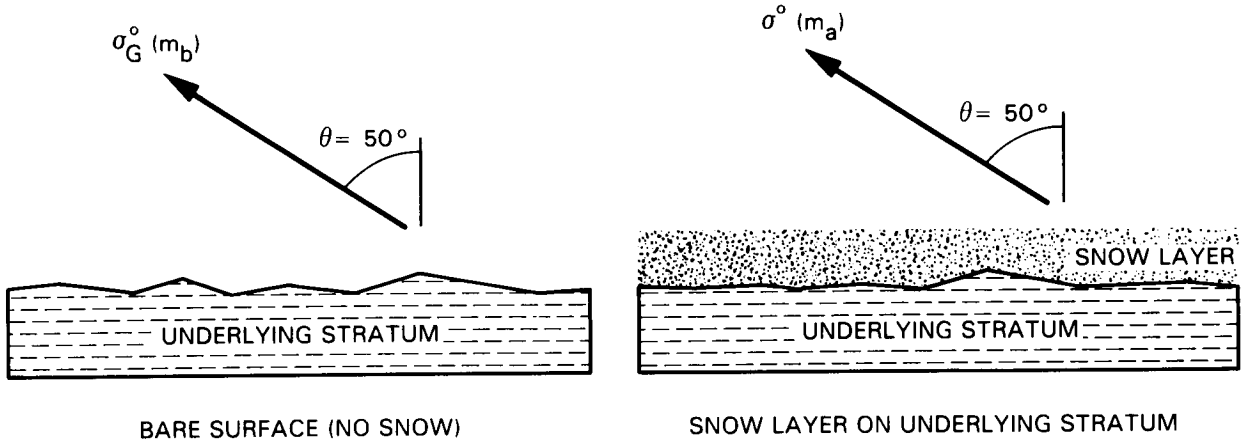

Figure A.6. Illustrating backscattering cross section measurement geometry before (left) and after (right) snowfall.

- $$D_{50} = \frac{B_{50}}{A_{50}} \qquad \text{(A-9)}$$

The next step in the process is to begin to observe the snowpack at L-, C-, and X-bands over the winter season and at night (when the snowpack is dry), starting from a no-snow condition. Because of the presence of the snow, the underlying stratum will now have a new moisture level m_a. We continue to observe at 50° incidence angle. If we make an L-band (f = 1.3 GHz) measurement, SAR will image only the underlying surface and, if absolutely calibrated, will give the following backscattering coefficient:

$$\sigma^\circ_G(\theta_{50},L) = \Gamma_{50}(m_a)[A_{50}-B_{50}] = \Gamma_{50}(m_a)A_{50}[1-D_{50}] \qquad \text{(A-10)}$$

from which we obtain

$$\Gamma_{50}(m_a)A_{50} = \frac{\sigma^\circ_G(\theta_{50},L)}{1-D_{50}} \qquad \text{(A-11)}$$

Thus, the radar return from the underlying surface at *any* frequency f is given by:

$$\sigma^\circ_G(\theta_{50},f) = \frac{\sigma^\circ_G(\theta_{50},L)}{1-D_{50}}\,[1-D_{50}e^{-C_{50}(f-1.3)}] \qquad \text{(A-12)}$$

It is noted that the constants D_{50} and C_{50} are independent of frequency. We can use Equation A-12 to obtain the backscattering coefficient of the underlying stratum at both C-band (f = 5) and X-band (f = 9.6).

We now use the SAR X-band channel (VV polarization) to make a measurement of the backscattering coefficient at a 50° incidence angle. It can be shown that this can be related to the albedo, the backscattering coefficient from the underlying surface, and the snowpack water equivalent SWE by the following relationship:

$$\sigma^\circ(\theta_{50},X) = \tfrac{3}{4}\,\omega(X,r)\cos\theta - [\tfrac{3}{4}\,\omega(X,r) - \sigma^\circ_G(\theta_{50},X)]e^{-2k_{em}(X,r)(SWE)\sec\theta} \qquad \text{(A-13)}$$

At the same time, we use the C-band channel (VV) to measure the backscattering coefficient from the snowpack, and relate this to the water equivalent as above:

$$\sigma^\circ(\theta_{50},C) = \tfrac{3}{4}\,\omega(C,r)\cos\theta - [\tfrac{3}{4}\,\omega(C,r) - \sigma^\circ_G(\theta_{50},C)]e^{-2k_{em}(C,r)(SWE)\sec\theta} \qquad \text{(A-14)}$$

In these equations,

$$\omega(f,r) = \text{snow albedo at frequency f (= 5 GHz or 9.6 GHz)} \qquad \text{(A-15)}$$

$$r = \text{ice particle radius} \qquad \text{(A-16)}$$

$$k_{em}(f,r) = \text{specific extinction coefficient (cm}^{-1}\text{)} = \text{extinction coefficient/snow density} \qquad \text{(A-17)}$$

$$\theta = 50°$$

Equations A-13 and A-14 can be solved using iterative techniques for the two unknowns, which are SWE (the snowpack water equivalent) and r (the ice particle radius). This is possible since the albedo and extinction coefficient can easily be calculated once the frequency and radius r are known. It should be noted that a *simultaneous measurement* at C- and X-band is required and that both measurements must be absolutely calibrated, i.e., the SAR image intensities must be expressed in terms of the radar backscattering coefficient σ°.

Equation A-14 can be rearranged to give a formal expression for the snow water equivalent:

$$SWE = \frac{\cos\theta}{2\,K_{em}} \log_e \left[\frac{\sigma^\circ_G(\theta_{50},C)^{-\frac{3}{4}}\,\omega(C,r)\cos\theta}{\sigma^\circ(\theta_{50},C)^{-\frac{3}{4}}\,\omega(C,r)\cos\theta} \right] \qquad \text{(A-18)}$$

A similar equation may be obtained for the X-band response. It is again noted that both the extinction coefficient k_{em} and the albedo are dependent on both frequency and ice particle radius. In Equation A-18, the C-band backscattering coefficient term in the numerator due to the underlying soil or ice is obtained from Equation A-12.

This completes the formalism for obtaining the snowpack water equivalent. These equations are based upon the assumption that the snowpack is electrically thick enough at C-band to distinguish the backscattering coefficient of the snowpack from that of the underlying surface. For fairly dry underlying moisture conditions and snowpacks over about 20 cm in thickness, this should be a good assumption.

In order to improve the estimate of SWE, a similar measurement would be made at an incidence angle of 30° and the results averaged with the 50° results.

Snow Wetness

The snow wetness m_v (expressed as a volumetric fraction) may be obtained from similar relationships to Equations A-13 and A-14 above, with the understanding that the relationships for σ° must now include a functional dependence on m_v as well as SWE. As shown in Figure A.5, the radar returns from a snowpack with a given water equivalent (depth) will be strongly modulated by the wetness. During midday, when the wetness is maximum, the radar echoes will be weakest and during the night, when the wetness is zero, the scattering will be strongest. If we observe this diurnal modulation at two frequencies (C- and X-bands), we can determine the wetness of the snowpack.

Diurnal observations of snowpacks will be necessary for accurate snowmelt runoff predictions. Figure A.7 illustrates the diurnal behavior of snowpack wetness (top curve) and the dependence of the radar scattering coefficient (bottom curve), during a typical melting day with liquid water appearing during the day (when temperatures are above freezing) and then refreezing during the night. The diurnal variation in backscatter may thus be directly related to snow wetness.

Implications for Absolute Radiometric Calibration

It is clear from Figure A.2 and Equation A-18 that SAR images must be absolutely calibrated in order to obtain the snowpack water equivalent. At X-band, a ±1 dB error in absolute calibration means an approximate ±20 cm error in water equivalent for thicker snowpacks. A detailed study of the quantitative requirement for absolute calibration at C-band has not yet been undertaken. It is clear, however, that errors in absolute calibration translate directly into errors in water equivalent and that Eos SAR should be absolutely calibrated to the maximum possible extent.

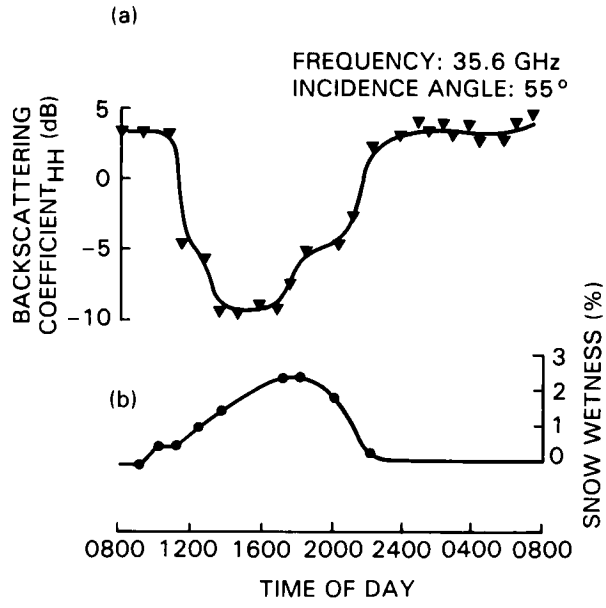

Figure A.7. Diurnal response and hysteresis effect of σ° from snow at 35.6 GHz and 55° angle of incidence (Ulaby and Stiles, 1978).

SEASAT SAR BEAUFORT SEA ICE DYNAMICS

Seasat SAR images of the Beaufort Sea ice pack have been utilized in a variety of applications (Weller *et al.*, 1983; Prinn *et al.*, 1985) and studies (Hall and Rothrock, 1981; Carsey, 1985; Curlander *et al.*, 1985; Fily and Rothrock, 1986; Teleki *et al.*, 1979; Leberl *et al.*, 1983). The sampling period for Seasat was during summer and fall 1978, at which time the system's operation was terminated by a power failure. Because of this unfortunate event and the timing of the successful portion of the mission, it was not possible to carry out the coordinated ground-truth program that had been planned. Nevertheless, analysis of the imagery (L-band, HH polarization, 20 m resolution) clearly showed that:

- Under most situations first-year and multi-year ice can be distinguished.
- A large variety of ice features can be identified on sequential images, thereby facilitating the determination of ice motions (Figure A.8).

Figure A.8. Seasat SAR images of central pack ice in the Beaufort Sea taken 3 days apart: (a) Rev. 1439, October 5, 1978; (b) Rev. 1482, October 8, 1978; (c) relative velocity vectors resulting from tracking over 750 common floes in (a) and (b) (Curlander *et al.*, 1985).

- Newly formed leads are clearly evident.
- The structure of the ice margin is clearly displayed.
- Pressure ridges and rubble fields are readily delineated.
- Ice islands, which are major operational hazards, can be distinguished.

Maps of ice motion are obtained from sequential imagery by simply tracking common ice features from image to image. Highly accurate information on spatial structure, scales of motion, and deformation in the ice velocity field can be obtained using geometrically corrected and Earth-located SAR imagery. Such information can be directly compared with larger-scale motions from buoys and used in circulation models of the ice-covered polar oceans. What is still under investigation is the sampling rate between sequential images that is needed to provide most of the variability for ice motion as well as automated algorithms that will derive the motion vectors.

SIR-B SOUTHERN OCEAN ICE

The SIR-B mission obtained SAR images (L-band, HH polarization, 25 m resolution) of the northern most reaches of the Antarctic ice pack during 8 days in October 1984 (Figure A.9). The only "ground-truth" observations available were hand-held photography taken by the astronauts. The ice showed band-like aggregates at the outermost margin similar to those observed in the Bering Sea but on a larger scale. Further south into the ice pack more fully developed ice floes were observed. Icebergs were resolvable in the open ocean but not when imbedded in sea ice (Carsey *et al.*, 1986). Ice concentrations derived from this SIR-B imagery and Nimbus-7 SMMR data showed favorable comparisons except at the outermost margin where changes in ocean surface roughness resulting from air-ice band interactions tended to blur the ice-water separation (Martin *et al.*, 1987).

KOSMOS-1500 IMAGERY

Probably the most instructive example of the scientific and operational utility of a satellite-based imaging radar system is the Soviet experience with the Kosmos-1500 satellite. This satellite, which was launched in December 1983, carries an X-band, real-aperture side-looking radar (SLAR) plus a scanning microwave radiometer and a multichannel scanner operating in the visible range. Even though the resolution of the SLAR system is significantly less than the SAR system proposed for Eos (1 km as contrasted to 30 m), the results have proven to be invaluable with the Arctic Ocean being selected as the principal research area. The SLAR images, which cover 450 km wide swaths, are processed at three main receiving stations and are supplied with slightly reduced resolution (2 km) to over 500 subsidiary reception points. The imagery is routinely used to assist in decision-making for ship routing in the Northern Sea in that large leads, polynyas, and floes can be identified and the movement of the ice studied. It has also proven generally possible to distinguish multi-year ice from first-year ice under most conditions, although the coarse resolution causes a number of data interpretation problems (Bushuyev *et al.*, 1985a, 1985b; Mitnik *et al.*, 1985; Aleksandrov and Loshchilov, 1985). Studies of the Antarctic ice sheet

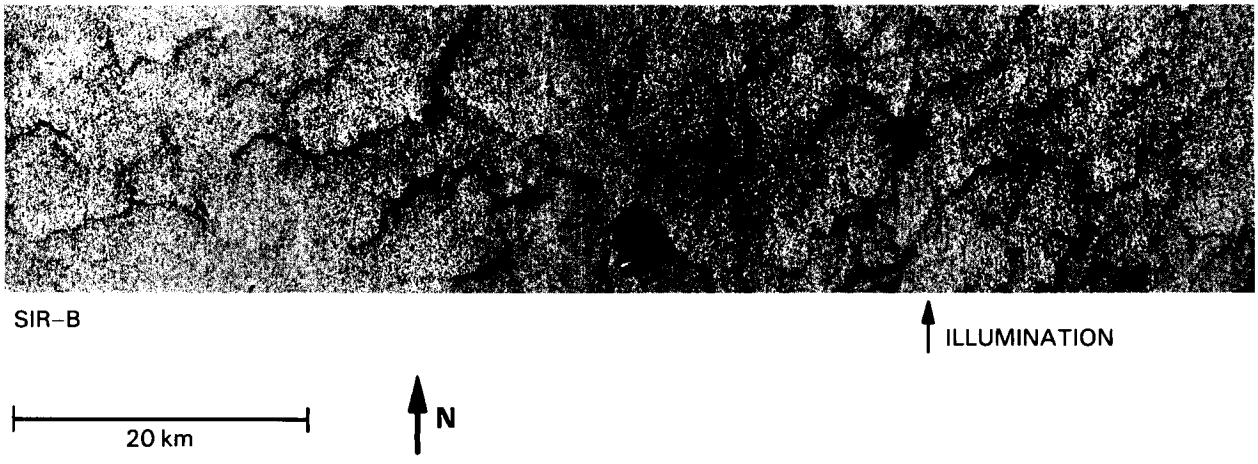

Figure A.9. SIR-B image of the outermost ice margin of the Weddell-Scotia Sea taken October 11, 1984 (data take 104.5). The dark central feature is Zavodovski Island. The dark curvilinear features are ice bands that are an aggregate of small floes. The ocean appears uniformly bright due to high winds.

(Burtsev *et al.*, 1985) have also proven to be very promising.

AIRBORNE SAR, SLAR, AND SCATTEROMETER MEASUREMENTS OF SNOW AND ICE

Many detailed assessments of the use of SAR for ice and snow studies have been done using airborne scatterometer and SLAR observations. These results are discussed for sea ice, lake and river ice, ice sheets and shelves, and snow.

Sea Ice

Figure A.10 is a C-band SAR image of sea ice, acquired on March 23, 1987 by a newly commissioned airborne (Convair-580) instrument operated by the Canada Centre for Remote Sensing. The data were collected in connection with the Labrador Ice Margin Experiment (LIMEX). Data acquisition was from 20,000 feet using HH polarization, 19 km swath width, and 12 m resolution; the near edge (top of image) corresponds to a 45° incidence angle. Included in the southwest corner of the image is the rugged northern tip of Newfoundland's Avalon Peninsula which, at this time, was surrounded by pack ice. Predominantly first-year ice had been compacted against the shore prior to the light by strong easterly winds resulting in the well defined ice edge clearly visible towards the eastern edge of the image. Adjacent to the land, distinct floes are visible that are agglomerations of much smaller floes, 5 to 30 m in diameter, and that are moving southward at rates up to a few kilometers per day depending on distance from the shore. The area of brighter returns, beginning approximately 10 km from the shore, delineates the shear zone beyond which the ice is made up of small individual floes or ice cakes surrounded by brash ice. This ice is moving much more rapidly with the generally southerly flow of the Labrador current. Although not visible in the ocean returns, gravity wave patterns are visible in the bright sea ice returns near the ice edge. It is believed that the small-scale, scalloped edge visible on the image arises from SAR imaging of the motion of the ice due to wave action. Ice surface and ocean information was collected from the CSS Baffin, a Bedford Institute of Oceanography ship, whose bright radar return is visible in the ice close to the ice edge. The adjacent bright return in the ocean is an associated radar artifact.

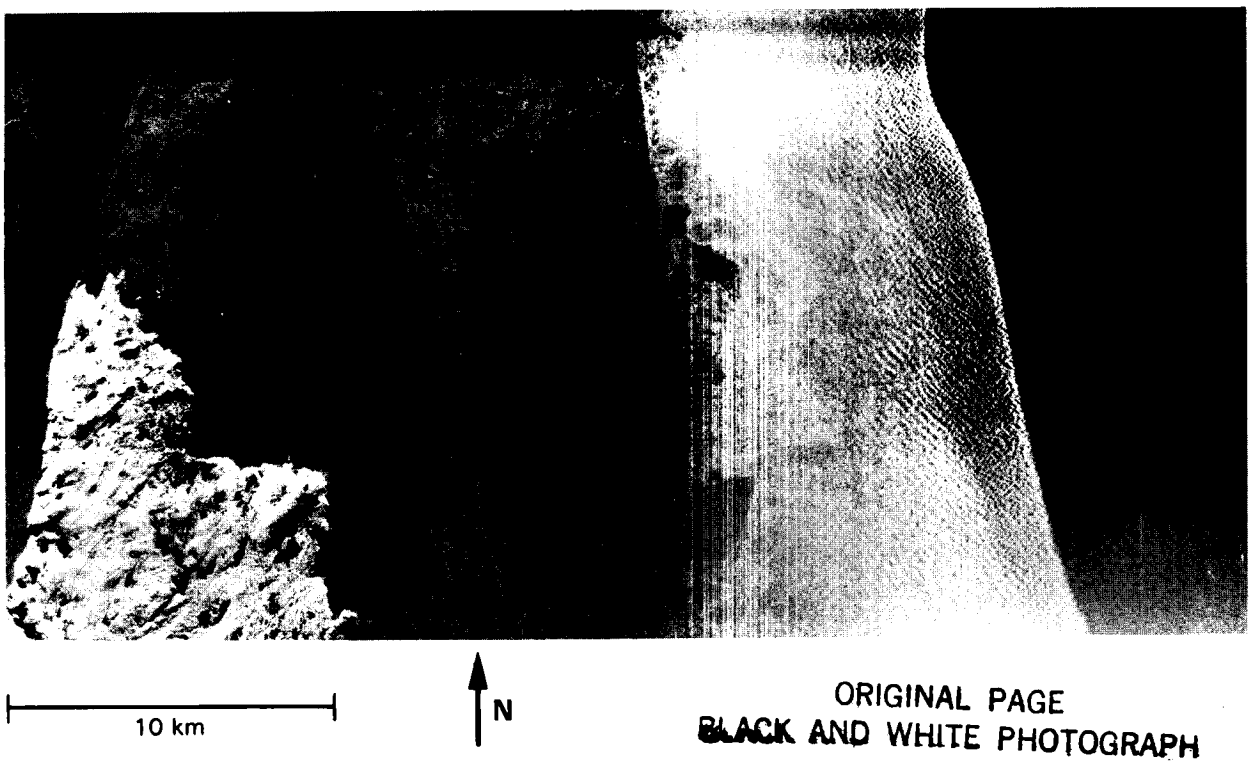

Figure A.10. Airborne C-band SAR imagery of sea ice near Newfoundland's Avalon Peninsula (data courtesy of Canada Centre for Remote Sensing).

Figures A.11a through A.11d shows 13.3 GHz (K_u-band) backscatter data acquired with an airborne scatterometer for a wide variety of ice types and conditions occurring during the Arctic winter (Gray *et al.*, 1981). The lowest return is from calm water and the next lowest originates from smooth first-year ice under winter conditions. At this frequency, multiyear ice can be readily discriminated from first-year and thin ice for incidence angles greater than 20°. The difference in $\sigma°$ between first-year and thin ice is highly variable and depends very much on the thickness of thin ice. The radar backscatter for thin ice can vary by about 15 dB as the ice thickness increases from less than 5 cm to 15 cm. This backscatter change is almost as large as the dynamic range found for all ice types. The phenomenon is, however, easily explained—the increase in radar backscatter associated with the increase in ice thickness is due to the formation of frost flowers (a rough surface ice "layer" grown from briny water found in and on the surface of thin ice). The effect of wind on the backscatter of the surrounding ocean causes some problems in interpretation of $\sigma°$ in the marginal ice zone, in polynyas, and in large leads. Depending on wind speed and incidence angle, the radar backscatter of open water can equal that of any ice type. The patterns of the returns, however, commonly allow the ice and water to be discriminated. At incidence angles above 30°, the multiyear ice/open water discriminated is assured even at wind speeds of 20 m/s.

During the early melt season (Figure A.12a), multiyear, first-year, and very likely thin ice, cannot be distinguished because of the presence of wet snow on the surface. At the time of freeze-up, thin ice can easily be distinguished from first-year and multiyear ice as shown in Figure A.9. The first-year ice that has survived two or more summers, is, as might be expected, indistinguishable based on microwave behavior.

Figures A.11e and A.11f depict the radar backscatter for different ice types and conditions at a frequency of 1.5 GHz (L-band) and 5.2 GHz (C-band) as a function of incidence angle. Figure A.11e shows the ability to discriminate between thick first-year ice, multiyear ice, and pressure ridges during winter conditions.

Figure A.12 depicts the frequency dependence of the Mould Bay data set for three ice types. The data were taken during the earlier part of October when the ice was close to the melting point. Figure A.12a gives the results for an incidence angle of 30° and Figure A.12b for 40°. A significant change in backscatter behavior occurs at X-band (near 11 GHz) where a jump of about 14 dB for multiyear and 9.6 dB for first-year ice takes place. On the average, the difference in backscatter between first-year and multiyear ice for a frequency of less than 10.5 GHz is about 2.5 dB and above 11.5 GHz about 5.4 dB.

At the lower end of the frequency spectrum (1 to 10 GHz) all frequencies do a poor job of discriminating between first-year and multiyear ice. It is only at frequencies greater than 11.5 GHz that discrimination between multiyear and first-year ice becomes reliable based on radar backscatter alone. The change in backscatter behavior near 11 GHz is probably due to the change from roughness scattering at higher frequencies to roughness plus structural properties at lower frequencies.

Lake and River Ice

Analysis of both X- and L-band side-looking airborne radar (SLAR) imagery indicate that it is commonly possible to discriminate water from ice, observe roughness elements on both the upper and lower ice surfaces, observe scattering elements within the ice, and determine if the ice is frozen to the lake bottom (Bryan and Larson, 1975; Weeks *et al.*, 1981).

Ice Sheets and Shelves

Like lake and river ice, glacial ice exhibits very low electromagnetic loss. Therefore, deep penetration into the ice is possible and depends strongly on the choice of electromagnetic frequency. Furthermore, the surface relfectivity is reasonably low, which also enhances the penetration of radar signals into ice sheets. It has been shown that when the viewing angle is greater than 20°, surface backscatter effects are negligible; hence, the radar returns is almost entirely a result of volume scattering from inclusions. An extreme example of the effects of volume scattering occurs over a portion of the Southern Greenland ice sheet. It is in this region where summer melting can occur, resulting in seepage of water into percolation channels. At some depth, the water distributes laterally when it refreezes to form ice lenses and ice glands. Both the number, density, and size of these inclusions are large, resulting in strong backscatter.

During October 1979, a 13 GHz scatterometer, set in a mode to collect scattering data as a function of viewing angle and polarization, was flown over the Greenland ice sheet along the transect shown in Figure A.13. The results for vertical polarization are also shown in Figure A.13. Here, the data collected at shallow viewing angles of 0° and 10° are primarily associated with surface scattering; whereas, volume scattering is the dominant mechanism at viewing angles of 20° or greater. At the relative time of 2,000 seconds (which can be geographically located by reference to the map), the scatterometer was flying over a region that seldom experiences summer melt conditions; the resultant radar return was fairly low. However, as the aircraft flew over the percolation zone where summer melt occurs, a gradual increase in backscatter is noted that couples with an increase in the number density of scatterers. There is approximately a 10 dB difference between minimum (2,000 seconds) and maximum (4,000 seconds) values of the radar return. The same general behavior can be expected with the Eos SAR X-band channel.

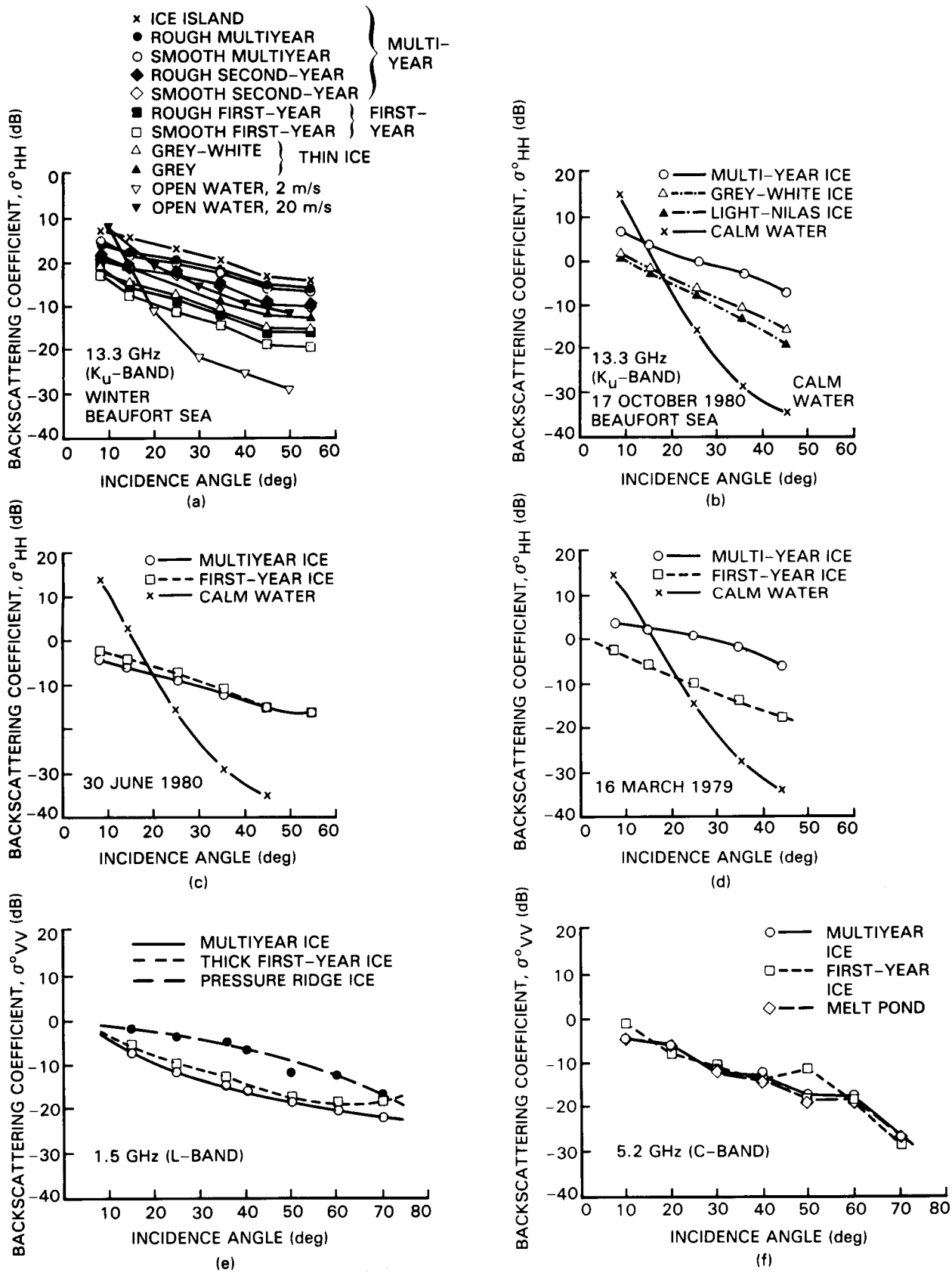

Figure A.11. Ice backscatter results at 13.3 GHz for ice types found in the Beaufort Sea (Gray *et al.*, 1981) and for open water with 2 and 20 m/s winds (Jones *et al.*, 1981). At this high frequency there is considerable difference in backscatter for the different ice.

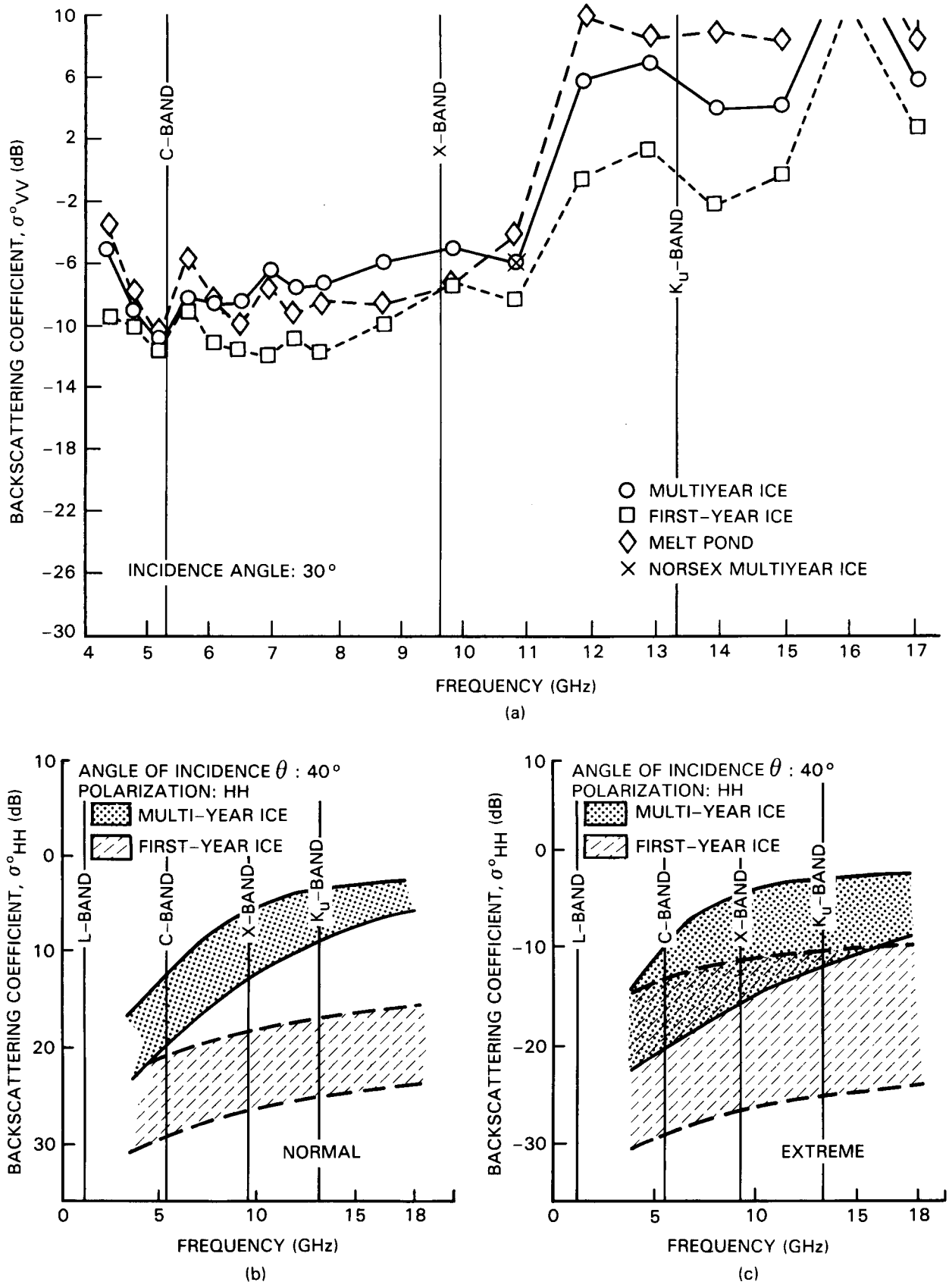

Figure A.12. (a) Frequency dependence of the backscatter coefficient for two incidence angles, (a) 30° and (b) 40°. Theoretical σ° for multiyear and first-year ice under normal (b) and extreme (c) conditions (Kim, 1984).

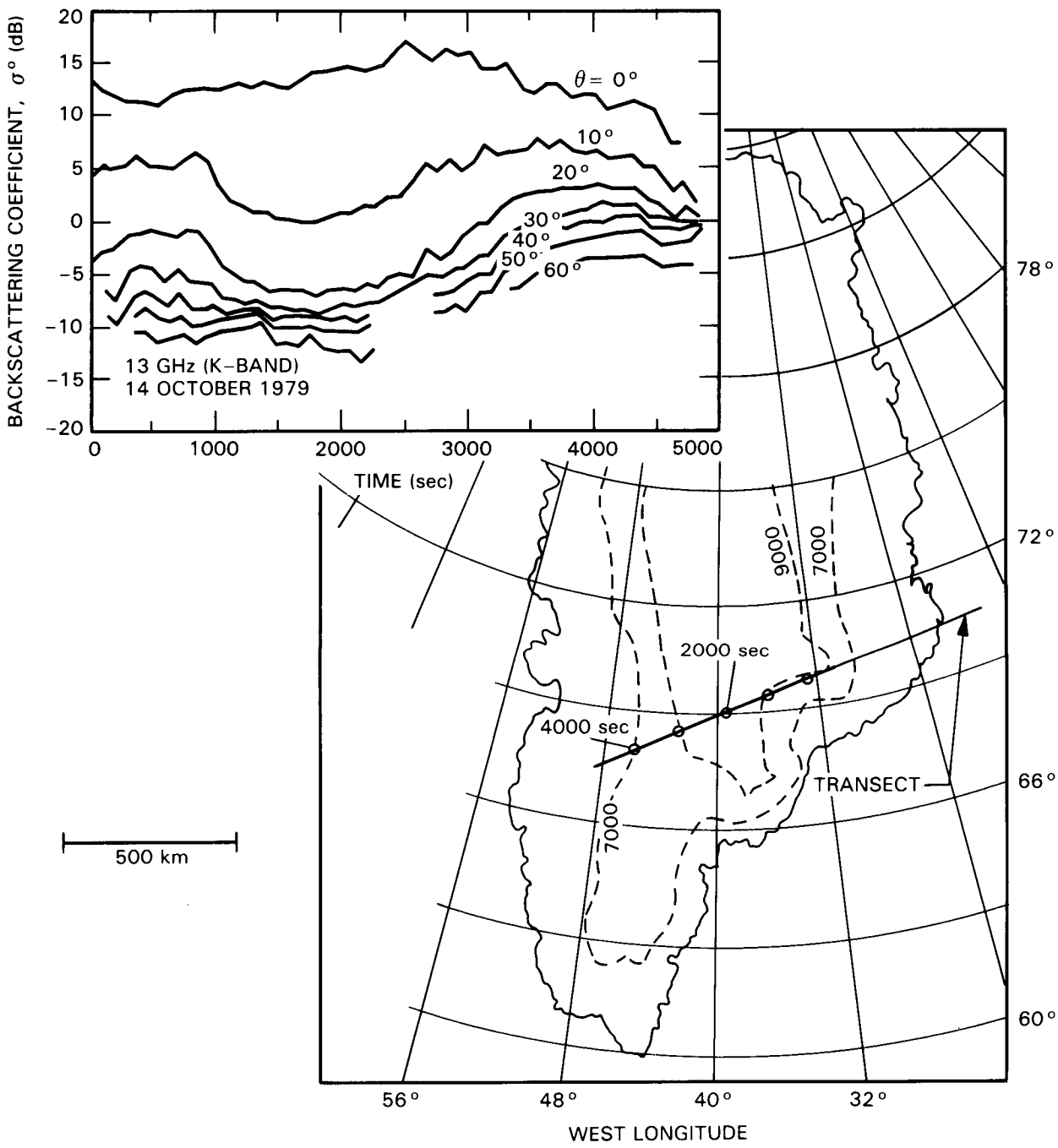

Figure A.13. Transect of 13 GHz airborne scatterometer over the Greenland ice sheet in October 1979 (Swift *et al.*, 1985b).

APPENDIX B: SOIL MOISTURE—ADDITIONAL INFORMATION

This Appendix presents additional information supporting the discussion in Chapter III of soil moisture remote sensing using SAR.

The basis for microwave sensitivity to soil moisture lies in the strong dependence of both radar backscatter and passive radiometric brightness temperatures on the dielectric constant of soil. Dry soil has a real dielectric constant (ϵ') of about 3 and water has an ϵ' of about 81. When these two materials are mixed, the resulting dielectric constant can range from 3 (for very dry soil) to over 25 (for very moist soil), as shown in Figure B.1. This relationship of dielectric constant to soil moisture is also highly dependent on soil texture, as shown.

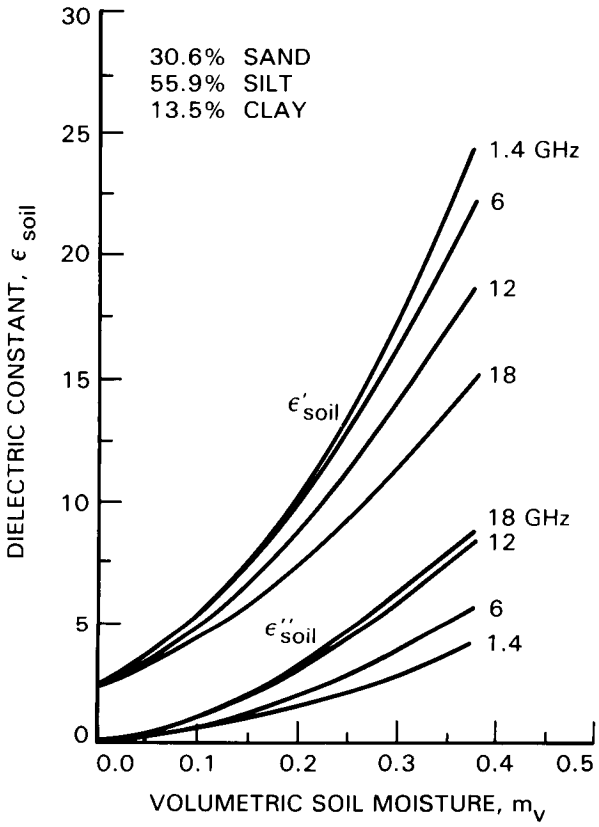

Figure B.1. Measured dielectric constant as a function of volumetric moisture content for a loamy soil at four microwave frequencies (Ulaby *et al.*, 1986).

There are two fundamental approaches to radar measurements of soil moisture. The first uses instantaneous estimation of absolute near-surface soil moisture and the second relies on change detection procedures to estimate increments (or decrements) to near-surface water content. The accuracy of the first approach is constrained by our capability to correct the estimated volumetric soil moisture (g/cm^3), m_v, for the effects of "target noise" on σ° as a function of sensor resolution; the main "target noise" components are: (1) vegetation cover, (2) surface roughness, and (3) surface slope. The change detection approach minimizes the impact of these scene variates as they tend to change slowly as functions of time. The surface slope is essentially constant—and the surface roughness changes abruptly only as a consequence of tillage and then decays quickly to a near steady state value, and vegetation cover varies over a seasonal phenologic calender marked by several distinctive phases of rapid change.

Assuming the selection of a transmit and receive polarization configuration (from polarization synthesis) to minimize the interaction term for scattering between soil and canopy trunk (or stalk), the following simplified model can be applied:

$$\sigma_T^\circ = \sigma_V^\circ + \frac{\sigma_S^\circ}{L^2} \qquad \text{(B-1)}$$

where σ_T°, σ_V°, σ_S°, and L^2 are the total backscatter observed by SAR (at some frequency, polarization, and angle of incidence), the backscatter contribution from vegetation, the backscatter contribution from the soil, and the two-way attenuation loss due to the canopy, respectively. The dependence of σ_S° on volumetric moisture is given by:

$$\sigma_S^\circ = R\,\alpha\,m_v \qquad \text{(B-2)}$$

where R is defined as a surface roughness coefficient and α is soil moisture sensitivity. Both R and α vary in an approximately known fashion as functions of frequency, polarization, and incidence angle. Since they are dependent upon local angle of incidence, they are sensitive to local slope.

Rigorous testing of empirically determined values of R (from scatterometry) versus physical characterization of roughness (in terms of RMS roughness $\varkappa_s$ and correlation length $\varkappa_l$), as required by theoretical scattering models, has been frustrated by an inadequate methodology for physically measuring $\varkappa_s$ and $\varkappa_l$. Improved measuring techniques such as a laser roughness system may make such tests possible with the required rigor.

Inserting Equation B-2 into Equation B-1 and inverting to calculate m_v yields:

$$m_v = \frac{L^2}{\alpha R}\,(\sigma_T^\circ - \sigma_V^\circ) \qquad \text{(B-3)}$$

It can be shown from scatterometer measurements that by using a certain combination of frequency, polarization, and angle of incidence, we can maximize α, minimize ΔR = f (roughness), and minimize the magnitude of σ_V° and L^2 for certain

classes of vegetation. However, a more robust inversion approach for use with Eos SAR would make use of multiple angles, frequencies, and polarizations to predict R, σ_v°, and L^2 for a given σ_T°. It is noted that σ_v° and L^2 are of interest themselves as separate retrievals for erosion studies in hydrology and surface drag in atmospheric studies. However, robust models for these parameters have yet to be demonstrated. Also, the error related to surface slope can be minimized using digital terrain data (or multi-angle SAR data itself to estimate local slope).

The second approach to soil moisture, i.e., by the use of change detection, does not require "multi" data except in the time domain. It assumes that σ_v°, L, and R exhibit negligible change over short time increments (for a given resolution element) and for fixed viewing geometry. In this case, the derivative of Equation B-3 with respect to time becomes:

$$\frac{dm_v}{dt} = -\frac{L^2}{\alpha R}\frac{d\sigma_T^\circ}{dt} \qquad \text{(B-4)}$$

The foregoing assumptions are generally true except during tillage operations, periods of rapid foliar development, and harvest of crops (or cutting of timber). In these cases, the changes tend to be specific to a local region and thus can be identified by spatial analysis. These techniques have been tested on Seasat data and applied to SIR-B data to differentiate changes in σ° resulting from (1) dR/dt, (2) $d\sigma_v^\circ/dt$ and dL/dt, and (3) dm_v/dt (Ulaby and Dobson, 1986).

Even so, Equation B-4 shows that the relationship between soil moisture changes (dm_v/dt) and total backscatter changes ($d\sigma_T^\circ/dt$) is still affected by the canopy attenuation L^2 and by surface roughness R. However, it has been found (1) that sensitivity to roughness is minimized in the vicinity of C-band and for angles of incidence less than 20° for agronomic roughness where 0.75 cm < s ≤ 4.0 cm and (2) that the between field variance in L^2 is small for grasses and agronomic crops (LAI ≤ 6) at L- and C-band frequencies. Hence, an L- or preferably C-band system operating at incidence angles of 15° to 20° should be best suited for this type of approach.

Some of the results obtained by truck scatterometer measurements are shown in Figures B.2 and B.3. Figure B.2 shows the dependence of HH-polarized radar backscattering coefficient (σ°) on surface roughness of non-vegetated soils as a function of incidence angle. Measurements were made over the range of common agronomic roughness scales ranging from smooth (rms roughness height of 1.1 cm) to very rough (rms roughness height = 4.1 cm). For each of the three frequencies shown in Figure B.2, the variance in σ° related to surface roughness is

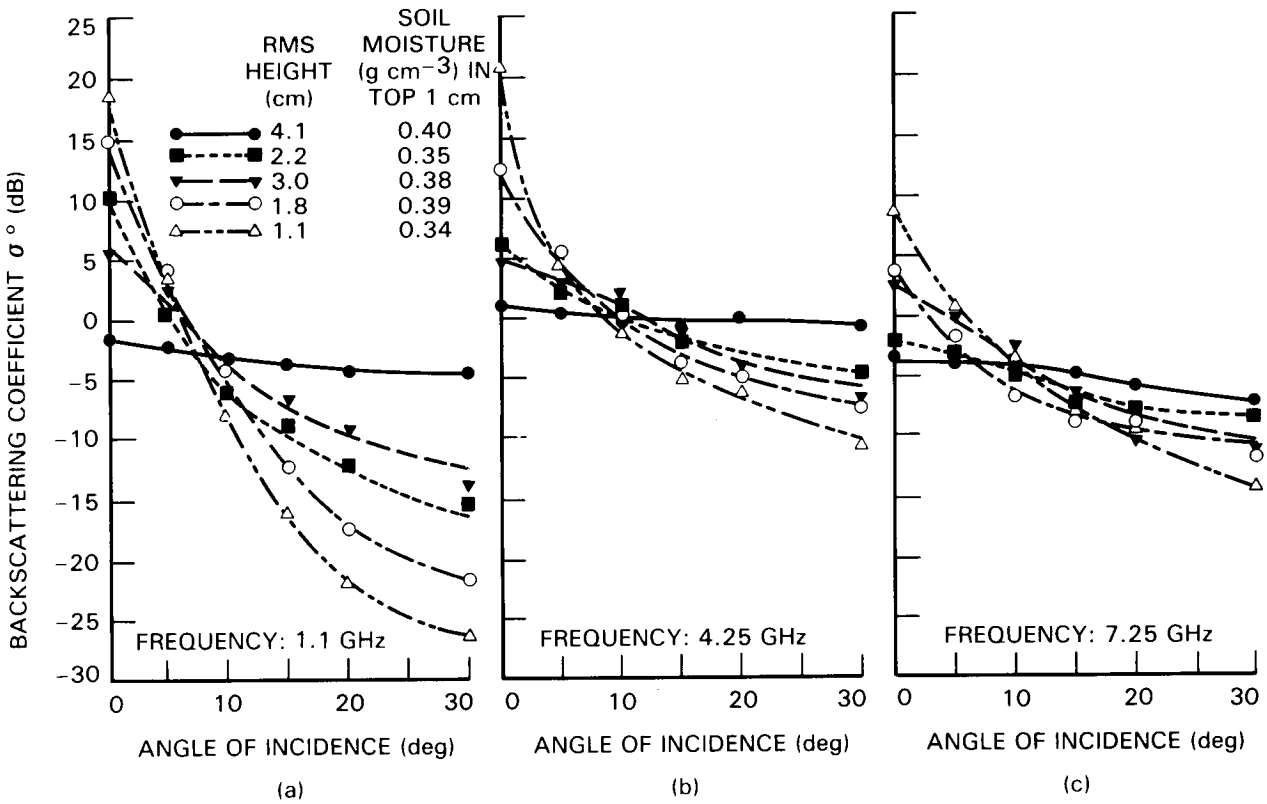

Figure B.2. Angular response of scattering coefficient for five fields for high levels of moisture content at (a) 1.1 GHz, (b) 4.25 GHz, and (c) 7.25 GHz (Ulaby *et al.*, 1986).

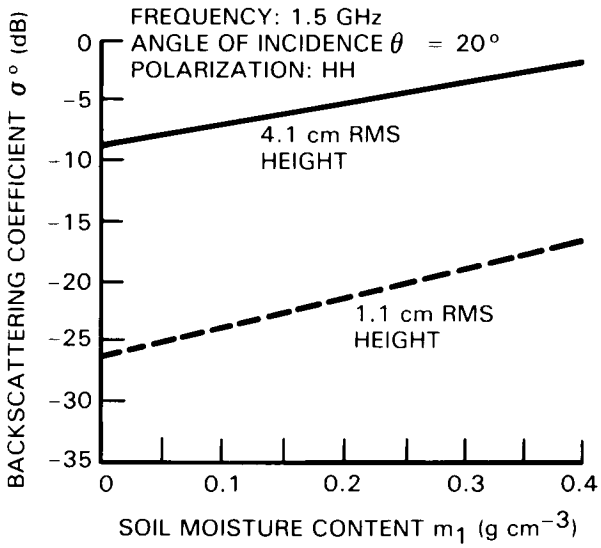

Figure B.3. Comparison of backscattering response from a smooth and a rough surface at 1.5 GHz and 20° incidence angle with HH polarization.

observed to be minimized in the vicinity of 7° to 10° incidence angles. Hence, SAR viewing angles near normal are expected to minimize the effects of surface roughness. In addition, the effects of agronomic surface roughness are observed to be greatest at L-band and to decrease at higher frequencies since all of the surfaces become increasingly rough relative to wavelength and thus more similar in their surface scattering characteristics. Thus, higher frequencies are preferred for reducing variance in σ° related to surface roughness; however, attenuation and scattering by vegetation canopies also increases with frequency. Figure B.3 shows surface roughness to contribute an additive bias to σ° in dB which can be of considerable magnitude. Consequently, failure to account for the effects of surface roughness can seriously reduce apparent correlation and sensitivity of σ° to soil moisture unless change detection approaches are used.

Aircraft estimates of soil moisture from radar scatterometers have been reported by Ulaby *et al.* (1979), Theis *et al.* (1982), and Jackson *et al.* (1981). Thus far, better results were obtained with the low-altitude airborne scatterometer experiments of Bradley and Ulaby (1981) and of Jackson and O'Neill (1985). The results reported by Moe *et al.* (1984) showed an excellent correlation between σ° and soil moisture at both 1.6 GHz and 4.75 GHz frequencies, based on the data taken over four small watersheds in Chickasha, Oklahoma during 1978 and 1980 (Figure B.4).

Early attempts to measure soil moisture from satellite altitudes were reported by Ulaby *et al.* (1974) using the Skylab 13.9 GHz scatterometer and by Blanchard *et al.* (1981) using the Seasat 1.275 GHz SAR. The radar scattering coefficients derived from the 13.9 GHz Skylab experiment showed only a weak

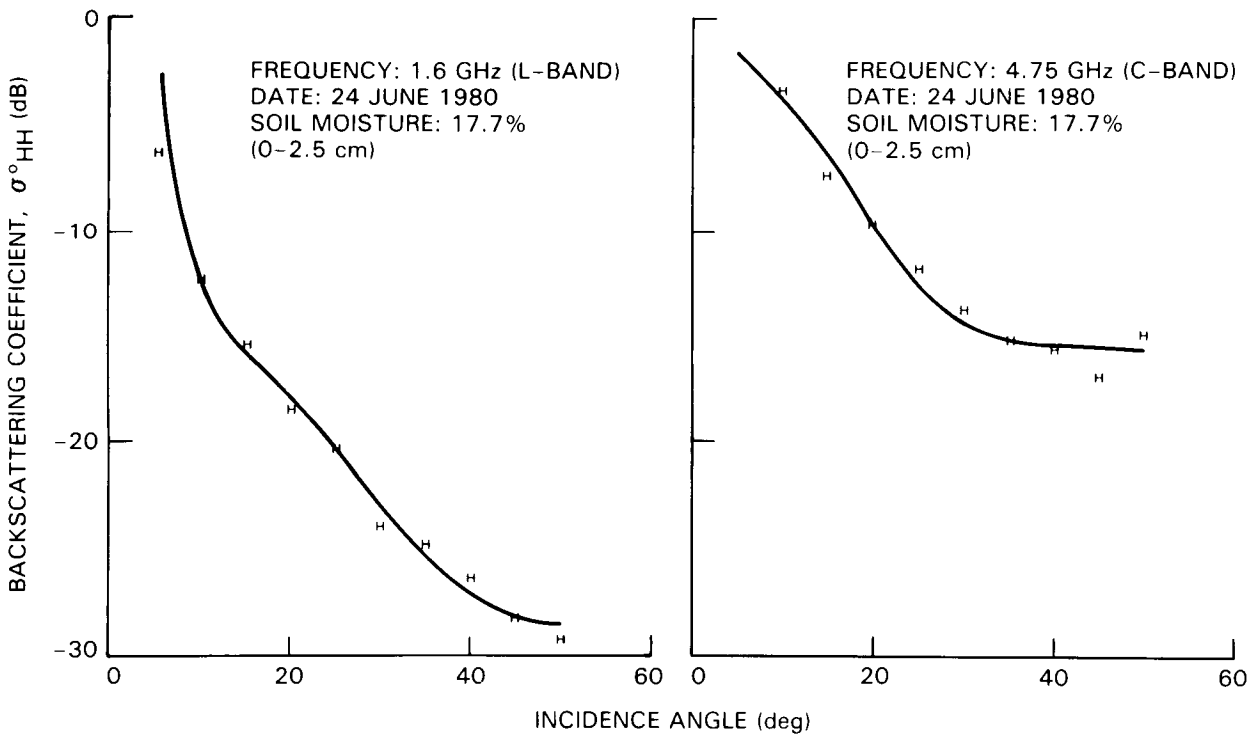

Figure B.4. Comparison of theoretical model calculations to data obtained from aircraft flights over a watershed in Chickasha, Oklahoma, at the frequencies of (a) 1.6 GHz and (b) 4.75 GHz.

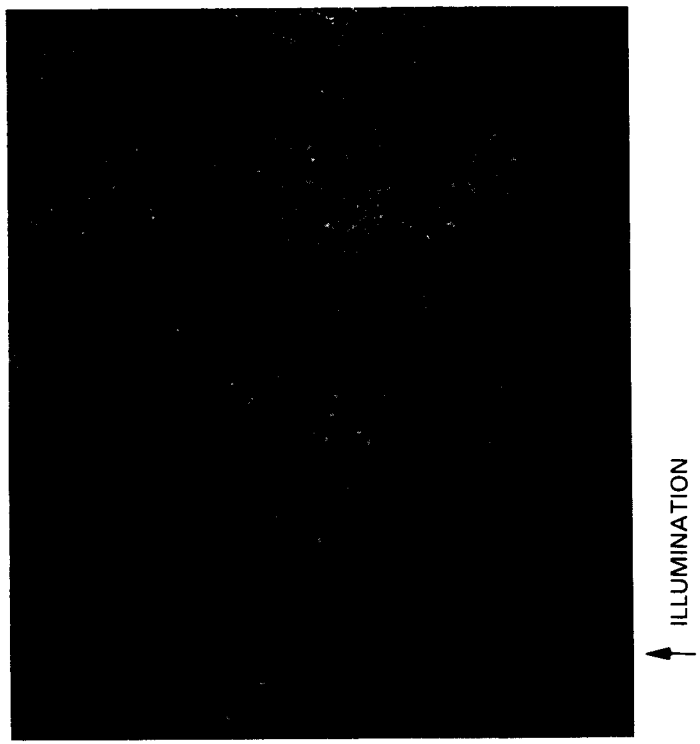

SEASAT SAR

ILLUMINATION

N

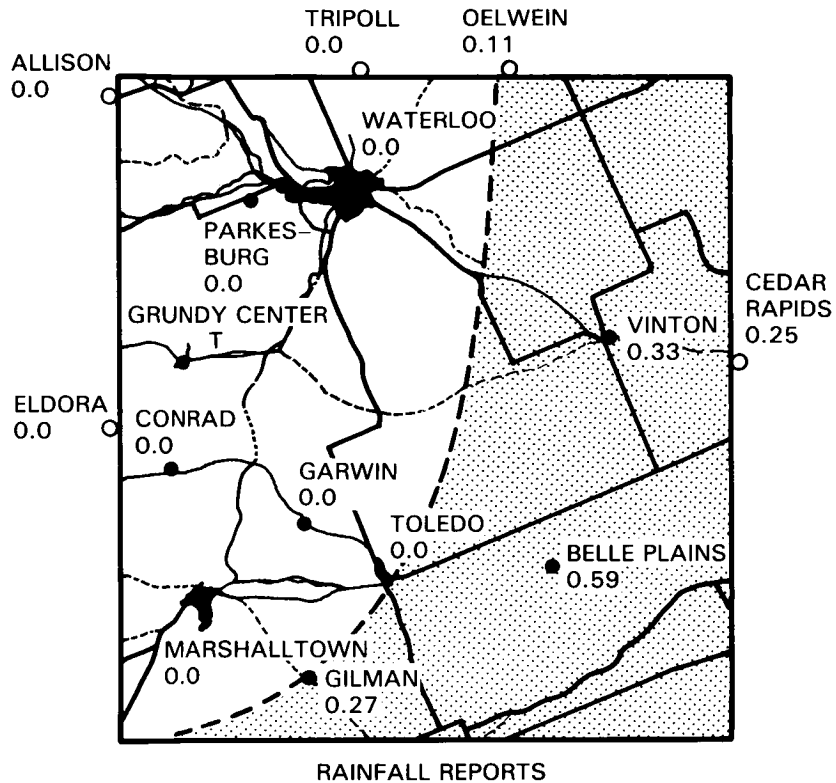

RAINFALL REPORTS

Figure B.5. Seasat SAR image of Ames, Iowa, showing soil moisture differences due to a recent series of rain squalls (Ulaby *et al.*, 1983).

correlation with soil moisture, mainly because the frequency was too high.

A number of Seasat SAR images demonstrated sensitivity to soil moisture; perhaps the most dramatic is that shown in Figure B.5, comparing a SAR image of a region in Iowa with rain gauge data taken immediately after a passing squall. The eastern portion of this scene exhibits a much brighter overall tone than the western portion. This is attributable to rainfall on the previous day; there is a clear correlation between the bright-return area seen in the eastern portion of the image and the rainfall amounts recorded in Cedar Rapids, Vinton, Belle Plains, and Oelwein. The measured rainfall ranged from 0.11 to 0.59 inches, which was enough to increase significantly the moisture content of the soil surface. Two additional areas of interest are observable in Figure B.5. First, although Grundy Center reported only a trace of rain, it appears as a region of brighter tone on the Seasat image. Secondly, the area north of Marshalltown also appears as a region of generally brighter tone although the recording stations reported no precipitation. This apparent discrepancy could be the consequence of rainfall occurring between the gauging stations in the area. Figure B.5 also shows a color enhancement of the Seasat scene; it has been incoherently averaged to a 250 m resolution.

Measurements of soil moisture using the L-band SAR on SIR-B were also quite successful (Figure B.6) (Wang *et al.*, 1986). The dependence of the SIR-B backscattering coefficient on soil moisture (gravimetric) is shown in Figure B.7. A linear regression excluding data points A, B, C, D, and E gave a correlation coefficient of 0.80 and a sensitivity of 2.3 dB per 0.1 g/cm^3. Similar results were obtained by other SIR-B investigations (Dobson and Ulaby, 1986). This sensitivity is comparable to those previously reported using truck scatterometer data. The absolute values of $\sigma°$ derived from SIR-B are difficult to compare to those from the Seasat SAR and those from the airborne scatterometer, due to calibration uncertainties.

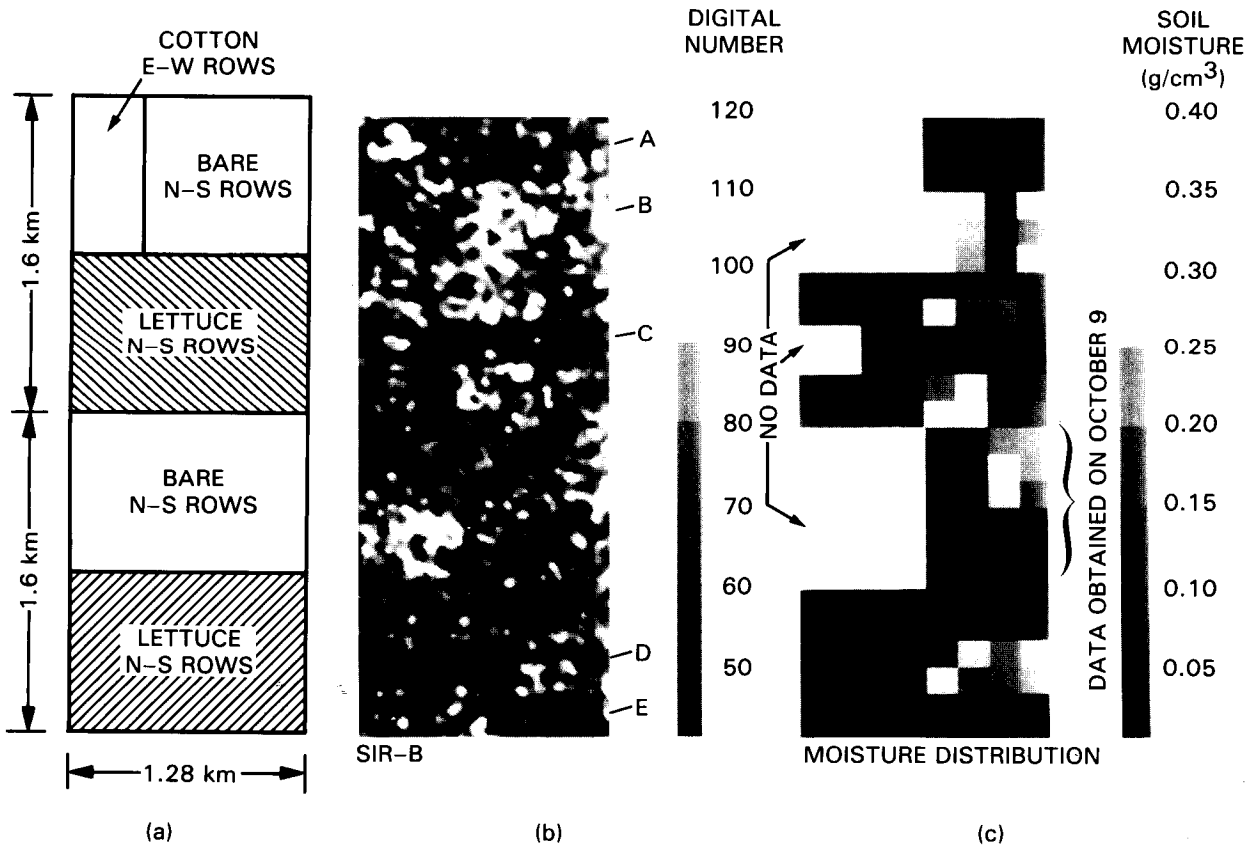

Figure B.6. SIR-B and related ground truth data for dry and irrigated fields (Wang *et al.*, 1986).

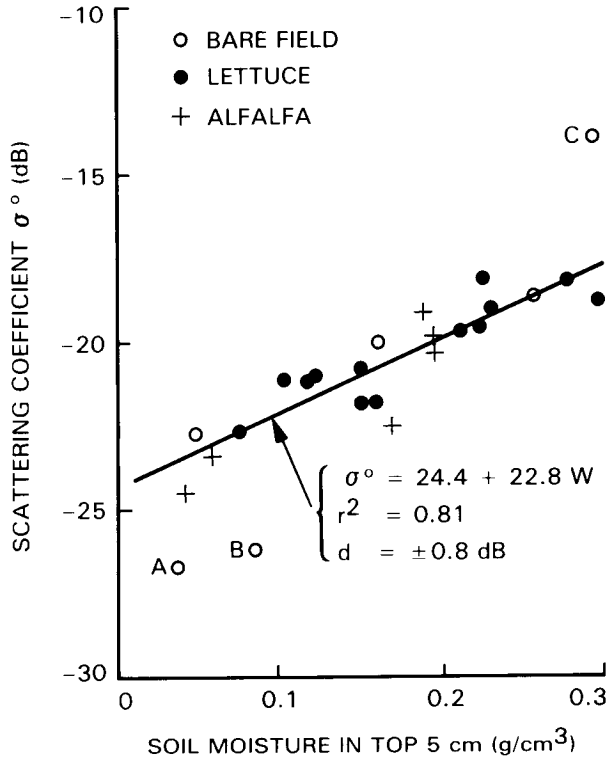

Figure B.7. Shuttle Imaging Radar-B backscattering coefficient plotted as a function of volumetric soil moisture (Wang *et al.*, 1986).

APPENDIX C: VEGETATION SCIENCE—ADDITIONAL INFORMATION

This appendix presents several case histories that are relevant to SAR observations of vegetation parameters as discussed in Chapter IV.

RADAR STUDIES OF MONOSPECIFIC AGRICULTURAL CANOPIES

In general, the backscattering coefficient of a closed agricultural canopy or shrub ecosystem consists of three terms: a term representing the scattering contributions by the vegetation volume, σ_V°, a second term representing the direct soil surface backscattering contribution, σ_S°, including two-way attenuation, and a third term representing interactions (multiple reflections) between the soil surface and the vegetation volume, σ_{SV}°:

$$\sigma_{canopy}^\circ = \sigma_V^\circ + T^2 \sigma_S^\circ + \sigma_{SV}^\circ \qquad \text{(C-1)}$$

where T is the canopy transmission coefficient. The relative magnitudes of these three contributions as a function of incidence angle are highly dependent on the foliar and woody biomass of the vegetation and the state of the soil layer. The soil term generally dominates near normal incidence and the volume term dominates for high-loss canopies at high angles of incidence.

Penetration Depth

Both the albedo and the optical thickness of a vegetation layer generally increase with increasing frequency, and both may be polarization-dependent if the canopy has components with specific orientations (such as vertical stalks). As an illustration, Figure C.1a presents the L-band penetration depth as a function of incidence angle for a fully grown corn canopy. The penetration depth defines the depth at which the incident power is attenuated by a factor of 1/e (37 percent). For H-polarization, which couples weakly to the vertical stalks, the attenuation is relatively small resulting in a penetration depth of about 5 m across the indicated angular range. In contrast, V-polarized waves are attenuated much more readily than H-polarized waves and the penetration depth is less than one-third as large at incidence angles greater than 60°. Consequently, H-polarization measurements provide information about primarily the underlying soil medium, and V-polarization data are related more to the canopy structure. In addition to the role of polarization, because the penetration depth varies with frequency, L-band observations are influenced by the entire canopy, whereas X-band observations are governed primarily by the top layer (Figure C.1b). It is significant to note that the ratios of maximum penetration depth (L-band with H-polarization) to minimum penetration depth (X-band with V-polarization) is about 5:1 for corn.

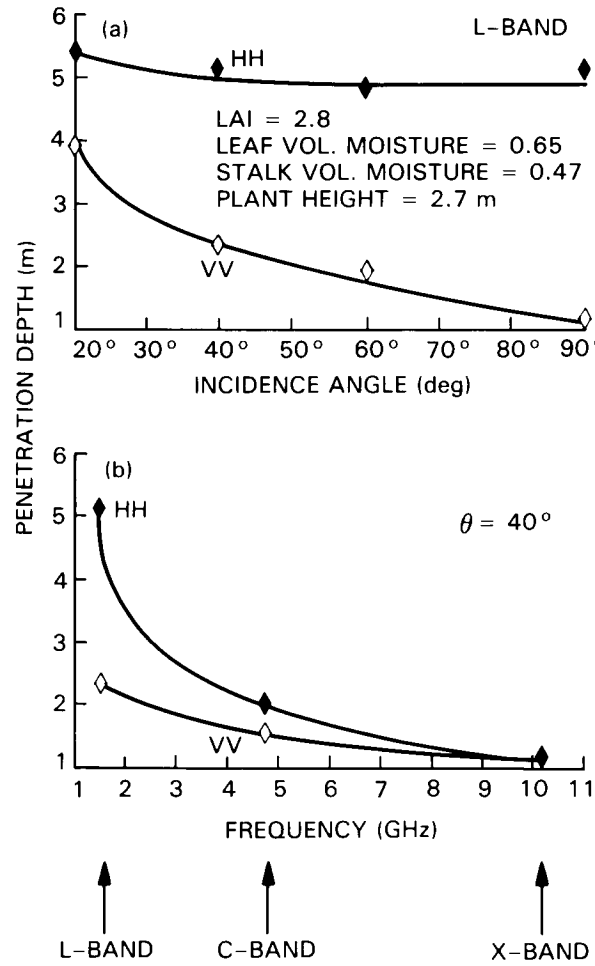

Figure C.1. Penetration depth of a corn canopy versus incidence angle for HH and VV polarization at (a) L-band and (b) 40° (Source: F.T. Ulaby, private communication).

At a given set of wave parameters (wavelength, incidence angle, and polarization configuration), the primary quantity governing the attenuation coefficient of a vegetation canopy is the water content per unit volume. Consequently, the temporal variation of the total attenuation loss is governed by the temporal variations of the plant height and its water content. Figure C.2 depicts the X-band vertical polarization one-way loss measured for a soybean canopy as a function of time (day of year) at an angle of incidence of 52°. The experimental results, which were found to be in good agreement with theoretical calculations, show that the loss increases with time during the early growth stage, then maintains a constant level (for about three weeks) after the canopy attains full height, and finally decreases to zero over a period of four weeks as the plants lose their water.

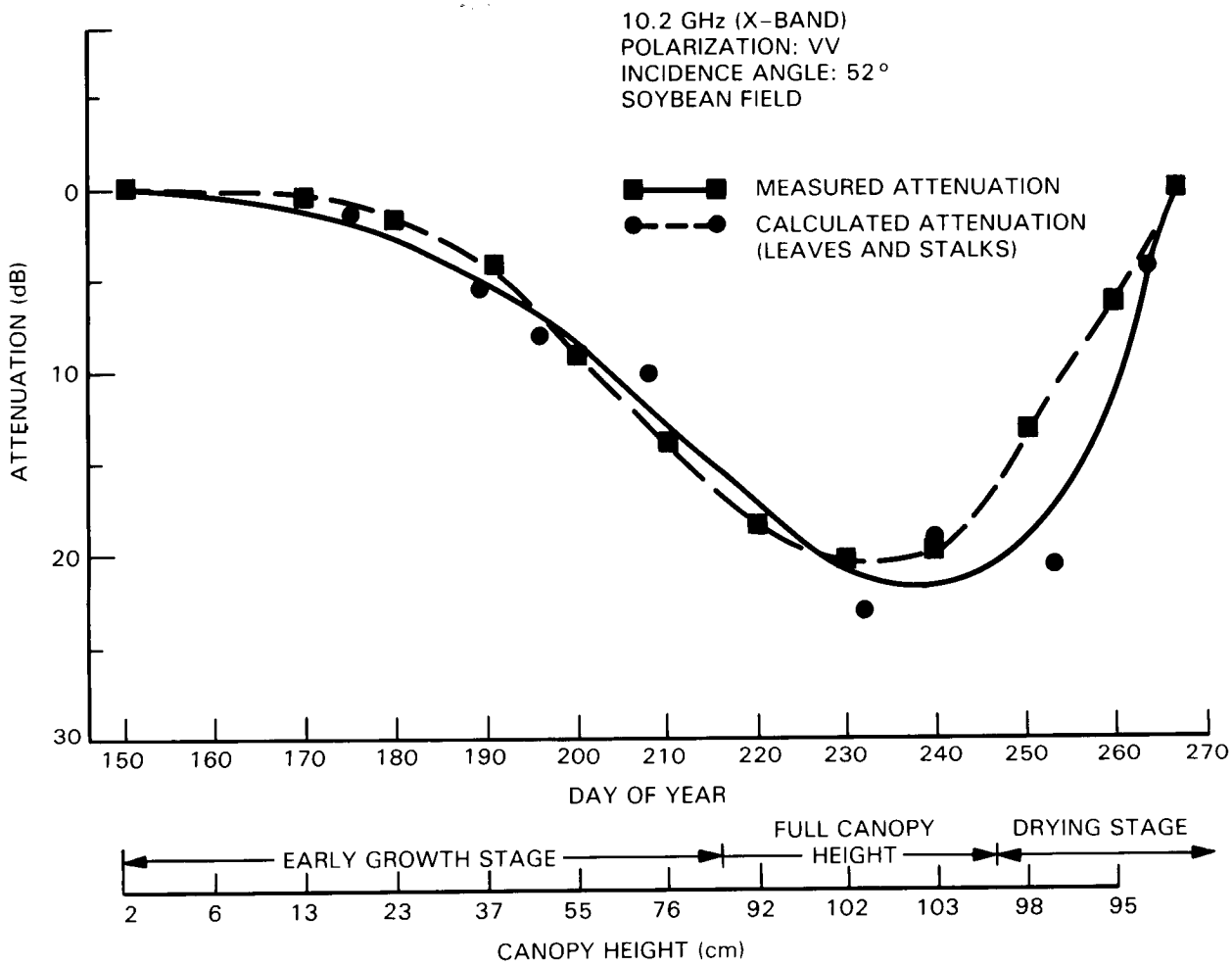

Figure C.2. Seasonal variation of the measured one-way attenuation at 10.2 GHz for a soybean canopy and the calculated attenuation due to absorption by leaves and stalks (Ulaby *et al.*, 1986).

Crop Type Classifications

Numerous studies have been conducted over the past 2 decades to evaluate the use of radar for crop type classification. One example is presented here in the form of Figure C.3. The test site, an agricultural region in the Netherlands, consisted of 182 fields comprising seven crop types (Figure C.3a). Part (b) of the figure shows a color composite image that was generated by merging three radar images of an agricultural test site. The images had been obtained on different dates using an airborne X-band real aperture imaging radar. Use of the multidate single-polarization (HH) image provided a correct classification accuracy of 88 percent (Figure C.3c).

Multidate Signatures

In general, the temporal pattern of the canopy backscattering coefficient may be modeled as the sum of contributions from the individual canopy constituents (leaves, stems, fruit, etc.) and the underlying soil surface. For winter wheat, for example, σ°_{canopy} has been modeled as the sum of a leaf term, σ°_{leaf}, a head term, σ°_{head}, and a soil term $T^2\,\sigma^\circ_S$. The relative importance of the three contributions is depicted in Figure C.4a, which shows that σ°_{canopy} is dominated by the leaf contribution until about day of year (DOY) 145, and by the head and soil contributions from there on until harvest. According to field observations, the green LAI decreases to a relatively small level by DOY 145. For the period preceding this date, σ°_{canopy} exhibits a strong sensitivity to LAI (Figure C.4b) over a wide range extending from about 1 to 9. It is relevant to note that optical sensors are sensitive to LAI also, but their response "saturates" above LAIs of 3.

Cross-Polarization

Multiple scattering is one of the primary mechanisms for the generation of cross-polarized energy. It therefore follows that the cross-polarized scattering coefficient of a given surface or volume should be

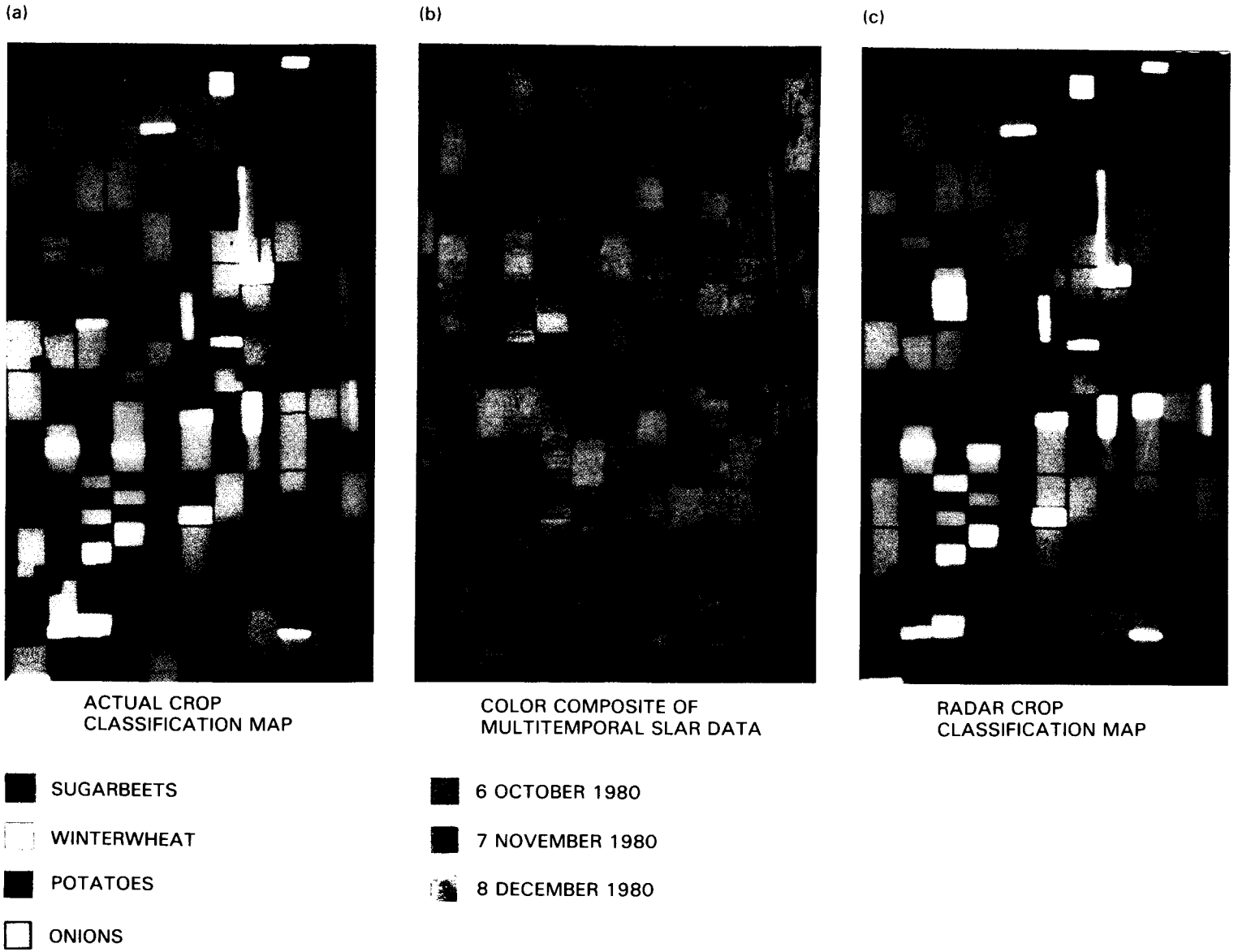

Figure C.3. Crop classifications using multitemporal radar data of a region containing 182 fields in the Netherlands. (a) The actual crop classification map; (b) A color composite generated using multidate radar data; and (c) A classification map generated using the radar data (Hoogeboom, 1983).

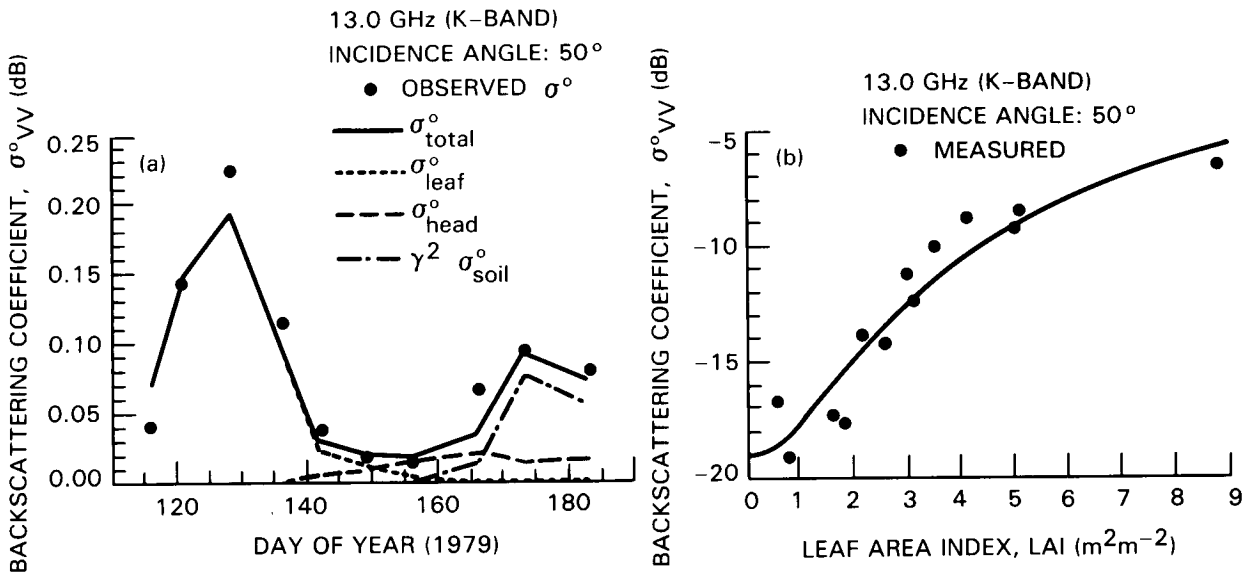

Figure C.4. Multidate backscatter coefficients for a winter wheat canopy. σ°_{pred} is the predicted total backscatter coefficient; σ°_{leaf} is the leaf term; σ°_{head} is the head term and $T^2\sigma^\circ_s$ is the soil term (Ulaby *et al.*, 1984b).

strongly associated with the degree of inhomogeneity of that surface or volume. The degree of inhomogeneity may be characterized by the ratio $(\sigma_\epsilon/\lambda)^2$, where σ_ϵ is the standard deviation associated with the dielectric constant variation of the boundary layer for a scattering surface and the spatial discontinuities within the volume for a medium such as vegetation, and g is the wavelength. Hence, depolarization in a vegetation canopy generally increases with increasing frequency.

The cross-polarized (HV or VH) scattering coefficient exhibits a much weaker angular dependence, particularly near normal incidence, than the like-polarized (HH or VV) scattering coefficients. This is evident from the curves shown in Figures C.5a and C.5b, which represent averages of several hundred observations of bare-soil surfaces (a) and crop canopies (b). Figure C.5c shows plots of the cross-polarization ratio (ratio of σ°_{HV} to σ°_{HH} expressed in dB) as a function of the incidence angle for bare soil and crop canopies at L-, C-, and X-band. The cross-polarization ratio increases with increasing incidence angle, is generally larger for crop canopies than for bare soil surfaces, and increases with increasing frequency for a given terrain category. This last observation is based, in part, on the behavior depicted by the data shown in Figure C.5d.

One of the consequences of the weaker angular dependence of σ°_{HV} (relative to σ°_{VV} and σ°_{HH}) is that the cross-polarized SAR images will be less sensitive to slope variations. Thus, cross-polarized images are more suitable for computer extraction of information from mountainous areas. Also, the ambiguities associated with the azimuthal variation of the backscattering coefficient for row crops may be either avoided or reduced considerably when cross-polarized images are available (in addition to HH and VV imagery).

Although the mechanisms responsible for the generation of cross-polarized energy in a vegetation canopy are not well understood, cross-polarized measurements have proven to be useful in several ways related to the monitoring of vegetation canopies. Whereas two crop types having similar geometries may be indistinguishable from each other on the basis of their like-polarization scattering properties alone, it may be possible to separate them when cross-polarized observations are used as well. This is illustrated by the data in Figure C.6, in which the HV channel is observed to play the primary role in discriminating wheat, barley, peas, and rapeseed.

In some cases, it is difficult to distinguish image pixels or areas corresponding to bare soil surfaces from those corresponding to vegetation- covered surfaces when using like-polarized images alone. This is true when the two types of targets exhibit comparable image tones and textures. Because vegetation canopies depolarize more strongly than bare surfaces, the cross-polarization ratio can prove very useful in achieving discrimination between bare and vegetation-covered surfaces.

RADAR STUDIES OF FOREST CANOPIES

The proposed Eos SAR will be capable of producing four types of radar images: HH, VV, HV, and VH (which according to the reciprocity principle should be identical) as well as images of the phase-difference between all the polarizations. For most

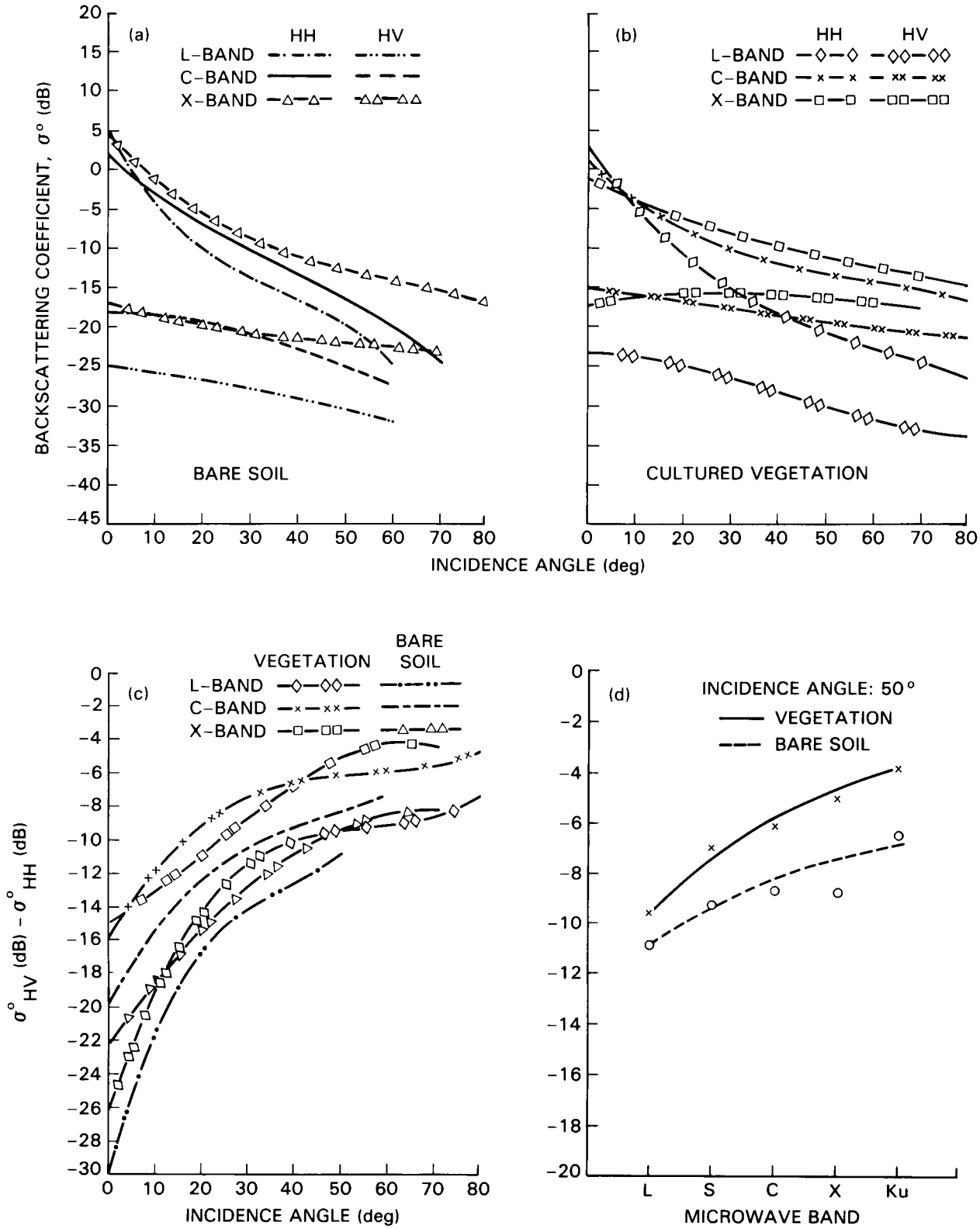

Figure C.5. (a) Mean backscattering coefficient of bare soil surfaces at L-, C- , and X-band. (b) Mean backscattering coefficient of vegetation canopies at L- , C-, and X-band. (c) Cross-polarization ratio for bare soil and vegetation canopies as a function of the incidence angle at L-, C-, and X-band. (d) Frequency variation of cross-polarization ratio at 50° incidence angle.

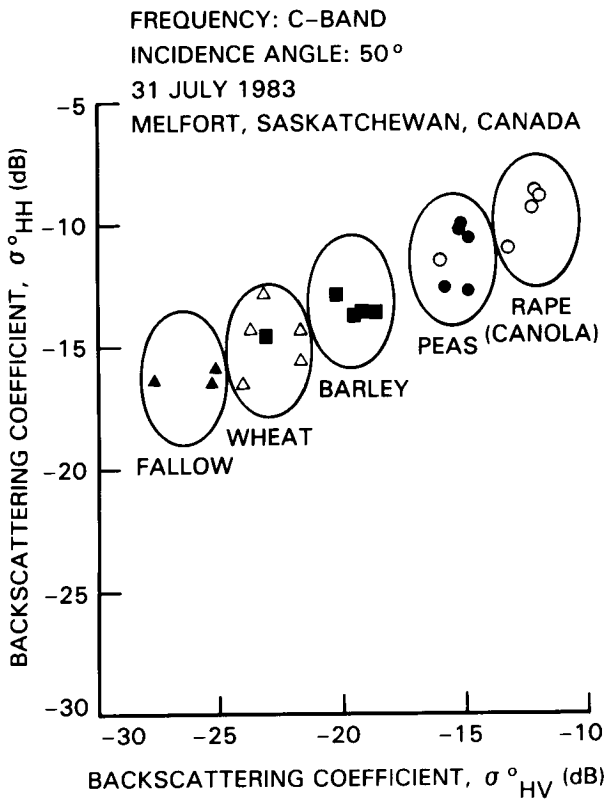

Figure C.6. Classification of five crop types using like- and cross-polarized backscattering measurements made with a C-band scatterometer at 50° (data courtesy of F.T. Ulaby).

conditions, the difference between VV and HH backscattering amplitudes of a given canopy is much smaller than the difference between either one of them and the cross-polarized return (Figure C.7). Among HH and VV, the latter polarization generally is more sensitive to the stalks of plants and to the trunks of trees because of their vertical orientation.

Polarization Phase-Difference

Referring to the polarization-phase difference image shown in Figure 28, the corn fields were clearly distinguishable from the other fields because they were the only type of cover exhibiting a phase difference that was significantly different from zero. Each corn field (which is comprised typically of about 500 pixels) has a phase difference distribution characterized by a single peak (Figure C.8a) located at approximately the mean value of the distribution. Figure C.8b compares values of phase difference plotted versus incidence angle to a theoretical curve calculated on the basis of a model developed by Ulaby *et al.* (1986). According to this model, the observed phase difference is due to the differential time delay between the VV and HH signals as they propagate through the corn canopy to the underlying soil surface and back. Because of the stronger coupling between the V-polarized wave and the vertical stalks (compared to the coupling for the H-polarization wave), its velocity of propagation in the canopy is slower than it is for the H signal. Moreover, because the coupling of the V-polarization increases with incidence angle and the coupling for the H-polarization is angle-independent, the phase difference, W_d, increases with increasing incidence angle.

The preceding study is one of very few investigations conducted to date to relate polarization phase difference to the scene parameters. It is anticipated that future studies will further establish the potential use of phase-difference information in monitoring vegetation canopies.

Relationship to Tree Height

In a study of L-band radar images of a test site in France consisting of several quasi-uniform areas of monospecific stands of pine trees, it was found that image tone (which is proportional to the scattering coefficient $\sigma°$) was correlated to tree height (Figure C.9). The extent to which such a relationship is applicable to forested areas in general is the subject of current research.

Relationship to Seasonal State

Observations of the backscattering coefficient of deciduous trees (Figure C.10) indicate that in the L-band region, radar is minimally sensitive to the presence of leaves and the backscatter is dominated by the branches, whereas at X-band the presence of leaves in the spring produced a scattering coefficient more than twice as large (3 to 4 dB) as was observed in the fall.

Relationship to Species Type and Species Structure

In a recent study conducted by Cimino *et al.* (1986), multi-angle SIR-B images of a forested area in Argentina were used to discriminate various forest species and various canopy structures within a single species on the basis of the angular signature of the observed radar return. Comparison of the color composite radar image shown in Figure C.11a with the corresponding vegetation maps of the region (Figure C.11b) has shown that use of the multi-angle data can provide good discrimination between species types (nire and lenga) and structure types of a single species (nire). Similar results are obtained by other researchers using SIR-B data of other regions around the world.

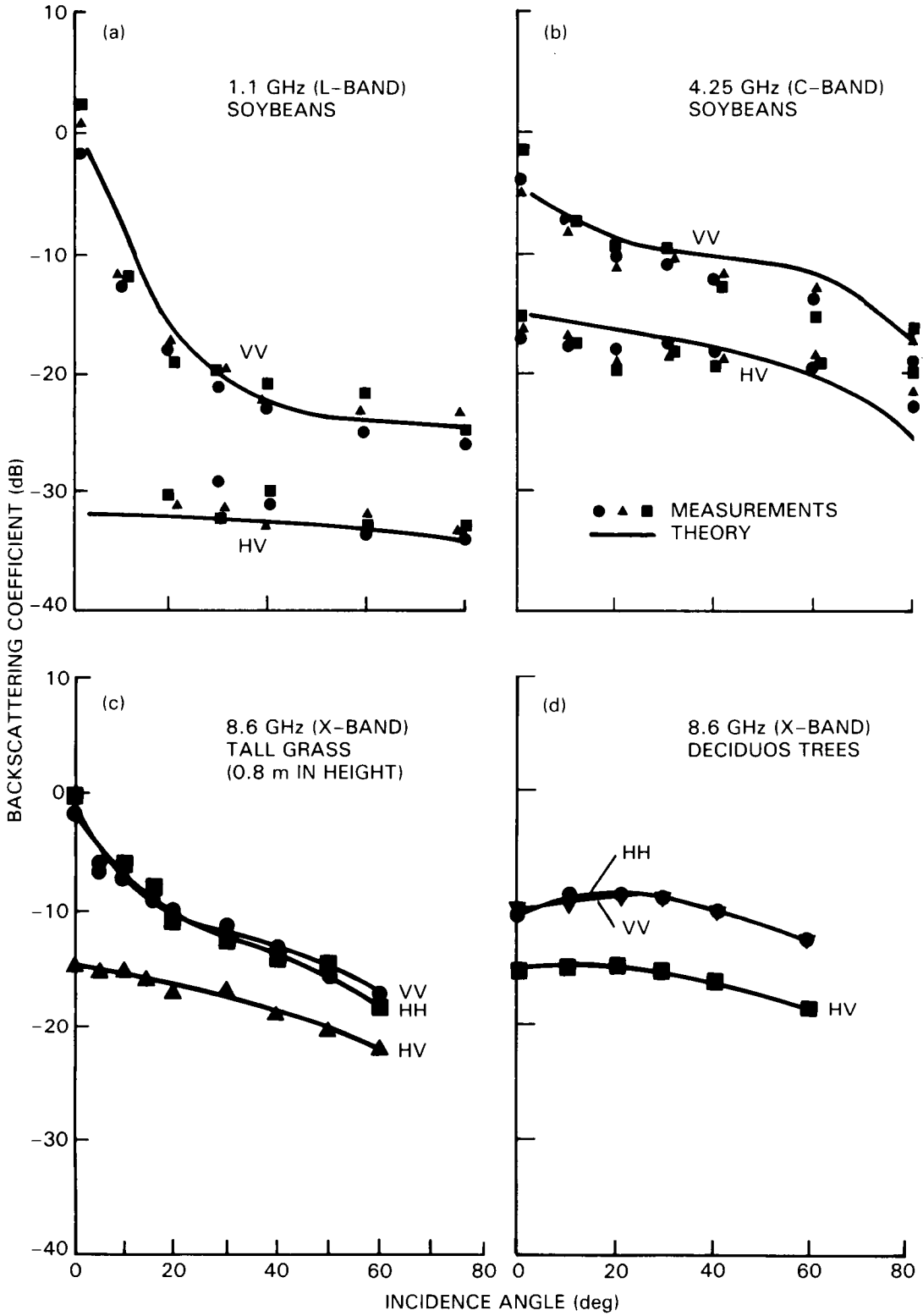

Figure C.7. Multipolarization data for (a) mature soybeans at L-band, (b) soybeans at C-band, (c) tall grass at X-band, and (d) deciduous trees at X-band (Ulaby *et al.*, 1986).

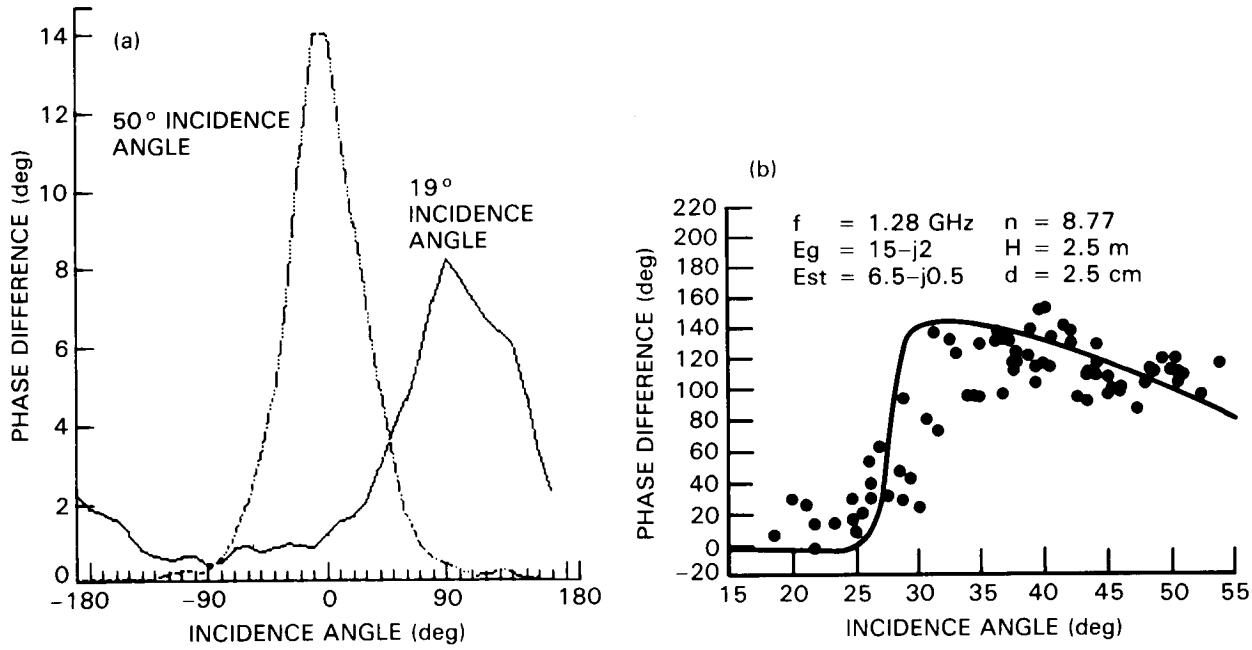

Figure C.8. (a) Polarization-phase-difference distribution for two corn fields located at incidence angles of 19° and 50°. (b) Variation of the mean phase difference with incidence angle for fields of standing corn. The data points were extracted from L-band SAR imagery and the solid curve is based on model calculation (Ulaby *et al.*, 1987).

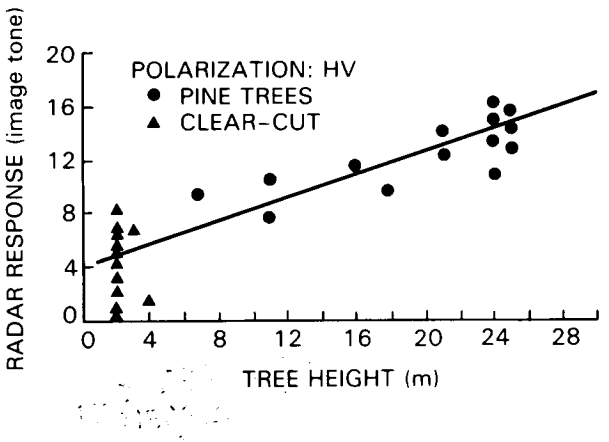

Figure C.9. Relationship between height of pine populations and radar image tone (from Riom and LeToan, 1981).

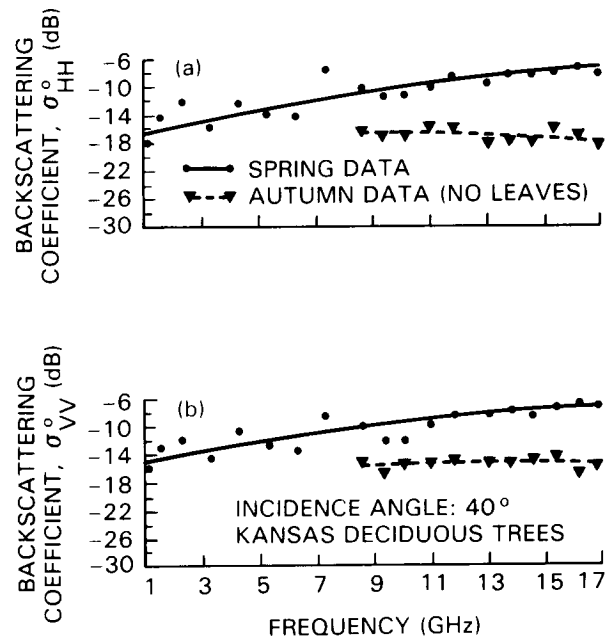

Figure C.10. Spectral response of (a) σ°_{HH} and (b) σ°_{VV} of trees measured at 40 incidence angle (Ulaby et al., 1986).

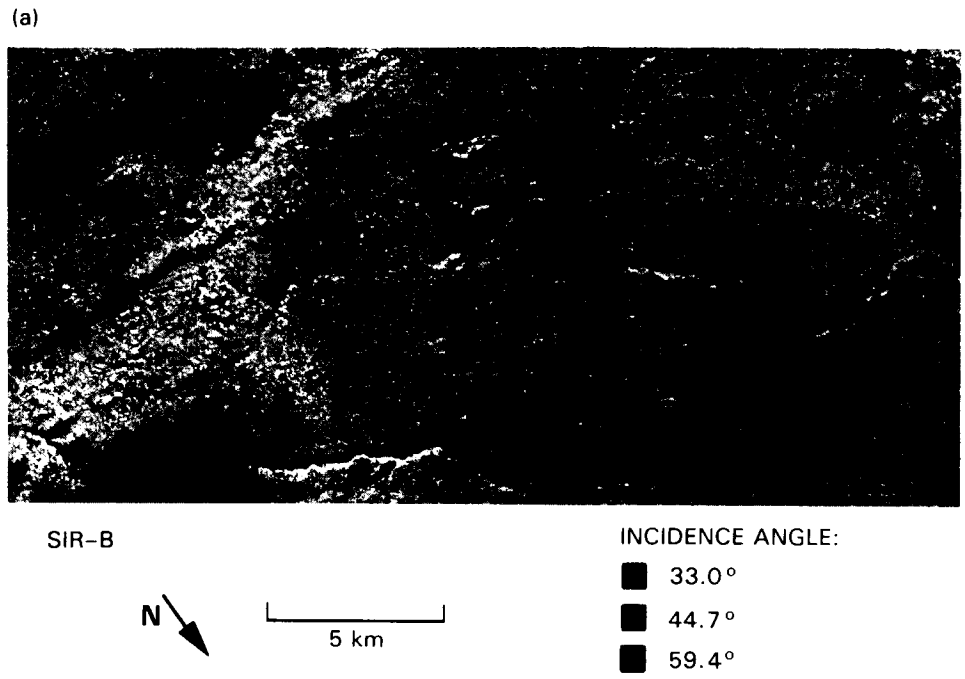

Figure C.11. (a) Color composite image of Cordon la Grasa region in Argentina generated using three of the four available multiple incidence angle images from SIR-B. A different color was assigned to each image: blue is data take 56.4 (33.0° incidence angle), green is data take 72.4 (44.7° angle), and red is data take 104.4 (59.4° angle). The variation in color indicates differences in the backscatter of the forest types as a function of incidence angle. (b) Vegetation map of the Cordon la Grasa region (Cimino *et al.*, 1986).

APPENDIX D: OCEANOGRAPHY—ADDITIONAL INFORMATION

This appendix provides additional information about SAR ocean wave imaging mechanisms and discusses Seasat SAR observations of current fronts, for some of the case histories discussed in Chapter V.

SAR OCEAN IMAGING MECHANISMS

Over the ocean, an imaging radar obtains an instantaneous map of the short gravity wave field (1 to 30 cm) that is present as well as the variations in these short waves induced by currents, longer waves, winds, and surfactants. Understanding how these variations are produced and interact with the electromagnetic radiation is critical in deriving quantitative information from radar imagery. At present, extensive research has been conducted in determining the theoretical basis for imaging of surface waves but the critical evaluation of these theories based on experimental results under a variety of conditions has been limited (see the thorough review by Hasselmann *et al.*, 1985; Alpers *et al.*, 1986). Theoretical work has also been done on internal wave and bathymetry imaging mechanisms (Alpers and Henning, 1984; Alpers, 1985) but little work has been conducted on circulation features and atmospheric-related mesoscale conditions such as rain cells and windows. With sound imaging theories substantiated by experimental conformation, it may be possible to determine directly from the radar data the energetics of the features in question. Algorithms could then be developed to utilize the quantitative information to derive useful geophysical data, in combination with other quantitative sensor data or alone, possibly on both a regional and global basis.

For SAR imaging the ocean over a range of incidence angles from about 20° to 70°, the radar backscatter is principally caused by a resonant mechanism, called Bragg scattering, where the radar energy is scattered by surface waves of approximately the same wavelength. The short surface waves are modulated by long waves and currents, causing sufficient variability that can be seen on the high-resolution radar imagery.

For SAR imaging of ocean waves, the modulation is caused by three principal processes, each of which varies in strength depending on the surface wave propagation direction with respect to the radar velocity vector (e.g., Table 2 in Hasselmann *et al.*, 1985). For range-traveling waves, image variability is mainly produced by surface tilt, which is the change in local incidence angle of the short waves present along the long wave and by hydrodynamic interactions (also called straining), where the long wave alters the amplitude of the surface waves by convergence and divergence and airflow variations (Figure D.1). For azimuth traveling waves, the principal cause of image variability results from velocity bunching where the orbital motion of the long waves themselves produces an azimuthal displacement of the Bragg waves in the image plane (Figure D.2). For ocean waves having a high-azimuth directional component, this mechanism also causes image smearing at higher azimuth wave numbers. Velocity bunching is linear for low-azimuth wave numbers (i.e., long low swell) (Alpers and Bruening, 1986; Alpers, 1983) and when the altitude of the SAR platform is less than about 300 km (Beal *et al.*, 1986a; Alpers *et al.*, 1986).

Other ocean features are imaged by SAR through a variety of mechanisms. The convergent and divergent current components of shallow internal waves modulate the short surface waves and accumulate surface films to produce both bright and dark bands on the ocean surface which are detectable by a radar (Alpers, 1985). Similar current mechanisms account for detection of bathymetry features (Alpers and Henning, 1984). Additionally, shallow bathymetric features may be detected by the internal waves generated by them and surface wave refraction around them. Currents, rings, and eddies are presumably imaged in the following ways: (1) variations of short waves at a current shear boundary caused by a discontinuity in wind velocity, or wave refraction, caused by the shear and/or convergence of the surface velocity field at the boundary; (2) a sharp temperature gradient, which may be present for all three types of features that alters the stability of air flow across the boundary and therefore sea surface roughness; and (3) the current motion which can produce measurable Doppler shifts in the azimuth direction. The third mechanism may only be applicable for current velocities higher than those of eddies (~ 1 m/s) and at incidence angles greater than approximately 40°. No extensive studies have been conducted on the first two mechanisms.

Understanding the physics of the interaction of radar waves and ocean features is critical to producing geophysical information from such observations. From numerous SAR studies on ocean waves, there is enough understanding to show that high quality information from ocean waves will be possible from the Eos altitude in certain situations. Fortunately, mapping of currents, eddies, fronts, internal waves, bathymetric features, and wind fields should not be critically affected by platform altitude. As a matter of fact, the wider swath resulting from the higher altitude is considered a benefit for feature mapping. Accurate wave spectra measurements, however, may not be possible at Eos altitudes, as explained below.

SAR will interpret the radial motion of a scatterer as a change in position since it depends on the accurate measurement of the target radial velocity to determine the azimuth location. A scatterer with a radial velocity will produce an azimuth displacement of:

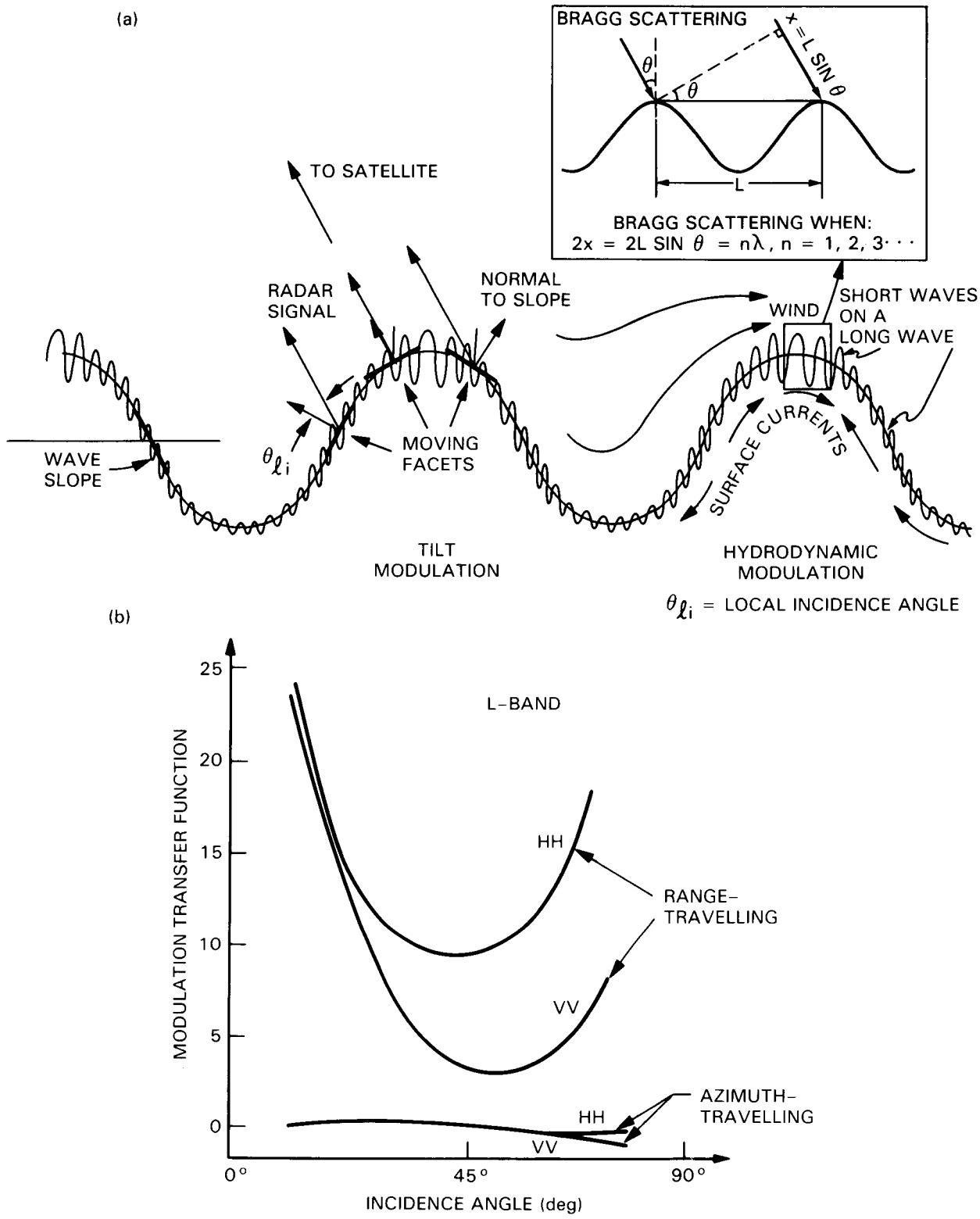

Figure D.1. (a) Illustration of surface tilt and hydrodynamic interactions that affect the SAR imaging of ocean waves. (b) Tilt modulation transfer function (dimensionless) as a function of incidence angle for HH and VV polarizations for both range-traveling and azimuth-traveling ocean waves (after Alpers *et al.*, 1981).

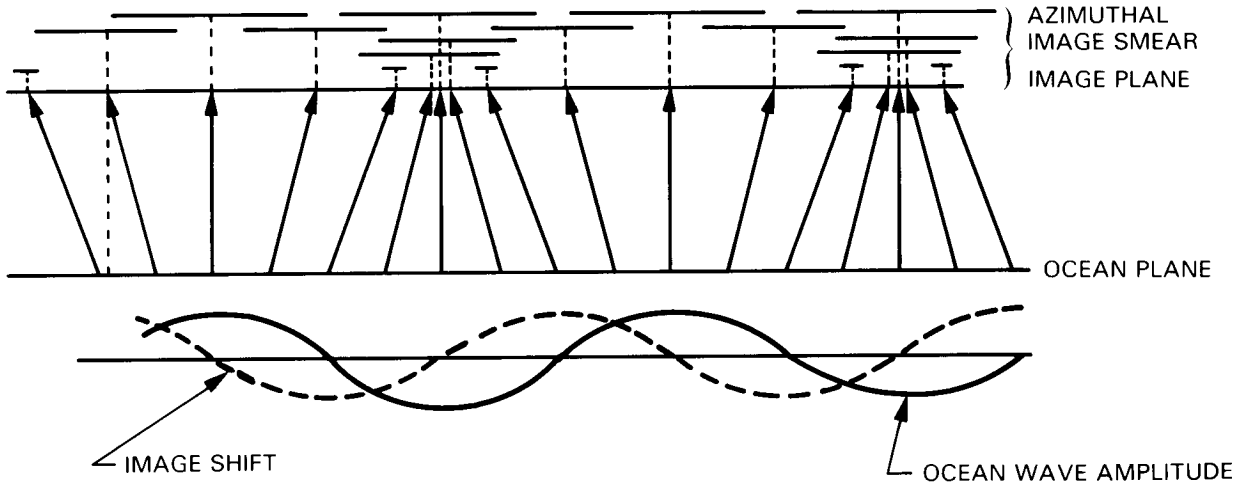

(a)

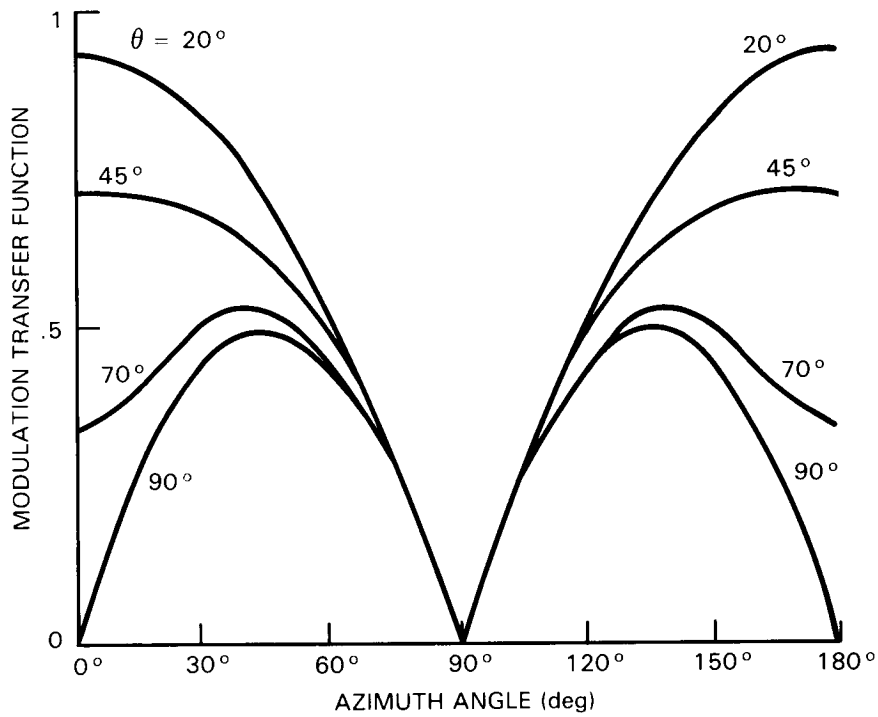

(b)

Figure D.2. (a) Illustration of velocity bunching for SAR imaging of azimuth-traveling ocean waves from a side view. Equally spaced components of the ocean surface wave or plane are non-uniformly displaced on the SAR image plane and have variable degrees of azimuth smearing (after Alpers, 1983). (b) Dependence of velocity bunching modulation transfer function (dimensionless) for SAR imaging of ocean waves on azimuth angle, defined as the angle between wave direction and spacecraft flight direction and SAR incidence angle.

$$x_d = (R/V)\, v_r \qquad \text{(D-1)}$$

where R/V is the range-to-velocity ratio of the platform and v_r is the radial velocity component. Thus, a low altitude SAR (250 to 300 km) could be a valuable adjunct to operational wave forecasting, but the increased Doppler contamination present at higher altitudes results in SAR wave spectra of limited utility, except for long low swell and waves traveling nearly perpendicular to the flight path of the satellite (Alpers and Bruening, 1986). The Seasat wave spectra acquired from an 800 km altitude clearly show

the effects of this contamination, with severe non-linearities occurring near hurricanes (Gonzales *et al.*, 1982; McLeish and Ross, 1983; Alpers, 1983), while the more recent SIR-B spectra acquired from a 225 km altitude confirm the expected improvement at low altitude (Alpers *et al.*, 1986; Beal *et al.*, 1986a). Unfortunately, even the low altitude Eos option of 542 km exceeds the optimum altitude for accurately measuring wave spectra by about a factor of two.

SOME SEASAT RESULTS

Current Boundaries, Oceanic Fronts, and Eddies

SAR imagery from Seasat demonstrated that current-system boundaries, oceanic fronts, and mesoscale eddies can be detected via their influence on the short gravity waves responsible for L-band microwave backscatter. Figure 37 shows the strong expression of a Gulf Stream eddy seen in Seasat SAR imagery. The mechanisms by which SAR detects these phenomena are not well understood. In at least some situations, it is likely that current gradients modify the spectrum of short waves, producing the microwave backscatter. In other instances, or perhaps concurrently, sea-state changes can also be induced by sea-surface temperature variations that alter the atmospheric boundary-layer stability, giving rise to local variations in wind drag. A third mechanism, azimuthal displacements in the SAR image plane due to Doppler frequency shifts from variable current components along the radar look direction, has also been advanced.

To illustrate the potential of SAR for circulation (i.e., current boundary) monitoring, Figure D.3

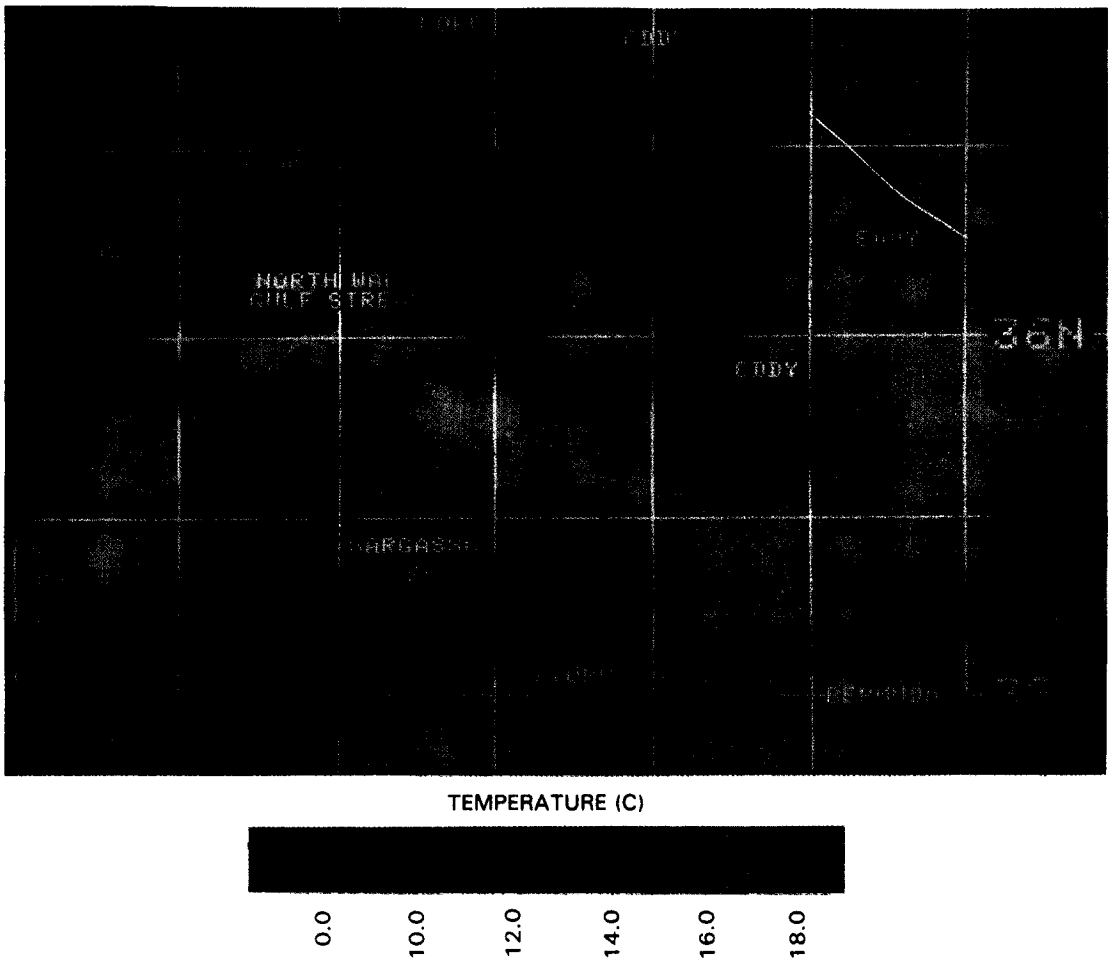

Figure D.3. NOAA-7 infrared false color image of the North Atlantic at 10.3 to 11.3 μm (from cover of *Trans. Amer. Geophys. Union, 66,* 1985).

shows the thermal structure of the Gulf Stream in April 1983 as measured by the NOAA-7 satellite in the 10 μm band. This region corresponds closely to one of those depicted in Figure 43 as one of the most highly variable areas in the world. The boxed areas in Figure D.3 correspond to regions imaged by the Seasat SAR in 1978, and shown in Figures 35, 36, 37, and D.4. This simple example indicates the strength of SAR for precisely locating current boundaries and bathymetric features with a precision and sensitivity unmatched by other sensors. The geostrophic sampling of the altimeter at 10 km along-track resolution (but many hundreds of km cross-track spacing), and the thermal sampling of the Advanced Very High Resolution Radiometer (AVHRR), HIRIS, and MODIS at similar or higher resolution, will all lack precise current boundary definition that could be provided by SAR. Additionally, in certain oceanic regions, for example the Gulf of Mexico, seasonal warming of surface waters drastically reduces any temperature contrast associated with current boundaries and eddies or meanders that normally would be detectable by AVHRR. Monitoring by a SAR of such regions in this warming period would reveal the location and movement of currents and eddies.

Figure D.4. This Seasat SAR image of Nantucket Shoals provides a dramatic example of bathymetric expressions occasionally evident over large areas. Most of the region included in this image is <40 m deep, a good fraction is <20 m deep, and portions are <2 m deep. The island of Nantucket is at the upper left.

Internal Waves

Internal waves in coastal oceans are among the oceanic phenomena most frequently observed by Seasat SAR. Shown in Figure 38 is a well-documented example in the Gulf of California (Fu and Holt, 1984). Clearly seen on the image is a series of wave packets generated by the strong tidal currents flowing through the islands. Each packet was generated during one tidal cycle. From the geometry characteristics of the wave packets as estimated from the image (e.g., distance between packets, number of crests in a packet, length of crest, etc.), Fu and Holt (1984) were able to estimate the amplitude of these waves and hence their rate of dissipation in the northern Gulf. Using SIR-B imagery and field observations along the New York Bight, Gasparovic *et al.* (1986) have shown favorable comparisons between observed SAR intensity signatures of internal waves with predicted signatures based on hydrodynamic and radar scattering models. Determining the wave amplitude and energy content of internal waves by their signatures on SAR will enable estimates to be made on the contribution of internal waves to coastal mixing.

Bottom Signatures

A number of investigators have noted a variety of SAR-observed ocean-surface patterns that are closely related to submerged bottom features (Kasischke *et al.*, 1984). Evidence of bottom-related signatures is widespread on Seasat SAR imagery (Figure D.4), although fortuitous tidal flows combined with low surface wind conditions are thought to be necessary. Valenzuela *et al.* (1985), in a study of backscatter related to bottom topography, found maximum surface manifestations when the surface winds were 7 m/s or less. This is consistent with the results of Lichy *et al.* (1981) on eddy signatures.

Atmospheric Effects

An excellent example of SAR's ability to acquire information about the interaction between the atmosphere and the ocean was acquired by Seasat SAR in the Gulf of Mexico.

Several tropical rain cells were imaged about 160 km east-southeast of New Orleans (Figure D.5a). The cell centers have a low radar return because the sea surface is smoothed by the heavy rainfalls that damp the short capillary/gravity waves, whereas the areas surrounding the cell centers have a high radar return because the sea surface is roughened by the wind squalls that carry the cold, descending air away from the cell centers. The distinct boundaries between the wind squalls and surrounding calm water are squall lines.

The enhanced GOES (Geostationary Operational Environmental Satellite) infrared image of this area (Figure D.5b), taken about 13 minutes before the

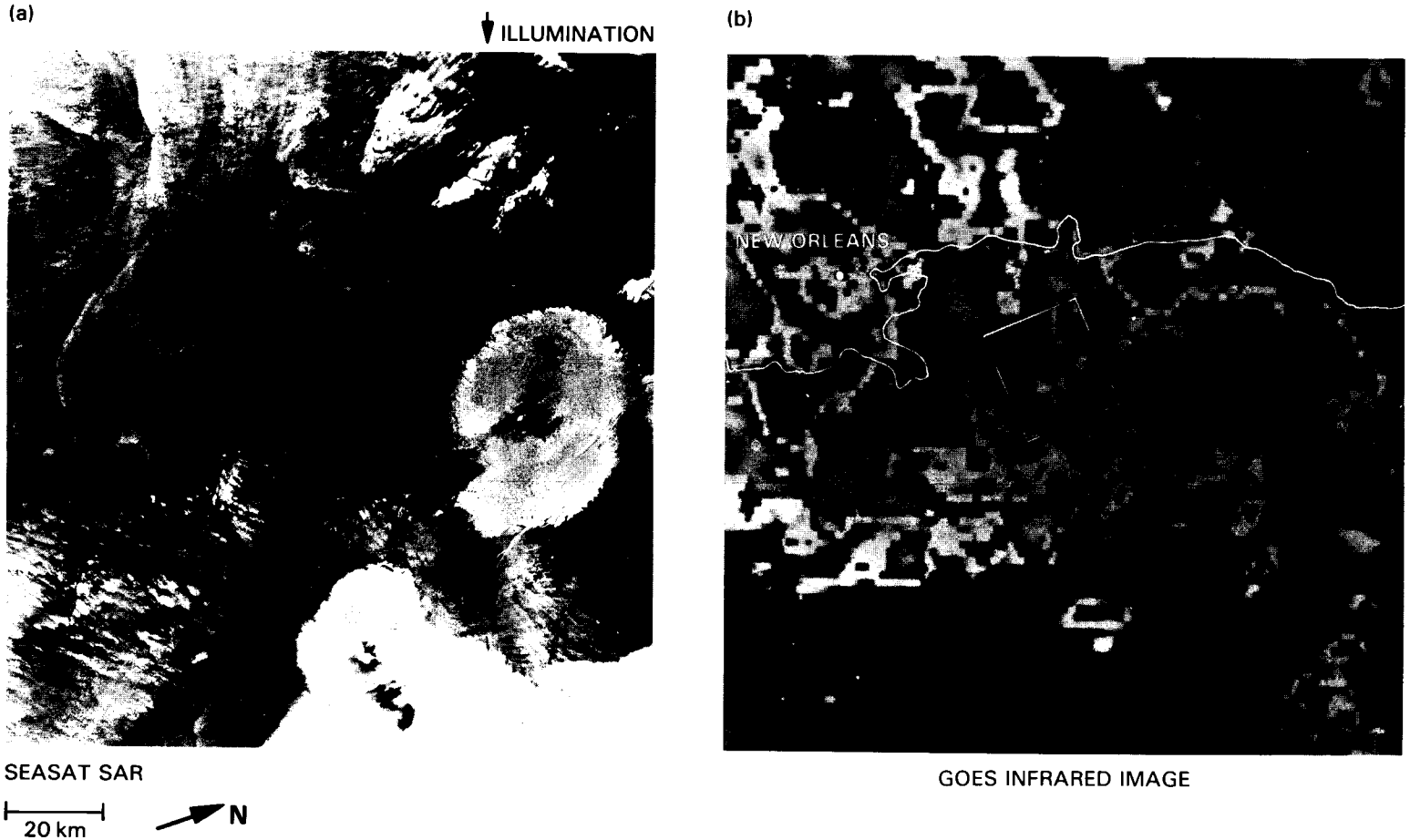

ORIGINAL PAGE
BLACK AND WHITE PHOTOGRAPH

Figure D.5 Tropical rain cells in the Gulf of Mexico as imaged by the Seasat SAR (Fu and Holt, 1982).

Seasat pass, indicates that the SAR-imaged area was on the western edge of a convective storm system (the elongated dark region) with cloud-top temperatures generally below -30°C. Note that the rain cells on the SAR image are represented by two dark spots (cold clouds) and a less distinct, brighter (warmer clouds) feature at their corresponding locations on the infrared image. This comparison indicates that the rain cell in the center of the SAR image was probably decaying.

APPENDIX E: GEOLOGY—ADDITIONAL INFORMATION

This appendix provides a brief discussion of some radar geology case histories that are relevant to the specific Eos science objectives discussed in Chapter VI.

CRUSTAL STRUCTURE AND PLATE TECTONICS

This section presents additional material, references, and radar images to support the discussion of crustal structure and plate tectonics. Plate tectonics provides a basis for understanding the distribution and origin of mineral and energy resources in space and time. The occurrence of energy and mineral deposits can be related to plate tectonics in three ways (Condie, 1982): (1) geological processes driven by energy liberated at plate boundaries control the formation of energy and mineral deposits; (2) such deposits form in specific tectonic settings, which are in turn controlled by plate tectonics; and (3) reconstruction of fragmented continents can be used in exploration of new mineral and energy deposits. The common surface indicators signaling mineralization include fracture zones, veins, and rock type associations. The sites of igneous plugs, or volcanic centers in general, are highly prospective for metal mineralization. The margins of discrete igneous intrusive bodies are similarly prospective, especially where dike swarms, radial faults, or other tensional fractures coincide (MacDonald, 1976). Figure 47 is an example of dikes appearing on a SIR-A image.

Geologic studies using radar imagery have delineated potential mineralization areas (Wing, 1970). However, few such investigations have been published owing to the fact that most commercial radar mapping programs are conducted "in-house" by energy and mineral companies. Areas of extensive radar mapping for mineral, land resource, and other commodities include Brazil, Venezuela, Colombia, Panama, Nicaragua, Indonesia, New Guinea, Australia, and sections of the United States (MacDonald, 1976). In 1972, President Rafael Caldera of Venezuela announced a new mineral find "of great importance," including iron and possible uranium, as a result of radar mapping of the southern one-third of Venezuela. Of course SAR imagery itself did not show mineral deposits, but indicated to geologists where ground surveys should occur, which were later carried out successfully.

Condie (1982) has pointed out that several requirements must be met in any tectonic setting for the production and accumulation of hydrocarbons such as oil and natural gas. The preservation of organic material requires restricted seawater circulation to inhibit oxidation and decomposition. High geothermal gradients are needed to convert organic matter into oil and gas. Finally, tectonic conditions must be such as to create traps for the hydrocarbons to accumulate. Several tectonic settings meet these requirements (Condie, 1982). One of the few published reports dealing specifically with radar mapping and petroleum exploration was completed in eastern Panama and northwestern Colombia (Wing and MacDonald, 1973).

The economic payoff for these investigations could be significant with development of more efficient mineral resource exploration techniques; the science payoff would be in gaining a better understanding of the crustal evolution and the tectonic overprint on a global scale. SAR sensors offer considerable potential and are often considered the sensor of choice for portraying crustal tectonic fabrics and other related landforms. This is mainly due to SAR's capability to provide its own illumination at various incidence and azimuth angles, and the sensitivity of microwave radiation to various scales of surface roughness (Dellwig *et al.*, 1968; MacDonald and Waite, 1970, 1973; Wing, 1970; MacDonald, 1976; Wadge and Dixon, 1984; Sabins, 1978, 1983; Ford, 1980; Ford *et al.*, 1980, 1983; Cimino and Elachi, 1982; Koopmans, 1983; American Society of Photogrammetry, 1983; Elachi *et al.*, 1982; Froidevaux, 1980). These sensitivities are illustrated by Figures 46 and 47, and Figures E.1 and E.2.

Stereo viewing (Leberl *et al.*, 1986), digital registering (Rebillard and Nguyen, 1982) and direct comparison (Chavez *et al.*, 1983; Ford *et al.*, 1983) of spaceborne SAR and Landsat imagery have also been shown to significantly enhance interpretability of the structural and other geologic aspects of a terrane as shown in Figures 48 and 60. Thus, one major objective for a thorough investigation of crustal evolution and plate tectonics using Eos SAR, in conjunction with other sensors such as HIRIS, is to understand better the association of tectonic features with major deposits of economic mineral resources, and thus to locate and develop new potential resource areas.

SIR-A Images of Indonesia

Indonesia was selected as a SIR-A test site for the following reasons (Sabins, 1983): (1) the persistent cloud cover has hampered acquisition of images and photographs in the visible spectrum from aircraft and satellites. Clouds and rain, however, are readily penetrated by radar sensors, such as SIR-A, to produce useful images; (2) Indonesia provides a representative test site for the geological utility of images of heavily vegetated terrain. Although radar does not completely penetrate the foliage due to volume scattering, geologic features are commonly enhanced on radar images by subtle changes in topog-

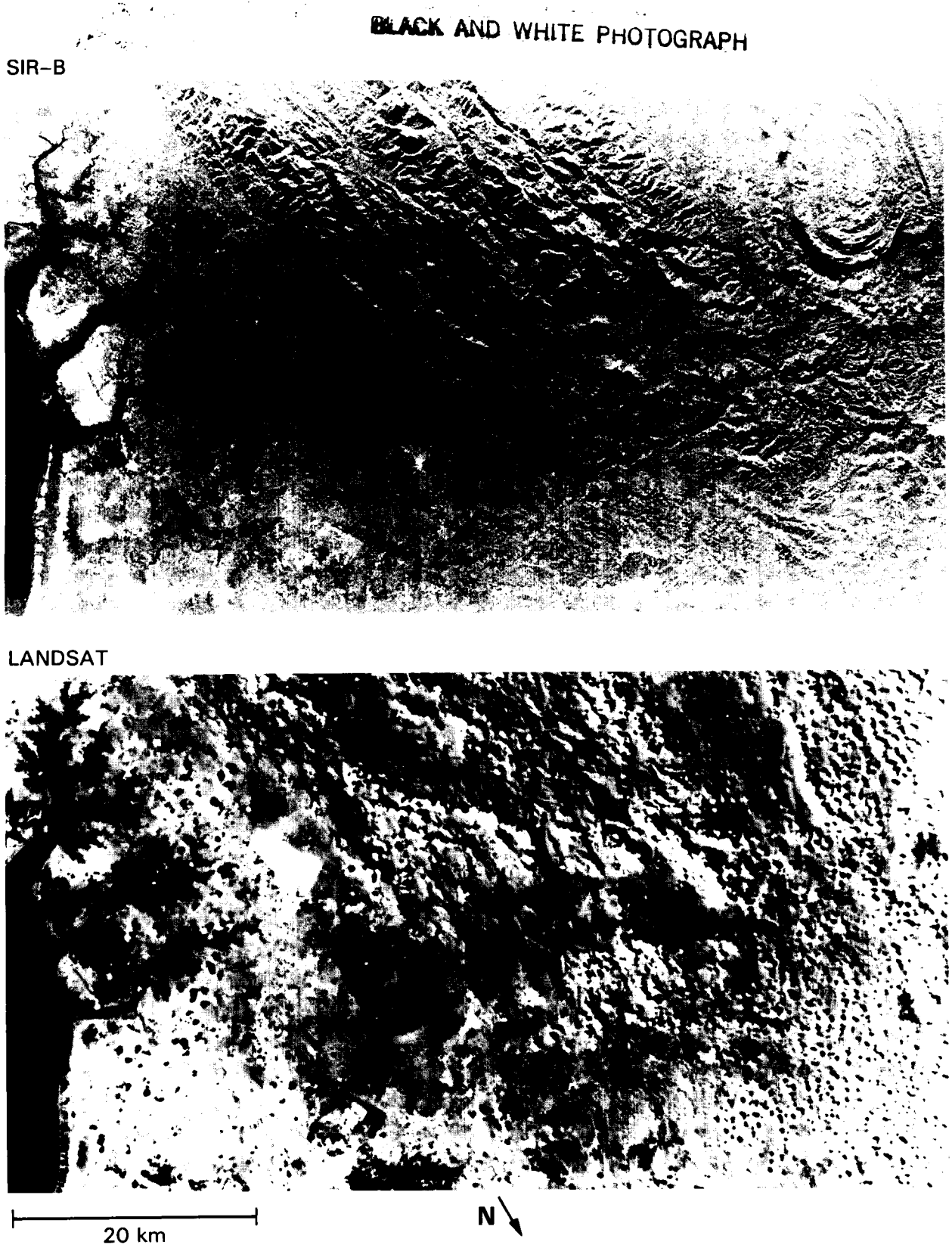

Figure E.1. SIR-B image of the Pasir Mountains and adjacent coastal lowlands located west of Balikpapan in East Kalimantan, Borneo. The SIR-B image enhances terrain features and reveals a widespread pattern of folded layered rocks in densely forested mountainous areas. The mountainous areas on the corresponding Landsat infrared image are partially obscured by cumulus clouds; complete cloud cover is very common in this region (from Ford *et al.*, 1986).

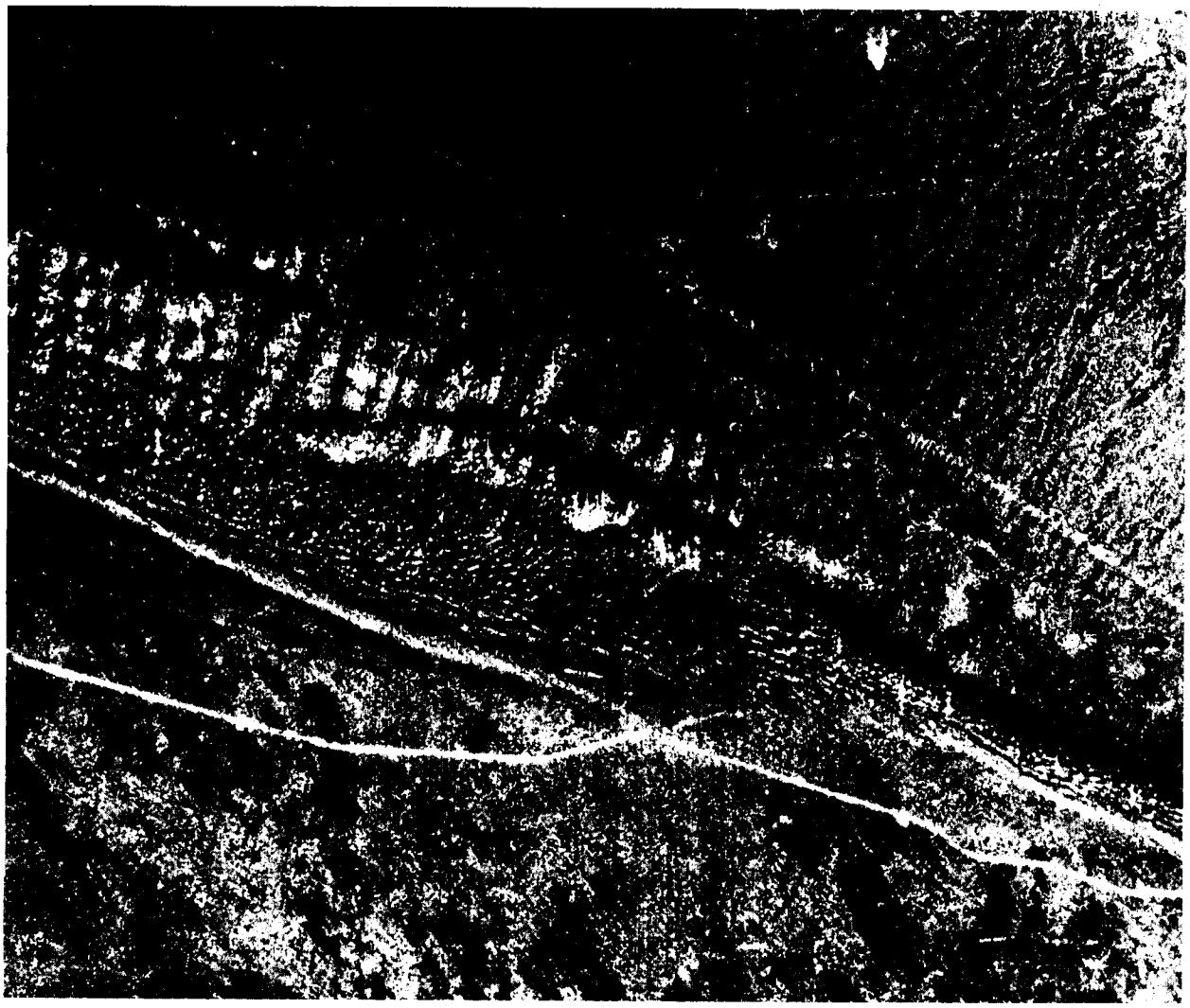

Figure E.2. Seasat image of the Algodones Dunes in southeastern California near the Arizona and Mexico border clearly showing the dune morphology at the low 20° incidence angle.

raphy underlying the vegetation canopy; (3) because of its present and potential petroleum reserves, Indonesia is an excellent site for evaluating satellite radar images for energy exploration; and (4) a wide variety of rock types and structures occurs in Indonesia, providing the opportunity to establish the radar signatures of these features.

SIR-A images of Indonesia have been classified by texture into six major terrain categories that correspond to carbonate rocks, clastic rocks, volcanic rocks, alluvial deposits, melange complexes, and metamorphic rocks. In the Vogelkop region (Figure E.3), the stratigraphic succession of four terrain categories was readily interpreted. Geologic structures were identified at two different scales: (1) major tectonic elements such as foldbelts, uplifts, and basins are recognizable because the 50 km wide SIR-A image strips cover hundreds of kilometers along the orbit path; and (2) individual structures, such as faults and folds, are detectable because the 40 m resolution of SIR-A is well-suited for displaying features with dimensions of hundreds to thousands of meters (Figure 46). In the Vogelkop region (Figure E.3), a prominent lineament marks the Sorong fault, and the left-lateral strike-slip nature of this fault is confirmed by presence in the SIR-A image of offset drainages, shutterridges, and scarps. The Koor fault shown in Figure E.3 is marked by a composite lineament of scarps and linear drainages. Sabins (1983) found that lineaments are generally expressed on the SIR-A images as escarpments, linear drainages, and aligned drainage segments. He found good correlation between image lineaments and previously mapped faults. Other reports describing the potential

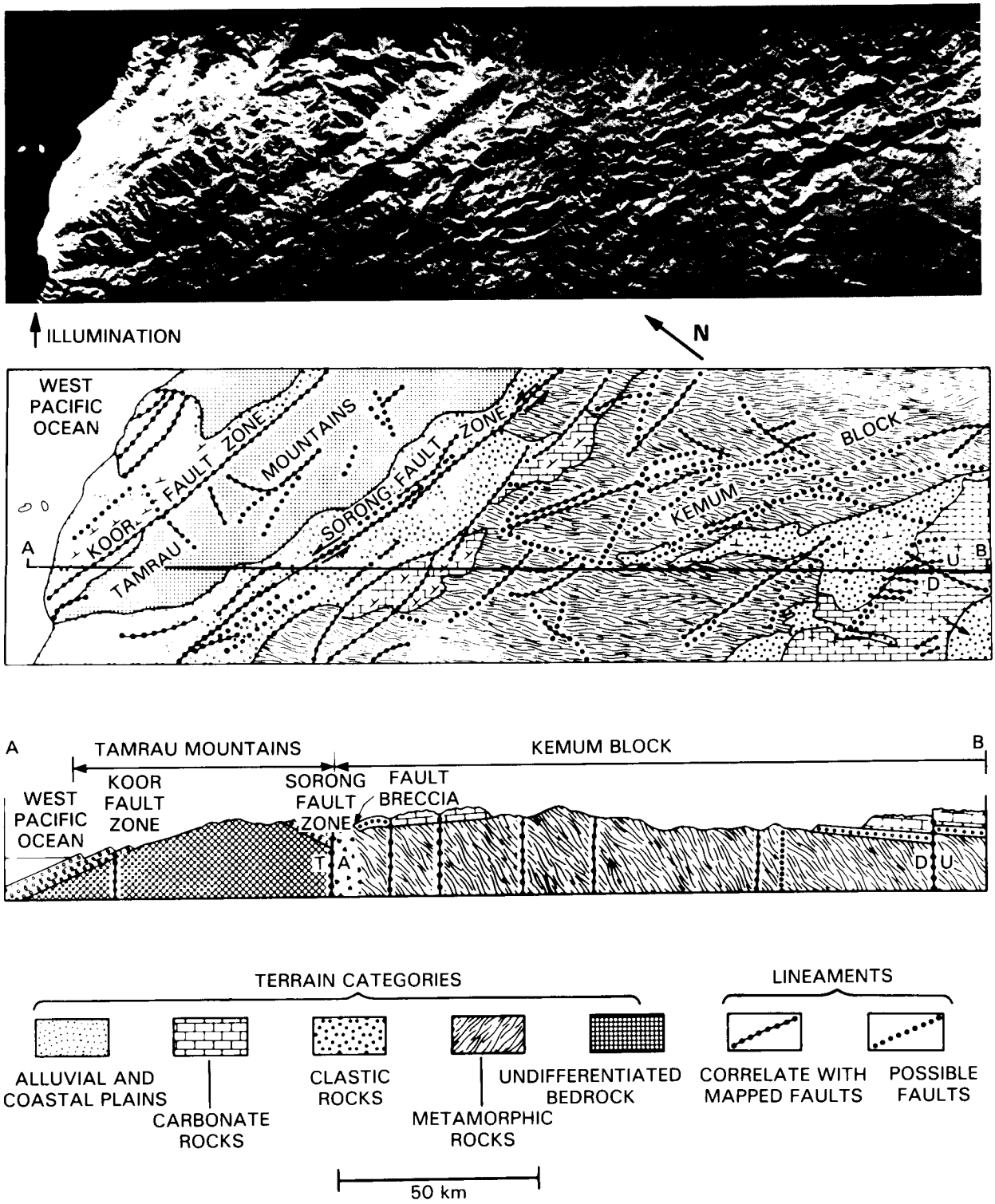

Figure E.3. Geologic map and cross section interpreted from SIR-A image in the Vogelkop region of Irian Jaya, Indonesia (Sabins, 1983.)

of spaceborne SAR images for geologic structure interpretations include those by Froidevaux (1980), Sabins *et al.* (1980), Wadge and Dixon (1984), Ford (1980), and Ford *et al.* (1980; 1983).

ARID LANDS SAR INVESTIGATIONS

Paleodrainages of the Eastern Sahara

SIR-A data revealed previously unknown paleodrainage networks in the shallow subsurface of the eastern Sahara in the extremely dry region of southern Egypt and northern Sudan (McCauley *et al.*, 1982). Although reduced in transmitted power because of technical malfunctions, SIR-B verified the findings of SIR-A in this region (McCauley *et al.*, 1986). Evidence of a long and complex fluvial history in this now hyperarid and uninhabited core of the Sahara is seen on radar images as well-defined networks of broad alluvial valleys, sets of braided channels inset into the aggraded floors of these valleys, and by long, narrow, bedrock-controlled channels incised in the adjacent interfluves. The topographic expression and the Landsat response of the broad alluvial valleys and superposed braided channels in southwest Egypt and northwest Sudan is so vague that these types of "radar rivers" were not recognized prior to SIR-A (Figures 49 and E.4). Parts of the incised channels, on the other hand, are visible on enhanced Landsat images, and are progressively better defined as the overlying eolian blanket becomes less continuous and overall aridity decreases in a southwestern direction toward Chad and Libya.

Extensive fluvial denudation of extreme southwest Egypt was suspected prior to the SIR experiment, based on regional field relations (McCauley *et al.*, 1981). However, the magnitude and geographic extent of the buried paleodrainages were not anticipated until the shallow subsurface imaging capabil-

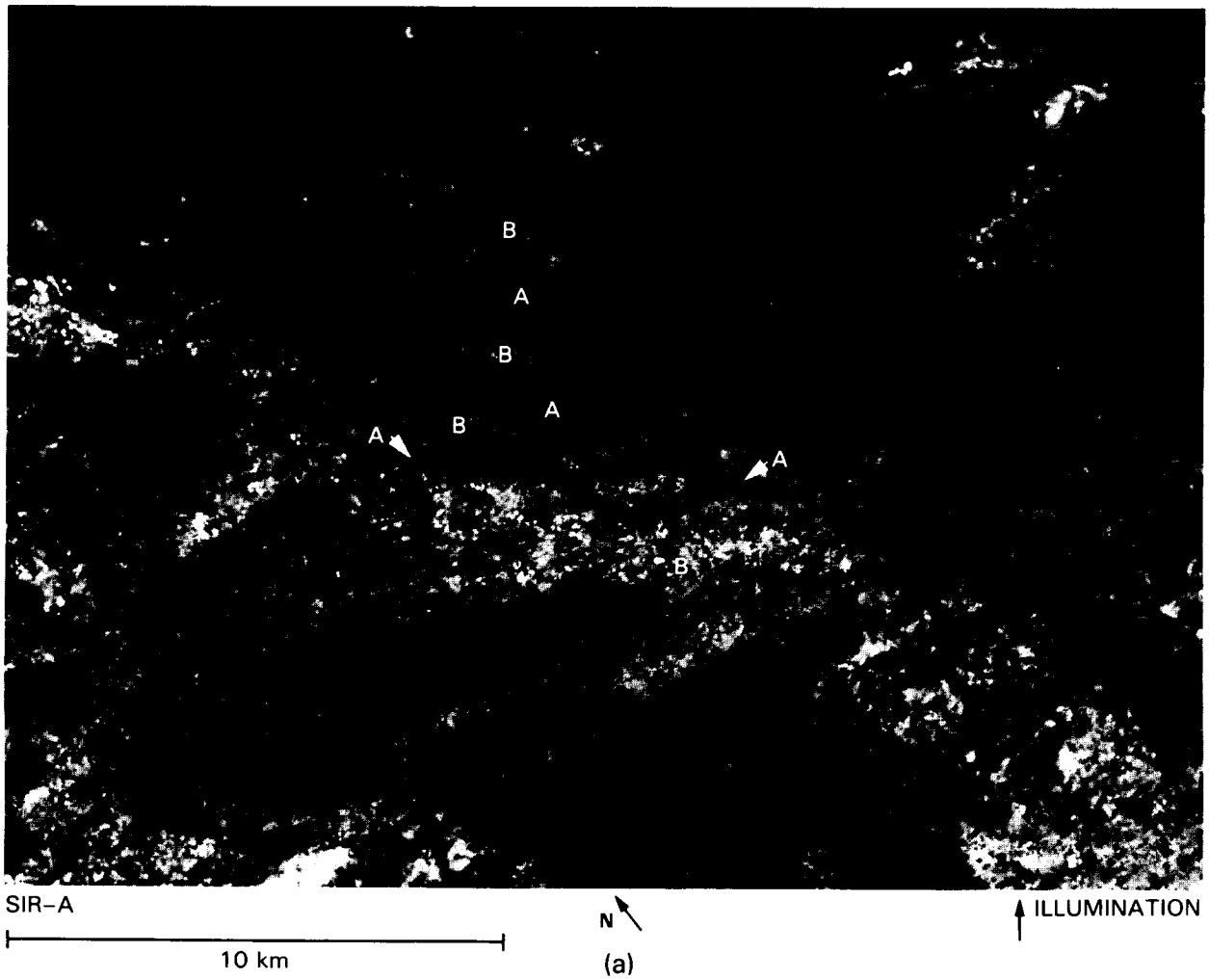

Figure E.4. Area south of Safsaf oasis in extreme south-central Egypt (Schaber *et al.*, 1986). (a) Part of the SIR-A image showing previously unknown braided stream channels of probable late Pleistocene age: (A) older fluvial sands cut by the channels and (B) abundant $CaCO_3$ nodules and rhizoliths (calcified root casts) in upper 1 to 2 m of surface cause significant volume scattering (above), (b) Part of Landsat-3 MSS band 7 image (following page). Note pervasive sand cover in area of braided channels revealed on SIR-A image.

ities of the SIR were brought to bear on the eastern Sahara. The SIR data, used together with Landsat pictures and supplemented by field studies, changed the common concept of the region from that of a surface reduced to its present essentially level configuration chiefly by wind erosion to that of a broad pediplane cut by major Tertiary river systems (10 to 30 million years ago), long before the onset of Quaternary aridity and takeover of the surface by eolian processes.

A major question to be considered is how the fluvial activity in the radar rivers relates to existing models of climate change in northeast Africa. The presence of high-bedload, braided channel complexes or strings of lakes of Late Quaternary age, inset into the older aggraded floors of the major river valleys, suggests a correlation between desert riparian environments and episodic Stone Age occupations. The large number of *in situ* stone artifacts found in the course of excavations in and near presumed radar river banks or terraces strengthens this inference (McCauley *et al.*, 1986).

Additional questions raised by the SIR-A results center around the ages of the various types of radar rivers, their sources, and debouchment areas. Answers to these questions would help determine whether any of the "radar rivers" were related to the ancestral Nile or to any of its relatively youthful descendents. The major alluvial valleys recognized to date on the SIR-A and SIR-B strips appear to trend west and south. SIR-based mapping of these paleodrainages, although incomplete, was used by McCauley *et al.* (1986) to reveal missing links in an area once thought to be devoid of master streams. A former trans-African master stream system is suggested by McCauley *et al.* (1986) to have possibly flowed from headwaters in the Red Sea Hills (Egypt and Sudan) southwestward across North Africa, discharging into the Atlantic at the Paleo-Niger delta, prior to the Neogene domal uplifts and building of volcanic edifices across the paths of these ancient watercourses.

Prior to the SIR missions, a few workers attempted pre-Nile reconstructions of the regional

(b)

paleodrainage, but these suffered from an unfortunate tendency to try to force the inferred rivers to the north and east—in accord with the present regional slope and drainages in northeast Africa. A further hindrance to this work was the lack of reliable junction angle data as well as maps or pictures, so that stream flow directions could not be determined. SIR-A provided good junction angle data but is ambiguous in places because of the sparse coverage. Future SIR experiments (SIR-C and SIR-D) will provide additional, yet limited, coverage of the eastern Sahara and other major desert areas, however complete maps of these arid regions are essential to the solution of problems such as these.

SIR Signal Penetration and Backscatter in the Eastern Sahara

Field examination of the "radar rivers" in the eastern Sahara subsequent to SIR-A has verified at least 12 separate surface and near-surface permittivity interfaces responsible for seven mappable variations in tone on the SIR data (Schaber *et al.*, 1986) (Figure E.4). Seventy-five hand-dug pits and 82 backhoe trenches were studied, sketch-mapped, and sampled in order to better define the radar response of various surface and subsurface materials and inhomogeneities in electrical properties. Volume scattering from calcium carbonate nodules and subsurface backscatter from more discrete carbonate and bedrock interfaces within the upper meter of alluvium were found, in conjunction with backscatter from isolated grazing outcrops, to play important roles in moderating the SIR signals, and thus enhancing detection of sand-buried stream channels (Schaber *et al.*, 1986) as shown in Figure E.4. The secondary carbonate horizons in this region of the eastern Sahara are developed within a sequence of alluvial and colluvial deposits; and are disconformably overlain by sand sheets, dunes, and sediments of mixed origin that record the important and little understood interplay of geologic processes under variable climatic conditions culminating in the present extreme aridity.

SIR signal penetration resulting in recorded subsurface backscatter (called "radar imaging depth" by Schaber) was documented from field investigations in the eastern Sahara to reach a maximum of 1.5 m in the eolian sand sheet and sand-to-small pebble alluvium, and between 2 and 3 m in active dune sands (Schaber *et al.*, 1986). These values are about 25 percent of the calculated electrical "skin depths" for these materials. Signal penetration and subsurface backscatter from shallow dielectric interfaces and volume scattering in the upper meter or so of the sand sheet are enhanced both by parameters of the SIR-A and SIR-B sensors (wavelength, incidence angle, HH polarization; Elachi *et al.*, 1984) and by the physical and chemical characteristics of the surficial deposits. Pertinent physical characteristics are (a) a favorable distribution of particle sizes and density of materials, (b) low clay content, and (c) extremely low moisture content. Laboratory measurements of electrical properties and modeling of DC conduction, water, and scattering losses for the eastern Sahara materials were used by Schaber *et al.* (1986) to show that the SIR-A and SIR-B frequency (1.3 GHz) is within the narrow optimum range (1 to 20 GHz) for both maximum penetration (minimum scattering losses) and for contrast between the eolian and alluvial sediments in this specific region. Geometric scattering is the dominant loss mechanism for these sediments in the absence of sufficient moisture to activate dielectric relaxation loss mechanisms associated with water.

This pioneering SIR investigation in the eastern Sahara has set the stage for subsequent experiments and provides a model for effective and vital coordination of radar data analysis of megageomorphic and geologic field investigations in deserts worldwide.

SAND DUNE INVESTIGATIONS, DESERTIFICATION

No SAR investigation has systematically addressed the critical problem of desertification. However, there have in recent years been some enlightening investigations of the radar responses from sand dunes (e.g., Breed *et al.*, 1982). Blom and Elachi (1981) compared Seasat SAR L-band images (23.5 cm wavelength; HH polarization), aircraft SAR X-band images (3 cm wavelength; HH polarization), Landsat images, and air photographs of five areas of sand dunes in the southwest United States and northwestern Mexico (Figure 51). The sand dunes studied were found to behave as smooth surfaces for both L- and X-band wavelengths; i.e., the reflection of radar energy from the dunes was specular. The measured surface irregularities on the dunes were found to be inadequate to cause either Bragg or incoherent (diffuse scattering) on the incident radar beam in the X- to L-band wavelength region. The fact that dunes are characterized by a total absence of small surface scatterers of high permittivity contrast with the sand (no rocks), no diffuse or volume scatter from buried inhomogeneities occurs and the surface appears smooth, although relief on the dunes can be hundreds of meters. This results in dunes that appear dark when imaged at incidence angles greater than the angle of repose because none of the dune faces are oriented properly (normal to the radar antenna beam) to reflect a specular response to the antenna (Figure 51d). Blom and Elachi (1981) found that imaging radar resolution must be adequate to define the changing morphology of dune faces. Linear dune features with interdune spacing of less than three to four resolution elements are not recognizable. They also found that distributed dune-types such as barchans or star dunes must be more than 10 resolution elements in each direction to be defined on SAR im-

agery. At least two SAR look azimuths were found to greatly facilitate interpretation of dune morphology and hence conclusions about causative wind regimes.

In the application of SAR image data to monitoring desertification, the radar-dark character of active sand sheets and dunes is a very positive attribute. The encroachment of dune sand and drift sand onto arable and other cultural regions should be easily monitored through changes in the spatial relations between brighter, higher backscattering terrains such as vegetation or natural rough surfaces, and radar-dark active drift sand. Of critical importance, however, is to acquire SAR data with maximum resolution and as many frequencies and look directions as possible.

APPENDIX F: SUMMARY OF SAR PRINCIPLES

Detailed discussions of the principles of SAR and SAR design techniques may be found in a number of books such as Hovanessian (1980) and Ulaby *et al.* (1982). Even though a treatment of SAR principles is outside the scope of this report, a brief summary of some of more critical elements is presented to amplify some of the points raised in Chapter VIII.

SAR is composed basically of a transmitter and modulator, an antenna, a receiver, a data recording and handling mechanism, and a processor whose output is a SAR image (Figure F.1). The Eos SAR will effectively be a suite of three SARs, one operating at L-band (1.248 GHz), a second at C-band (5.298 GHz), and a third at X-band (9.600 GHz). To illustrate the operation of SAR, we will consider the C-band channel operating at 5.298 GHz. The output of the transmitter is a train of pulses; a switch directs a pulse to the antenna which then transmits the pulse to the Earth's surface where it is then scattered. The backscattered signal (radar echo) is detected by the antenna and directed by the switch to the receiver. The receiver's output is then a train of received radar echo pulses that are fed to the correlator.

ACHIEVING FINE CROSS-TRACK RESOLUTION

An imaging radar transmits a continuous sequence of pulses at a PRF of typically 1,500 pulses per second; each pulse would have a carrier frequency of 5.298 GHz and a pulse-width τ of typically 50 μs (Figure F.2).

Each transmitted pulse is scattered by the Earth's surface and thus a series of much weaker radar echoes arrives back at the SAR receiver. The time required for the pulse to make the round trip from SAR to a target at slant range R and back to SAR is

$$T = 2R/c \qquad \text{(F-1)}$$

where c is the speed of light and the factor of 2 is due to the round trip (see Figure F.3).

The resolution r_r along the slant range direction is determined by the pulse width, i.e.,

$$r_r = c\tau/2 \qquad \text{(F-2)}$$

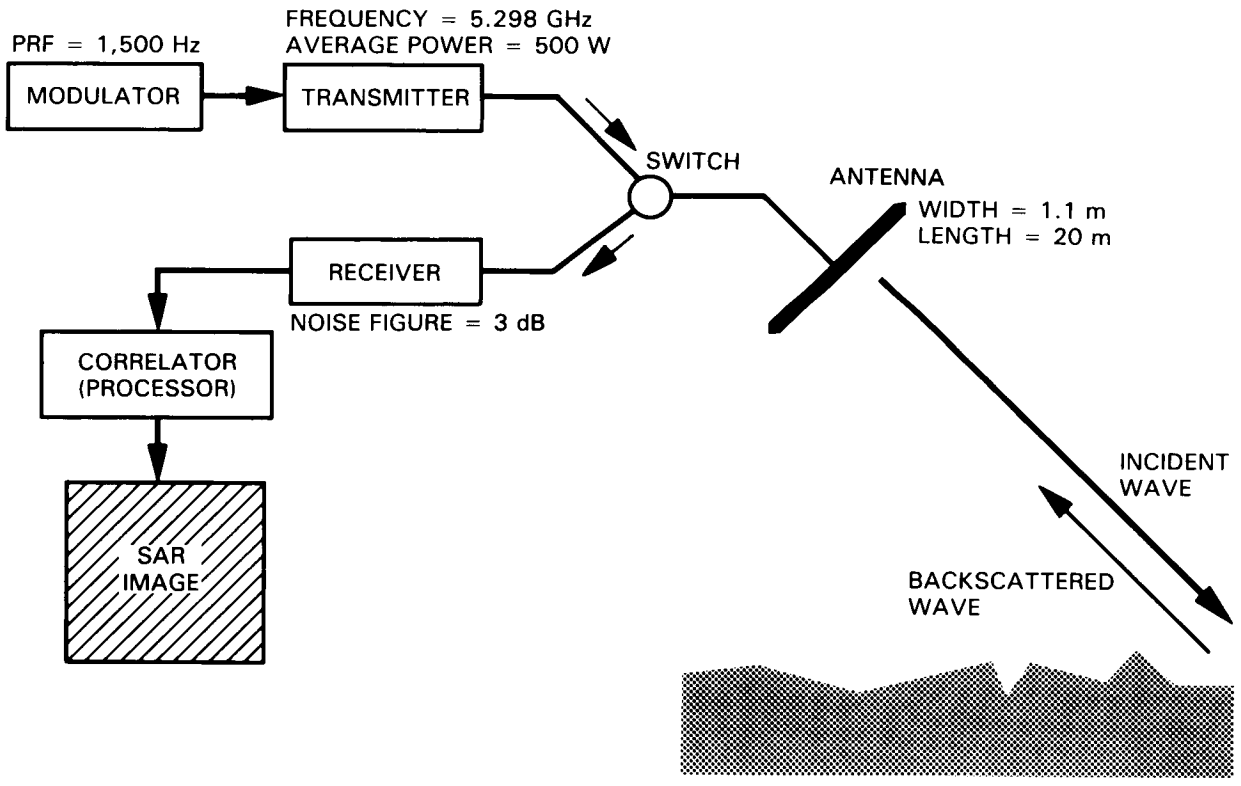

Figure F.1. Simplified diagram of a synthetic aperture radar; typical values are given for a C-band SAR.

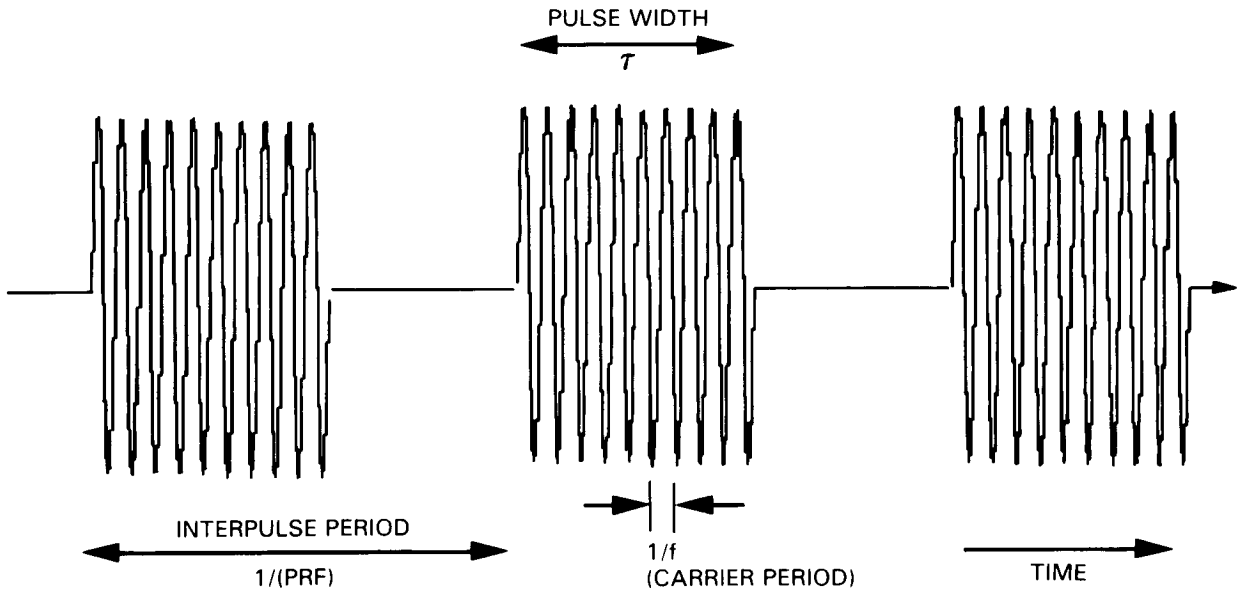

Figure F.2. A train of radar pulses with carrier frequency f, interpulse period 1/PRF, and pulse width τ. The sketch is not to scale, since the pulse width is much smaller than the interpulse period.

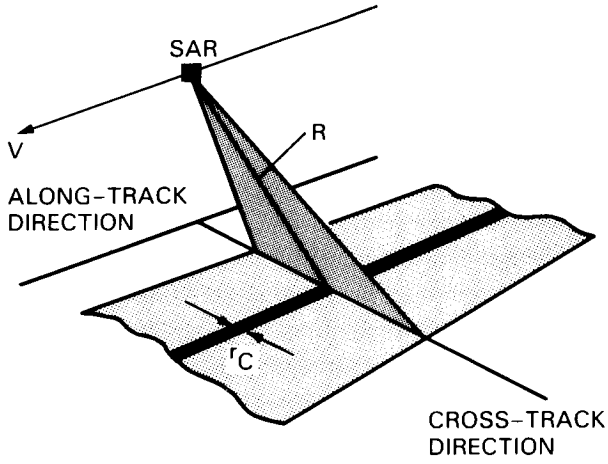

Figure F.3. Illustrating the cross-track resolution of a SAR.

Thus the resolution in the cross-track direction is given by

$$r_c = c\tau/(2 \sin \theta) \qquad \text{(F-3)}$$

where Θ is the angle of incidence. Thus, the range resolution is governed by the pulse width and incidence angle; range resolution is best at large incidence angles.

The pulse width is determined by the transmitter bandwidth; larger bandwidths produce narrower pulses and thus finer-range range resolution. Fine-range resolution is obtainable when the transmitted pulses are chirp modulated (linear FM) and the receiver bandwidth is sufficient to allow matched filtering of the received radar echoes.

ACHIEVING FINE ALONG-TRACK RESOLUTION

In order to achieve fine along-track resolution from imaging radars at orbital altitudes, it is necessary to utilize a Doppler beam-sharpening approach. This basic principle of SAR was first developed by Carl Wiley in the early 1950s. The basic SAR technique is to record a series of radar echoes that are received from a ground target and that are Doppler shifted due to the motion of the radar, focus these returns through a special processor and thereby achieve fine along-track resolution.

We can explain the principle by considering the response of SAR to a single bright point target such as a corner reflector or metal building. As the SAR with spacecraft velocity V passes over a given ground target at a fixed slant range R, a series of echoes will be received beginning with the first echo from the leading edge of the antenna along-track footprint and ending with the last echo at the trailing edge of the footprint (Figure F.4).

The length of this along-track footprint is given approximately by

$$L_a = \beta_a R \qquad \text{(F-4)}$$

where β_a is the along-track antenna beamwidth and

R is the range. The along- track antenna beamwidth is given approximately by

$$\beta_a = \lambda/h_a \qquad \text{(F-5)}$$

where λ is the wavelength and h_a is the antenna length (along-track); h_a = 20 m for the Eos SAR design. The time required for the target to traverse the antenna along-track footprint is given by

$$T_a = L_a/V \qquad \text{(F-6)}$$

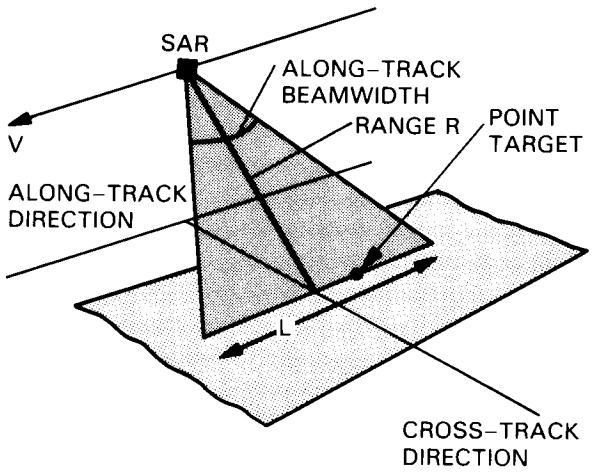

Figure F.4. Illustrating along-track acquisition of target.

As the antenna beam first acquires the target, the radar echoes are negatively Doppler shifted; as SAR travels just over the target the Doppler frequency is zero and as the target departs the beam, the echoes are positively Doppler shifted. The voltage output from the SAR receiver due to this point target is given by

$$v_s(t) = \exp[j2\pi V^2t^2/(\lambda R)] \qquad \text{(F-7)}$$

where V is the spacecraft ground velocity, t is time, λ is the wavelength (6 cm for the C-band channel), R is the slant range, and $j = \sqrt{-1}$. Equation F-7 describes a signal whose frequency varies quadratically with time; the frequency is zero as the target passes just under SAR and rises to a maximum at either end of the along-track footprint of the antenna.

By passing this received signal v_s along with an appropriate fixed reference signal through a correlation device (essentially a suite of narrow-bandwidth filters), it is possible to achieve fine along-track resolution (typically 25 m) at orbital altitudes. Early versions of SAR used an optical correlator with a lens designed to "focus" the above quadratically varying frequencies to a point. SIR-A also used an optical correlator. SIR-B, SIR-C, and Eos will all utilize digital correlators which accomplish the same focusing action by use of a Fast Fourier Transform (FFT) technique. The along-track resolution obtainable by SAR is determined by the Doppler bandwidth B_D of the filter, i.e.,

$$r_a = (\lambda R/2V)\, B_D \qquad \text{(F-8)}$$

The maximum attainable along-track resolution for a point target is given by

$$r_a = h_a/2 \qquad \text{(F-9)}$$

Thus, for h_a = 20 m, the maximum along-track resolution is 10 m.

SAR images of interest for Earth observations are composed of many point targets or scatterers. Under the coherent illumination provided by SAR, the addition of backscattered energy from a collection of scatterers gives rise in the SAR image to speckle, which is a form of image noise characteristic of all coherent imaging devices. It is usually desirable to minimize speckle; this can be accomplished by effectively dividing the SAR along-track beam into four to eight subbeams, each giving independent "looks" at the scene. By recording and incoherently averaging the output from each of these looks, the speckle can be reduced, at the expense of decreased resolution.

For these distributed scenes, the resolution is given approximately by

$$r_a = N\, h_a/2 \qquad \text{(F-10)}$$

Thus for an antenna with 20 m length and for N = 4 looks, the azimuth resolution would be approximately 40 m.

SAR POWER CONSIDERATIONS

The received signal to noise ratio (SNR) is the ratio of the received signal power to the thermal noise power generated in the receiver; generally, for good image quality it is desirable to achieve an SNR of at least 3:1. The SNR for SAR is given by

$$\text{SNR} = \frac{P_{av}G^2\lambda^3\sigma^\circ r_c}{2(4\pi)^3R^3kT^\circ FV} \qquad \text{(F-11)}$$

where P_{av} is the average transmit power (W), G is the antenna gain, σ° is the radar backscattering coefficient of the scene, r_c is the cross-track resolution (m), R is the slant range (m), k = Boltzman's constant = 1.38×10^{-23} J K^{-1}, T° is the physical temperature of the antenna (K), F is the receiver noise figure, and V is the spacecraft ground velocity. The peak transmit power is related to the average power by

$$P_p = \frac{P_{av}}{\tau\,(\text{PRF})} \qquad \text{(F-12)}$$

Equation F-11 indicates that the SNR varies with the inverse cube of the spacecraft range to target, with the inverse cube of the wavelength and proportionally to the radar scattering coefficient $\sigma°$. This means that SNR quickly decreases as the range increases (either spacecraft altitude or look angle), and for a given transmit power and $\sigma°$, the SNR rapidly degrades as the frequency increases. In fact, the reason that K_u-band SARs are impractical from orbital altitudes is that high-power space qualified transmitters are not currently available.

Equation F-12 indicates that low PRFs correspond to high peak power. For an average power of 100 W, a pulse width τ = 35 μs, and a PRF = 1,500 Hz, a peak power of 1.9 kW would be obtained.

The example given above was for the simple case of a fixed point target. Distributed scenes of interest for Eos SAR are composed of many such point targets or scatterers, each generating its own signal of the form given in Equation F-6. Thus, after along-track and cross-track correlation, each scatterer is focused to a point.

AMBIGUITIES

As indicated earlier, the radar echoes are passed through a series of narrow-band filters in the correlator (processor) in order to focus the image. Ambiguities in these filters occur when the sampling rate (PRF) is not high enough to satisfy the Nyquist sampling criterion. Essentially, "ghosts" or "aliases" of the desired radar echoes appear within the filter passband.

Since these ambiguities produce undesired aliases or noises in the SAR image, it is desirable to reduce them to a minimum level. The ambiguity level, which is the ratio of the power in all the undesired alias radar echoes to the power in the desired echoes is normally kept low, e.g., -20 dB. This is accomplished in part by correct sizing of the SAR antenna.

To avoid significant ambiguity noise, it is necessary to provide a minimum antenna aperture area given approximately by

$$\text{Area} = h_a h_c > k_d (4 V R \tan \theta)/f \quad \text{(F-13)}$$

where V is the spacecraft velocity, R is the range to the swath midpoint, θ is the incidence angle, f is the frequency, and k_d is an antenna illumination factor taken here as 1.5. Thus, as the incidence angle increases it is necessary to increase the antenna area. However, in order to maintain wide swaths, it is desirable to keep the antenna width h_c as small as possible. Thus, for SAR images at large incidence angles and with low ambiguities, the antenna length h_a must be increased. Consider an example where V = 7 km/s, R = 1,000 km, and f = 5.298 GHz; if the maximum incidence angle is 45°, then the minimum area would be 5.3 m^2; thus, if the antenna width were h_c = 0.75 m, then the minimum antenna length would be 10.6 m. If the maximum incidence angle were now increased to 60° (tan 60° = 1.732), then with the same antenna width, the minimum antenna length would have to be increased to 10.6 × 1.732 = 18.4 m.

REFERENCES

Aleksandrov, V.Y., and V.S. Loshchilov, Quantitative interpretation of satellite radar images of sea ice using a priori data, *Issledovaniye Zemli iz Kosmosa, 3,* 28, 1985.

Alpers, W.R., Monte Carlo simulations for studying the relationship between ocean wave and Synthetic Aperture Radar image spectra, *J. Geophys. Res., 88C3,* 1745, 1983.

Alpers, W.R., Imaging ocean surface waves by Synthetic Aperture Radar-A review, in *Satellite Microwave Remote Sensing,* edited by E. D. Allan, Chapter 6, Ellis Horwood Ltd., England, 1983.

Alpers, W.R., Theory of radar imaging of internal waves, *Nature, 314,* 245, 1985.

Alpers, W.R., and C. Bruening, On the relative importance of motion-related contributions to the SAR imaging mechanism of ocean surface waves, *IEEE Trans. Geosci. Remote Sens., GE-24,* 873, 1986.

Alpers, W.R., C. Bruening, and K. Richter, Comparison of simulated and measured Synthetic Aperture Radar image spectra with buoy-derived ocean wave spectra during the Shuttle Imaging Radar B Mission, *IEEE Trans. Geosci. Remote Sens., GE-24,* 559, 1986.

Alpers, W.R., and I. Henning, A theory of the imaging mechanism of underwater bottom topography by real and Synthetic Aperture Radar, *J. Geophys. Res., 89(C6),* 10,529, 1984.

Alpers, W.R., D.B. Ross, and C.L. Rufenach, On the detectability of ocean surface waves by real and Synthetic Aperture Radar, *J. Geophys. Res., 86(C7),* 6481, 1981.

American Society of Photogrammetry, *Manual of Remote Sensing, Volume 11,* 2nd edition, Falls Church, VA, p. 2174, 1983.

Babaev, A.G., and N.S. Orlovskii, Some results of investigations of desert problem in the tenth five-year plan period, *Problemy Osvoeniya Pustyn,* Allerton Press Inc., p. 3, 1981.

Beal, R.C., P.S. DeLeonibus, and I. Katz (Eds.), *Spaceborne Synthetic Aperture Radar for Oceanography,* The Johns Hopkins Press, 216 pp., 1981.

Beal, R.C., F.M. Monaldo, D.G. Tilley, D.E. Irvine, E.J. Walsh, F.C. Jackson, D.W. Hancock, III, D.E. Hines, R.N. Swift, F.I. Gonzalez, D.R. Lyzenga, and L.F. Zambresky, A comparison of SIR-B directional ocean wave spectra with aircraft scanning radar spectra, *Science, 232,* 1531, 1986a.

Beal, R.C., T.W. Gerling, D.E. Irvine, F.M. Monaldo, and D.G. Tilley, Spatial variations of ocean wave directional spectra from the Seasat Synthetic Aperture Radar, *J. Geophys. Res., 91(C2),* 2433, 1986b.

Blanchard, B.J., A.J. Blanchard, S. Theis, W.D. Rosenthal, C.L. Jones, Seasat SAR response for water resources parameters, Final Report 3891, Remote Sensing Center, Texas A&M University, Texas, 1981.

Blom, R., and C. Elachi, Spaceborne and airborne imaging radar observations of sand dunes, *J. Geophy. Res., 86(B4),* 3061, 1981.

Bradley, G.A., and F.T. Ulaby, Aircraft radar response to soil moisture, *Remote Sens. Environ., 11,* 419, 1981.

Breed, C.S., J.F. McCauley, G.G. Schaber, A.S. Walker, and G.L. Berlin, Dunes on SIR-A images, in *Shuttle Imaging Radar-A (SIR-A) Experiment,* edited by J.B. Cimino and C. Elachi, California Institute of Technology, *JPL 82-77,* p. 4-52, 1982.

Bretherton, F., *et al.,* Earth System Science: A Program for Global Change, Report of the Earth System Sciences Committee, NASA Advisory Council, Washington, D.C., 1986.

Bryan, M.L., and R.W. Larson, The study of fresh water lake ice using multiplexed imaging radar, *J. Glaciol., 14(72),* 445, 1975.

Burtsev, A.I., V.A. Krovotyntsev, M. Nazirov, P.A. Nikitin, and Y.G. Spiridonov, Radar maps of Arctic and Antarctic from data of Kosmos-1500 Satellite and preliminary results of analyses, *Issledovaniye Zemli iz Kosmosa, 3,* 54, 1985.

Bushuyev, A.V., V.D. Grishchenko, and A.D. Masanov, Interpreting sea ice on satellite radar images, *Issledovaniye Zemli iz Kosmosa, 3,* 9, 1985.

Butler, D., *et al.,* Earth Observing System: Science and Mission Requirements Working Group Report Vol. I, *NASA TM 86129,* 51 pp., 1984.

Butler, D., *et al.,* From Pattern to Process: The Strategy of the Earth Observing System, Report of the Eos Science Steering Committee, Vol. II, 1987.

Carsey, F.D., Summer Arctic sea ice character from satellite microwave data, *J. Geophys. Res., 90(C3),* 5025, 1985.

Carsey, F.D., and B. Holt, Beaufort-Chukchi ice margin data from Seasat: Ice motion, *J. Geophys. Res., 92(C7),* 7163, 1987.

Carsey, F.D., B. Holt, S. Martin, L. McNutt, D.A. Rothrock, V.A. Squire, and W.F. Weeks, Weddell-Scotia Sea marginal ice zone observations from space October, 1984, *J. Geophys. Res., 91(C3),* 3920, 1986.

Carsey, F.D., K. Jezek, J. Miller, W. Weeks, and G. Weller, The Alaska SAR Facility Project, Eos Transactions, *Amer. Geophys. Union, 68,* 593, 1987.

Carsey, F.D., R.O. Ramseier, and W.F. Weeks, Sea ice mission requirements for the U.S. FIREX and Canada Radarsat programs, NASA/JPL, 72 pp., 1982.

Chase, R., *et al.,* Earth Observing System Data and Information System, Report of the Eos Data Panel, Volume IIa, *NASA TM 87777,* 1986.

Chavez, P.S., Jr., and E. Sanchez, Digital combination of Landsat and Seasat images, *Eos, 62,* 294, 1981.

Chavez, P.S., Jr., G.L. Berlin, and M.A. Tarabzouni, Discriminating lithology and surficial deposits in the Al Hisma Plateau region of Saudi Arabia with digitally combined Landsat MSS and SIR-A images, in *Remotely Sensed/Geographic Information Systems in Geologic Applications,* 1983 Nat'l. Conf. Resour. Mgmt. Appl., p. 22, 1983.

Cheney, R.E., A search for cold water rings, in *Spaceborne Synthetic Aperture Radar for Oceanography,* edited by R.C. Beal, P.S. DeLeonibus, and I. Katz, Johns Hopkins University Press, Baltimore, MD, 215 pp., 1981.

Cimino, J.B., and C. Elachi, The SIR-B Radar on the Shuttle, *Proceedings of the Second Thematic Conference: Remote Sensing for Exploration Geology,* Fort Worth, Texas, 1982.

Cimino, J., A. Brandani, D. Casey, J. Rabassa, and S.D. Wall, Multiple incidence angle SIR-B experiment over Argentina: mapping of forest units, *IEEE Trans. Geosci. Remote Sens.,* 1986.

Cohen, S.C., and J.J. Degnan, Spaceborne laser ranging from Eos, *Proceedings of IGARSS'87,* Ann Arbor, Michigan, 1987.

Condie, D.C., *Plate Tectonics and Crustal Structure,* (2nd Edition), Pergamon Press, New York, 310 pp., 1982.

Curlander, J.C., B. Holt, and K.J. Hussen, Determination of sea ice motion using digital SAR imagery, *IEEE J. of Oceanic Eng., OE-10,* 4, 358, 1985.

Curran, R.J., *et al.,* LASA: Lidar Atmospheric Sounder and Altimeter Instrument Panel Report, Volume IId, 1987.

Daily, M., C. Elachi, T.G. Farr, and G.G. Schaber, Discrimination of geologic units in Death Valley using dual frequency and polarization imaging radar data, *Geophys. Res. Letters, 5,* 889, 1978.

Dellwig, L.F., H.C. MacDonald, and J.N. Kirk, The potential of radar in geological exploration, *Proceedings of the Fifth Symposium on Remote Sensing of Environment,* Institute of Science and Technology, University of Michigan, Ann Arbor, 747, 1968.

De Martonne, E., Regions of interior-basin drainage, *Geogr. Rev., 17,* 397, 1927.

Dobson, M.C., and F.T. Ulaby, Preliminary evaluation of the SIR-B response to soil moisture, surface roughness, and crop canopy cover, *IEEE Trans. Geosci. Remote Sens.,* 1986.

Dozier, J., S.R. Schneider, and D.F. McGinnis, Jr., "Effect of grain size and snowpack water equivalence on visible and near-infrared satellite observations of snow," *Water Resour. Res., 17,* 1213, 1981.

Dregne, H.E., Soils of arid lands, Dev. in *Soil Science,* Chapter 6, Elsevier Sci. Publ. Co., New York, p. 13, 1976.

Dregne, H.E., Desertification of Arid Lands, *Economic Geography, 3,* 329, 1977.

Elachi, C., W.E. Brown, J.B. Cimino, T. Dixon, D.L. Evans, J.P. Ford, R.S. Saunders, C. Breed, H. Masursky, J.F. McCauley, G. Schaber, L. Dellwig, A. England, H. MacDonald, P. Martin-Kaye, and F. Sabins, Shuttle Imaging Radar Experiment, *Science, 218,* 996, 1982.

Elachi, C., L.E. Roth, and G.G. Schaber, Spaceborne radar subsurface imaging in hyperarid regions, *IEEE Trans. Geosci. Remote Sens., GE-22,* 383, 1984.

Engman, E.T., Remote sensing applications in watershed modeling in applied modeling in catchment hydrology, *Proceedings of the International Symposium of Rainfall-Runoff Modeling,* Mississippi State, Mississippi, p. 473, 1981.

Esaias, W., *et al.,* MODIS: Moderate-Resolution Imaging Spectrometer Instrument Panel Report, Report of the MODIS Panel, Volume IIb, 1986.

Evans, D.L., Geological applications of multipolarization SAR data, in *The Second Spaceborne Imaging Radar Symposium,* 1986, Pasadena, California, 1986.

Evans, D.L., *et al.,* Multipolarization radar images for geologic mapping and vegetation discrimination, *IEEE Trans. Geosci. Remote Sens., GE-24,* 246, 1986.

Farr, T.G., and D.L. Evans, Geologic applications of multisensor remote sensing, *Geol. Soc. Amer. Abs. with Prog., 18,* 598, 1986.

Fily, M., and D.A. Rothrock, Extracting sea ice data from satellite SAR imagery, *IEEE J. Geosci. Remote Sens., GE-24,* 849, 1986.

Ford, J.P., Seasat orbital radar imagery for geologic mapping: Tennessee-Kentucky-Virginia, *Am. Assoc. Petrol. Geol., 64,* 2064, 1980.

Ford, J.P., Resolution versus speckle relative to geologic interpretability of spaceborne radar images: A survey of user preference, *IEEE Trans. Geosci. Remote Sens., GE-20,* 434, 1982.

Ford, J.P., R.G. Blom, M.L. Bryan, M.I. Daily, T.H. Dixon, C. Elachi, and E.C. Xenos, Seasat views North America, the Caribbean, and western Europe with imaging radar, California Institute of Technology, *JPL 80-67,* 141 pp., 1980.

Ford, J.P., J.B. Cimino, and C. Elachi, Space Shuttle Columbia views the world with imaging radar: the SIR-A experiment, California Institute of Technology, *JPL 82-95,* 179 pp., 1983.

Ford, J.P., J.B. Cimino, B. Holt, M. Ruzek, Shuttle imaging radar views the Earth from Challenger: The SIR-B Experiment, California Institute of Technology, *JPL 86-10,* 135 pp., 1986.

Fownes, J.H., and J.D. Aber, Forest canopy chemistry from Blackhawk Island, Wisconsin, in *Proceedings of the Airborne Imaging Spectrometer Data Analysis Workshop,* edited by G. Vane and A.F.H. Goetz, *JPL 85-41,* Pasadena, CA, 1985.

Froideaux, C.M., Radar, an optimum remote-sensing tool for detailed plate tectonics analysis and its application to hydrocarbon exploration (an example in Irian Jaya, Indonesia), in *Radar Geology: An Assessment,* California Institute of Technology, *JPL 80-61,* 457, 1980.

Fu, L.L., and B. Holt, Seasat views oceans and sea with Synthetic Aperture Radar, *JPL 81-120,* 200 pp., 1982.

Fu, L.L., and B. Holt, Some examples of detection of oceanic mesoscale eddies by the Seasat Synthetic Aperture Radar, *J. Geophys. Res., 88(C3),* 1844, 1983.

Fu, L.L., and B. Holt, Internal waves in the Gulf of California: Observations from a spaceborne radar, *J. Geophys. Res., 89(C2),* 2053, 1984.

Fung, A.K., and F.T. Ulaby, Matter-energy interactions in the microwave region, in *Manual of Remote Sensing,* 2nd Edition, Amer. Soc. Photogram., edited by R.N. Colwell, Sheridan Press, p. 115, 1983.

Gasparovic, R.F., J.R. Apel, D.R. Thompson, and J.S. Tochko, A comparison of SIR-B Synthetic Aperture Radar data with ocean internal wave measurements, *Science, 232,* 1529, 1986.

Gerling, T.W., Fine scale structure of the surface wind field from the Seasat SAR, *J. Geophys. Res., 91(C2),* 2308, 1986.

Goetz, A.F.H., and M. Herring, The High-Resolution Imaging Spectrometer (HIRIS) for Eos, *Proceedings of IGARSS'87,* Ann Arbor, MI, 1987.

Gonzalez, F.I., T.W. Thompson, W.E. Brown, Jr., and D.E. Weissman, Seasat wind and wave observations of Northeast Pacific Hurricane Iva, August 13, 1978, *J. Geophys. Res., 87(C5),* 3431, 1982.

Gray, A.L., R.K. Hawkins, C.E. Livingstone, and L.D. Arsenault, Seasonal effects on the microwave signatures of Beaufort Sea ice, *Proceedings of 15th International Symposium on Remote Sensing of the Environment,* ERIM, Ann Arbor, MI, 1981.

Gurney, R.J., J.P. Ormsby, and D.K. Hall, A comparison of remotely sensed surface temperature and biomass estimates for aiding evapotranspiration determination in Central Alaska, *Proceedings of the Permafrost: Fourth International Conference,* 1983.

Hall, R.T., A test of the AIDJEX ice model using Landsat images, in *Sea Ice Processes and Models,* edited by R.S. Pritchard, University Washington Press, p. 89, 1980.

Hall, R.T., and D.A. Rothrock, Sea ice displacement from Seasat Synthetic Aperture Radar, *J. Geophys. Res., 86,* 11078, 1981.

Hasselmann, K., R.K. Raney, W.J. Plant, W. Alpers, R.A. Schuchman, D.R. Lyzenga, C.L. Rufenach, and M.J. Tucker, Theory of Synthetic Aperture Radar ocean imaging: A MARSEN view, *J. Geophys. Res., 90(C3),* 4659, 1985.

Hoffer, R., D.F. Lozano-Garcia, D.D. Gillespie, P.W. Mueller, and M.J. Ruzek, Analysis of multiple incidence angle SIR-B data for determining forest stand characteristics, 2nd Space-Borne Imaging Radar Symposium, May 1986, JPL, Pasadena, CA, 1986.

Holt, B., and S. Digby, Processes and imagery of first-year sea ice during the melt season, *J. Geophys. Res., 90(C3),* 5045, 1985.

Hoogeboom, P., Classification of agricultural crops in radar images, *IEEE Trans. Geosci. Remote Sens., GE-21,* 329, 1983.

Hovanessian, S.A., *Introduction to Synthetic Array and Imaging Radars,* Artech House, Inc., Dedham, MA, 156 pp., 1980.

Imhoff, M., M. Story, C. Vermillion, F. Khan, and F. Polcyn, Forest canopy characterization and vegetation penetration assessment with spaceborne radar, *IEEE Trans. Geosci. Remote Sens., GE-24,* 535, 1986.

Jackson, T.J., A. Chang, and T.J. Schmugge, Active microwave measurements for estimating soil moisture in Oklahoma, *Photogram. Eng. Remote Sens., 47,* 801, 1981.

Jackson, T.J., and P.E. O'Neill, Aircraft scatterometer observations of soil moisture on rangeland watersheds, *Int. J. Remote Sens., 6,* 1135, 1985.

Jensen, K.H., and T. Jonch-Clausen, Unsaturates flow and evapotranspiration modeling as a component of the European hydrologic system (SHE), in *Modeling Components of Hydrologic Cycle,* Water Resources Publication, Littleton, CO, p. 235, 1982.

Jones, W.L., V.E. Delnore, and E.M. Bracalente, The study of mesoscale ocean winds, in *Spaceborne Synthetic Aperture Radar for Oceanography,* edited by R.C. Beal, P.S. DeLeonibus, and I. Katz, Johns Hopkins University Press, Baltimore, MD, 215 pp., 1981.

Kasischke, E.S., G.A. Meadows, and P.L. Jackson, *The Use of Synthetic Aperture Radar Imagery to Detect Hazards to Navigation,* Environmental Research Institute of Michigan, *169200-2-F,* 194 pp., 1984.

Kaupp, V.H., L.R. Gaddis, P.J. Mouginis-Mark, B.A. Darryberry, H.C. MacDonald, and W.P. Waite, Preliminary analyses of SIR-B radar data for recent Hawaii lava flows, *Remote Sens. Environ.,* (in press), 1987.

Kennett, R., A study of the global over-land K_u-band backscatter coefficients using data from the SEASAT scatterometer, (in preparation), 1987.

Keyte, G.E., and J.T. Macklin, SIR-B observations of ocean waves in the NE Atlantic, *IEEE Trans. Geosci. Remote Sens., GE-24,* 1986.

Kharin, N.G., Actual problems in desertification control of arid territories, *Problemy Osvoeniya Pustyn, 1,* 8, 1985.

Kim, Y.S., Theoretical and Experimental Study of Radar Backscatter from Sea Ice, Ph.D. Dissertation, University of Kansas, Lawrence, KS, 1984.

Koopmans, B.N., Side-looking radar, a tool for geological surveys, in *Remote Sensing Reviews,* edited by G.P. DeLoor, Harwood Academic Publishers, New York, *1,* 19, 1983.

Le Houerou, H.N., Desertification problems in northern China: An overview, in *Delegation Trip Report-Arid Lands in China,* America Assoc. Adv. Sci., Washington D.C., p. 5, 1984.

Leberl, F., A. Domik, J. Raggam, and M. Kobrick, Radar stereomapping techniques and application to SIR-B images of Mt. Shasta, *IEEE Trans. Geosci. Remote Sens., GE-24,* 473, 1986.

Leberl, F., J. Raggam, C. Elachi, and W.J. Campbell, Sea ice motion measurements from Seasat-SAR images, Seasat Special Issue II, Scientific Results, J. Geophys. Res., 88(C3), 1915, 1983.

Li, R.Y., F.T. Ulaby, and J.R. Eyton, Crop classification with a Landsat-Radar sensor combination, in *Proceedings of the 1980 Symposium on Machine Processed Remotely Sensed Data,* Purdue Univ., West Lafayette, IN, June 2-6, 1980.

Lichy, D.E., M.G. Mattie, and L.J. Mancini, Tracking of a warm water ring, in *Spaceborne Synthetic Aperture Radar for Oceanography,* (edited by R.C. Beal, P.S. DeLeonibus, and I. Katz), p. 171, The Johns Hopkins Press, 1981.

Lingle, C.S., and T.J. Brown, A subglacial aquifer bed model and water pressure dependent basal sliding relationship for the West Antarctic ice stream, in *Dynamics of the West Antarctic Ice Sheet* (edited by C.J. Van der Veen and J. Oerlemans), p. 249, Reidel Publishing Co., 1987.

MacDonald, H.C., Use of radar in Geology, Part VI in Remote Sensing of the Electromagnetic Spectrum, Forum of the Remote Sensing Committee of the Assoc. of Amer. Geographers, *3,* 93, 1976.

MacDonald, H.C., J.N. Kirk, L.F. Dellwig, and A.J. Lewis, The influence of radar look direction on the detection of selected geologic features, in *Proceedings of the Sixth Symposium on Remote Sensing of Environment,* University of Michigan, Ann Arbor, p. 637, 1969.

MacDonald, H.C., and W.P. Waite, Optimum radar depression angles for geological analysis, *Modern Geol., 2,* 179, 1970.

MacDonald, H.C., and W.P. Waite, Imaging radars provide terrain texture and roughness parameters in semi-arid environments, *Modern Geol., 4,* 2, 145, 1973.

Martin, S., B. Holt, D. Cavalieri, and V.A. Squire, Shuttle Imaging Radar-B (SIR-B) Weddell Sea Ice observations: A comparison of SIR-B and SMMR ice concentrations, *J. Geophys. Res., 92(C7),* 7173, 1987.

McCauley, J.F., C.S. Breed, and M.J. Grolier, The interplay of fluvial, mass-wasting, and eolian processes in the eastern Gilf Kebir region, *Annal. Geol. Surv. Egypt, XI,* 207, 1981.

McCauley, J.F., C.S. Breed, G.G. Schaber, W.P. McHugh, C.V. Haynes, B. Issaw, M.J. Grolier, and A. El-Kilani, Paleodrainages of the eastern Sahara—the radar rivers revisited, *IEEE Trans. Geosci. Remote Sens., GE-24,* 1986.

McCauley, J.F., G.G. Schaber, C.S. Breed, M.J. Grolier, C.U. Haynes, B. Issawi, C. Elachi, and R. Blom, Subsurface valleys and geoarcheology of the Eastern Sahara revealed by Shuttle Radar, *Science, 218,* 1004, 1982.

McLeish, W., and D.B. Ross, Imaging radar observations of directional properties of ocean waves, *J. Geophys. Res., 88(C7),* 4407, 1983.

Meigs, P., World distribution of arid and semi-arid homoclimates, in *UNESCO, Review of Research on Arid Zone Hydrology, Arid Lands Res.,* 1, 203, 1953.

Mitnik, L.M., G.I. Desyatova, V.V. Kovbasynk, Determination of characteristics of ice cover of the Sea of Okhotsk in winter of 1983-1984 from radar probing data, *Issledovaniye Zemli iz Kosmosa, 3,* 16, 1985.

Moe, T., T.J. Schmugge, and T.J. Jackson, Calculations of radar backscattering coefficient of vegetative-covered soils, *Remote Sens. Environ., 15,* 119, 1984.

Mognard, N.M., and W.J. Campbell, Comparison of sea surface wind speed fields by Seasat radar altimeter, scatterometer, and microwave radiometer, with an emphasis on the southern ocean, in *Proceedings of IGARSS'1984,* Strasbourg, France, 403, 1984.

Mollo-Christensen, E., Surface signs of internal ocean dynamics, in *Spaceborne Synthetic Aperture Radar for Oceanography,* edited by R.C. Beal, P.S. DeLeonibus, and I. Katz, Johns Hopkins University Press, Baltimore, MD, 215 pp., 1981.

National Research Council, A Strategy for Earth Science from Space in the 1980's. Part I: Solid Earth and Oceans, National Academy of Sciences, Washington, D.C., 99 pp., 1982.

National Research Council, Opportunities for research in the geologic sciences, National Academy of Sciences, Washington, D.C., 95 pp., 1983.

National Research Council, A Strategy for Earth Science from Space in the 1980's and 1990's. Part II: Atmosphere and Interactions with the Solid Earth, Oceans, and Biota, National Academy of Sciences, Washington, D.C., 149 pp., 1985.

National Research Council, Global Change in the Geosphere-Biosphere: Initial Priorities for an IGBP, National Academy of Sciences, Washington, D.C., 91 pp., 1986a.

National Research Council, Remote Sensing of the Biosphere, National Academy of Sciences, Washington, D.C., 135 pp., 1986b.

PIPOR Science Working Group, A Programme for International Polar Oceans Research (PIPOR), *ESA SP-1074,* 42 pp., 1985.

Price, J.F., E.A. Terray, and R.A. Weller, Upper ocean dynamics, *Rev. Geophys., 25,* 193, 1987.

Rango, A. (Chairman), Plan of Research for Integrated Soil Moisture Studies, Recommendations of the Soil Moisture Working Group, National Aeronautics and Space Administration, Washington, D.C., 70 pp., 1980.

Rebillard, P., and T.P. Nguyen, An exploitation of coregistered SIR-A, Seasat and Landsat images, in *Proceedings of the International Symposium on Remote Sensing of Environment,* Environmental Research Institute of Michigan, Ann Arbor, 109, 1982.

Riom, J., and T. LeToan, Relations Entre des Types de Forets de Pins Maritimes et la Retrodiffusion Radar en Bande, in *Proceedings of ISP International Colloquium on Spectral Signatures of Objects in Remote Sensing,* Avignon, France, 455, 1981.

Rufenach, C., and C. Smith, Observation of internal waves in Landsat and Seasat satellite imagery, *Int. J. Remote Sensing, 6,* 1201, 1985.

Sabins, F.F., Jr., *Remote Sensing—Principles and Interpretation,* W.H. Freeman and Co., San Francisco, 426 pp., 1978.

Sabins, F.F., Jr., Geologic interpretation of Space Shuttle radar images of Indonesia, *Amer. Assoc. Petrol. Geologists Bulletin, 67,* 2076, 1983.

Sabins, F.F., Jr., R. Blom, and C. Elachi, Seasat radar images of San Andreas fault, California, *Amer. Assoc. Petrol. Geol., 64,* 619, 1980.

Salomonson, V.V., W. Barnes, H. Montgomery, and H. Ostrow, Modis: Advanced Facility Instrument for Studies of the Earth as a System, in *Proceedings of IGARSS'87,* Ann Arbor, Michigan, 1987.

Saxton, K.E., H.P. Johnson, and R.H. Shaw, Modeling evapotranspiration and soil moisture, *Trans. ASAE, 17,* 673, 1974.

Schaber, G.G., C. Elachi, and T. Farr, Remote sensing data of S. P. Mountain and S. P. lava flow in north-central Arizona, *Remote Sens. Environ., 9,* 149, 1980.

Schaber, G.G., J.F. McCauley, C.S. Breed, and G.R. Olhoeft, Shuttle imaging radar: physical controls on signal penetration and subsurface backscatter in the eastern Sahara, *IEEE Trans. Geosci. Remote Sens., GE-24,* 1986.

Sheridan, D., Desertification of the United States, Council on Environmental Quality; Superintendent of Documents, U.S. Government Printing Office, Washington, D.C., 142 pp., 1981.

Shuchman, R.A., and E.S. Kasischke, Refraction of coastal ocean waves, in *Spaceborne Synthetic Aperture Radar for Oceanography,* edited by R.C. Beal, P.S. DeLeonibus, and I. Katz, Johns Hopkins University Press, Baltimore, MD, 215 pp., 1981.

Smith, E., J.B. Cimino, and D.J. Casey, Eos altitude study report, *JPL D-4127,* 1987.

Spanner, M.A., D.L. Peterson, W. Acevedo, and P. Matson, High resolution spectrometry of leaf canopy chemistry for biogeochemical cycling, in *Proceedings of the Airborne Imaging Spectrometer Data Analysis Workshop,* edited by G. Vane and A.F.H. Goetz, *JPL 85-41,* 1985.

Stiles, W.H., and F.T. Ulaby, The active and passive microwave response to snow parameters, Part I: Wetness, *J. Geophys. Res., 85,* 1037, 1980.

The SWAMP Group, *Ocean Wave Modeling,* 256 pp., Plenum Publishers, New York, NY, 1985.

Swift, C.T., *et al.,* Observations of the polar regions from satellites using active and passive microwave techniques, *Advances Geophys., 27,* 335, 1985a.

Swift, C.T., P.S. Hayes, J.S. Herd, W.L. Jones, and V.E. Delnore, Airborne microwave measurements of the Southern Greenland ice sheet, *J. Geophys. Res., 90,* 1983, 1985b.

Teleki, P.G., W.J. Campbell, R.O. Ramseier, and D. Ross, The offshore environment: A perspective from Seasat SAR data, in *Proceedings of the 11th Annual Offshore Technology Conference, Houston, TX, 215,* 1979.

Theis, S.W., M.J. McFarland, W.D. Rosenthal, and C.L. Jones, Microwave remote sensing of soil moisture, Texas A&M University, College Station, TX, *RSC-3458k-129,* 1982.

Thomas, R.H., *et al.,* Satellite remote sensing for ice sheet research, NASA, *TM-86233,* 32 pp., 1985.

Ulaby, F.T., C.T. Allen, G. Eger, III, and E. Kanemasu, Relating the microwave backscattering coefficient to leaf area index, *Remote Sens. Environ., 14,* 113, 1984b.

Ulaby, F.T., J. Barr, A. Sobti, and R. K. Moore, Soil moisture detection by Skylab's microwave sensors, in *Proceedings of URSI Commission II Specialist Meeting,* p. 205, Berne, Switzerland, September 1974.

Ulaby, F.T., G.A. Bradley, and M.C. Dobson, Microwave backscatter dependence on surface roughness, soil moisture and soil texture, Part II: Vegetation-covered soil, *IEEE Trans. Geosci. Electron., GE-17,* 33, 1979.

Ulaby, F.T., B. Brisco, and M.C. Dobson, Improved spatial mapping of rainfall events with spaceborne SAR imagery, *IEEE Trans. Geosci. Remote Sens. Let., GE-21,* 118, 1983.

Ulaby, F.T., and M.C. Dobson, SIR-B measurements and modeling of vegetation, The Second Spaceborne Imaging Radar Symposium, *JPL 86-26,* April 28-30, Pasadena, CA, 1986.

Ulaby, F.T., D. Held, M.C. Dobson, K.C. McDonald, and T.B.A. Senior, Relating polarization phase difference of SAR signals to scene properties, *IEEE Trans. Geosci. Remote Sens., GE-25,* 82, 1987.

Ulaby, F.T., R.K. Moore, and A.K. Fung, *Microwave Remote Sensing: Active and Passive: Volume 1,* Addison-Wesley, 456 pp., 1981.

Ulaby, F.T., R.K. Moore, and A.K. Fung, *Microwave Remote Sensing: Active and Passive: Volume II,* Addison-Wesley, 607 pp., 1982.

Ulaby, F.T., R.K. Moore, and A.K. Fung, *Microwave Remote Sensing: Active and Passive, Volume III,* Artech House, Inc., MA, 1986.

Ulaby, F.T., W.H. Stiles, and M. Abdelrazik, Snow cover influence on backscatter from terrain, *IEEE Trans. Geosci. Remote Sens., GE-22,* 126, 1984a.

Ulaby, F.T., W.H. Stiles, A.K. Fung, H.J. Eom, and M. Abdelrazik, Observations and modeling of the radar backscatter from snowpacks, University of Kansas Center for Research, Lawrence, KS, *RSL Tech. Report 527-4,* 1982.

Untersteiner, N., The cryosphere, in *The Global Climate,* edited by J.T. Houghton, Cambridge University Press, p. 121, 1984.

Valenzuela, G.R., W.J. Plant, D.L. Schuler, D.T. Chen, and W.C. Keller, Microwave probing of shallow water bottom topography in Nantucket Shoals, *J. Geophys. Res., 90,* 4931, 1985.

van Zyl, J.J., H.A. Zebker, and C. Elachi, Imaging radar polarization signatures: Theory and observation, submitted to Radio Science, June 1986.

Vesecky, J.F., and R.H. Steward, The observation of ocean-surface phenomena using imagery from the Seasat Synthetic Aperture Radar, *J. Geophys. Res., 87,* 3397, 1982.

Wadge, G., and T.H. Dixon, A geological interpretation of Seasat SAR imagery of Jamaica, *J. Geol., 92,* 561, 1984.

Wang, J.R., E.T. Engman, J.C. Shiue, M. Ruzek, and C. Steinmeier, *IEEE Trans. Geosci. Remote Sens., GE-24,* 510, 1986.

Waring, R.H., J.B. Aber, J.M. Melillo, and B. Moore, III, Precursors of change in terrestrial ecosystems, *Bioscience, 36,* 433, 1986.

Weeks, W.F., A.J. Gow, and R.J. Schertler, Ground-truth observations of ice covered North Slope lakes imaged by radar, *CRREL Report 81-19,* 17 pp., 1981.

Weller, G., F. Carsey, B. Holt, D.A. Rothrock, and W.F. Weeks, Science program for an imaging radar receiving station in Alaska, *JPL 400-207,* 45 pp., 1983.

Wing, R.S., Cholame area-San Andreas fault zone, California: A study in SLAR, *Modern Geology, 1,* 173, 1970.

Wing, R.S., and H.C. MacDonald, Radar geology, petroleum exploration technique, Eastern Panama and northwestern Colombia, *Amer. Assoc. Pet. Geol. Bulletin, 57,* 825, 1973.

ADDITIONAL SAR REFERENCES

Bernstein, R. (Editor), SEASAT Special Issue I, *J. Geophys. Res., 87(C5),* 1982.

Cimino, J.B., and C. Elachi (Editors), Shuttle Imaging Radar-A (SIR-A) experiment, California Institute of Technology, *JPL 82-77,* 174 pp., 1982.

Ford, J.P., R.G. Blom, M.G. Bryan, M.I. Daily, T.H. Dixon, C. Elachi, and X.C. Xenos, Seasat views North America, the Caribbean, and Western Europe with imaging radar, California Institute of Technology, *JPL 80-67,* 141 pp., 1980.

Ford, J.P., J.B. Cimino, and C. Elachi, Space Shuttle Columbia views the world with imaging radar: The SIR-A experiment, California Institute of Technology, *JPL 82-95,* 179 pp., 1983.

Ford, J.P., J.B. Cimino, B. Holt, and M.R. Ruzek, Shuttle imaging radar views the Earth from Challenger: The SIR-B experiment, California Institute of Technology, *JPL 86-10,* 135 pp., 1983.

Fu, L., and B. Holt, Seasat views the oceans and sea ice with Synthetic Aperture Radar, California Institute of Technology, *JPL 81-120,* 200 pp., 1982.

Imaging Radar Science Working Group, The SIR-B science plan, California Institute of Technology, *JPL 82-78,* 1982.

Johns Hopkins APL Technical Digest, Special issue on ocean science II, *6,* 1985.

Kirwan, A.D., T.J. Ahrens, and G.H. Bern (Editors), SEASAT special issue II, *J. Geophys. Res., 88(C3),* February 28, 1983.

Ottl, H., and F. Valdoni, The X-SAR science plan, Deutsche Forschungs- und Versuchsanstalt fur Luft- und Raumfahrt-Mitteiliung, *85-17,* 160 pp., 1985.

Pravdo, S.H., B. Huneycutt, B. Holt, and D.H. Held, Seasat Synthetic Aperture Radar data user's manual, California Institute of Technology, JPL 82-90, 1983. Proceedings of the Symposium Measuring Ocean Waves from Space, Johns Hopkins APL Technical Digest, *8,* 1987.

The second spaceborne imaging radar symposium, California Institute of Technology, *JPL 86-26,* 1986.

The Shuttle Imaging Radar-C science plan, California Institute of Technology, *JPL 86-29,* 1986.

Spaceborne Imaging Radar Symposium, California Institute of Technology, *JPL 83-11,* 1983.

Weller, G., F. Carsey, B. Holt, D. Rothrock, and W. Weeks, Science program for an imaging radar receiving station in Alaska, California Institute of Technology, JPL Publication, 45 pp., 1983.

GLOSSARY

Albedo: Ratio of electromagnetic radiation reflected by a body to the amount of radiation incident upon the body

Alluvial Fan: Cone-shaped deposit formed where a stream issues from mountains onto lowlands

Andesite: Rock composed essentially of andesine and one or more mafic constituents, as applied to volcanic rocks

Anisotropic: Having physical or optical properties that vary in different directions

Anticline: Folded-rock structure whose limbs dip away from the fold axis

Azimuth: Bearing of a line measured clockwise from geographic north

Azimuth: Along-track direction of image acquisition, in reference to ambiguity level (see figure)

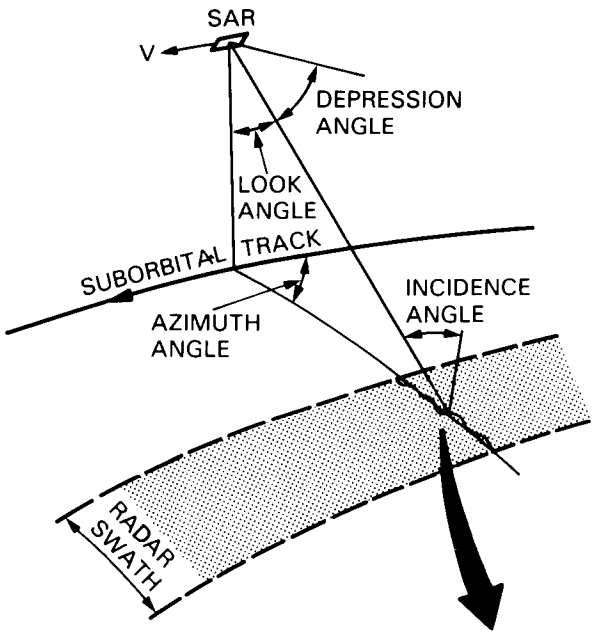

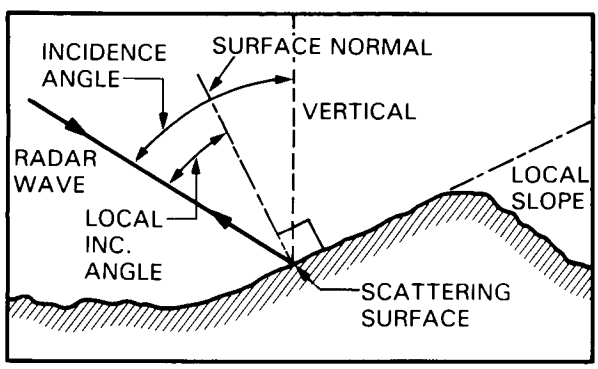

Azimuth: Angle formed by line from subsatellite point to a target on the Earth's surface and the line along the cross-track direction

Backscatter: Portion of microwave energy scattered by the Earth's surface that is reflected back to the radar antenna

Backslope: Slope that is inclined away from an incident radar beam

Band: An interval in the electromagnetic spectrum whose boundaries are marked by a lower and an upper limiting wavelength, or frequency

Bandwidth: Frequency range used to modulate a transmitted carrier frequency

Barchan: A dune having a crescentic ground plan, with the convex side facing the wind

Basalt: Rock composed essentially of calcic plagioclase and pyroxene, as applied to fine-to-medium-grained volcanic rocks

Bathymetry: Measurement of ocean depth

Beamwidth: Angle subtended by the two points on the main beam of the antenna pattern at which the received (or transmitted) power is one-half of that on the peak of the pattern

Biomass: Total mass (or weight) of living matter per unit area or volume

Biome: A major ecological community of organisms occupying a large area (e.g., tropical rainforest, tundra)

Bragg Scattering: Enhanced scattering in a given direction from a periodically rough surface which results when the electrical pathlength difference between radar returns from adjacent surface peaks corresponds to an integral number of half-wavelengths

Dielectric Constant: A measure of the ability of a given material to store and reflect electric energy; identical with the term dielectric permittivity

Dike: Tabular body of intrusive rock that crosscuts the structure of the host rock

Dip: Angle at which a bed or other planar feature is inclined from horizontal

Dome: Any structural deformation characterized by approximately circular local uplift

Doppler Effect: Apparent change of frequency of electromagnetic waves varying with relative velocity of source and observer

Ecotone: Transitional zone between two adjacent communities containing species characteristic of both zones as well as other species occurring only within the zone

Electromagnetic Spectrum: An ordered progression of radiations that includes cosmic, gamma, X, ultraviolet, visible, infrared, microwave, and radiowave energy

Elevation: Inclination of the sun to horizontal

Emissivity: The ability of a surface to radiate electromagnetic energy relative to that of an ideal blackbody with the same surface shape and temperature

Eolian: Eroded or deposited by wind action

Evapotranspiration: Loss of water from the Earth's surface by evaporation from lakes, streams, and soil surfaces and by transpiration of plants

Floeberg: A mass of hummocked ice formed by the piling up of many ice floes by lateral pressure; may be more than 15 m high and resemble an iceberg

Foliar: Relating to leaf or leaves

Geocoded: Plotted on an Earth-fixed coordinate system

Geomorphology: The science dealing with origins of Earth's topography and landforms

Georeferenced: Located according to a geographic reference system

Geostrophic: A force producing deflection as a result of the Earth's rotation

Gneiss: Coarse grained rock with alternating bands of granular and schistose material

Hysteresis: A lag of effect when the forces acting on a body are changed

Ice Floe: Relatively flat piece of sea ice 20 m or more across

Incidence: Angle between the incident radar beam at the ground and the normal to the ground surface at the point of incidence (see figure)

Isotropic: Having the same physical or optical properties regardless of the angular orientation or direction of the measuring device

Kosmos: Russian satellite used to observe ice

Landsat: A series of five orbital imaging satellites that have measured and recorded reflectance from the Earth's surface at visible and infrared wavelengths

Lead: Fracture through sea ice that is navigable by surface vessels

Lignin: A complex organic substance that binds cellulose fibers in wood and strengthens cell walls

Look Angle: Angle between the vertical plane and the line that links an imaging-radar antenna to a feature on the ground (see figure)

Lossy: Describing the dissipation of electromagnetic energy by a material

Microwave: Any electromagnetic wave having a wavelength in the interval between one millimeter and one meter

Mie Scattering: Scattering of electromagnetic energy by spherical particles

Nilas: Thin elastic crust of gray-colored ice formed on calm sea

Paleodrainage: Ancient stream systems

Permittivity: Dielectric constant

Phenology: The study of periodically recurring natural phenomena and their relation to climate and changes in season

Phreatic Zone: Subsurface zone in which water fills the interstices and is under pressure greater than atmospheric pressure

Pixel: Single sample of data or picture element in a digital image

Pleistocene: From 2 million to 10,000 B.P.

Polarimeter: A radar for which the polarization states of both transmitted and received waves can be arbitrarily specified

Polynya: Area of open water surrounded by sea ice

Quaternary: Younger of two periods of the Cenezoic era, lasting from 600,000 B.P. until present

Radar: Radio Detection And Ranging

Range: Across-track direction of image acquisition

Rayleigh Scattering: Scattering by particles small in size compared with the wavelength being scattered

Sastrugi: Long, wavelike ridges of hard snow formed perpendicular to the direction of wind

Scatterometer: A calibrated radar that measures the radar backscattering coefficient as a function of angle

Senescence: That phase of plant growth extending from full maturity to death

Shutterridges: Ridge formed by displacement of a fault traversing a ridge-and-valley topography with the displaced part of a ridge shutting in the adjacent ridge or canyon

Spectral Reflectance: Reflectance of electromagnetic energy at specified wavelength intervals

Specular: Describing surfaces that are electrically flat or near flat

Syncline: Folded-rock structure whose limbs dip toward the fold axis

Telescience: The conduct of geoscientific inquiry by telecommunication and remote interaction with a bank of scientific or engineering data

Terrane: A geologic formation or series of formations

Terrain: Topographical features

Waveguide: A hollow conducting pipe used for efficient transmission of microwaves